

①

AD-A283 531

PL-TR-93-2266



**ULTRASENSITIVE INFRARED
CHEMILUMINESCENCE DETECTION**

**W.T. Rawlins
M.E. Fraser
K.W. Holtzclaw
W.J. Marinelli
H.C. Murphy
L.G. Piper**

**Physical Sciences Inc.
20 New England Business Center
Andover, MA 01810**

October 1993

**Final Report
September 1988-September 1993**

**DTIC
ELECTE
AUG 22 1994
S G D**

Approved for public release, distribution unlimited.

94-24574
 538

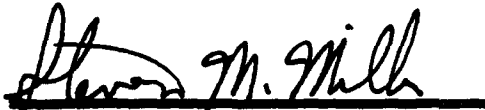
DTIC QUALITY INSPECTED 5



**PHILLIPS LABORATORY
Directorate of Geophysics
AIR FORCE MATERIEL COMMAND
HANSCOM AFB, MA 01731-3010**

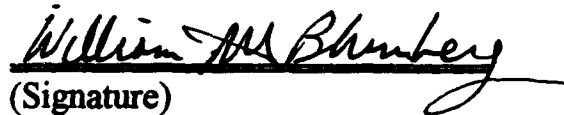
94 8 19 090

"This technical report has been reviewed and is approved for publication"



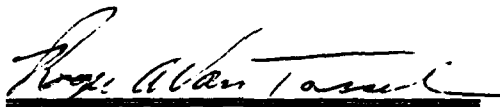
(Signature)

Steven M. Miller
Contract Manager
Simulations Branch
Optical Environmental Division



(Signature)

William A.M. Blumberg, Branch Chief
Simulations Branch
Optical Environmental Division



(Signature)

ROGER A. VAN TASSEL, DIRECTOR
Optical Environmental Division

This report has been reviewed by the ESC Public Affairs Office (PA) and is releasable to the National Technical Information Service (NTIS).

Qualified requestors may obtain additional copies from the Defense Technical Information Center (DTIC). All others should apply to the National Technical Information Service (NTIS).

If your address has changed, if you wish to be removed from the mailing list, or if the addressee is no longer employed by your organization, please notify PL/TSI, 29 Randolph Road, Hanscom AFB, MA 01731-3010. This will assist us in maintaining a current mailing list.

Do not return copies of this report unless contractual obligations or notices on specific document requires it to be returned.

REPORT DOCUMENTATION PAGE			Form Approved OMB No 0704-0188	
Public reporting burden for this collection of information is estimated to average 1 hour per response, including the time for reviewing instructions, searching existing data sources, gathering and maintaining the data needed, and completing and reviewing the collection of information. Send comments regarding this burden estimate or any other aspect of this collection of information, including suggestions for reducing this burden, to Washington Headquarters Services, Directorate for Information Operations and Reports, 1215 Jefferson Davis Highway, Suite 1204, Arlington, VA 22202-4302, and to the Office of Management and Budget, Paperwork Reduction Project (0704-0188), Washington, DC 20503.				
1. AGENCY USE ONLY (Leave blank)	2. REPORT DATE October 1993	3. REPORT TYPE AND DATES COVERED Final Technical Report (9/88-9/93)		
4. TITLE AND SUBTITLE Ultrasensitive Infrared Chemiluminescence Detection		5. FUNDING NUMBERS PE 61102F PR 2310 TA G4 WUBY F19628-88-C-0173		
6. AUTHOR(S) W.T. Rawlins, M.E. Fraser, K.W. Holtzclaw, W.J. Marinelli, H.C. Murphy, L.G. Piper				
7. PERFORMING ORGANIZATION NAME(S) AND ADDRESS(ES) Physical Sciences Inc. 20 New England Business Center Andover, MA 01810-1077		8. PERFORMING ORGANIZATION REPORT NUMBER PSI-1059/TR-1277		
9. SPONSORING/MONITORING AGENCY NAME(S) AND ADDRESS(ES) Phillips Laboratory 29 Randolph Road Hanscom AFB, MA 01731-3010 Contract Manager: Steve Miller/GPOS		10. SPONSORING/MONITORING AGENCY REPORT NUMBER PL-TR-93-2266		
11. SUPPLEMENTARY NOTES				
12a. DISTRIBUTION/AVAILABILITY STATEMENT approved for public release; distribution unlimited			12b. DISTRIBUTION CODE	
13. ABSTRACT (Maximum 200 words) This document is the Final Report for a 5-year project dedicated to investigations of chemical processes related to the excitation of infrared chemiluminescent radiation in the upper atmosphere. The effort has included experimental measurements of molecular infrared fluorescence, from 2 to 25 μm , excited by energetic chemical reactions involving upper atmospheric and aurorally excited species. Observed IR radiators include electronically excited molecular nitrogen, vibrationally excited N_2O , and rovibrationally excited $\text{CO}(\text{v},\text{J})$ and $\text{NO}(\text{v},\text{J})$. Additional experimental measurements in a discharge-flow reactor quantified the kinetics and spectroscopy of energetic IR precursor species including metastable electronic states of molecular oxygen, molecular nitrogen, and atomic nitrogen. Results from the experimental measurements were included in a critical review of nitric oxide kinetics, and were applied to predictive modeling of nitric oxide excitation in the auroral upper atmosphere.				
14. SUBJECT TERMS Infrared emission, Chemiluminescence, Nitrogen, Nitric oxide, Molecular dynamics, Vibrational excitation, Atmospheric background, Mesospheric chemistry			15. NUMBER OF PAGES 368	
			16. PRICE CODE	
17. SECURITY CLASSIFICATION OF REPORT Unclassified	18. SECURITY CLASSIFICATION OF THIS PAGE Unclassified	19. SECURITY CLASSIFICATION OF ABSTRACT Unclassified	20. LIMITATION OF ABSTRACT Unlimited	

Contents

	<u>Page</u>
List of Figures	iv
List of Tables	v
1. SUMMARY	1
2. COCHISE INFRARED MEASUREMENTS AND DATA BASE	3
2.1 Summary of IR Data Base	4
2.2 LWIR N_2^+ Spectroscopy	8
2.3 LLWIR Measurements	9
2.4 Dynamics of $NO(v,J)$	11
3. FLOW REACTOR INVESTIGATIONS OF METASTABLE CHEMISTRY	17
4. MODELS OF AURORAL EXCITATION	19

List of Appendices

A - Branching Ratios for Infrared Vibrational Emission from $NO(X^2, v' = 2-13)$..	21
B - The Dipole Moment and Infrared Transition Strengths of Nitric Oxide	35
C - N_2O Production Mechanism from the Interaction of Discharged-Excited Species ..	57
D - The Ratio A_{00}/A_{01} for the Infrared Atmospheric Bands of Molecular Oxygen ..	65
E - The Stability of $N_2(A'^5\Sigma_g^+)$	89
F - Further Observations of the Nitrogen Orange Afterglow	101
G - Re-evaluation of the Transition-Moment Function and Einstein Coefficients for the $N_2(A^3\Sigma_u^+ - X^1\Sigma_g^+)$ Transition	131
H - Energy Transfer Studies of $N_2(X^1\Sigma_g^+, v)$ and $N_2(B^3\Pi_g)$	141
I - Electronic Transition Moment Variation and Einstein Coefficients for the $NO(B^2\Pi - X^2\Pi)$ System	149
J - Experimental Determination of the Einstein Coefficient for the $N(^2P - ^4S)$ Transition	161
K - The Reactions of $N(^2P)$ with O_2 and O	177
L - Review of the Chemistry of Vibrationally Excited Nitric Oxide in the Disturbed Upper Atmosphere	185
M - The Aeronomy of Aurorally Excited Infrared Fluorescence from Rovibrationally Excited Nitric Oxide	319

List of Figures

<u>Figure No.</u>		<u>Page</u>
1	Schematic of COCHISE Facility	3
2	COCHISE Reaction Chamber	4
3	$N_2O(00^{\circ}1 \rightarrow 10^{\circ}0)$ Excited by N_2 Energy Transfer in COCHISE	8
4	Data (light line) and Fit (dark line) to 3-2 $N_2(W^3\Delta \rightarrow B^3\pi)$ Emission . . .	10
5	Data (light line) and Fit (dark line) to 3-2 $N_2(W^3\Delta \rightarrow B^3\pi)$ and 0-1, 1-2, 2-3 $N_2(w^1\Delta \rightarrow a^1\pi)$	10
6	Identified Sources of $NO(v,J)$ Infrared Chemiluminescence	14
7	Energy Transfer Excitation of $NO(v,J)$ N^* , $N_2^* + NO \rightarrow NO(v,J)$ Average Populations	15

List of Tables

<u>Table No.</u>		<u>Page</u>
1	COCHISE Experimental Database - August 1990	5
2	N ₂ O(v) Excitation	9
3	Possible Energy Transfer Mechanisms	16

Accession For	
NTIS CRA&I	<input checked="" type="checkbox"/>
DTIC TAB	<input type="checkbox"/>
Unannounced	<input type="checkbox"/>
Justification	
By	
Distribution /	
Availability Codes	
Dist	Avail and/or Special
A-1	

THIS PAGE INTENTIONALLY LEFT BLANK

1. SUMMARY

This document is the Final Report for a 5-year project dedicated to investigations of chemical processes related to the excitation of infrared chemiluminescent radiation in the upper atmosphere. The effort has included experimental measurements and interpretations of the dynamics of infrared fluorescence from atmospheric gases using microwave discharge techniques. These studies required operation of the Air Force's COCHISE facility as well as supporting experimental and analytical investigations.

A wide variety of high-sensitivity, spectrally resolved infrared chemiluminescence measurements were performed on the COCHISE facility, over the wavelength range 2 to 25 μm . These included spectral surveys of the SWIR, MWIR, and LWIR regions for fluorescence which could be excited by chemical interactions of metastable oxygen and nitrogen with atmospheric species. In many instances these surveys revealed previously unobserved band systems, such as LWIR transitions of electronically excited N_2^* or vibrationally excited $\text{N}_2\text{O}(\text{v})$. In addition, species previously thought to be formed, such as $\text{NO}(\text{a}^4\text{II})$, were found to be unimportant.

We also used the COCHISE facility to perform a comprehensive series of investigations of the radiative and collisional dynamics of rovibrationally excited $\text{NO}(\text{v},\text{J})$. Previous COCHISE work has demonstrated the formation of $\text{NO}(\text{v},\text{J})$ from the reactions of metastable $\text{N}(\text{2D}, \text{2P})$ with O_2 ; those results have major implications for the production of $\text{NO}(\text{v},\text{J})$ in the disturbed atmosphere, and for the concomitant atmospheric radiation signatures in the SWIR and MWIR. In the present effort, we have obtained new data showing the excitation of $\text{NO}(\text{v},\text{J})$ by an energy transfer mechanism involving active nitrogen; this can also be an upper atmospheric process under certain conditions. We have also obtained unique, new data on the collisional deactivation of $\text{NO}(\text{v},\text{J})$, which will provide essential guidance to interpretations of high-altitude spectral measurements. Finally, we have performed a comprehensive set of measurements, data analysis, and theoretical computations dedicated to the determination of the IR transition strengths and uncertainties for $\text{NO}(\text{v},\text{J})$ in the fundamental and first overtone transitions. This effort has determined experimentally the dipole moment function for NO, and has for the first time placed the evaluation of the infrared transition strengths of NO on quantitatively solid footing.

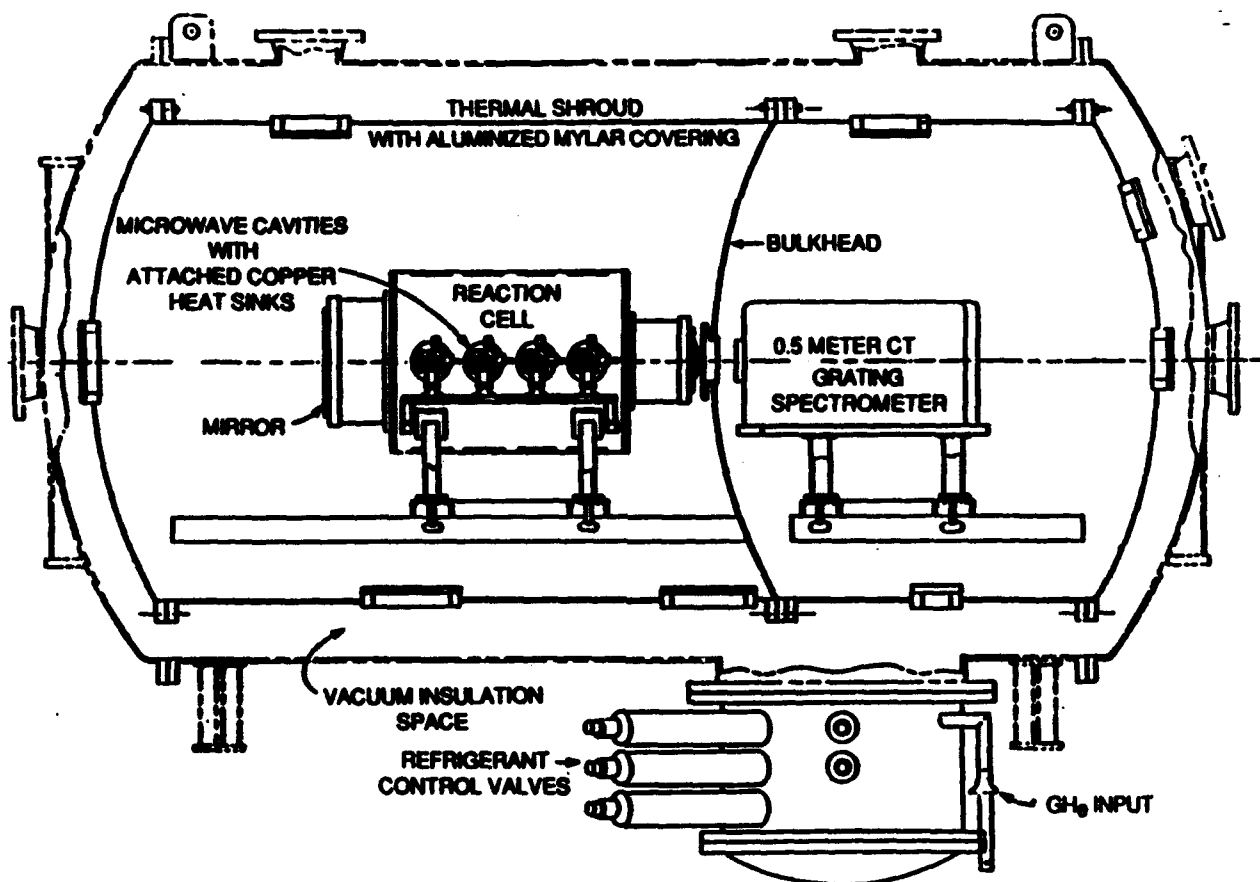
In support of the COCHISE investigations of IR chemiluminescent processes, we have used discharge-flow methods to investigate the reaction and quenching kinetics and spectroscopy of electronically excited metastable species which can act as precursors to atmospheric IR fluorescence. This work has included experimental measurements of the kinetics and spectroscopy of electronically excited states of molecular nitrogen, molecular oxygen, nitric oxide, and metastable atomic nitrogen. We have also investigated reaction product channels for the formation of NO^+ , N_2O and $\text{NO}(\text{v},\text{J})$ from reactions of electronically excited species.

To relate the results of the laboratory experiments to observations and predictions of high-altitude phenomena, we have used the laboratory results to construct simple models of

auroral excitation and deactivation processes, particularly for $\text{NO}(v,J)$. This work has resulted in a comprehensive critical review of the relevant chemical kinetics data base and uncertainties. We have also assembled a predictive steady-state kinetic model for auroral $\text{NO}(v,J)$ excitation, to guide the interpretation of high-altitude field observations in terms of excitation mechanisms.

2. COCHISE INFRARED MEASUREMENTS AND DATA BASE

Infrared fluorescence experiments on the COCHISE facility at PL/GPDS are focussed on the dynamics and spectroscopy of the excitation of infrared-radiating species by processes involving excited-state/metastable precursors. COCHISE has the capability to measure spectrally resolved fluorescence between 2 and 25 μm from very low concentrations of vibrationally and electronically excited species at gas phase temperatures of 80 to 100 K and pressures of a few mt. Energetic precursors, created in a set of microwave discharges, expand into a low-pressure, cryopumped reaction volume where they interact with opposing jets of reagent (counterflow) species under near-single-collision conditions. The resulting infrared fluorescence is viewed by a highly sensitive scanning monochromator/Si:As detector combination. The apparatus and reaction cell are diagrammed in Figures 1 and 2. The measurements performed have focussed on (1) dynamics of $\text{NO}(\nu, J)$ excitation, radiative transition probabilities, and collisional deactivation; (2) surveys of fluorescence excitation arising from energy transfer from metastable N_2^* and O_2^* ; and (3) extension of the capabilities of the apparatus into the LLWIR (16 to 25 μm).



B-6243

Figure 1
Schematic of COCHISE Facility

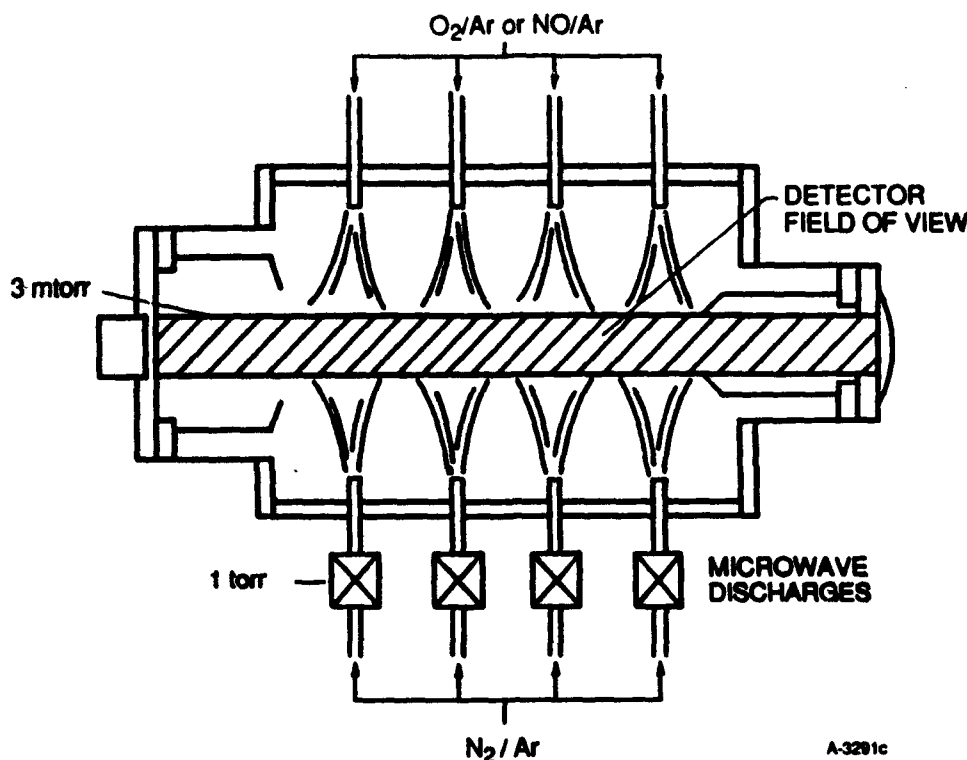


Figure 2
COCHISE Reaction Chamber

A-3291c

2.1 SUMMARY OF IR DATA BASE

The COCHISE infrared data base is summarized in Table 1. Measurements in the SWIR/MWIR region have addressed $\text{NO}(\nu, J)$ dynamics, N_2 electronic transitions, and N_2O , CO , and OH excitation phenomena. Measurements of $\text{NO}(\nu, J)$ phenomena are discussed further below. Measurements of the $\text{N}_2(\text{W} \rightarrow \text{B}) (2,1)/(2,0)$ intensity ratio give a value ≈ 2 times larger than the theoretical value of Werner et al, suggesting an unpredicted inflection in the transition moment. Discharge-excited N_2^* was observed to excite $\text{N}_2\text{O}(\nu_3)$ by energy transfer to N_2O , probably from $\text{N}_2(\nu)$ emanating from the discharge. Discharge-excited O_2^* excited $\text{CO}(\nu=1)$ weakly, and did not form any vibrationally excited N_2O upon interaction with an N_2 counterflow. In an experiment employing codischarged $\text{Ar}/\text{H}_2/\text{O}_2$ mixtures, we observed fluorescence from $\text{OH}/\text{H}_2\text{O}$ near $2.7 \mu\text{m}$ and H_2O at 6 to $7 \mu\text{m}$, but no clearly identifiable high- N rotational transitions of OH .

Measurements in the LWIR have focussed on N_2^* spectroscopy and attempts to identify vibration-rotation bands of $\text{NO}(\text{a}^4\Pi)$. We have observed the $\text{N}_2(\text{W} \rightarrow \text{B}) (3,2)$ band at $9.6 \mu\text{m}$, and the $(\text{w} \rightarrow \text{a}) (0,1), (1,2),$ and $(2,3)$ bands between 9.5 and $11 \mu\text{m}$. Observation of the $(\text{W} \rightarrow \text{B}) (3,2)$ band can contribute to the determination of the $(\text{W} \rightarrow \text{B})$ transition moment through measurements of the $(3,2)/(3,1)$ branching ratio. Similarly, the data for the $(\text{w} \rightarrow \text{a})$ transitions can be combined with SWIR data on $(\text{w} \rightarrow \text{a})$ transitions to determine branching ratios and transition moment variations with r -centroid. These are discussed further below.

Table 1
COCHISE Experimental Database - August 1990

SWIR/MWIR (1 to 8 μm)

Subject	Data Entries	Database Status	Comments
1 to 8 μm			
NO F/O ratios, High P	Aug 1988 Sep 1988	Complete	Five matched pairs at 10 mT; bandhead contribution negligible. Appendix A,B
NO(v,J) Pressure Effect	Sep 1988 Sep 1989	Complete	Variation in fund. bands, temporal behavior 2 to 10 mT. Bandheads, low, high v levels have different pressure dependencies.
N ₂ (W-B) Pressure Effect	Jan 1990	Complete	2 to 10 mT data to be used to support NO(v,J) pressure studies.
N ₂ (W-B) Trans. Moment	Aug 1988 Oct. 1988	Incomplete	2-1/2-0 ratio 2x larger than Werne. et al. Results imply sharp inflection in transition moment. Will need more data at similar r_e (e.g., 3-2/3-1) and compare to LABCEDE lifetimes.
N ₂ (w-a) Branching Ratios	Jan 1989 Feb 1989	Incomplete	Presence of 0-1, 1-2, and 2-3 w-a bands at 9.5 to 11 μm makes branching ratio determination possible. A dedicated run will be needed.
N ₂ ⁺ + NO	Oct 1988 May 1989 Jun 1989	Incomplete	Observe N ₂ O(ν_3), NO(v,J), and 6.5 to 7.5 μm mystery continuum. N ₂ O from impurities. Some NO(v,J) real. Data will have to be taken in pairs to correct for background.
N ₂ ⁺ + N ₂ O	Aug 1989	Complete	Observed N ₂ O(ν_3) only. No NO(v,J) or mystery continuum. Failed to see N ₂ O(ν_1) at 7.8 μm .
O ₂ ⁺ + CO	Dec 1988	Complete	Only weak CO(1-0) emission produced.
O ₂ ⁺ + N ₂ → N ₂ O	Dec 1988	Complete	No N ₂ O(ν_3). Issue resolved.
N ₂ ⁺ + CO Pressure Effect	Feb 1990	Complete	All data taken DC. CO funds increase with pressure as with NO (v dep. not yet determined). No effect on bandheads. Pressure range 2 to 10 mT.

Table 1
COCHISE Experimental Database - August 1990 (Continued)

Subject	Data Entries	Database Status	Comments
Discharged Ar/H ₂ /O ₂	Mar 1990	Complete	Observe 2.7 μ m and 6 to 7 μ m emissions. The 6 to 7 μ m emission probably due to H ₂ O(ν_2).
Other Studies: O ₂ ⁺ + NO O ₂ ⁺ , N ₂ ⁺ + CO ₂ O ₂ + N ₂ O	None None None		
Co-discharged N ₂ /O ₂ /Ar \rightarrow N ₂ O	Old data only		
8 to 16 μ m			
N ₂ ⁺ Spectroscopy	Jan 1989 Feb 1989	Incomplete	3-2 W-B observed at 9.6 μ m. 0-1, 1-2, 2-3 w-a transitions seen in 9.5 to 11 μ m region. More data necessary to check branching ratios. 16 to 17 μ m feature presently believed to be real.
N ₂ ⁺ + CO Survey	Jan 1989	Incomplete	No new emission systems seen.
NO(a ⁴ II)	Feb 1989	Complete	Tried N ₂ ⁺ + O ₂ , NO without success. Data allows upper limit for NO(a ⁴ II) branching ratio to be determined. We do observe N ₂ O combination band at 10.6 μ m from N ₂ O impurities.
Other Studies: O ₃ (v) transition moment O ₃ (v) high pressure	None None		
16 to 25 μ m			
Ar Rydberg Survey	Aug 1990	Incomplete	Data from May, June 1990 compromised by cracked filter. Thus, data from these runs were multiple orders. Data from Aug 1990 were taken with 8 μ m filter. All previously observed 9 to 16 μ m lines were seen here as well. Another partial entry will be needed to properly observe all the new lines.

Table 1
COCHISE Experimental Database - August 1990 (Continued)

	Data Entries	Database Status	Comments
N ₂ [*] Survey	Aug 1990	Incomplete	Aug 1990 data indicates broad system 16 to 19 μm . Will need a new filter to verify and check the 22 to 25 μm range.
Other Surveys:			
NO [*]	Aug 1990	Incomplete	No emissions observed from N ₂ [*] + O ₂ . Should also check N ₂ [*] + NO.
N ₂ O(ν_2)	Aug 1990	Incomplete	Only a small out-of-phase feature seen at $\sim 15 \mu\text{m}$ from discharged Ar/air. Need to look again and try N ₂ [*] + N ₂ O.
OH(J)	Aug 1990	Incomplete	Tried discharged Ar/O ₂ /H ₂ in Aug 1990 with no success. Try again.
CO [*]	None	Incomplete	Must try in a near-term data set.

The NO($a^4\Pi$) state is the lowest metastable state of NO, lying at $\approx 5 \text{ eV}$. It is known to be formed in three-body $\text{N} + \text{O} + \text{M}$ recombination. Its fundamental vibration-rotation transitions are predicted to occur from 10 to 15 μm , and its first overtone should lie between 5 and 7 μm . From theoretical arguments, we would expect NO($a^4\Pi$) to be formed from the reaction of N(^2P) with O₂ via an adiabatic, fully allowed reaction path. The exoergicity of the reaction would be sufficient to populate $v=0,1$ of the $a^4\Pi$ state. Similarly, it is possible that energy transfer from triplet N₂^{*} states to NO could excite NO($a^4\Pi$) in a spin-allowed process. We performed experiments in COCHISE to probe the 10 to 15 μm region for radiation arising from discharged N₂/Ar + O₂ and discharged N₂/Ar + NO configurations, and observed no NO($a^4\Pi, v$) fluorescence in either case. This places upper bounds to the branching ratios for NO($a^4\Pi, v \geq 1$) formation of $\leq 10^{-3}$ for N(^2P) + O₂, and $\leq 10^{-2}$ for N₂($A^3\Sigma$, $W^3\Delta$) + NO.

Additional LWIR measurements have identified the 10.6 μm $\nu_3 \rightarrow \nu_1$ band of N₂O, excited by VV energy transfer from discharge-excited N₂(v). The observed spectrum is shown in Figure 3. This observation has implications for the possibility of N₂O LWIR radiation in prolonged bombardments, since we know that N₂O can be formed from bombarded air (see below). These implications are summarized in Table 2.

The COCHISE measurement capabilities have been extended into the LLWIR (16 to 25 μm) through procurement and installation of antireflection coated KRS-5 (thallium

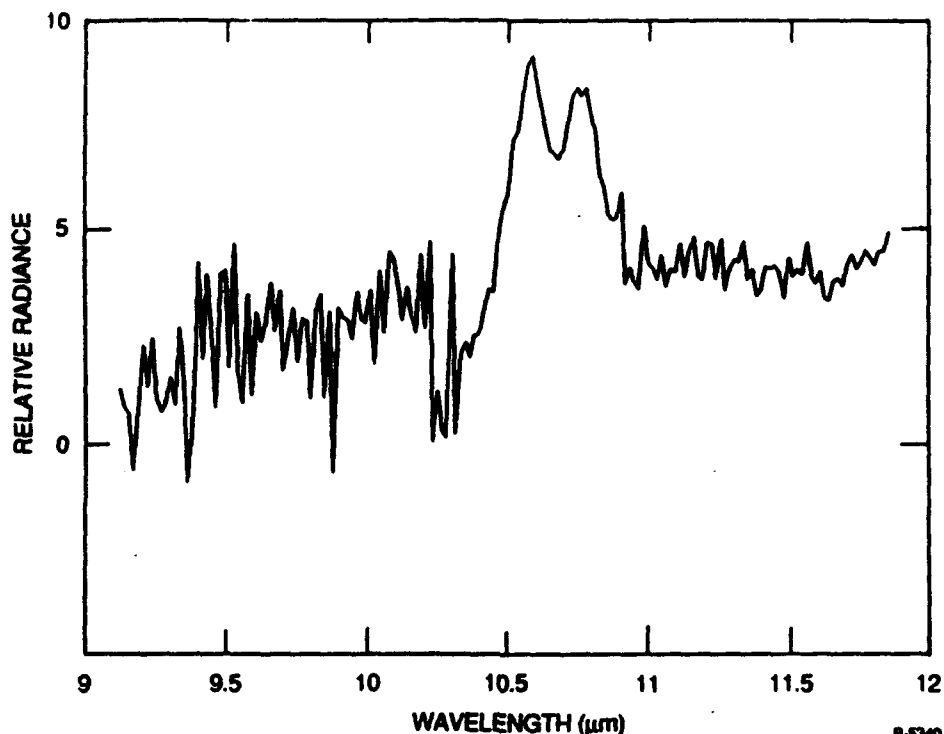


Figure 3
 $\text{N}_2\text{O}(00^0 1 \rightarrow 10^0 0)$ Excited by N_2 Energy Transfer in COCHISE

bromiodide) optics. The operation and calibration of the apparatus in this wavelength region have been tested, and a series of preliminary survey fluorescence experiments has been performed. These are summarized in Table 1. An initial series of experiments was compromised by a crack in the order-sorting filter, and a second series was limited to the use of a filter optimized for the 8 to 16 μm region. However, good data were obtained for N_2^* and Ar(I) fluorescence features in the 9 to 20 μm region.

2.2 LWIR N_2^* SPECTROSCOPY

One of the COCHISE objectives is the examination of N_2^* spectroscopy. As shown in Table 1, we have examined the 8 to 16 μm region for nitrogen electronic features. Although this analysis is not yet complete, we have identified previously unobserved $\text{N}_2(\text{w}^1\Delta - \text{a}^1\pi)$ features in the 9.5 to 11 μm region.

The SWIR (2 to 4 μm) region has been carefully examined for N_2 electronic features by COCHISE. We have identified emission arising from $\text{N}_2(\text{W}^3\Delta, v=2-5 \text{ to } \text{B}^3\pi, v=0-3)$ and $\text{N}_2(\text{w}^1\Delta, v=0-2 \text{ to } \text{a}^1\Delta, v=0-2)$. Many of the bands are overlapped such that identification proved difficult. This was particularly true of the 3.6 μm region which contains the 3,1 W-B and 0,0 w-a bands superimposed. Owing to different discharge N_2 mole fraction dependencies, we were able to positively distinguish both emission systems.

The 9.5 to 11 μm region is similarly complex and the emissions arise from branches of the same radiators encountered at 3.6 μm . The 3,2 W-B transition is centered at 9.4 μm while the 0,1 w-a transition falls at 9.25 μm . The 1,2 and 2,3 w-a bands occur at 10.2 and

Table 2
N₂O(v) Excitation

- N₂O is formed in bombarded N₂/O₂
 - Flow reactor experiments => four possibilities:

$$\text{N}_2(v \geq 15) + \text{O}_2(^1\Delta) \rightarrow \text{N}_2\text{O} + \text{O}(^1\text{D})$$

$$\text{N}_2(v \geq 8) + \text{O}_2(^1\Delta) \rightarrow \text{N}_2\text{O} + \text{O}(^3\text{P})$$

$$\text{N}_2(v \geq 13) + \text{O}_2(^1\Sigma) \rightarrow \text{N}_2\text{O} + \text{O}(^1\text{D})$$

$$\text{N}_2(v \geq 6) + \text{O}_2(^1\Sigma) \rightarrow \text{N}_2\text{O} + \text{O}(^3\text{P})$$
 - N₂(A, v > 3) + O₂ is still unknown
- Auroral/nuclear production of N₂O is unknown by 10⁶ without better kinetics.
 - Production rates are probably slow to medium
 - Chemical losses negligible, local loss will be limited by transport
 - Suggests gradual buildup, 120 to 150 km, as with NO but more slowly
- N₂O(00°1) is very efficiently excited by N₂(v) energy transfer (COCHISE, LABCEDE data) => potential 10.6 μm radiator above 100 km

11.36 μm, respectively. We have previously identified the 3,2 W-B feature in spectra of discharged nitrogen. Figures 4 and 5 show that to accurately reproduce the observed spectral intensities in the 9.5 to 11 μm region requires more than W-B contribution. Figure 4 shows an experimental spectrum with a fit to only 3,2 W-B emission. Figure 5 shows the same data but with w-a features included. These features are quite clearly present but a dedicated run should be performed to examine them in greater detail, e.g., N₂ mole fraction dependence, branching ratios, etc.

2.3 LLWIR MEASUREMENTS

As indicated in Table 1 we have successfully performed the first COCHISE examination of LLWIR emissions. In the wavelength region beyond 16 μm we have identified new Ar Rydberg emissions as well as broad features possibly arising from N₂*. These data were taken with the 8 μm filter. The cut-on for this filter is 8 μm with the cut-off at approximately 22 μm. An earlier filter that had a 13.7 μm cut-on and 25 μm cut-off shattered during thermal cycling. A consequence of using the 8 μm filter is the serious

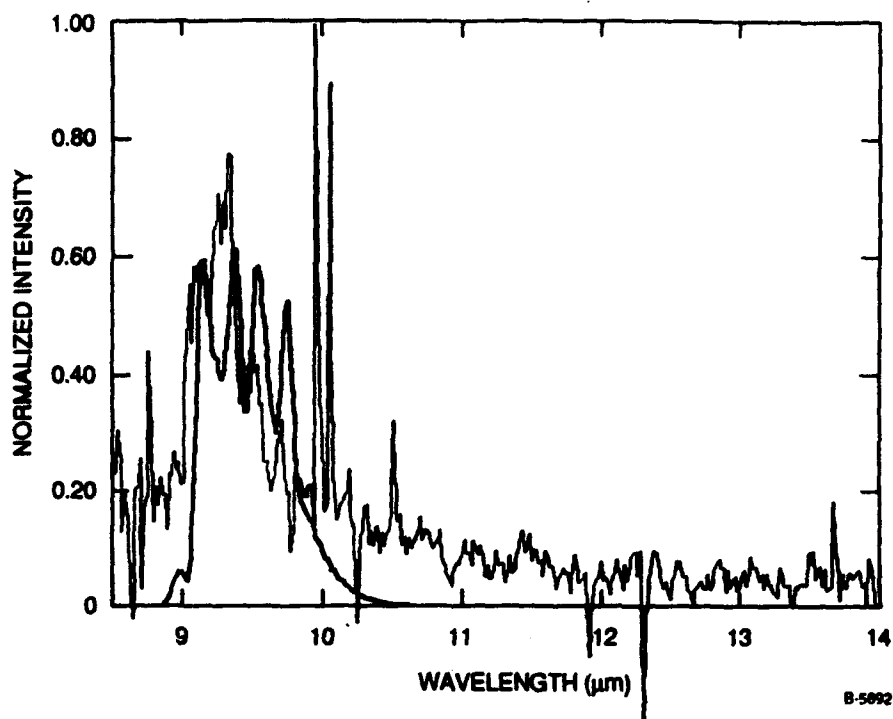


Figure 4
Data (light line) and Fit (dark line) to 3-2 $N_2(W^3\Delta \rightarrow B^3\pi)$ Emission

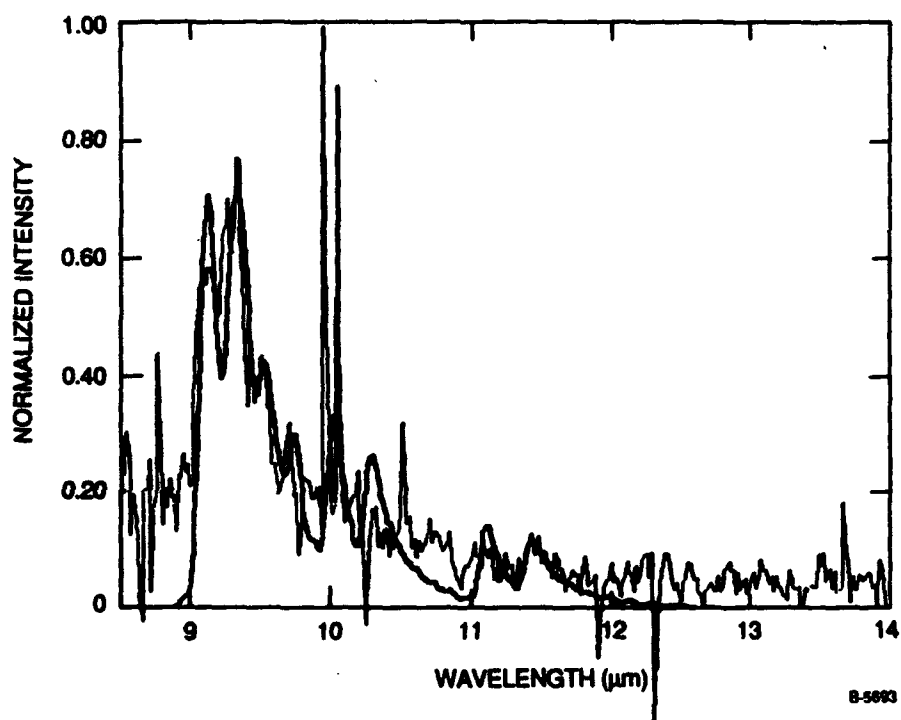


Figure 5
Data (light line) and Fit (dark line) to 3-2 $N_2(W^3\Delta \rightarrow B^3\pi)$ and 0-1, 1-2, 2-3 $N_2(w^1\Delta \rightarrow a^1\pi)$

potential of second order interference at wavelengths longer than $16\text{ }\mu\text{m}$. To address this issue we have purchased another filter ($14\text{ }\mu\text{m}$ cut-on and $22\text{ }\mu\text{m}$ cut-off) for examination in the next run. Use of this filter will help establish how much of the observed 16 to $19\text{ }\mu\text{m}$ N_2^* emission is first order.

We will take precautions to avoid cracking this filter during cool-down. These precautions include greater clearance in the filter holder and extensive testing prior to the COCHISE run. In these cooling tests, the filter and holder assembly will be slowly cooled to LN_2 temperature inside a vacuum chamber. These tests should be sufficient to indicate whether the new filter can withstand the COCHISE cryogenic environment.

Even if the new filter is successful, we will still require another for a thorough examination of the LLWIR. Because the present filters are constructed on Germanium substrates, the wavelength cut-offs occur at $22\text{ }\mu\text{m}$. We will require another filter on a CdTe substrate to access the 22 to $25\text{ }\mu\text{m}$ region (with a wavelength cut-on at about 13 to $14\text{ }\mu\text{m}$). We can presently find no stock commercial source for such filters which leaves commissioning a company to produce one to our specs, as was done for the 2 , 4 , and $8\text{ }\mu\text{m}$ filters.

2.4 DYNAMICS OF $\text{NO}(v,J)$

We have performed an extensive series of COCHISE experiments dedicated to quantitative determinations of the IR transition strengths and excitation characteristics of rovibrationally excited $\text{NO}(v,J)$. A series of experiments determined the overtone/fundamental branching ratios for $v=2-12$ for low rotational temperatures, $T = 60\text{ K}$. This work was published in J. Chem. Phys.; the manuscript is given in Appendix A.

In continuing analysis, we extracted an empirical dipole moment function for $\text{NO}(X^2\Pi)$ from COCHISE data on the overtone/fundamental branching ratios. We verified and extended our earlier preliminary results for this analysis, and established uncertainty bounds on the final results. The method of analysis used a nonlinear least squares fitting procedure to determine the empirical, polynomial representation of the dipole moment function giving the best fit between computed and observed Einstein coefficient ratios. The computed overtone and fundamental band Einstein coefficients were calculated by transition moment integrals using RKR wavefunctions for the upper and lower states, together with the assumed form of the dipole moment function. Since the COCHISE data were obtained at low rotational temperatures, 60 K , it was not necessary to treat the effects of spin uncoupling and centrifugal distortion in this analysis.

The COCHISE data extend to $v=13$, limiting the validity of the dipole moment function to internuclear distances between 0.9 and $1.5\text{ }\text{\AA}$. The empirical results over that range are in good agreement with the ab initio calculations of Langhoff et al. We used quadratic and cubic empirical dipole moment functions, derived from the COCHISE data, to compute rotationless Einstein coefficients (A-factors) for the fundamental and first, second,

and third overtone bands of NO. These coefficients are valid for use at low to moderate rotational temperatures. A viewgraph presentation of these results is given in Appendix B.

Extrapolations of the A-factors to higher vibrational levels require assumptions about the functional form of the dipole moment function at larger and smaller internuclear distances. This is especially problematic for larger internuclear distances, $r > 1.5$ Å, since it is necessary to describe the "rollover" in the function as the system approaches dissociation. Since there are no experimental data to support such a description at these internuclear distances, the uncertainties in the A-factors for high vibrational levels ($v = 20$ to 26) are in the range of a factor of ≈ 3 for the fundamental band and are substantially larger for the first and higher overtones. The fits to the COCHISE data give two alternate functions, expressed as a cubic and a quadratic polynomial respectively. These functions agree well within the range of internuclear separation covered by the COCHISE data, but diverge from each other at larger internuclear separations. In order to define the magnitude of the uncertainties in A-factors resulting from uncertainties in dipole moment functions at large internuclear separation, we have computed rotationless A-factors for both empirical functions as well as for ab initio functions published in the literature. A manuscript describing the determination of the empirical dipole moment function and rotationless A-factors is now in preparation for submission to the Journal of Chemical Physics.

We have also used the COCHISE empirical dipole moment functions for NO to perform rigorous calculations of the rotational line strengths as a function of J . The purpose of these calculations is to examine the effects of the dipole moment function, spin uncoupling (transition from Hund's Case (a) to Case (b)), and centrifugal distortion on the P- and R-branch line strengths at high J ($J = 80$ to 120). Calculations were performed for the COCHISE quadratic and cubic empirical dipole moment functions as well as for the ab initio functions of Langhoff et al, Billingsley, and Peyerimhoff et al. The calculations incorporate the spin uncoupling treatment of Hill and Van Vleck, and treat centrifugal distortion effects rigorously using RKR wavefunctions for the upper and lower rotational states of each transition.

It appears that spin uncoupling is a relatively weak effect for NO, even at high J , however centrifugal distortion of the rovibrational wavefunctions significantly perturbs the transition moment integrals. The effects of centrifugal distortion on rotational intensity scaling are small for the fundamental band, but are significant for the first and higher overtones. Specifically, centrifugal distortion at high- J causes a factor-of-two increase in the R-branch transition intensities of the first overtone; this can increase the integrated overtone/fundamental band intensity ratios in cases where significant high- J radiation is present. The choice of dipole moment function affects the magnitude of the centrifugal distortion effects at high- J , and also causes factor-of-two variations in the computed magnitudes of the band-integrated A-factors for the fundamental band at high- v and for the first overtone band.

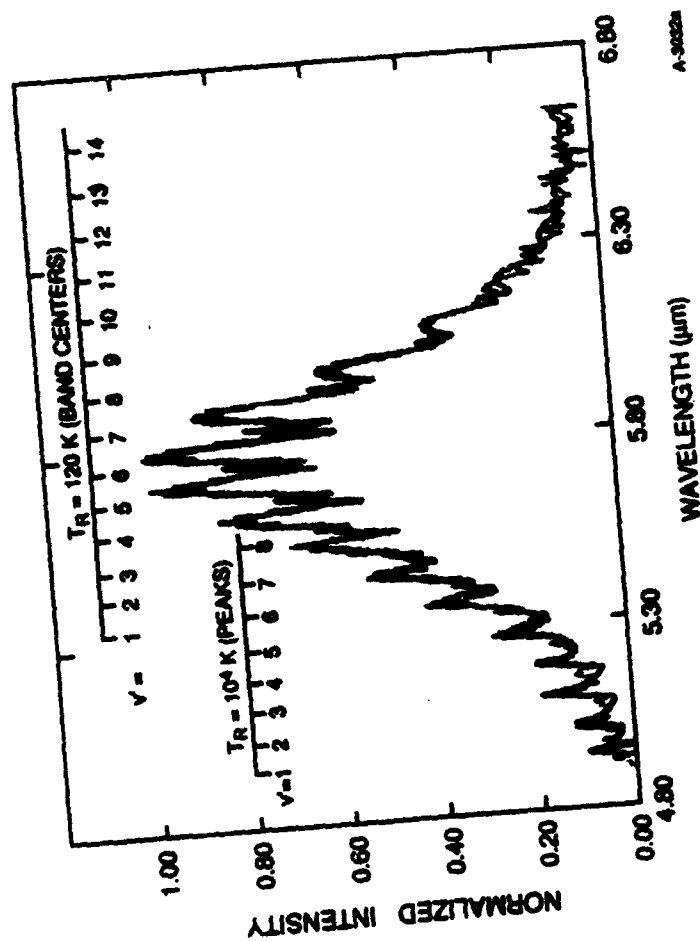
We have compared the results for the different dipole moment functions, and have computed thermally averaged A-factors for rotational temperatures up to $10,000$ K, $v = 1-26$,

fundamental and first overtone. The thermally averaged A-factors show a weak temperature dependence which results primarily from the ν^3 factor in the rotational line intensity. We are preparing a manuscript reporting the high-J effects and the thermally averaged A-factors for submission to the Journal of Quantitative Spectroscopy and Radiative Transfer. We are continuing to examine the behavior of the second and third overtone bands in order to define a series of laboratory measurements which would improve the empirical dipole moment accuracy at larger internuclear distances. Such measurements would resolve current discrepancies near 1.5 Å and would enable much more reliable calculations of the A-factors for high vibrational levels ($v \approx 15$ to 26).

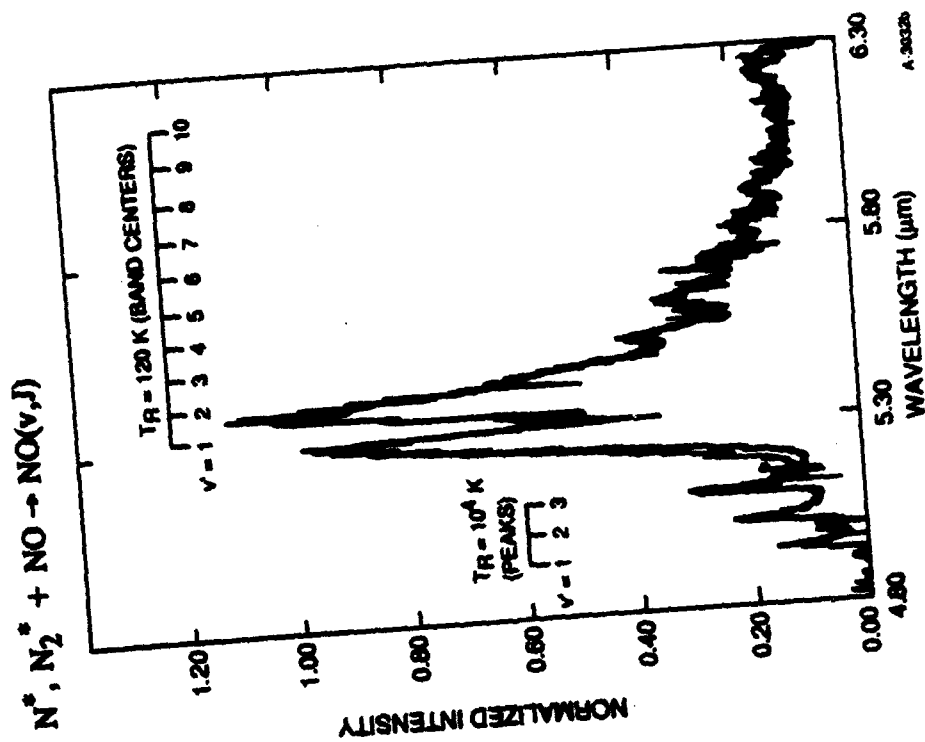
In another series of measurements, we observed NO(v, J) fluorescence spectra from the energy transfer interaction of discharged N₂/Ar mixtures with NO counterflows. These measurements employed variations in discharge and counterflow component mixing ratios in an attempt to identify the precursors to the excited NO fluorescence. We observed fluorescence from at least seven vibrational levels having thermal rotational distributions and three vibrational levels having rotationally "hot" (high-J) distributions. An example spectrum (compared to a spectrum from N⁺ + O₂) and population distribution are shown in Figures 6 and 7. Large contributions to the rotationally thermal NO($v=1$) populations from N₂(v) VV energy transfer could be identified; however the mechanism(s) for excitation of the remainder of the fluorescence is still uncertain. Spectral fits to the observed spectra indicate energy transfer of up to 1.7 eV to account for the observed states. The vibrational state population distributions are nearly the same for the thermal and rotationally hot components, and conform with a modeled distribution based on NO(A \rightarrow X) radiative cascade following formation of NO(A) by energy transfer from N₂(A). However, excitation of the high rotational states requires excitation of NO(A, v , high-J) by energy transfer from N₂(A, $v \leq 8$), a process which has never been investigated or observed. An alternative mechanism with sufficient energetics is energy transfer via N(²D) + NO, which can occur through N-atom exchange. Possible energy transfer mechanisms are compared in Table 3. We have completed a detailed analysis of this data, and a manuscript is in preparation.

We have also performed several series of experiments dedicated to the investigation of collisional deactivation of high-J states, particularly for NO(v, J). These measurements were performed by systematically varying the pressure of background He in the reaction cell and using phase-sensitive detection to obtain NO(v, J) spectra at two phase settings. By observing both in-phase and out-of-phase components, it is possible to reconstruct phase-summed and phase-dependent spectra which can be analyzed to determine detailed state populations for the rotationally thermal and hot components. The NO(v, J) measurements were performed for the N⁺ + O₂ reaction. As the pressure was increased from 2 to 10 mt, the rotationally hot component was observed to shift out of phase with the thermal component. Phase-summed spectra showed the disappearance of the high-J component with increasing pressure, and a concomitant increase in the lower vibrational levels of the rotationally thermal component. To support the interpretation of these data, we also obtained phase-sensitive, pressure-dependence data on N₂(W \rightarrow B) emission (a prompt radiator excited by the discharge) and CO(v, J) excited by N₂ energy transfer. Comprehensive analysis of these data will provide new information on the rotational deactivation dynamics of high-J states.

Excitation Mechanisms:



Discharged Nitrogen + O₂ Chemiluminescence



Discharged Nitrogen + NO Energy Transfer

Figure 6
Identified Sources of NO(v,J) Infrared Chemiluminescence

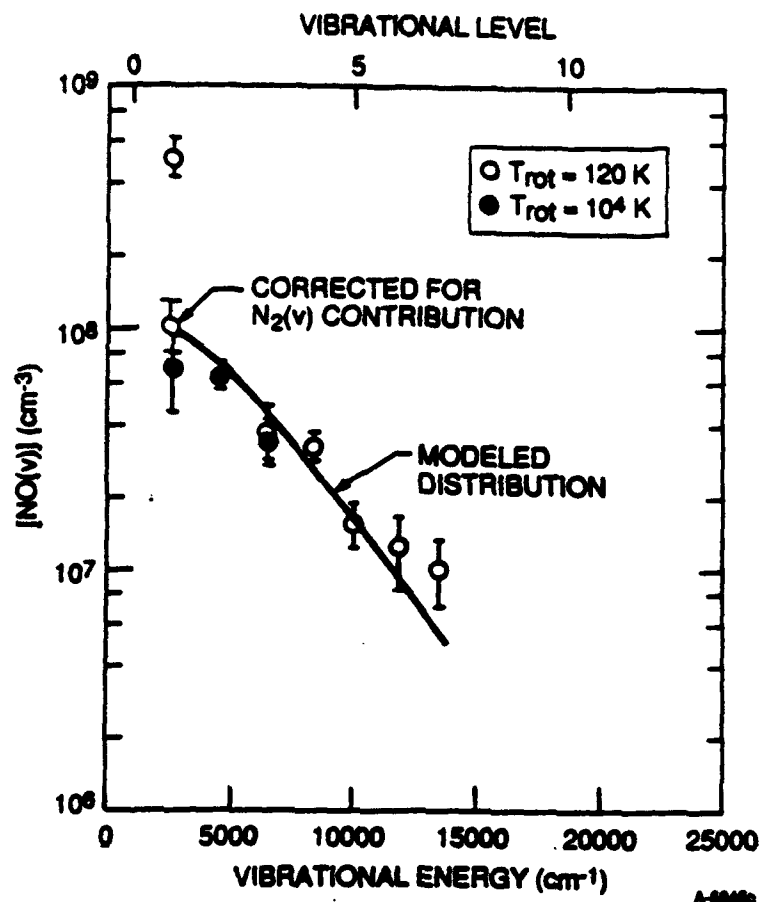


Figure 7
Energy Transfer Excitation of NO(v,J): N^* , $N_2^* + NO \rightarrow NO(v,J)$ Average Populations

- NO(v=1) must be corrected for $N_2(v) + NO(v=0) \rightarrow NO(v=1) + N_2(v-1)$ contribution
- $v \leq 7$ rotationally thermalized bands; $v \leq 3$ rotational band heads observed
- Indicate energy transfer of ≤ 1.7 eV
- Modeled distribution is for $N_2(A) + NO \rightarrow NO(A) \rightarrow NO(v,J)$

Table 3
Possible Energy Transfer Mechanisms

Comparison of predicted versus actual NO(v,J) densities
in COCHISE experiment

Species	Energetics (eV)	Rate Constant (cm ⁻³ s ⁻¹)	Required for NO(v,J) Excitation	Estimated for Interaction Zone	Comments
N(² D)	2.38	6 x 10 ⁻¹¹	4.7 x 10 ⁸	3-10 x 10 ⁹	May occur through atom exchange N(² D) + NO → NO(v) + N
N(² P)	3.576	3 x 10 ⁻¹¹	9.3 x 10 ⁸	1-3 x 10 ⁸	No attractive potentials for atom exchange
N ₂ (W ³ Δ)	7.36	No data	3 x 10 ⁸	3 x 10 ⁸	Unlikely; would require gas kinetic rate constant
N ₂ (w ¹ Δ)	7.35	No data	3 x 10 ⁸	1 x 10 ⁸	Unlikely; would require gas kinetic rate constant
N ₂ (a ¹ π)	8.4	~ 3 x 10 ^{-10*}	1.0 x 10 ⁸	2 x 10 ⁶	Insufficient number density
N ₂ (a' ¹ Σ _u ⁻)	8.55	3.6 x 10 ⁻¹⁰	8 x 10 ⁷	3 x 10 ⁹	Possible but channels to form NO(A), NO(X) unknown
N ₂ (A ³ Σ)	6.315	6.6 x 10 ⁻¹¹	4 x 10 ⁸	1-3 x 10 ⁹	Known to form NO(A) with majority of the energy defect in vibration and rotation
* Assumed					

3. FLOW REACTOR INVESTIGATIONS OF METASTABLE CHEMISTRY

Using discharge flow reactor techniques, we have performed several investigations of the quenching kinetics, spectroscopy, radiative lifetimes, and reactions of electronically excited and metastable species relevant to auroral excitation in the upper atmosphere. This work has resulted in several journal articles which are included here as appendices.

Observations of N_2O formation from reactions of discharge-excited $\text{N}_2^* + \text{O}_2^*$ are described in a manuscript in Appendix C. A viewgraph presentation on the branching ratio for (0,0)/(0,1) emission from $\text{O}_2(^1\Delta)$ is given in Appendix D. Investigations of N_2^* dynamics include: a search for $\text{N}_2(^5\Sigma)$, Appendix E; investigations of the N_2 orange afterglow, Appendix F; the transition moment, Einstein coefficients, and radiative lifetime of $\text{N}_2(\text{A})$, Appendix G; and energy transfer between $\text{N}_2(\text{X},v)$ and $\text{N}_2(\text{B})$, Appendix H. A determination of the transition moment for the $\text{NO}(\text{B} \rightarrow \text{X})$ transition is described in Appendix I. Investigations of metastable N-atom kinetics include a determination of the Einstein coefficient for the $\text{N}(^2\text{P} \rightarrow ^4\text{S})$ transition, viewgraph presentation in Appendix J, and rate coefficients for quenching of $\text{N}(^2\text{P})$ by O_2 and by O (including NO^+ production from the latter), Appendix K.

We have performed discharge-flow reactor experiments to determine $\text{NO}(v,J)$ yields from the reactions of $\text{N}(^2\text{D})$ and $\text{N}(^2\text{P})$ with O_2 . In these experiments, metastable atoms generated by a microwave discharge react with rapidly flowing O_2 in an argon bath at pressures near or below 1 Torr and room temperature. The NO formed from these reactions is interrogated by tunable-UV laser-induced fluorescence (LIF) to determine the vibrational and rotational populations in the ground electronic state. Analysis of preliminary laser-induced fluorescence spectra for the $\text{X} \rightarrow \text{A}$ system (γ -bands) resulted in the identification of $\text{NO}(\text{X}, v=22)$, undoubtedly produced by the reaction $\text{N}(^2\text{P}) + \text{O}_2$ (the corresponding $\text{N}(^2\text{D})$ reaction has insufficient exoergicity to form this state). This is an important finding, since theorists have previously argued that $\text{NO}(\text{X})$ cannot be formed in the reaction of $\text{N}(^2\text{P})$ with O_2 due to the unavailability of adiabatic potential surfaces.

In subsequent experiments we observed LIF in the $\text{X} \rightarrow \text{B}$ system of NO (β -bands), and simultaneously monitored $\text{N}(^2\text{D})$ and $\text{N}(^2\text{P})$ optically. We detected $\text{N}(^2\text{D})$ by vacuum-ultraviolet (VUV) resonance absorption at 149 nm, and $\text{N}(^2\text{P})$ by both VUV resonance absorption at 174 nm and passive fluorescence at 346 nm. The experiments were performed in fast flows of Ar and He buffer gases at pressures near 0.5 Torr and reaction times near 1 ms (downstream from the O_2 injection). The specific $\text{X} \rightarrow \text{B}$ bands observed to date are $(v', v'') = (1, 6)$ and $(6, 21)$. The observation of the (6,21) band near 560 nm provides further identification of high- v $\text{NO}(v,J)$ which can be produced by reaction of $\text{N}(^2\text{P})$ but not by $\text{N}(^2\text{D})$. The data show that the LIF intensity of this band correlates linearly with the $\text{N}(^2\text{P})$ number density, indicating that the reaction of $\text{N}(^2\text{P})$ with O_2 is indeed responsible for the formation of $\text{NO}(v=21)$. At present, our experiments do not distinguish whether $\text{NO}(v=21)$ is formed directly from the reaction or via near-resonant collisional deactivation of high- J $\text{NO}(v,J)$ formed as the primary product. However, the latter alternative is consistent with our previous experiments in COCHISE, which show initial formation of high- J $\text{NO}(v,J)$, no

detectable $\text{NO}(v \geq 15)$, and moderately efficient deactivation of the high-J states by collisions with He.

Based on the COCHISE observations of deactivation of the high-J states at tens of milliTorr, we expect any high-J $\text{NO}(v,J)$ to be present at greatly reduced number densities under the conditions of these flow reactor experiments. However, owing to the sensitivity of the LIF technique, it may be possible to detect the presence of high-J states if they are sufficiently robust against collisional deactivation. Some low-intensity features observed in the LIF spectra may be due to high-J states, however conclusive assignments are difficult owing to uncertainties in the term energies for high-J states in the lower and upper electronic manifolds. To aid in the analysis and identification of the LIF spectra, we have adapted an LIF spectral prediction code developed in Prof. Ron Hanson's group at Stanford University. We have upgraded this capability to incorporate the highly accurate spectroscopic constants for $\text{NO}(X)$ reported by Amiot and coworkers. Comparisons of simulated and measured LIF spectra in the $X \rightarrow B$ (1,6) band near 280 to 285 nm confirm the observation of $J \approx 25$ transitions, but at near-thermal intensity distributions. The simulations show that high-J transitions for the (2,4) band overlap this spectral region, however we have not clearly identified any of these transitions in the spectra observed to date. We are continuing to pursue these measurements along the same lines, to (1) quantify the relationship between the kinetic behavior of high- v $\text{NO}(v,J)$ and that of $\text{N}(^2\text{P})$, and (2) establish whether detectable levels of high-J $\text{NO}(v,J)$ are present.

4. MODELS OF AURORAL EXCITATION

We have related the laboratory data to upper atmospheric auroral excitation phenomena and observations by developing simple kinetic models of the excitation and deactivation processes. In particular, we have focussed on the excitation of $\text{NO}(v,J)$ by chemistry induced by energetic electron bombardment of the lower thermosphere. As a part of this effort, we have compiled a critical review of recommended values and uncertainties for kinetic parameters of elementary reactions associated with the formation, destruction, excitation, and deactivation of nitric oxide in the quiescent and bombarded upper atmosphere. This review, dated November 1991, is included here as Appendix L. An update of this review is in progress for submission to the open literature.

We have also performed a variety of model calculations and predictions for comparison to field data and scaling to other auroral strengths, altitudes, and atmospheric (atomic oxygen) compositions. These predictions are made by a steady state model calculation which balances the excitation and deactivation rates for $\text{NO}(v,J)$ and its metastable precursors, given a set of atmospheric composition and dosing profiles. The predicted vibrational populations for the rotationally thermalized and hot components are then used to compute detailed, high resolution spectra of the $\text{NO}(v,J)$ fluorescence as it would be observed in the atmosphere. These predictions are compared to field data, such as that obtained by the Field Widened Interferometer (FWI).

The principal assumption in these calculations is that the rotationally thermal component, $\text{NO}(v)$, originates from the reaction $\text{N}(^2\text{D}) + \text{O}_2$, while the rotationally hot component, $\text{NO}(v,J)$, arises from the reaction $\text{N}(^2\text{P}) + \text{O}_2$, as postulated based on COCHISE laboratory results. We therefore must treat the formation of $\text{N}(^2\text{D}, ^2\text{P})$ from electron impact processes and their quenching kinetics with O , O_2 , N_2 , and electrons. We also treat the collisional and radiative deactivation of $\text{NO}(v)$ and $\text{NO}(v,J)$. This gives predicted altitude profiles of the individual vibrational state number densities, which can be integrated to compare with the overhead column densities observed by FWI. In general, we find that the $\text{N}(^2\text{P}) + \text{O}_2$ mechanism only gives large $\text{NO}(v,J)$ yields when the atomic oxygen number density is low and the aurora penetrates to ≈ 100 km. This is because O quenches $\text{N}(^2\text{P})$ more efficiently than O_2 , and at higher altitudes the increasing O/O_2 ratio discriminates against $\text{NO}(v,J)$ formation. Thus the altitude of peak $\text{NO}(v,J)$ production is near 100 to 120 km, and $\text{NO}(v,J)$ production via $\text{N}(^2\text{P}) + \text{O}_2$ is predicted to decrease sharply with increasing altitude. While the predicted $\text{NO}(v,J)/\text{NO}(v)$ yields agree with FWI data for the likely $[\text{O}]$ and dosing conditions of the flight, there remains a significant possibility for an additional, previously unknown mechanism which might produce $\text{NO}(v,J)$ at higher altitudes. A viewgraph presentation, illustrating the FWI spectral data, the kinetics of the key reactions, the predicted species profiles and spectra, and potential additional excitation reactions, is included in Appendix M.

THIS PAGE INTENTIONALLY LEFT BLANK

APPENDIX A

Branching Ratios for Infrared Vibrational Emission from $\text{NO}(X^2, v' = 2-13)$

W.T. Rawlins
M.E. Fraser
S.M. Miller
W.A.M. Blumberg

J. Chem. Phys. 96, 7555 (1992)

(SR-576 reproduced in its entirety)

THIS PAGE INTENTIONALLY LEFT BLANK

Reprinted from

THE JOURNAL OF CHEMICAL PHYSICS

VOLUME 96

NUMBER 10

15 MAY 1992

Branching ratios for infrared vibrational emission from $\text{NO}(X^2\Pi, v=2-13)$

W. T. Rawlins and M. E. Fraser

Physical Sciences Incorporated, 20 New England Business Center, Andover, Massachusetts 01810

S. M. Miller and W. A. M. Blumberg

Phillips Laboratory/Geophysics Directorate, Hanscom Air Force Base, Massachusetts 01731

pp. 7555-7563

Published by the

AMERICAN INSTITUTE OF PHYSICS

AIP

THIS PAGE INTENTIONALLY LEFT BLANK

Branching ratios for infrared vibrational emission from $\text{NO}(X^2\Pi, v' = 2-13)$

W. T. Rawlins and M. E. Fraser

Physical Sciences Incorporated, 20 New England Business Center, Andover, Massachusetts 01810

S. M. Miller and W. A. M. Blumberg

Phillips Laboratory/Geophysics Directorate, Hanscom Air Force Base, Massachusetts 01731

(Received 14 November 1991; accepted 30 January 1992)

The ratios of overtone and fundamental vibrational Einstein coefficients for $\text{NO}(X^2\Pi)$ have been measured by spectrally resolved infrared chemiluminescence near 2.7–3.3 μm and 5.2–6.8 μm . The reactions of $\text{N}(^2D, ^2P)$ with O_2 , in the presence of a small background of He in a cryogenic low-pressure reactor, generated vibrationally excited, rotationally cold (60 K) $\text{NO}(v)$, whose emission spectra were recorded with high spectral resolution. Least-squares spectral fitting analysis of the observed overtone and fundamental spectra gave vibrational band intensities, whose ratios at each emitting vibrational level v' yielded the $(\Delta v = 2)/(\Delta v = 1)$ Einstein coefficient ratios for $v' = 2-13$. The results provide comparisons to previous theoretical and experimental data, and reflect the behavior of the dipole moment function for $\text{NO}(X^2\Pi)$. The measured ratios indicate an overtone Einstein coefficient $A_{2,0} = 0.94 \pm 0.11 \text{ s}^{-1}$ for an assumed fundamental value $A_{1,0} = 13.4 \text{ s}^{-1}$.

1. INTRODUCTION

The nitric oxide molecule plays key roles in the chemistry and radiative behavior of air-breathing combustion systems, chemical lasers, discharge plasmas, and the earth's atmosphere. In all of these applications, the infrared vibrational transition probabilities for NO are important for diagnostic applications and investigations of energy/radiation transfer. Owing to the high temperatures and nonequilibrium conditions in which NO radiation is often encountered, the emitting species can be highly internally excited, requiring knowledge of vibration-rotation transition moments at large internuclear separations. This information for NO is available only from theory, with little or no experimental validation. In this paper, we present experimental data for the branching ratios of fundamental and first overtone emission from highly vibrationally excited NO, as observed in a cryogenic chemiluminescence reactor. These data provide insight into the shape of the electric dipole moment function, as well as an indirect determination of the absolute $(v' = 2) \rightarrow (v'' = 0)$ overtone transition probability.

In the specification of absolute emission intensities and spectral distributions, one requires the vibrational emission rates (Einstein coefficients, $A_{v',v''}$), averaged over all thermally populated rotational levels, for all the vibrational states of interest. While many ground state absorption measurements have determined values for the $(v', v'') = (1, 0)$ and $(2, 0)$ transition strengths, the scaling of $A_{v',v''}$ with v' is only partially understood. Previous empirical determinations^{1,2} of the dipole moment near equilibrium internuclear separation provided limited information for low v' . In a definitive theoretical treatment, Billingsley³⁻⁶ performed an *ab initio*, multiconfiguration self-consistent-field (MCSCF) calculation of the dipole moment function of $\text{NO}(X^2\Pi)$, and rigorously evaluated the rotationally dependent and

thermally averaged Einstein coefficients for the fundamental ($\Delta v = 1$) and first overtone ($\Delta v = 2$) transitions over a large range of v' and J' ($v' = 1-20, J' = 0.5-33.5$). The overlap of the *ab initio* dipole moment function and the $\text{NO}(X^2\Pi)$ potential is illustrated in Fig. 1. The absolute values and relative scalings given by this work have been widely utilized; however the absolute values of $A_{v',v''}$ are now known to be erroneously small.⁷

In the only previous experimental investigation of vibrational dependence, Green *et al.*⁸ determined Einstein coefficient branching ratios for $\text{NO}(v' = 2-9)$ from $\Delta v = 1$ and $\Delta v = 2$ fluorescence spectra in electron-bombarded N_2/O_2 mixtures. These measurements confirmed Billingsley's⁶ predicted vibrational scaling of the branching ratios for $v' = 3-7$, and established that the dipole moment function of Michels¹ was incorrect. However, the experimental data leave considerable uncertainty for the $(2, 0)/(2, 1)$ ratio, and are not definitive for $v' > 8$. Nevertheless, the data of Green *et al.*⁸ verify the shape (second derivative) of the *ab initio* dipole moment function at intermediate nuclear separation. Thus, a reasonable approach for selecting values of $A_{v',v''}$ is to apply the Billingsley⁶ vibrational scalings to absolute values of $A_{1,0}$ and/or $A_{2,0}$ determined from careful absorption measurements.^{2,9,10} This approach was adopted by Rothman *et al.*⁷ to evaluate absorption strengths for both the fundamental and the first overtone; the resulting absolute values were slightly modified by Rawlins *et al.*¹¹ for the analysis of $\text{NO}(\Delta v = 1)$ chemiluminescence spectra.

We have previously reported¹¹ detailed laboratory investigations of the vibrational chemiluminescence from nascent $\text{NO}(v, J)$ formed by reactions of metastable atomic nitrogen with O_2 , as originally observed by Kennealy *et al.*¹² In the recent experiments,¹¹ extensive rotational and vibrational excitation was observed in nitric oxide formed under nearly collisionless conditions by the reactions

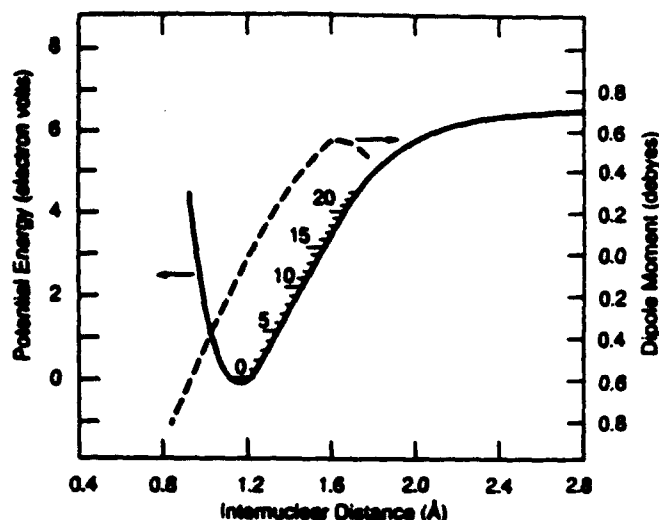
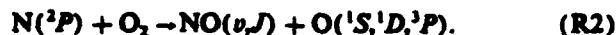


FIG. 1. *Ab initio* dipole moment function of Billingsley (Refs. 3 and 4) compared to potential curve for NO($X^2\Pi$).



The NO(ν) distributions from (R1) peak near $\nu = 7$, and are detectable to $\nu = 14$. Reaction (R1) is responsible for auroral chemiexcitation of NO(ν),^{13,14} and for most of the production of NO in the earth's thermosphere.¹⁵

Reaction (R2) produces NO(ν, J) with a high degree of rotational excitation in each of several (at least eight) vibrational levels.¹¹ The spectral data exhibit distinctive *R*-branch band heads, which signify substantial populations of rotational states in the range $J = 60.5$ – 120.5 (i.e., > 1 eV of rotational energy). Similar band heads have been observed in high-altitude auroral spectra of NO emission,¹⁶ indicating a significant role for (R2) and/or similar chemiexcitation processes in the particle-bombarded upper atmosphere.

In the analysis of spectral distributions for the high vibrational and rotational states populated by reactions (R1) and (R2), it is necessary to probe the dipole moment function over a much larger range of the NO potential surface than has previously been examined experimentally. In addition, it is often important to specify the overtone spectral distribution corresponding to that of the fundamental, or vice versa. To these ends, we have used the infrared chemiluminescence approach, previously applied to determine the nascent product distributions for reactions (R1) and (R2), to simultaneously observe $\Delta\nu = 1$ and $\Delta\nu = 2$ spectral distributions from those reactions. To eliminate complications due to multimodal rotational distributions and spectral band overlap, we introduced low levels of helium bath gas which caused extensive rotational cooling and slight vibrational deactivation of the initial state distributions. This effect, combined with the cryogenic temperature of the reaction chamber, resulted in extremely low-temperature Boltzmann rotational distributions, which permitted accurate determinations of the $(\Delta\nu = 2)/(\Delta\nu = 1)$ branching ratios over the

range $\nu' = 2$ – 12 . The results clarify previous determinations at low ν' , and indicate significant departure from Billingsley's⁶ scaling at high ν' .

A subsequent paper¹⁷ will address the analysis of the branching ratios to determine an empirical dipole moment function for NO and the corresponding Einstein coefficients. We describe here the experimental methods, spectral analysis, and branching ratio results as compared with previous work.

II. EXPERIMENTAL MEASUREMENTS

The experiments were performed in the cryogenic COCHISE (cold chemiluminescent infrared stimulation experiment) facility at the Geophysics Directorate. The design and operation of this facility are described in detail elsewhere;¹⁸ the measurement conditions were essentially the same as those for the previous NO chemiluminescence investigation.¹¹ In brief, the reaction cell and surrounding radiative environment are cooled to approximately 15–20 K, which eliminates background radiation and provides rapid cryopumping of the reagent gases. The infrared detection system consists of a cryogenic, scanning grating monochromator and a liquid-helium-cooled Si:As detector, focused to infinity along the axis of the reaction cell. Reagent gases, at 80 K, enter the cell through a series of four opposing jets, and mix along the cell axis as illustrated in Fig. 2. In the present case, nitrogen metastables, generated by microwave discharge of flowing N₂/Ar (12% N₂) mixtures near 1 Torr, enter from one side of the cell and mix along the centerline with a mass-balanced opposing flow of O₂. This results in a rapid chemical reaction producing chemiexcited NO(ν, J), which radiates in infrared bands near 5.4 ($\Delta\nu = 1$) and 2.7 ($\Delta\nu = 2$) μm . The discharges are modulated with a 23 Hz square wave, and the emission from the reaction zone is observed via phase-sensitive detection.

In other applications of this technique,^{19–21} the pressure in the reaction zone is typically 3–5 mTorr, approaching single collision conditions. For the present experiments, he-

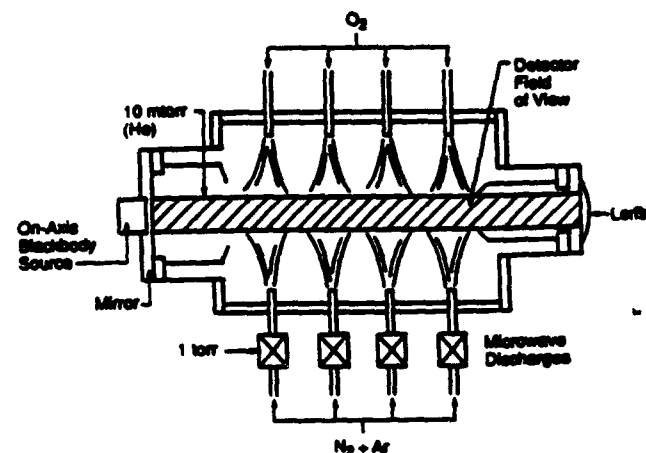


FIG. 2. Diagram of COCHISE reaction chamber.

limum was admitted to achieve a steady state (static) pressure of 10 mTorr, quenching out the high- J states. Preliminary measurements in the absence of He gave overtone spectra which were difficult to analyze unambiguously, owing to the extensive spectral overlap between poorly resolved high- J and thermalized rotational components of adjacent vibrational bands. The addition of small amounts of He resulted in significant rotational cooling, and a pressure of 10 mTorr was sufficient to eliminate the high- J components. This is demonstrated by the absence of R -branch band heads in the $\Delta\nu = 1$ spectra, and by the conformity of the rotational distributions to a single-temperature Boltzmann form for all vibrational levels.

Spectra of the $\Delta\nu = 1$ and $\Delta\nu = 2$ emission were recorded sequentially, as matched pairs, using order-sorting interference filters to isolate each band. A total of four matched pairs were recorded, all for essentially the same conditions of pressure, temperature, flow rates, and discharge operation. All spectra were obtained at a resolution of $0.0067\ \mu\text{m}$ (full width at half-maximum), corresponding to approximately $2.3\ \text{cm}^{-1}$ for the fundamental band and $9.2\ \text{cm}^{-1}$ for the overtone band. The uncertainty in the observed wavelengths is $\pm 0.003\ \mu\text{m}$ due to a periodic fluctuation in the monochromator scan rate at cryogenic temperature.

Before and after the spectral measurements, the optical system was calibrated for absolute and relative spectral response using a blackbody radiation source imbedded in the mirror at the end of the reaction cell. The calibrations employed blackbody temperatures between 350 and 400 K, with a temperature measurement uncertainty of $\pm 3\ \text{K}$. This results in a systematic uncertainty of $\pm 12\%$ in the measured $(\Delta\nu = 2)/(\Delta\nu = 1)$ intensity ratios.

A representative spectral pair is shown in Fig. 3, with the NO transition band centers labeled. Note the logarithmic intensity scale illustrating a dynamic range of approximately two orders of magnitude. The NO($\Delta\nu = 1$) system is clearly resolved up to $v' = 13$, with no apparent interfering radiators. However, several additional features appear with the NO($\Delta\nu = 2$) system. The (5,2) and (2,0) bands of the $\text{N}_2(W^3\Delta_u - B^3\Pi_g)$ electronic transition²² are evident near 2.6 and $3.3\ \mu\text{m}$, respectively; the $3.3\ \mu\text{m}$ band ultimately limits the range of v' for which the analysis can be carried out. In addition, several Rydberg transitions of Ar are observable as scattered light from the discharges.²³ In particular, a weak Ar line near $2.69\ \mu\text{m}$ partially obscures the NO($2 \rightarrow 0$) emission, necessitating a factor of ≈ 2 downward correction in the observed intensity of this band.

III. ANALYSIS AND RESULTS

The spectra were analyzed using a linear least-squares spectral fitting method which we have employed extensively in the past.^{11,12,15,19-21} The NO line positions and strengths were calculated with the spectroscopic constants given in Rawlins *et al.*¹¹ (as modified slightly from those of Goldman and Schmidt²⁴) using the assumption of Hönl-London scaling of the rotational line strengths.²⁵ From the predictions of Billingsley,²⁶ the Hönl-London assumption should be accurate for the low- J levels sampled in these measure-

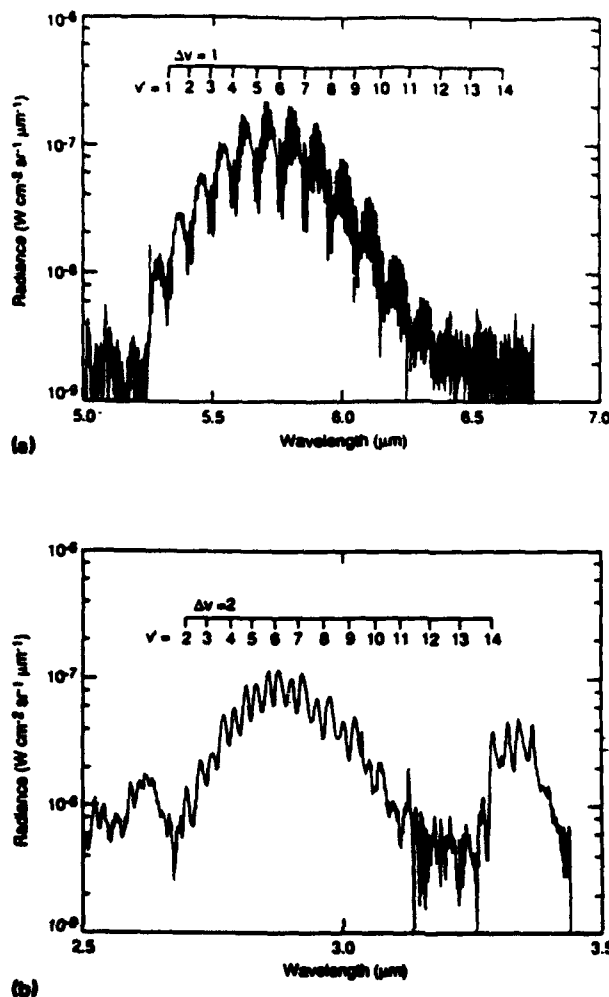


FIG. 3. Observed fundamental and overtone emission spectra. Band centers of the individual vibrational transitions are indicated.

ments. In particular, spin-uncoupling and vibration-rotation interactions will not impact the analysis of the data. Matching of the observed rotational envelopes to the computed spectra gives a uniform rotational temperature of 60 K, signifying that the presence of He causes significant thermal coupling between the 80 K reagent gases and the 20 K reactor wall. At 60 K, the third rotational level carries the maximum population, and 99% of the population lies in the lowest ten rotational levels. Examples of the computed spectral fits are shown in Figs. 4 and 5.

The least-squares solutions to the spectral fitting procedure are the integrated intensities for each vibrational transition, $[\text{NO}(\nu')]A_{\nu',\nu''}$, as plotted in Fig. 6 for a matched pair of overtone and fundamental spectra. By taking ratios of these values at each v' for a given spectral pair, we determine the Einstein coefficient ratios $A_{\nu',\nu''-2}/A_{\nu',\nu''-1}$, which represent the branching ratios between $\Delta\nu = 2$ and $\Delta\nu = 1$ transitions. The observed Einstein coefficients are thermally

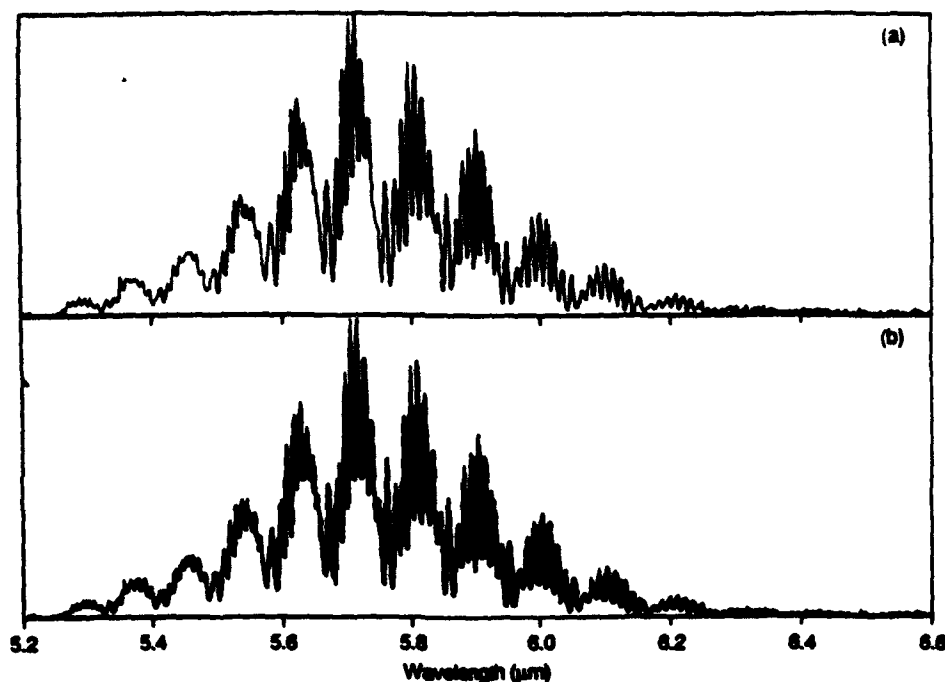


FIG. 4. Data (light line, shown with best fit and separately above) and least-squares fit (dark line) to NO($\Delta\nu = 1$) emission spectrum. Rotational temperature and spectral resolution are 60 K and 0.0067 μm . The standard deviation of the spectral fit is 0.048.

averaged at 60 K. However, since Hönl–London scaling applies (no spin uncoupling), these Einstein coefficients are equivalent to the rotationless Einstein coefficients of the molecule, and are independent of temperature to at least 600 K as shown by Billingsley.⁶ The observed ratios for all the

data, and average values for each ν' , are tabulated in Table I. The uncertainties given in Table I are statistical errors determined for the fitting and averaging procedures, and do not incorporate the systematic uncertainty of the relative response calibration.

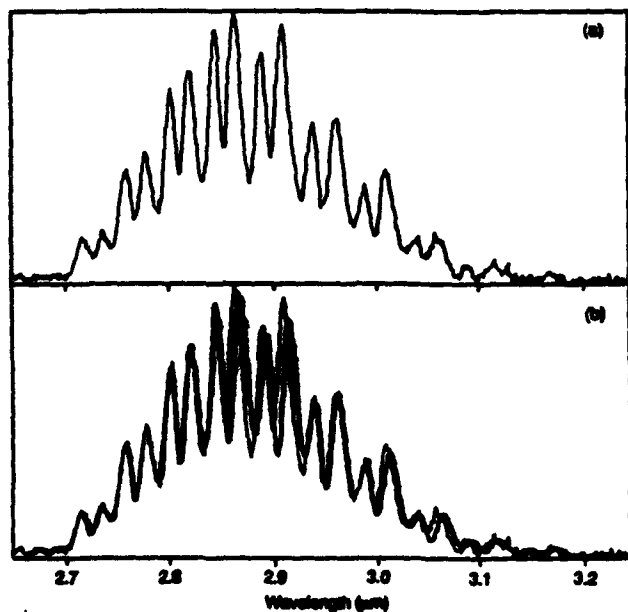


FIG. 5. Data (light line shown with the best fit and separately above) and least-squares fit (dark line) to NO($\Delta\nu = 2$) emission spectrum. Rotational temperature and spectral resolution are 60 K and 0.0067 μm . The slight mismatches near 2.9 and 3.1 μm result from nonlinearity in the cryogenic grating drive. The standard deviation of the spectral fit is 0.15.

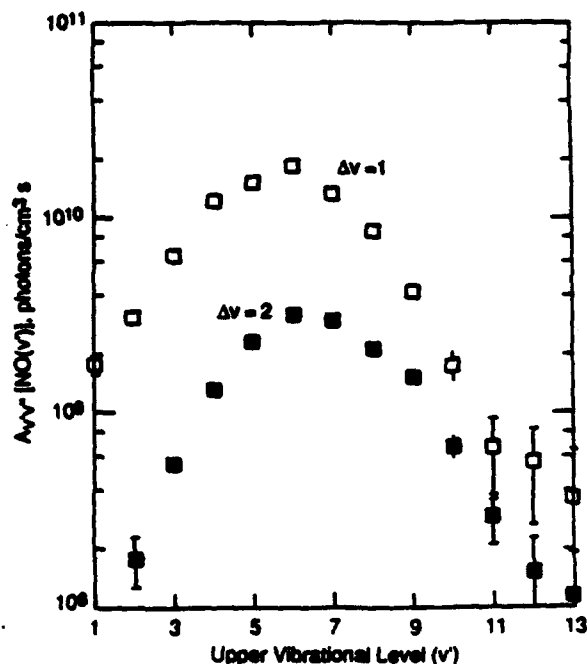


FIG. 6. Vibrational band intensities determined from a least-squares fit of fundamental and overtone spectra. Error bars denote $\pm 1\sigma$ standard deviation.

TABLE I. Experimental $(\Delta v = 2)/(\Delta v = 1)$ branching ratios.

v'	$A_{v',v'-1}/A_{v',v'-1} (\pm 1\sigma)$	Weighted average $(\pm 1\sigma)$
2	0.041 \pm 0.017 0.031 \pm 0.026 0.036 \pm 0.011 0.036 \pm 0.016	0.037 \pm 0.001
3	0.060 \pm 0.011 0.084 \pm 0.016 0.086 \pm 0.009 0.096 \pm 0.020	0.078 \pm 0.007
4	0.096 \pm 0.007 0.107 \pm 0.008 0.107 \pm 0.005 0.096 \pm 0.010	0.103 \pm 0.003
5	0.131 \pm 0.006 0.120 \pm 0.006 0.152 \pm 0.005 0.131 \pm 0.009	0.136 \pm 0.008
6	0.152 \pm 0.006 0.146 \pm 0.006 0.172 \pm 0.004 0.147 \pm 0.008	0.158 \pm 0.007
7	0.193 \pm 0.008 0.215 \pm 0.010 0.221 \pm 0.007 0.165 \pm 0.010	0.202 \pm 0.012
8	0.202 \pm 0.011 0.215 \pm 0.015 0.247 \pm 0.012 0.180 \pm 0.016	0.214 \pm 0.014
9	0.295 \pm 0.034 0.331 \pm 0.042 0.359 \pm 0.031 0.263 \pm 0.036	0.315 \pm 0.022
10	0.289 \pm 0.066 0.258 \pm 0.063 0.378 \pm 0.074 0.263 \pm 0.075	0.293 \pm 0.027
11	0.380 \pm 0.234 0.319 \pm 0.197 0.439 \pm 0.222 0.425 \pm 0.265	0.384 \pm 0.029
12	0.387 \pm 0.357 0.315 \pm 0.353 0.279 \pm 0.204 0.223 \pm 0.267	0.286 \pm 0.030
13	0.572 \pm 0.732 0.298 \pm 1.001 0.318 \pm 0.345 0.082 \pm 0.406	0.262 \pm 0.088

IV. DISCUSSION

A. Comparisons to previous data

The equations relating Einstein emission coefficients to the dipole moment function are discussed in detail by Billingsley.⁶ The band Einstein coefficients $A_{v',v'}$ represent thermal averages, for a given rotational temperature, of the individual state-specific Einstein coefficients for a given vibrational transition. These state-specific Einstein coefficients are proportional to the square of the dipole moment integral connecting the two states.

$$\left| \int_0^\infty \psi'(r) \mu(r) \psi''(r) dr \right|^2,$$

where $\psi'(r)$ and $\psi''(r)$ are the wave functions of the upper and lower states and $\mu(r)$ is the dipole moment as a function of internuclear distance r . For an electrically harmonic system, where $\mu(r)$ is linear, the magnitudes of the $\Delta v = 1$ transition probabilities are determined from the first derivative of the dipole moment function, while those for the overtone transitions are determined solely by the mechanical anharmonicity of the system, i.e., the nonorthogonality of the wave functions ψ' and ψ'' . As the dipole moment function acquires curvature, increases in the second and third derivatives strongly increase the overtone transition probabilities. In the case of OH($X^2\Pi$), the dipole moment function is strongly curved near equilibrium internuclear separation, and as a result the $\Delta v = 2$ Einstein coefficients exceed those for $\Delta v = 1$ at unusually low v' .²⁶⁻³⁰

For NO($X^2\Pi$), the dipole moment function is small and only mildly curved near equilibrium separation.²⁻⁴ Thus we expect the $\Delta v = 1$ Einstein coefficients to be primarily sensitive to the slope of $\mu(r)$, and fairly insensitive to its shape. The scaling of $A_{v',v'-1}$ with v' should be close to harmonic (i.e., $\propto v'$) near the bottom of the potential well, and will tail off at higher v' due to the increasing effects of mechanical anharmonicity in the wave functions. In addition, increasing curvature in $\mu(r)$ at large r will affect the $\Delta v = 1$ values at some high (but unknown) v' . In contrast, even modest curvature in $\mu(r)$ will profoundly affect the absolute values and v' scaling of the $\Delta v = 2$ Einstein coefficients. Thus the measurement of $(\Delta v = 2)/(\Delta v = 1)$ branching ratios over a wide range of v' provides information on the curvature of the dipole movement function over a large range of r .

The average $(\Delta v = 2)/(\Delta v = 1)$ ratios are plotted in Fig. 7, together with previously measured and predicted values. The agreement with Green *et al.*⁸ is excellent over the range $4 < v' < 7$, where their data have reasonable precision. The COCHISE measured values deviate significantly from the Billingsley scaling at both low and high v' , and indicate the presence of a broad maximum near $v' = 11$. The existence of such a maximum could have significant implications for the shape of the dipole moment function at large internuclear separation and for the behavior of $A_{v',v'}$ at high v' and/or J' . Unfortunately, due to the limited precision (low signal/noise) of our spectra in this region, we cannot obtain sufficiently accurate $v' = 13$ data to define the apparent downturn in the ratios for $v' > 12$. Nevertheless, the data clearly show significant deviations from the shape of the *ab initio* dipole moment function for both equilibrium and large internuclear separations.

The ratio values in Table I are appropriate for rotational temperatures below ≈ 100 K, and are probably reliable for temperatures up to at least 300 K. Billingsley^{3,6} found that the individual line strengths departed only slightly from Hönl-London scaling, and as a result the thermally averaged Einstein coefficients were virtually independent of temperature up to 600 K. The extension of these values to higher J' and temperature requires further investigation. At some

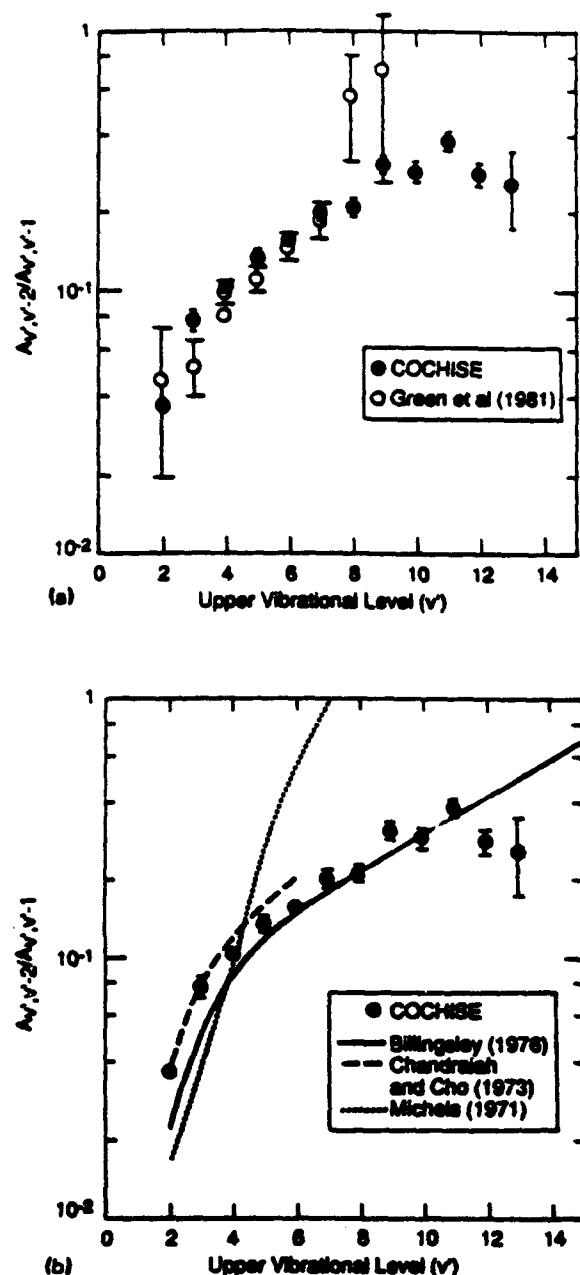


FIG. 7. Comparison of experimental branching ratios to (a) previous measurements and (b) predictions from dipole moment functions. Solid circles: weighted averages from Table I, with error bars signifying $\pm 1\sigma$ standard deviation from the weighted mean. Open circles: data from Green *et al.*, Ref. 8. Solid curve: Billingsley, Ref. 6. Dashed curve: Chandraiah and Cho, Ref. 2 (calculated in Ref. 6). Dotted curve: Michels, Ref. 1 (calculated in Ref. 6).

temperature, $A_{\nu, \nu-2}$ will become sensitive to rotational distribution, since the scaling of $A(J')$ diverges from Hönl-London as J' increases.⁵ It is possible that the high- J distributions resulting in R -branch band heads¹¹ are significantly affected, since the effects of spin-uncoupling and vibration-rotation interactions may be substantial, and further since

these states sample the extremes of internuclear separation where curvature in the dipole moment function is more pronounced. Further analysis of the COCHISE data to infer an empirical dipole moment function, examine high- J effects, and compute $A_{\nu, \nu-2}(T)$ will be reported elsewhere.¹⁷

B. Absolute Einstein coefficients: $A_{1,0}$ and $A_{2,0}$

Most of the experimental data base on NO(ν) transition probabilities comes from absorption measurements on the (1,0) and (2,0) transitions. A list of previously published experimental and theoretical values for the absorption strengths and Einstein coefficients for these transitions is given in Table II. The measurements for the (1,0) transition fall into three groups: those with $A_{1,0} \approx 13$ –14 s⁻¹, those with 12–13, and a few early measurements of 7–8. The work of Holland *et al.*,¹⁰ together with the extrapolated line-by-line data of Mandin *et al.*⁹ as reported by Rothman *et al.*,⁷ give consistent values of $A_{1,0}$ of 13.6 and 13.3 s⁻¹, respectively. A discussion comparing these values to previous measurements can be found in Holland *et al.*¹⁰ In brief, the high spectral resolution and higher measurement precision of Refs. 9 and 10 indicate a significant discrepancy with the previous lower values, and strongly support a value for $A_{1,0}$ between 13 and 14 s⁻¹. Indeed, Rothman *et al.*⁷ invoked the extrapolated line-by-line data of Mandin *et al.*⁹ in their compilation of atmospheric line absorption parameters. We have adopted the value $A_{1,0} = 13.4$ s⁻¹ at 300 K. This value is further supported by recent shock tube measurements of spectrally resolved NO($\Delta\nu = 1$) emission between 800 and 2500 K, which give $A_{1,0} = 13.2$ s⁻¹ ($\pm 10\%$).³¹

The (2,0) transition probability is less well determined. Experimental values range from 0.8 to 1.1 s⁻¹. The most careful measurements are those of Chandraiah and Cho,² whose empirical dipole moment function provides good agreement with the COCHISE branching ratios at low ν' (see Fig. 7). We note, however, that their result for the (1,0) band appears to be about 10–12% low.

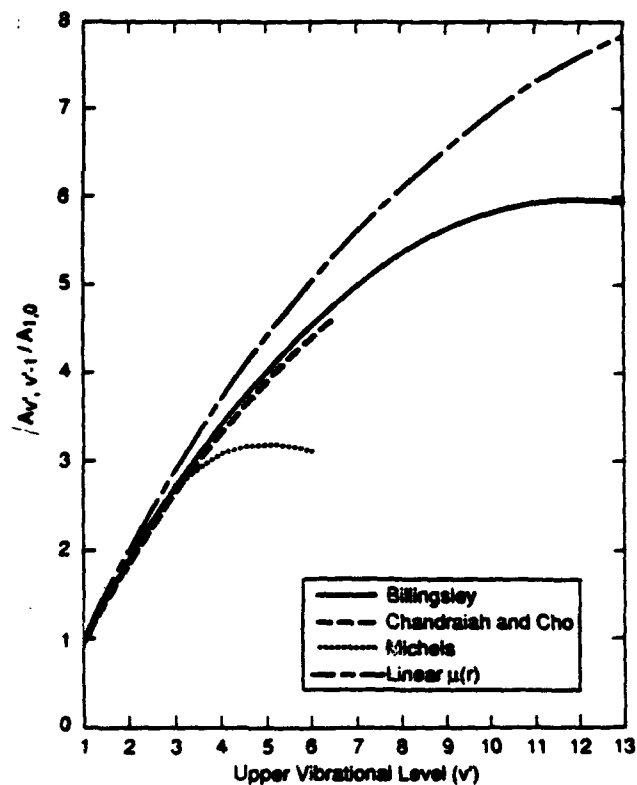
The COCHISE data give an accurate value of $A_{2,0}/A_{2,1}$ ($\pm 2\sigma = 7.9\%$, cf. Table I), which can be used to determine $A_{2,0}$ with good precision. Billingsley⁶ gives the ratio $A_{2,1}/A_{1,0} = 1.90, 1.89,$ and 1.92 for the dipole moment functions of Refs. 4, 2, and 1, respectively. Since the dipole moment function is nearly linear near equilibrium internuclear separation, this particular ratio is dominated by the mechanical anharmonicity of NO (i.e., the radial wave functions for $\nu = 0, 1, 2$), and is relatively independent of the details of slope and shape of the dipole moment function. Thus the $A_{2,1}/A_{1,0}$ ratio is ≈ 1.9 for three very different dipole moment functions, and is probably quite accurate. We can then determine from the experimental data the ratio $A_{2,0}/A_{1,0} = 0.070$, which is identical to that determined by Chandraiah and Cho² and about 1.6 times that computed by Billingsley.⁶ {In comparison, the experimental value for this ratio is 2.4 times larger than for the electrically harmonic [linear $\mu(r)$] case.} Application of our recommended value for $A_{1,0}$ gives the determination

$$A_{2,0} = 0.94 \pm 0.11 \text{ s}^{-1},$$

where the indicated error is the systematic uncertainty in the

TABLE II. Absorption coefficients and Einstein coefficients for the $\Delta v = 1$ and $\Delta v = 2$ transitions of NO.

Investigator	Citation	$S(0-1)$ $\text{cm}^{-2} \text{Ama}^{-1}$	$S(0-2)$ $\text{cm}^{-2} \text{Ama}^{-1}$	$A(1-0)$ s^{-1}	$A(2-0)$ s^{-1}
Havens (1938)	Ph.D. Dissertation, U. of Wisconsin	121		12.0	
Dinsmore and Crawford (1949)	U. of Minnesota Report No. NR-019-104	145 ± 29		14.3 ± 2.9	
Dinsmore (1949)	Ph.D. thesis, U. of Minnesota		2.57 ± 0.51		1.0 ± 0.2
Penner and Weber (1953)	J. Chem. Phys. 21, 649	70 ± 7	2.3 ± 0.6	6.9 ± 0.7	0.9 ± 0.2
Vincent-Geisse (1954)	Compt. Rend. 239, 251	82		8.1	
Breene (1958)	J. Chem. Phys. 28, 11; 29, 512	70	2.7	6.9	1.1
Schurin and Clough (1963)	J. Chem. Phys. 38, 1855	111 ± 7		11.0 ± 0.7	
Breeze and Ferriso (1964)	J. Chem. Phys. 41, 3420	76 ± 7	2.8 ± 0.5	7.5 ± 0.7	1.1 ± 0.2
James (1964)	J. Chem. Phys. 40, 762	138 ± 6		13.6 ± 0.6	
Fukuda (1965)	J. Chem. Phys. 42, 521	74 ± 4		7.3 ± 0.4	
Ford and Shaw (1965)	Appl. Opt. 4, 1113	115 ± 9		11.4 ± 0.9	
Alamichel (1966)	J. Phys. (Paris) 27, 345	132 ± 3		13.0 ± 0.3	
Schurin and Ellis (1966)	J. Chem. Phys. 45, 2528		2.11 ± 0.1		0.82 ± 0.04
Varanasi and Penner (1967)	J. Quant. Spectrosc. Radiat. Transfer 7, 279	128 ± 10		12.6 ± 1.0	
Oppenheim et al. (1967)	Appl. Opt. 6, 1305	125 ± 8		12.4 ± 0.8	
Feinberg and Camac (1967)	J. Quant. Spectrosc. Radiat. Transfer 7, 581	124 ± 22		12.3 ± 2.2	
Green and Tien (1970)	J. Quant. Spectrosc. Radiat. Transfer 10, 805	125		12.4	
Michels (1971)	Ref. 1	134 ± 2	2.0 ± 0.6	13.2 ± 0.2	0.78 ± 0.23
King and Crawford (1972)	J. Quant. Spectrosc. Radiat. Transfer 12, 443	135 ± 5		13.3 ± 0.5	
Chandraiah and Cho (1973)	Ref. 2	121 ± 6	2.17 ± 0.11	12.0 ± 0.6	0.84 ± 0.04
Garside et al. (1976)	Appl. Opt. 16, 398	124 ± 9		12.3 ± 0.9	
Billingsley (1976)	Ref. 6	113.3	1.31	10.78	0.46
Kunimori et al. (1977)	J. Quant. Spectrosc. Radiat. Transfer 19, 127	122 ± 6		12.1 ± 0.6	
Mandin et al. (1980)	Ref. 7, 9	134.4		13.3	
Holland et al. (1980)	Ref. 10	137.3 ± 4.6		13.6 ± 0.5	

FIG. 8. Relative scaling of $\Delta v = 1$ Einstein coefficients with v' . Solid curve: Billingsley, Ref. 6. Dashed curve: Chandraiah and Cho, Ref. 2 (calculated in Ref. 6). Dotted curve: Michels, Ref. 1 (calculated in Ref. 6). Dash/dot curve: computed for a linear dipole moment function.

relative response calibration. This value is 12% higher than (but within experimental uncertainty of) that measured by Chandraiah and Cho,² and is a factor of 2 larger than predicted from the dipole moment function of Billingsley.⁶ The relatively large value for $A_{2,0}$ indicates that the dipole moment function has more curvature near equilibrium internuclear separation than was predicted from the *ab initio* theory.

Potentially, the assumption of Billingsley scaling of $A_{\nu',\nu'-1}$ can be used with the COCHISE data to infer $A_{\nu',\nu'-2}$ values to higher ν' ; however, this procedure will have increasing uncertainty at higher ν' as curvature in the dipole moment function plays more of a role in the ν' dependence of $A_{\nu',\nu'-1}$. To evaluate the validity of this procedure, we examine the predicted $A_{\nu',\nu'-1}$ scalings as shown in Fig. 8. Predictions for the dipole moment functions of Refs. 1, 2, and 4 were taken from Ref. 6. In addition, we have plotted the predicted scaling for a linear dipole moment function as computed using Rice-Ramsperger-Kassel (RKR) wave functions for NO($X^2\Pi$). (While the absolute values of $A_{\nu',\nu'-1}$ depend on the assumed slope of $\mu(r)$, the relative values $A_{\nu',\nu'-1}/A_{1,0}$ do not.) It is clear from Fig. 7 that the relative A factors for the fundamental band are fairly insensitive to modest variations in $\mu(r)$ curvature for $\nu' < 4$. Furthermore, the close agreement between our $A_{2,0}/A_{1,0}$ ratio and that of Chandraiah and Cho,² together with the similarity in ν' scaling of the A factors for $\Delta\nu = 1$ computed by Billingsley⁶ from the *ab initio*⁴ and empirical² dipole moment functions, suggest that the Billingsley scaling is indeed reliable, at least up to $\nu' = 6$.

With the caveat that curvature in $\mu(r)$ at large r can affect the $A_{\nu',\nu'-1}/A_{1,0}$ scaling at high ν , we tentatively conclude that Billingsley scaling is a good approximation for the fundamental band, with an uncertainty increasing with ν' to perhaps $\pm 20\%$ near $\nu' = 12$. (However, we note that there is no firm basis for extending this scaling to higher ν' , say $\nu' = 20$.) Accordingly, we have applied this scaling of $A_{\nu',\nu'-1}$ to estimate values for $A_{\nu',\nu'-2}$ using a quartic least-squares fit to the branching ratio data of Table I. The results are listed in Table III. Given the combined uncertainties in

the branching ratio measurements and the $A_{\nu',\nu'-1}$ scaling, we conservatively estimate uncertainties in $A_{\nu',\nu'-2}$ ranging from $\pm 12\%$ for $\nu' = 2$ to $\pm 40\%$ for $\nu' = 13$.

V. SUMMARY AND CONCLUSIONS

We have used the infrared chemiluminescence technique, in a cryogenic reaction vessel, to measure the overtone/fundamental branching ratios for vibrational emission from NO($X^2\Pi, \nu$). A combination of low rotational temperature and high spectral resolution eliminated complications of non-Boltzmann rotational distributions, and minimized spectral overlap between adjacent bands. The spectral resolution also reduced complications in the analysis due to interference from other radiating species. The measurements cover ranges of 2–13 in ν' and 0–12 in ν'' , and extend the previous experimental data base to both lower and higher vibrational levels. The agreement with predictions from a previous *ab initio* calculation is generally favorable, but detailed comparison indicates significant differences in slope and curvature of the dipole moment function at equilibrium and large internuclear separations. These differences will affect the magnitudes and ν' scaling of the $\Delta\nu = 1$ and $\Delta\nu = 2$ Einstein coefficients, the more significant effect being on the overtone transitions. An experimental value derived for $A_{2,0}$ agrees with previous determinations and shows the theoretical value to be a factor of 2 too low. Further details of these effects, as well as the scaling of transition strengths for high vibrational and rotational excitation, must be addressed through derivation of an empirical dipole moment function.

ACKNOWLEDGMENTS

The authors are grateful to J. C. Person, B. D. Green, L. G. Piper, and G. E. Caledonia for informative technical discussions, and to H. C. Murphy and D. Sinclair for assistance with the laboratory experiments. The work was performed under Contract No. F19628-88-C-0173 with the Air Force Geophysics Laboratory, and was sponsored by the U.S. Air Force Office of Scientific Research under Task 2310G4 and by the Defense Nuclear Agency under Project SA, Task SA, Work Unit 115.

TABLE III. Einstein coefficients for NO($\Delta\nu = 2$) transitions.

ν'	$A_{\nu',\nu'-2}, s^{-1}$	
	Estimated from COCHISE	<i>Ab initio</i> (Ref. 6)
2	0.94 ($\pm 12\%$)	0.46
3	2.74	1.51
4	4.8	3.10
5	7.1	4.90
6	9.8	7.29
7	13.0	9.63
8	16.6	12.50
9	20.2	15.68
10	23.9	19.14
11	26.5	22.94
12	27.9	27.15
13	27.2 ($\pm 40\%$)	31.88

¹ H. H. Michels, J. Quant. Spectrosc. Radiat. Transfer 11, 1735 (1971).

² G. Chandraiah and C. W. Cho, J. Mol. Spectrosc. 47, 134 (1973).

³ F. P. Billingsley II, J. Chem. Phys. 62, 864 (1975).

⁴ F. P. Billingsley II, J. Chem. Phys. 63, 2267 (1975).

⁵ F. P. Billingsley II, AFRL-TR-75-0586, Air Force Geophysics Laboratory, Hanscom AFB, MA 01731, 13 Nov 1975.

⁶ F. P. Billingsley II, J. Mol. Spectrosc. 61, 53 (1976).

⁷ L. S. Rothman, A. Goldman, J. R. Gillis, R. R. Gamache, H. M. Pickett, R. L. Poynter, N. Husson, and A. Chedin, Appl. Opt. 22, 1616 (1983).

⁸ B. D. Green, G. E. Caledonia, and R. E. Murphy, J. Quant. Spectrosc. Radiat. Transfer 26, 215 (1981).

⁹ J. Y. Mandin, C. Amiot, and G. Guelachvili, Ann. Phys. (Paris) 5, 91 (1980).

¹⁰ R. F. Holland, M. C. Vasquez, W. H. Beattie, and R. S. McDowell, J. Quant. Spectrosc. Radiat. Transfer 29, 435 (1983).

¹¹ W. T. Rawlins, M. E. Fraser, and S. M. Miller, J. Phys. Chem. 93, 1097 (1989).

¹² J. P. Kennealy, F. P. Del Greco, G. E. Caledonia, and B. D. Green, J. Chem. Phys. 69, 1574 (1978).

¹³ G. E. Caledonia and J. P. Kennealy, Planet. Space Sci. 30, 1043 (1982).

- ¹⁴W. T. Rawlins, G. E. Caledonia, J. J. Gibson, and A. T. Stair, Jr., *J. Geophys. Res.* **86**, 1313 (1981).
- ¹⁵D. E. Siskind, C. A. Barth, and R. G. Roble, *J. Geophys. Res.* **94**, 16885 (1989).
- ¹⁶R. H. Picard, J. R. Winick, R. D. Sharma, A. S. Zachor, P. J. Espy, and C. R. Harris, *Adv. Space Res.* **7**, 23 (1987).
- ¹⁷W. T. Rawlins, J. C. Person, M. E. Fraser, and W. A. M. Blumberg, *J. Chem. Phys.* (submitted).
- ¹⁸W. T. Rawlins, H. C. Murphy, G. E. Caledonia, J. P. Kennealy, F. X. Robert, A. Corman, and R. A. Armstrong, *Appl. Opt.* **23**, 3316 (1984).
- ¹⁹M. E. Fraser, W. T. Rawlins, and S. M. Miller, *J. Chem. Phys.* **92**, 1758 (1990).
- ²⁰W. T. Rawlins and R. A. Armstrong, *J. Chem. Phys.* **87**, 5202 (1987).
- ²¹W. T. Rawlins, G. E. Caledonia, and R. A. Armstrong, *J. Chem. Phys.* **87**, 5209 (1987).
- ²²M. E. Fraser, W. T. Rawlins, and S. M. Miller, *J. Chem. Phys.* **88**, 538 (1988).
- ²³W. T. Rawlins, A. Gelb, and R. A. Armstrong, *J. Chem. Phys.* **82**, 681 (1985).
- ²⁴A. Goldman and S. C. Schmidt, *J. Quant. Spectrosc. Radiat. Transfer* **15**, 127 (1975).
- ²⁵G. Herzberg, *Molecular Spectra and Molecular Structure. I. Spectra of Diatomic Molecules* (Van Nostrand, Toronto, 1950).
- ²⁶S. R. Langhoff, H. J. Werner, and P. Rosmus, *J. Mol. Spectrosc.* **118**, 507 (1986).
- ²⁷D. N. Turnbull and R. P. Lowe, *J. Chem. Phys.* **89**, 2763 (1988).
- ²⁸D. D. Nelson, Jr., A. Schiffman, D. J. Nesbitt, and D. J. Yaron, *J. Chem. Phys.* **90**, 5443 (1989).
- ²⁹D. D. Nelson, A. Schiffman, and D. J. Nesbitt, *J. Chem. Phys.* **90**, 5455 (1989).
- ³⁰D. D. Nelson, Jr., A. Schiffman, and D. J. Nesbitt, *J. Chem. Phys.* **93**, 7003 (1990).
- ³¹W. T. Rawlins, R. R. Foutter, and T. E. Parker (in preparation).

THIS PAGE INTENTIONALLY LEFT BLANK

APPENDIX B

The Dipole Moment and Infrared Transition Strengths of Nitric Oxide

W.T. Rawlins
J.C. Person
K.W. Holtzclaw
M.E. Fraser

(Quarterly No. 17 reproduced in its entirety)

THIS PAGE INTENTIONALLY LEFT BLANK

**THE DIPOLE MOMENT AND INFRARED TRANSITION
STRENGTHS OF NITRIC OXIDE**

Quarterly Status Report No. 17

For the Period

1 September to 30 November 1992

Under Air Force Contract No. F19628-88-C-0173

Prepared by:

W.T. Rawlins, J.C. Person, K.W. Holtzclaw, and M.E. Fraser

Sponsored by:

Air Force Geophysics Laboratory
Air Force Systems Command
U.S. Air Force
Hanscom Air Force Base, MA 01731

January 1993

THIS PAGE INTENTIONALLY LEFT BLANK

Nitric oxide is an important source of infrared radiation in the thermosphere. During auroral depositions or other energetic particle bombardments, nitric oxide is produced with copious excess internal energy, resulting in non-thermal population of a wide range of vibrational and rotational states. The corresponding infrared fluorescence spectra extend from 5 to 9 μm in the fundamental band ($\Delta v=1$), and from 2.5 to nearly 4 μm in the first overtone band. Reliable prediction and analysis of the excited state radiant intensities and spectral distributions requires accurate values for the infrared transition strengths (Einstein A coefficients) as functions of initial and final vibrational and rotational state. Using recently published overtone/fundamental branching ratio measurements, we have applied a non-linear least squares fitting technique to determine an empirical electric dipole moment function for $\text{NO}(X^2\Pi)$ over the range 1.7 to 3.0 bohr in internuclear distance. We then used this dipole moment function to compute state-to-state Einstein coefficients, taking into account the effects of spin uncoupling and vibration-rotation interaction for high rotational energies. We discuss the results of these calculations, and their implications for the modeling and analysis of rovibrationally excited $\text{NO}(v,J)$ fluorescence in the electron-irradiated upper atmosphere.

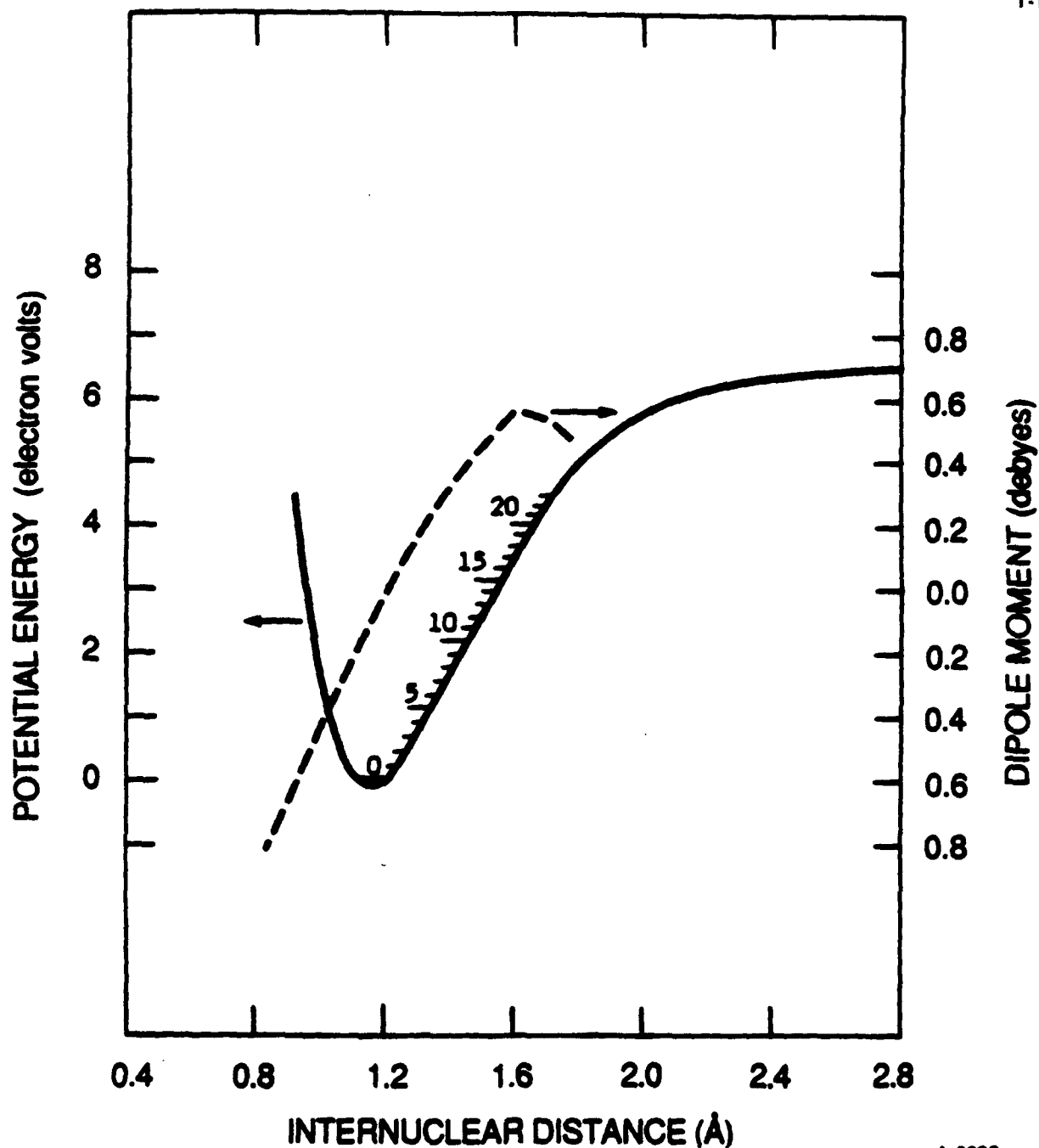
KEYS FOR THERMOSPHERIC NO(v , J) ANALYSIS

T-14136

- Overtone transition strengths
- Scaling of $A_{\Delta v=1}$, $A_{\Delta v=2}$ with v' and J'
 - Shape of $\mu(r)$
- Effects of super-high J on $A(J)$ scaling, P/R ratios
- Band-integrated A -factors
 - Effects of high T_{ROT}
 - Uncertainties at high v

NO($X^2\Pi$) DIPOLE MOMENT FUNCTION BILLINGSLEY THEORY, 1975

T-1241



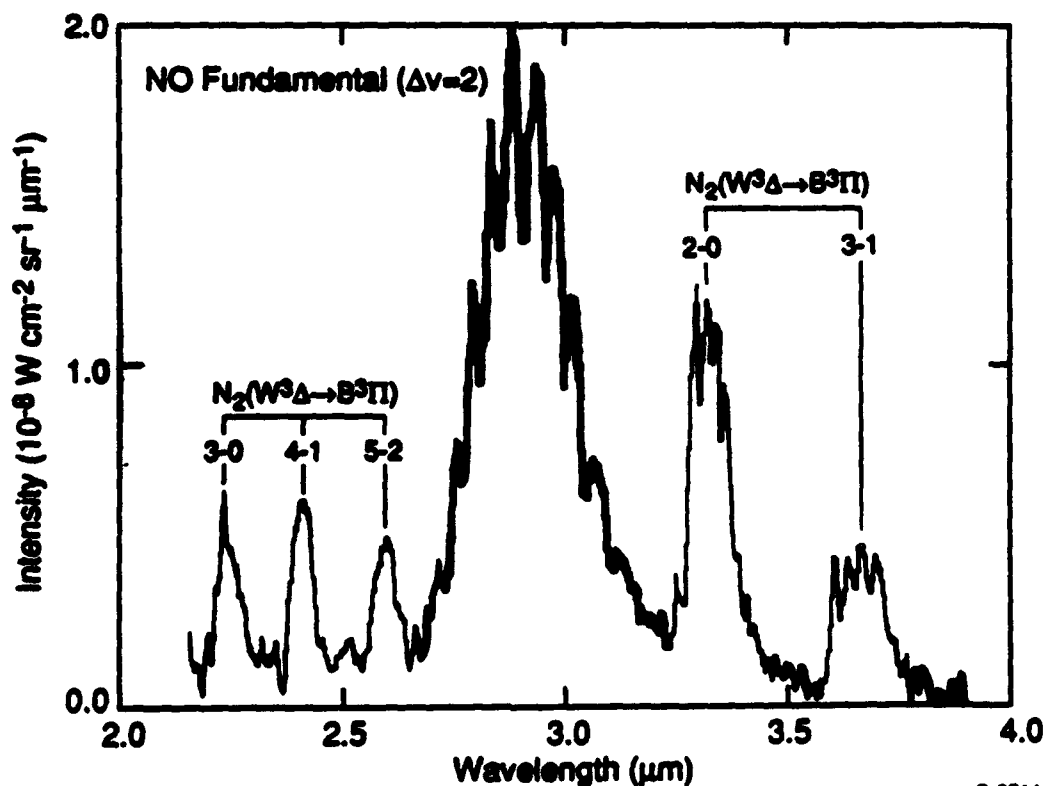
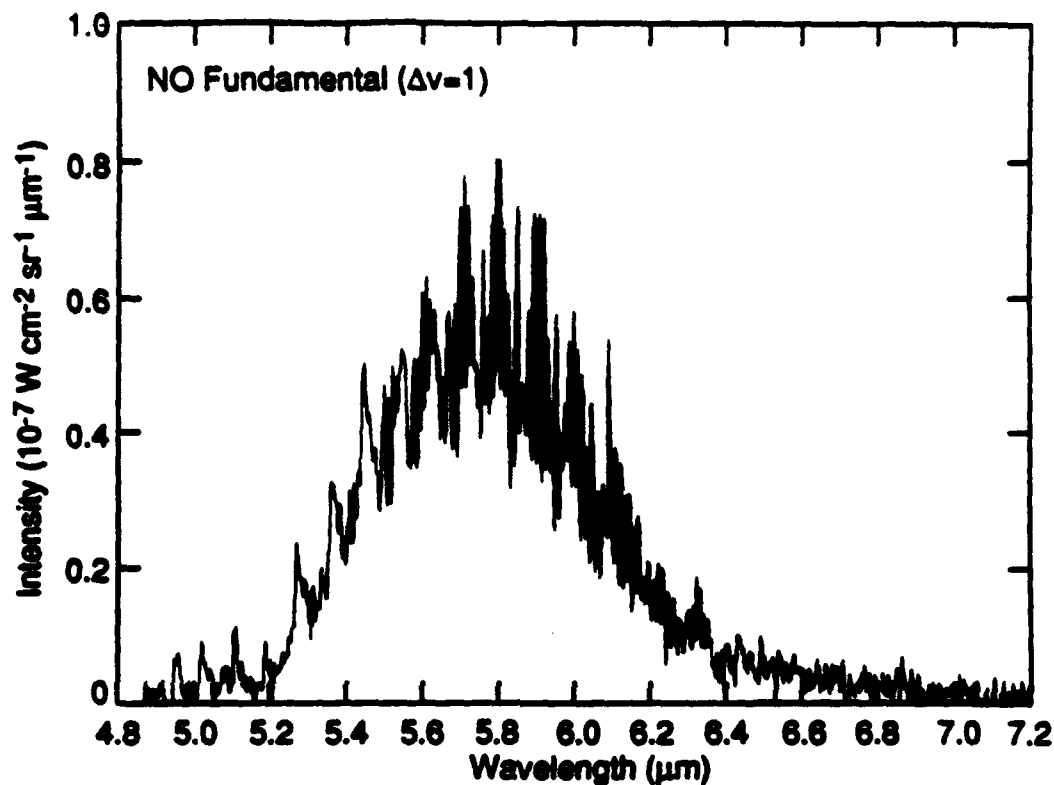
A-8222

- High v , high J sample large and small r
- $A(\Delta v=1) \propto$ 1st derivative (slope)
- $A(\Delta v=2) \propto$ 2nd derivative (curvature)

COCHISE SPECTRA OF NO(V, J) FLUORESCENCE

$N(^2D, ^2P) + O_2 \rightarrow NO(v, J) + O$

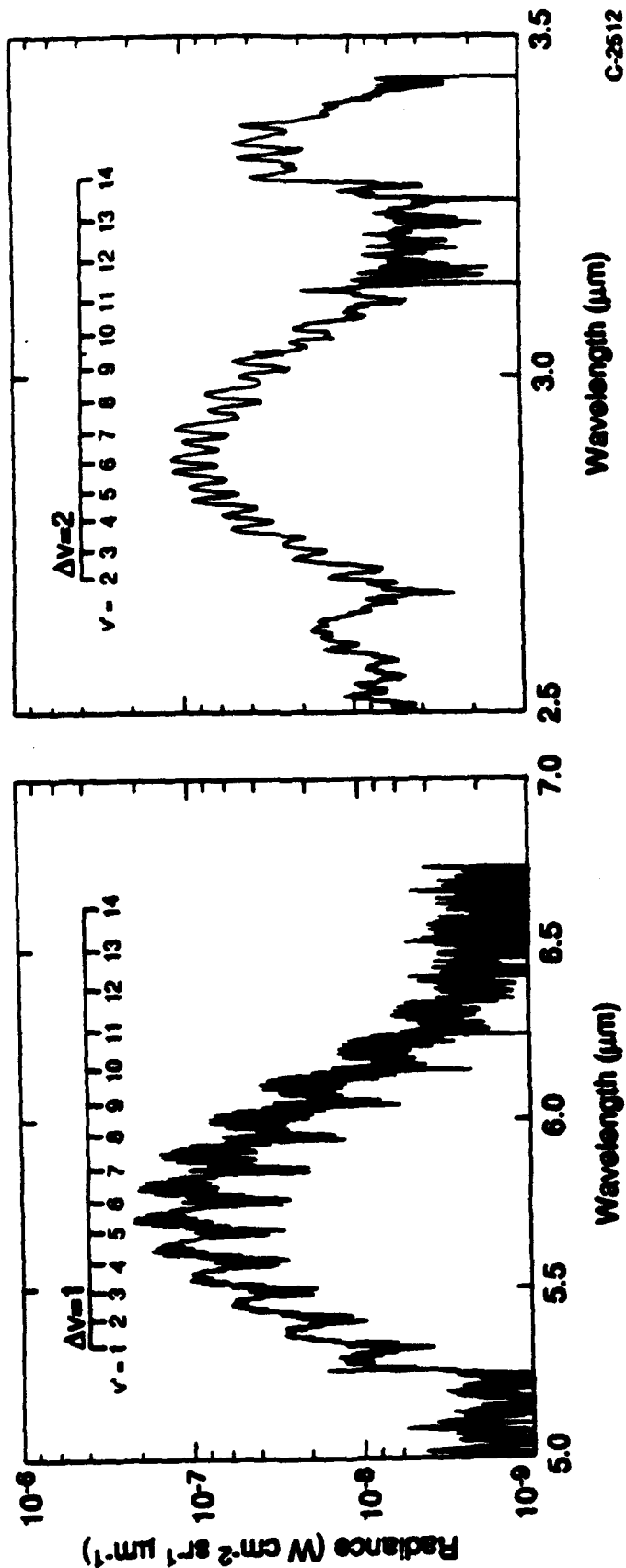
T-14137



C-2511

ROTATIONALLY THERMALIZED NO(v) SPECTRA (10 mtorr He)

T-14138



DETERMINATION OF $\mu(r)$

T-14139

$$\bullet \quad A(v' j' \Omega' \longrightarrow v'' j'' \Omega'') = \frac{64 \pi^4 \nu^3}{3 h} \times \left| \int \psi(v' j' \Omega') \mu(r) \psi(v'' j'' \Omega'') dr \right|^2$$

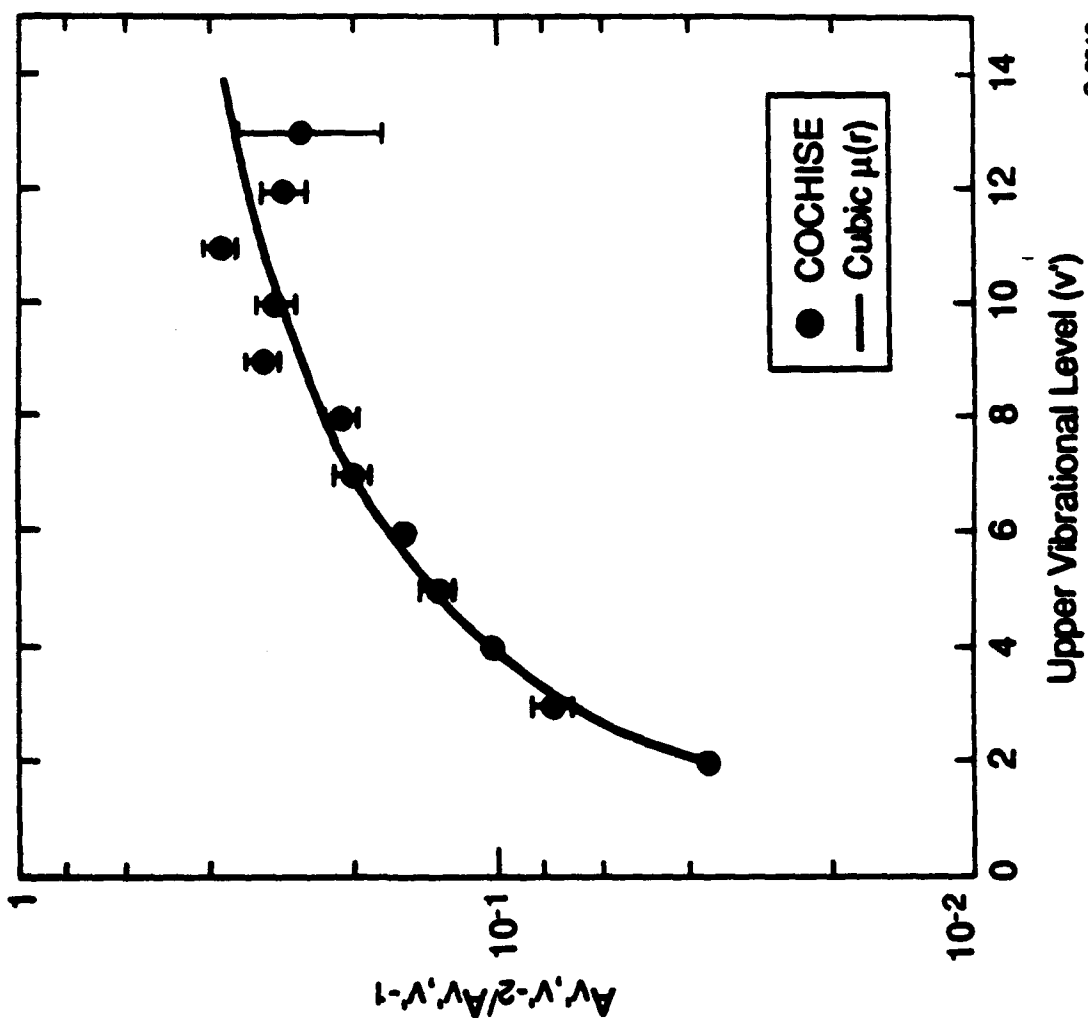
- Determine ψ by RKR method
 - Hurlburt - Hirschfelder potential from spectroscopic constants
 - Numerov - Cooley inversion:

$$\mathcal{H}\psi = E\psi$$

- Solve $\mu(r)$ to fit A-ratio data
 - $\mu(r) = a + br + cr^2 + dr^3$
 - Constraints: static dipoles, A₁₀, A₂₀
- Compute rotationless A-factors

OVERTONE/FUNDAMENTAL BRANCHING RATIOS

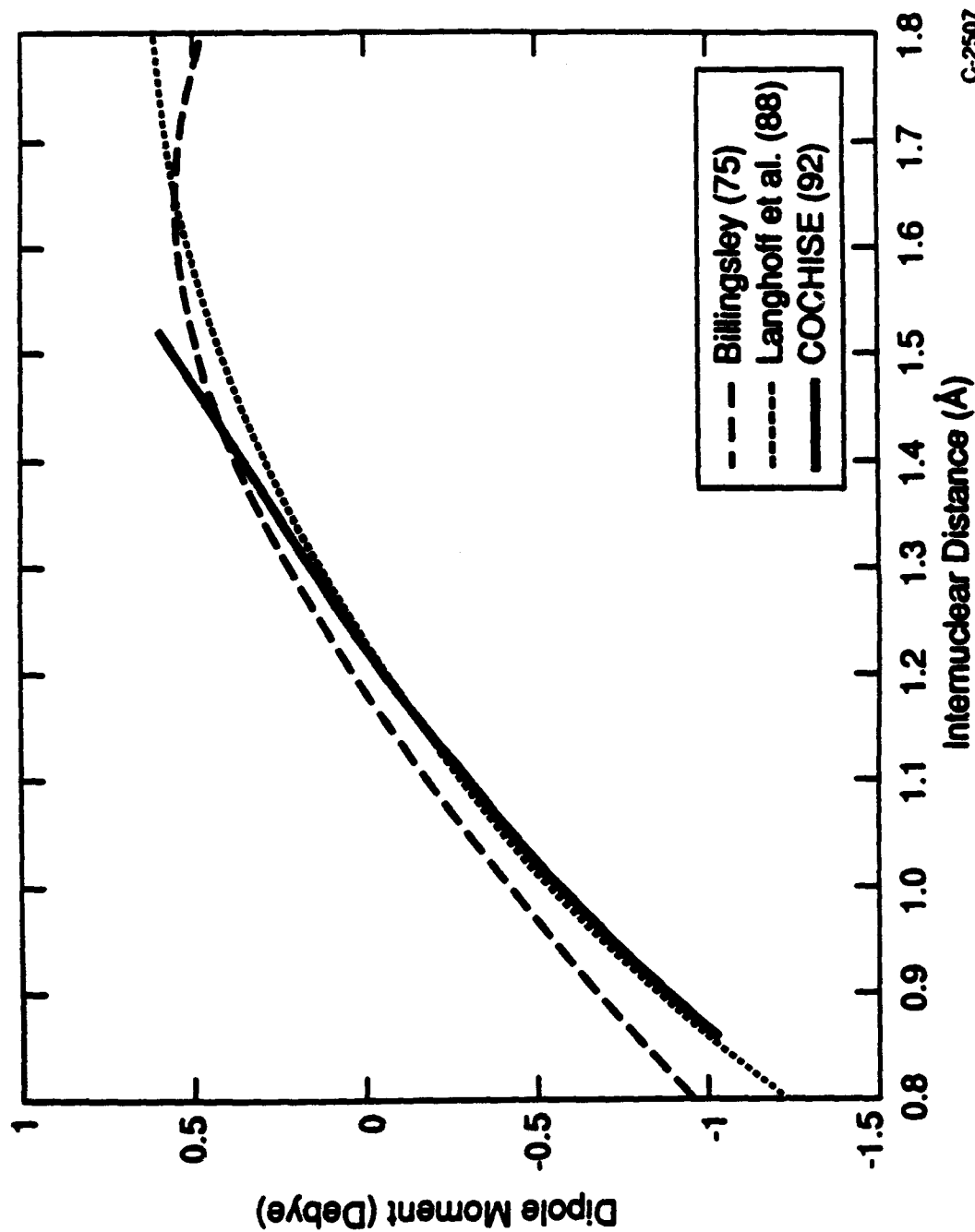
T-14140



C-2513

NO (χ^2 Π) DIPOLE MOMENT FUNCTION

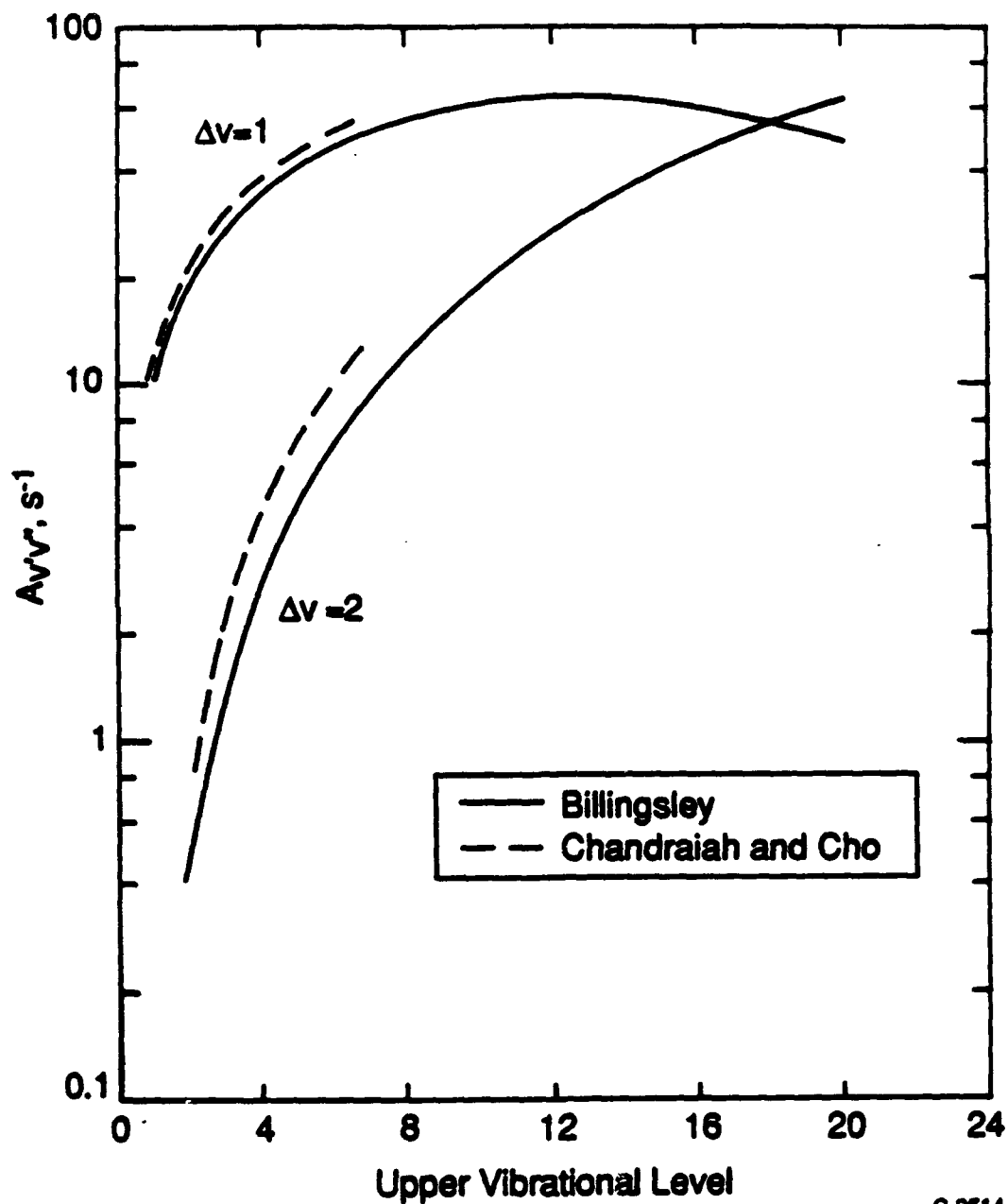
T-14141



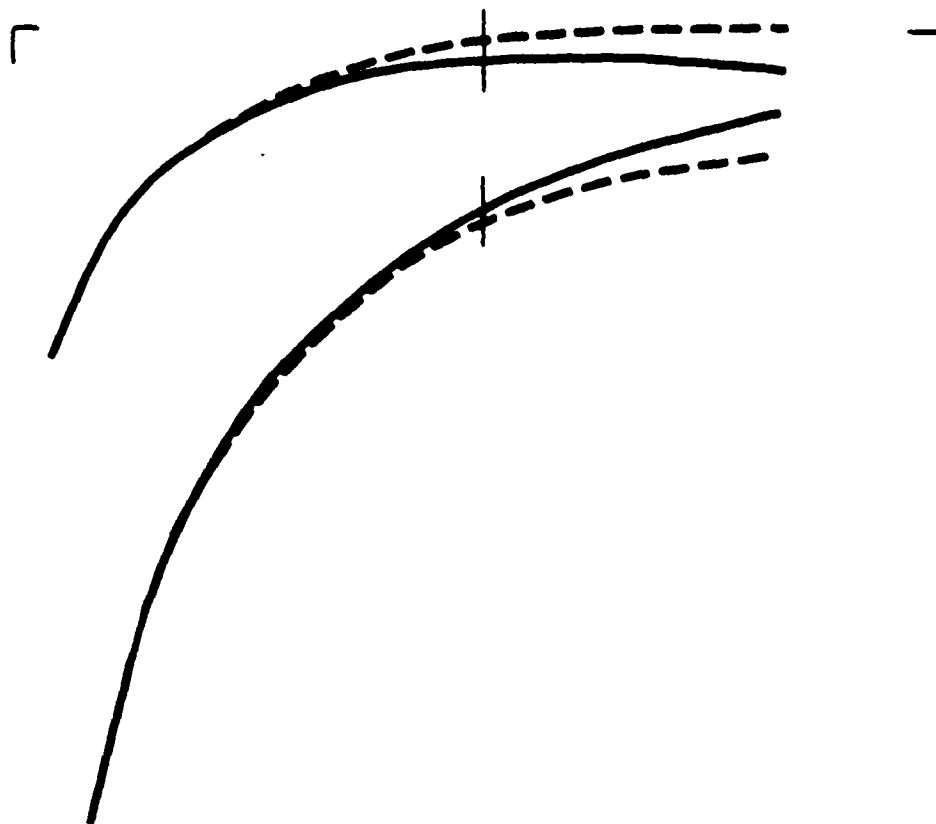
C-2507

EINSTEIN COEFFICIENTS FOR NO ($X^2\Pi$)

T-14142



C-2514

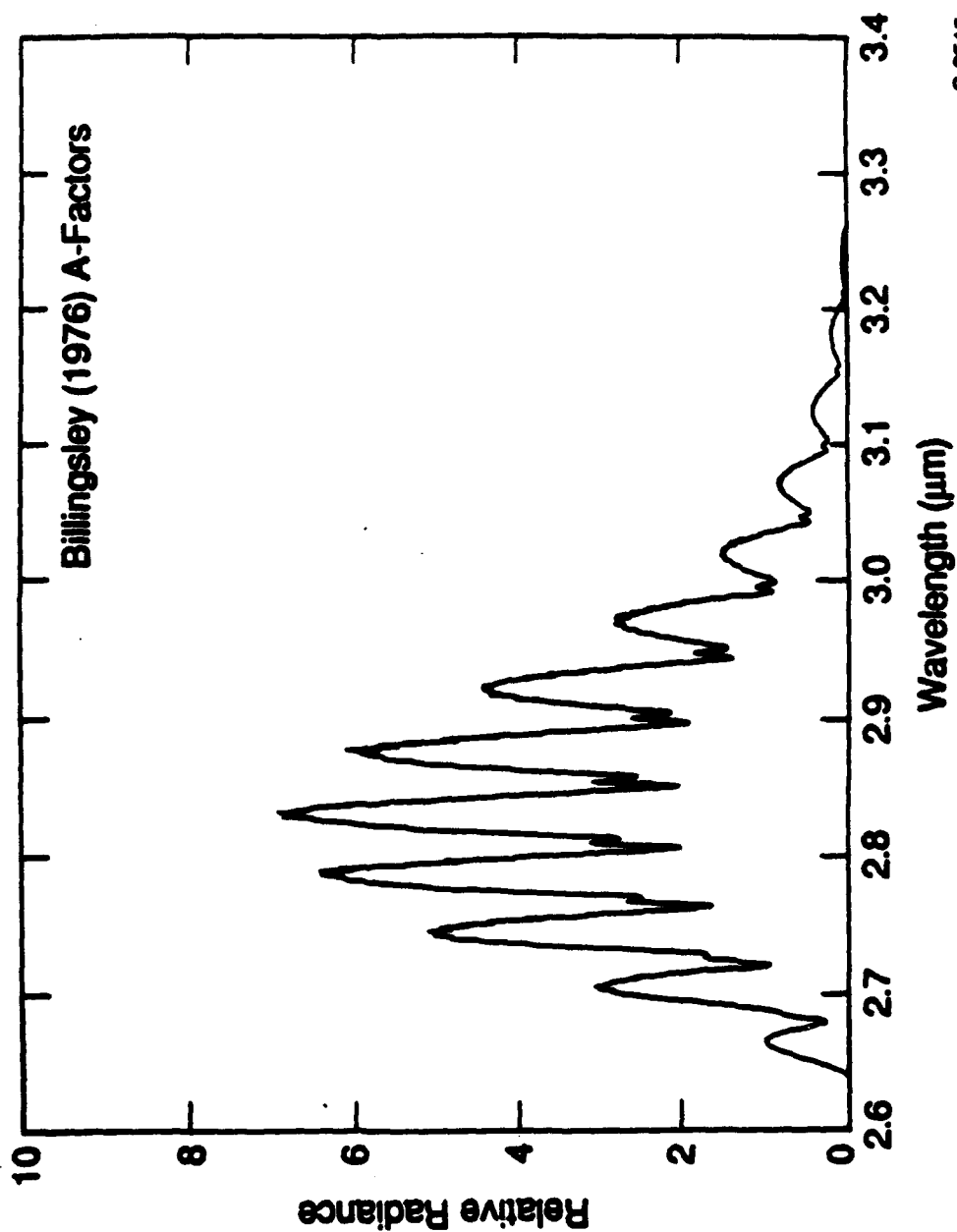


COCHISE Values From $\mu(r)$ Fit:

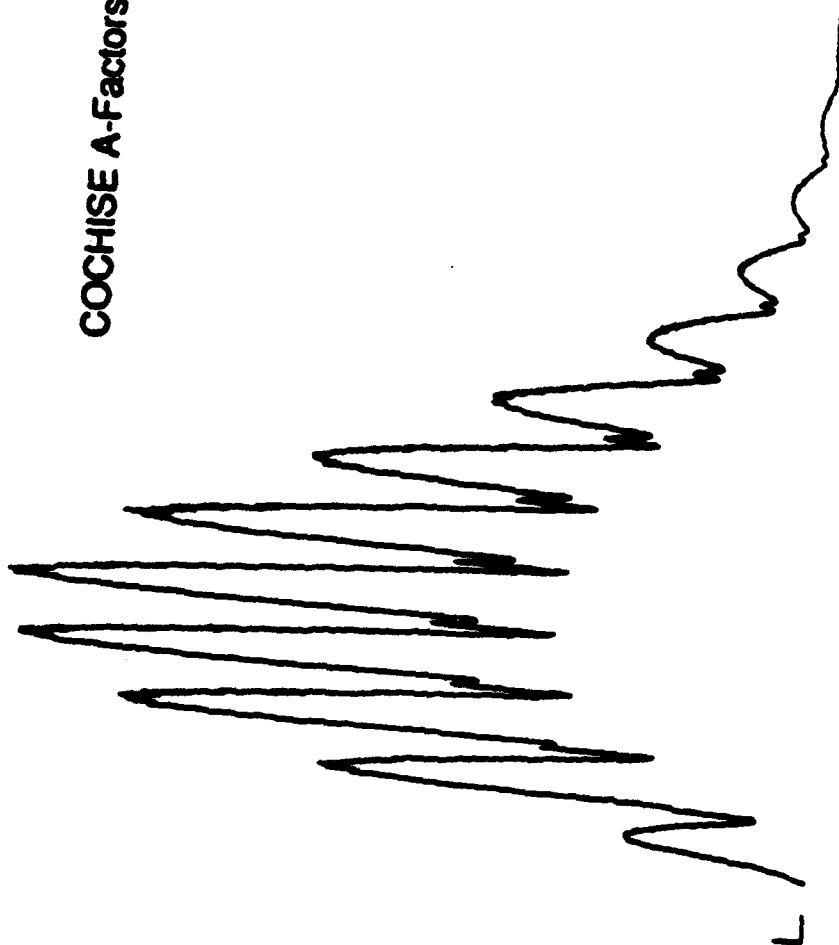
—	Quadratic
- -	Cubic

PREDICTED NO($\Delta v=2$) SPECTRUM FOR N(2D) + O₂, $z \geq 120$ km

T-14170



COCHISE A-Factors



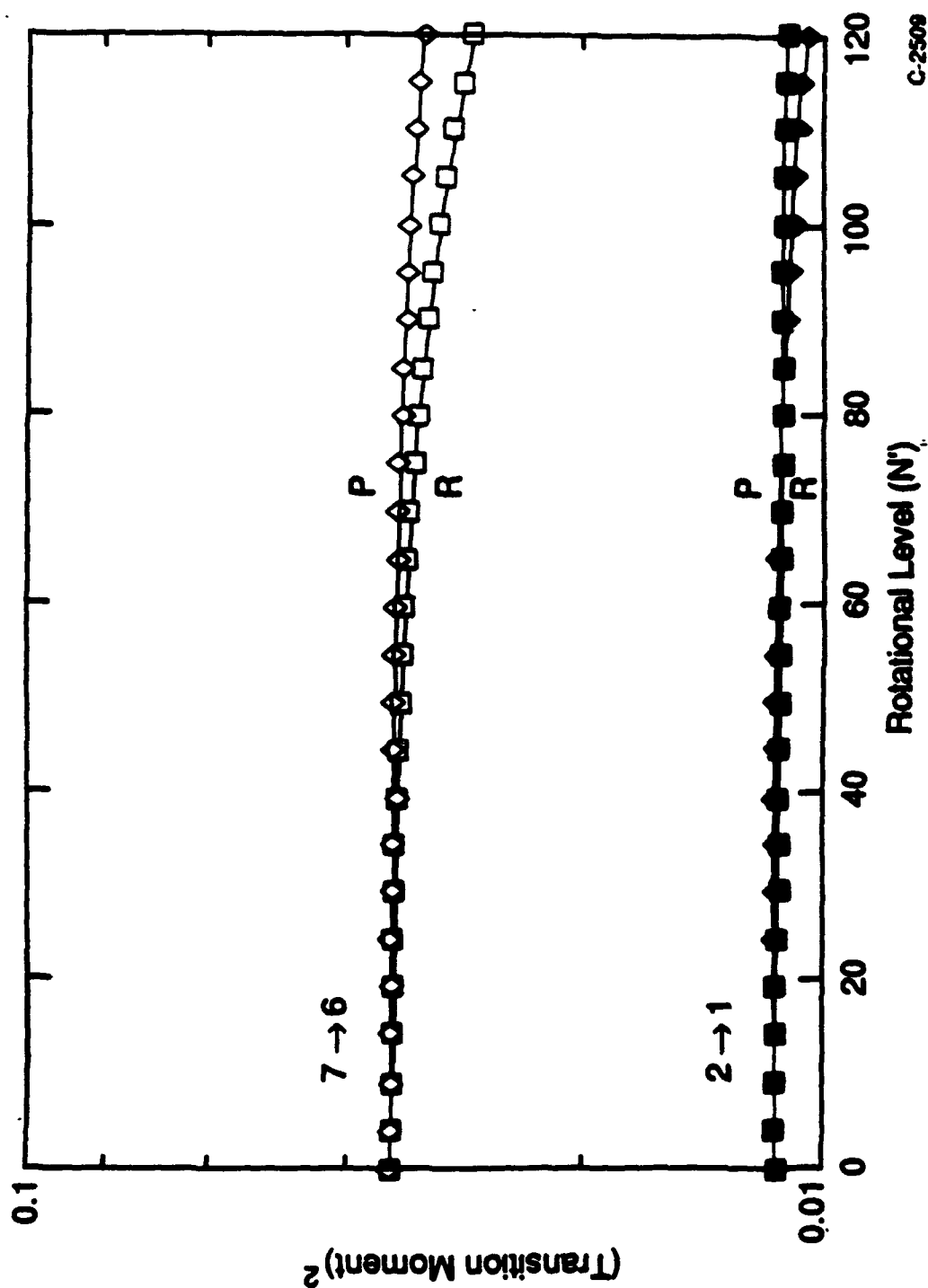
FACTORS AFFECTING $A(J)$ SCALING

T-14143

- Curvature in $\mu(r)$ at larger r
- Vibration-rotation interaction
- Spin uncoupling (Hund's Case (a) \rightarrow (b))
- Lambda doubling (neglected)

ROTATIONAL INTENSITY SCALING NO FUNDAMENTAL BAND

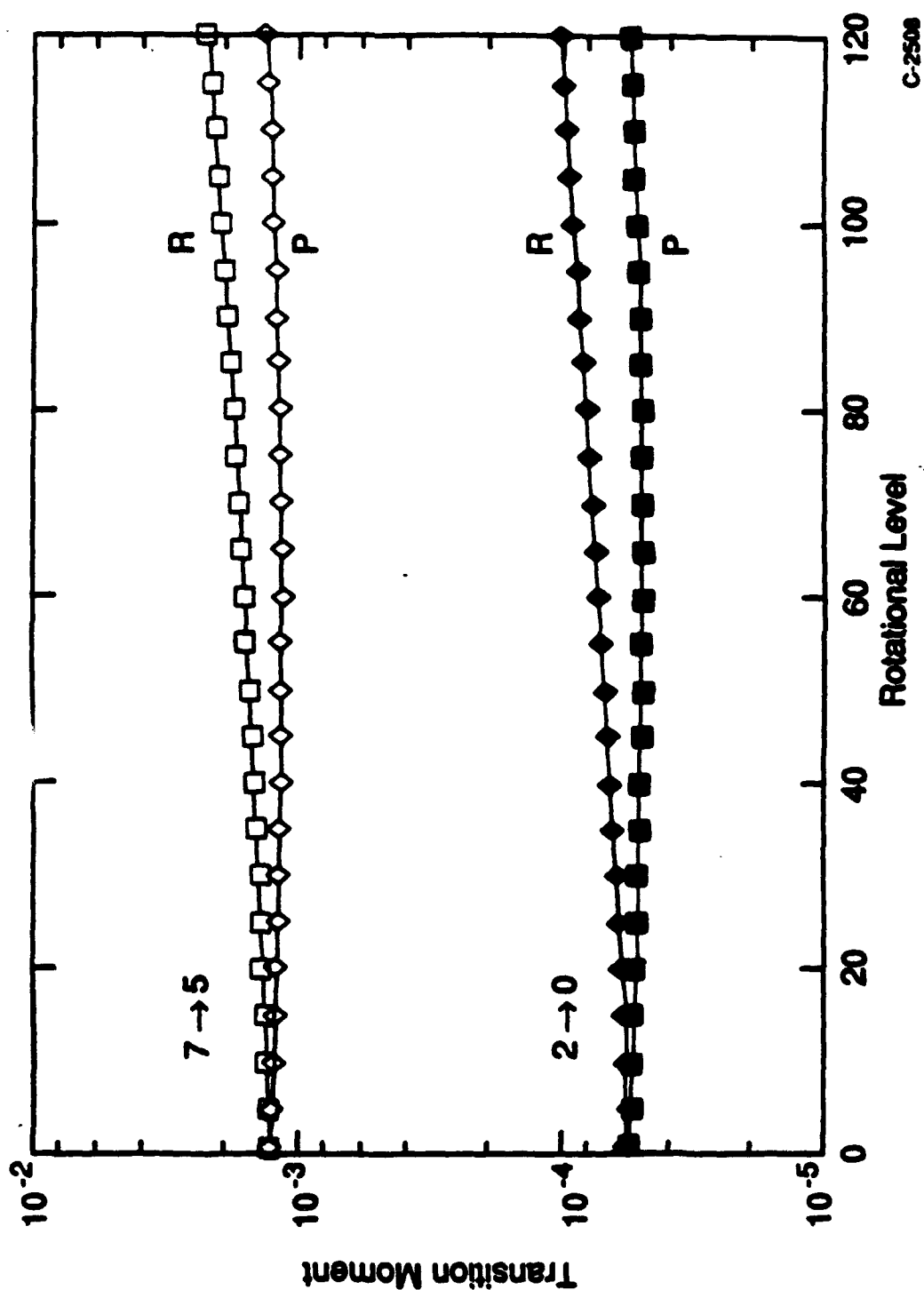
T-14144



C-2509

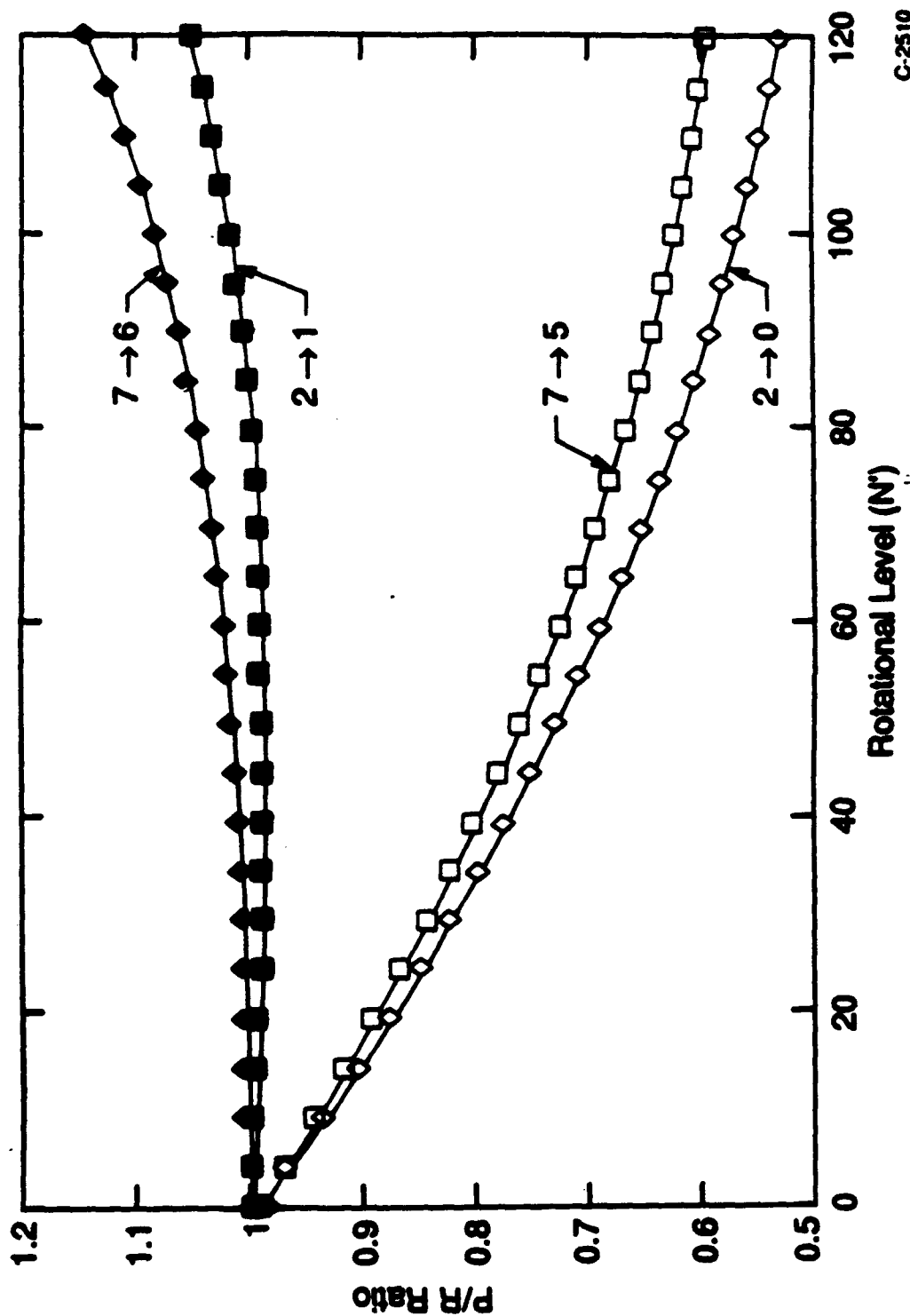
ROTATIONAL INTENSITY SCALING NO FIRST OVERTONE BAND

T-14145



ROTATIONAL INTENSITY SCALING P/R RATIOS RELATIVE TO HONL-LONDON

T-14148



C-2510

CONCLUSIONS

T-14147

- Dipole moment function determined for $r = 0.9$ to 1.5 \AA
 - A-factors for $\Delta v = 1$ to 4 , $v' \leq 12$
- Fundamental band: no surprises
- First overtone band: new and different
 - New $A(v)$ values affect analysis of 2.5 to $3 \text{ }\mu\text{m}$ fluorescence
 - Non-HL $A(J)$ scaling effects analysis of high- J spectral components, 3 to $4 \text{ }\mu\text{m}$ fluorescence
- Require more data to evaluate scaling to high $v(v = 13$ to $26)$

THIS PAGE INTENTIONALLY LEFT BLANK

APPENDIX C

N₂O Production Mechanism from the Interaction of Discharged-Excited Species

M.E. Fraser
T.R. Tucker
L.G. Piper
W.T. Rawlins

J. Geophys. Res. 95, 18,611 (1990)

(SR-457 reproduced in its entirety)

THIS PAGE INTENTIONALLY LEFT BLANK

N₂O PRODUCTION MECHANISM FROM THE INTERACTION
OF DISCHARGE-EXCITED SPECIESMark E. Fraser, Thomas R. Tucker, Lawrence G. Piper,
and Wilson T. Ravlins

Physical Sciences Inc., Andover, Massachusetts

Abstract. We have examined the interaction of discharge effluents to understand the formation mechanism of N₂O in the upper atmosphere and in published studies employing discharge-flow systems. N₂O production rates were determined under various discharge-flow conditions and are consistent only with a process in which both N₂ and O₂ species are excited and are present in large relative concentrations. We postulate N₂(v≥15) + O₂(a¹Δ or b¹Σ) as the responsible mechanism.

1. Introduction

N₂O production from lightning [Hill et al., 1984; Levine and Shaw, 1983] and discharged [Donohue et al., 1977; Brandvold and Martinez, 1989; Eliasson and Kogelschatz, 1986; Levine et al., 1979] or irradiated [Hartack and Dondes, 1956] N₂/O₂ mixtures is well-documented but the formation mechanisms are not understood. N₂O plays an important role in both the upper and lower atmosphere as a photochemical precursor to odd nitrogen (NO_x) and as an infrared radiator/absorber. N₂O is produced copiously via ground-based biological activity and fossil fuel combustion, and these sources are generally considered to control the global atmospheric N₂O budget. However, a variety of observations of N₂O formation in discharge-excited N₂/O₂ mixtures has led to considerable speculation about possible mechanisms for local atmospheric sources of N₂O which would impact the chemistry of tropospheric electrical discharges, stratospheric NO_x production, and auroral energy deposition. In particular, Prasad and Zipf [1981] have suggested that the reaction of N₂(A³Σ_g⁺) with O₂ was responsible for laboratory observations of N₂O production in electron-irradiated N₂/O₂ [Zipf, 1980a], and have used this idea to model chemical N₂O production in the upper stratosphere/lower mesosphere (via solar-pumped N₂(A) [Zipf and Prasad, 1982] and in the auroral D and E regions (via electron-impact-excited N₂(A)) [Zipf, 1980b]. In addition, Hill et al. [1984] have applied this mechanism to models of tropospheric N₂O production in lightning, point discharges below thunderclouds, and high voltage power line coronas.

Recent laboratory investigations of the N₂(A) + O₂ interaction indicate the branching ratio for N₂O formation to be small [Iannuzzi et al., 1982; Black et al., 1983; DeSousa et

al., 1985], probably near zero [Fraser and Piper, 1989]. Furthermore, additional exploratory measurements in our laboratory showed that readily detectable N₂O levels were formed, not from interactions of discharge-excited N₂ with O₂ or excited O₂/O₂ with N₂, but with co-discharged N₂/O₂ mixtures. This observation suggests that the reaction(s) responsible for N₂O formation observed in discharges requires the presence of metastable excited states of both N₂ and O₂:



This type of reaction can be expected to be a far less productive source of N₂O than the Zipf-Prasad mechanism in most atmospheric scenarios.

We report here an investigation of the interaction of discharge-excited O₂ and N₂ in order to determine the kinetic behavior and identify the N₂O production mechanism. Our measurements establish copious N₂O production via reaction of N₂^{*} with O₂^{*}, and indicate that previous inferences [Hill et al., 1984; Levine and Shaw, 1983; Zipf, 1980a; Zipf and Prasad, 1982; Zipf, 1980b] of atmospheric effects from N₂^{*} + O₂ or O₂^{*}/O₂ + N₂ reactions are incorrect.

2. Experimental Techniques

The experiments were performed in a 5-cm-diameter, 50-cm-long quartz flow tube equipped with a Pyrex trap. A diagram of the experimental apparatus is shown in Figure 1. The total flow rate was 1900 μmole s⁻¹ at a pressure of 2.6 torr and a linear flow velocity of 670 cm s⁻¹. The nitrogen flow ranged from 0 to 200 μmole s⁻¹ (typically 100 μmole s⁻¹) and the oxygen flow varied from 2 to 56 μmole s⁻¹ (typically 2 μmole s⁻¹). The input oxygen and argon gases were purified by flowing them through cryogenic traps of 5-Å molecular sieve prior to their entry into the reactor. The argon was further purified using a commercial scrubber. Nitrogen was used without purification.

These experiments employed both microwave and hollow-cathode dc discharges. The microwave discharges were operated at 2450 MHz and 40 to 50 W power. The hollow-cathode discharge source was of conventional design [Clyne and Nip, 1979], operating at 240 V dc and 3 mA.

The excited species created in the discharges interacted for 75 ms between the mixing point and the point of N₂O collection. The N₂O product was collected in a pyrex trap immersed in liquid nitrogen. Typical trapping times were 5 min. The gas flows were

Copyright 1990 by the American Geophysical Union.

Paper number 90JD00818.
0148-0227/90/90JD-00818\$05.00

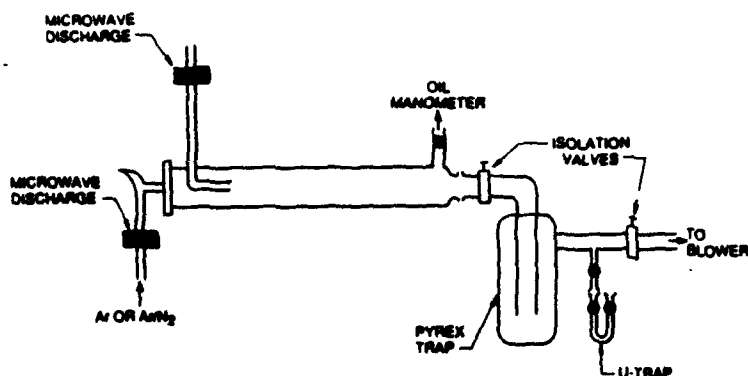


Fig. 1. Diagram of the experimental apparatus.

then shut off and the trapped products were transferred to a second trap. The contents of the transfer trap were analyzed for N₂O by gas chromatography with mass spectrometric detection (GCMS). Details of the analysis and calibration procedures have been published previously [Fraser and Piper, 1989].

All of the determined N₂O production rates were corrected for background levels of N₂O arising from oxygen impurity in the nitrogen gas. For the microwave discharges this impurity was 3×10^{-4} $\mu\text{moles s}^{-1}$ and for the dc experiments the N₂O background was undetectable.

3. Results

The results of our experiments are summarized in Table 1. Typically 10 to 20 measurements were performed for each discharge configuration. The error limits shown with the data represent the total scatter in the data over the entire nitrogen mole fraction range. The data are presented in this manner because the N₂O yields were found to be relatively constant over all nitrogen mole fraction conditions. The data in Table 1 are uncorrected for N₂O loss mechanisms which are likely to be small for our experimental conditions.

The greatest N₂O yields were observed from co-discharged N₂/O₂ mixtures. For the co-discharged system, roughly 1 percent of the initial O₂ was converted to N₂O. Dis-

charging the nitrogen and oxygen separately with subsequent mixing downstream produced yields that were reduced by a factor of two. The yields for this configuration are significant, especially considering the increased surface quenching of excited state precursors for this system. Discharged nitrogen with "cold" oxygen added downstream produced N₂O yields that were further reduced by an order of magnitude. The yields of N₂O from discharged oxygen with "cold" nitrogen added downstream were below detection limits. The results from these three discharge configurations indicate that discharged nitrogen is essential to N₂O formation and discharging the oxygen improves the yield by a factor of ten.

In an attempt to isolate the excited state species contributing to N₂O formation, experiments were conducted with modified discharge conditions. Glass wool was placed downstream from the Ar/N₂ discharge to remove completely discharge-created electronic states of N₂ such as N₂(A³Σ_g⁺, A' ³Σ_g⁺). This has the additional effect of reducing the number density of vibrationally excited ground-state nitrogen significantly and that of ground-state N-atom number density slightly [Morgan and Schiff, 1963; Piper et al., 1989]. As shown in Table 1, the addition of glass wool to the Ar/N₂ discharge caused a reduction in the N₂O yield by a factor of about four. This is commensurate with the reduction that might be expected for

TABLE 1. Results for N₂O Formation

Experiment	N ₂ O Production Rate ($\mu\text{mole s}^{-1}$)
Co-discharged Ar/N ₂ /O ₂	0.053 ± 0.12
MW Ar/N ₂ + MW Ar/O ₂	0.022 ± 0.003
MW Ar/N ₂ + MW Ar/O ₂ + w/Ni screen	0.0103 ± 0.003
MW Ar/N ₂ w/glass wool + MW Ar/O ₂	0.0056 ± 0.0013
MW Ar/N ₂ w/glass wool + MW Ar/O ₂ w/Ni screen	0.0027 ± 0.00065
MW Ar/N ₂ + O ₂	0.0019 ± 0.0004
MW Ar/N ₂ w/glass wool + O ₂	0.00056 ± 0.00011
Ar metastables + N ₂ O ₂	< 10 ⁻³
MW Ar/O ₂ + N ₂	0.0

MW = microwave discharge

N₂(v) under these conditions. If excited electronic states of N₂ were involved, a much greater decrease should have been observed.

Similarly, a nickel screen was placed downstream of the Ar/O₂ discharge. The nickel screen quenches discharge-produced metastables and catalytically recombines the atomic oxygen to form electronically excited O₂, e.g., O₂(A³Σ_u⁺, b¹Σ_g⁺, a¹Δ_g) [Kenner and Ogryzlo, 1983; Ali et al., 1986]. This procedure caused only a factor of two decrease in the N₂O yield implying that electronic metastables of O₂ are involved in the production mechanism.

The remaining discharge configurations failed to produce N₂O in excess of background levels. This includes microwave discharged Ar/O₂ with N₂ added downstream and argon metastables added to N₂/O₂ mixtures.

4. Discussion

The results clearly show that efficient N₂O formation requires excited O₂ and excited N₂. The measured N₂O production rates indicate the minimum concentrations of the responsible excited species. Estimates of the discharge effluent number densities and their flow rates at the mixing point are listed in Table 2. The number densities shown in Table 2 are accurate to within a factor of 2 to 10. The factors that influence the absolute number densities include O₂, N₂ mole fraction, extent of wall and collisional deactivation prior to mixing, and microwave power. The dependence on microwave power is large from 0 to 30 W but less than a factor of two from 50 to 90 W [Piper et al., 1989]. The estimates shown here are for 50 W microwave power.

The N₂ and O₂ flow rates were measured directly from flow meters. The remaining data in Table 2 derive from direct measurements of microwave discharged Ar/N₂ and Ar/O₂ mixtures performed in our laboratory or from studies reported in the literature. The data

for N(⁴S) and O(³P) shown in Table 2 reflect our measurements of the dissociation of N₂ and O₂ in microwave discharges [Piper and Rawlins, 1986]. The number densities for N₂(X,v) are derived from direct measurements of these populations in discharge-excited N₂ mixtures [Piper et al., 1989]. The data in Table 2 are for an N₂ mole fraction of 0.1 which yields a modified Treanor vibrational distribution of characteristic temperature 3500 K [Treanor et al., 1967; Caledonia and Center, 1971]. Cook and Miller [1974] have determined the O₂(a¹Δ) yield to be 5 to 10 percent of the O₂ density. We have directly measured the N(²D), N(²P) yields from discharged nitrogen [L.G. Piper, unpublished, 1989]. The data in Table 2 reflect the measured ratio [N(²D)]/[N₂] = 10⁻⁵ and [N(²P)]/[N(²D)] = 0.2. Observation of N₂(A³Σ - X¹Σ) Vegard-Kaplan emission has set the N₂(A) number density to be ~ 10⁹ molecules cm⁻³ with vibrational populations predominantly in the lowest two vibrational levels. These studies [Piper and Marinelli, 1989] have also indicated the density of other N₂ electronic states to be <10⁹ molecules cm⁻³.

We have excluded ion concentrations from Table 2. Although ion concentration may be high within the active discharge region (~10¹¹ cm⁻³), recombination rapidly drops the ion number densities to <10⁷ cm⁻³ [e.g., Nelson and Tardy, 1988]. Even if ions were to form N₂O with unit efficiency in our various discharge configurations, the formation rates would be several orders of magnitude below the data shown in Table 1.

It can be seen from Table 2 that number densities of N₂(A) and other electronically excited forms of N₂^{*} are too small to account for the observed N₂O production rate. Thus, the most likely nitrogenous N₂O precursor appears to be N₂(v). The most abundant molecular effluents of the Ar/O₂ discharge are O₂(a,b); O₂(A,A',c) are significantly less abundant and are therefore unlikely to

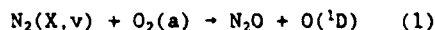
TABLE 2. Discharge Effluents

Species	Approximate Concentration (molecules cm ⁻³)	Radiative Lifetime, τ _{rad}	Flow Rate (μmole s ⁻¹)
N ₂	4.8 × 10 ¹³	-	100
O ₂	9.6 × 10 ¹³	-	2
N(⁴ S)	10 ¹³ - 10 ¹⁴	-	0.1 - 1
O(³ P)	~3 × 10 ¹³	-	0.65
N ₂ (v≥7)	~7 × 10 ¹³	-	1.5
N ₂ (v≥15)	~3 × 10 ¹³	-	0.6
O ₂ (a ¹ Δ)	10 ¹³	65 min	0.22
O ₂ (b ¹ Σ)	10 ¹²	12s	2.2 × 10 ⁻²
N(² D)	~5 × 10 ¹⁰	12 hr	10 ⁻³
N(² P)	~1 × 10 ¹⁰	12s	2 × 10 ⁻⁴
N ₂ (A)	10 ⁹	2s	2.2 × 10 ⁻⁵
Other N ₂ electronically excited species	<10 ⁹	<<1s	<10 ⁻³

Concentrations are rough estimates for the effluents of the discharged Ar/N₂ and Ar/O₂ prior to mixing.

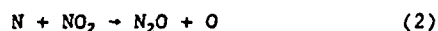
be involved. The observation of slight N₂O formation when the O₂ is not discharged suggests a serial process in which the O₂ must first be excited by collisions with N₂⁺ before it can react to form N₂O.

We therefore conclude that N₂O is indeed formed in discharge-excited nitrogen/oxygen mixtures at low pressures, and that the most likely reaction involves vibrationally excited N₂(X) and electronically excited O₂(a or b). In order for the spin-allowed reaction

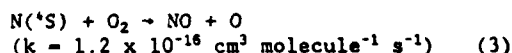


to be exoergic, N₂(v≥15) is required. The occurrence of a spin-forbidden reaction path forming O(³P) or the involvement of O₂(b) lowers this energetic requirement by seven or two quanta, respectively. For our results to be accounted for by reaction (1) requires a lower bound to its rate coefficient, on the order of 10⁻¹⁴ cm³ s⁻¹. The actual rate coefficient could well be much larger than this limit owing to precursor quenching effects and competitive reactions that we have not yet evaluated.

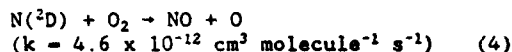
In performing these experiments we have been cautious to minimize N₂O production from the reaction



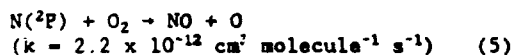
which has a rate coefficient [Glyne and Ono, 1982] for all product branches of 3 × 10⁻¹² cm³ molecule⁻¹ s⁻¹. We have chosen an O₂:N₂ ratio of 1:50 in order to minimize NO and, hence the NO₂ that can form from the recombination of NO and O. For our experimental conditions the reactions



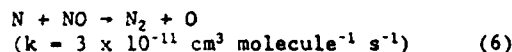
[Becker et al., 1969],



[Piper et al., 1987],



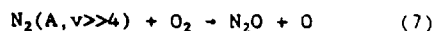
[Piper et al., 1989], and



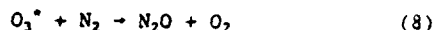
[Glyne and McDermid, 1975; Husain and Slater, 1980; Lee et al., 1978] yield a steady-state number density for NO of ~1.3 × 10⁹ molecules cm⁻³. Even if all the NO were converted to N₂O by either gas phase or heterogenous processes, the N₂O yield would be 10⁻³ μmole s⁻¹. This is significantly lower than the N₂O yields presented in Table 1. Thus, we conclude this source does not contribute significantly to our results.

As alternatives to reaction (1) there are other suggested mechanisms for N₂O

formation in electric discharges. These include



and



that have been postulated by Zipf [private communication, 1987] and Prasad [1981], respectively. Table 2 shows that the total number density of N₂(A) is insufficient to account for the N₂O yields observed here. However, we note that the possibility of N₂O formation via reaction of N₂(A, v≥4) with O₂ is not addressed in the present experiments (N₂(A) concentrations are too small), nor can it be ruled out on the basis of the previous kinetic studies [Iannuzzi et al., 1982; Black et al., 1983; DeSousa et al., 1985; Fraser and Piper, 1989] of N₂(A, low v). Thus there are still no direct or conclusive measurements to confirm or deny the occurrence of this process.

Reaction (8) is also unlikely under our experimental conditions since ozone formed by three-body recombination of O and O₂ cannot reach sufficient number densities to account for the observed results. Additionally, no N₂O was observed from the interaction of discharged oxygen with nitrogen, indicating excited N₂ to be key to N₂O formation.

5. Conclusions

Although it is well known that co-discharged N₂/O₂ mixtures efficiently produce N₂O, our observation that the responsible mechanism requires both the N₂ and O₂ species to be excited is unique. Due to the requirement that both reactants are excited, an N₂O formation mechanism of the form



severely restricts the range of its importance in natural atmospheric processes.

This process is probably responsible for N₂O formation in lightning and cloud discharges, and may have provided an important source of N₂O in the primordial atmosphere. In addition, this reaction may contribute to N₂O formation in coronal discharges around high voltage transmission lines, previously suggested by Hill et al. [1984] (on the basis of N₂(A) + O₂) to be a significant global source of N₂O. Clearly, the kinetics of tropospheric electrical discharges need to be re-evaluated in light of the present results.

However, stratospheric/mesospheric effects due to solar excitation of both N₂⁺ and O₂⁺ (directly or indirectly via collisional energy transfer from more efficiently excited species) will be negligible. This is consistent with the upper atmospheric data base [NASA, 1985], in which the observed N₂O profiles above 40 km show no sign of the local enhancement in production rate predicted by Zipf and Prasad [1982].

Similarly, in auroras the N₂⁺ + O₂⁺ reaction will not be significant except at the strongest dosing levels, probably IBC Class III-IV in intensity. This level of

auroral dosing could produce significant molecular excitation below 100 km, i.e., at altitudes where quenching of the excited species by atomic oxygen would be diminished. Under these conditions, N₂O formation would probably be observable through fluorescence in its infrared vibrational bands at 4.5, 7.8 and 17 μ m. Unfortunately, the auroral data base for such high dosing levels is limited [Stair et al., 1983], and there is as yet no clear evidence for N₂O formation under these conditions.

It appears from the present results that N₂⁺ + O₂⁺ interactions are the primary source of N₂O formation in discharge-excited air, and that other processes involving N₂(A, high v) need not be invoked. We hope to pursue this issue further in future experimental investigations.

Acknowledgments. The authors would like to acknowledge advice provided by B.D. Green. This work was performed under Contract F19628-88-C-0173 with the Air Force Geophysics Laboratory and was sponsored by the U.S. Air Force Office of Scientific Research under Task 2310G4 and the Defense Nuclear Agency under project SA, task SA, work unit 213.

References

- Ali, A.A., E.A. Ogryzlo, Y.Q. Shen, and P.T. Wassel, The formation of O₂(a¹ Δ_g) in homogeneous and heterogeneous atom recombination, *Can. J. Phys.*, **64**, 1614-1620, 1986.
- Becker, K.H., W. Groth, and D. Kley, The rate constant of the aeronomic reaction N + O₂, *Z. Naturforsch.*, **A24**, 1280-1281, 1969.
- Black, G., R.M. Hill, R.L. Sharpless, and T.G. Slanger, Laboratory studies of N₂O relevant to stratospheric processes, *J. Photochem.*, **22**, 369-372, 1983.
- Brandvold, D.K., and P. Martinez, The NO_x/N₂O fixation ratio from electrical discharges, *Atmos. Environ.*, **22**, 2477-2480, 1989.
- Caledonia, G.E. and R.E. Center, Vibrational distribution functions in anharmonic oscillators, *J. Chem. Phys.*, **55**, 552-561, 1971.
- Clyne, M.A.A. and Y. Ono, Determination of the rate constant of reaction of N(⁴S_{3/2}) with NO₂ using resonance fluorescence in a discharge flow system, *Chem. Phys.*, **69**, 381-388, 1982.
- Clyne, M.A.A. and W.S. Nip, Generation and measurement of atom and radical concentrations in flow systems, in *Reactive Intermediates in the Gas Phase*, edited by D.W. Setser, pp. 1-57, Academic Press, San Diego, Calif., 1979.
- Clyne, M.A.A. and I.S. McDermid, Mass spectrometric determinations of the rates of elementary reactions of NO and NO₂ with ground state N⁴S atoms, *J. Chem. Soc. Faraday Trans. 1*, **71**, 2189-2202, 1975.
- Cook, T.J. and T.A. Miller, Production of ¹A_g O₂ from microwave discharges in CO₂, NO₂ and SO₂, *Chem. Phys. Lett.*, **25**, 396-398, 1974.
- DeSousa, A.R., M. Touzeau, and M. Petitdidier, Quenching reactions of metastable N₂(A³ Σ^- , v=0,1,2) molecules by O₂, *Chem. Phys. Lett.*, **121**, 423-428, 1985.
- Donohoe, K.G., F.H. Shair, and O.R. Wulf, Production of O₃, NO, and N₂O in a pulsed discharge at 1 atm, *Ind. Eng. Chem. Fundam.*, **16**, 208-215, 1977.
- Eliasson, B. and U. Kogelschatz, N₂O formation in ozonizers, *J. Chem. Phys.*, **83**, 279-282, 1986.
- Fraser, M.E. and L.G. Piper, Product branching ratios from the N₂(A³ Σ_u^+) + O₂ interaction, *J. Phys. Chem.*, **93**, 1107-1111, 1989.
- Harteck, P. and S. Dondes, Fixation of nitrogen by ionizing radiation as nitrogen dioxide and nitrous oxide, *J. Chem. Phys.*, **24**, 619, 1956.
- Hill, R.D., R.G. Rinker, and A. Coucouvinos, Nitrous oxide production by lightning, *J. Geophys. Res.*, **89**, 1411-1421, 1984.
- Husain, D. and N.K.H. Slater, Kinetic study of ground state atomic nitrogen N(2⁴S_{3/2}) by time-resolved atomic resonance fluorescence, *J. Chem. Soc. Faraday Trans. 2*, **76**, 606-619, 1980.
- Iannuzzi, M.P., J.B. Jeffries, and F. Kaufman, Product channels of the N₂(A³ Σ_u^+) + O₂ interaction, *Chem. Phys. Lett.*, **87**, 570-574, 1982.
- Kenner, R.D. and E.A. Ogryzlo, Quenching of O₂(C¹ Σ_u^-) v=0 by O(³P), O₂(a¹ Δ_g), and other gases, *Can. J. Chem.*, **61**, 921-926, 1983.
- Lee, J.H., J.V. Michael, W.A. Payne, and L.J. Stief, Absolute rate of the reaction of N(⁴S) with NO from 196 to 400 K with DF-RF and FP-RF techniques, *J. Chem. Phys.*, **69**, 3069-3076, 1978.
- Levine, J.S. and E.F. Shaw, Jr., In situ aircraft measurements of enhanced levels of N₂O associated with thunderstorm lightning, *Nature*, **303**, 312-314, 1983.
- Levine, J.S., R.E. Hughes, W.L. Chameides, and W.E. Howell, N₂O and CO production by electric discharge: atmospheric implications, *Geophys. Res. Lett.*, **6**, 557-559, 1979.
- Morgan, J.E. and H.I. Schiff, The study of vibrationally excited N₂ molecules with the aid of an isothermal calorimeter, *Can. J. Chem.*, **41**, 903-912, 1963.
- NASA, Atmospheric Ozone 1985: Assessment of Our Understanding of the Processes Controlling its Present Distribution and Change, *WMO Rep.*, **16**, Chapter 10, 1985.
- Nelson, T.O. and D.C. Tardy, On the ion contamination of atoms produced in a microwave discharge, *Int. J. Chem. Kinet.*, **20**, 187-190, 1988.
- Piper, L.G. and W.J. Marinelli, Excitation of IF(B³ Π_{0+}) by active nitrogen, *J. Phys. Chem.*, **93**, 4073, 1989.
- Piper, L.G. and W.T. Rawlins, O-Atom yields from microwave discharges in N₂O/Ar mixtures, *J. Phys. Chem.*, **90**, 320-325, 1986.
- Piper, L.G., M.E. Donahue, and W.T. Rawlins, Rate coefficients for N(⁴D) reactions, *J. Phys. Chem.*, **91**, 3883-3888, 1987.
- Piper, L.G., K. Donohue, W.J. Kessler, T.R. Tucker, W.J. Marinelli, and S.J. Davis, Laser-based diagnostics for N₂(X,v), *Rep. PSI-1045/TR-960*, final report under Air

- Force Weapons Laboratory contract F29601-87-C-0056, prepared by Physical Sciences Inc., 1989.
- Prasad, S.S., Excited ozone as a possible source of atmospheric N₂O, Nature, **289**, 386-389, 1981.
- Prasad, S.S. and E.C. Zipf, Atmospheric nitrous oxide produced by solar protons and relativistic electrons, Nature, **291**, 564-566, 1981.
- Rawlins, W.T., L.G. Piper, M.E. Fraser, H.C. Murphy, T.R. Tucker, and A. Gelb, CANOES II: Dynamics of atmospheric infrared thermochemical excitation, Rep. PSI-9032/TR-901, under Air Force Geophysics Laboratory contract F19628-85-C-0032, prepared by Physical Sciences Inc., 1989.
- Stair, A.T., Jr., J. Pritchard, I. Coleman, C. Bohne, W. Williamson, J. Rogers, and W.T. Rawlins, The rocketborne cryogenic (10 K) high resolution interferometer spectrometer flight-HIRIS: Atmospheric and auroral infrared emission spectra, Appl. Opt., **22**, 1056-1069, 1983.
- Treanor, C.E., J.W. Rich, and R.G. Rehm, Vibrational relaxation of anharmonic oscillators with exchange-dominated collisions, J. Chem. Phys., **48**, 1798-1807, 1968.
- Zipf, E.C., A laboratory study on the formation of nitrous oxide by the reaction N₂(A³Σ_g⁺) + O₂ → N₂O + O, Nature, **287**, 523-524, 1980a.
- Zipf, E.C. Production of nitrous oxide in the D and E regions, Nature, **287**, 1980b.
- Zipf, E.C. and S.S. Prasad, A mesospheric source of nitrous oxide, Nature, **295**, 133-135, 1982.
-
- M.E. Fraser, T.R. Tucker, L.G. Piper, and W.T. Rawlins, Physical Sciences Inc., 20 New England Business Center, Andover, Massachusetts.

(Received November 6, 1989;
revised February 27, 1990;
accepted April 3, 1990.)

APPENDIX D

The Ratio A_{00}/A_{01} for the Infrared Atmospheric Bands
of Molecular Oxygen

L.G. Piper
W.T. Rawlins

(Quarterly No. 7 reproduced in its entirety)

THIS PAGE INTENTIONALLY LEFT BLANK

THE RATIO A_{00}/A_{01} FOR THE
INFRARED ATMOSPHERIC BANDS OF MOLECULAR OXYGEN

Quarterly Status Report No. 7

For the Period

1 March to 31 May 1990

Under Air Force Contract No. F19628-88-C-0173

Prepared by:

L.G. Piper and W.T. Rawlins

Physical Sciences Inc.
20 New England Business Center
Andover, MA 01810

Sponsored by:

Air Force Geophysics Laboratory
Air Force Systems Command
U.S. Air Force
Hanscom Air Force Base, MA 01731

September 1990

THIS PAGE INTENTIONALLY LEFT BLANK

Previously, values for the ratio A_{00}/A_{01} for the $O_2(a^1\Delta_g \rightarrow X^3\Sigma_g^-)$ transition have been reported to be either about 80 or about 50. Both laboratory and aeronomic determinations fall into each group. We have re-examined this Einstein coefficient ratio both in the laboratory and from data taken on a recent orbital mission. Our laboratory measurements involve scanning the spectrum of an afterglow of an oxygen discharge between 1000 and 1600 nm. We calibrated the relative spectral response of our detection system by scanning the spectral output of the three different standard radiation sources, obtaining good agreement from all three. Our laboratory measurements give a ratio of 85 ± 8 . Since the accepted value for A_{00} is $2.6 \times 10^{-4} \text{ s}^{-1}$, A_{01} will be $3.0 \times 10^{-6} \text{ s}^{-1}$. Analysis of the field data requires correcting each spectral scan for differences in altitude, in some instances near dawn and dusk for differences in local time, as well as for spectral overlap from neighboring hydroxyl emissions.

The following viewgraphs were presented at the 1990 Spring Meeting of the American Geophysical Union in Baltimore.

**Explanatory Text Accompanying
"The Ratio A00/A01 for the Infrared Atmospheric Bands of Molecular Oxygen"
by Lawrence G. Piper**

1. Title viewgraph including acknowledgment of sponsoring agencies.
2. Why is $O_2(a)$ important? It is a major species involved in upper atmospheric photochemistry. In the day glow, $[O_2(a)]$ tracks $[O_3]$ while in the nightglow it tracks $[O]$. One can use ground-based observations of $O_2(a)$ profiles to deduce the profiles of O_3 and O .
3. The problem we are addressing is that emission in the 0,0 band at 1269 nm is absorbed by the O_2 in the earth's atmosphere. From the ground, therefore, one must monitor the 0,1 band at 1581 nm. In order to analyze one's data, one must have an accurate value for the ratio of Einstein coefficients of the 0,0 to 0,1 bands. Previous values of this Einstein coefficient are in conflict. Several groups reported a value of about 50 while others have suggested that the ratio is about 80. Theoretical considerations based upon Franck-Condon factors suggest that the ratio might be as high as 146.
- 4.,5. Our experiments were performed in a discharge-flow apparatus in which about 4 Torr of O_2 was discharged in a side arm and then flowed into the observation tube. The emission from the flow tube was monitored with a 0.5m monochromator employing a 300 l mm^{-1} grating blazed at 1000 nm and a LN_2 -cooled intrinsic Ge detector. The relative response of the detection system was calibrated with quartz-halogen lamps and a 1250 K black body source.
6. The data were analyzed using the equation on this viewgraph. Since the emission features at 1269 and 1581 nm have the same upper level, the ratio of emission intensities of the two features gives the Einstein-coefficient ratio directly.

7. This viewgraph shows a typical spectrum of emission from the flow reactor. Note that the vertical sensitivity has increased by a factor of 33 at 1320 nm.
8. We took 13 spectra between 1200 and 1600 nm under varying conditions. The emission features at 1269 and 1581 nm were integrated numerically. The experimental ratio derived from the measurements is 52 ± 6 , where the uncertainty is an r.m.s. average of the statistical uncertainty ($2\sigma = 10$ percent) and the estimated uncertainty in the instrument calibration (5 percent).
9. We also looked at a number of earth-limb scans taken by a satellite in mid-latitude orbit. The satellite used a LN_2 -cooled CVP spectrometer to scan the wavelength region between 0.7 and $5.0 \mu\text{m}$. The data we analyzed were taken just after noon, local time, and at dusk, just before sunset local time.
10. This shows a typical spectral scan. The two emission features at 1269 and 1581 were readily apparent, rising above the baseline which is Rayleigh-scattered sunlight. We have overlaid scans taken above and below the O_2^* layer to show how the baseline can be subtracted readily from the data.
- 11.,12. This shows how the ratio of the band intensities varied with local time for upleg and downleg traversals of the earth's limb. The upleg data are significantly higher than the data taken on the downleg. This is most likely because of the detector's slow recovery from saturation after the instrument had been looking at the hard earth. Averages of the downleg data gave a result of 41 ± 7 from the noon scans, and 56 ± 8 from the dusk scans. A weighted average of the two sets of data results in a ratio of 50 ± 11 from the field measurements, in good agreement with the laboratory data.

13. This table compares our results with those of previous workers. Our data from both the laboratory and field measurements shows that the previous reports of a ratio around 50 are correct, while those around 80 are erroneous for some reason.
14. In conclusion, our data show that the ratio of the Einstein coefficients of the 0,0 to 0,1 bands of the infrared atmospheric bands of O_2 is 52 ± 6 . Given that the accepted value of the Einstein coefficient for the 0,0 band is $2.6 (\pm 15 \text{ percent}) \times 10^{-4} \text{ s}^{-1}$, we calculate that the 0,1 Einstein coefficient is $5.0 (\pm 19 \text{ percent}) \times 10^{-6} \text{ s}^{-1}$. If we assume that the transition moment function is linear, we can determine the parameters of the function from the Einstein coefficient ratio and the absolute value of the Einstein coefficient for the 0,0 band. For a linear function, the transition moment function in units of Debye is either $6.28 \times 10^{-5} - 8.56 \times 10^{-4} r(v'v'')$ or else $4.50 \times 10^{-4} - 3.34 \times 10^{-4} r(v'v'')$.

THE RATIO A_{00}/A_{01} FOR THE INFRARED ATMOSPHERIC BANDS OF MOLECULAR OXYGEN*

**Lawrence G. Piper
Physical Sciences Inc.
20 New England Business Center
Andover, MA 01810**

20 April 1990

***Sponsored by Air Force Office of Scientific Research
and the Defense Nuclear Agency**

IMPORTANCE OF $O_2(a^1\Delta_g)$

VG90-301

- $O_2(a^1\Delta_g)$ a major species in upper atmospheric photochemistry
 - Day glow: $[O_2(a)]$ tracks $[O_3]$
 - Night glow: $[O_2(a)]$ tracks $[O(^3P)]$
- Ground-based observations of $O_2(a)$ coupled with photochemical model can give $[O_3]$ and $[O]$ profiles

PROBLEM STATEMENT

VG90-301

- 1269 nm radiation, $O_2(a^1\Delta_g, v'=0-X^3\Sigma_g^-, v''=0)$, absorbed by earth's atmosphere
- 1581 nm radiation, $O_2(a^1\Delta_g, v'=0-X^3\Sigma_g^-, v''=0)$, optically thin
- Therefore, ground-based measurements of $O_2(a)$ profiles require observations at 1581 nm and an accurate ratio A_{00}/A_{01}
- Previous reports of A_{00}/A_{01} in conflict
 - Two laboratory measurements and one estimate from photochemical model: $A_{00}/A_{01} \approx 50$
 - One laboratory/one field measurement: $A_{00}/A_{01} \approx 80$
 - Franck-Condon factor prediction: $A_{00}/A_{01} \approx 146$

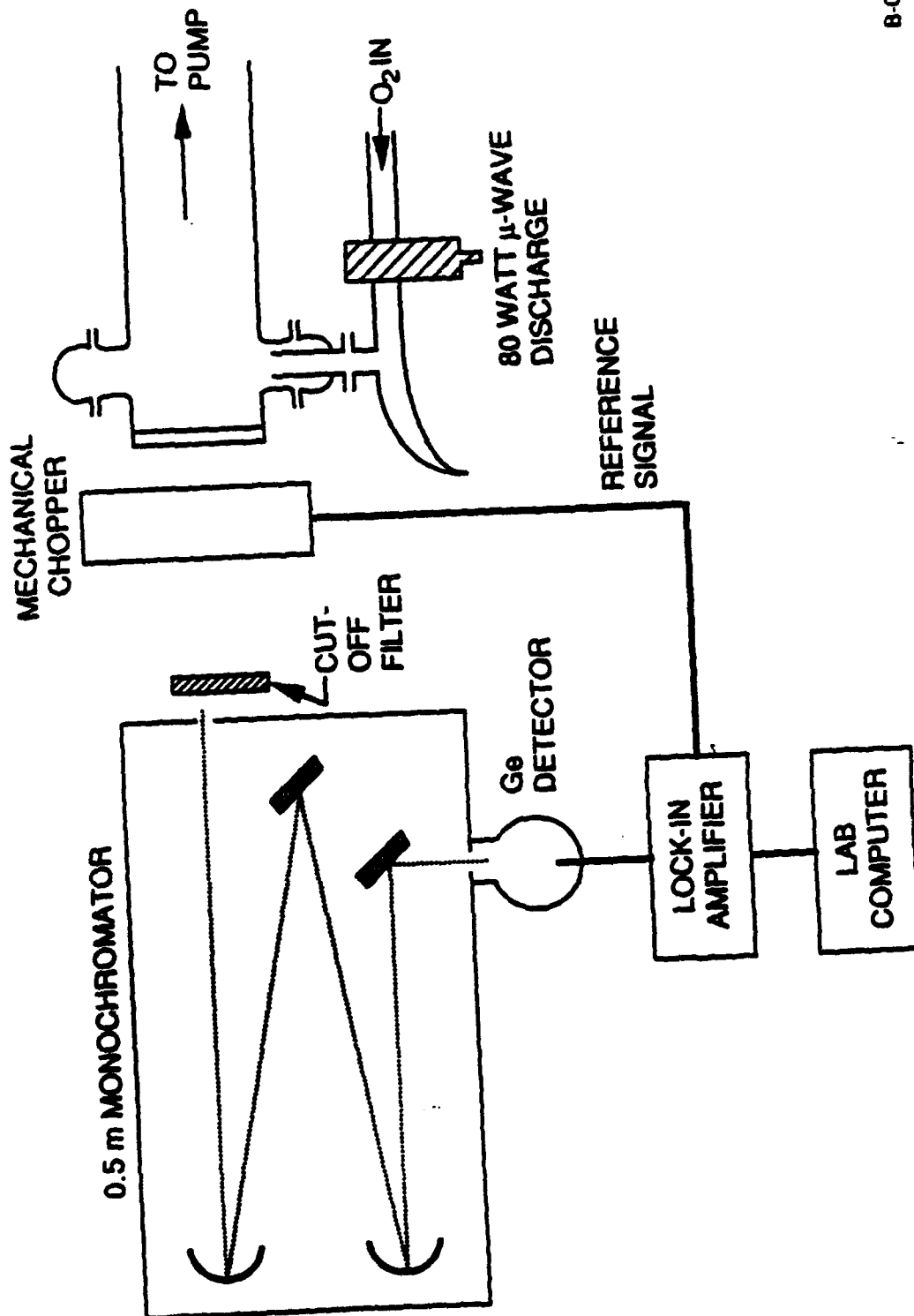
EXPERIMENTAL CONDITIONS

VG90-301

- Discharge-flow reactor
 - 3.8 Torr pure O₂
- 0.5m monochromator
 - 300 ℓ mm⁻¹ grating with 1000 nm blaze
 - ℓ N₂ cooled intrinsic Ge detector
- Relative spectral response from quartz-halogen lamp and 1200 K black body cavity

SCHEMATIC OF DISCHARGE-FLOW APPARATUS FOR GENERATING $O_2(a^1\Delta_g)$

VG90-301



B-0144a

ANALYSIS OF LABORATORY DATA

VG90-301

- Intensity of emission band

$$I_{v'v''} = N_{v'} A_{v'v''} = \frac{64\pi^4}{3h} N_{v'} q_{v'v''}^3 R_e^2(\bar{r}_{v'v''})$$

$N_{v'}$ = number density of emitters

$A_{v'v''}$ = Einstein coefficient for spontaneous radiation

$q_{v'v''}$ = Franck-Condon factor

$\nu_{v'v''}$ = transition frequency in cm

R_e = electronic transition moment

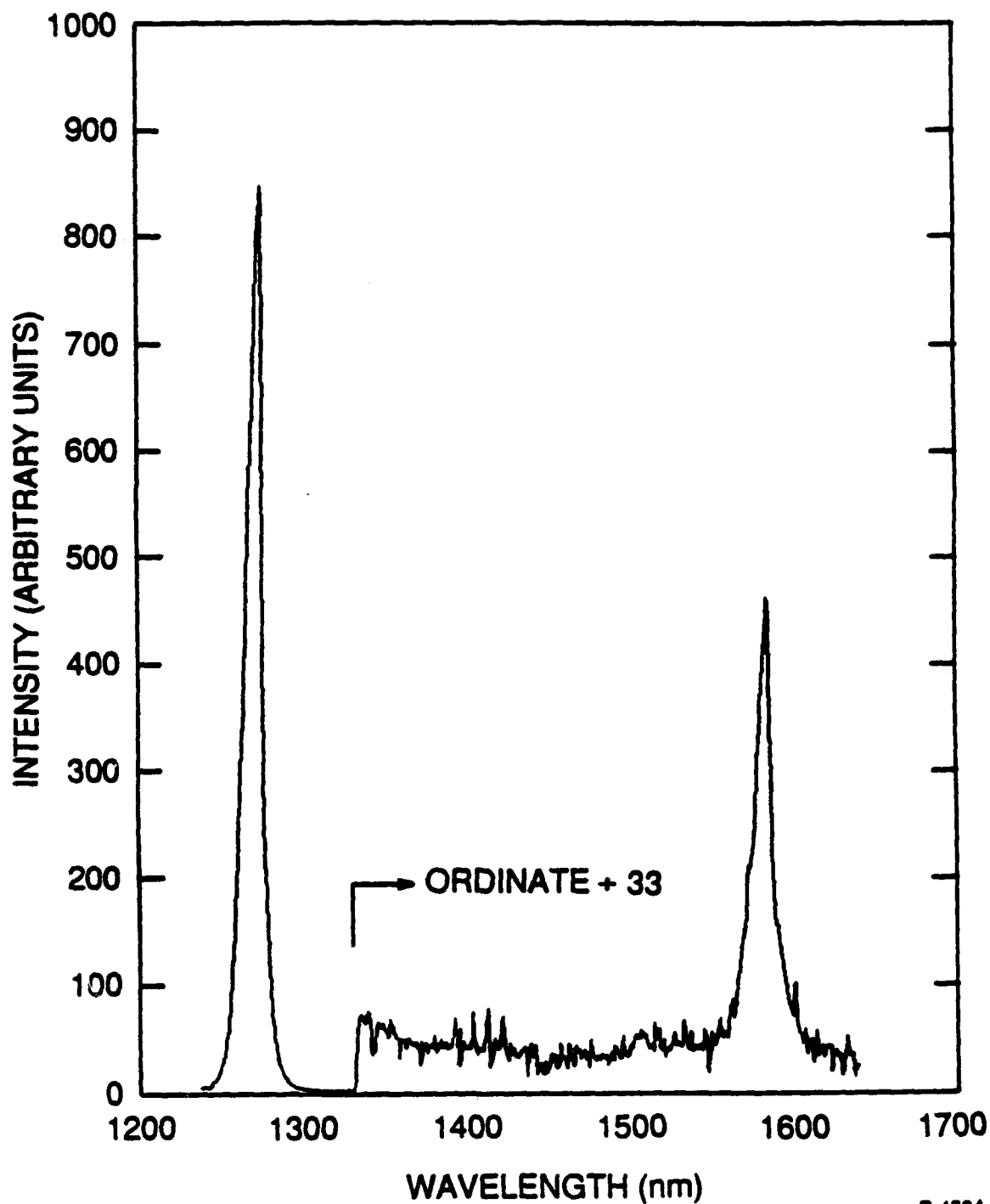
$r_{v'v''}$ = r-centroid for transition

Transitions from common upper level v' to lower levels v'' and v''' :

$$\frac{I_{v'v''}}{I_{v'v'''}} = \frac{A_{v'v''}}{A_{v'v'''}} = \frac{q_{v'v''}^3 R_e^2(\bar{r}_{v'v''})}{q_{v'v'''}^3 R_e^2(\bar{r}_{v'v'''})}$$

OXYGEN AFTERGLOW SPECTRUM

VG90-301



B-4504

RESULTS OF LABORATORY MEASUREMENTS

VG90-301

- Thirteen scans between 1200 and 1600 nm
- Spectral resolution varied between 4 and 8 nm
- Numerical integration of bands at 1269 and 1581 nm
 $A_{00}/A_{01} = 52 \pm 6$
- Uncertainty is r.m.s. of
 - $\pm 2\sigma$ for reproducibility
 - ± 5 percent for calibration uncertainty

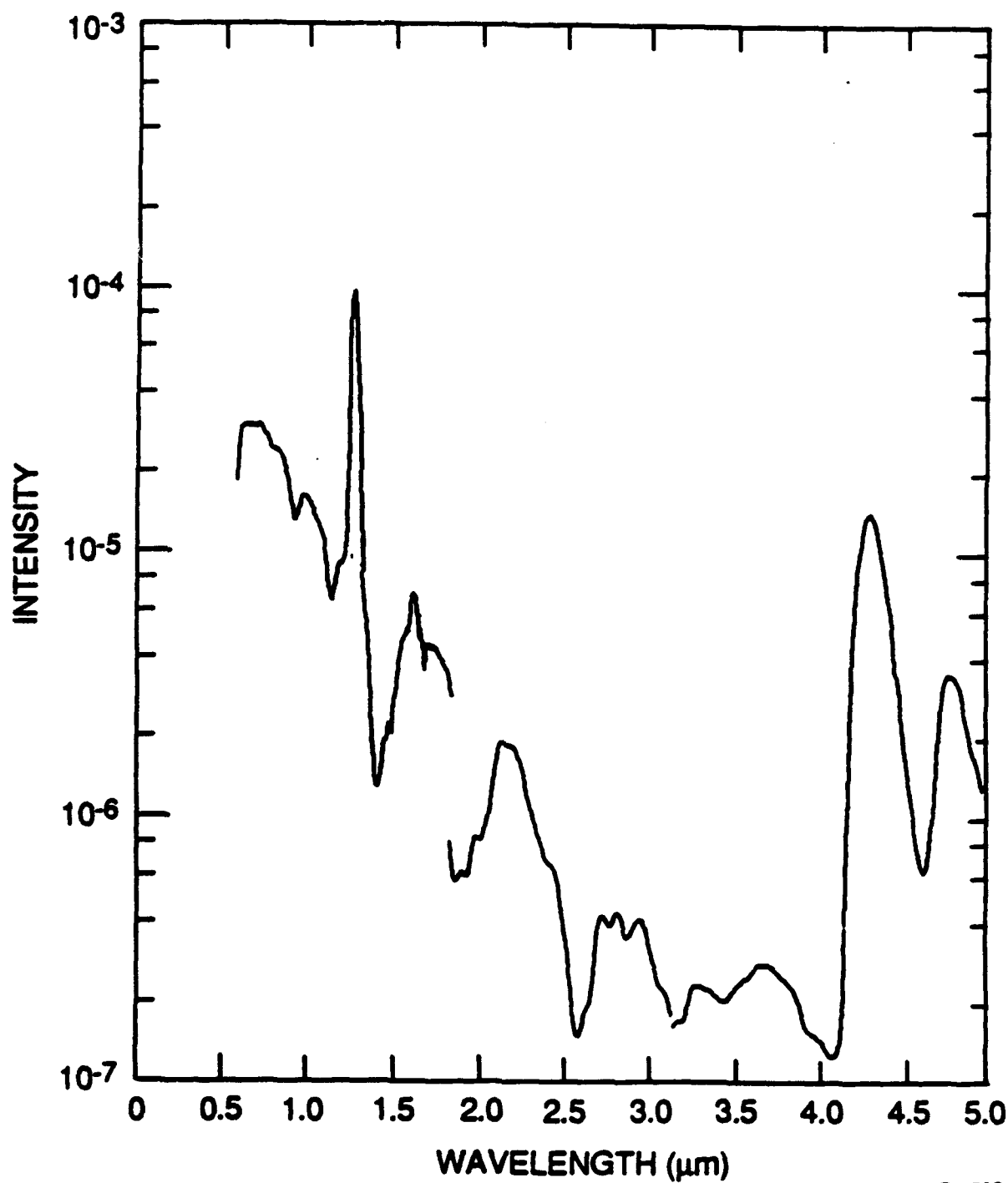
FIELD MEASUREMENTS

VG90-301

- Earth limb scans from satellite
 - Noon scans: 4 measurements on upleg scans
7 measurements on downleg scans
 - Dusk scans: 7 measurements on upleg scans
11 measurements on downleg scans
- Mid-latitude orbit
- N_2 -cooled CWF spectrometer
 - Spectral coverage: 0.7 to 5.0 μm
 - Resolution: 2.5 to 3 percent of wavelength

**EARTH-LIMB SCAN NEAR NOON
LOCAL TIME AT A TANGENT
HEIGHT OF ABOUT 65 km**

VG90-301



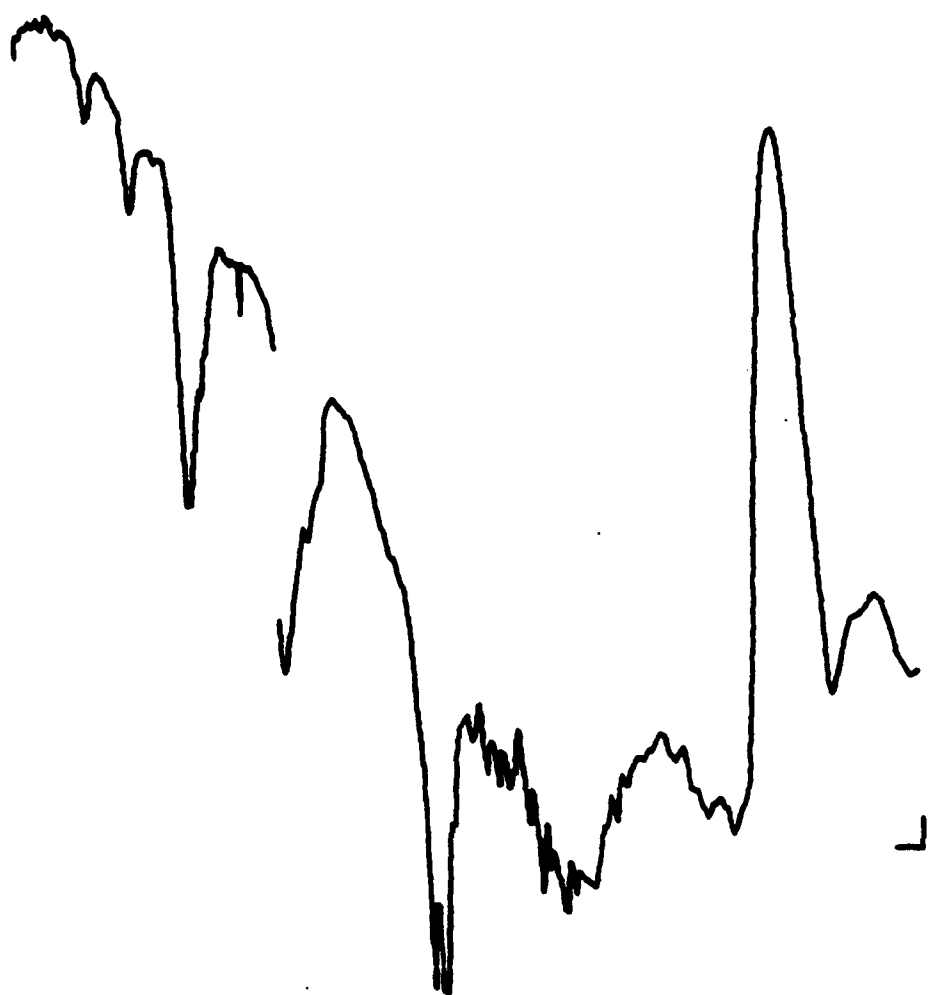
B-4502

L

L

L

L



Overlay B

┐

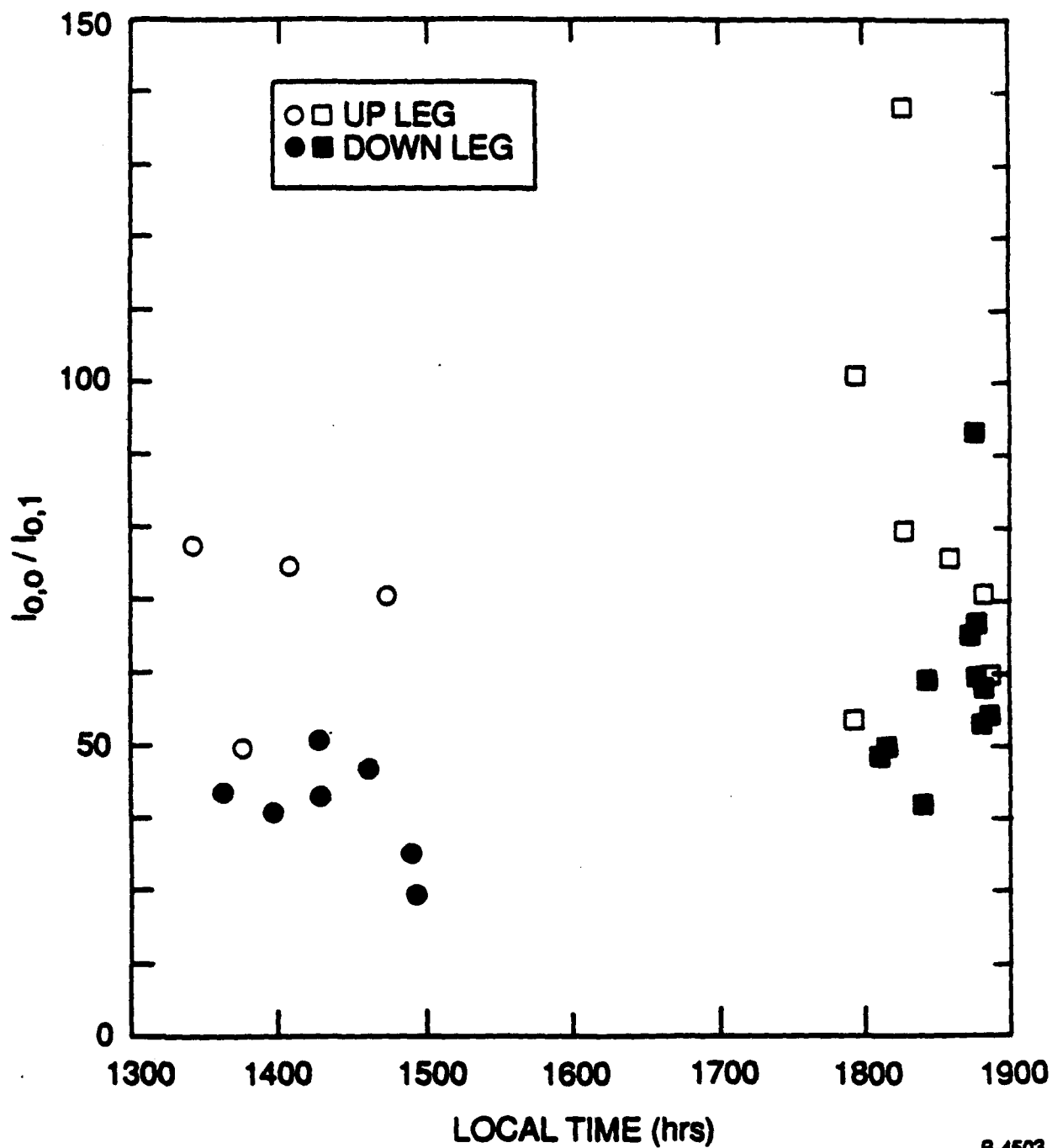
┐

┐

┐

VARIATIONS IN THE RATIO $I_{0,0}/I_{0,1}$ WITH CHANGES IN LOCAL TIME FOR UPLEG SCANS AND DOWNLEG SCANS

VG90-301



B-4503

RESULTS OF FIELD MEASUREMENTS

VG80-301

- Upleg results skewed by detector saturation when looking at hard earth
- Downleg results
 - Noon: $A_{00}/A_{01} = 41 \pm 7$
 - Dusk: $A_{00}/A_{01} = 56 \pm 8$
 - Weighted average: $A_{00}/A_{01} = 50 \pm 11$

COMPARISON WITH PREVIOUS DETERMINATIONS

VG90-301

Laboratory Measurements Using Discharge-Flow Reactors

Group	Detector	A_{00}/A_{01}
Haslet and Fehsenfeld (1963)	Calibrated photometers	80 ± 20
Findlay (1969)	Grating monochromator &N ₂ -cooled Ge detector	46.0 ± 0.7
Becker et al. (1971)	CVF spectrometer 196 K PbS detector	49.5 ± 4
Present results (1990)	Grating monochromator &N ₂ -cooled Ge detector	52 ± 6

Field Measurements

Group	Instrument	A_{00}/A_{01}
Pick et al. (1971)	Balloon-borne grating spectrometer; T.E. cooled PbS detector	80 ± 15
Winick et al. (1985)	CVF spectrometer at 1581 nm coupled with photochemical model of O ₃ ; &N ₂ -cooled InSb detector	52 ± 25
Present results (1990)	CVF spectrometer between 700 and 5000 nm; &N ₂ -cooled InSb detector	50 ± 11

CONCLUSIONS

VG90-301

- $A_{00}/A_{01} = 52 \pm 6$
- Since $A_{00} = 2.6 (\pm 15\%) \times 10^{-4} \text{ s}^{-1}$,
 $A_{01} = 5.0 (\pm 19\%) \times 10^{-6} \text{ s}^{-1}$
- Assuming linear transition-moment function
 $R_e(r) \text{ (in Debye)} = 6.28 \times 10^{-5} - 8.56 \times 10^{-5} \bar{r}_{VV''}$
or
 $4.50 \times 10^{-4} - 3.34 \times 10^{-4} \bar{r}_{VV''}$

APPENDIX E

The Stability of $N_2(A'^5\Sigma_g^+)$

W.J. Marinelli
W.J. Kessler
A.M. Woodward
W.T. Rawlins

J. Chem. Phys. 92, 1796 (1990)

(SR-429 reproduced in its entirety)

THIS PAGE INTENTIONALLY LEFT BLANK

Reprinted from

THE JOURNAL OF CHEMICAL PHYSICS

VOLUME 92

NUMBER 3

1 FEBRUARY 1990

The stability of $N_2(A'^5\Sigma_g^+)$

W. J. Marinelli, W. J. Kessler, A. M. Woodward, and W. T. Rawlins
Physical Sciences Inc., 20 New England Business Center, Andover, Massachusetts 01810

pp. 1796-1803

Published by the

AMERICAN INSTITUTE OF PHYSICS

THIS PAGE INTENTIONALLY LEFT BLANK

The stability of $N_2(A'^3\Sigma_g^+)$

W. J. Marinelli, W. J. Kessler, A. M. Woodward, and W. T. Rawlins
Physical Sciences Inc., 20 New England Business Center, Andover, Massachusetts 01810

(Received 4 August 1989; accepted 26 September 1989)

The energy and stability of the "high spin" $^3\Sigma_g^+$ and $^3\Sigma_g^-$ states of N_2 have been the subject of many theoretical efforts. These states play an important role in N-atom recombination. The collisional coupling of these states to other excited electronic states strongly influences the electronic emission spectrum of N_2 observed in atom recombination. Since these states are not dipole coupled to lower excited electronic states of N_2 , they are considered metastable and are possible candidates for high energy density storage media. We have examined the stability of $N_2(^3\Sigma_g^+)$ state in a discharge flow reactor. The $^3\Sigma_g^+$ state is produced from the $N_2(A'^3\Sigma_g^+)$ energy pooling reaction and probed via laser-induced fluorescence on the $C''^3\Pi_g-A'^3\Sigma_g^+$ transition. While no laser-induced fluorescence from excitation of the A' state is observed, comparison of signal levels with laser-induced fluorescence on the $B^3\Pi_g-A'^3\Sigma_g^+$ transition enables us to establish an upper limit on the gas phase lifetime of this state at pressures of a few Torr. Experimental evidence is presented which suggests that the primary mode of A' -state quenching is through collisional coupling to the $B^3\Pi_g$ state. However, other matrix isolation experiments suggest that the A' state may be stabilized in cryogenic rare gas matrices.

INTRODUCTION

Experimental investigations of "active" nitrogen have long postulated the existence of a high-energy metastable electronic state of N_2 responsible for the excitation of many species. Various reports indicate the state has a low heterogeneous deactivation probability on glass and metal surfaces and lives for several milliseconds in the gas phase. Matrix isolation studies have shown that chemiluminescence from "active" nitrogen trapped at 10 to 35 K may radiate for many seconds.¹ The existence of such a long-lived metastable state would have important consequences for our understanding of upper atmospheric chemistry, chemical lasers, energy storage and high voltage switching.

Recently, several theoretical efforts have focused on the stability of the high spin $^3\Sigma_g^+$ and $^3\Sigma_g^-$ electronic states of N_2 . These states arise from the pairing of two $N(^4S)$ atoms to form an N_2 molecule in which all or all but two of the electron spins remain unpaired in the resulting molecular orbitals. These states are characterized by the formation of a weakly bound (several cm^{-1}) van der Waals minimum at long r_e and a somewhat more strongly covalently bound minimum at shorter r_e . Since these configurations are the lowest energy of each of the spin multiplicities, they should be stable with respect to decay via dipole radiation and perhaps metastable with respect to collisional deactivation. However, collisional coupling between the $^3\Sigma_g^+$ and $B^3\Pi_g$ states was postulated by Kistiakowsky and co-workers² as a key step in the mechanism for three-body recombination of atomic nitrogen.

Early calculations on the stability of the $^3\Sigma$ state were conducted by Vanderslice, Mason, and Lippincott³ and were refined by Meador.⁴ These investigators obtained 13.4 and 14.7 cm^{-1} , respectively, for the depth of the covalent well. Subsequent calculations by Ferrante and Stwalley⁵ and Capitelli and co-workers⁶ obtained well depths of 43 and 188

cm^{-1} , respectively. Recently, Partridge, Langhoff, and Bauschlicher⁷ performed SD-CI *ab initio* calculations and obtained a well depth of 21 cm^{-1} . Though this well depth is large enough to support a stable molecule at cryogenic temperatures, spin-orbit and spin-spin interactions may quickly cause this state to couple to other electronic states of N_2 .

The potential of the $^3\Sigma_g^+$ state was initially investigated by Mulliken,⁸ who predicted a covalent well depth of $\sim 2300 \text{ cm}^{-1}$. Subsequent calculations by Krauss and Neumann⁹ predicted a shallower potential with a well depth much closer to 850 cm^{-1} . Siegbahn¹⁰ calculated that D_e was approximately 1450 cm^{-1} . Experimental evidence for the existence of a stable $^3\Sigma$ state is limited to the effects it may have on the predissociation of the $B^3\Pi_g$ and $a'^1\Pi_g$ states. The proposition advanced by Berkowitz *et al.*,² that the $^3\Sigma$ state is responsible for these predissociations, is bolstered by the evidence of Carroll,¹¹ who derived a well depth of 850 cm^{-1} from predissociation and airglow data.

Recently, Partridge and co-workers¹² performed complete active space self-consistent field (CASSCF/MRCI) *ab initio* calculations on the $^3\Sigma_g^+$ and $^3\Pi_g$ states of N_2 . Their calculations for the $^3\Sigma$ state (designated A') revealed a covalent well depth of approximately 3450 cm^{-1} and a van der Waals minimum with a binding energy of 47 cm^{-1} . A barrier of approximately 500 cm^{-1} with respect to dissociation to form two $N(^4S)$ atoms further enhances the stability of the covalently bound state. Recombining $N(^4S)$ atoms, a primary mechanism for formation of the A' state, must traverse this barrier to enter the covalently bonded well. The potential supports seven bound vibrational levels with a spacing of approximately 630 cm^{-1} . The potential for the $^3\Pi_g$ state (designated C'') was also found to be more deeply bound than previously estimated. The C'' state well depth is calculated to be 10 505 cm^{-1} with a vibrational spacing of approximately 925 cm^{-1} . A potential energy diagram of these states is shown schematically in Fig. 1.

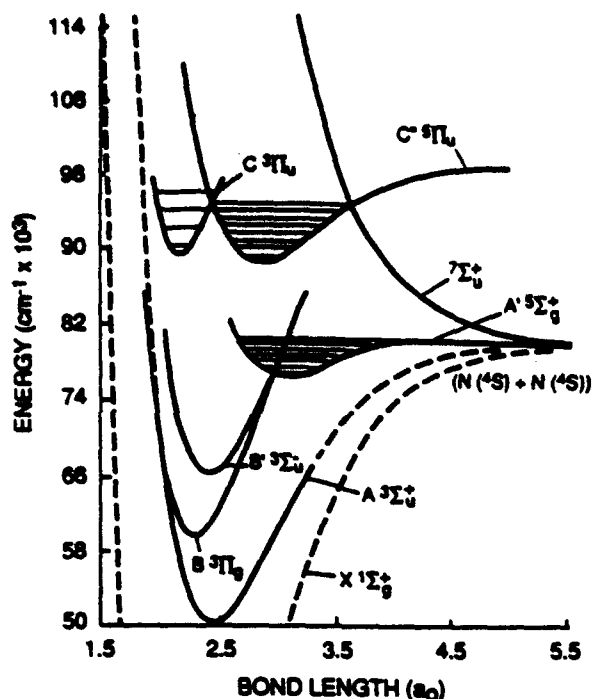


FIG. 1. Potential energy diagram for the excited quintet and triplet states of N_2 (from Ref. 12). The vibrational levels of the $C^3\Pi_u$ and $A'^3\Sigma_u^+$ states are indicated.

Perhaps the most important result from the Partridge study was the assignment of the previously unassigned Herman infrared (HIR) band system of N_2 to the $C^3\Pi_u - A'^3\Sigma_u^+$ transition. This assignment was subsequently confirmed by Fourier-transform infrared (FTIR) studies of Huber and Vervloet.¹³ The HIR bands are observed in the 650 to 900 nm region as a result of an energy pooling reaction between two $N_2(A'^3\Sigma_u^+)$ molecules.¹⁴⁻¹⁶ Emission from the $C^3\Pi_u$ and $B^3\Pi_u$ states is also observed from the energy pooling process. The calculated radiative lifetime of the $C^3\Pi_u$ state is 4.3 μs ,¹² similar to the $B^3\Pi_u - A'^3\Sigma_u^+$ first-positive bands.¹⁷ The calculated lifetime is in conflict with experimental observations¹⁴ that the ratio of $C^3\Pi_u/C$ state emission intensities is unchanged over a pressure range of a few Torr. This would place the lifetime of the $C^3\Pi_u$ state nearer the 37 ns lifetime of the C state and raises the possibility that the $C^3\Pi_u$ state derives its lifetime from collisional coupling to the C state.

The assignment of the N_2 HIR bands to the $C^3\Pi_u - A'^3\Sigma_u^+$ transition coupled with the 3450 cm^{-1} well depth establishes a means of production and indirect evidence for the stability of the A' state. The 9.45 eV electronic term energy of the A' state is more than sufficient to excite many of the states observed in "active" nitrogen. However, the magnitude of the intersystem collisional transfer processes and nonradiative spin-orbit and spin-spin couplings to other electronic states in the N_2 manifold, which decrease the A' state lifetime, have not been addressed. The experiments reported in this paper employ a discharge-flow laser induced fluorescence technique to quantitatively explore the stability of the A' state in the gas phase. Under conditions

where the production rate of $N_2(A')$ can be rigorously quantified, we are unable to detect its presence even with reasonably sensitive detection limits. This places an upper bound on the collisional lifetime of $N_2(A')$ in our apparatus, and has implications for the rate of collisional coupling of $N_2(A')$ with neighboring states of N_2 .

EXPERIMENTAL

Our approach to determining the collisional stability of the $A'^3\Sigma_u^+$ state of N_2 was as follows: We employed energy pooling of two $N_2(A'^3\Sigma_u^+)$ molecules to produce the $C^3\Pi_u$ state. Radiative cascade through the $C^3\Pi_u - A'$ HIR bands results in production of the A' state. The production rate can be determined absolutely via quantitative observation of the HIR band emission intensity. Laser-induced fluorescence (LIF) on the $C^3\Pi_u - A'$ transition is employed to probe for the presence of the A' state. Calibration of the LIF detection system is accomplished approximately by comparison with LIF signals from the nearby $B^3\Pi_u - A'^3\Sigma_u^+$ transition. The $N_2(A'^3\Sigma_u^+)$ population may be inferred from HIR band emission intensities using the HIR energy pooling rate coefficient or directly using $N_2(A'-X)$ Vegard-Kaplan band emission intensities. A simple kinetic model, tied to absolute population measurements, is used to predict the A' state population. The HIR band LIF intensities were compared with intensities predicted by the calibrated computer model. The gas phase $N_2(A')$ lifetime required to explain the observed signal level was then determined from the model. The experiment is described in more detail below.

The discharge flow apparatus is shown schematically in Fig. 2. The apparatus consists of an $N_2(A'^3\Sigma_u^+)$ generator, a short flow section, diagnostics section, and pumping facility. The flow section was provided to allow the $N_2(A')$ to build to maximum concentration, to reduce scattered light from the discharge, and to add various reagents. The diagnostics section provided for observation of passive emission and LIF at the same point in the flow reactor. Passive emission was detected using a 0.35 m monochromator (McPherson 270) equipped with a cooled GaAs PMT (HTV R943-02) operat-

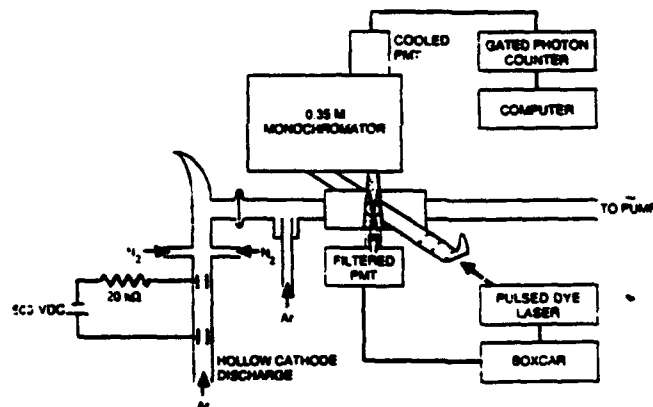


FIG. 2. Schematic diagram of the discharge flow reactor and LIF detection system used in the experiments.

ed in photon counting mode. A rate meter on the photon counter (Pacific Photometrics) was interfaced to a laboratory computer for signal acquisition. The absolute sensitivity of the detection system was calibrated using the well known O/NO air afterglow in the 400 to 900 nm region.^{16,18} The absolute calibration was extended to 200 nm by comparison with deuterium and quartz halogen irradiation standards.

A Nd:YAG pumped tunable dye laser (Quantel YG581C/TDL50) operating with LDS 698 dye was used to excite fluorescence from the $N_2(A')$ state and A state in the diagnostics section. The section is internally blackened with a Teflon coating and equipped with long baffle arms to reduce scattered light. The LIF is detected with a baffled and filtered PMT (HTV R955). An $f/2$ lens was used to image fluorescence onto the PMT photocathode. The combination of a Schott RG-9 color filter and 750 nm long-pass interference filter, along with the PMT long-wavelength cutoff, limited the wavelength range of the detection system to 750 to 900 nm. Approximately 50% of the emission from $N_2(B, v=3)$ and $N_2(C'', v=2)$, the levels pumped in the LIF detection experiments, occurs in this wavelength region. Signals from the PMT were fed to a high-speed current amplifier (Ithaco 1211) and then to a boxcar signal averager. The LIF signals were recorded with a laboratory computer and corrected for variations in laser intensity.

The $N_2(A'^3\Sigma_g^-)$ used in this study was produced by energy transfer from metastable $Ar(^3P_{0,2})$ to N_2 . This technique has been described extensively in the literature.^{16,19,20} The metastable Ar was produced by passing Ar through a low power DC discharge (500 VDC, 2 mA) at a flow rate of approximately $4000 \mu\text{mol s}^{-1}$. Small flows of N_2 (10 to $250 \mu\text{mol s}^{-1}$) were added downstream of the discharge. In some experiments a 5% Ar in He mixture was passed through the discharge in order to use He as the buffer gas. A small flow of O_2 could be injected downstream of the $N_2(A'^3\Sigma_g^-)$ generator in order to quench the $N_2(A')$. This was done occasionally in order to eliminate all chemiluminescence and check for the presence of scattered light from the discharge. In all cases flows were measured using calibrated mass flow meters. Cell pressures were measured using a calibrated capacitance manometer. All reagent gases were ultra-high purity (UHP) (99.999%) and were used without further purification. The flow reactor was pumped by two 17 cfm and one 27 cfm mechanical vacuum pumps connected in a parallel manifold. In this configuration flow velocities in excess of 3700 cm s^{-1} at pressures of 2 Torr were attainable.

RESULTS

Initial experiments were conducted using Ar as a buffer gas at pressures of approximately 4 Torr. Observation of N_2 HIR emission showed that the intensity was maximized under these conditions at N_2 mole fractions of approximately 0.05. An emission spectrum of the region from 610 to 820 nm, recorded at a point 5 ms downstream of the $N_2(A')$ generator, is shown in Fig. 3. The spectrum includes the data and a fit to the data indicating the presence of both the $N_2(C''-A')$ HIR bands and the $N_2(B-A)$ first positive bands. The transition probabilities calculated by Partridge *et al.*¹²

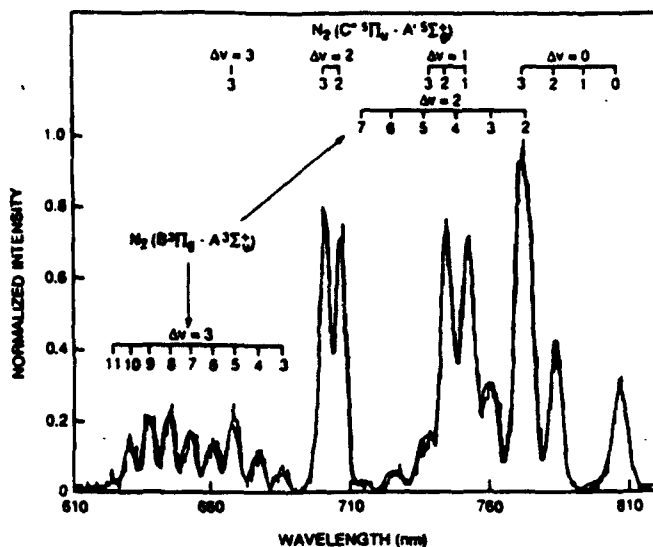
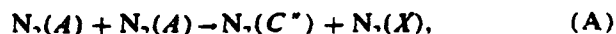


FIG. 3. Visible emission spectrum of N_2 resulting from the $N_2(A')$ energy pooling reaction in Ar. The important $C''-A'$ and $B-A$ transitions are indicated. Heavy line is fit and light line is data.

were used in calculating the fitted spectrum. It is evident that these parameters do quite a good job of reproducing the experimental spectrum. The spectrum of the $C''-A'$ transition is dominated by emission from vibrational levels 2 and 3. Previous studies by Piper¹⁶ showed that these levels are produced nearly exclusively by the energy pooling reactions involving combinations of $N_2(A, v=0)$ and $N_2(A, v=1)$.

A lower limit on the $N_2(A')$ production rate is given by the $C''-A'$ emission intensity. This emission intensity can also be used to determine the $N_2(A)$ concentration at that point in the flow reactor. The total $N_2(A')$ concentration at any point in the flow reactor is the integral of $N_2(A')$ production and loss processes from the $N_2(A)$ generator to that location. Initially, we assume that only quenching at the walls of the flow reactor is responsible for the loss of $N_2(A')$. The production and loss of $N_2(A)$ and $N_2(A')$ can be described approximately by the set of reactions:



We have neglected quenching of $N_2(C'')$ based on experimental observations that it is insignificant at our operating pressures.^{14,16} Other collisional and noncollisional pathways for deactivation of $N_2(A')$ can be described by inclusion of an additional pseudofirst-order loss term:



The radiative rate of the C'' state is sufficiently large so that the C'' -state concentration is considered to be in steady state in the field of view of the detection system. Hence, the rate of reaction (A) can be set equal to the rate of reaction (D):

$$k_A [N_2(A)]^2 = k_4 [N_2(C'')] = I_{\text{HIR}} \quad (1)$$

where I_{HIR} is simply the total Herman-infrared band volume emission rate. Thus, the $N_2(A)$ concentration may be determined from the HIR band absolute emission rate,

$$[N_2(A)] = \{I_{\text{HIR}}/k_A\}^{1/2} \quad (2)$$

The energy pooling rate coefficients for the formation of the $N_2(C'')$ state have been measured by Piper.¹⁶ The rate coefficients and the vibrational levels of the C'' state that are excited depend on the degree of vibrational excitation present in the $N_2(A)$. Under our experimental conditions the $N_2(A)$ is produced primarily in $v=0$. Hence, we have used Piper's rate coefficient for pooling of two $N_2(A, v=0)$ molecules, $8.1 \pm 2.3 \times 10^{-11} \text{ cm}^3 \text{ molecule}^{-1} \text{ s}^{-1}$, in determining the $N_2(A)$ number density. Thus, under typical experimental conditions the HIR band emission measurement gives an $N_2(A)$ number density of $9 \times 10^9 \text{ molecules cm}^{-3}$ 5 ms downstream of the generator.

This estimate of the $N_2(A)$ number density is confirmed by direct observation of the $N_2(A-X)$ Vegard-Kaplan Bands. Figure 4 shows a spectrum of the region from 200 to 400 nm. The fit to the spectrum clearly identifies features from $N_2(A, v=0,1)$ and $N_2(C, v=0-3)$. The $N_2(C)$ emission is produced from the $N_2(A)$ energy pooling reaction.¹⁶ The emission from the $\text{NO}(A-X)$ transition evident in the spectrum is due to excitation of small amounts of discharge-produced NO by $N_2(A)$.²¹ Also present, but not identified in the spectrum, is emission from the $\text{OH}(A-X)$ transition which is also due to a low-level impurity. The direct determination of $N_2(A)$ concentrations from the $A-X$ band intensities in general indicated $N_2(A)$ concentrations consistent with HIR emission intensity determinations.

The decay of $N_2(A)$ in the flow reactor can be modeled to determine the initial $N_2(A)$ concentration at the exit of the generator. This concentration must be determined in or-

der to calculate the total $N_2(A')$ production up to the observation point. The decay of $N_2(A)$ is given by the expression

$$\frac{d[N_2(A)]}{dt} = -(k_A + k_B)[N_2(A)]^2 - k_C[N_2(A)], \quad (3)$$

where the factor of 2 usually found in the rate expression reflecting the loss of two $N_2(A)$ molecules per pooling event has been excluded. This is done to account for the fact that, under most experimental conditions, one $N_2(A)$ molecule is regenerated from the pooling reaction via radiative cascade through the $C^3\Pi_u$ and $B^3\Pi_g$ states. The rate coefficient for wall loss in a diffusion dominated regime k_1 is given by²²

$$k_C = 3.66 D/a^2, \quad (4)$$

where D is the diffusion coefficient of $N_2(A)$ in the buffer gas and a is the tube radius. The diffusion coefficient can be calculated approximately from kinetic theory²³ to be $160 \text{ cm}^2 \text{ s}^{-1}$ at a pressure of 1 Torr in Ar and scales inversely with pressure. Under our conditions k_C typically has a value of 80 s^{-1} . The value of k_B , the energy pooling rate coefficient for production of all products other than the C'' state, is estimated by Piper¹⁶ to be approximately $3 \times 10^{-10} \text{ cm}^3 \text{ molecule}^{-1} \text{ s}^{-1}$. Thus, it is clear that at these $N_2(A)$ concentrations wall loss is primarily responsible for the loss of $N_2(A)$. Expression (3) can be solved analytically by neglecting pooling or exactly using a simple numerical model to yield the $N_2(A)$ concentration at the generator exit port.

The equation governing the production and loss of $N_2(A')$ is given by

$$\frac{d[N_2(A')]}{dt} = k_D[N_2(C'')] - \{k_E + k_F\}[N_2(A')], \quad (5)$$

where the value of k_E , wall loss rate coefficient for the A' state, is assumed to be the same as for the $N_2(A)$ state and $k_D[N_2(C'')]$ is shown in expression (1) to be the total HIR band emission intensity. By substitution of expression (1) into expression (5) one can relate the expected A' -state concentration to the $N_2(A)$ concentration:

$$\frac{d[N_2(A')]}{dt} = k_A[N_2(A)]^2 - \{k_E + k_F\}[N_2(A')]. \quad (6)$$

Given the initial $N_2(A)$ concentration determined from expression (3), the concentration of $N_2(A')$ can be calculated at any point in the flow reactor using a simple numerical model. It was initially assumed that other loss processes were negligible ($k_F = 0$). The model predicted that $N_2(A')$ concentrations on the order of $4 \times 10^7 \text{ molecules cm}^{-3}$ could be expected in the observation region, 5 ms downstream of the injector. As shown below, this is readily detectable by laser-induced fluorescence in the HIR bands.

Approximate calibration of the LIF detection system was accomplished by observing the LIF produced by pumping the $N_2(B^3\Pi_g - A^3\Sigma_u^+, 3-0)$ band. The origin of the band is at 685.83 nm. This is a spectral region where no absorption is expected from the $N_2(C'' - A')$ transition. A typical spectrum of LIF from the 3-0 band is shown in Fig. 5. The transition is a $^3\Pi(\text{case a}) - ^3\Sigma$ transition with 27 possible branches. Several of the main branches and satellite branches are indicated in the figure. The signal intensity at the P_{11} branch

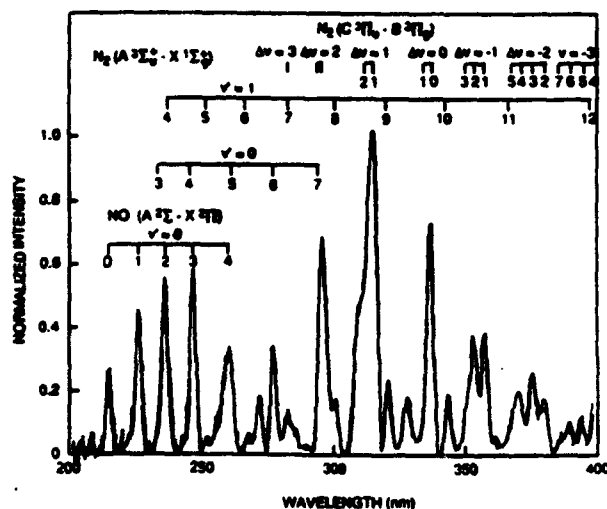


FIG. 4. UV emission spectrum of N_2 from $N_2(A)$ energy pooling. Features of the $A-X$ and $C-X$ transitions are indicated. Also present are features from the $\text{NO}(A-X)$ and $\text{OH}(A-X)$ transitions resulting from the presence of low-level impurities. The heavy line is the fit and the light line is the data.

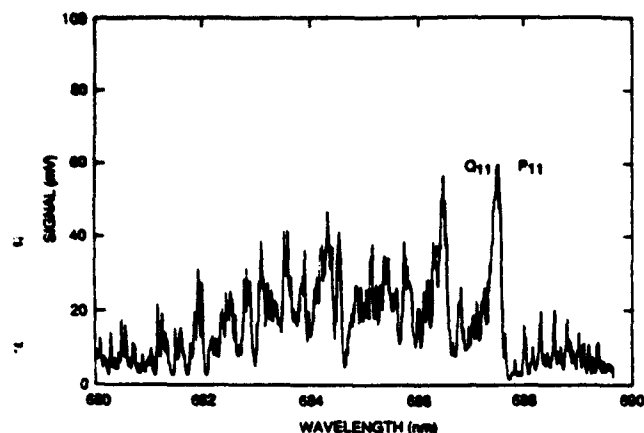


FIG. 5. LIF excitation spectrum of the $B^3\Pi_g-A'^1\Sigma_g^+$ 3,0 band transition observed in the discharge flow reactor. The Q_{11} and P_{11} branch band heads are indicated in the figure.

head was chosen for determining the detection sensitivity. The absolute $N_2(A'^1\Sigma, v=0)$ concentration was determined by the techniques described above.

Several issues must be considered in using this method to determine the sensitivity of the LIF technique for detecting the A' state. The primary issue is the actual oscillator strength of the $C''-A'$ transition relative to the $B-A$ transition. As mentioned in the introduction, the calculated radiative lifetime for the $C''-A'$ transition, 4.3 μ s, conflicts with some of the data on quenching of C'' -state emission. The quenching data suggests that the lifetime of the C'' state is closer to 40 ns. This lifetime would imply a much stronger absorption oscillator strength for the transition. The discrepancy will be addressed further in the discussion session; however, the primary effect of an increased oscillator strength for the $C''-A'$ transition would be a lowering of the detection limit for the A' state by approximately a factor of 100. Thus, observation of $N_2(A')$, coupled with the theoretical radiative lifetime, would give a result which is an upper limit on the A' -state concentration and hence a lower bound on the effective loss rate.

An LIF spectrum of the region from 700 to 710 nm is shown in Fig. 6. The 2-0 and 3-1 bands of the $C''-A'$ transition should be excited in this wavelength region. Though absorption features are observed in this region, they can be assigned to the $N_2(B-A, 8-6)$ transition. This assignment is confirmed by resolving the fluorescence excited by the laser. A typical resolved emission spectrum is shown in Fig. 7. The only discernible emission features are due to transitions originating from $v=8$ and $v=7$ of the B state. Population of $N_2(B, v=7)$ is due to vibrational relaxation of $B, v=8$ by the Ar buffer. Thus, no emission from the $N_2(C''-A')$ system is excited by the laser within the detection limits of the system. The detection sensitivity used in the LIF spectrum of the 700 to 710 nm region is a factor of 1000 better than the sensitivity used in recording the spectrum of the $N_2(B-A, 3-0)$ band. Observation of the poorly populated and weakly absorbing $v=6$ level of the A' state illustrates the detection limits of the system. Comparison of the noise levels

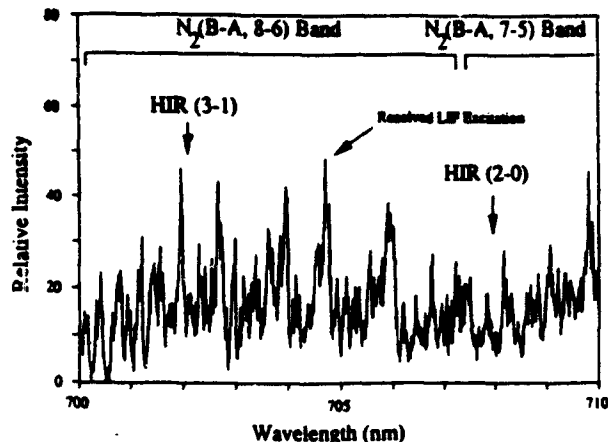


FIG. 6. LIF excitation spectrum for the region from 700 to 710 nm. Features of the $B-A$, 8,6, and 7,5 transition are identified. Arrows show the expected location of the HIR 3,1 and 2,0 bands. The excitation point for the spectrum of Fig. 7 is shown.

observed in this spectrum with the signal levels obtained in the spectrum of Fig. 4, corrected for the differences in the absorption strengths for the $B-A$, 3-0 and $C''-A'$, 2-0 bands, establishes a detection sensitivity for $N_2(A')$ of approximately 1×10^6 molecules cm^{-3} .

The simple numerical model used to predict the expected $N_2(A')$ densities at the observation point in the discharge flow reactor can be used to determine a lower limit on the loss rate (k_r) for $N_2(A')$ consistent with a concentration at our detection limit. The traces in Fig. 8 show the expected temporal profile for $N_2(A')$ when only wall loss (trace a) and a loss rate of 3200 s^{-1} (trace b) is included in the model. When the loss rate of 3200 s^{-1} is incorporated in the model an $N_2(A')$ concentration equivalent to the estimated detection limit is predicted at the detection point. Hence, we can place an upper limit on the A' -state lifetime of approximately 0.3 ms at pressures of approximately 4 Torr of Ar. In our

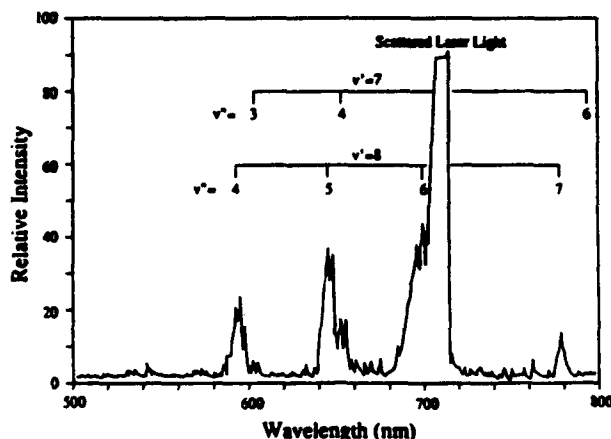


FIG. 7. Resolved LIF spectrum for one of the absorption bands of Fig. 6. The features present can all be identified as originating from the $B-A$ transition. Excitation of the 8,6 band is clearly indicated. Emission from $B, v=7$ is probably due to vibrational relaxation of the B state.

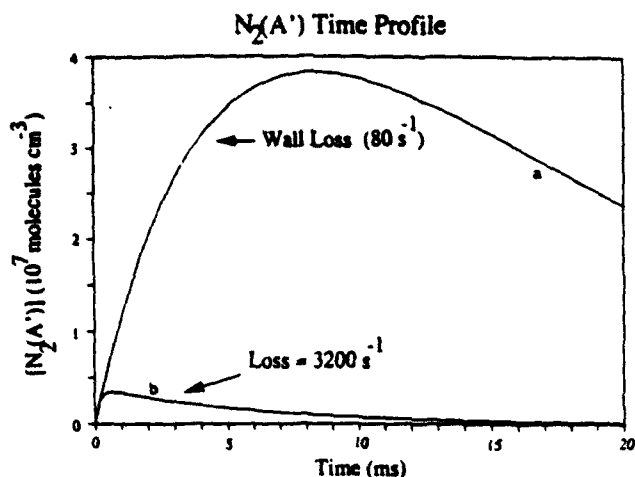


FIG. 8. Model predictions for the temporal evolution of the $N_2(A')$ population in the discharge flow reactor. Trace a shows the behavior expected if wall loss was the only mechanism responsible for quenching of the A' state. Trace b shows the behavior expected for a loss rate of 3200 s^{-1} . This rate produces a concentration of A' at our detection limits.

experiments we explored a range of N_2/Ar mixture ratios (1% to 20% N_2), discharge conditions (300 to 600 VDC), and pressures (2 to 5 Torr). In addition, we passed N_2/Ar and $N_2/\text{Ar}/\text{He}$ mixtures directly through the DC discharge. This method of production enhances the observed $N_2(C''-A')$ emission intensity at the expense of producing N atoms and perhaps other metastable states of N_2 . In addition, He/Ar mixtures were codischarged and N_2 was added downstream. Ratios of He/Ar in excess of 100 were employed in these studies. Under no set of conditions was LIF on the $C''-A'$ transition observed.

DISCUSSION

We have conducted a series of experiments to determine the gas-phase lifetime of the A' state of N_2 . Though the LIF calibration method employed in the study was not precise, the experiments do infer a lifetime for the $^4\Sigma$ state which is much shorter than expected for a spin-forbidden decay process. Our experiments do not provide any direct evidence for any of the possible decay mechanisms. However, some indirect evidence provides support for a collisional decay channel through the $B^3\Pi_g$ state.

An expanded potential energy diagram for the A' state and near isoenergetic levels of the $B^3\Pi_g$ and $A'^4\Sigma_g^+$ states is shown in Fig. 9. The diagram shows that the lowest vibrational level of the A' state is near resonant with $v = 10$ of the $B^3\Pi_g$ state. Also, the barrier to predissociation for the A' state occurs at $v = 13$ of the B state. The latter observation provides evidence for invoking curve crossing to the A' state as the mechanism for predissociation of the B state.² Thus, both collisional and spin-orbit coupling to the B state might be evident in the spectrum of levels 10–12. A recent study of the high-resolution LIF spectrum from the $N_2(B^3\Pi_g-A'^4\Sigma_g^+, 10-6)$ transition revealed no apparent perturbations in the rotational levels of the B state.²⁴ In addition, no other studies have reported any perturbations in the

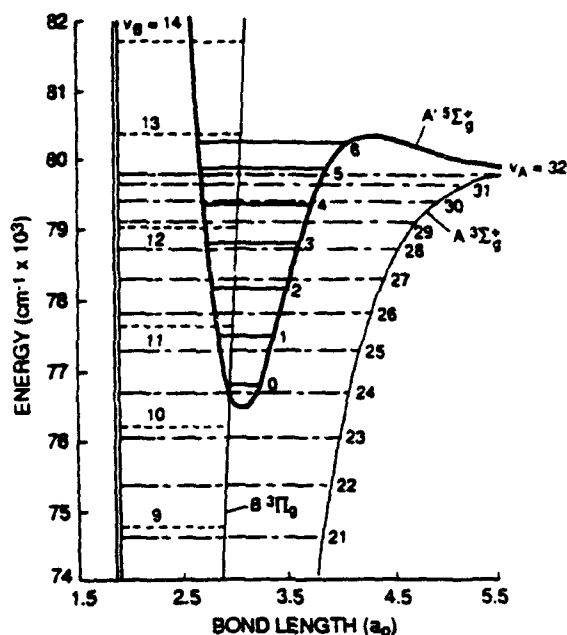


FIG. 9. Expanded energy level diagram of the A' state redrawn from the results of Partridge *et al.* (Ref. 12). The figure illustrates the potential for coupling of the A' and B states.

spectra of levels 10–12.²⁵ Thus, there appears to be no direct evidence from the spectroscopy of the B state to indicate spin-orbit coupling to the A' state.

Possible evidence for collisional coupling of the B state to the A' state comes from measurements of the energy pooling rate coefficient to form the B state. If the energy pooling reaction is studied using an Ar buffer gas, much of the information on the distribution of vibrational levels populated in the B state is washed-out by rapid vibrational relaxation. If He is employed as a buffer gas, vibrational relaxation is less efficient, and much of the nascent vibrational distribution is preserved in the emission spectrum. A typical spectrum of emission from the energy pooling reaction from 560 to 720 nm using He as a buffer gas is shown in Fig. 10. In contrast to the spectrum of Fig. 3, a strong enhancement in the population of $v = 10$ of the B state is observed. This enhancement has been previously observed.²⁶ Thus, it would appear that collisional coupling from low levels ($v = 0-4$) of the A' state to high levels ($v \sim 10-12$) of the B state may be an important mechanism for the decay of the A' state.

If the main loss of $N_2(A')$ is through collisional transfer to $N_2(B)$, then a major fraction of the apparent $N_2(B)$ excitation from $N_2(A)$ energy pooling may actually proceed through the $N_2(C'')$ channel via cascade to A' and collisional transfer to B . Indeed, the energy pooling rate coefficient for "direct" production of $N_2(B)$ by two $N_2(A, v = 0)$ molecules as measured by Piper,²⁶ is $(7.7 \pm 1.1) \times 10^{-11} \text{ cm}^3 \text{ molecule}^{-1} \text{ s}^{-1}$, comparable to his value¹⁶ of $(8.1 \pm 2.3) \times 10^{-11} \text{ cm}^3 \text{ molecule}^{-1} \text{ s}^{-1}$ for production of $N_2(C'')$. However, it appears from Piper's data²⁶ that substantial, truly direct production of $N_2(B)$ must also occur since the reaction gives enhanced production of $N_2(B, \bar{v} = 2)$ and vibrationally excited $N_2(A)$ clearly favors pro

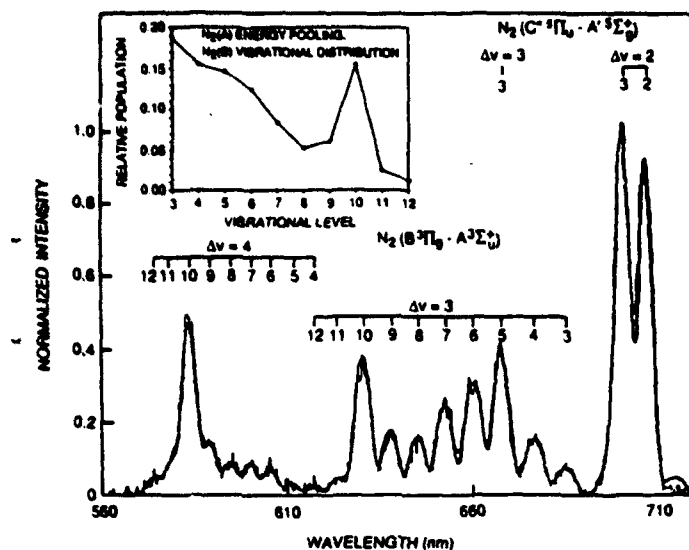


FIG. 10. Visible emission spectrum of N_2 due to $N_2(A')$ energy pooling in a dominantly He buffer gas. The enhancement of the population of $v = 10$ of the B state is indicated in the inset plot of the vibrational distribution.

duction of $N_2(B, v < 6)$ over $N_2(B, v = 9-11)$. Thus it appears that only a fraction of the $N_2(A')$ produced is converted to $N_2(B, v)$. The remainder may be quenched through some other pathway, or may appear in the neighboring $W^3\Delta_u$ or $B'^1\Sigma_u^-$ states, which are known to be rapidly collisionally coupled to the $B^3\Pi_g$ state.²⁷

The upper limit on the stability of the A' state is uncertain, to a large degree, due to the apparent discrepancy in the theoretical¹² and experimentally inferred¹⁴ radiative lifetimes of the C'' state. Predissociation of the C'' state can be excluded as the cause for the apparent reduced lifetime. The energy pooling rate coefficient would have to be significantly larger than gas kinetic in order to produce a C'' -state population for which the predissociation rate was 100 times greater than the fluorescence rate. Similarly, direct coupling of the C and C'' states is unlikely. At the pressures employed in most of the experiments which have investigated this system, radiative decay of the C state should be much more efficient than collisional energy transfer. On the other hand, the most quantitative experimental measurements cover a limited pressure range, and are not inconsistent with a longer radiative lifetime and an inefficient (e.g., $< 10^{-12}$ gas kinetic) rate coefficient for electronic quenching by the inert bath gas. Clearly, further investigation of this problem is warranted.

Our experiments in which we vary the N_2 concentration indicate that N_2 is not primarily responsible for coupling of the two manifolds. At the lowest N_2 concentrations employed, a gas-kinetic coupling rate coefficient would be required to couple the levels and significant variations in the B state, $v = 10$ enhancement would have been observed. It would appear more likely that Ar or He, which are both present in much greater concentrations, may be responsible for the coupling. In this case the effective quenching rate coefficient could be as small as 3×10^{-14} cm³ molecule⁻¹

s⁻¹. The production of $N_2(A')$ in either a supersonic jet or in a rare gas matrix may reduce the collisional coupling to the B state and enable a more rigorous determination of the stability of this state.

CONCLUSIONS

We have observed production of the $A'^1\Sigma_g^+$ state of N_2 via $(C''^3\Pi_u \rightarrow A'^1\Sigma_g^+)$ radiative cascade from the energy pooling of $N_2(A'^1\Sigma_g^+)$ molecules. However, laser-induced fluorescence on the $C''^3\Pi_u - A'^1\Sigma_g^+$ transition failed to detect the presence of A' -state molecules. Based on simple kinetic arguments, we place an upper limit on the lifetime of the A' state under our experimental conditions of 0.3 ms. Observation of enhanced emission from $v = 10$ of the $B^3\Pi_g$ state suggests that collisional coupling of the A' to the B state is responsible for the decay of this state. This coupling provides a significant pathway into the upper triplet manifold of N_2 in energy pooling and atom recombination, via a mechanism analogous to that originally proposed by Bayes and Kistiakowsky.²

ACKNOWLEDGMENTS

This work was supported by the Air Force Astronautics Laboratory under Contract No. F04611-86-C-0077. We are also grateful to the Air Force Geophysics Laboratory for additional support (Contract No. F19628-88-C-0173) including the use of the dye laser system. We would also like to thank L. G. Piper, S. J. Davis, and B. D. Green at PSI for helpful discussions of our results.

- ¹See, for example, *Formation and Trapping of Free Radicals*, edited by A. M. Bass and H. P. Broida (Academic, New York, 1960).
- ²J. Berkowitz, W. A. Chupka, and G. B. Kistiakowsky, *J. Chem. Phys.* **25**, 457 (1956); K. D. Bayes and G. B. Kistiakowsky, *J. Chem. Phys.* **32**, 992 (1960).
- ³J. T. Vanderslice, E. A. Mason, and E. R. Lippincott, *J. Chem. Phys.* **30**, 129 (1959).
- ⁴W. E. Meador, NASA Tech. Rep. TR-R-68 (1960).
- ⁵R. F. Ferrante and W. C. Stwalley, *J. Chem. Phys.* **78**, 3107 (1983).
- ⁶M. Capitelli, U. T. Lamanna, C. Guidotti, and G. P. Arrighini, *J. Chem. Phys.* **79**, 5210 (1983).
- ⁷H. Partridge, S. R. Langhoff, and C. W. Bauschlicher, Jr., *J. Chem. Phys.* **84**, 6901 (1986).
- ⁸R. S. Mulliken, *J. Chem. Phys.* **37**, 809 (1962).
- ⁹M. Krauss and D. B. Neumann, *Mol. Phys.* **32**, 101 (1976).
- ¹⁰P. E. M. Siegbahn, *Int. J. Quantum Chem.* **23**, 1869 (1983).
- ¹¹P. K. Carroll, *J. Chem. Phys.* **37**, 805 (1962).
- ¹²H. Partridge, S. R. Langhoff, and C. W. Bauschlicher, Jr., *J. Chem. Phys.* **88**, 3174 (1988).
- ¹³K. P. Huber and M. Vervloet, *J. Chem. Phys.* **89**, 5957 (1988).
- ¹⁴I. Nadler, D. W. Setser, and S. Rosenwaks, *Chem. Phys. Lett.* **72**, 536 (1980).
- ¹⁵I. Nadler, A. Rotem, and S. Rosenwaks, *Chem. Phys.* **69**, 375 (1982).
- ¹⁶L. G. Piper, *J. Chem. Phys.* **88**, 231 (1988).
- ¹⁷E. E. Eyler and F. M. Pipkin, *J. Chem. Phys.* **79**, 3654 (1983).
- ¹⁸A. Fontijn, C. B. Meyer, and H. I. Schiff, *J. Chem. Phys.* **40**, 64 (1964).
- ¹⁹D. W. Setser, D. H. Stedman, and J. A. Coxon, *J. Chem. Phys.* **53**, 1004 (1970).
- ²⁰D. H. Stedman and D. W. Setser, *Chem. Phys. Lett.* **2**, 542 (1968).

- ²¹L. G. Piper, L. M. Cowles, and W. T. Rawlins, *J. Chem. Phys.* **85**, 3369 (1986).
- ²²E. E. Ferguson, F. C. Fehsenfeld, and A. L. Schmeltekopf, *Adv. At. Mol. Phys.* **V**, 1 (1970).
- ²³J. O. Hirschfelder, C. F. Curtiss, and R. B. Bird, *Molecular Theory of Gases and Liquids* (Wiley, New York, 1954).
- ²⁴H. Geisen, D. Neuschäfer, and Ch. Ottinger, *Z. Phys. D* **4**, 263 (1987).
- ²⁵A. Lofthus and P. H. Krupenie, *J. Phys. Chem. Ref. Data* **6**, 113 (1977).
- ²⁶L. G. Piper, *J. Chem. Phys.* **88**, 6911 (1988).
- ²⁷A. Rotem, I. Nadler, and S. Rosenwaks, *Chem. Phys. Lett.* **83**, 281 (1981).

APPENDIX F

Further Observations of the Nitrogen Orange Afterglow

L.G. Piper

J. Chem. Phys., submitted for publication, 1994

(SR-548 reproduced in its entirety)

THIS PAGE INTENTIONALLY LEFT BLANK

FURTHER OBSERVATIONS ON THE NITROGEN ORANGE AFTERGLOW

Lawrence G. Piper

Physical Sciences Inc.

20 New England Business Center

Andover, MA 01810

ABSTRACT

We have extended earlier observations on the nitrogen orange afterglow that results from the excitation of $N_2(B\ ^3\Pi_g, v'=1-12)$ in energy transfer reaction between $N_2(A\ ^3\Sigma_u^+)$ and $N_2(X, v \geq 4)$. Spectral observations out to 1550 nm show that $N_2(B, v'=0)$ accounts for about 38% of the total $N_2(B)$ excitation. This makes the rate coefficient for $N_2(B)$ excitation in the energy-transfer reaction between $N_2(A)$ and $N_2(X, v \geq 4)$ $(4 \pm 2) \times 10^{-11} \text{ cm}^3 \text{ molecule}^{-1} \text{ s}^{-1}$. Experiments involving $^{14}N_2(A)$ and isotopically labeled $^{15}N_2(X, v)$ show $^{15}N_2(B)$ is the principal product. This demonstrates that the mechanism involves electronic energy transfer from the $N_2(A)$ to the $N_2(X, v)$. The vibrational distributions of $N_2(B, v \geq 4)$ are qualitatively similar whether $^{15}N_2(v)$ or $^{14}N_2(v)$ is excited, being characterized roughly as a 5200 K, Boltzmann distribution, although the magnitude of $^{15}N_2(B, v \geq 4)$ excitation is about 20% larger. In contrast, the vibronic levels of $^{14}N_2(B, v=0-2)$ are substantially more excited than are those of $^{15}N_2(B, v=0-2)$. Interestingly, the overall excitation rates for both $^{14}N_2(X, v)$ and $^{15}N_2(X, v)$ are the same to within 20%. Adding $^{14}N_2(X)$ to the mixture of $N_2(A)$ with $^{15}N_2(X, v)$ results in quenching of $^{15}N_2(B)$ and the concomitant excitation of $^{14}N_2(B)$. The rate coefficient for this electronic energy exchange reaction is $(8 \pm 2) \times$

$10^{-11} \text{ cm}^3 \text{ molecule}^{-1} \text{ s}^{-1}$, about 2.5 times greater than the rate coefficient for $\text{N}_2(\text{B})$ removal by N_2 .

1. INTRODUCTION

The nitrogen orange afterglow can be produced in a discharge flow apparatus by flowing dilute mixtures of nitrogen in helium or argon rapidly through a low power microwave or radio frequency discharge.¹ It has also been generated in a high voltage, low current discharge in static mixtures of nitrogen highly dilute in argon or helium.² This afterglow is distinctively different from the other, better known, nitrogen afterglows, the Lewis-Rayleigh, pink, blue and green afterglows.^{3,4} In common with the well-known Lewis-Rayleigh afterglow, the orange afterglow's primary emission features to the red of 500 nm are the nitrogen first-positive bands, $\text{N}_2(\text{B}^3\Pi_g - \text{A}^3\Sigma^+_u)$. However, the vibrational level populations of the first-positive bands in the orange afterglow decrease monotonically with increasing vibrational level, in contrast to the Lewis-Rayleigh afterglow, where the populations of vibrational levels 10 through 12 are elevated relative to the populations of the other vibrational levels. Generally, the N_2 B-state vibrational level populations in the orange afterglow can be characterized roughly by a 5000 K Boltzman distribution.

Spectral observations of the orange afterglow in the ultraviolet reveal the nitrogen Vegard-Kaplan bands, $\text{N}_2(\text{A}^3\Sigma^+_u - \text{X}^1\Sigma^+_g)$. Ordinarily, these bands are difficult to detect in nitrogen afterglows because $\text{N}_2(\text{A})$ has quite a long radiative lifetime,⁵ about 2.5s, and is readily quenched by nitrogen atoms.⁶ Nitrogen atoms are generated in abundance in most nitrogen discharges, but flowing the gases rapidly shortens the residence time in the

discharge sufficiently to reduce the production of atomic nitrogen. As a result, metastable $N_2(A)$ can persist in the flow several tens of milliseconds downstream from the discharge.

Another species abundant in the orange afterglow is highly vibrationally excited, ground-electronic-state nitrogen. Several years ago, we applied a Penning-ionization diagnostic to the orange afterglow.^{7,8} This diagnostic involves introducing metastable $He(2^3S)$ to the afterglow. A Penning-ionization reaction between $He(2^3S)$ and vibrationally excited nitrogen results in excitation of the nitrogen first-negative bands, $N_2^+(B^2\Sigma_u^+ - X^2\Sigma_g^+)$. The vibrational distribution of the $N_2^+(B)$ is related to that of ground state nitrogen through the Franck-Condon factors that couple the two states. The $N_2^+(B, v)$ distribution observed in the Penning-ionization process can be inverted to give the vibrational distribution of the vibrationally excited, neutral, ground electronic state nitrogen. Our investigations showed that even a modest discharge power of 50W was sufficient to raise more than half of the discharged nitrogen to excited vibrational levels.⁸ Under certain conditions, the Penning-ionization reaction also produced some $N_2^+(C)$, thereby demonstrating the presence of ground electronic state nitrogen molecules carrying at least 3.8 eV in vibrational energy.

In a series of observations in which $N_2(A)$ and $N_2(X, v)$ were generated in separate sources and combined subsequently, we have shown that the orange afterglow is excited in an energy-pooling reaction between $N_2(A)$ and $N_2(X, v)$.¹ Exciting $N_2(B, v=1)$ requires $N_2(X, v \geq 5)$ whereas $N_2(X, v \geq 13)$ is required to generate $N_2(B, v=12)$. We have since used this energy transfer reaction to study the quenching of vibrational energy in ground electronic state nitrogen by a variety of molecules.⁹

This paper reports additional observations related to the orange afterglow. We have extended spectral observations to 1550 nm in order to quantify the contribution of emission from $N_2(B, v' = 0)$ to the afterglow radiation. In addition, we have mixed isotopically labeled $^{15}N_2(X, v)$ with $^{14}N_2(A)$ to demonstrate that the excitation mechanism of the orange afterglow involves energy transfer from $^{14}N_2(A)$ to $^{15}N_2(X, v)$ to produce $^{15}N_2(B)$. Further, we find adding $^{14}N_2(X)$ to quench the $^{15}N_2(B)$ results in excitation of $^{14}N_2(B)$ in vibrational levels lower than those of the $^{15}N_2(B)$ initially excited.

2. EXPERIMENTAL

The experimental apparatus (see Figure 1) is a 2-in. diameter discharge-flow reactor configured to allow spectral observations along the flow tube axis. The $N_2(A)$ and $N_2(X, v)$ entered the main flow reactor from opposing side arms at the reactor's upstream end. This end of the flow tube was sealed with a CaF_2 window having uniform transmission over the spectral range investigated in these studies, 200 to 1800 nm.

The $N_2(A)$ was generated by the energy transfer reaction between metastable $Ar^*(^3P_{0,2})$ and N_2 .^{10,11} This reaction produces $N_2(C^3\Pi_u)$ which radiates immediately to the $N_2(B^3\Pi_g)$ state. Subsequent radiative and collisional cascade from $N_2(B^3\Pi_g)$ makes the highly metastable $N_2(A^3\Sigma_u^+)$. A low-power, hollow-cathode discharge, sustained in a flow of 5 to 10% argon in helium, produces the Ar^* . The N_2 then is mixed with the Ar^* downstream from the discharge.

A microwave discharge sustained in a flow of 0.5 to 5% nitrogen in helium generates the $N_2(X, v)$. The discharge efflux flows through a nickel screen prior to entering the main

reactor. The nickel screen removes molecular metastables other than $N_2(X,v)$ and recombines most of the nitrogen atoms produced in the discharge.^{7,12}

Either mass-flow meters or rotameters measured gas flow rates. All flow meters had been calibrated either by measuring the variation of pressure with time when the gases flowed into a calibrated volume, or by comparison with a standard mass flow meter. The cylinders of nitrogen used for generating the $N_2(X,v)$ were connected to a T-valve which could be rotated to admit either $^{14}N_2$ or $^{15}N_2$ into the discharge. This allowed the isotopic sources of $N_2(X,v)$ to be switched rapidly to allow comparison between the two $N_2(X,v)$ sources under otherwise similar conditions.

A 0.5m monochromator was used to make spectral observations along the axis of the main flow tube. For measurements between 200 and 900 nm, the monochromator had a 1200 line mm^{-1} grating blazed at 250 nm. A thermoelectrically cooled HTV R943-02 photomultiplier tube, connected to a photon-counting rate meter and lab computer, detected the photons. For spectral observations between 700 and 1500 nm, the monochromator had a 300 line mm^{-1} grating blazed at 1.0 μm and a liquid nitrogen cooled, intrinsic germanium detector measured fluorescence. In the infrared measurements, light from the flow reactor was chopped prior to entering the monochromator, and a lock-in amplifier connected to the lab computer processed the signals from the intrinsic germanium detector.

The spectra observed under the various sets of conditions were analyzed using the spectral fitting procedure we have detailed previously.¹³ Synthetic spectra are generated by first multiplying a set of vibronic level populations by a set of basis functions representing the intensity of a unit population of each vibronic level as a function of wavelength. The intensities of each band at each wavelength increment are then summed to determine an

overall spectral intensity. A least squares program varies the populations of each vibronic level to determine the set giving a spectrum that best matches the one observed experimentally. The important spectral features between 200 and 400 nm were the nitrogen Vegard-Kaplan bands, $N_2(A^3\Sigma_u^+ - X^1\Sigma_g^+)$, nitrogen second-positive bands, $N_2(C^3\Pi_u - B^3\Pi_g)$, and nitric oxide gamma bands, $NO(A^2\Sigma^+ - X^2\Pi)$. The only significant spectral features in the visible and infrared were the nitrogen first-positive bands, $N_2(B^3\Pi_g - A^3\Sigma_u^+)$.

The spectral fitting procedure was essential to the analysis because emissions from $^{14}N_2(B)$ are highly overlapped with those from $^{15}N_2(B)$. Our spectra cover a number of different vibronic sequences, however, and the degree of overlap between vibronic levels in one sequence is quite different from those in the other sequences.

We used the spectroscopic constants of Roux et al.^{14,15} or Lofthus and Krupenie¹⁶ in generating the synthetic nitrogen spectra. Einstein coefficients for $N_2(A-X)$ were from Shemansky,¹⁷ those for $^{14}N_2(B-A)$ from Piper et al.,¹³ $N_2(C-B)$ from Lofthus and Krupenie,¹⁶ and $NO(A-X)$ from Piper and Cowles.¹⁸ We calculated a set of Einstein coefficients for $^{15}N_2(B-A)$ using the transition-moment function of Piper et al.¹³ and a set of Franck-Condon factors that we calculated for $^{15}N_2(B-A)$ using procedures outlined previously.¹⁹ The Einstein coefficients for $^{15}N_2(B-A)$ differed little from those for $^{14}N_2(B-A)$.

3. RESULTS

We showed previously that mixing flows of $N_2(X,v)$ and $N_2(A^3\Sigma_u^+)$ generates the orange afterglow of nitrogen¹ which is characterized by nitrogen first-positive emission,

$N_2(B^3\Pi_g - A^3\Sigma_u^+)$. Mixing $^{15}N_2(X,v)$ with $^{14}N_2(A)$ also generates the orange afterglow, but in this case the emission is predominantly from $^{15}N_2(B)$. Adding increasing amounts of vibrationally cold $^{14}N_2(X)$ to the reactor shifts the spectrum from $^{15}N_2(B)$ emission to that from $^{14}N_2(B)$. Pravilov et al.²⁰ noted similar behavior in their study on $N_2(B)$ fluorescence excited by N-atom recombination involving ^{15}N and ^{14}N .

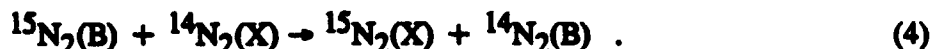
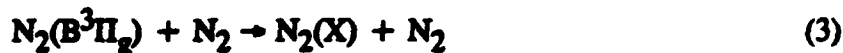
The experimental procedure consisted of measuring nitrogen first-positive spectra generated using first $^{15}N_2(X,v)$ and then $^{14}N_2(X,v)$ as a function of the number density of added cold $^{14}N_2(X)$. This procedure allowed direct comparison of the two $N_2(X,v)$ sources at constant conditions. It also permitted extrapolation of the spectral intensities of the $^{15}N_2(B-A)$ to zero partial pressure of $^{14}N_2$. Studies between 200 and 900 nm also involved scanning the Vegard-Kaplan bands for each set of conditions to correct for variations in $N_2(A)$ number density. The experimental conditions for the infrared studies exactly matched those for the visible/UV measurements to ensure comparable number densities of $N_2(A)$ and $N_2(X,v)$.

The number densities of $N_2(X,v)$ in the observation region were deemed to vary linearly with the flow rate of N_2 in the microwave discharge. We confirmed this supposition (see Figure 2) by observing that the intensities of several nitrogen first-positive bands increased linearly with the flow rate of nitrogen through the microwave discharge under otherwise constant conditions. This behavior is expected because the effective vibrational temperature of $N_2(X,v)$ varies little at low nitrogen mole fractions in the discharge,⁸ $\lesssim 0.05$. This proportionality allowed us to normalize our observations to common conditions.

Figures 3 and 4 show how the visible spectrum of nitrogen first-positive bands, excited from $N_2(A)$ energy transfer to $^{15}N_2(X,v)$, changes when a substantial amount of cold

$^{14}\text{N}_2$ is added to the reactor. Figures 5 and 6 show near infrared spectra under conditions similar to those of Figures 3 and 4. The shift from primarily $^{15}\text{N}_2(\text{B-A})$ bands at a $^{14}\text{N}_2$ partial pressure of 19 mtorr to primarily $^{14}\text{N}_2(\text{B-A})$ bands at a $^{14}\text{N}_2$ partial pressure of 132 mtorr is particularly noticeable in the shorter wavelength spectra. The variation at longer wavelengths is more subtle, but significant enough that the spectral fitting procedure can differentiate the two isotopic emissions easily. Relative populations for $\text{N}_2(\text{B}, v=1-5)$ under constant conditions are the same whether determined from spectral scans between 500 and 900 nm or 700 and 1500 nm.

The following set of reactions provides a framework for analyzing these observations:



The first three reactions can be subdivided depending upon whether $^{15}\text{N}_2(\text{X}, v)$ or $^{14}\text{N}_2(\text{X}, v)$ flows into the reactor, and will be denoted in subsequent kinetic equations by $^{15}k_1$, $^{14}k_1$, etc., when necessary.

The rate of change in the number density of $\text{N}_2(\text{B})$ with time is

$$\frac{d[\text{N}_2(\text{B})]}{dt} = k_1[\text{N}_2(\text{A})][\text{N}_2(\text{X}, v)] - \{k_2 + k_3[\text{N}_2]\}[\text{N}_2(\text{B})] \quad (5)$$

This reaction is in steady state within the field of view so that the excitation and decay rates can be equated. As a result

$$[N_2(B)] = \frac{k_1[N_2(A)][N_2(X,v)]}{k_2 + k_3[N_2]} \quad (6)$$

Since the intensity of molecular fluorescence equals the product of the excited state number density and its radiative decay rate, Eq. (6) can be rearranged to give

$$\frac{[N_2(A)][N_2(X,v)]}{I_{N_2(B)}} = \frac{1}{k_1} + \frac{k_3}{k_1 k_2} [N_2] \quad (7)$$

A plot of the left-hand side of Eq. (7) against the N_2 number density should be linear with an intercept that is the reciprocal of the excitation rate coefficient, and a slope that is proportional to the total quenching rate coefficient. Only relative excitation rate coefficients can be determined unless one measures absolute photon emission rates. In this study we determined relative excitation rate coefficients by dividing the product of the relative number densities of $N_2(A)$ and $N_2(X,v)$ by the observed band intensities and extrapolating this quantity to zero $^{14}N_2$ partial pressure.

Figure 7 shows how the relative excitation rate coefficients vary with $N_2(B)$ vibrational level. We normalized the relative rate coefficient for $N_2(B, v'=0)$ to the others by multiplying it by the ratio of the relative rate coefficients for $N_2(B, v=1-5)$ determined in spectral scans between 500 and 900 nm to those determined from scans between 700 and 1500 nm. The relative rate coefficients for $N_2(B, v'=0)$ excitation are essentially the same for excitation from $^{15}N_2(X)$ as from $^{14}N_2(X)$ excitation, but substantial differences exist for most of the other vibrational levels. Vibrational levels 1 and 2 are excited much more efficiently from $^{14}N_2(X,v)$ than from $^{15}N_2(X,v)$, while for most of the remaining vibrational levels excitation from $^{15}N_2(X,v)$ is more efficient.

The relative excitation rate coefficients for vibrational levels $v' = 4$ and above essentially follows a Boltzmann distribution with a vibrational temperature of roughly 5200 K for both $N_2(X,v)$ isotopes. In large part, the distribution in excitation rate coefficients with vibrational level is determined by the number densities of the $N_2(X,v)$ vibrational levels from which the $N_2(B,v)$ were excited. We have shown previously that the $N_2(X,v)$ distribution does not follow a Boltzmann distribution, rather a modified Treanor distribution.^{7,8} Interestingly, the characteristic temperature of this modified Treanor distribution is on the order of 5000 K for discharge conditions similar to those used in these studies.

Figures 8 and 9 show the variation in the ratio of the product of the number densities of $N_2(A)$ and $N_2(X,v)$ to the total N_2 first-positive band intensity as a function of $^{14}N_2$ number density. Figure 8 is for the excitation of vibrational levels zero through five, the near infrared data, and Figure 9 for the visible data, vibrational levels one through twelve. Both plots include data from $^{15}N_2(B)$ excitation and, for comparison purposes, from $^{14}N_2(B)$ excitation. The intercepts on each plot for the $^{14}N_2$ data and the $^{15}N_2$ data are essentially the same. This indicates that the total rate coefficient for $^{15}N_2(X,v)$ excitation is the same as that for $^{14}N_2(X,v)$ excitation within the limits of experimental error which are $\pm 20\%$.

The ratio of the slope for $^{15}N_2(B)$ excitation to that for $^{14}N_2(B)$ excitation is the same in both Figures 8 and 9. This ratio indicates the rate coefficient for $^{15}N_2(B)$ quenching by $^{14}N_2$ is 2.6 ± 0.3 times greater than that for $^{14}N_2(B)$ quenching by $^{14}N_2$. We suspect that the reason for this large difference is because $^{15}N_2(B)$ can be removed not only by electronic quenching to $N_2(A)$ or $N_2(X)$, but also by energy transfer to lower vibrational levels of $^{14}N_2(B)$. While this latter process undoubtedly occurs in $^{14}N_2(F)$ as well, it is indistinguishable from a lack of quenching.

In the case of $^{14}\text{N}_2(\text{B})$ excitation by energy transfer from $^{15}\text{N}_2(\text{B})$ to $^{14}\text{N}_2(\text{X})$, the differential equation for the rate of change in the $^{14}\text{N}_2(\text{B})$ number density as a function time is

$$\frac{d[^{14}\text{N}_2(\text{B})]}{dt} = k_4[^{15}\text{N}_2(\text{B})][^{14}\text{N}_2] - \{^{14}k_2 + ^{14}k_3[\text{N}_2]\}[^{14}\text{N}_2(\text{B})] \quad (8)$$

Here again, the $^{14}\text{N}_2(\text{B})$ is in steady state so that we can equate its formation and destruction rates. Rearranging Eq. (8) gives

$$\frac{[^{15}\text{N}_2(\text{B})]}{[^{14}\text{N}_2(\text{B})]} = \frac{^{14}k_3}{k_4} + \frac{^{14}k_2}{k_4[\text{N}_2]} \quad (9)$$

Figure 10 shows our data plotted in a form compatible with Eq. (9). The slope in Figure 10 indicates that $k_4 = (8.0 \pm 2.0) \times 10^{-11} \text{ cm}^3 \text{ molecule}^{-1} \text{ s}^{-1}$. Multiplying this rate coefficient, i.e., k_4 , by the intercept in Figure 10 gives the rate coefficient for $^{14}\text{N}_2(\text{B})$ quenching by N_2 , $(3.2 \pm 0.4) \times 10^{-11} \text{ cm}^3 \text{ molecule}^{-1} \text{ s}^{-1}$. This rate coefficient agrees nicely with other reported values for global quenching rate coefficients of $\text{N}_2(\text{B})$ by N_2 .^{9,21-23} Note also that the ratio of these two rate coefficients, k_4/k_3 , is 2.4 ± 0.3 , the same as the ratio obtained from the analysis related to Figures 8 and 9.

4. SUMMARIZING REMARKS

Table 1 summarizes the results of this study. Initially¹ we had reported k_1 as $3 \times 10^{-11} \text{ cm}^3 \text{ molecule}^{-1} \text{ s}^{-1}$, but subsequently revised this value upwards by 16% to correct for having discounted $\text{N}_2(\text{B})$ quenching by CH_4 .⁹ Our recent revision of the $\text{N}_2(\text{A-X})$ Einstein coefficients⁵ indicates we underestimated $\text{N}_2(\text{A})$ number densities by about 25% in our earlier study. The results of this study show that $\text{N}_2(\text{B}, v'=0)$ accounts for about 40% of the total $\text{N}_2(\text{B})$ excitation. Incorporating this value with the two above mentioned corrections makes the total rate coefficient for excitation into all vibrational levels of $\text{N}_2(\text{B})$ $k_1 = (4 \pm 2) \times 10^{-11} \text{ cm}^3 \text{ molecule}^{-1} \text{ s}^{-1}$.

Our results show that a substantial fraction of $\text{N}_2(\text{B})$ quenching by ground electronic state nitrogen is an energy exchange reaction where molecules in higher vibrational levels of $\text{N}_2(\text{B})$ transfer some of their energy to the quenching molecule exciting it to a lower B-state vibrational level. This process is in effect a form of vibrational relaxation in the B state. Interestingly, $\text{N}_2(\text{B})$ vibrational distributions excited in processes such as N-atom recombination²⁴ or $\text{N}_2(\text{A})$ energy pooling²¹ are relaxed only modestly at high nitrogen partial pressures, although the overall emission rates are significantly diminished. This is quite unlike the situation in an argon bath where significant distortion of the nascent $\text{N}_2(\text{B})$ vibrational distribution from these two excitation processes is evident even at pressures as low as 1 torr.^{21,24}

Another product channel for $\text{N}_2(\text{B})$ quenching by N_2 will be the reverse of reaction 1, i.e., the production of $\text{N}_2(\text{A})$ and $\text{N}_2(\text{X}, v)$. This undoubtedly is the major pathway by which nitrogen that is excited by metastable argon energy transfer^{10,11} is channeled into the A state. Metastable argon excites $\text{N}_2(\text{C}^3\Pi_u)$ which radiates to $\text{N}_2(\text{B}^3\Pi_g)$ in about 40 ns.¹⁶

However, further radiative cascade from $N_2(B)$ to $N_2(A)$ via first-positive emission is too slow to compete with collisional processes at normal nitrogen partial pressures downstream from a metastable argon producing discharge. Thus the $N_2(A)$ must be produced predominantly by collisional processes. It is not coincidental, therefore, that our measured rate coefficients for reaction 1 and its reverse (essentially reaction 3) are identical.

ACKNOWLEDGEMENTS

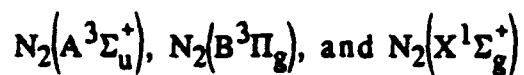
We appreciate partial financial support from the Air Force Office of Scientific Research (Task 2310G4) and the Defense Nuclear Agency (Project SA, Task SA/SDI, work unit 00175) through a contract with the Phillips Laboratory, Geophysics Directorate, F19628-88-C-0173.

REFERENCES

1. L.G. Piper, J. Chem. Phys. 91, 864 (1989).
2. C. Kenty, Proceedings of the 3rd International Conference on Physics of Electronic and Atomic Collisions, M.C.R. McDowell, ed., Amsterdam: North Holland, p. 1133 (1964).
3. A.N. Wright and C.A. Winkler, Active Nitrogen, New York: Academic Press (1968).
4. O. Oldenberg, J. Opt. Soc. Amer. 61, 1092 (1971).
5. L.G. Piper, J. Chem. Phys. 99 XXXX (1993).
6. L.G. Piper, J. Chem. Phys. 90, 7087 (1989).
7. L.G. Piper and W.J. Marinelli, J. Chem. Phys. 89, 2918 (1988).
8. L.G. Piper, K. Donohue, W.J. Kessler, T.R. Tucker, W.P. Cummings, W.J. Marinelli, and S.J. Davis, "Laser Based Diagnostics for N₂(X,v)," Contract F-29601-87-C-0056. Available through NTIS as WL-TR-90-45 (1990).
8. L.G. Piper and W.P. Cummings, manuscript in preparation.
9. L.G. Piper, J. Chem. Phys. 97, 270 (1992).
10. D.H. Stedman and D.W. Setser, Chem. Phys. Lett. 2, 542 (1968).
11. D.W. Setser, D.H. Stedman, and J.A. Coxon, J. Chem. Phys. 53, 1004 (1970).

12. L.G. Piper, J. Phys. Chem. 95, 3965 (1991).
13. L.G. Piper, K.W. Holtzclaw, B.D. Green, and W.A.M. Blumberg, J. Chem. Phys. 90, 5337 (1989).
14. F. Roux, D. Cerny, and J. Verges, J. Mol. Spectrosc. 97, 302 (1982).
15. F. Roux and F. Michaud, J. Mol. Spectrosc. 116, 43 (1986).
16. A. Lofthus and P. Krupenie, J. Phys. Chem. Ref. Data 6, 113 (1977).
17. D.E. Shemansky, J. Chem. Phys. 51, 689 (1969).
18. L.G. Piper and L.M. Cowles, J. Chem. Phys. 85, 2419 (1986).
19. W.J. Marinelli and L.G. Piper, J. Quant. Spectrosc. Radiat. Transfer 34, 121 (1985).
20. A.M. Pravilov, L.G. Smirnova, and A.F. Vilesov, Chem. Phys. Lett. 144, 469 (1988).
21. L.G. Piper, J. Chem. Phys. 88, 6911 (1988).
22. D.E. Shemansky, J. Chem. Phys. 64, 565 (1976).
23. R.A. Young, T.G. Slanger, and G. Black, J. Chem. Phys. 50, 303 (1969).
24. R.L. Brown, J. Chem. Phys. 52, 4064 (1970).

Table 1. Rate Coefficients for Energy-Transfer Reactions Involving



Reaction	Rate Coefficient ^a
$\text{N}_2(\text{A}) + \text{N}_2(\text{X}, \nu) \xrightarrow{k_1} \text{N}_2(\text{B}^3\Pi_g) + \text{N}_2(\text{X})$	4 ± 2
$\frac{k_1(^{15}\text{N}_2(\text{X}, \nu))}{k_1(^{14}\text{N}_2(\text{X}, \nu))}$	1.0 ± 0.2
$^{15}\text{N}_2(\text{B}) + ^{14}\text{N}_2(\text{X}) \rightarrow ^{14}\text{N}_2(\text{B}) + ^{15}\text{N}_2(\text{X})$	8 ± 2
$^{14}\text{N}_2(\text{B}) + \text{N}_2(\text{X}) \rightarrow 2\text{N}_2(\text{X}) \text{ or } \text{N}_2(\text{A}) + \text{N}_2(\text{X})$	3.2 ± 0.4
a. Units of rate coefficients are $10^{-11} \text{ cm}^3 \text{ molecule}^{-1} \text{ s}^{-1}$.	

Figures Captions

- Figure 1. Discharge-flow reactor for observing fluorescent emissions from metastable energy transfer processes.
- Figure 2. Variation in the intensity of several N_2 first-positive bands excited from the interaction of $N_2(A)$ with $N_2(X,v)$ as a function of the nitrogen mole fraction in the discharge.
- Figure 3. Nitrogen first-positive emission between 700 and 900 nm generated from the reaction of $^{15}N_2(X,v)$ with $N_2(A)$ in the presence of 19 mtorr of $^{14}N_2(X)$. The light line is the experimental spectrum while the heavy line shows the synthetic fit to the experimental spectrum.
- Figure 4. Nitrogen first-positive emission between 700 and 900 nm generated from the reaction of $^{15}N_2(X,v)$ with $N_2(A)$ in the presence of 132 mtorr of $^{14}N_2(X)$.
- Figure 5. Nitrogen first-positive emission between 1000 and 1500 nm generated from the reaction of $^{15}N_2(X,v)$ with $N_2(A)$ in the presence of 19 mtorr of $^{14}N_2(X)$.
- Figure 6. Nitrogen first-positive emission between 1000 and 1500 nm generated from the reaction of $^{15}N_2(X,v)$ with $N_2(A)$ in the presence of 240 mtorr of $^{14}N_2(X)$.
- Figure 7. Relative rate coefficients for exciting $N_2(B,v)$ in the energy transfer reaction between $N_2(A)$ and $N_2(X,v)$.
- Figure 8. Stern Volmer quenching plot for $^{15}N_2(B,v'=0-5)$ and $^{14}N_2(B,v'=0-5)$.
- Figure 9. Stern Volmer quenching plot for $^{15}N_2(B,v'=1-12)$ and $^{14}N_2(B,v'=1-12)$.
- Figure 10. Ratio of the number densities of $^{15}N_2(B)$ to $^{14}N_2(B)$ as a function of the reciprocal of the $^{14}N_2$ number density.

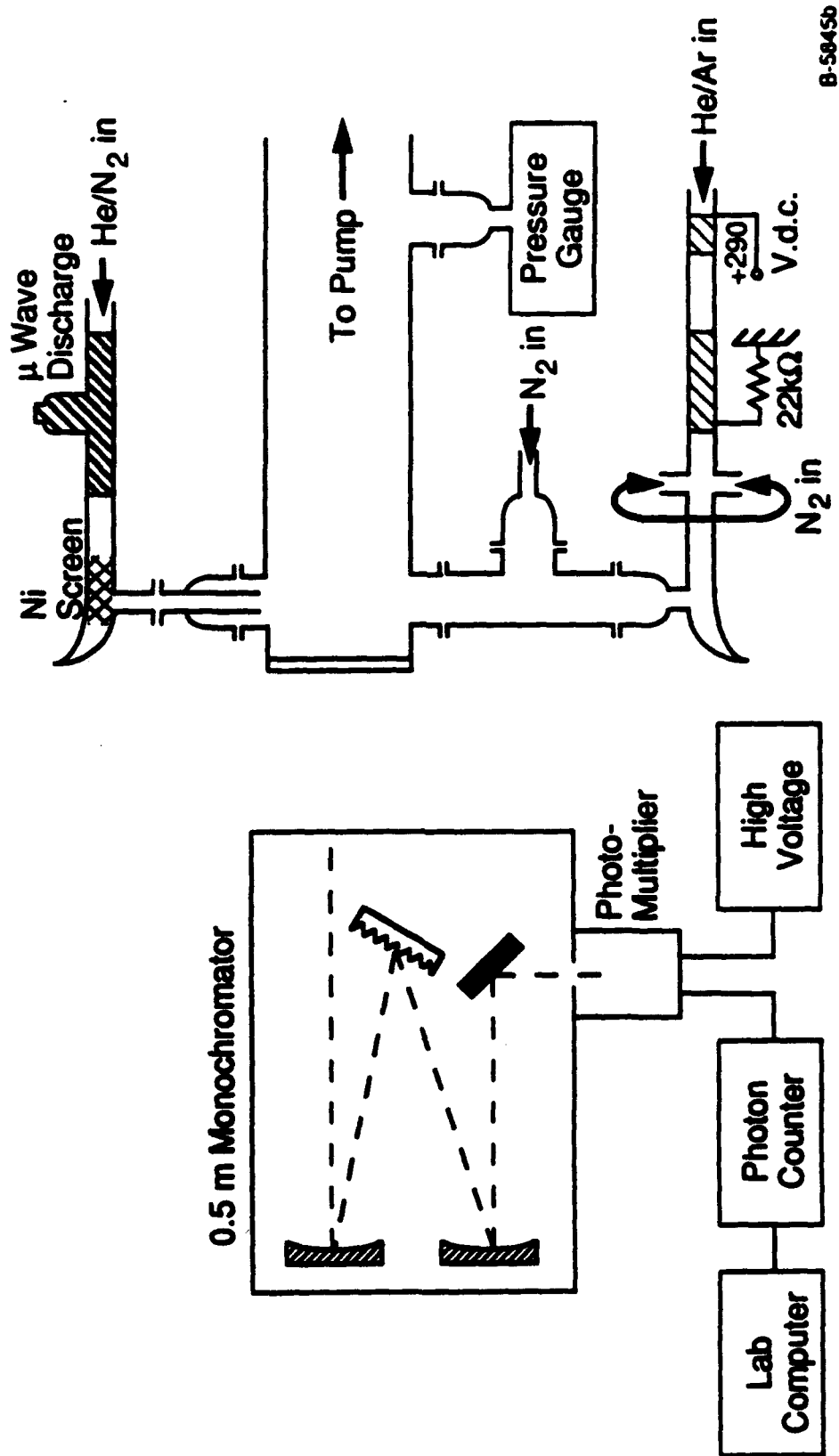


Figure 1

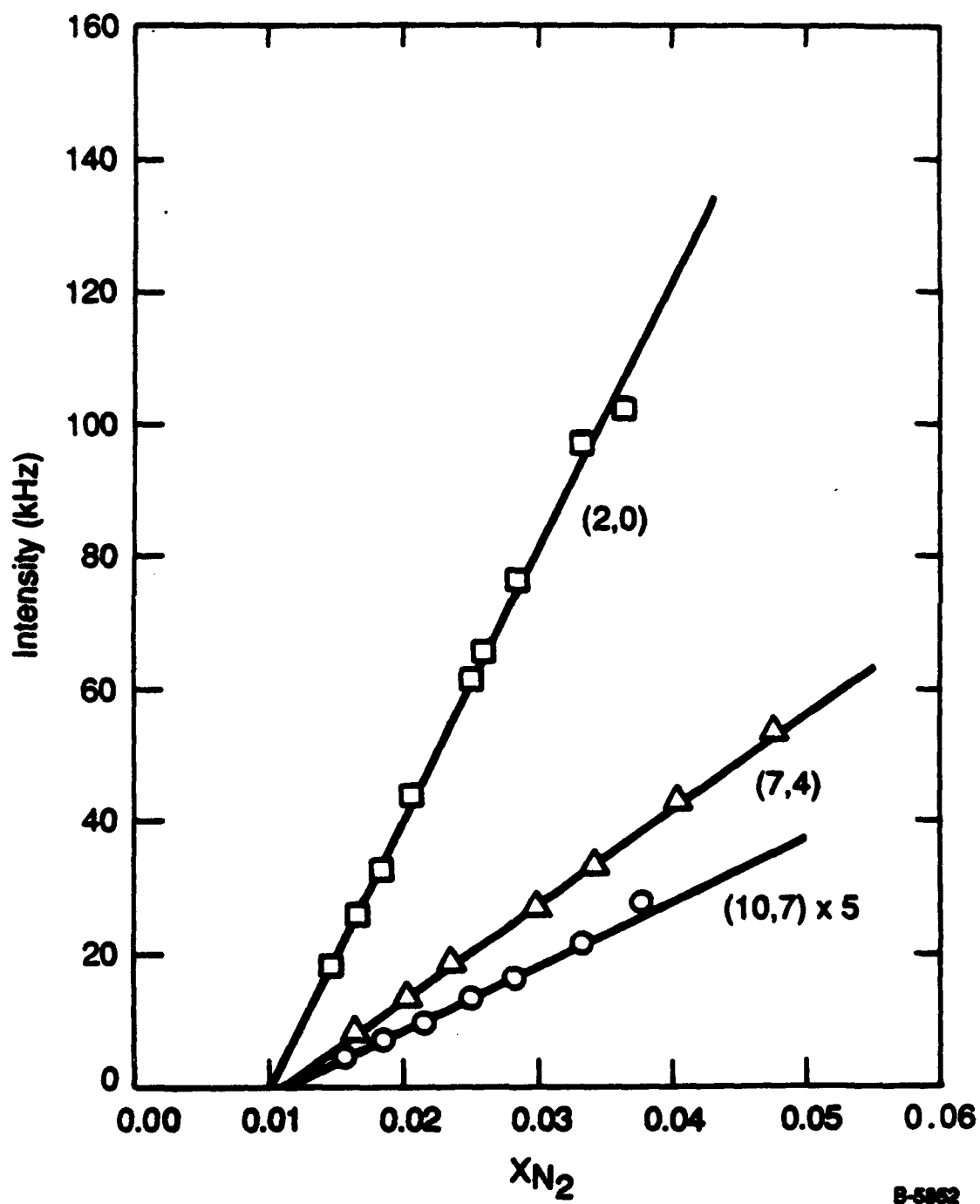
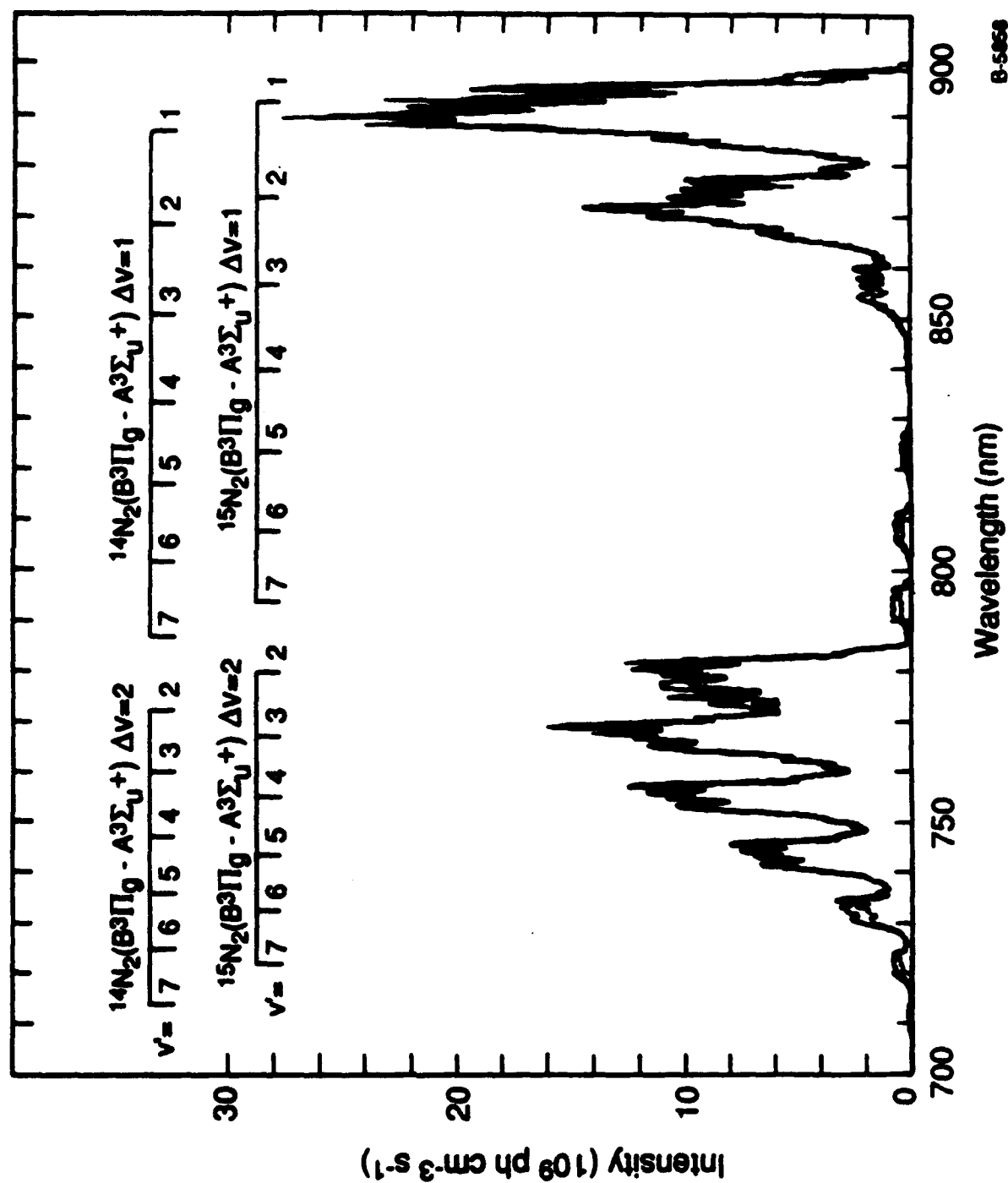


Figure 2



B-5053

Figure 3

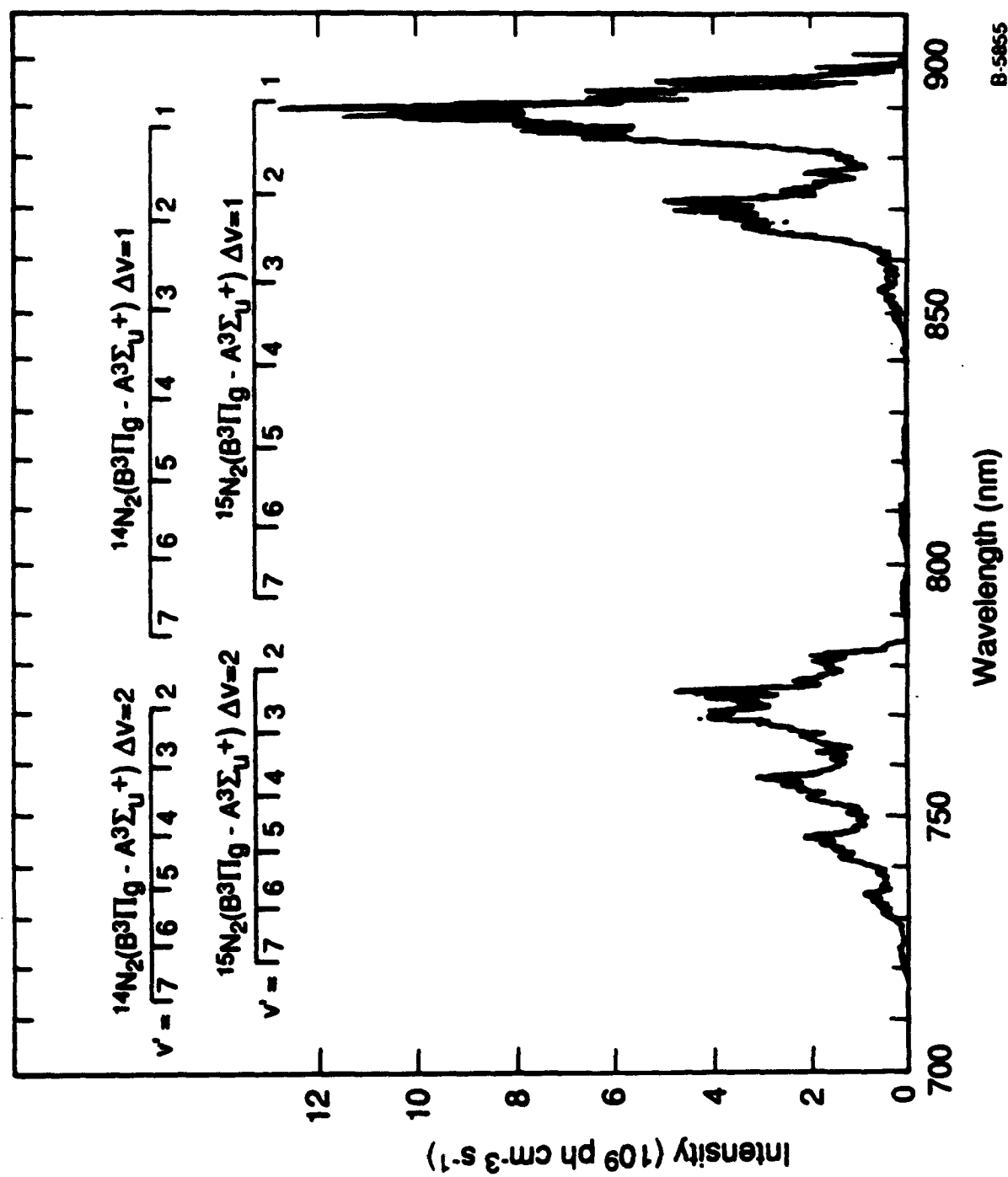
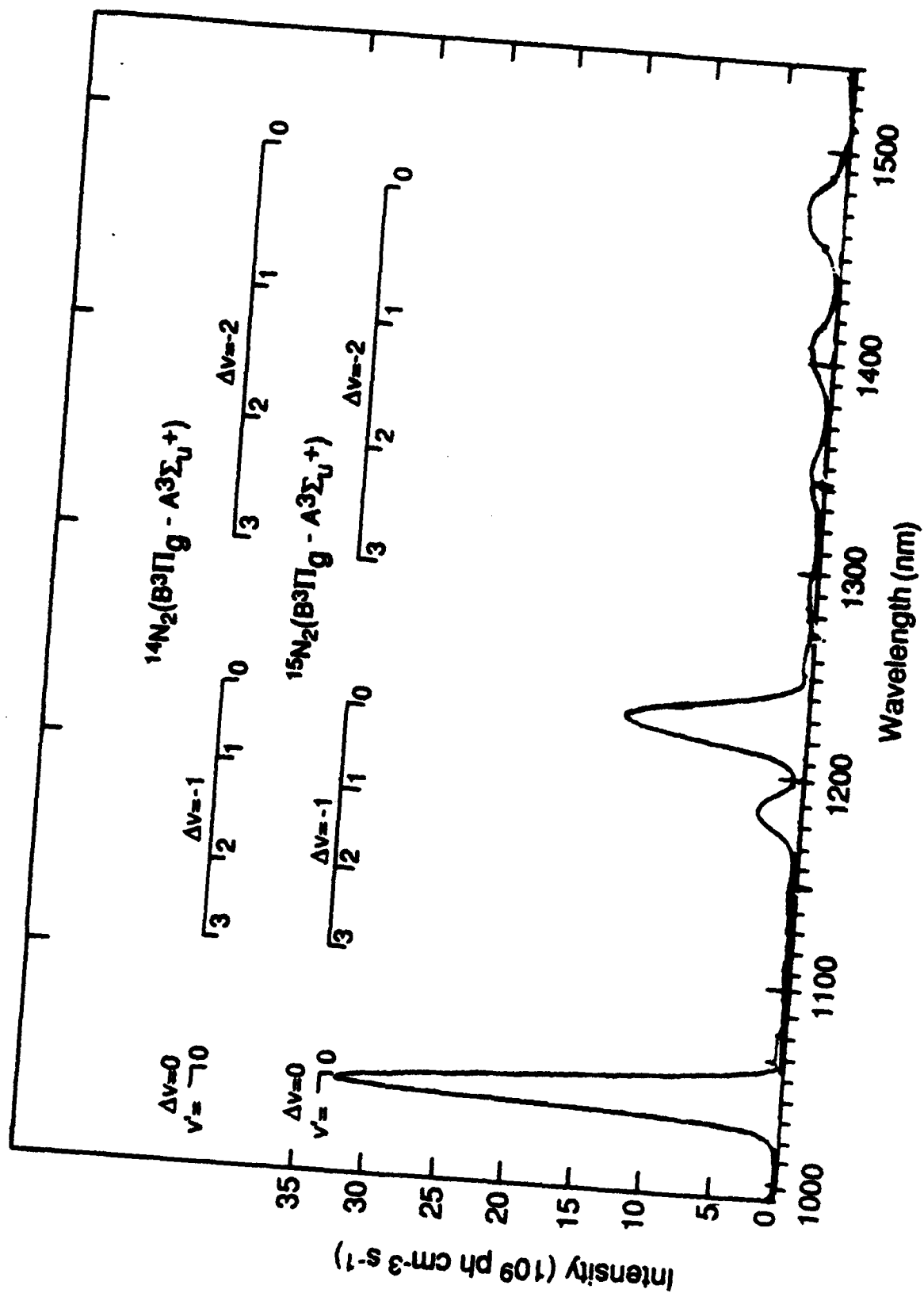


Figure 4



B-5857

Figure 5

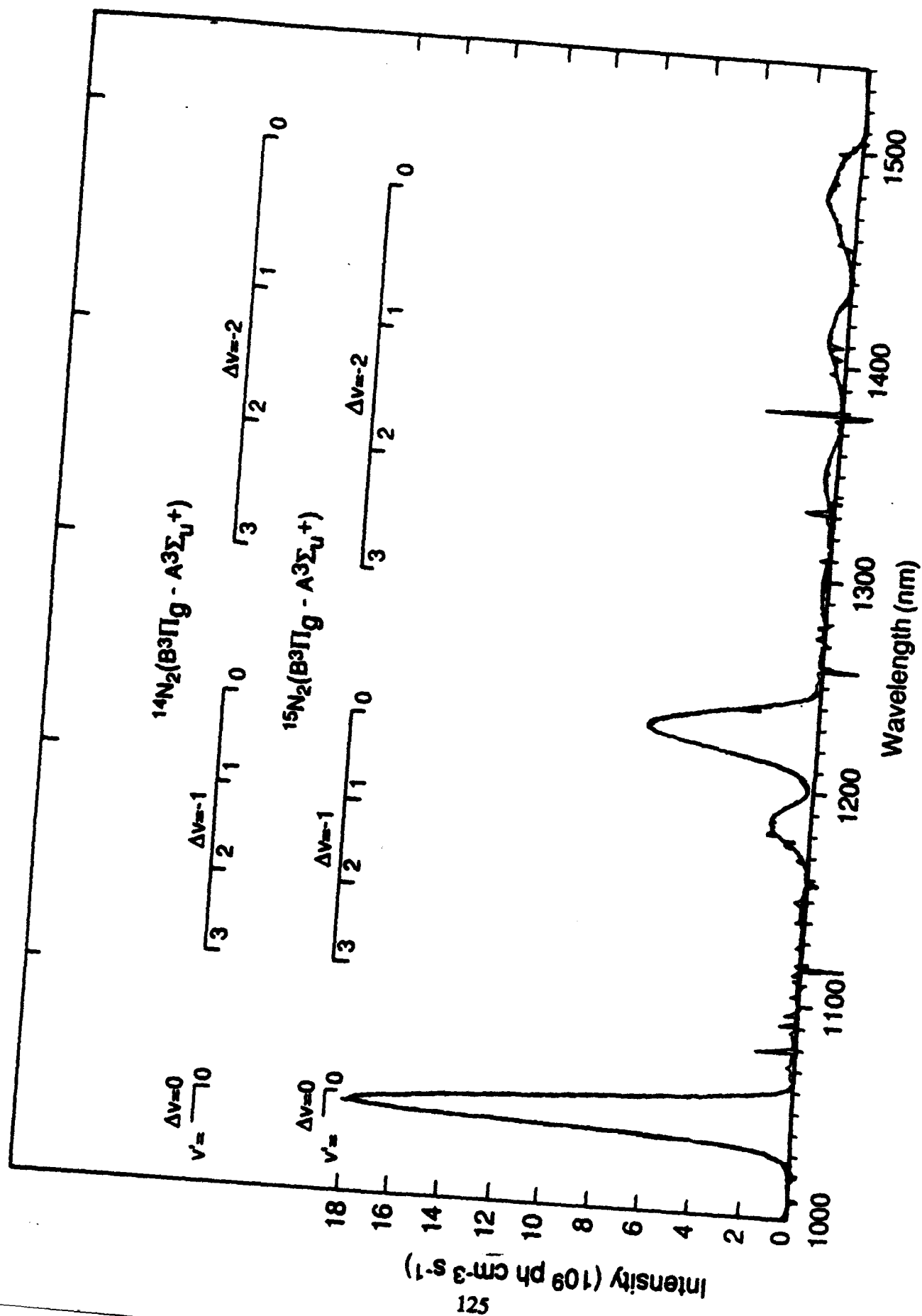
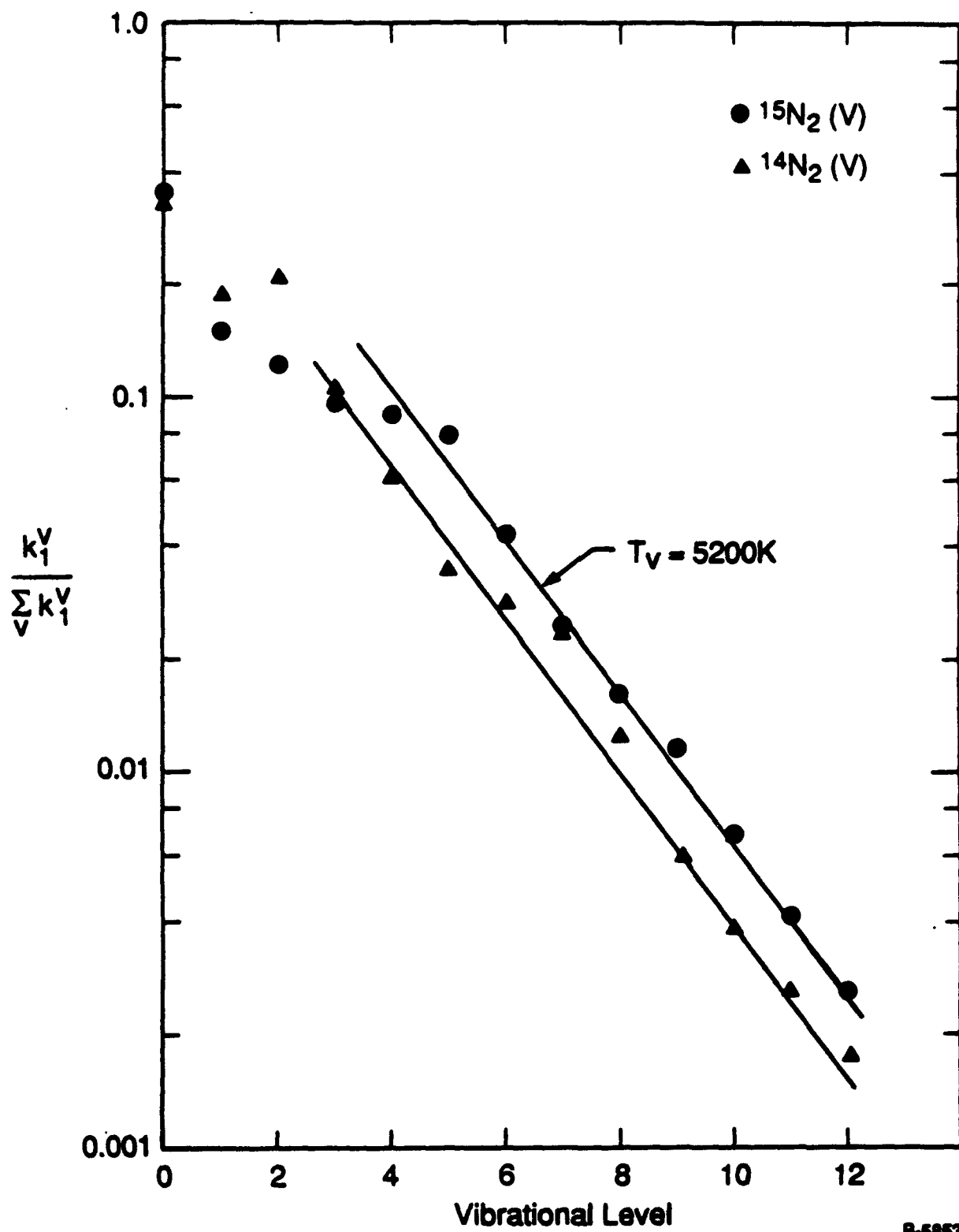


Figure 6

B-5859



B-5853

Figure 7.

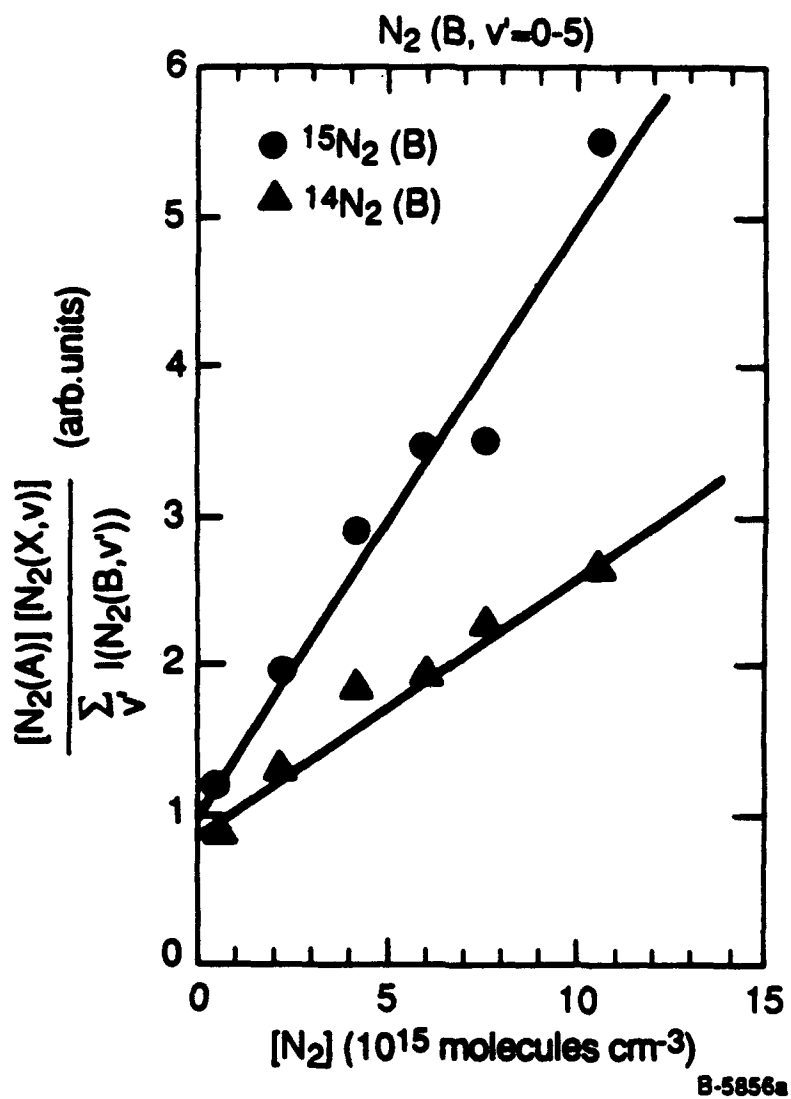


Figure 8

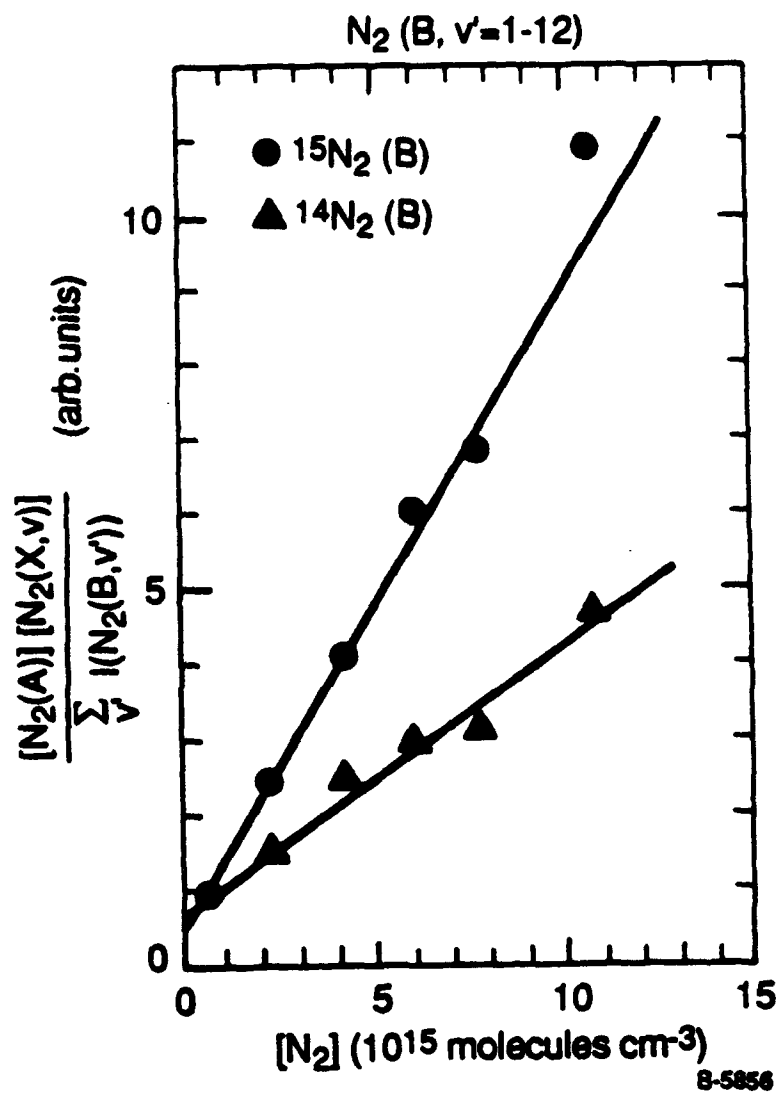


Figure 9

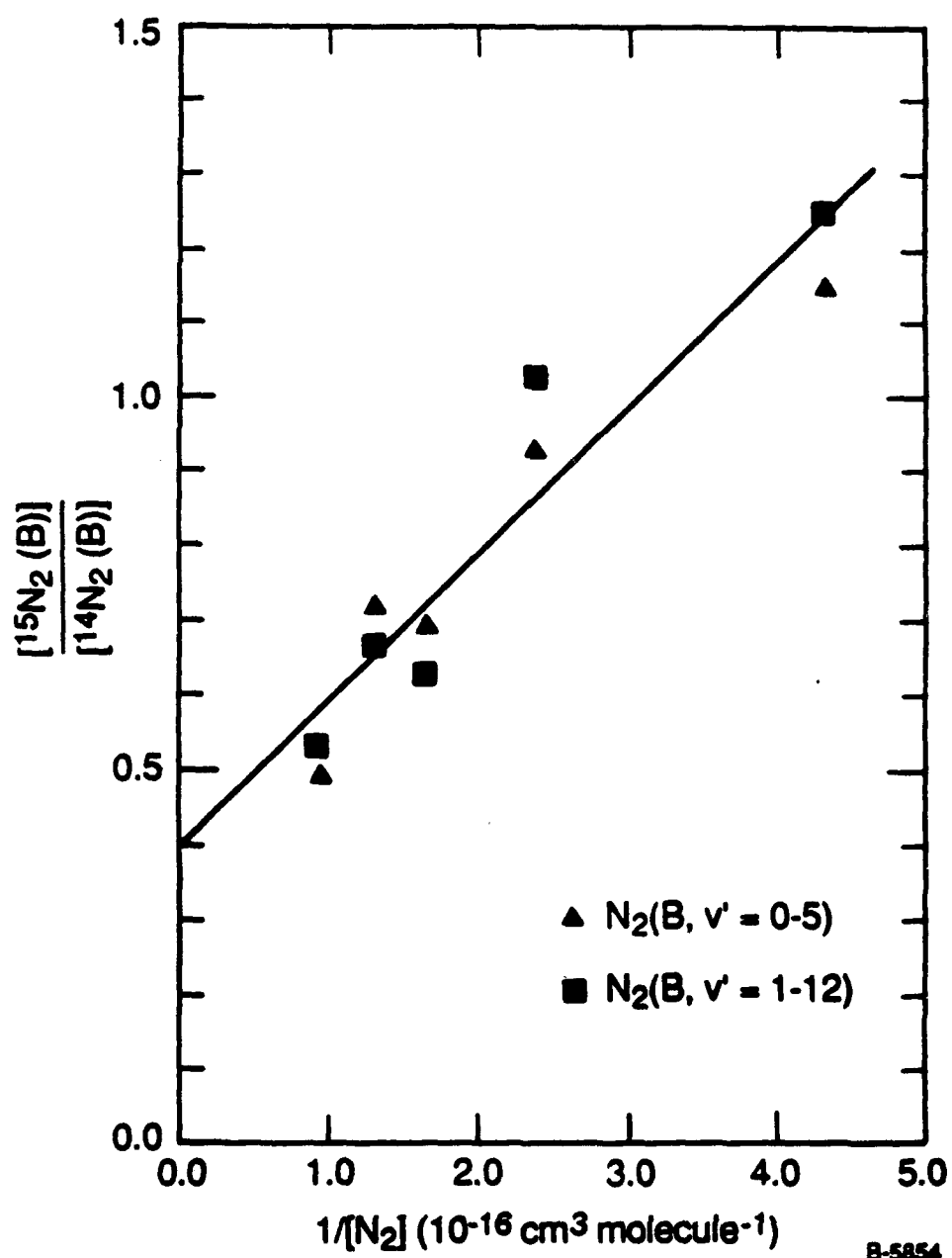


Figure 10

THIS PAGE INTENTIONALLY LEFT BLANK

APPENDIX G

Re-evaluation of the Transition-Moment Function and Einstein Coefficients
for the $N_2(A^3\Sigma_u^+ - X^1\Sigma_g^+)$ Transition

J. Chem. Phys. 99, 3174 (1992)

L.G. Piper

(SR-594 reproduced in its entirety)

THIS PAGE INTENTIONALLY LEFT BLANK

Reevaluation of the transition-moment function and Einstein coefficients for the $N_2(A^3\Sigma_u^+ - X^1\Sigma_g^+)$ transition

Lawrence G. Piper

Physical Sciences Inc., Andover, Massachusetts 01810

(Received 4 December 1992; accepted 28 April 1993)

We have measured the relative intensities of the nitrogen Vegard-Kaplan bands $N_2(A^3\Sigma_u^+ - X^1\Sigma_g^+)$ for transitions covering a range in r centroids between 1.22 and 1.48 Å. With this data we constructed a relative electronic transition moment function that diverges significantly from previously reported functions. We place our data on an absolute basis by normalizing our relative function by the experimentally determined Einstein coefficient for the $v'=0$ to $v''=6$ transition. Combining our normalized data from 1.22 to 1.48 Å with absolute transition moment data measured by Shemansky between 1.08 and 1.14 Å results in a function covering the range between 1.08 and 1.48 Å. The radiative lifetimes calculated from this function are longer than those currently accepted by amounts varying between 25% for $v'=0$ –50% for $v'=4$ –6.

I. INTRODUCTION

For most of the last 20 years, the radiative lifetime of $N_2(A^3\Sigma_u^+)$ has been accepted to be 1.9 s. This lifetime and the associated Einstein coefficients for $N_2(A^3\Sigma_u^+ - X^1\Sigma_g^+)$ transitions, the Vegard-Kaplan bands, are based on Shemansky's¹ measurements of the absorption coefficients of the 6–0 through 12–0 Vegard-Kaplan bands in the vacuum ultraviolet and his reanalysis² of a measurement by Carleton and Oldenberg³ of the Einstein coefficient of the 0–6 transition.

Carleton and Oldenberg³ simultaneously measured the absolute photon-emission rate of the 0–6 Vegard-Kaplan band and the absolute number density in $v'=0$ of the A state via resonance absorption on the 1–0 transition of the nitrogen first-positive system $N_2(B^3\Pi_g - A^3\Sigma_u^+)$. Shemansky and Carleton² corrected the original data with an improved set of line strength factors needed to analyze the absorption measurements correctly. Assuming that the experimental observations of Carleton and Oldenberg are accurate, and that the reanalysis of the absorption measurements is correct, then the derived Einstein coefficient for the 0,6 Vegard-Kaplan band depends directly on the accuracy of the Einstein coefficient for the 1,0 band of the first-positive system. Shemansky and Carleton used the value of $8.48 \times 10^4 \text{ s}^{-1}$ calculated by Shemansky and Vallance Jones⁴ using the Franck-Condon factors of Benesch *et al.*⁵ and Jeunehomme's⁶ transition-moment function.

Several years ago, we questioned the accuracy of some of the input data used to analyze the Carleton and Oldenberg experiment⁷ and suggested that the radiative lifetime of $N_2(A, v=0)$ could be 40% larger than the accepted value. Werner *et al.*⁸ *ab initio* calculations of the electronic transition moment for the $N_2(B^3\Pi_g - A^3\Sigma_u^+)$ transition appeared to support our contention. Their results indicated the accepted values for the radiative lifetimes of the lowest vibrational levels of $N_2(B)$ were probably seriously in error, perhaps being as much as 40% too low. This suggested to us that the Einstein coefficient for the $N_2(B-A)$ 1,0 transition could be in error by a like amount. The result then would be a 40% error in the $N_2(A)$ lifetime

derived from the Carleton and Oldenberg experiment.

Our subsequent experimental determination⁹ of the $N_2(B-A)$ transition-moment variation confirmed Werner *et al.* set of theoretically calculated lifetimes. The corrected value of the 1,0 Einstein coefficient of the N_2 first-positive system $7.48 \times 10^4 \text{ s}^{-1}$, however, is only 12% less than that of Shemansky and Vallance Jones. This reasonable agreement between the two Einstein coefficients is fortuitous because the two transition-moment functions happen to be close together at the internuclear separation appropriate to the 1,0 transition. They diverge widely at other internuclear separations and give much different Einstein coefficients for other important transitions.

The uncertainty in the data used to derive the Einstein coefficients for the Vegard-Kaplan bands is stated¹ to be about 20%. Making a 12% correction to these Einstein coefficients, therefore, hardly seems justified. However, our difficulties fitting Vegard-Kaplan spectra, particularly at wavelengths larger than 400 nm, indicated that the shape of the transition-moment function might be errant. A re-investigation therefore seemed warranted.

We have measured relative intensities in a number of Vegard-Kaplan bands covering a range of wavelengths between 220 and 500 nm. The transition moment function we derive from these data differs significantly from those previously proposed.^{10–12} Einstein coefficients calculated with our transition-moment function are up to 60% smaller than those Shemansky published and our calculated radiative lifetimes are between 25% and 60% longer for $v'=0$ –6.

II. EXPERIMENT

The experimental apparatus (see Fig. 1) is a 2 in. diameter discharge-flow reactor configured to allow spectral observations along the flow tube axis. $N_2(A)$ entered the observation vessel from a sidearm normal to the flow tube axis, but parallel with and just in front of the slits of the monochromator used for the spectral measurements. A CaF_2 window sealed the upstream end of the flow tube. The window transmission is nearly uniform over the spec-

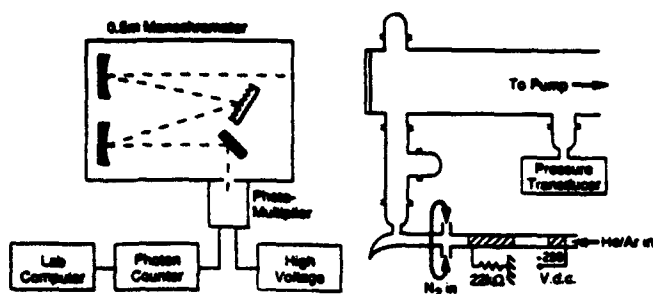


FIG. 1. Discharge-flow reactor for observing $N_2(A^3\Sigma_u^+ - X^1\Sigma_g^+)$ emission.

tral range investigated in these studies 220–500 nm. Small reductions in transmission at the shortest wavelengths were incorporated into the data analysis.

The energy transfer reaction between metastable $Ar^*(^3P_{0,2})$ and N_2 (Refs. 13 and 14) generated $N_2(A)$. This reaction produces $N_2(C^3\Pi_u)$ which radiates immediately to the $N_2(B^3\Pi_g)$ state. Subsequent radiative and collisional cascade from $N_2(B)$ makes the highly metastable $N_2(A^3\Sigma_u^+)$. A low-power, hollow-cathode discharge, sustained in a flow of argon or 5%–10% argon in helium produced Ar^* . N_2 mixed with Ar^* downstream from the discharge. Helium bath gas relaxes the vibrational distribution of $N_2(A)$ so that only $v' < 2$ is observed (see Fig. 2). In an argon bath gas, emission from $v' < 4$ is readily observed (see Fig. 3).

A 0.5 m monochromator having a 1200 line mm^{-1} grating blazed at 250 nm collected and dispersed radiation emanating from the flow tube. A thermoelectrically cooled HTV R943-02 photomultiplier tube connected to a photon-counting rate meter and lab computer detected the dispersed radiation.

The relative variation in monochromator response as a function of wavelength was determined from measurements of the spectra emitted from standard D_2 (180–400 nm) and quartz-halogen lamps (280–500 nm) (Op

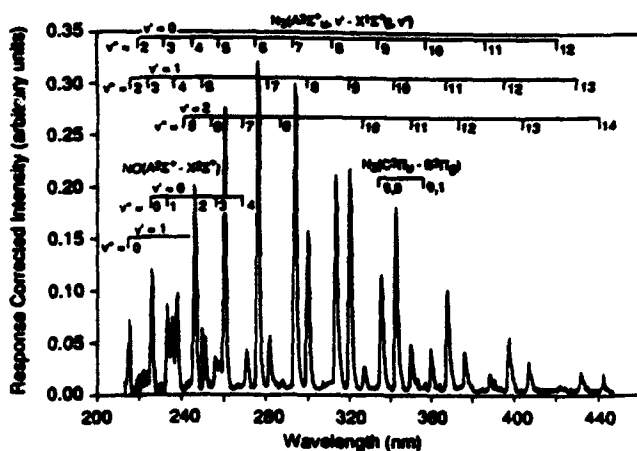


FIG. 2. Emission between 215 and 450 nm from $N_2(A)$ in helium. Note that the 0,1 band of the $N_2(C-B)$ system is barely visible at 358 nm.

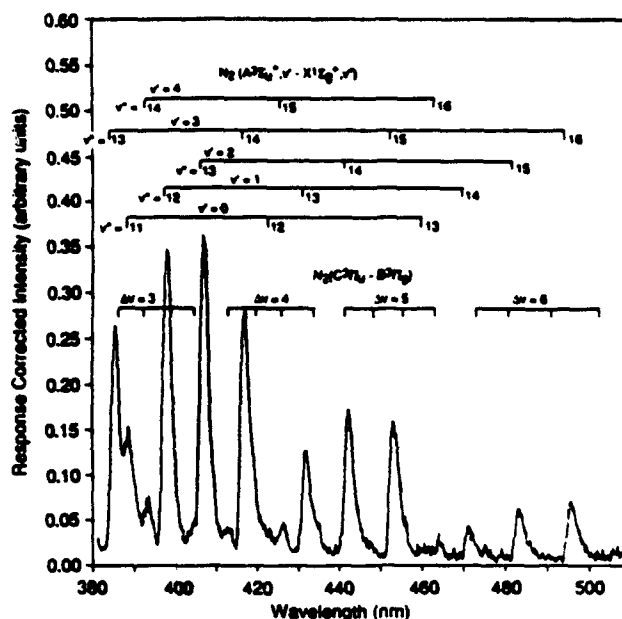


FIG. 3. Emission between 380 and 500 nm from $N_2(A)$ in argon.

Laboratories). The lamp output was reflected into the monochromator off a uniformly scattering, diffuse white target (Spectralon). This procedure ensured that the monochromator optics were filled and eliminated possible errors resulting from such things as nonuniformities in reflectivity across the face of the grating or in sensitivity across the face of the photomultiplier. The two lamps gave congruent response functions (within 5%) over the spectral region common to them both, 280–400 nm.

Most of the spectra were generated at conditions that minimized, as much as possible, interfering emissions from the nitrogen second-positive bands $N_2(C^3\Pi_u - B^3\Pi_g)$ and the NO gamma bands $NO(A^2\Sigma^+ - X^2\Sigma^-)$. $N_2(A)$ energy pooling reactions generate the second-positive emission¹⁵ while the energy transfer reaction between $N_2(A)$ and NO excites the gamma bands.⁷ The hollow cathode discharge makes small number densities of NO from the impurities in the gases used. The advantage of the axial observation configuration is that band intensity measurements with good signal to noise ratio can be made with $N_2(A)$ number densities sufficiently low that $N_2(C^3\Pi_u)$ production from $N_2(A)$ energy pooling is relatively minor, and at total pressures low enough to keep NO production rates in the d.c. discharge small.

A spectral fitting procedure we have detailed previously⁹ aided data analysis. Synthetic spectra are generated by first multiplying a set of vibronic level populations by a set of basis functions representing the intensity of a unit population of each vibronic level as a function of wavelength. The intensities of each band at each wavelength increment are then summed to determine an overall spectral intensity. A least squares solution determines the set of vibronic level populations giving a predicted spectrum that best matches the experimental one. The important spectral features between 200 and 500 nm are the nitrogen Vegard-

Kaplan bands $N_2(A^3\Sigma_u^+-X^1\Sigma_g^+)$, nitrogen second-positive bands $N_2(C^3\Pi_u-B^3\Pi_g)$, and nitric oxide gamma bands $NO(A^2\Sigma^+-X^2\Pi)$.

To generate synthetic spectra, we used the spectroscopic constants of Roux *et al.*^{16,17} for the A and B electronic states of N_2 , those in Lofthus and Krupenie¹⁸ for the C and X states of N_2 , and those tabulated in Huber and Herzberg¹⁹ for NO A and X . Einstein coefficients used in the fit were from Lofthus and Krupenie for $N_2(C-B)$ (Ref. 18) and Piper and Cowles for $NO(A-X)$.²⁰ We calculated a set of Franck-Condon factors and r centroids for $N_2(A-X)$ using procedures we have outlined previously.²¹ These Franck-Condon factors are quite similar to those calculated by Benesch *et al.*⁵ which are tabulated in Lofthus and Krupenie.¹⁸

III. TRANSITION MOMENT VARIATIONS

Our data analysis is based on the r -centroid approximation as first described by Fraser²² and developed by Nicholls²³ and McCallum.²⁴ The intensity of radiative emission from an electronic transition is given by the product of the upper state number density and the Einstein coefficient for spontaneous radiation

$$I_{\nu'\nu''} = N_{\nu'} A_{\nu'\nu''}. \quad (1)$$

The Einstein coefficient $A_{\nu'\nu''}$ can be written as

$$A_{\nu'\nu''} = \frac{64\pi^3}{3h} q_{\nu'\nu''} \nu_{\nu'\nu''}^3 |R_e(\bar{r}_{\nu'\nu''})|^2, \quad (2)$$

where $q_{\nu'\nu''}$ is the Franck-Condon factor for the transition; $\nu_{\nu'\nu''}$ is the transition frequency in cm^{-1} ; $R_e(\bar{r})$ is the electronic transition moment, a function of internuclear separation; and $\bar{r}_{\nu'\nu''}$ is the r centroid of the transition, an average internuclear separation for the transition. Determining Einstein coefficients requires that the variation in the transition moment as a function of internuclear separation be established over the range of important transitions and that the absolute value of the transition moment be determined for at least one point.

Relative variations in the transition moment function usually can be determined over a wide range of internuclear separations from measurements of relative band intensities in a progression from a common upper level. Dividing the measured band intensities by $q_{\nu'\nu''} \nu_{\nu'\nu''}^3$ results in reduced intensities that are a function only of the square of the transition moment

$$\frac{I_{\nu'\nu''}}{q_{\nu'\nu''} \nu_{\nu'\nu''}^3} = \kappa N_{\nu'} |R_e(\bar{r}_{\nu'\nu''})|^2, \quad (3)$$

where $\kappa = 64\pi^3/3h$. The form of the transition moment function is then given by a fit of the square roots of the reduced intensities to their corresponding r centroids which are, in essence, effective internuclear separations at which each transition occurs.

The relative function often can be normalized so that the sum of Einstein coefficients in a progression yield the reciprocal of the radiative lifetime of the state under investigation. In the present case, no accurate lifetime measure-

ments of the A state of nitrogen exist. What is available is Carleton and Oldenberg's³ determination of the Einstein coefficient of the 0,6 band of $N_2(A)$ as reanalyzed by Shemansky and Carleton² and corrected here for the improved value of the $N_2(B-A)$ Einstein coefficient.

Another method for obtaining absolute transition moment values is from oscillator strengths determined from absorption measurements. The transition moment in this case is given by

$$R_e(\bar{r}_{\nu'\nu''}) = \left(\frac{f_{\nu'\nu''}}{1.5\kappa q_{\nu'\nu''} \nu_{\nu'\nu''}} \right)^{1/2}. \quad (4)$$

Shemansky measured a set of oscillator strengths for the absorptions from $\nu''=0$ of the X state to $\nu'=5-12$ of the A state. These values can be converted to transition moments over the range of internuclear separations between 1.084 and 1.129 Å.

Our measurements of relative intensities of bands in four different progressions of the Vegard-Kaplan band system establish the shape of the transition moment function. Shemansky and Carleton's Einstein coefficient for the 0,6 band normalizes our data to give an absolute transition moment function for internuclear separations between 1.22 and 1.48 Å. Finally, combining our normalized data with the results of Shemansky's absorption measurements results in a transition moment function covering the range of internuclear separations between 1.08 and 1.48 Å.

IV. RESULTS

We fit our spectra in a number of segments each containing no more than one Vegard-Kaplan emission band from each of the progressions emanating from $\nu'=0-3$. Figures 2 and 3 show two of the spectra we took for this study, while Figs. 4 and 5 show small spectral segments to illustrate the fitting procedure. The spectral fits give relative intensities within each progression. Dividing these relative intensities by the product $q_{\nu'\nu''} \nu_{\nu'\nu''}^3$ converted them to a set of reduced intensities covering a range of wavelengths, or equivalently, r centroid values. The square root of the reduced intensities vary from one another with changes in r centroid in the same fashion that the transition moment function varies as a function of internuclear separation. Our data set consisted of the transitions $\nu'=0$ to $\nu''=2-13$; $\nu'=1$ to $\nu''=4, 5, 7-14$; $\nu'=2$ to $\nu''=6-8, 10-15$; and $\nu'=3$ to $\nu''=13-16$.

Our data fitting procedure involved fitting the data from just one of the progressions first. A quadratic function represented the data adequately. The other progressions were then normalized by the factor that resulted in the smallest sum of the squares of the relative residuals between the data and the initial quadratic function. The relative residual is

$$\chi = \frac{|R_e|_{fit} - |R_e|_{measured}}{|R_e|_{fit}}. \quad (5)$$

We then refit this combined data set to a new quadratic function and then renormalized the reduced intensities in each progression to minimize again the sum of squares of

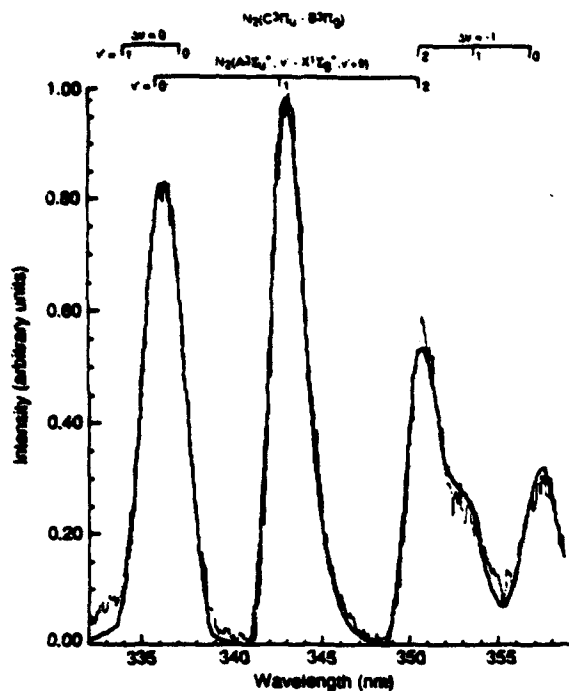


FIG. 4. $N_2(A^3\Sigma_u^+ - X^1\Sigma_g^-)$, $\Delta v = -9$ sequence in argon carrier. The contribution of the $N_2(C^3\Pi_u, v' = 0 - B^3\Pi_g, v'' = 0)$ band to the $N_2(A, v' = 0 - X, v'' = 9)$ band at 337 nm can be removed in the spectral fitting analysis by including the $N_2(C, v' = 0 - B, v'' = 1)$ band at 357 nm in the spectral fit. The light line represents the data and the heavy line the spectral fit.

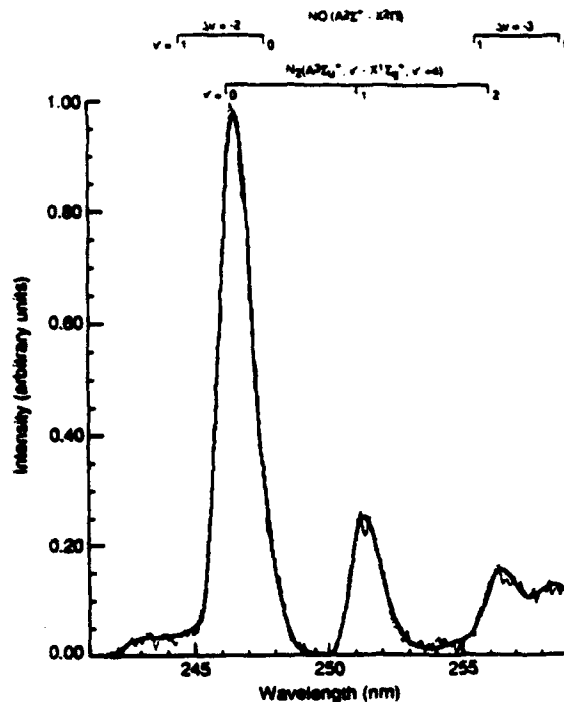


FIG. 5. $N_2(A^3\Sigma_u^+ - X^1\Sigma_g^-)$, $\Delta v = -4$ sequence in helium. Extending the fit to 259 nm includes enough of the $NO(A^2\Sigma^+, v' = 0 - X^2\Pi, v'' = 3)$ band to allow an accurate assessment of the contribution of the $NO(A, v' = 0 - X, v'' = 2)$ band to the emission at 246 nm which is primarily the $N_2(A, v' = 0 - X, v'' = 4)$ band.

the residuals between the renormalized data and the new quadratic function. After several iterations, the renormalization procedure failed to improve the sum of squares of the residuals to any significant extent.

We then established absolute values for our relative data by multiplying each point by the factor necessary to make the value of the relative transition moment function at 1.294 Å, the r centroid for the 0,6 transition, equal to the value determined in Shemansky's reanalysis of Carleton and Oldenberg's measurement of the 0,6 Einstein coefficient, i.e., 0.0901 s^{-1} . This value has been corrected for the updated value of the $N_2(B, v' = 1 - A, v'' = 0)$ transition probability. Finally, combining our absolute values with absolute transition moment values calculated from Shemansky's oscillator strength measurements determined the transition moment function between 1.084 and 1.476 Å.

Figure 6 shows the fit of these two sets of transition moment values. The data quite nicely fit the function

$$R_e(r) = 0.00443 - 0.00582r + 0.00175r^2, \quad (6)$$

where R_e is in units of Debye and r is in Angstroms. Table I lists the Einstein coefficients calculated from the transition moment function represented by Eq. (6). Table I also lists the other spectroscopic properties—Franck-Condon factors, r centroids, and band origins.

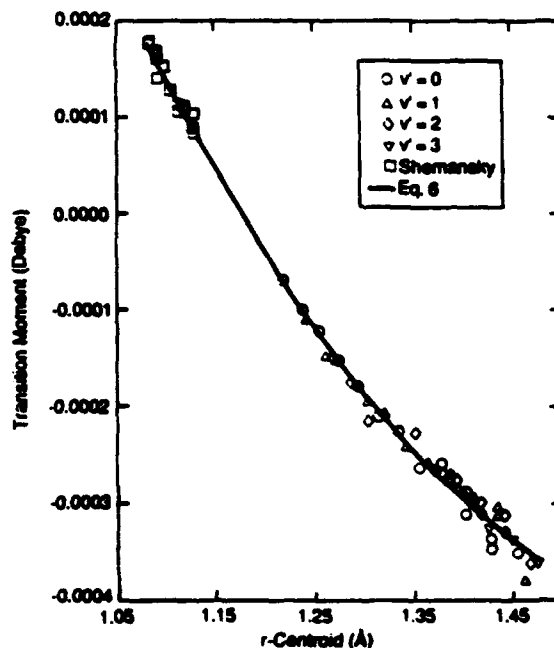


FIG. 6. Electronic transition moment data and the associated quadratic least squares fit [Shemansky (Ref. 1)].

TABLE I. $N_2(A^3\Sigma_u^+ - X^1\Sigma_g^+)$ Einstein coefficients.

v'	v''	Wave-length (nm)	$q_{v',v''}$	r centroid (Å)	Branching ratio	$A_{v',v''}$ (s^{-1})
0	0	200.99	0.000 97	1.185	0.000 02	0.000 008
	1	210.86	0.008 00	1.202	0.001 18	0.000 499
	2	221.61	0.031 94	1.219	0.010 77	0.004 544
	3	233.37	0.079 16	1.237	0.044 31	0.018 705
	4	246.26	0.139 70	1.255	0.107 40	0.045 332
	5	260.47	0.184 50	1.274	0.176 88	0.074 662
	6	276.20	0.190 50	1.294	0.212 22	0.089 579
	7	293.70	0.157 30	1.314	0.190 26	0.080 308
	8	313.28	0.106 40	1.335	0.133 87	0.056 506
	9	335.34	0.059 19	1.356	0.073 91	0.031 197
	10	360.36	0.027 42	1.379	0.033 11	0.013 976
	11	388.97	0.010 50	1.402	0.011 77	0.004 968
	12	422.00	0.003 30	1.428	0.003 36	0.001 419
	13	460.54	0.000 87	1.455	0.000 77	0.000 327
	14	506.07	0.000 20	1.479	0.000 15	0.000 063
	15	560.66	0.000 04	1.499	0.000 02	0.000 010
	16		0.000 01	1.533	0.000 00	0.000 001
Sum = 1.000 00			Lifetime = 2.37 s			
1	0	195.36	0.005 18	1.175	0.000 00	0.000 002
	1	204.68	0.031 85	1.191	0.001 94	0.000 734
	2	214.79	0.087 25	1.208	0.020 42	0.007 714
	3	225.81	0.131 20	1.225	0.059 93	0.022 636
	4	237.87	0.111 60	1.242	0.076 36	0.028 844
	5	251.10	0.040 87	1.260	0.037 04	0.013 991
	6	265.68	0.000 03	1.281	0.000 04	0.000 014
	7	281.84	0.036 47	1.303	0.048 48	0.018 311
	8	299.82	0.109 80	1.322	0.153 20	0.057 869
	9	319.96	0.150 10	1.342	0.212 26	0.080 179
	10	342.66	0.134 70	1.364	0.188 35	0.071 145
	11	368.44	0.088 84	1.387	0.118 70	0.044 839
	12	397.94	0.045 35	1.410	0.055 67	0.021 030
	13	432.03	0.018 46	1.435	0.020 27	0.007 657
	14	471.85	0.006 10	1.461	0.005 78	0.002 185
	15	518.97	0.001 67	1.487	0.001 31	0.000 497
	16	575.56	0.000 38	1.513	0.000 24	0.000 090
Sum = 0.999 85			Lifetime = 2.65 s			
2	0	190.14	0.014 76	1.164	0.000 86	0.000 298
	1	198.95	0.065 13	1.180	0.000 33	0.000 114
	2	208.50	0.113 30	1.197	0.013 85	0.004 807
	3	218.87	0.082 21	1.213	0.026 21	0.009 097
	4	230.17	0.011 24	1.227	0.005 69	0.001 976
	5	242.54	0.014 83	1.254	0.014 18	0.004 921
	6	256.12	0.077 37	1.269	0.086 41	0.029 990
	7	271.10	0.081 23	1.287	0.104 65	0.036 319
	8	287.70	0.021 88	1.304	0.030 16	0.010 466
	9	306.20	0.003 70	1.340	0.006 38	0.002 213
	10	326.92	0.062 30	1.352	0.098 59	0.034 218
	11	350.30	0.127 80	1.372	0.193 91	0.067 299
	12	376.86	0.138 00	1.394	0.196 55	0.068 217
	13	407.30	0.100 50	1.418	0.131 09	0.045 498
	14	442.51	0.053 90	1.442	0.062 01	0.021 522
	15	483.69	0.022 29	1.468	0.021 97	0.007 627
	16	532.49	0.007 28	1.495	0.005 93	0.002 058
	17	591.20	0.001 91	1.524	0.001 23	0.000 428
Sum = 0.999 63			Lifetime = 2.88 s			
3	0	185.29	0.030 14	1.155	0.006 30	0.002 032
	1	193.65	0.093 36	1.170	0.001 39	0.000 450
	2	202.68	0.091 09	1.186	0.002 99	0.000 963
	3	212.46	0.015 29	1.200	0.002 47	0.000 797
	4	223.10	0.015 21	1.224	0.008 11	0.002 617
	5	234.70	0.072 27	1.239	0.055 27	0.017 831
	6	247.39	0.045 87	1.255	0.045 50	0.014 682
	7	261.34	0.000 04	1.276	0.000 06	0.000 018

TABLE I. (Continued.)

v'	v''	Wave-length (nm)	$q_{v',v''}$	r centroid (Å)	Branching ratio	$A_{v',v''}$ (s^{-1})
4	8	276.73	0.042 17	1.297	0.063 81	0.020 587
	9	293.80	0.080 66	1.314	0.127 50	0.041 135
	10	312.83	0.036 47	1.332	0.058 46	0.018 861
	11	334.17	0.000 12	1.357	0.000 19	0.000 062
	12	358.26	0.046 25	1.382	0.075 98	0.024 514
	13	385.66	0.116 60	1.403	0.176 51	0.056 950
	14	417.09	0.134 20	1.426	0.183 12	0.059 081
	15	453.48	0.098 84	1.450	0.117 92	0.038 045
	16	496.10	0.052 19	1.476	0.052 90	0.017 066
	17	546.68	0.020 85	1.503	0.017 31	0.005 584
	18	607.65	0.006 47	1.532	0.004 23	0.001 365
Sum = 0.998 09			Lifetime = 3.10 s			
5	0	180.77	0.048 55	1.146	0.023 65	0.007 298
	1	188.71	0.099 80	1.161	0.010 45	0.003 226
	2	197.28	0.041 69	1.176	0.000 00	0.000 000
	3	206.54	0.002 79	1.201	0.000 56	0.000 171
	4	216.58	0.058 74	1.211	0.019 52	0.006 026
	5	227.49	0.041 21	1.226	0.023 41	0.007 226
	6	239.40	0.000 37	1.246	0.000 34	0.000 104
	7	252.44	0.048 71	1.265	0.059 03	0.018 220
	8	266.77	0.053 12	1.281	0.073 26	0.022 610
	9	282.60	0.002 30	1.303	0.003 72	0.001 147
	10	300.16	0.030 80	1.325	0.054 20	0.016 729
	11	319.75	0.076 34	1.342	0.132 38	0.040 859
	12	341.74	0.037 68	1.361	0.063 42	0.019 575
	13	366.58	0.000 08	1.387	0.000 13	0.000 039
	14	394.86	0.047 13	1.413	0.073 76	0.022 764
	15	427.33	0.117 70	1.434	0.162 64	0.050 199
	16	464.97	0.131 50	1.458	0.157 53	0.048 620
	17	509.12	0.092 46	1.484	0.093 31	0.028 799
	18	561.59	0.045 96	1.512	0.037 78	0.011 660
	19	624.95	0.017 03	1.540	0.010 91	0.003 367
Sum = 0.993 96			Lifetime = 3.24 s			
6	0	176.55	0.067 26	1.137	0.062 28	0.018 734
	1	184.12	0.085 52	1.152	0.026 51	0.007 974
	2	192.27	0.006 54	1.163	0.000 49	0.000 148
	3	201.05	0.032 50	1.185	0.001 01	0.000 304
	4	210.55	0.053 13	1.199	0.009 00	0.002 707
	5	220.85	0.000 95	1.215	0.000 38	0.000 113
	6	232.06	0.038 26	1.236	0.029 63	0.008 914
	7	244.29	0.045 01	1.251	0.045 11	0.013 570
	8	257.68	0.000 12	1.270	0.000 16	0.000 048
	9	272.42	0.040 74	1.291	0.063 57	0.019 122
	10	288.71	0.050 86	1.307	0.083 57	0.025 139
	11	306.79	0.002 10	1.311	0.003 02	0.000 909
	12	326.97	0.031 81	1.353	0.058 62	0.017 634
	13	349.64	0.073 47	1.371	0.128 15	0.038 550
	14	375.27	0.030 25	1.389	0.048 76	0.014 667
	15	404.48	0.001 50	1.442	0.002 61	0.000 785
	16	438.05	0.059 04	1.443	0.081 28	0.024 451
	17	477.02	0.124 40	1.467	0.147 11	0.044 252
	18	522.79	0.125 10	1.493	0.123 28	0.037 086
	19	577.27	0.079 99	1.520	0.063 50	0.019 102
	20	644.63	0.035 98	1.549	0.021 97	0.006 609
Sum = 0.984 54			Lifetime = 3.32 s			
7	0	172.61	0.082 11	1.128	0.121 91	0.036 835
	1	179.84	0.057 88	1.143	0.036 69	0.011 085
	2	187.60	0.001 56	1.168	0.000 05	0.000 015
	3	195.96	0.054 52	1.175	0.000 03	0.000 010
	4	204.97	0.016 26	1.187	0.000 72	0.000 216
	5	214.72	0.016 72	1.210	0.005 63	0.001 702
	6	225.29	0.048 19	1.224	0.026 12	0.007 892
	7	236.80	0.001 94	1.228	0.001 09	0.000 328

TABLE I. (Continued.)

v'	v''	Wave-length (nm)	$q_{v',v''}$	r centroid (Å)	Branching ratio	$A_{v',v''}$ (s^{-1})
	8	249.37	0.033 07	1.261	0.039 16	0.011 833
	9	263.15	0.040 04	1.276	0.053 71	0.016 230
	10	278.31	0.000 00	1.297	0.000 01	0.000 002
	11	295.08	0.042 63	1.318	0.074 41	0.022 482
	12	313.70	0.043 60	1.334	0.075 63	0.022 851
	13	334.51	0.000 17	1.358	0.000 31	0.000 094
	14	357.90	0.041 00	1.382	0.071 88	0.021 720
	15	384.37	0.069 43	1.400	0.111 34	0.033 641
	16	414.56	0.017 80	1.417	0.025 21	0.007 617
	17	459.30	0.008 43	1.461	0.011 57	0.003 495
	18	489.67	0.079 97	1.477	0.090 34	0.027 296
	19	537.16	0.132 50	1.502	0.123 30	0.037 255
	20	594.97	0.114 40	1.529	0.084 48	0.025 526
	21	664.60	0.063 93	1.558	0.036 09	0.010 906
	22	751.24	0.025 13	1.589	0.010 33	0.003 120
Sum = 0.849 73						
Lifetime = 3.31 s						

V. DISCUSSION

A. Relative transition moment function comparison

Three other groups have reported relative transition moment functions based on measurements of relative Vegard-Kaplan band intensities.¹⁰⁻¹² We have reanalyzed all three sets of relative intensity measurements because our RKR-based (Rydberg-Klein-Rees) Franck-Condon factors are substantially different from the Franck-Condon factors used by Carleton and Papaliolios¹⁰ and Chandraiah and Shepherd.¹¹ Broadfoot and Maran¹² do not list the Franck-Condon factors they used in their analysis, but since they came from the widely disseminated, albeit unpublished compendium of Albritton *et al.*,²³ they are most likely quite similar to the ones we have calculated.

We find that all three sets of band intensity measurements give relative transition moment values that are consistent with each other. However, they are not at all consistent with our measurements nor, for that matter, with Shemansky's transition moment function. Figure 7 compares the data from these three earlier sets of measurements, normalized to each other at 1.294 Å, to Shemansky's quadratic function and to our functional fit from Eq. (6). The previous measurements all show a slight, but clearly identifiable convex curvature, whereas Shemansky's function and ours are both concave.

The origin of the difference between the earlier data and Shemansky's function is unclear. He depended only on the data of Broadfoot and Maran in the region between 1.27 and 1.43 Å, and Broadfoot and Maran's analysis used Franck-Condon factors that most likely were good ones. Nevertheless, those data and Shemansky's function are of opposite curvature.

The differences between the earlier data and our own must relate to disparate intensity measurements or data analysis. Since we have analyzed all four sets of intensity measurements with a common set of Franck-Condon factors, r centroids, and transition frequencies, the disagree-

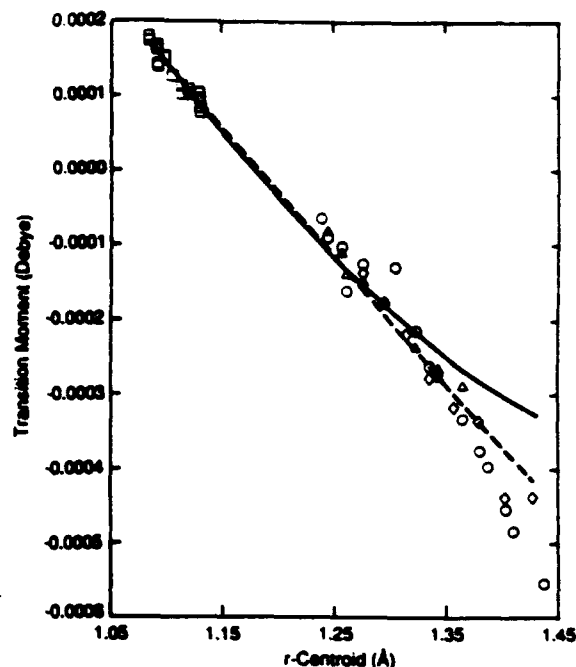


FIG. 7. A comparison of the relative transition moment data of Carleton and Papaliolios (Ref. 10) (Δ), Chandraiah and Shepherd (Ref. 11) (\circ), and Broadfoot and Maran (Ref. 12) (\diamond) with Shemansky's (Ref. 1) transition moment data (\square), his transition moment function (—), and that calculated from Eq. (6) (—). The relative data have been normalized to Shemansky's function at 1.294 Å.

ment must reside either in the intensity measurements themselves or in reducing the actual measured quantities, e.g., the current flowing out of a photomultiplier anode, to physical units, such as photons s^{-1} .

The most common source of measurement error arises in calibrating the spectroscopic measuring system for sensitivity as a function of wavelength. These calibrations involve measuring the spectrum of a lamp whose irradiance is known as a function of wavelength. Because all three of the earlier groups recorded a set of relative band intensities that were compatible with each other, we can assume that they all calibrated their spectroscopic systems with similar standards.

Our calibrations differ from those of the other groups in that our calibration standard was a deuterium lamp between 200 and 400 nm and a quartz-halogen lamp for wavelengths longer than 400 nm. The two sources agreed excellently in the region of spectral overlap 280–400 nm. The other three groups all used a tungsten strip lamp for their irradiance standard. Perhaps the root of the problem lies in these different standards. The deuterium lamp is strictly an ultraviolet standard, whereas the tungsten lamps are very faint at wavelengths shorter than about 300 or 350 nm. Thus, making accurate intensity measurements at the shortest wavelengths is particularly difficult.

A common problem arises in accounting satisfactorily for scattered light within the monochromator. Scattered light generally will lead one to overestimate calibration lamp intensities at the shorter wavelengths. Such an error

will cause band intensity measurements to be undercorrected. As a result, response corrected band intensities at short wavelengths will appear to be smaller with respect to longer wavelength band intensities than is actually the case. Such a trend is consistent with the discrepancies between the earlier data and our own.

In the present case, however, this argument is probably insufficient to rationalize the differences in the various band-intensity measurements. The discrepancies between our data and those of the other groups become most pronounced at the longer wavelengths where the standard lamp calibrations are more likely to be accurate. Another possibility might reside in augmentation of apparent band intensities by overlap with other band systems, primarily the nitrogen second-positive bands which are excited in $N_2(A)$ energy-pooling processes. Although the other groups recognized this problem and tried to apply appropriate corrections, we think our spectral fitting analysis likely accommodates overlapping emissions more accurately.

We are confident our response calibration and data analysis are correct. Using a similar approach to study the $NO(B^2\Pi - X^2\Pi)$ (Ref. 26) and $N_2(B^3\Pi_g - A^3\Sigma_u^+)$ (Ref. 8) band systems, we have determined transition moment functions that match the best available *ab initio* transition moment functions for^{8,27} these band systems to within 5%. In addition, the variation in radiative lifetime with vibrational level calculated from our transition moment functions for these two band systems follows the experimentally determined lifetime variations^{28,29} to within 5%.

B. Absolute transition moment function comparison

Figure 7 also compares our transition moment function with that proposed by Shemansky.¹ The two functions agree fairly well between 1.08 and 1.25 Å, but then begin to diverge as the internuclear distance increases further. As a result of this divergence, band intensity calculations using Einstein coefficients calculated from Shemansky's transition moment function will predict much more radiation at long wavelengths, compared to radiation levels at short wavelengths, than would be the case using Einstein coefficients calculated from our function. This difference amounts to almost a factor of 2 for transitions around 450 nm.

The difference in the shapes of the transition moment functions also results in a much steeper increase in radiative lifetime with increasing vibrational level for lifetimes calculated from our function compared to those reported by Shemansky. Table II compares radiative lifetimes calculated from the two transition moment functions. Our radiative lifetimes are larger than Shemansky's by about 25% for $v'=0$ and the discrepancy increases to almost 60% for $v'=4-6$.

C. Other considerations

Shemansky has shown that the three substates of the $N_2(A)$ state do not all have the same radiative lifetime, or equivalently, each band consists of three degenerate tran-

TABLE II. Radiative lifetimes^a of $N_2(A^3\Sigma_u^+, v)$.

Vibrational level	Present results	Shemansky ^b
0	2.37	1.91
1	2.65	1.97
2	2.88	2.02
3	3.10	2.05
4	3.24	2.08
5	3.32	2.10
6	3.31	2.13

^aUnits of seconds. These values are averaged over all spin substates.

^bReference 1.

sitions not all having the same Einstein coefficient. In most practical cases, the sublevels are in collisional equilibrium, so that each transition has only one effective radiative lifetime. Shemansky's table of Einstein coefficients gives values only for one sublevel. Our Einstein coefficients should be multiplied by a factor of 1.5 for comparison with Shemansky's values. The values in Table I are the average values for the collisionally coupled substates, and therefore need be corrected only for the unusual cases in which the differences in the behavior of the sublevels can be distinguished. Such cases require ambient pressures below about 10^{-7} Torr. For atmospheric applications, this corresponds to altitudes above about 150 km.

Studies aimed at determining product branching ratios in $N_2(A)$ energy transfer reactions generally use Vegard-Kaplan band intensity measurements to determine $N_2(A)$ number densities. Using our Einstein coefficients will result in somewhat larger $N_2(A)$ number densities than are obtained from Shemansky's Einstein coefficients. The larger $N_2(A)$ number densities will translate to smaller excitation rate coefficients or branching ratios. The magnitude of the correction depends on how the Vegard-Kaplan photometry has been accomplished.

In some cases, $N_2(A)$ number densities are determined by observing a single Vegard-Kaplan band, e.g., the 0,6 band for $v'=0$ and the 1,9 or 1,10 bands for $v'=1$. In this case, the appropriate corrections can be determined directly by comparing the Einstein coefficients in Table I with those in Table VI of Shemansky's paper,¹ being sure to apply the factor of 1.5 correction to put the two sets on a common basis.

In our work, we usually use spectral fitting techniques to determine the $N_2(A)$ number densities. The discrepancies in number densities calculated using the two different Einstein coefficient sets will then depend on the range in wavelengths over which the Vegard-Kaplan spectra have been fit. Fits over the wavelength range between 200 and 260 nm using the two different sets of transition probabilities will give $N_2(A, v'=0,1,2)$ number densities that differ from each other by less than 10%. On the other hand, fits between 400 and 500 nm will result in number densities of $N_2(A, v=0)$ 45%–50% and $N_2(A, v'=1,2,3)$ almost 60% larger using our Einstein coefficients instead of Shemansky's.

The more normal situation is for the Vegard-Kaplan spectra to begin between 220 and 250 nm and extend to

between 370 and 400 nm. In this situation, our transition probabilities will give number densities for $N_2(A, v'=0)$ 15%–20%, $N_2(A, v'=1)$ 25%–35%, and $N_2(A, v'=2)$ 40%–50% larger than those calculated from Shemansky's transition probabilities. Given a typical vibrational distribution of 1:0.6:0.2 for $v'=0,1,2$, respectively, as calculated using Shemansky's Einstein coefficients, overall $N_2(A)$ number densities will be about 25% larger if calculated using our transition probabilities. This will result in product excitation rate coefficients or branching ratios^{7,30–35} about 25% smaller than published values. In the case of $N_2(A)$ energy-pooling studies,^{15,36} where the square of the $N_2(A)$ number density is important, the rate coefficients will decrease by about 50%. If state specific product measurements have been made, then the product formation rate coefficients have to be corrected appropriately for the individual vibrational levels.

For example, the current studies were initiated because we observed a rate coefficient for exciting $NO(A)$ by $N_2(A, v'=0)$ that was about 40% greater than the total rate coefficient for $N_2(A, v'=0)$ quenching by NO .⁷ This discrepancy initially led us to suspect a problem with the Einstein coefficients of either the nitrogen first-positive or the Vegard–Kaplan systems. Our current results indicate that $N_2(A)$ number densities in our study of the excitation of $NO(A)$ by $N_2(A)$ were underestimated by about 20%. Using the Einstein coefficients in Table I to correct the earlier results makes the rate coefficient for $NO(A)$ excitation by $N_2(A)$ $(8.3 \pm 2.5) \times 10^{-11} \text{ cm}^3 \text{ molecule}^{-1} \text{ s}^{-1}$, which is more in accord with the rate coefficient for $N_2(A)$ quenching by NO $(6.6 \pm 1.0) \times 10^{-11} \text{ cm}^3 \text{ molecule}^{-1} \text{ s}^{-1}$ although still, annoyingly, 25% larger.

Those studies also indicated that $N_2(A, v'=1)$ excited $NO(A)$ 22% more rapidly than does $N_2(A, v'=0)$. Correcting these results for our Einstein coefficients results in only an 8% increased efficiency for $N_2(A, v'=1)$. This difference is smaller than the experimental uncertainty in the measurements. On the other hand, $N_2(A, v'>2)$ was determined to be only 55% as efficient at exciting $NO(A)$ as $N_2(A, v'=0)$. Correcting this ratio will reduce this number to 45%.

Subsequent to the $N_2(A)/NO$ work, we and others^{31–33} noted excess product formation in several other $N_2(A)$ energy transfer systems in which the $N_2(A)$ number densities were determined by $N_2(A)$ Vegard–Kaplan emission. In most instances, correcting the previous results with our Einstein coefficients is insufficient to resolve these discrepancies. This problem appears more to result from an addi-

tional, so far unobserved metastable produced in the energy transfer reaction between $Ar^*(^3P_{2,0})$ and N_2 .

ACKNOWLEDGMENTS

We appreciate financial support from the Air Force Office of Scientific Research (Task 2310G4) and the Defence Nuclear Agency (Project SA, Task SA/SDI, work unit 00175) through a contract with the Phillips Laboratory/Geophysics Directorate F19628-88-C-013.

- ¹D. E. Shemansky, *J. Chem. Phys.* **51**, 689 (1969).
- ²D. E. Shemansky and N. P. Carleton, *J. Chem. Phys.* **51**, 682 (1969).
- ³N. P. Carleton and O. Oldenberg, *J. Chem. Phys.* **36**, 3460 (1967).
- ⁴D. E. Shemansky and A. Vallance Jones, *Planet. Space Sci.* **16**, 1115 (1968).
- ⁵W. Benesch, J. T. Vanderslice, S. G. Tilford, and P. G. Wilkinson, *Astrophys. J.* **143**, 408 (1966).
- ⁶M. Jeunehomme, *J. Chem. Phys.* **45**, 1805 (1966).
- ⁷L. G. Piper, L. M. Cowles, and W. T. Rawlins, *J. Chem. Phys.* **85**, 3369 (1986).
- ⁸H. J. Werner, J. Kalcher, and E. A. Reinsch, *J. Chem. Phys.* **81**, 2420 (1984).
- ⁹L. G. Piper, K. W. Holtzclaw, B. D. Green, and W. A. M. Blumberg, *J. Chem. Phys.* **90**, 5337 (1989).
- ¹⁰N. P. Carleton, and C. Papaliolios, *J. Quant. Spectrosc. Radiat. Transfer* **2**, 241 (1962).
- ¹¹G. Chandraiah and G. G. Shepherd, *Can. J. Phys.* **46**, 221 (1968).
- ¹²A. L. Broadfoot and S. P. Maran, *J. Chem. Phys.* **51**, 678 (1969).
- ¹³D. H. Stedman and D. W. Setser, *Chem. Phys. Lett.* **2**, 542 (1968).
- ¹⁴D. W. Setser, D. H. Stedman, and J. A. Coxon, *J. Chem. Phys.* **53**, 1004 (1970).
- ¹⁵L. G. Piper, *J. Chem. Phys.* **88**, 231 (1988).
- ¹⁶C. Effantin, C. Amiot, and J. Verges, *J. Mol. Spectrosc.* **76**, 221 (1979).
- ¹⁷F. Roux, F. Michaud, and J. Verges, *J. Mol. Spectrosc.* **97**, 253 (1983).
- ¹⁸A. Lofthus and P. Krupenie, *J. Phys. Chem. Ref. Data* **6**, 113 (1977).
- ¹⁹K. P. Huber and G. Herzberg, *Constants of Diatomic Molecules* (Van Nostrand Reinhold, New York, 1977).
- ²⁰L. G. Piper and L. M. Cowles, *J. Chem. Phys.* **85**, 2419 (1986).
- ²¹W. J. Marinelli and L. G. Piper, *J. Quant. Spectrosc. Radiat. Transfer* **34**, 121 (1985).
- ²²P. A. Fraser, *Can. J. Phys.* **32**, 515 (1954).
- ²³R. W. Nicholls, *J. Quant. Spectrosc. Radiat. Transfer* **14**, 233 (1974).
- ²⁴J. C. McCallum, *J. Quant. Spectrosc. Radiat. Transfer* **21**, 563 (1979).
- ²⁵D. L. Albritton, A. L. Schmeltekopf, and R. N. Zare (unpublished, 1971).
- ²⁶L. G. Piper, T. R. Tucker, and W. P. Cummings, *J. Chem. Phys.* **94**, 7667 (1991).
- ²⁷S. R. Langhoff, H. Partridge, R. W. Bauschlicher, and A. Komornicki, *J. Chem. Phys.* **94**, 6638 (1991).
- ²⁸G. E. Gadd and T. G. Slanger, *J. Chem. Phys.* **92**, 2194 (1990).
- ²⁹E. E. Eyler and F. M. Pipkin, *J. Chem. Phys.* **79**, 3654 (1983).
- ³⁰M. E. Fraser and L. G. Piper, *J. Phys. Chem.* **93**, 1107 (1989).
- ³¹L. G. Piper, *J. Chem. Phys.* **90**, 7087 (1989).
- ³²T. D. Dreiling and D. W. Setser, *Chem. Phys. Lett.* **74**, 211 (1980).
- ³³L. G. Piper, W. J. Marinelli, W. T. Rawlins, and B. D. Green, *J. Chem. Phys.* **83**, 5602 (1985).
- ³⁴L. G. Piper, *J. Chem. Phys.* **77**, 2373 (1982).
- ³⁵L. G. Piper, *J. Chem. Phys.* **91**, 864 (1989).
- ³⁶L. G. Piper, *J. Chem. Phys.* **88**, 6911 (1988).

APPENDIX H

Energy Transfer Studies of $N_2(X^1\Sigma_g^+, v)$ and $N_2(B^3\Pi_g)$

L.G. Piper

J. Chem. Phys. 97, 270 (1992)

(SR-467 reproduced in its entirety)

THIS PAGE INTENTIONALLY LEFT BLANK

Energy transfer studies on $N_2(X^1\Sigma_g^+, v)$ and $N_2(B^3\Pi_g)$

Lawrence G. Piper

Physical Sciences Inc., 20 New England Business Center, Andover, Massachusetts 01810

(Received 25 March 1991; accepted 20 March 1992)

We have developed a novel discharge-flow technique for studying the quenching of $N_2(X^1\Sigma_g^+, v'' > 5)$ and $N_2(B^3\Pi_g)$ by a variety of molecules. The technique involves adding small number densities of $N_2(A^3\Sigma_u^+)$ to a flow of $N_2(X, v)$ producing, thereby, $N_2(B)$. By comparing $N_2(B)$ fluorescence intensities generated when a quencher is added to the $N_2(X, v)$ flow 2–3 ms before $N_2(A)$ addition with intensities observed after the $N_2(X, v)$ and quencher have been mixed for times of 10–30 ms, we can separate the effects of $N_2(B)$ fluorescence quenching from effects of $N_2(X, v)$ quenching. Our results indicate that CH_4 , CO_2 , CO , O_2 , and N_2O quench $N_2(B)$ at rates approaching gas kinetic while H_2 , N_2 , SF_6 , and CF_4 are about ten times slower. Rate coefficients for $N_2(X, v'' > 5)$ quenching by H_2 and N_2 are on the order of 10^{-15} cm³ molecule⁻¹ s⁻¹, those for CO_2 , CH_4 , and CF_4 roughly an order of magnitude faster, and CO and N_2O yet another order of magnitude faster.

I. INTRODUCTION

We have developed a technique for determining global quenching rate coefficients for $N_2(X, v'')$ in vibrational levels $v'' > 5$. This technique involves monitoring nitrogen first-positive fluorescence, $N_2(B^3\Pi_g - A^3\Sigma_u^+)$, excited in the energy transfer reaction between $N_2(A)$ and $N_2(X, v'')$. The first-positive emission intensity is proportional to the number density of $N_2(X, v'')$.¹ Molecules added to the reactor can quench both the $N_2(X, v'')$ and the first-positive emission. This paper describes techniques for separating the two processes.

Vibrationally excited, ground-electronic state nitrogen plays an important role in a number of areas including laser excitation,² discharge physics,³ semiconductor processing,⁴ and upper atmospheric chemistry.⁵ Determining the role of $N_2(X, v)$ in these various processes is difficult, however, due to $N_2(X, v)$'s diabolical resistance to detection. A number of laser-based techniques for detecting $N_2(X, v)$ have been developed in recent years,^{6–8} but these techniques tend to be prohibitively expensive for most budgets, insensitive ($\geq 10^{14}$ molecules cm⁻³), or they defy ready quantification. The technique we have developed is sensitive ($\geq 10^{11}$ molecules cm⁻³) and easy to implement. Although our approach cannot quantify $N_2(X, v)$ number densities exactly, it can specify them within factors of 2 or 3.

II. EXPERIMENT

These experiments used the 4.6 cm i.d., quartz, discharge-flow reactor we have described in detail previously¹ (see Fig. 1). Briefly, the $N_2(X, v'')$ is generated in a microwave discharge through a flowing mixture of nitrogen dilute in helium. The effluents from the discharge pass through a nickel screen prior to entering the upstream end of the flow reactor. The screen removes the atoms and deactivates electronically excited metastables, but has relatively little effect on vibrationally excited N_2 .

$N_2(A)$ enters at the downstream end of the flow reactor through an axial injector. The $N_2(A)$ is prepared in a side

arm off the flow tube from the reaction between metastable $Ar(^3P_{2,0})$ and N_2 .^{7,8} A hollow cathode, dc discharge in a flow of a few percent Ar in He makes the $Ar(^3P_{2,0})$. Nitrogen intercepts the argon metastables just after they flow out from the cathode. A loop injector that can be moved along the length of the flow tube adds the quenching reagent.

A monochromator sensitive to radiation between 200 and 900 nm detects emissions diagnostic of $N_2(X, v'')$ and $N_2(A)$. The important spectral features are the N_2 first-positive bands, $N_2(B^3\Pi_g - A^3\Sigma_u^+)$ between 560 and 900 nm, excited in the $N_2(A)$ plus $N_2(X, v'')$ energy-transfer reaction, and the N_2 Vegard-Kaplan bands, $N_2(A^3\Sigma_u^+ - X^1\Sigma_g^+)$, between 250 and 370 nm. The $N_2(X, v'')$ number density is proportional to the ratio of the first-positive to Vegard-Kaplan intensities.¹ A least-squares, spectral fitting procedure, that we have described in some detail previously,⁹ determines band intensities from the spectra.

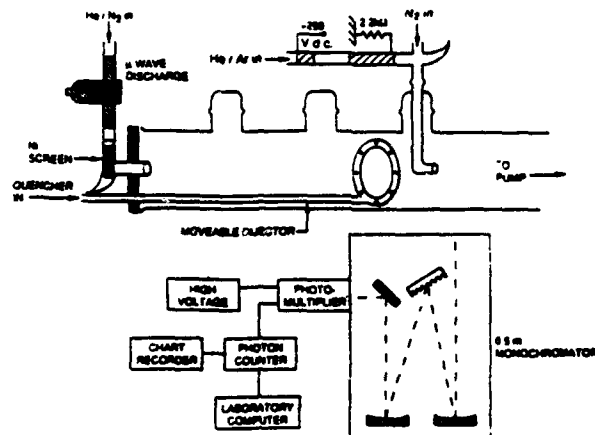


FIG. 1. Discharge-flow reactor for studying $N_2(B)$ and $N_2(X, v)$ quenching.

III. EXPERIMENTAL TECHNIQUE

When quencher is injected immediately behind the N₂ (*A*) inlet, the number density of N₂ (*X*, *v*^{*}) remains essentially unchanged. This is because vibrational quenching is a relatively slow process ($k_q \lesssim 10^{-14}$ cm³ molecule⁻¹ s⁻¹) and reagents are mixed for too short a time (≈ 2 ms) to effect significant quenching. Any diminution in the first-positive emission, therefore, results from quenching N₂ (*B*), or, in some cases, N₂ (*A*). Injecting the reagent into the upstream end of the flow reactor allows adequate time (~ 10 – 30 ms) for some of the N₂ (*X*, *v*^{*}) to be quenched, unless its quenching rate coefficients are exceedingly small. Any difference in diminution of the first-positive emission with the injector in the upstream position as compared to the downstream position can be attributed to quenching of the N₂ (*X*, *v*^{*}) by added reagent.

These concepts are described mathematically as follows. In the absence of added quencher, the intensity of the N₂ first-positive emission is given by¹

$$I_0 = k_r [N_2(B)] = k_{ex} [N_2(X, v^*)] [N_2(A)], \quad (1)$$

where, k_{ex} is the rate coefficient for N₂ (*B*, *v*^{*} > 1) excitation in the reaction between N₂ (*A*) and N₂ (*X*, *v*^{*}), 3.5×10^{-11} cm³ molecule⁻¹ s⁻¹ (see below), and k_r is the N₂ (*B*) radiative decay rate, taken here for the global measurements to be 1.5×10^5 s⁻¹.⁹ These experiments were run at low pressures (~ 1 Torr), primarily of helium. This reduces bath-gas quenching of N₂ (*B*) in the flow tube to less than a 20% effect.¹⁰ We have neglected bath-gas quenching, therefore, in Eq. (1).

When the quencher is introduced into the flow reactor with the injector in the downstream position, the first-positive emission intensity is given by

$$I = k_r [N_2(B)] = \frac{k_{ex} [N_2(A)] [N_2(X, v^*)]}{1 + k_Q [Q] / k_r}, \quad (2)$$

where k_Q is the rate coefficient for N₂ (*B*) quenching by the quencher *Q*. For the moment we ignore quenching of the N₂ (*A*). Taking the ratio of the first-positive intensity in the absence of quencher to that in the presence of quencher gives the classical Stern–Volmer formula¹¹ for electronic quenching, viz.,

$$\Gamma = I_0 / I = 1 + k_Q [Q] / k_r. \quad (3)$$

The rate coefficient for N₂ (*B*) quenching is given, therefore, by the product of the N₂ (*B*) radiative decay rate times the slope of a plot of Γ vs $[Q]$ for data taken with the injector in the downstream position.

With the injector in the upstream position, quenching of the N₂ (*X*, *v*^{*}) also becomes possible, and the first-positive emission intensity becomes

$$I = k_r [N_2(B)] = \frac{k_{ex} [N_2(A)] [N_2(X, v^*)]_0 e^{-k_q [Q] \Delta t}}{1 + k_Q [Q] / k_r}, \quad (4)$$

where k_q is the rate coefficient for N₂ (*X*, *v*^{*}) quenching, Δt is the time the quencher and the N₂ (*X*, *v*^{*}) are mixed, and the subscript *o* refers to conditions in the absence of added

quencher. The N₂ (*X*, *v*^{*}) quenching rate coefficients can be determined, therefore, from the natural log of the ratio of Stern–Volmer factors, Γ , at long to short delay times divided by quencher number density and reaction time:

$$k_q = \frac{\ln(\Gamma_u / \Gamma_d)}{[Q] \Delta t}, \quad (5)$$

where the subscripts *u* and *d* refer to intensity measurements with the injector in the upstream and downstream positions, respectively.

These formalisms presume that the added N₂ (*A*) is not diminished upon injecting the quencher. This is not necessarily always the case. When the *A* state also is quenched, the actual *A*-state number density must be determined by measuring Vegard–Kaplan intensities for each set of experimental conditions, and then divided into the corresponding first-positive intensities. This procedure corrects for *A*-state quenching, and therefore makes this technique applicable for studies of quenchers which react rather efficiently with N₂ (*A*), e.g., N₂O. Because of the rather short time that N₂ (*A*) is actually in the flow reactor before the fluorescence is observed, *A*-state quenching generally is not large even for efficient *A*-state quenchers.

IV. RESULTS

Figure 2 shows typical spectra generated in the quenching of N₂ (*B*) and N₂ (*X*, *v*) by CO₂. Clearly the longer mix-

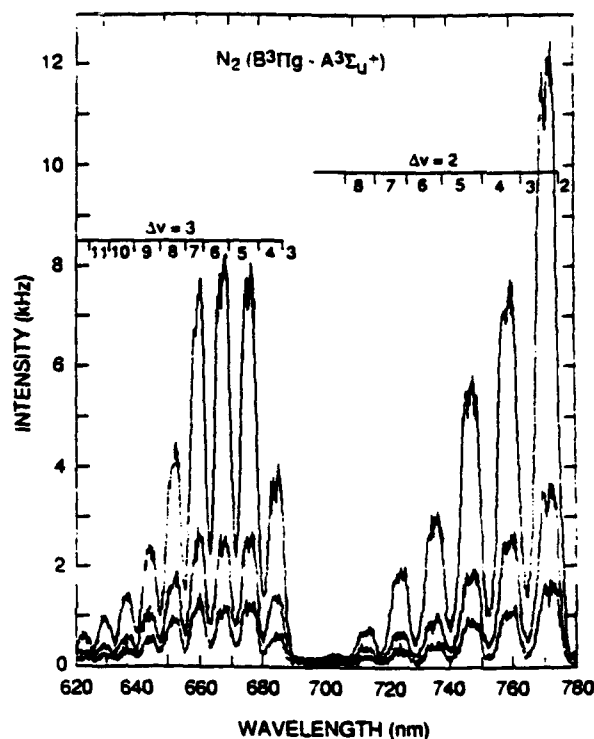


FIG. 2. N₂ (*B*³Π_g–*A*³Σ_u⁺) spectra excited in the energy transfer reaction between N₂ (*A*) and N₂ (*X*, *v*) at different number densities of added CO₂ and varying reaction times. In order of decreasing intensity the conditions are [CO₂] = 0, $\Delta t = 2.5$ ms; [CO₂] = 9.6×10^{14} molecules cm⁻³, $\Delta t = 2.5$ ms; [CO₂] = 9.6×10^{14} molecules cm⁻³, $\Delta t = 19.4$ ms. The spectra are not corrected for monochromator spectral response.

ing time further decreases the first-positive emission intensities from the levels at short mixing times. Most of our observations were survey measurements designed primarily to determine relative quenching efficiencies. Thus the majority of N₂(B) and N₂(X,v^{*}) quenching rate coefficients were determined by monitoring changes in the N₂(B) band intensities in the presence and absence of a single quencher number density at the two different injector positions. In a few cases, spectra were taken at two different quencher number densities with agreement between the two sets of data better than 20%.

To assess the validity of our procedure, we studied the quenching of N₂(B) by CH₄ in more detail than the other molecules investigated. Figure 3 shows the Stern-Volmer quenching plot for two of the four bands of the first-positive system that were monitored as a function of added CH₄. The rate coefficients for quenching N₂(B) by CH₄ range from about 3×10^{-10} cm³ molecule⁻¹ s⁻¹, for v' = 2 and 3, to 4 and 5×10^{-10} cm³ molecule⁻¹ s⁻¹ for v' = 6 and 8, respectively. The good linearity of these Stern-Volmer plots indicates that the two- or three-point measurements for all other quenchers should not give grossly inaccurate results.

Table I summarizes the global quenching rate coefficient measurements. Since we were interested primarily in relative quenching efficiencies, the experimental values can have absolute uncertainties up to a factor of 2. In relative terms, the numbers should be good to $\pm 25\%$. Table II shows that rate coefficients for quenching individual vibrational levels of N₂(B) can vary considerably for some molecules.

The values reported for N₂(X,v) quenching (also Table I) are not state specific. The energetics of the N₂(A) plus N₂(X,v) reaction restrict N₂(X,v) to vibrational levels no

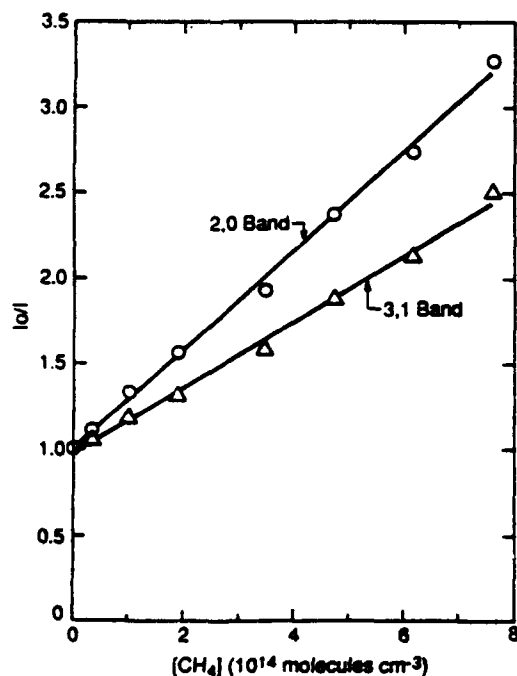


FIG. 3. Stern-Volmer plot for N₂(B) quenching by CH₄.

TABLE I. Global rate coefficients^a for quenching of N₂(B) and N₂(X,v^{*}).

Quencher	N ₂ (B)	N ₂ (X,v [*])
CH ₄	3×10^{-10}	1×10^{-16}
H ₂	5×10^{-11}	2×10^{-13}
CO ₂	2×10^{-10}	4×10^{-16}
N ₂	3×10^{-11}	2×10^{-13}
CF ₄	4×10^{-11}	1×10^{-16}
SF ₆	$\sim 1 \times 10^{-11}$...
N ₂ O	4×10^{-10}	3×10^{-13}
CO	2×10^{-10}	7×10^{-16}
O ₂	2×10^{-10}	...

^a Units of cm³ molecule⁻¹ s⁻¹ at 300 K.

smaller than five for N₂(B, v = 1) excitation, and at least as great as 13 to excite N₂(B, v = 12). Undoubtedly each B-state vibrational level is excited by several X-state levels.

In our initial studies on the reaction between N₂(A) and N₂(X,v^{*}), we studied the variation in B-state excitation as a function of A-state vibrational level.¹ We added CH₄ to our reactor to relax the vibrational energy in the A state. In our analysis, we included the effects of some vibrational relaxation of the N₂(X,v^{*}) by the CH₄, but presumed no electronic quenching of the N₂(B) state. The current studies show that this supposition was in error and that, in fact, CH₄ is quite efficient at quenching first-positive emission.

Correcting the data of Ref. 1 for N₂(B) quenching by CH₄ has only a small effect on the rate coefficient for exciting N₂(B, v' = 1-12) in the reaction between N₂(A) and N₂(X, v' = 5-15). The revised value for this rate coefficient is $(3.5 \pm 1.5) \times 10^{-11}$ cm³ molecule⁻¹ s⁻¹, a 16% increase over the value reported previously.

V. DISCUSSION

A. N₂(B) quenching

Most gases studied quenched N₂(B) quite strongly, with rate coefficients for quenching by CH₄, CO, CO₂, O₂, and N₂O being roughly gas kinetic. N₂, H₂, CF₄, and SF₆ quenched N₂(B) about 10 times more slowly.

TABLE II. Vibrational level dependent N₂(B) quenching rate coefficients.^a

v'	N ₂	CO	CO ₂	N ₂ O	CH ₄	CF ₄	SF ₆	H ₂	O ₂
1	0.16	2.1	2.0	3.1	2.3	0.29	0.08	0.34	1.5
2	0.21	2.0	2.0	4.6	2.5	0.59	...	0.39	1.5
3	0.29	1.7	1.8	4.5	1.6	0.20	0.53	0.50	1.5
4	0.31	1.2	2.1	5.1	1.6	0.14	0.23	0.48	1.7
5	0.35	0.7	2.5	6.5	2.0	0.16	0.66	0.54	1.6
6	0.35	1.0	2.3	6.6	2.4	0.59	0.33	0.56	2.2
7	0.36	1.1	1.6	5.2	2.3	0.23	...	0.50	2.3
8	0.39	...	1.4	5.8	2.7	0.65	...	0.57	2.7
9	0.36	0.5	2.1	7.4	3.1	0.73	0.38	0.73	1.9
10	0.29	1.6	2.0	7.5	3.6	0.60	0.20	0.69	4.0
11	0.30	0.7	1.7	9.1	4.9	0.45	0.39	0.82	3.2
12	0.22	3.0	1.6	7.4	5.1	1.3	0.28	0.61	2

^a Units of 10^{-10} cm³ molecule⁻¹ s⁻¹.

Young *et al.*¹² reported the most extensive set of $N_2(B)$ quenching rate coefficients in the literature. Their values, in units of $\text{cm}^3 \text{ molecule}^{-1} \text{ s}^{-1}$, were 4.6×10^{-11} , 8.5×10^{-11} , 1.5×10^{-10} , 2.7×10^{-11} , 1.1×10^{-10} , and 1.6×10^{-10} for $N_2(B)$ quenching by H_2 , CO , CO_2 , N_2 , O_2 , and N_2O , respectively. Their rate coefficients for quenching by N_2 and H_2 agree quite well with ours, but their other values are about 50% smaller. Their value for $N_2(B)$ quenching by He , $8 \times 10^{-13} \text{ cm}^3 \text{ molecule}^{-1} \text{ s}^{-1}$, is similar to that which we reported previously.¹⁰

Young *et al.*'s rate coefficient measurements were relative to their rate coefficient for $N_2(B)$ quenching by N_2O . Since the value for N_2O quenching is about half the one we measured, their rate coefficients should be doubled for proper comparison. Agreement between the two sets of measurements then is quite good for CO , CO_2 , and O_2 while their rate coefficients for quenching by H_2 and N_2 are roughly double ours.

Both Young *et al.*'s measurements and our global quenching-rate coefficients are not state specific and might, therefore, have been most sensitive to different groups of $N_2(B)$ vibrational levels. This could then explain the reported differences if the individual $N_2(B)$ vibrational levels were quenched at markedly disparate rates. Table II shows that in cases where significant variation with vibrational level exists, the lower levels tend to quench more slowly. Our global quenching rate coefficients are weighted towards the lower vibrational levels, $v' = 1-3$, whereas Young *et al.*'s experiment was most sensitive to middle levels, $v' = 4-7$. One would expect, therefore, that our results would be smaller than those of Young *et al.* In the present case, however, the average rate coefficients for quenching $v = 4-8$ by both H_2 and N_2 and is essentially the same as the global rate coefficients.

Lee and Suto¹³ reported $N_2(B)$ quenching rate coefficients by H_2 and N_2 to be $2.4 \times 10^{-11} \text{ cm}^3 \text{ molecule}^{-1} \text{ s}^{-1}$ and $2.1 \times 10^{-11} \text{ cm}^3 \text{ molecule}^{-1} \text{ s}^{-1}$, respectively. While their rate coefficient for quenching by N_2 is consistent with ours, their H_2 quenching rate coefficient is outside the combined uncertainties of the two studies. Their experiment was most sensitive to $N_2(B, v' = 6-12)$. For this range of vibrational levels, our H_2 quenching rate coefficients are two to three times larger than theirs.

Our data for the individual vibrational levels (see Table II) indicate little variation with vibrational level for $N_2(B)$ quenching by CO_2 and N_2 . In contrast, CH_4 , CF_4 , H_2 , O_2 , and N_2O show a tendency for quenching rate coefficients to increase with increasing vibrational level. The increase between $v' = 2$ and $v' = 12$ is roughly a factor of 2-3.

Our results on quenching by N_2 are consistent with our previous study¹⁴ which indicated $N_2(B)$ quenching rate coefficients by N_2 ranged between 2 and $3 \times 10^{-11} \text{ cm}^3 \text{ molecule}^{-1} \text{ s}^{-1}$ for most vibrational levels. We had observed previously, however, that vibrational levels 7-9 were quenched two to three times faster than the other vibrational levels. Shemansky reported similar observations.¹⁵ Shemansky's investigation and our earlier studies were more extensive than the current investigation, and should be more reliable.

Global observations cannot provide mechanistic information related to $N_2(B)$ -state quenching. Thus the observed rate of removal of a lower vibrational level of $N_2(B)$ might be moderated by collisional cascade from higher $N_2(B)$ vibrational levels. The measured global quenching rate coefficient for these low v' levels would then be somewhat less than one would measure in a single state selected study. The cascade could be either direct removal of vibrational energy from N_2 molecules in the B state or it could involve electronic quenching into one or more of the electronic states nested within the $N_2(B)$ manifold, the primary ones being $A(^3\Sigma_u^+, v \geq 7)$, $B(^3\Sigma_u^-)$, $W(^3\Delta_u)$, or $X(^1\Sigma_g^+)$, followed by collisional intersystem crossing back to lower vibrational levels of the B state. An additional mechanism for quenching by N_2 is electronic energy exchange where a molecule in the B state transfers some of its electronic energy to a ground state molecule, leaving the receptor molecule in a lower vibrational level of the B state. This process has been demonstrated in isotopic studies by Pravilov *et al.*¹⁶ and more recently by us.¹⁷ For most cases of practical interest, e.g., discharge or auroral excitation of $N_2(B)$, the effective, global rate coefficient describes better the overall system behavior.

B. $N_2(X, v')$ quenching

Nitrous oxide and carbon monoxide quench $N_2(X, v)$ rather efficiently, roughly 0.1% gas kinetic. Rate coefficients for quenching by CO_2 , CF_4 , and CH_4 are roughly an order of magnitude, and H_2 and N_2 two orders of magnitude smaller than N_2O and CO . The primary mode of de-excitation is undoubtedly $v-v$ transfer, although our measurement technique cannot distinguish single quantum from multi-quantum relaxation.

The process being identified as vibrational quenching essentially involves the difference between removal of vibrational energy in levels 5-13 to vibrational levels 4 and below and energy resident in vibrational levels greater than 13 into levels 5-13. It is thus a net vibrational quenching, and the reported quenching rate coefficients should be taken to be lower limits to the true values. Because the higher vibrational levels of the B state can be excited only from larger vibrational levels of the ground state, one can determine, in a qualitative sense, relative quenching efficiencies for the X -state vibrational levels involved by examining changes in the $N_2(B, v)$ distribution under the different sets of conditions.

The $N_2(B, v)$ distributions with the injector placed in the upstream position are essentially identical ($\pm 15\%$) to those with the injector in the down stream position for $N_2(X, v)$ quenching by N_2 and CO_2 . This result suggests that the relative $N_2(X, v)$ distributions do not change with added N_2 or CO_2 , but that the overall $N_2(X, v)$ number density is diminished.

With H_2 , CH_4 , and CF_4 , quenchers, the relative vibrational distributions of the five lowest $N_2(B, v)$ are similar for both injector positions, as are the relative distributions of the six highest $N_2(B, v)$. Relative to each other, however, the magnitude of the emission from the high vibrational level group diminishes twice as much as the lower vibrational level group when the injector is in the upstream position. The

observations suggest that these molecules quench $N_2(X)$ vibrational levels greater than about 9 about twice as efficiently as levels 5–9.

On the other hand, N_2O and CO quenchers decrease the relative $N_2(B, v)$ more for the lower six vibrational levels than for the higher ones when the reagent injector is moved to the upstream position. Such behavior would result if the $N_2(X, v)$ levels most responsible for $N_2(B, v = 1-6)$ excitation are quenched more rapidly than the higher $N_2(X, v)$.

An alternative explanation of our observations might be that the added quenchers just rearrange population within ground state vibrational levels 5–13 from vibrational levels more efficiently excited to the B state by $N_2(A)$ into levels that are excited less efficiently. If this were the case, however, one would expect that the quenched $N_2(B)$ vibrational distributions with the injector in the upstream position would differ from those with the injector in the downstream position. In reality, as we have mentioned, for some quenchers the $N_2(B, v)$ distributions do not vary with injector position while for other quenchers changes are readily apparent.

SF_6 and O_2 behaved anomalously. In the global sense, SF_6 quenched $N_2(B)$ only modestly with the injector in the downstream position. With the injector in the upstream position, adding SF_6 actually increased the total $N_2(B)$ number density. The first-positive vibrational distributions in the absence and presence of SF_6 were quite different, however, with some levels increasing in intensity as SF_6 was added, while others diminished in intensity. This observation appears to indicate that SF_6 relaxes vibrational energy within the B -state manifold. The increase in $N_2(B)$ with the injector in the upstream position indicates that SF_6 relaxes higher vibrational levels of $N_2(X, v)$ into those for which our diagnostic is most sensitive, most likely $v' = 5-15$. However, SF_6 apparently does not relax the observed levels efficiently.

In the case of O_2 , the $N_2(B, v)$ intensity was reduced by the addition of O_2 at both injector positions. However, the diminution was less with the injector in the upstream position. Unlike the case of SF_6 , $N_2(B, v)$ quenching by O_2 was fairly uniform over the range of vibrational levels at both injector positions. These observations would suggest that O_2 is an inefficient quencher of the $N_2(X, v)$ important for $N_2(B)$ excitation process, but that it does quench higher $N_2(X, v)$.

Morgan and Schiff¹⁸ used a catalytic probe to monitor vibrationally excited nitrogen in a discharge afterglow. They deduced rate coefficients for vibrational relaxation by N_2 , CO_2 , and N_2O to be $< 5 \times 10^{-18}$, 7.2×10^{-15} , and 2.6×10^{-14} cm^3 molecule⁻¹ s⁻¹, respectively. Their results for quenching by CO_2 and N_2O are roughly an order of magnitude smaller than what we have determined, while their upper-bound rate coefficient for relaxation by nitrogen is smaller by three orders of magnitude. Their diagnostic was sensitive to all excited vibrational levels of nitrogen, whereas our diagnostic monitors only $v > 5$. Thus our technique in essence monitors relaxation from levels > 5 to any of the vibrational levels $v < 4$. Morgan and Schiff's technique, on the other hand measures only quenching to $v'' = 0$. Since the $CO_2(v)$ and $N_2O(v)$ that are created from $N_2(v)$ quenching can re-excite $N_2(v = 0)$ back to $N_2(v = 1)$, the overall

quenching rates of $N_2(v)$ by CO_2 and N_2O will be retarded. McNeal *et al.*¹⁹ demonstrated this effect for CO_2 by showing that the effective rate of $N_2(v)$ quenching diminished as the N_2 partial pressure increased.

McNeal *et al.*¹⁹ and Starr and Shaw²⁰ also reported rate coefficients for $N_2(v)$ quenching by CO_2 and N_2O . Starr and Shaw noted that $N_2(v)$ excited atomic potassium fluorescence at a number of wavelengths. They monitored diminution of the 404.4 nm potassium line as a function of increasing CO_2 or N_2O number density. This state of potassium can be excited only by $N_2(v > 11)$, so their experiment measured quenching of vibrational levels above those for which we are most sensitive. Nonetheless, their values of 8×10^{-16} and 1.4×10^{-13} cm^3 molecule⁻¹ s⁻¹ for CO_2 and N_2O , respectively, are in reasonable accord with our values.

McNeal *et al.*¹⁹ monitored $N_2(v)$ by photoionization of N_2 at wavelengths too long to ionize $N_2(v = 0)$. Although their signals were for ionization of $N_2(v > 1)$, their diagnostic was heavily weighted towards $N_2(v = 1)$. They measured effective rate coefficients for quenching at a number of N_2 partial pressures and found the effective rate coefficients for $N_2(v)$ quenching by CO_2 and N_2O increased as the N_2 partial pressure decreased. In the low N_2 partial pressure limit, they determined rate coefficients of $(2 \pm 1) \times 10^{-13}$ and $(9 \pm 4) \times 10^{-14}$ cm^3 molecule⁻¹ s⁻¹ for CO_2 and N_2O , respectively. Since our diagnostic monitors only $N_2(v > 5)$, we should not be affected by back relaxation from $CO_2(v)$.

In summary, we have presented a novel technique for measuring the quenching of $N_2(X, v'')$ and $N_2(B)$ by a variety of quenchers. Our observations indicate that most species studied quench $N_2(B)$ at near gas-kinetic rates, whereas even efficient vibrational quenching of $N_2(X, v'')$ generally proceeds at rates four or more orders of magnitude less than gas kinetic.

ACKNOWLEDGMENTS

We appreciate partial financial support from the Air Force Weapons Laboratory under Contract No. F29601-87-C-0056, and the Air Force Office of Scientific Research (Task 2310GA) and the Defense Nuclear Agency (Project SA, Task SA/SDI work unit 00175) through a contract with the Phillips Laboratory/Geophysics Directorate, F12628-88-C-013. We are grateful for Bill Cummings' analytical support.

¹ L. G. Piper, *J. Chem. Phys.* **91**, 864 (1989).

² B. F. Gordiets, A. I. Osipov, and L. A. Shelepin, *Soviet Phys. JETP* **34**, 299 (1972).

³ J. P. Boef and E. E. Kunhardt, *J. Appl. Phys.* **60**, 915 (1986).

⁴ G. Luckovsky, P. D. Richard, D. V. Tsu, S. Y. Lin, and R. J. Markunas, *J. Vac. Sci. Technol. A* **4**, 681 (1986).

⁵ V. A. Vlaskov and K. Henriksen, *Planet. Sp. Sci.* **33**, 141 (1985).

⁶ L. G. Piper, K. Donohue, W. J. Kessler, T. R. Tucker, W. P. Cummings, and W. J. Marinelli, *Laser Based Diagnostics of $N_2(X, v)$* , PSI-1045/TR-960 (1990), and references therein. Also published as WL-TR-90-45 by the Weapons Laboratory (AFSC) and is available from NTIS.

⁷ D. H. Stedman and D. W. Setser, *Chem. Phys. Lett.* **2**, 542 (1968).

⁸ D. W. Setser, D. H. Stedman, and J. A. Coxon, *J. Chem. Phys.* **53**, 1004 (1970).

⁹ L. G. Piper, K. W. Holtzclaw, B. D. Green, and W. A. M. Blumberg, *J.*

- Chem. Phys. 98, 5337 (1989).
- ¹⁰ S. J. Davis and L. G. Piper, J. Phys. Chem. 94, 4515 (1990).
- ¹¹ O. Stern and M. Volmer, Phys. Z. 20, 183 (1919).
- ¹² R. A. Yung, G. Black, and T. G. Slinger, J. Chem. Phys. 50, 303 (1969).
- ¹³ L. C. Lee and M. Suto, J. Chem. Phys. 80, 4718 (1984).
- ¹⁴ L. G. Piper, J. Chem. Phys. 89, 6911 (1988).
- ¹⁵ D. E. Shemansky, J. Chem. Phys. 64, 565 (1976).
- ¹⁶ A. M. Pravilov, L. G. Smirnova, and A. F. Vilesov, Chem. Phys. Lett. 144, 469 (1988).
- ¹⁷ L. G. Piper (manuscript in preparation, 1991).
- ¹⁸ J. E. Morgan and H. I. Schiff, Can. J. Chem. 41, 903 (1963).
- ¹⁹ R. J. McNeal, M. E. Whitson, and G. R. Cook, J. Chem. Phys. 57, 4752 (1972).
- ²⁰ W. L. Starr and T. M. Shaw, J. Chem. Phys. 44, 4181 (1966).

APPENDIX I

Electronic Transition Moment Variation and Einstein Coefficients for the $\text{NO}(\text{B}^2\Pi - \text{X}^2\Pi)$ System

L.G. Piper
T.R. Tucker
W.P. Cummings

J. Chem. Phys. 94, 7667 (1991)

(SR-447 reproduced in its entirety)

THIS PAGE INTENTIONALLY LEFT BLANK

Electronic transition moment variation and Einstein coefficients for the $\text{NO}(B^2\Pi-X^2\Pi)$ system

Lawrence G. Piper,^{a)} Thomas R. Tucker,^{b)} and William P. Cummings^{c)}
Physical Sciences Inc., 20 New England Business Center, Andover, Massachusetts 01810

(Received 27 February 1990; accepted 26 February 1991)

This paper details an investigation of the variation in the electronic transition moment with internuclear separation for the $\text{NO}(B^2\Pi-X^2\Pi)$ transition. Measurements of the relative intensities of a number of $\text{NO } B-X$ vibronic transitions having a common upper level were used to construct a relative transition-moment function between 1.27 and 1.60 Å. After normalizing this relative function by experimentally determined radiative lifetimes, the transition-moment function was extended down to 1.23 Å by incorporating data from oscillator strength measurements. In contrast to empirical transition-moment functions that have been proposed previously, the function in this paper decreases with increasing internuclear separation. Unlike these other functions, however, this one is consistent with theoretical predictions, with most available oscillator strength data, and with the observed trend in B -state radiative lifetimes as a function of vibrational level.

1. INTRODUCTION

The $\text{NO}(B^2\Pi-X^2\Pi)$ system gives rise to the well-known β bands of NO . These bands are prominent in air and nitric oxide discharges and are excited in a number of chemiluminescent processes, most notably the three-body recombination of oxygen and nitrogen atoms. Surprisingly, the quantitative spectroscopic aspects of this system have not been well characterized.

Robinson and Nicholls¹ reported that the electronic transition moment, $R_e(r)$, of the $\text{NO}(B-X)$ system increased linearly with increasing internuclear separation. They based their conclusions upon observations of relative intensities of a number of $\text{NO } \beta$ bands that had common upper vibrational levels. Thirty years later, using a similar experimental approach and analysis, Vilesov and Matveev² determined a transition-moment function that was almost identical to that of Robinson and Nicholls. In the interim, Kuz'menko *et al.*³ derived a substantially different electronic transition moment function, but one that also increased with increasing internuclear separation, although much more strongly than the other two functions. They relied on absorption oscillator strength measurements for small values of internuclear separation and absolute emission measurements derived from shock-tube experiments for large values of internuclear separation.

All three of these transition-moment functions predict that the radiative lifetimes of the $\text{NO } B$ state vibrational levels will increase with increasing vibrational level. Such a trend is contrary to all published experimental measurements⁴⁻⁶ which show clearly that the lifetimes of the higher vibrational levels are shorter than those of the lower levels. Furthermore, if the two linear transition-moment functions

are normalized so as to yield a radiative lifetime of 2.0 μs for $v' = 0$ as given by the recent measurement of Gadd and Slanger,⁶ they underpredict the absorption oscillator strengths for the 0-0 through 6-0 transitions by more than a factor of two compared to all available experimental data.⁷⁻⁹ Kuz'menko *et al.*'s transition-moment function predicts radiative lifetimes for $\text{NO}(B)$ which are even more discordant with available experimental measurements than the other two empirical functions.

In contrast to the experimentally based transition-moment functions, the results from three *ab initio* calculations¹⁰⁻¹² indicate that the electronic transition moment of the $\text{NO}(B-X)$ system decreases with increasing internuclear separation. Cooper's¹⁰ *ab initio* function falls very rapidly, dropping a factor of 2 between 1.22 and 1.3 Å. The decrease in $R_e(r)$ then moderates somewhat, dropping another factor of 2 between 1.3 and 1.5 Å. de Vivie and Peyerimhoff's function,¹¹ on the other hand, is essentially linear, dropping roughly a factor of 2 between 1.3 and 1.6 Å. Langhoff *et al.* have proposed a function that combines a steep drop in the transition moment function at small r (almost a factor of 2 between 1.20 and 1.27 Å) with a much more moderate decline at larger r (about a third between 1.30 and 1.60 Å).

The plethora of inconsistent results has led us to reinvestigate the $\text{NO}(B-X)$ system. We use a branching-ratio technique to determine the relative variation in the electronic transition moment with internuclear separation. This allows us to normalize our relative data to the radiative lifetime measurements of Gadd and Slanger. We then extend our function to shorter internuclear distances by incorporating $R_e(r)$ values determined from oscillator-strength measurements.^{7,8}

Our transition moment function has a slope opposite that proposed by all three previous experimentally derived functions, but in accord with *ab initio* calculations. Our function is consistent, furthermore, with most available absorption oscillator strength and radiative lifetime measurements.

^{a)} Author to whom correspondence should be addressed.

^{b)} Mailing address: 550 S. Ruston, Evansville, IN 47714.

^{c)} Current address: Dept. of Physics, University of Georgia, Athens, Georgia.

II. EXPERIMENT

The NO- β bands were excited in a discharge-flow apparatus from the recombination of O and N atoms in argon.¹³ A microwave discharge through a flow of nitrous oxide in argon produced the atoms.¹⁴ The mole fraction of N₂O was kept low (less than 1%) in order to avoid production of NO in the discharge. The NO destroys the N atoms quite efficiently.¹⁵

Spectra were recorded between 200 and 530 nm at moderate resolution ($\Delta\lambda \approx 0.25$ nm) using a 0.5 m scanning monochromator that was equipped with a thermoelectrically cooled photomultiplier and a photon-counting rate meter. A computer-based data acquisition system digitized the output of the photon counter and stored the data for subsequent analysis. Figure 1 displays a portion of one of the spectra recorded for this study. Bands from all seven of the vibrational levels of NO(B) that are below the predissociation limit, i.e., $v' = 0-6$, radiate over the spectral range studied, 200 to 530 nm. Relative populations of the emitting levels vary with pressure and with the third body. They are more relaxed at higher buffer gas pressures and also more relaxed in nitrogen than in argon. In 2.5 torr of argon, the relative populations of $v' = 0$ to 6, respectively, are 100:14:20:30:11:7:8.

The variation in the response of the detection system as a function of wavelength was determined by resolving the output of standard quartz-halogen and deuterium lamps. A BaSO₄ screen reflected the lamp emission into the monochromator, thereby ensuring that the optics were filled. The small drop in the reflectivity of the screen at shorter wavelengths was included in the response function calculations.^{16,17} Calibrations obtained from the two lamps agreed excellently in the region of spectral overlap, 300 to 400 nm. The only optical element between the flow reactor and the entrance slit of the monochromator was a CaF₂ window which transmits uniformly over the relevant spectral region. This procedure ensured that the relative response determined from the lamps would not be modified by the presence

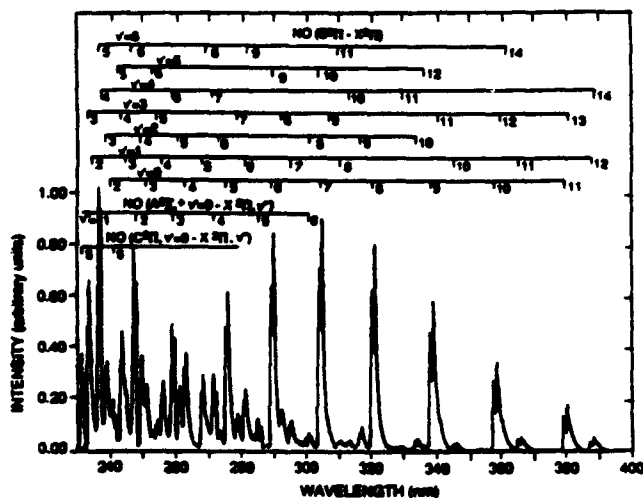


FIG. 1. The chemiluminescence spectrum generated from the recombination of O and N atoms in argon between 230 and 400 nm.

of other optical elements, such as a collection lens or even a curved flow reactor wall.

Spectral analysis involved dividing each spectrum into a number of discrete segments. Each segment contained only one transition from each of the seven upper levels of NO(B). These segments were then fit by computer to determine the intensities of each of the bands in the spectral segment. This spectral-fitting procedure allows intensities to be determined unambiguously in cases of partial overlap between bands. In a few cases the overlap was so great that reliable intensities could not be determined. Such bands were not included in the analysis. Figure 2 shows one of the spectral segments along with its associated synthetic fit. Without the spectral fitting analysis, we would have been unable to determine the intensities of any of the bands in this spectral region except that of the 2,16 band.

We have described our spectral-fitting procedure in some detail previously.^{18,19} A least-squares-fitting routine adjusts the populations of each vibrational level in a computer-generated synthetic spectrum of the NO- β bands so as to match best the experimentally determined spectrum. We used spectral constants tabulated in Huber and Herzberg²⁰ to calculate the synthetic spectrum. Incorporating the variation in the spin-orbit coupling constant with vibrational level was imperative to obtaining adequate fits.

III. RESULTS

A. Fit to branching-ratio measurements

The intensity of emission from a given band is the product of the number density in the upper state, N_v , and the Einstein coefficient for spontaneous radiation, $A_{v,v'}$. Generally, one can separate the Einstein coefficient into a product of several factors²¹ including the Franck-Condon factor, $q_{v,v'}$, the cube of the transition frequency, $\nu_{v,v'}$, and the square of the electronic transition moment, $R_e(r)$. This latter quantity is a function of the internuclear separation, r . The internuclear separation appropriate to a given transition is known as the r centroid of that transition, $\bar{r}_{v,v'}$. Thus,

$$I_{v,v'} = N_v A_{v,v'} = \kappa N_v q_{v,v'} \nu_{v,v'}^3 \times \frac{(2 - \delta_{0,\Lambda'} + \Lambda')}{(2 - \delta_{0,\Lambda})} R_e^2(\bar{r}_{v,v'}), \quad (1)$$

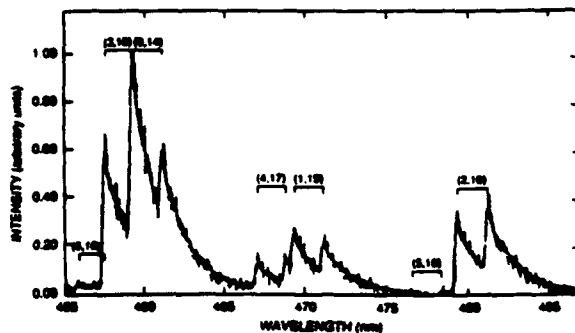


FIG. 2. A portion of the NO($B^2\Pi - X^2\Pi$) spectrum excited by the recombination of O with N in argon. The light line represents the data while the heavy line is the best-fit synthetic spectrum. The band heads are marked for each band (v', v'').

where κ is a constant ($\kappa = 64\pi^4/3h$ for ν in cm^{-1}), and the subscripts, Λ , on the Kronecker delta characterize the orbital angular momentum of the electronic states. This definition of the Einstein coefficient²² is consistent with the recommendations of Whiting *et al.*²³

The reduced intensities of bands in a progression having a common upper level,

$$\frac{I_{v'v''}}{q_{v'v''}\nu_{v'v''}^3} = \kappa N_{v'} R_e^2(\bar{r}_{v'v''}), \quad (2)$$

are a function only of the electronic-transition moment. The square root of the ratios of these reduced intensities to that of a single band in the progression vary from one another, therefore, in the same way that the electronic transition moment varies with internuclear separation. The conditions under which this analysis is valid have been documented extensively in the literature over the past 35 years.^{21,24-27} Although the r -centroid approximation is only strictly valid when $R_e(r)$ is a linear function, Fraser²⁰ and McCallum²⁴ have shown that the r -centroid approximation describes the electronic transition moment function quite well for most molecules even when higher-order polynomial or exponential functions are used to model $R_e(r)$.

We calculated the reduced intensities using the band intensities determined from the spectral fitting procedure described above and the Franck-Condon factors and band origins calculated by Albritton *et al.*²⁸ The r centroids needed for the analysis also derive from Albritton *et al.*'s calculations. These Franck-Condon factors are based on a Rydberg-Klein-Rees (RKR) potential and agree to better than 10 percent with the RKR based Franck-Condon factors of Jain and Sahni.²⁹ The Morse potential based Franck-Condon factors of Nicholls³⁰ and Ory *et al.*³¹ agree with those of Albritton *et al.* to better than 20 percent for Franck-Condon factors ≥ 0.02 . Sizeable disagreements occur for smaller Franck-Condon factors, but such bands contribute negligibly to the observed intensities. In general, RKR-based Franck-Condon factors tend to be more accurate than those that use Morse potential functions in their calculation.

Figure 3 shows data for bands originating from levels $v' = 0-3$ plotted together. Transitions used in the fit included the following: $v' = 0, v'' = 2-15$; $v' = 1, v'' = 3-7, 10-16$; $v' = 2, v'' = 2-5, 8-16$; and $v' = 3, v'' = 1-5, 7, 8, 11, 12$, and $15-18$. The line through the data is a least-squares-fit to the function

$$R_e(\bar{r}_{v'v''})|_{\text{rel}} = 1.40 - 0.40\bar{r}_{v'v''} + 1.508 \times 10^5 \exp(-10.07\bar{r}_{v'v''}). \quad (3)$$

A least-squares routine adjusted the normalization factor for each progression to minimize the difference between the data for each progression and the function describing the variation with r centroid for all progressions. The procedure was to fit just one progression initially and then adjust the normalization factors for each of the other progressions so that they would match, as closely as possible, this initial fit. The criterion for the fitting procedure was minimization of the sum of the squares of the differences between the analytical function and the individual data points (the residuals). All of the adjusted data then were refit to determine a new

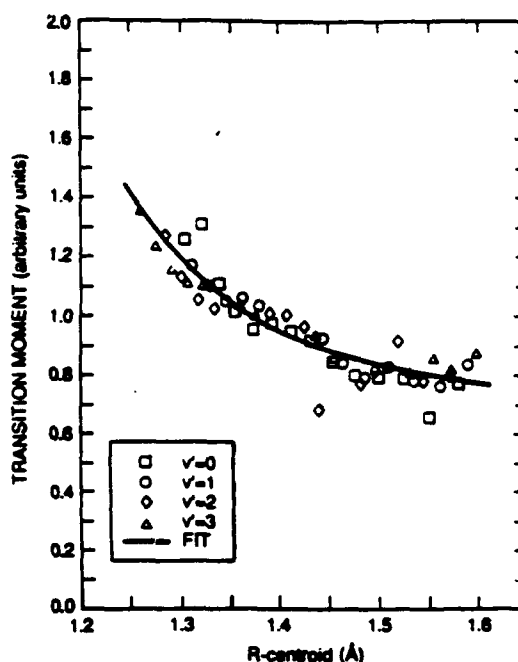


FIG. 3. Relative variation in the transition moment for the $\text{NO}(B^2\Pi-X^2\Pi)$ system as a function of internuclear separation.

best-fit function. The individual progressions then were readjusted to reduce further the sum of the squares of the residuals. After several iterations, no further improvements in the fit could be realized. The variance of the final fit indicated that the function reproduced the data to within about 5%.

The data could be fit just as well to a quadratic function or to an exponential function that didn't have a linear term in $\bar{r}_{v'v''}$. A quadratic polynomial fit to our data goes through a minimum at $\bar{r} \sim 1.55$ Å and then increase at larger \bar{r} . This is physically unreasonable since R_e must vanish at large internuclear separations. A simple exponential function also is physically unreasonable because it becomes constant at large r . The exponential function with the linear term, on the other hand, decreases in value throughout the range of internuclear separation that is important for determining Einstein coefficients.

We used Gadd and Slanger's radiative lifetime values for $v' = 0-3$ to place our relative transition-moment function on an absolute basis. The reason for restricting the normalization procedure to vibrational levels three and below is that our data provide a transition-moment function that is valid only over the range $1.27 \text{ Å} < r < 1.60 \text{ Å}$. This range encompasses well over 90% of the important vibronic transitions from $v' = 0-3$, whereas more than 40% of important transitions from $v' = 4-6$ occur outside this range.

The inverse of the radiative lifetime is given by

$$\tau_{v'}^{-1} = \zeta \sum_{v''} q_{v'v''} \nu_{v'v''}^3 |R_e(\bar{r}_{v'v''})|_{\text{rel}}^2, \quad (4)$$

where the scaling factor, ζ , is chosen so that τ in Eq. (4) gives the experimentally determined value. The average scal-

ing factor determined from Eq. (4) gives calculated radiative lifetimes for $v' = 0-3$ that agree with Gadd and Slinger's experimental values to within $\pm 4\%$.

B. Limits of validity of branching ratio fit

Equation (3) is a reasonably good representation of our data over the range of its validity, 1.27 to 1.60 Å. The least-squares-fit indicates an overall uncertainty of about 5%. Extrapolation of our function outside this region could lead to problems, however (*vide infra*). Most important transitions from $v' = 0-3$ occur within this range of internuclear separations, so that determining the lifetimes and Einstein coefficients of transitions involving these levels should not be subject to serious extrapolation error.

For the higher vibrational levels, the sum of the Franck-Condon factors for transitions from a given upper level to all lower levels is somewhat smaller than the value of unity that is required by quantum mechanical sum rules. This indicates that our sum over Einstein coefficients could be incomplete, and that if a greater range of lower levels were included in the summation, the radiative lifetime might be even smaller than those we calculate using our transition-moment function.

Any errors in radiative lifetime introduced by the incomplete summation, however, will be small because the missing transitions occur at longer wavelengths. The ν^j factor in Eq. (1) is sufficiently small at these longer wavelengths that transition probabilities will be small even for transitions with sizable Franck-Condon factors. For example, if we assumed that the Franck-Condon factor for the 6,20 band were 0.423, i.e.,

$$1 - \sum_{v''=0}^{19} q_{vv''},$$

the resulting Einstein coefficient would add less than 4% to the total radiative decay rate of $v' = 6$. In reality, the sum of the Franck-Condon factors for the 6,21 and 6,22 bands is only 0.27,³² so that the uncertainty arising from the incomplete set of Franck-Condon factors is somewhat less than 4%.

A more serious problem is that our transition moment-function by itself probably underpredicts values at the smaller internuclear separations. Mixing between the *B* and *C* states becomes important at an internuclear separation around 1.25 Å.¹² This mixing causes a fairly abrupt change in slope of the transition-moment function. The increase in R_v values with decreasing internuclear separation becomes much more rapid below 1.25 Å than it was above 1.25 Å. Since our experimental data provide a transition-moment function that is valid only down to 1.27 Å, using our function to calculate Einstein coefficients for transitions at smaller internuclear separations may result in values that are too small and will predict radiative lifetimes that are somewhat too long.

The vibrational levels that would be most affected by an extrapolation error are the higher ones, $v' = 4-6$, and only for sequences $\Delta v = 6$ through $\Delta v = 2$. Our function should provide reasonably accurate Einstein coefficients for all important transitions from the other vibrational levels, as well

as for those transitions from the higher vibrational levels occurring in sequences smaller than $\Delta v > 2$.

C. Extension of transition-moment function

In order to reduce extrapolation errors associated with our function, we extended it to smaller internuclear distances by including results from oscillator-strength measurements. The oscillator strength, $f_{v'v''}$, is determined from absorption measurements and will give the transition moment at a given internuclear distance directly,²²

$$R_v(\bar{r}_{v'v''}) = \left\{ \left(\frac{2 - \delta_{0,\Lambda}}{2 - \delta_{0,\Lambda} + \Lambda} \right) \frac{f_{v'v''}}{1.5\kappa q_{v'v''} \nu_{v'v''}} \right\}^{1/2}, \quad (5)$$

where c is the speed of light and κ is as defined above in presenting Eq. (1). Each oscillator strength measurement results in a discrete point on a plot of transition moment as a function of internuclear separation.

The scaling factor, ζ , determined from Eq. (4) allows us to convert our relative transition-moment data into absolute units. Combining our absolute branching ratio data with the oscillator strength data allows us to extend the transition-moment function, because all transitions involved in the oscillator strength measurements have r centroids smaller than 1.27 Å.

Plotting our renormalized data and the oscillator-strength measurements together, showed that our data faired smoothly into the data of Bethke,⁹ who used low resolution absorption at high pressure, and of Farmer *et al.*⁸ who used the hook method. The higher resolution measurements of Hasson and Nicholls,⁹ however, give transition moments that appear to be about 25 to 30% too low. Our data, when normalized by Gadd and Slinger's lifetimes,⁶ could be reconciled with Hasson and Nicholl's results only if the transition-moment function were not monotonic, but rather turned over at about 1.3 Å and started to decrease at shorter internuclear separations. This functional behavior, however, would lead to radiative lifetimes for the higher vibrational levels that were much longer than those observed experimentally. Interestingly, if the lifetime of NO(*B*, $v' = 0$) were 3.1 μ s, as was reported by Jeunehomme³ and by Brzozowski *et al.*,⁴ our function would favor Hasson and Nicholl's oscillator strengths over those of the other two groups. We believe Gadd and Slinger's lifetime determinations are more reliable than the other two, so we discounted Hasson and Nicholl's oscillator strengths when we made the functional fit to the extended data set.

A least-squares-fit to the combination of our adjusted $R_v(r)$ data between 1.27 and 1.60 Å with Bethke and Farmer *et al.*'s data from 1.22 to 1.26 Å gives R_v in Debye as

$$R_v(r) = 0.350 - 0.104\bar{r}_{v'v''} + 3.69 \times 10^4 \exp(-10.1 \bar{r}_{v'v''}). \quad (6)$$

Radiative lifetimes calculated from this function for $v' = 0-5$ are consistent with Gadd and Slinger's measurements to better than $\pm 4\%$. The radiative lifetime for $v' = 6$ that results from R_v described by Eq. (6) is about 17% too long. Table I lists the Einstein coefficients determined from this procedure along with other relevant information.

TABLE I. NO Beta-band Einstein coefficients.

v'	v''	Wavelength nm	$q v' v''$	r centroid Å	$Re(r)$ Debye	Branching ratio	$A v' v''$
0	0	220.09	0.000 02	1.269	0.3181	0.0001	5.269E + 01
	1	229.57	0.000 26	1.285	0.3014	0.0012	6.029E + 02
	2	239.73	0.001 76	1.302	0.2865	0.0066	3.290E + 03
	3	250.67	0.007 64	1.319	0.2735	0.0230	1.138E + 04
	4	262.46	0.023 54	1.336	0.2619	0.0565	2.802E + 04
	5	275.20	0.054 71	1.354	0.2517	0.1052	5.216E + 04
	6	289.01	0.099 55	1.372	0.2425	0.1534	7.608E + 04
	7	304.01	0.145 34	1.391	0.2344	0.1798	8.914E + 04
	8	320.38	0.173 05	1.411	0.2271	0.1717	8.513E + 04
	9	338.28	0.169 86	1.432	0.2205	0.1350	6.692E + 04
	10	357.95	0.138 39	1.453	0.2145	0.0879	4.356E + 04
	11	379.64	0.093 92	1.475	0.2091	0.0475	2.353E + 04
	12	403.67	0.053 12	1.499	0.2040	0.0213	1.054E + 04
	13	430.42	0.024 99	1.524	0.1992	0.0079	3.901E + 03
	14	460.36	0.009 73	1.550	0.1947	0.0024	1.185E + 03
	15	494.08	0.003 11	1.579	0.1902	0.0006	2.927E + 02
	16	532.31	0.000 81	1.610	0.1858	0.0001	5.816E + 01
	Sum =		0.998 0				
1	0	215.24	0.000 14	1.260	0.3283	0.0008	4.746E + 02
	1	224.30	0.001 69	1.276	0.3105	0.0079	4.530E + 03
	2	234.00	0.009 33	1.292	0.2949	0.0348	1.986E + 04
	3	244.40	0.031 21	1.309	0.2811	0.0929	5.297E + 04
	4	255.60	0.069 68	1.326	0.2688	0.1659	9.454E + 04
	5	267.67	0.107 25	1.343	0.2579	0.2048	1.167E + 05
	6	280.71	0.111 44	1.360	0.2484	0.1710	9.748E + 04
	7	294.85	0.069 50	1.378	0.2400	0.0859	4.899E + 04
	8	310.21	0.015 32	1.394	0.2334	0.0154	8.770E + 03
	9	326.97	0.002 78	1.432	0.2204	0.0021	1.211E + 03
	10	345.31	0.048 05	1.443	0.2173	0.0303	1.729E + 04
	11	365.45	0.112 08	1.463	0.2120	0.0568	3.238E + 04
	12	387.66	0.143 72	1.485	0.2069	0.0581	3.313E + 04
	13	412.27	0.127 20	1.508	0.2021	0.0408	2.326E + 04
	14	439.65	0.084 03	1.533	0.1975	0.0212	1.210E + 04
	15	470.31	0.042 80	1.560	0.1931	0.0084	4.812E + 03
	16	504.83	0.017 01	1.589	0.1888	0.0026	1.478E + 03
	Sum =		0.993 23				
2	0	210.67	0.000 59	1.252	0.3390	0.0035	2.286E + 03
	1	219.34	0.005 85	1.267	0.3202	0.0275	1.783E + 04
	2	228.60	0.025 54	1.283	0.3036	0.0952	6.182E + 04
	3	238.53	0.063 59	1.299	0.2890	0.1890	1.227E + 05
	4	249.18	0.095 86	1.315	0.2760	0.2281	1.481E + 05
	5	260.63	0.082 26	1.332	0.2647	0.1573	1.021E + 05
	6	272.98	0.028 01	1.347	0.2553	0.0434	2.815E + 04
	7	286.33	0.000 28	1.369	0.2441	0.0003	2.229E + 02
	8	300.80	0.037 36	1.389	0.2352	0.0367	2.382E + 04
	9	316.53	0.081 18	1.407	0.2286	0.0646	4.197E + 04
	10	333.69	0.062 42	1.425	0.2226	0.0402	2.610E + 04
	11	352.46	0.010 68	1.439	0.2182	0.0056	3.643E + 03
	12	373.08	0.008 62	1.480	0.2079	0.0035	2.251E + 03
	13	395.81	0.069 86	1.496	0.2046	0.0228	1.479E + 04
	14	420.99	0.129 03	1.518	0.2002	0.0335	2.174E + 04
	15	449.02	0.133 74	1.543	0.1958	0.0274	1.777E + 04
	16	480.37	0.093 77	1.570	0.1915	0.0150	9.735E + 03
	17	515.66	0.052 70	1.594	0.1880	0.0066	4.260E + 03
	Sum =		0.981 34				
3	0	206.35	0.001 75	1.244	0.3503	0.0105	7.665E + 03
	1	214.65	0.014 09	1.259	0.3302	0.0665	4.873E + 04
	2	223.52	0.047 63	1.274	0.3127	0.1785	1.308E + 05
	3	233.00	0.084 14	1.290	0.2973	0.2517	1.845E + 05
	4	243.15	0.074 95	1.305	0.2838	0.1798	1.318E + 05
	5	254.05	0.021 00	1.320	0.2728	0.0408	2.991E + 04
	6	265.77	0.002 69	1.350	0.2540	0.0040	2.895E + 03
	7	278.40	0.046 79	1.359	0.2491	0.0576	4.220E + 04
	8	292.07	0.063 90	1.375	0.2413	0.0639	4.684E + 04
	9	306.87	0.018 57	1.390	0.2350	0.0152	1.113E + 04
	10	322.97	0.004 31	1.426	0.2221	0.0027	1.980E + 03
	11	340.52	0.054 40	1.436	0.2191	0.0283	2.074E + 04
	12	359.73	0.072 60	1.455	0.2141	0.0306	2.242E + 04

TABLE I. (continued).

	13	380.82	0.024 16	1.472	0.2099	0.0082	6.044E + 03
	14	404.07	0.002 23	1.501	0.2035	0.0006	4.391E + 02
	15	429.82	0.058 66	1.530	0.1980	0.0124	9.085E + 03
	16	458.47	0.126 31	1.554	0.1941	0.0211	1.549E + 04
	17	490.51	0.134 20	1.576	0.1906	0.0177	1.296E + 04
	18	526.54	0.097 10	1.604	0.1866	0.0099	7.263E + 03
	Sum =		0.949 48				
4	0	202.25	0.004 08	1.236	0.3619	0.0248	2.026E + 04
	1	210.23	0.026 30	1.250	0.3408	0.1271	1.039E + 05
	2	218.72	0.067 48	1.265	0.3224	0.2570	2.102E + 05
	3	227.79	0.078 12	1.280	0.3061	0.2375	1.943E + 05
	4	237.48	0.029 77	1.295	0.2926	0.0730	5.970E + 04
	5	247.87	0.000 70	1.308	0.2815	0.0014	1.143E + 03
	6	259.01	0.040 43	1.331	0.2649	0.0626	5.123E + 04
	7	271.00	0.053 44	1.346	0.2558	0.0674	5.512E + 04
	8	283.93	0.008 36	1.358	0.2494	0.0087	7.128E + 03
	9	297.90	0.013 82	1.389	0.2355	0.0111	9.095E + 03
	10	313.05	0.057 57	1.403	0.2301	0.0381	3.116E + 04
	11	329.51	0.033 57	1.419	0.2246	0.0182	1.485E + 04
	12	347.46	0.000 15	1.438	0.2186	0.0001	5.361E + 01
	13	367.10	0.042 82	1.467	0.2110	0.0148	1.209E + 04
	14	388.66	0.071 38	1.485	0.2069	0.0200	1.632E + 04
	15	412.42	0.023 97	1.502	0.2034	0.0054	4.433E + 03
	16	438.73	0.003 68	1.561	0.1929	0.0006	5.086E + 02
	17	467.98	0.054 20	1.563	0.1926	0.0075	6.153E + 03
	18	500.68	0.124 90	1.587	0.1890	0.0136	1.115E + 04
	19	537.43	0.132 20	1.615	0.1851	0.0112	9.151E + 03
	Sum =		0.867 14				
5	0	198.37	0.007 99	1.228	0.3742	0.0498	4.495E + 04
	1	206.03	0.041 34	1.242	0.3520	0.2035	1.837E + 05
	2	214.19	0.076 33	1.257	0.3325	0.2984	2.693E + 05
	3	222.88	0.050 11	1.271	0.3157	0.1567	1.415E + 05
	4	232.15	0.001 71	1.278	0.3089	0.0045	4.090E + 03
	5	242.06	0.025 53	1.306	0.2830	0.0501	4.523E + 04
	6	252.68	0.051 54	1.320	0.2726	0.0825	7.445E + 04
	7	264.07	0.010 50	1.332	0.2644	0.0139	1.251E + 04
	8	276.33	0.012 09	1.360	0.2487	0.0123	1.112E + 04
	9	289.55	0.050 49	1.373	0.2424	0.0425	3.834E + 04
	10	303.84	0.019 27	1.386	0.2365	0.0133	1.205E + 04
	11	319.33	0.005 38	1.421	0.2238	0.0029	2.596E + 03
	12	336.16	0.051 03	1.431	0.2208	0.0228	2.054E + 04
	13	354.50	0.034 54	1.446	0.2163	0.0126	1.138E + 04
	14	374.57	0.000 23	1.472	0.2098	0.0001	6.043E + 01
	15	396.59	0.046 10	1.497	0.2043	0.0107	9.673E + 03
	16	420.86	0.066 92	1.515	0.2008	0.0126	1.135E + 04
	17	447.70	0.022 37	1.531	0.1979	0.0034	3.062E + 03
	18	477.53	0.005 25	1.562	0.1927	0.0006	5.618E + 02
	19	510.84	0.076 06	1.600	0.1871	0.0069	6.268E + 03
	Sum =		0.654 78				
6	0	194.68	0.013 68	1.220	0.3869	0.0869	8.706E + 04
	1	202.06	0.055 52	1.235	0.3635	0.2786	2.790E + 05
	2	209.90	0.070 25	1.249	0.3431	0.2801	2.805E + 05
	3	218.23	0.018 75	1.262	0.3265	0.0602	6.032E + 04
	4	227.11	0.006 70	1.284	0.3024	0.0164	1.640E + 04
	5	236.59	0.047 15	1.296	0.2918	0.0950	9.511E + 04
	6	246.72	0.021 55	1.309	0.2811	0.0355	3.555E + 04
	7	257.58	0.004 06	1.336	0.2617	0.0051	5.105E + 03
	8	269.23	0.043 30	1.345	0.2565	0.0457	4.579E + 04
	9	281.76	0.019 79	1.358	0.2494	0.0172	1.727E + 04
	10	295.28	0.005 12	1.390	0.2350	0.0034	3.446E + 03
	11	309.88	0.045 30	1.399	0.2315	0.0257	2.570E + 04
	12	325.70	0.019 56	1.412	0.2267	0.0091	9.127E + 03
	13	342.90	0.006 05	1.450	0.2154	0.0022	2.185E + 03
	14	361.64	0.051 24	1.459	0.2131	0.0154	1.543E + 04
	15	382.12	0.026 00	1.473	0.2095	0.0064	6.417E + 03
	16	404.60	0.003 65	1.498	0.2041	0.0007	7.202E + 02
	17	429.33	0.048 24	1.527	0.1986	0.0075	7.541E + 03
	18	456.69	0.062 57	1.545	0.1955	0.0079	7.875E + 03
	19	487.07	0.007 98	1.552	0.1943	0.0008	8.182E + 02
	Sum =		0.576 66				

TABLE II. Radiative lifetimes of NO($B^2\Pi, v'$).^a

v'	Present results	Gadd and Slinger (Ref. 6)	Brzozowski <i>et al.</i> (Ref. 4)	Jeunehomme and Duncan (Ref. 5)	Robinson and Nicholls (Ref. 1) or Vilesov and Matveev (Ref. 2) ^b	Kuz'menko <i>et al.</i> (Ref. 3)	de Vivie and (Ref. 11)	Cooper (Ref. 10)	Langhoff <i>et al.</i> (Ref. 12)
0	2.02	2.00	3.1 ± 0.2	3.1 ± 0.6	2.00	0.32	2.63	5.52	1.99
1	1.75	1.82	2.9 ± 0.2	2.3 ± 0.3	2.02	0.35	2.32	4.49	1.79
2	1.54	1.52	2.8 ± 0.2	2.2 ± 0.4	2.05	0.38	2.08	3.66	1.60
3	1.36	1.46	2.6 ± 0.2		2.09	0.41	1.89	2.85	1.41
4	1.22	1.19	2.5 ± 0.2		2.17	0.46	1.75	2.18	1.23
5	1.11	1.07	2.3 ± 0.2		2.35	0.52	1.64	1.70	1.05
6	1.00	0.85	2.3 ± 0.2		2.41	0.55	1.53	1.34	0.87

^a Units are 10^{-6} s.^b $R_e(r)$ normalized so that $r(v' = 0) = 2.00 \times 10^{-6}$ s.

IV. DISCUSSION

A. Transition moment functions

Figure 4 compares our transition-moment function with others that have appeared in the literature. The three functions determined from *ab initio* calculations¹⁰⁻¹² behave qualitatively like our function, i.e., the value of the transition moment decreases with increasing internuclear separation. We had to divide Cooper's transition moment values by a factor of two in order to have a consistent degeneracy normalization between all sets of data.^{21,22}

Cooper's¹⁰ function decreases somewhat too steeply over the range common to both his function and ours, but appears to represent experimental oscillator strengths quite well. Over the range 1.3 to 1.45 Å, the relative variation of de Vivie and Peyerimhoff's¹¹ function is consistent with ours, to within a few percent. Their function, however, is inadequate at $r < 1.3$ Å and decreases too rapidly for $r > 1.45$ Å.

Langhoff *et al.* found, that if they shifted their *ab initio* function 0.025 Å to larger internuclear separations, they could reproduce Gadd and Slinger's radiative lifetimes for all vibrational levels up through $v' = 6$ to better than $\pm 4\%$. Langhoff *et al.* "shifted" transition-moment function agrees with ours to better than $\pm 4\%$ between 1.24 and 1.60 Å.

The three previously published, experimentally derived functions all predict a variation in transition moment with internuclear separation that is contrary to our findings. Kuz'menko *et al.*³ function results primarily from fits to absolute emission measurements in shock heated air.³³ Those experiments did not have sufficient sensitivity and spectral resolution to provide positive identification of the NO β bands. A chronic problem with shock-tube measurements is that they tend to be plagued by interference from impurity emissions. This effect results in absolute photon-emission rates that are too large.

The functions of Robinson and Nicholls¹ and Vilesov and Matveev² derive from an approach that is similar to ours, so rationalizing the differences between their findings and ours is not so straightforward. The three major sources of error in using a branching-ratio technique to construct a transition-moment function are (1) incorrect band intensity measurements, because of spectral overlap problems with

impurity emissions or other vibrational levels of the band being studied; (2) incorrect values of Franck-Condon factors and r centroids; or (3) incorrect calibrations of the response of the detection system as a function of wavelength.

Our use of spectral fitting for determining band intensities reduces problems with spectral overlap significantly. These problems are most pronounced at longer wavelengths and could lead to overestimates of intensities of bands with larger r centroid values.

Robinson and Nicholls list the Franck-Condon factors

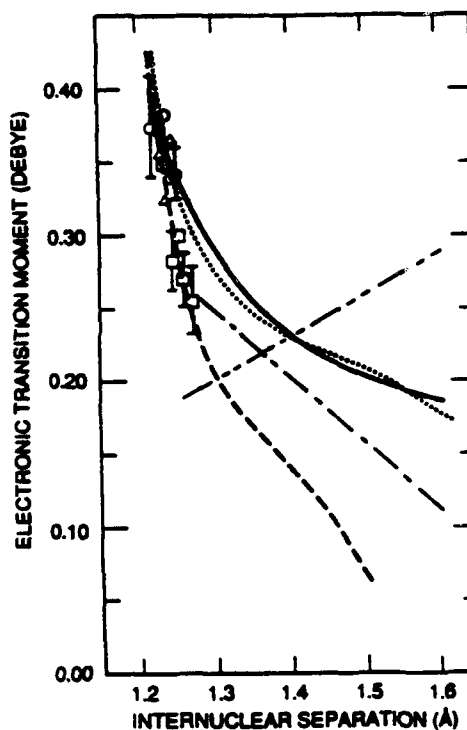


FIG. 4. Comparison between the various NO(B-X) transition-moment functions. Present results (—); Langhoff *et al.* (Ref. 12) (—); de Vivie and Peyerimhoff¹¹ (---); Cooper (Ref. 10) (-.-.-); Vilesov and Matveev (Ref. 2) (....); Bethke (Ref. 7) (O); Farmer *et al.* (Ref. 8) (Δ); Hesson and Nicholls (Ref. 9) (\square).

and r centroids used in their analysis. Although their values are based upon Morse potentials, they are similar to the values we used. Vilesov and Matveev's Franck-Condon factors and r centroids come from Jain and Sahni³¹ and also are almost identical to those used here.

Response calibration problems can result either from failure to fill monochromator optics or from neglect to correct standard lamp outputs from units of Watts to photons s^{-1} . Mixing intensity units tends to skew corrected intensities to be higher at longer wavelengths or larger r centroids. Underfilling monochromator optics can lead to response function errors if the photomultiplier varies in sensitivity across its face. Predicting how this effect will influence intensity measurements, however, is difficult.

Some sort of systematic error in the experiments of Robinson and Nicholls and Vilesov and Matveev seems likely. Dividing $R_e(\bar{F}_{v'v''})$ determined from their function by the wavelength of each transition gives relative branching ratios for $v' = 0$ to $v'' = 2-16$ that agree with ours to better than ± 5 percent.

B. Radiative lifetimes

Table II compares the radiative lifetimes derived from our transition-moment function with experimentally measured lifetimes and those determined from other proposed transition-moment functions. The agreement with the recent results of Gadd and Slinger⁶ is excellent for all vibrational levels except $v' = 6$. Most likely the cause of this discrepancy is because the function described by Eq. (6) does not increase rapidly enough below 1.25 Å.

Agreement with the radiative lifetimes determined by Brzozowski *et al.*⁴ and Jeunehomme and Duncan⁵ is, of course, not so good. Naturally, had we normalized our transition-moment function appropriately, some overlap between our calculated lifetimes and those measured by these two groups would have occurred. Our transition-moment function, however, indicates that the reduction in radiative lifetime with increasing vibrational level is much stronger than reported by Brzozowski *et al.*

Both Brzozowski *et al.* and Jeunehomme and Duncan monitored fluorescence decays following excitation in a pulsed discharge. A potential problem with this approach is the possibility that collisional or radiative cascade from higher states, that are also excited in the discharge, will continue to generate the state under study after termination of the discharge. This effect generally results in radiative lifetimes that are too long. Another potential problem is that radiation from the state under study might not be isolated adequately from radiation from other states. Neither of these potential problems will affect the measurements of Gadd and Slinger. They prepared the various vibrational levels of NO(*B*) by laser excitation. Thus, only one vibronic state was excited and only one radiated.

Table II also lists radiative lifetimes determined from other proposed transition-moment functions. The experimentally derived functions of Robinson and Nicholls,¹ Vilesov and Matveev,² and Kuz'menko *et al.*³ all predict that radiative lifetimes will increase with increasing vibrational

level in contradiction to all radiative lifetime measurements. In addition, as noted above, the transition-moment function of Robinson and Nicholls or Vilesov and Matveev is inconsistent with absorption oscillator strength measurements.

Radiative lifetimes we compute from de Vivie and Peyerimhoff's and Cooper's *ab initio* functions are longer than those measured by Gadd and Slinger, although those we compute from de Vivie and Peyerimhoff's function are only 30 percent too long for $v' = 0-3$. We compute radiative lifetimes from de Vivie and Peyerimhoff's function that are shorter by a factor of $\sqrt{2}$ than the values they list in their Table VIII. Although the computations used to calculate Einstein coefficients are based upon the appropriate equation in their paper, we may have misinterpreted their normalization to account for degeneracy effects. For comparison with our function, the absolute value of their function is less important than the qualitative trends it predicts. In a relative sense, the lifetimes calculated from their function decrease with increasing vibrational level about 20 percent more slowly than ours. The major problem with their function, however, is that it doesn't predict the sharp increase in the transition-moment function that commences at about 1.25 Å.

In contrast to de Vivie and Peyerimhoff, Cooper's¹⁰ function predicts the sharp increase below 1.25 Å, but his function doesn't flatten out enough at larger internuclear separations. As a result, his function predicts a much greater change in radiative lifetime with vibrational level than is observed experimentally.

As noted above, Langhoff *et al.*'s calculations predict both the magnitude and the variation in radiative lifetime with increasing vibrational level to within about $\pm 4\%$ for all vibrational levels, $v' = 0-6$.

C. Other issues

Gadd and Slinger excited NO(*B*, $v' = 6$) with a laser and scanned the resulting fluorescence spectrum. They converted the relative intensities to a set of branching ratios from $v' = 6$ to ground-state vibrational levels. These branching ratios then were converted to absolute Einstein coefficients by dividing each by the measured radiative lifetime of $v' = 6$.

Our Einstein coefficients for $v' = 6$ to $v'' = 0$ to 3 and 5 are within $\pm 10\%$ of Gadd and Slinger's. For all other transitions, Gadd and Slinger's values are larger than ours by factors ranging from 1.3 to 4. We see some evidence that a systematic error in Gadd and Slinger's measurements is the cause of the discrepancies.

Figure 5 shows the ratio of Gadd and Slinger's Einstein coefficients to ours plotted as a function of the wavelength of each transition. The ratios for the first fourteen transitions separate themselves into three distinct groups. The transition having Einstein coefficients on the order of $10^3 s^{-1}$ are the ones that agree with ours to within $\pm 10\%$. Those transitions for which $A_{6,v'}$ is on the order of $10^4 s^{-1}$ have ratios near 1.5, while the ratios are roughly 2.5 for transition having $A_{6,v'} \sim 10^5 s^{-1}$. This grouping of discrepancies according to the magnitude of the Einstein coefficient suggests an incomplete baseline subtraction for the weaker bands, or per-

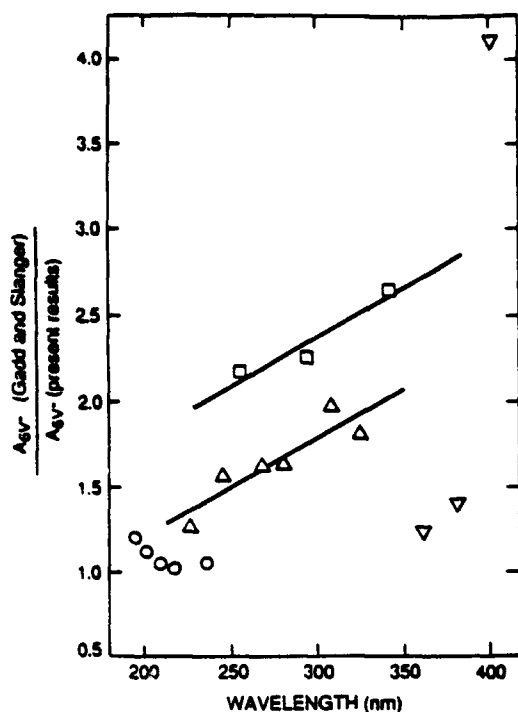


FIG. 5. Variation in the ratio of Einstein coefficients from $v' = 6$ to $v' = 0$ through 16 calculated by Gadd and Slanger to those we have derived, as a function of transition wavelength. \circ , $A_{6v'} \sim 10^3 \text{ s}^{-1}$; Δ , $A_{6v'} \sim 10^4 \text{ s}^{-1}$; \square , $A_{6v'} \sim 10^5 \text{ s}^{-1}$.

haps, a nonlinearity in changing signal amplifier ranges.

Figure 5 also shows evidence of a second systematic error in Gadd and Slanger's measurements. The ratios for the two groups of transitions having Einstein coefficients on the order of 10^4 and 10^5 s^{-1} increase linearly with increasing wavelength and, in addition, have similar slopes. The ratios of the 10^3 s^{-1} group decrease slightly with increasing wavelength. These trends could result from an error in calibrating the relative response of their monochromator as a function of wavelength. This seems likely since dividing the ratios of Gadd and Slanger's $A_{6v'}$ to those we have derived by the transition wavelength results in a set of values that are constant to within $\pm 5\%$ both for the 10^4 s^{-1} group and for the 10^5 s^{-1} group. Interestingly, the discrepancies in the Einstein coefficient ratios scale with wavelength in the same manner as the discrepancies between our transition-moment function and those of Robinson and Nicholls and Vilesov and Matveev.

Gadd and Slanger computed a set of radiative lifetimes for $v' = 0$ through 5 using the branching ratios for the $v', 0$ transitions calculated by Langhoff *et al.* and the oscillator strengths measured by Hasson and Nicholls⁹ and by Farmer *et al.*⁸ They found generally good agreement with their measured radiative lifetimes, especially with those lifetimes calculated from Hasson and Nicholls' oscillator strengths. As we have already noted, our transition-moment function is incompatible with transition moments derived from Hasson and Nicholls oscillator strength measurements. Einstein coefficients calculated from these measurements, therefore, ought also to be incompatible with our measurements. Our

radiative lifetimes, however, agree rather well with those of Gadd and Slanger.

We don't understand how Gadd and Slanger arrived at the lifetime values they calculated. We wonder if a systematic error might explain the discrepancy between the radiative lifetimes we calculate from both sets of oscillator-strength measurements and those calculated by Gadd and Slanger. We find that the ratio of the lifetimes we calculate to those calculated by Gadd and Slanger is 1.62 to within 2.5% for all transitions. The constancy in the ratio shows that our branching ratios for the $A_{v'0}$ are compatible with those used by Gadd and Slanger. Since Hasson and Nicholls and Farmer *et al.* list both oscillator strengths and Einstein coefficients for each transition, computational errors in converting from one quantity to the other also should not be an issue. The discrepancy of 1.62 (which just happens to be $16/\pi^2$) remains to be discovered.

V. SUMMARY

We have used a branching ratio technique to establish the variation in the electronic transition moment as a function of internuclear separation for the $\text{NO}(B^2\Pi-X^2\Pi)$ system. Although our transition-moment function differs significantly from previously published empirical functions, our function agrees to better than $\pm 5\%$ with the best available measurements of radiative lifetimes,⁶ of absorption oscillator strengths,^{7,8} and with the most recent and detailed *ab initio* computation.¹²

ACKNOWLEDGMENTS

Financial support from the Air Force Geophysics Laboratory through Contract No. F-19628-85-C-0032, sponsored by the Defense Nuclear Agency (Project SA, Task SA/SDI, Work Unit 00175) and by the Air Force Office of Scientific Research (Task 2310G4) was most welcome. We thank Don Setser (Kansas State University) for sending the Franck-Condon factors. We appreciate the comments and advice of our PSI colleagues Mark E. Fraser, B. David Green, W. Terry Rawlins, and George E. Caledonia, and were grateful for Stephen Langhoff's advice and insight.

¹ D. Robinson and R. W. Nicholls, *Proc. Phys. Soc.* **71**, 957 (1958).

² A. F. Vilesov and A. A. Matveev, *Opt. Spectrosc. (USSR)* **64**, 258 (1988).

³ N. E. Kuz'menko, L. A. Kuznetsova, A. P. Monyakina, and Yu. Ya. Kuz'yakov, *J. Quant. Spectrosc. Radiat. Transfer*, **24**, 219 (1980).

⁴ J. Brzozowski, P. Erman, and M. Lyyra, *Phys. Scr.* **14**, 290 (1976).

⁵ M. Jeunehomme and A. B. F. Duncan, *J. Chem. Phys.* **41**, 1692 (1964).

⁶ G. E. Gadd and T. G. Slanger, *J. Chem. Phys.* **92**, 2194 (1990).

⁷ G. Bethke, *J. Chem. Phys.* **31**, 662 (1959).

⁸ A. J. D. Farmer, V. Hasson, and R. W. Nicholls, *J. Quant. Spectrosc. Radiat. Transfer* **12**, 635 (1972).

⁹ V. Hasson and R. W. Nicholls, *J. Phys. B*, **4**, 1769 (1971).

¹⁰ D. M. Cooper, *J. Quant. Spectrosc. Radiat. Transfer* **27**, 459 (1982).

¹¹ R. de Vivie and S. D. Peyerimhoff, *J. Chem. Phys.* **89**, 3028 (1988).

¹² S. R. Langhoff, H. Partridge, C. W. Bauschlicher, Jr., and A. Komornicki, *J. Chem. Phys.* **94**, 6638 (1991).

¹³ R. A. Young and R. L. Sharpless, *J. Chem. Phys.* **39**, 1071 (1963).

¹⁴ L. G. Piper and W. T. Rawlins, *J. Phys. Chem.* **90**, 320 (1986).

¹⁵ F. Kaufman and J. R. Kelso, *J. Chem. Phys.* **27**, 1209 (1957).

¹⁶ F. Grum and G. W. Luckey, *Appl. Opt.* **7**, 2289 (1968).

¹⁷ F. Grum and T. E. Wightman, *Appl. Opt.* **16**, 2775 (1977).

- ¹⁸ L. G. Piper, W. J. Marinelli, W. T. Rawlins, and B. D. Green, *J. Chem. Phys.* **83**, 5602 (1985).
- ¹⁹ L. G. Piper, K. W. Holtzclaw, B. D. Green, and W. A. M. Blumberg, *J. Chem. Phys.* **90**, 5337 (1989).
- ²⁰ K. P. Huber and G. Herzberg, *Constants of Diatomic Molecules* (Van Nostrand Reinhold, New York, 1979).
- ²¹ P. A. Fraser, *Can. J. Phys.* **32**, 515 (1954).
- ²² A. Schadee, *J. Quant. Spectrosc. Radiat. Transfer* **19**, 451 (1978).
- ²³ E. E. Whiting, A. Schadee, J. B. Tatum, J. T. Hougen, and R. W. Nicholls, *J. Mol. Spectrosc.* **80**, 249 (1980).
- ²⁴ R. W. Nicholls, *J. Quant. Spectrosc. Radiat. Transfer* **14**, 233 (1974).
- ²⁵ J. C. McCallum, *J. Quant. Spectrosc. Radiat. Transfer* **21**, 563 (1979).
- ²⁶ S. M. Yazykova and E. V. Butyrskaya, *J. Phys. B.* **13**, 3361 (1980).
- ²⁷ N. E. Kuz'menko and A. V. Stolyarov, *J. Quant. Spectrosc. Radiat. Transfer* **35**, 415 (1986).
- ²⁸ D. L. Albritton, A. L. Schmeltekopf, and R. N. Zare (private communication via D. W. Setser, 1985).
- ²⁹ D. C. Jain and R. C. Sahni, *Trans. Faraday Soc.* **64**, 3169 (1968).
- ³⁰ R. W. Nicholls, *J. Res. NBS* **68A**, 535 (1964).
- ³¹ H. A. Ory, A. P. Gittleman, and J. P. Maddox, *Astrophys. J.* **139**, 346 (1964).
- ³² T. G. Slanger (private communication, 1990).
- ³³ J. C. Keck, J. C. Camm, B. Kivel, and T. Wentink, Jr., *Ann. Phys.* **7**, 1 (1959).

APPENDIX J

Experimental Determination of the Einstein Coefficient for the $N(2P - 4S)$ Transition

L.G. Piper
W.T. Rawlins

(Quarterly No. 10 reproduced in its entirety)

THIS PAGE INTENTIONALLY LEFT BLANK

**EXPERIMENTAL DETERMINATION OF THE EINSTEIN
COEFFICIENT FOR THE $N(2P - 4S)$ TRANSITION**

Quarterly Status Report No. 10

For the Period

1 December 1990 to 28 February 1991

Under Air Force Contract No. F19628-88-C-0173

Prepared by:

**L.G. Piper and W.T. Rawlins
Physical Sciences Inc.
20 New England Business Center
Andover, MA 01810**

Sponsored by:

**Air Force Geophysics Laboratory
Air Force Systems Command
U.S. Air Force
Hanscom Air Force Base, MA 01731**

August 1991

THIS PAGE INTENTIONALLY LEFT BLANK

1. INTRODUCTION

We have begun a series of laboratory measurements to determine the Einstein coefficient for the $N(^2P - ^4S)$ transition. Although emission from $N(^2P)$ is prominent in the aurora, the Einstein coefficients for its forbidden emission lines at 346.6 and 1040 nm are known only through two theoretical calculations, performed roughly 30 years apart. The purpose of this work was either to verify the theoretical calculations or else to provide a more accurate value of this important Einstein coefficient for use in modeling disturbed atmospheres.

Our experiment involves measuring absolute photon emission rates from the 346.6 nm line with a simultaneous determination of the $N(^2P)$ number density in the fluorescence observation region using vacuum ultraviolet resonance absorption measurements. We established the absolute spectral response of our monochromator and optical system by measuring intensities in the observation region of air afterglow emission, whose absolute photon emission rates have been established under conditions where O and NO number densities are known. Preliminary results give a value of $5.1 \times 10^{-3} \text{ s}^{-1}$, in excellent agreement with the most commonly used theoretical value of $5.4 \times 10^{-3} \text{ s}^{-1}$.

The measurements and data analysis are described in the following viewgraph presentation.

IMPORTANCE OF $N(^2P)$

T-5209

- $N(^2P)$ is a bright auroral radiator
- Auroral altitude from $I_{N(^2P)} / I_{N_2^+}$
- $N(^2P) + O$ probable source of NO^+
- $N(^2P) + O_2$ may be source of highly rotationally excited $NO(v)$
- Only theoretical values of $A(^2P - ^4S)$ available

EXPERIMENTAL APPROACH

T-5210

- Intensity = Einstein Coefficient x Number Density

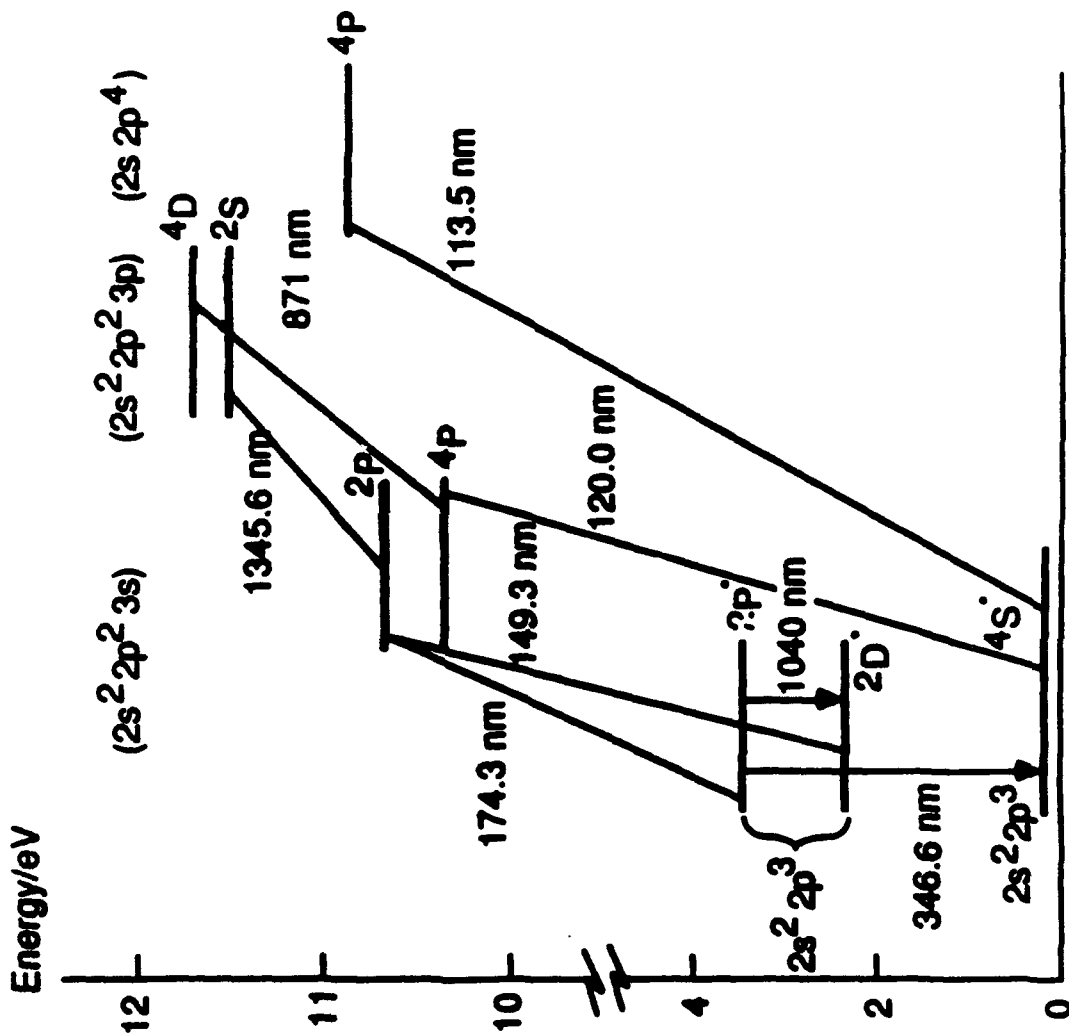
$$I = AN$$

$$A = I/N$$

- N measured by VUV resonance absorption
- I measured on instrument calibrated for absolute photon emission rates

ENERGY-LEVEL DIAGRAM OF ATOMIC NITROGEN

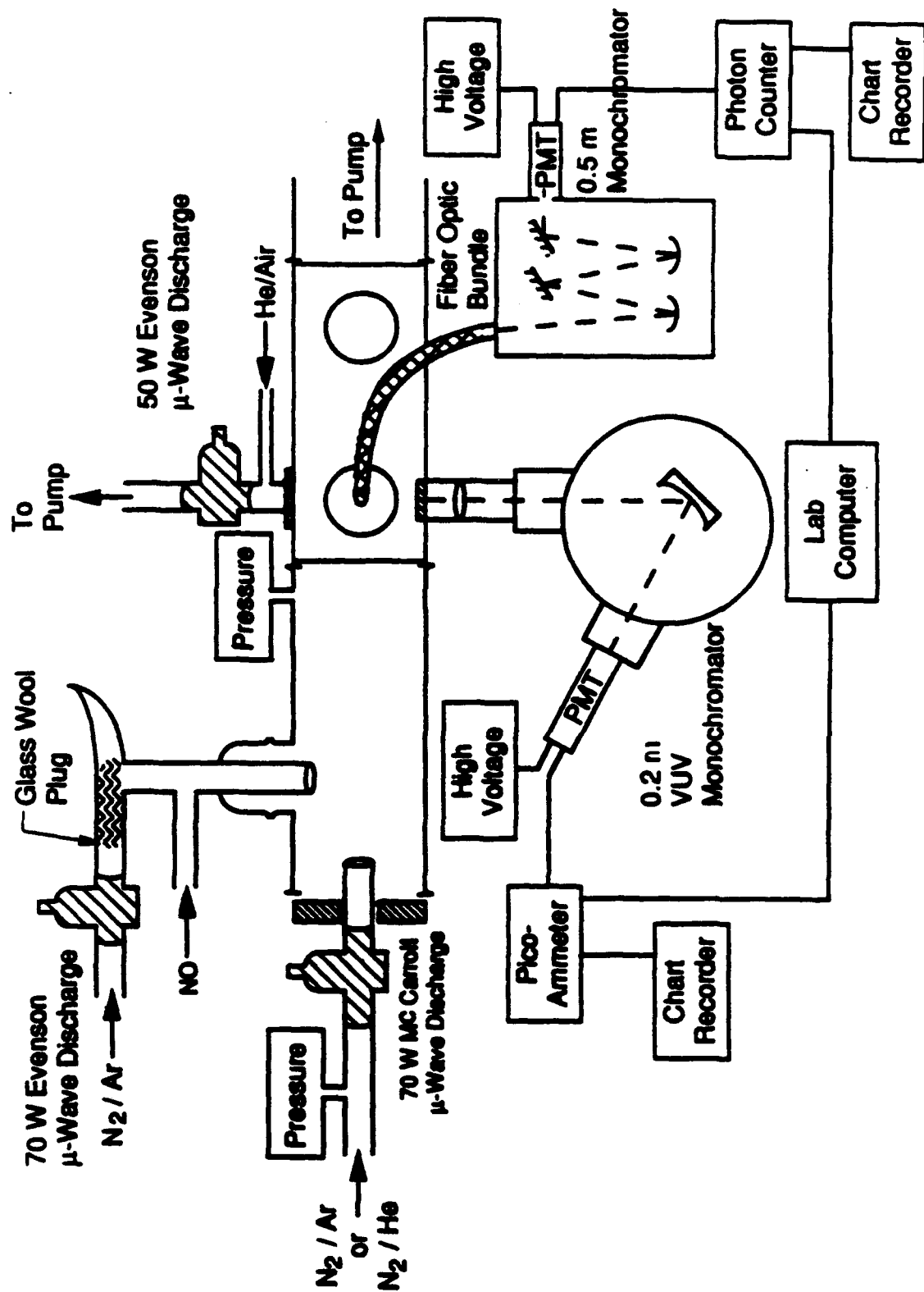
T-5211



B-0354a

SCHEMATIC OF APPARATUS FOR MEASURING $A(2P-4S)$ FOR $N(2P)$

T-5212



B-7486

RESONANCE ABSORPTION MEASUREMENTS

T-5213

- Resonance absorption

$$B = \frac{I_{\text{init}} - I_{\text{trans}}}{I_{\text{init}}}$$

- 174.3 nm emission line two unresolved doublets

$$B = \frac{\sum_i I_{\text{init}}^i - I_{\text{trans}}^i}{\sum_i I_{\text{init}}^i}$$

- A reasonable approximation

$$B \approx \frac{k_0 l}{(1 + \alpha^2)^{1/2}}$$

$k_0 l$ is optical depth

α is ratio of lamp to absorber linewidths

T-5213a

- $$B \approx \frac{k_o \ell}{(1 + \alpha^2)^{1/2}}$$

- $k_o \ell$: optical depth

$$k_o \ell = C f_{ul} N_\ell \ell$$

f_{ul} is oscillator strength

N_ℓ is number density

- $$\alpha^2 = \frac{\text{emission line width}}{\text{absorption line width}}$$

- Doppler broadened lines

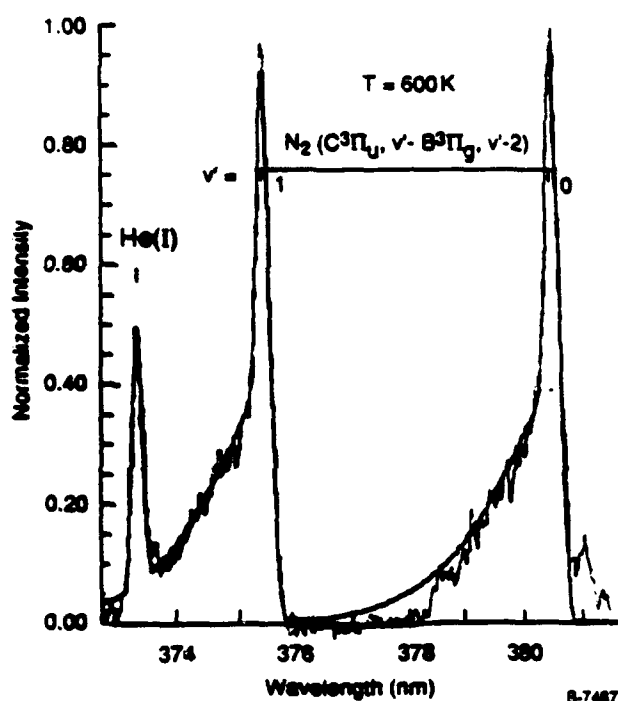
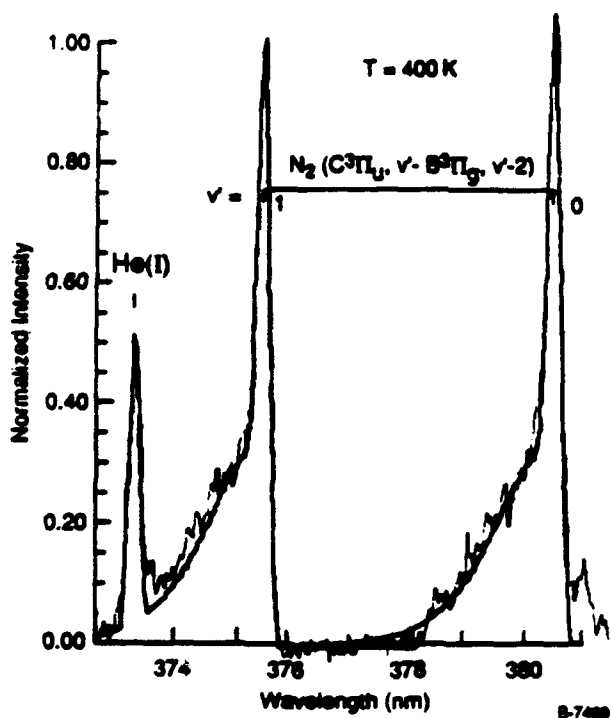
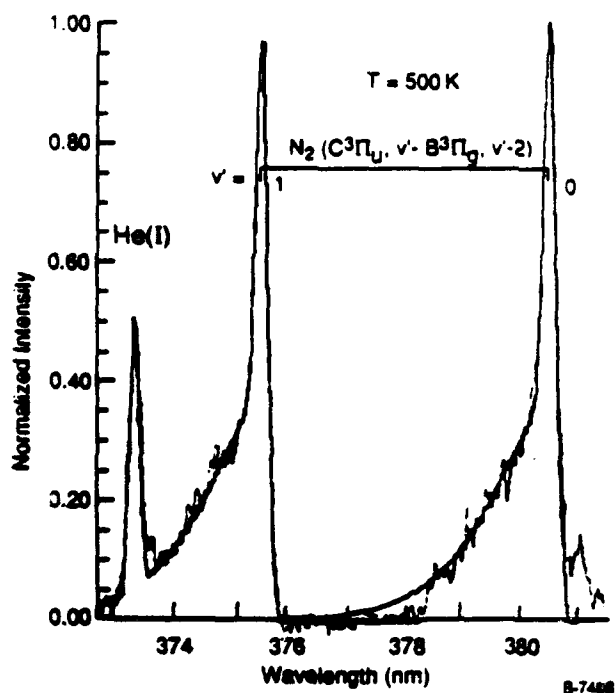
$$\Rightarrow \alpha^2 = \frac{T_{\text{emission}}}{T_{\text{absorption}}}$$

- $T_{\text{absorption}}$ = room temperature
 - T_{emission} = plasma kinetic temperature

DISCHARGE LAMP KINETIC TEMPERATURE

T-5214

- Translational and Rotational temperatures in equilibrium
- T_{rot} determined from spectral fit to N_2 second positive bands
- $T = 500 \text{ K}$ clearly superior to 400 or 600 K



ABSOLUTE PHOTOMETRIC CALIBRATION

T-5215

- Absolute calibration in situ using air afterglow



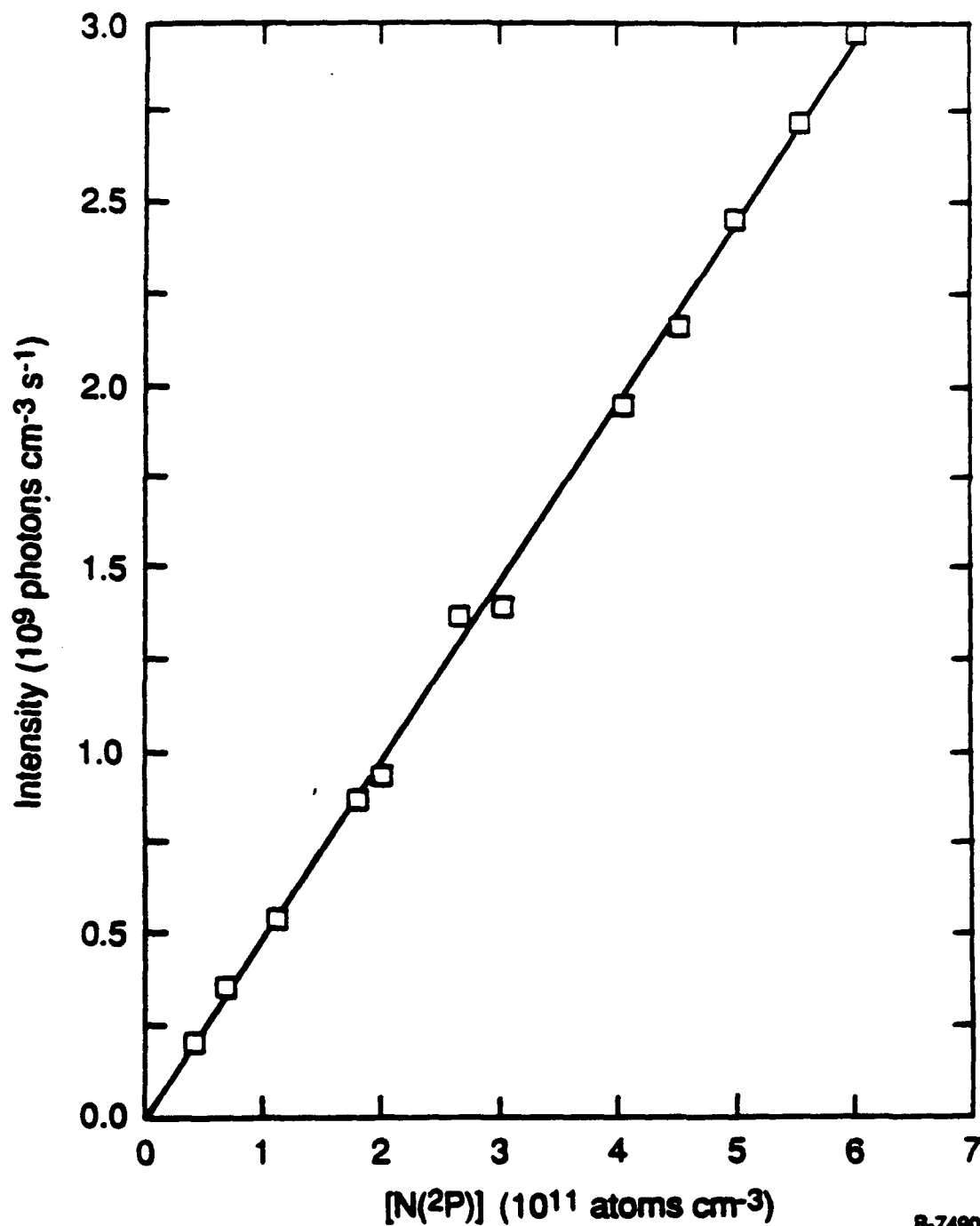
$$I_{\text{O/NO}} = k_\lambda [\text{O}][\text{NO}] \Delta\lambda \text{ VT}_\lambda \eta_\lambda$$

$\text{VT}_\lambda \eta_\lambda$ – Wavelength dependence - standard lamp

– Absolute - $I_{\text{O/NO}}$ with known $[\text{O}]$, $[\text{NO}]$

EMISSION OF $N(2P - 4S)$ 347 nm INTENSITY AS A FUNCTION OF $[N(2P)]$

T-5216



8-7490

PRELIMINARY RESULTS

T-5217

Radiative Decay
Rate (s)

Group and Method

Present results (1990)	- Experiment	$5.5(\pm 40\%) \times 10^{-3}$
Garstang (1956)	- Theory	5.4×10^{-3}
Godefroid and Froese Fischer (1984)	- Theory	4.8×10^{-3}

Conclusion: Theory and experiment appear to agree excellently

THIS PAGE INTENTIONALLY LEFT BLANK

APPENDIX K

The Reactions of $N(^2P)$ with O_2 and O

L.G. Piper

J. Chem. Phys. 98, 8560 (1993)

(SR-556 reproduced in its entirety)

THIS PAGE INTENTIONALLY LEFT BLANK

The reactions of $N(^2P)$ with O_2 and O

Lawrence G. Piper

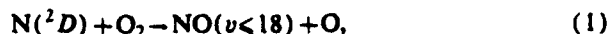
Physical Sciences Inc., Andover, Massachusetts 01810

(Received 4 December 1992; accepted 3 February 1993)

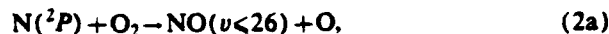
We have studied the kinetics of metastable $N(^2P)$ with atomic and molecular oxygen. The measurements were made in a discharge flow apparatus in which $N(^2P)$ was generated from the energy transfer reaction between $N_2(A)$ and ground state $N(^4S)$ and was monitored either by vacuum ultraviolet resonance fluorescence at 174 nm or else by observing the forbidden $N(^2P-^4S)$ emission at 347 nm. The rate coefficient for $N(^2P)$ quenching by O_2 is $(2.2 \pm 0.4) \times 10^{-12}$ $\text{cm}^3 \text{ molecule}^{-1} \text{ s}^{-1}$ and that for quenching by O is $(1.7 \pm 0.4) \times 10^{-11}$ $\text{cm}^3 \text{ molecule}^{-1} \text{ s}^{-1}$. One channel of the reaction between $N(^2P)$ and atomic oxygen appears to produce NO^+ via a chemi-ionization mechanism.

I. INTRODUCTION

The reaction between $N(^2D)$ and O_2 ,

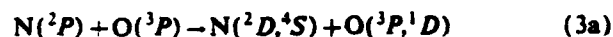


is the primary source of NO in the upper atmosphere and of vibrationally excited NO in the disturbed upper atmosphere.¹ Although much less abundant, the more energetic atomic nitrogen metastable, $N(^2P)$, can react with molecular oxygen to produce NO with significantly more internal energy,



While reaction (1) is well characterized in most regards,²⁻⁹ published values of the total rate coefficient for reaction (2) vary by a factor of 2.^{4,5,10,11} The products of reaction (2) have not been characterized at all, although Rawlins *et al.* have suggested that highly rotationally excited NO is the principal product.⁹

The reaction between $N(^2P)$ and atomic oxygen,



is even more poorly characterized. Only one experimental measurement of the rate coefficient for reaction (3) has been published,¹⁰ although the rate coefficient has been estimated from laboratory¹² and aeronomical¹³ observations. These estimates differ by nearly an order of magnitude. Theoretical considerations apparently favor channel (3a) over (3b),^{14,15} but experimental support is lacking.

This paper describes the measurements of the rate coefficients for $N(^2P)$ quenching by atomic and molecular oxygen. In addition we present evidence in support of channel (3b).

II. EXPERIMENT

The apparatus is a modification of one we have used previously in a number of other studies.^{8,16,17} It consists of a 2 in. i.d. flow tube pumped by a Leybold-Heraeus Roots blower/forepump combination capable of producing near velocities up to 5×10^3 cm s^{-1} at a pressure of 1 Torr. The

flow tube design incorporates separate source, reaction, and detection sections clamped together with O-ring joints (see Fig. 1).

The $N(^2P)$ was made in the upstream section of the flow reactor by adding a flow of nitrogen atoms to a flow containing metastable $N_2(A^3\Sigma_u^+)$.¹⁶ A low power, hollow-cathode dc discharge through a flow of argon produced metastable $Ar^*(^3P_{0,2})$. Downstream from this discharge, molecular nitrogen was mixed with the Ar^* , and the resulting energy transfer reaction between these two species ultimately made $N_2(A)$.^{18,19}

Atomic nitrogen was generated in a microwave discharge through a flow of nitrogen and argon in an 8 mm i.d. fixed point injector. Atomic nitrogen number densities were determined from NO titrations using procedures we have detailed previously.^{20,21} To ensure complete conversion of $N_2(A)$ to $N(^2P)$ prior to the reaction zone, we monitored the spectral region between 250 and 350 nm using a 0.5 m monochromator placed ~ 10 cm downstream from the N-atom injector. We adjusted the N-atom flow to be as small as possible while still ensuring complete removal of the Vegard-Kaplan band emission, $N_2(A^3\Sigma_u^+ - X^1\Sigma_g^+)$, diagnostic of $N_2(A)$. This procedure minimized both $N(^2P)$ losses from N-atom quenching and $N(^2P)$ production from N-atom recombination.²³

Molecular oxygen entered the flow tube through a movable loop injector consisting of a 0.25 in. diam length of stainless steel tubing capped with a perforated Teflon loop epoxied into its downstream end. The zero of the scale relating the distance between the injector and the detection region was calibrated by measuring the point at which the scattered light from the resonance fluorescence lamp suddenly increased as the injector was moved into the detection region.

To measure $N(^2P)$ quenching by atomic oxygen, we added O-atoms through a downstream fixed injector. The atomic oxygen was produced in the injector by titrating N atoms with NO. A microwave discharge through a flow of nitrogen in argon produced the N-atoms in the upstream end of the injector.

Mass flow meters monitored the flow rates of most gases, although rotameters were used for a few minor species. All flow meters were calibrated by measuring rates of

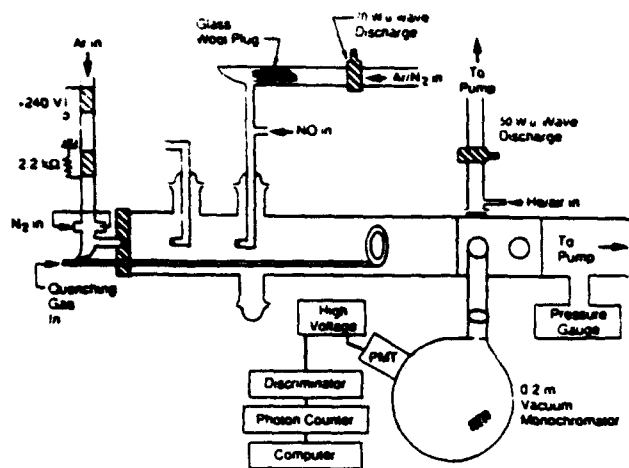


FIG. 1. Schematic of discharge-flow apparatus for studying $N(^2P)$ quenching kinetics.

increase in pressure with time into 6.5 or 12 ℓ flasks, using appropriate differential-pressure transducers (Validyne DP-15) which had themselves been calibrated with silicon oil or mercury manometers. Typically the flow rates for argon or helium, nitrogen, and quencher were 2000–5000, 50, and 0–120 $\mu\text{mol s}^{-1}$, respectively. The total pressure was generally 1–3 Torr, and the flow velocity was 1000–3500 cm s^{-1} .

Metastable $N(^2P)$ number densities were measured by resonance-fluorescence.^{8,22} Because the resonance lines of both $N(^2D)$ and $N(^2P)$ originate from a common upper state, one of the lines must be removed from the lamp so that the two metastables can be distinguished from each other. A suprasil window between the lamp and the flow reactor passed the 174 nm emission for $N(^2P)$ pumping, but rejected the 149 nm emission absorbed by $N(^2D)$. The combination of a 0.2 m vacuum monochromator, a photomultiplier with a CsI photocathode (120–185 nm sensitivity), and a photon-counting rate meter measured the resonance-fluorescence intensities in the flow tube.

III. RESULTS

A. $N(^2P)$ quenching by O_2

With the $N_2(A)$ off, some $N(^2P)$ still persisted in the flow reactor. This $N(^2P)$ was generated by transfer from $N_2(A)$ created by N -atom recombination.²³ The contribution to the total $N(^2P)$ signal from this secondary process, therefore, had to be subtracted to obtain unequivocal measurements. As a result, we monitored the decay of $N(^2P)$ as a function of added quencher both with the $N_2(A)$ on and with it off. The difference between the two sets of measurements, then, represents the quenching of the directly introduced $N(^2P)$. For the measurements on O_2 quenching this correction was small, generally < 10%.

Rate coefficients were determined from measurements of the change in the natural log of the metastable nitrogen number density as a function of number density of added

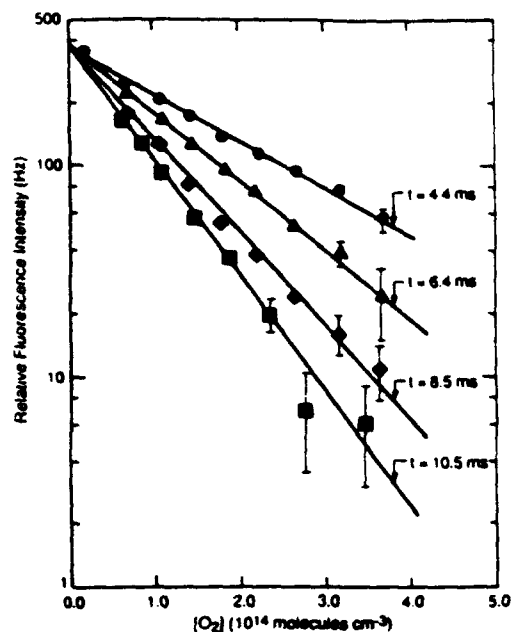


FIG. 2. Decay of $N(^2P)$ as a function of added molecular oxygen at four different reaction times.

quenching reagent with fixed reaction distance z , or time, z/\bar{v} ,⁸

$$-\frac{d \ln[N(^2P)]}{d[Q]} = 0.62 k_Q z / \bar{v} = \Gamma(z), \quad (4)$$

where the factor of 0.62 is a fluid mechanical correction needed to account for a parabolic velocity distribution in the flow tube.²⁴ The decay coefficient, Γ , requires corrections to the reaction distance, z , to account for imperfect mixing at the injector. Thus, one must measure decay coefficients at several different distances with all other conditions fixed, and then determine the rate coefficient from a plot of Γ vs z .

Figure 2 shows some typical decay plots for $N(^2P)$ quenching by molecular oxygen. The slopes of the lines in Fig. 2 are the decay coefficients at different reaction times. Plotting the decay coefficients as a function of reaction time, as shown in Fig. 3, corrects for imperfect mixing at the injector. The slope of the line in Fig. 3 is the rate coefficient for reaction (2) and the intercept is the effective O_2 mixing time in our reactor. Our results indicate that the rate coefficient for $N(^2P)$ quenching by molecular oxygen is $(2.2 \pm 0.4) \times 10^{-12} \text{ cm}^3 \text{ molecule}^{-1} \text{ s}^{-1}$. The error bars are a root-mean-square (rms) combination of the statistical uncertainty ($2\sigma = 14\%$) and the systematic uncertainty, 10%.

Our result agrees, within the limits of quoted error, with Hussain *et al.*⁵ measurement of $(2.6 \pm 0.2) \times 10^{-12} \text{ cm}^3 \text{ molecule}^{-1} \text{ s}^{-1}$ and the more recent measurement of Phillips *et al.*,¹¹ $(1.8 \pm 0.2) \times 10^{-12} \text{ cm}^3 \text{ molecule}^{-1} \text{ s}^{-1}$. Iannuzzi and Kaufman's⁴ value of $(3.5 \pm 0.5) \times 10^{-12} \text{ cm}^3 \text{ molecule}^{-1} \text{ s}^{-1}$ is somewhat larger than a consensus value based upon the other three sets of measurements.

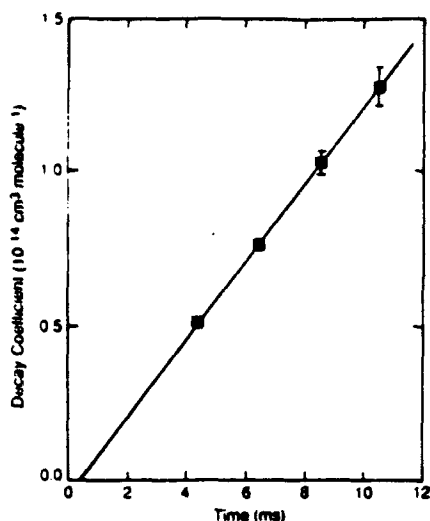


FIG. 3. Decay coefficients for $N(^2P)$ quenching by molecular oxygen as a function of reaction time.

B. $N(^2P)$ quenching by O

The procedure for measuring $N(^2P)$ quenching by O was similar to that given above for the quenching of $N(^2P)$ by O_2 . The decay of $N(^2P)$ was monitored as a function of added NO with the $N_2(A)$ discharge on and with it off. NO quantitatively converts N atoms to O, so the flow of O into the reactor will equal the flow of NO titrant added to the injector sidearm. The difference between the two decay curves was taken to represent the true rate of $N(^2P)$ quenching by O-atoms. Figure 4 shows two decay plots and their associated difference plot. Even though neither of the two raw decays are linear on the semilog plot, the difference between them is. The slope of this difference decay is the decay coefficient for quenching $N(^2P)$ by O as given in Eq. (4).

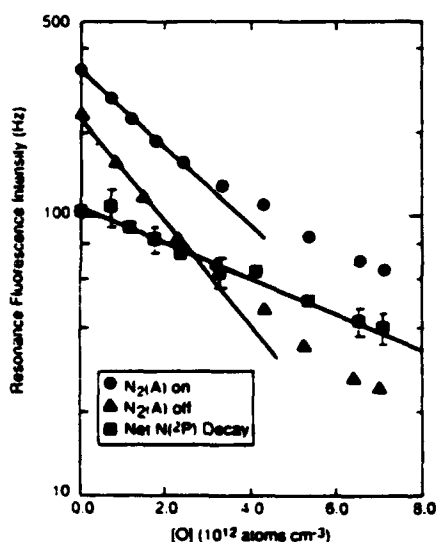


FIG. 4. Decay of $N(^2P)$ resonance-fluorescence intensity as a function of added atomic oxygen.

The N-atom number density required to make sufficient O for these measurements was several times greater than that required just to produce $N(^2P)$. Thus, the $N(^2P)$ generated from N-atom recombination was a much larger fraction of the total, as much as two-thirds of the total $N(^2P)$. Because the NO titration reaction reduced overall N-atom number densities, the background component decreased considerably, and nonexponentially, as the added NO increased.

Because the fixed injector does not give perfect mixing, we next determined a decay coefficient for $N(^2P)$ quenching by O_2 added through the same injector under otherwise similar flow conditions. The rate coefficient for O-atom quenching of $N(^2P)$ is then the ratio of the two decay coefficients times the previously determined rate coefficient for $N(^2P)$ quenching by O_2 . Our measurements show that the ratio of the two rate coefficients is 7.6 ± 1.1 , making the rate coefficient for $N(^2P)$ quenching by O $(1.7 \pm 0.4) \times 10^{-11} \text{ cm}^3 \text{ molecule}^{-1} \text{ s}^{-1}$.

The $N(^2P) + O$ rate coefficient has been estimated by Golde and Thrush¹² to be quite fast, $k_3 \sim 7 \times 10^{-11} \text{ cm}^3 \text{ molecule}^{-1} \text{ s}^{-1}$, and by Young and Dunn¹⁰ to be somewhat slower, but still fast, $k_3 \sim 1 \times 10^{-11} \text{ cm}^3 \text{ molecule}^{-1} \text{ s}^{-1}$. This is one of the few cases for which $N(^2P)$ quenching is reported to be faster than the corresponding quenching reaction with $N(^2D)$ ($k = 1.1 \times 10^{-12} \text{ cm}^3 \text{ molecule}^{-1} \text{ s}^{-1}$).¹⁷

C. Chemi-ionization from $N(^2P) + O$

Several groups have suggested that the interaction between $N(^2P)$ and O might be a chemi-ionization reaction producing NO^+ ,¹³ although others have argued on theoretical grounds that this mechanism is not likely.^{14,15} If it is a chemi-ionization reaction, this would explain the fast quenching of $N(^2P)$ by O. We tested for ionization by inserting electrodes into our flow reactor and measuring the resultant ion current. The electrodes consisted of a 1 in. diam loop centered along the flow tube axis upstream from the O-atom injector and a similarly sized circular electrode covered with nickel screen 10–20 cm downstream from the injector. The upstream electrode was biased positively while the downstream electrode, the collector, was at ground potential.

Figure 5 shows the variation in the collector current as a function of the potential difference between the two electrodes. The current rises quite steeply at low voltages, then levels off as the collector becomes saturated, and finally rises again as energetic ions and electrons in the gas begin to ionize the background argon.

Figure 6 demonstrates that the current collected in the plateau region ($\sim 75 \text{ V}$) varies linearly with the number density of $N(^2P)$. Additional measurements also showed that the current tracked linearly with the O-atom number density. In the absence of either $N(^2P)$ or O atoms, the ion current vanished. This evidence presents a strong case that chemi-ionization is at least one channel of the $N(^2P)$ plus O reaction. Our apparatus was not equipped with a mass spectrometer to identify NO^+ ions unequivocally, however, they seem the most likely candidate.

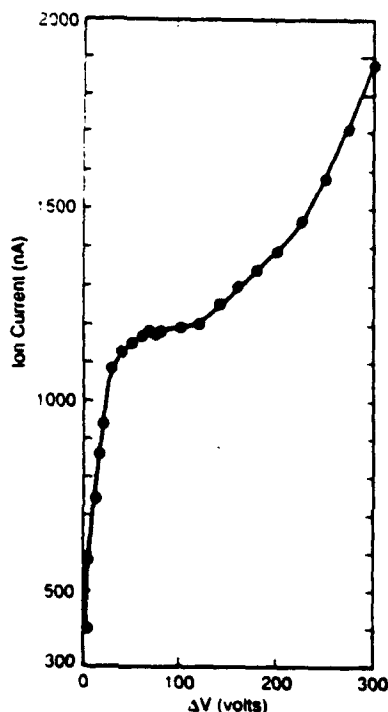


FIG. 5. Ion collection as a function of potential difference across electrodes.

The electrodes were not designed to collect the total ion current generated in the flow reactor. As a result, the magnitude of the ion current can only be used to determine a lower limit to the efficiency of the chemi-ionization chan-

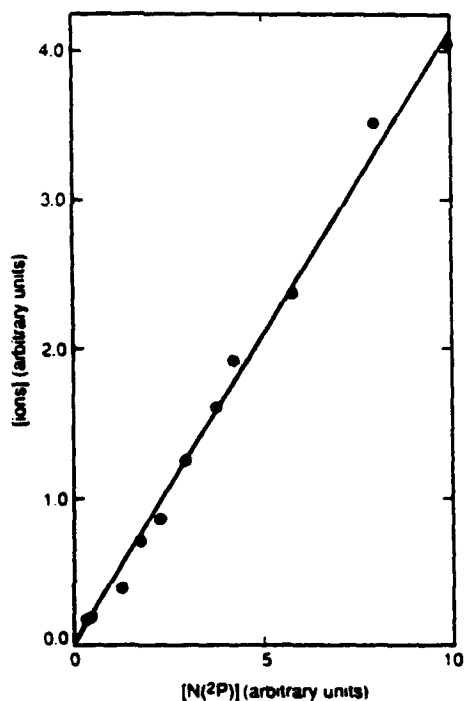


FIG. 6. Relationship between saturated ion current and $[N(^2P)]$ for fixed $[O]$.

nel. We estimate that at least 10% of the $N(^2P)$ atoms removed from the reactor are converted to ions. The true efficiency could be much higher than this.

IV. DISCUSSION

The reaction between $N(^2P)$ and O atoms is exoergic by ~ 0.3 eV for the channel to make NO^+ . Any other likely ions in the reactor would require somewhat more energy to produce. Support for the chemi-ionization channel comes from the experiments of Gatz *et al.*²⁵ They observed ion production when they added oxygen atoms to active nitrogen. By varying the potential between their electrodes, they were able to measure the mobility of the ions produced in their reactor. The mobility was exactly that which would obtain for NO^+ .

The principle removal mechanism for NO^+ ions is dissociative recombination with thermal electrons and the branching ratio for $N(^2D)$ production in NO^+ dissociative attachment is essentially unity.²⁶ Thus, if reaction (3b) is indeed the primary channel for $N(^2P)$ quenching by atomic oxygen, then the effects resulting from $N(^2P)$ production in the upper atmosphere would be indistinguishable from those resulting from $N(^2D)$ production. This is because $N(^2P)$ atoms will be predominantly converted to $N(^2D)$ either by dissociative recombination of NO^+ with electrons, reaction (3b), or via radiation to $N(^2D)$ at 1040 nm.

The principal processes for $N(^2P)$ removal at altitudes above 100 km are quenching by O atoms and, above 180 km, radiative decay. $N(^2P)$ radiates both in the infrared at 1040 nm to $N(^2D)$ and in the ultraviolet at 346.6 nm to $N(^4S)$. The transition probability of the 1040 nm transition is 16 times that of the 346.6 nm transition.²⁷ Thus, 94% of the $N(^2P)$ that radiates will end up as $N(^2D)$.

Overall $N(^2D)$ production rates in an aurora are much larger than those for $N(^2P)$ (Ref. 28) and $N(^2P)$ quenching by O atoms is an order of magnitude faster than is quenching by O_2 . Thus, only in a deeply penetrating aurora should $NO(v)$ production from the reaction of $N(^2P)$ with O_2 be important.

Rawlins *et al.*⁹ have observed high J rotational bandheads in the infrared spectrum of $NO(v,J)$ produced in the interaction of discharged nitrogen with O_2 . They speculated that these bandheads arose because a large fraction of the exoergicity of reaction (2) ended up as rotational energy in the product NO . They hypothesized that the rotationally hot $NO(v,J)$ could lead to significant emission in infrared bandpasses generally thought to be devoid of radiation.

Some support for the production of $NO(v,J)$ bandheads in a disturbed atmosphere issues from the interferometric observation of an aurora by Espy *et al.*²⁹ They observed several emission peaks to the blue of the main $NO(v,J)$ emission band. These peaks matched the location of the rotational bandheads observed by Rawlins *et al.*

Vallance Jones and Gattinger³⁰ have discussed how the mean altitude of an aurora can be determined by comparing the emission intensity of the $N(^2P \rightarrow ^2D)$ emission at 1040 nm to that from the N_2 first-negative system.

$N_2^+(B^2\Sigma_u^- - X^2\Sigma_g^+)$, or some other radiative feature known to be in fixed ratio with the $N_2^+(B-X)$ emission. The $N_2^+(B)$ emission intensity is a measure of the ion-pair production rate in an aurora. The primary production process for $N(^2P)$ is dissociative excitation of N_2 by the electrons.²⁸ This process has a cross-section energy dependence similar to that of N_2^+ production, so the ratio of excitation rates of $N(^2P)$ to N_2^+ should remain relatively constant over the range of typical auroral excitation conditions. $N_2^+(B)$ has a radiative lifetime of 65 ns and will not suffer quenching at any auroral altitudes. Any diminution in the ratio of emission intensities of $N(^2P)$ to $N_2^+(B)$, therefore, will be related to the local O-atom number density. The local altitude of the observed emission can be determined using a model atomic oxygen altitude profile.

Zipf *et al.*¹³ used a variation of this approach to estimate the rate coefficient, k_3 . They determined changes in the $N(^2P)$ to $N_2^+(B)$ intensity ratio as a function of altitude from data taken during a rocket flight. Combining their intensity ratio observations with an assumed O-atom number density profile allowed them to infer a value for k_3 of $1 \times 10^{-11} \text{ cm}^3 \text{ molecule}^{-1} \text{ s}^{-1}$, in reasonable accord with our direct measurement.

V. SUMMARY

We have determined rate coefficients for $N(^2P)$ quenching by O_2 and O to be $(2.2 \pm 0.4) \times 10^{-12}$ and $(1.7 \pm 0.4) \times 10^{-11} \text{ cm}^3 \text{ molecule}^{-1} \text{ s}^{-1}$, respectively. Our observation of ion production in the $N(^2P)/O$ atom system indicates chemi-ionization to form NO^+ is probably a significant reaction channel in this system, in contradiction to theoretical arguments.

ACKNOWLEDGMENTS

We appreciate financial support from the Defence Nuclear Agency (Project SA, Task SA/SDI, work unit 00175) and the Air Force Office of Scientific Research (Task 2310G4) through Contract No. F19628-88-C-0173 with the Phillips Laboratory, Geophysical Directorate. We were grateful to receive correspondence from Sir David Bates and Harvey Michels. The advice, comments, and

criticisms of PSI colleagues Dave Green, George Caledonia, Terry Rawlins, Bill Marinelli, and Mark Fraser were most welcome.

- ¹G. E. Caledonia and J. P. Kennealy, *Planet. Space Sci.* **30**, 1043 (1982).
- ²J. P. Kennealy, F. P. DelGreco, G. E. Caledonia, and B. D. Green, *J. Chem. Phys.* **69**, 1574 (1978).
- ³C. L. Lin and F. Kaufman, *J. Chem. Phys.* **55**, 3760 (1971).
- ⁴M. P. Iannuzzi and F. Kaufman, *J. Chem. Phys.* **73**, 4701 (1980).
- ⁵D. Husain, S. K. Mitra, and A. N. Young, *J. Chem. Soc. Faraday Trans. II* **70**, 1721 (1974).
- ⁶G. Black, T. G. Slanger, G. A. St. John, and R. A. Young, *J. Chem. Phys.* **51**, 116 (1969).
- ⁷T. G. Slanger, B. J. Wood, and G. Black, *J. Geophys. Res.* **76**, 8430 (1971).
- ⁸L. G. Piper, M. E. Donahue, and W. T. Rawlins, *J. Phys. Chem.* **91**, 3883 (1987).
- ⁹W. T. Rawlins, M. E. Fraser, and S. M. Miller, *J. Phys. Chem.* **93**, 1097 (1989).
- ¹⁰R. A. Young and O. J. Dunn, *J. Chem. Phys.* **63**, 1150 (1975).
- ¹¹C. M. Phillips, J. I. Steinfeld, and S. M. Miller, *J. Phys. Chem.* **91**, 5001 (1987).
- ¹²M. F. Golde, and B. A. Thrush, *Discuss. Faraday Soc.* **53**, 233 (1972).
- ¹³E. C. Zipf, P. J. Espy, and C. F. Boyle, *J. Geophys. Res.* **85**, 687 (1980).
- ¹⁴D. R. Bates, *Planet. Space Sci.* **37**, 1145 (1989).
- ¹⁵H. H. Michels, *Adv. Chem. Phys.* **45**, 225 (1972).
- ¹⁶L. G. Piper, *J. Chem. Phys.* **90**, 7087 (1989).
- ¹⁷L. G. Piper, *J. Chem. Phys.* **91**, 3516 (1989).
- ¹⁸D. W. Setser, D. H. Stedman, and J. A. Coxon, *J. Chem. Phys.* **53**, 1004 (1970).
- ¹⁹D. H. Stedman and D. W. Setser, *Chem. Phys. Lett.* **2**, 542 (1968).
- ²⁰L. G. Piper, G. E. Caledonia, and J. P. Kennealy, *J. Chem. Phys.* **75**, 2847 (1981).
- ²¹L. G. Piper and W. T. Rawlins, *J. Phys. Chem.* **30**, 320 (1986).
- ²²W. T. Rawlins and L. G. Piper, *Proc. Soc. Photo-Opt. Instrum. Eng.* **279**, 58 (1981).
- ²³A. Taghipour and W. Brennan, *Chem. Phys.* **37**, 363 (1979).
- ²⁴E. E. Ferguson, F. C. Fensfeld, and A. L. Schmeltekopf, in *Advances in Atomic and Molecular Physics V*, edited by D. R. Bates (Academic, New York, 1970).
- ²⁵C. R. Gatz, R. A. Young, and R. A. Sharpless, *J. Chem. Phys.* **39**, 1234 (1963).
- ²⁶J. L. Queffelec, B. R. Rowe, M. Morlais, J. C. Gomet, and F. Vallee, *Planet. Space Sci.* **33**, 263 (1985).
- ²⁷(a) R. H. Garstang, *The Airglow and the Aurora*, edited by Armstrong and A. Dalgarno (Pergamon, New York, 1956); (b) M. Godefroid and C. Froese Fischer, *J. Phys. B* **17**, 681 (1984).
- ²⁸M. H. Rees and G. J. Romick, *J. Geophys. Res.* **90**, 9871 (1985).
- ²⁹P. J. Espy, C. R. Harris, A. J. Steed, J. C. Ulwick, and R. A. Haycock, *Planet. Space Sci.* **36**, 543 (1988).
- ³⁰A. Vallance Jones and R. L. Gattinger, *J. Geophys. Res.* **84**, 1315 (1979).

THIS PAGE INTENTIONALLY LEFT BLANK

APPENDIX L

Review of the Chemistry of Vibrationally Excited Nitric Oxide in the Disturbed Upper Atmosphere

W.T. Rawlins

(Quarterly No. 12 reproduced in its entirety)

THIS PAGE INTENTIONALLY LEFT BLANK

**REVIEW OF THE CHEMISTRY OF VIBRATIONALLY EXCITED
NITRIC OXIDE IN THE DISTURBED UPPER ATMOSPHERE**

Quarterly Status Report No. 12

For the Period

1 June to 31 August 1991

Under Air Force Contract No. F19628-88-C-0173

Prepared by:

**W.T. Rawlins
Physical Sciences Inc.
20 New England Business Center
Andover, MA 01810**

Sponsored by:

**Air Force Geophysics Laboratory
Air Force Systems Command
U.S. Air Force
Hanscom Air Force Base, MA 01731**

November 1991

THIS PAGE INTENTIONALLY LEFT BLANK

TABLE OF CONTENTS

<u>Section</u>	<u>Page</u>
1. INTRODUCTION	1
2. ELECTRON-INITIATED CHEMISTRY	3
2.1 Precursor Formation	3
2.1.1 Auroral Bombardment	3
2.1.2 Nuclear Bombardment	6
2.1.3 Recommendations	8
2.2 Precursor Loss	9
2.3 NO Formation	14
2.4 NO Loss Processes	18
3. THERMALLY INITIATED CHEMISTRY	21
3.1 Precursor Formation	21
3.2 NO Formation	22
3.3 NO Removal	24
3.4 Recommendations	25
4. EXCITATION OF NO(v,J)	26
4.1 Chemiexcitation	26
4.2 Energy Transfer	34
4.3 Radiative Excitation	37
4.4 Recommendations	39
5. DEACTIVATION OF NO (v,J)	41
5.1 Collisional Deactivation	41

TABLE OF CONTENTS (Continued)

<u>Section</u>		<u>Page</u>	
5.2	Radiative Deactivation	46	-
5.3	Recommendations	50	
6.	SUMMARY AND CONCLUSIONS	52	
7.	REFERENCES	57	

LIST OF FIGURES

<u>Figure</u>		<u>Page</u>
1	Auroral N(² D) production rates as modeled by Caledonia and Kennealy [5] for an ICB II aurora	93
2	Auroral N(² P) production efficiencies based on data from Zipf et al. [8] and multiples of the U.S. Standard Atmosphere [11] atomic oxygen profile	94
3	Recommended rate coefficients and uncertainties for quenching of N(² D, ² P) by O	95
4	Recent measurements of the rate coefficient for N(² D) + O ₂ quenching at 300 K	96
5	Rate coefficients and uncertainties for reaction of N(² D) with O ₂	97
6	Measurements of the rate coefficient for N(² P) + O ₂ quenching at 300 K	98
7	Rate coefficients and uncertainties for reaction of N(² P) with O ₂	99
8	Recommended rate coefficients for quenching of N(² D)	100
9	Recommended rate coefficients for quenching of N(² P)	101
10	Evaluated rate coefficients for O ₂ + M dissociation, extracted from Baulch et al.	102
11	Evaluated rate coefficients for N ₂ + M dissociation, extracted from Baulch et al.	103
12	Recommended rate coefficients and uncertainties for O ₂ + M and N ₂ + M dissociation	104
13	Rate coefficients for the reaction of N(⁴ S) with O ₂ , extracted from Baulch et al.	105
14	Comparison of recommended rate coefficients for reaction of O ₂ with N(⁴ S), N(² D), and N(² P)	106

LIST OF FIGURES (Continued)

<u>Figure</u>		<u>Page</u>
15	Rate coefficient data for the reaction of O with N ₂ , extracted from Hanson and Salimian	107
16	Recommended rate coefficients and uncertainties for the N + O ₂ and O + N ₂ reactions	108
17	Rate coefficient data for the reaction of O with NO, extracted from Hanson and Salimian	109
18	Rate coefficient data for NO + M dissociation, extracted from Hanson and Salimian	110
19	Evaluated rate coefficients for NO + M dissociation, extracted from Baulch et al.	111
20	Recommended rate coefficients and uncertainties for NO removal reactions	112
21	Potential energy curves for the low-lying states of NO, extracted from Kenner and Ogryzlo	113
22	Recommended rate coefficients and uncertainties for two-body recombination of N and O	114
23	Relative NO(v) populations produced in the energy transfer between N ₂ (A ³ Σ _u ⁺) and NO, from the data of Piper and co-workers	115
24	Predicted excitation rates for NO(v=1) in the undisturbed upper atmosphere	116
25	Estimated rate coefficients for collisional excitation of NO(v) by O, compared to the rate coefficient for chemical reaction	117
26	Recommended rate coefficients and uncertainties for deactivation of NO(v) by O	118

LIST OF FIGURES (Continued)

<u>Figure</u>		<u>Page</u>
27	Comparison of temperature dependences for deactivation of NO($v=1$) by O ₂ , N ₂ , NO, and Ar	119
28	Theoretical dipole moment function of Billingsley [104] (dashed curve) compared to potential curve for NO(X ² Π)	120
29	Comparison of observed and predicted overtone/fundamental branching ratios	121
30	NO Einstein coefficients for the fundamental and first overtone sequences	122

LIST OF TABLES

<u>Table</u>		<u>Page</u>
1	High Altitude NO Chemistry	66
2	Recommended Average N^* Production Rates, Atoms/Ion Pair	68
3	Representative Kinetic Parameters Relevant to N^* Production	69
4	Gilmore Mixing Rules for Ion and Excited State Production Rates by Electron Bombardment in Dissociated or Ionized Air	71
5	Recommended Kinetic Parameters for N^* Collisional Loss Processes	72
6	Recommended Kinetic Parameters for NO Formation Reactions	74
7	Recommended Kinetic Parameters for NO Removal Processes	75
8	Recommended Kinetic Parameters for High-Temperature NO Formation and Removal Reactions	76
9	Surprisal Predictions of Relative Initial Populations of NO(v) in the Reactions of $N(^2D, ^2P)$ with O_2	77
10	Energy Transfer Kinetics for $N_2(A^3\Sigma_u^+ + NO$	78
11	Initial NO($X^2\Pi, v$) Populations from $N_2(A^3\Sigma_u^+) + NO$	79
12	Estimated Rate Coefficients for Excitation of NO(v) by $O + NO(v=0)$ Collisions	80
13	Suggested Kinetic Parameters for NO(v,J) Excitation Processes	81
14	Measured Rate Coefficients for Deactivation of NO(v) by N_2 and O_2 at 300 K	83
15	Absorption Coefficients and Transition Probabilities for the $\Delta v=1$ and $\Delta v=2$ Transitions of NO	84

LIST OF TABLES (Continued)

<u>Table</u>		<u>Page</u>
16	Predicted Einstein Coefficients for NO($\Delta v=1,2$) Transitions	86
17	Suggested Einstein Coefficients for NO($\Delta v=1,2$) Transitions, $T < 1000$ K	87
18	Recommended Kinetic Parameters for Deactivation of NO(v)	88
19	Key Unknown Factors in High-Altitude NO(v) Chemistry	89

THIS PAGE INTENTIONALLY LEFT BLANK

1. INTRODUCTION

Nitric oxide, NO, is an upper atmospheric trace species which plays a vital role in the chemical and radiative budgets of the quiescent, auroral, and nuclear-disturbed upper atmosphere. NO can be formed in situ from solar/UV photochemistry, electron bombardment chemistry, and high temperature air dissociation typical of a high altitude nuclear burst. In the normal thermosphere, its abundance varies widely depending on conditions of insolation, geomagnetic activity, and horizontal and vertical transport. Its prolific infrared and ultraviolet radiation bands can be excited by a wide variety of mechanisms, with very different spectral distributions depending on the energy dynamics of the excitation process. Infrared radiation from the fundamental vibration-rotation band at $5.3\ \mu\text{m}$ is the main cooling mechanism for the thermosphere, and IR radiation from this band and the first overtone at $2.7\ \mu\text{m}$ presents serious background discrimination problems in nuclear burst scenarios. To predict NO radiation levels for a variety of nuclear-disturbed conditions, one must model the detailed kinetics of NO formation and excitation in electron-bombarded and high temperature conditions. The credibility of such predictions is limited by uncertainties in the relevant chemical reaction kinetics, including experimental uncertainties in previously measured kinetic parameters, validity of extrapolations into unmeasured physicochemical regimes, and the possibility of missing or unknown chemical processes.

The purpose of this report is to provide a comprehensive and critical review of the known chemical kinetics of NO relevant to excitation of $2.7\ \mu\text{m}$ and 5 to $11\ \mu\text{m}$ radiation in the nuclear-disturbed upper atmosphere. Our objective is to determine a set of recommended kinetic parameters and confidence limits for use in predictive modeling and sensitivity studies, and to identify major gaps or uncertainties in the data base which need to be resolved. The temperature range of interest is nominally 200 to 8000 K. Since the altitude range of interest is above $\sim 100\ \text{km}$, we will not address three-body recombination chemistry, nor will we consider bimolecular reactions involving N_2O , NO_2 , or O_3 , on the premise that these species have no known bimolecular production

reactions involving diatomic precursors, and will thus play no significant role in the chemistry of NO at low pressure. However, we note that it is conceivable that such reactions will someday be demonstrated (some have already been suggested), and it may eventually be necessary to reconsider the role of triatomic species such as N_2O in the high altitude chemistry of NO.

The relevant chemical reactions are listed in Table 1. The reactions fall into two basic classes: those which involve excited state species formed from electron impact processes, and those which occur at high temperatures. Data for the excited state chemistry come mainly from laboratory experiments near room temperature and auroral aeronomic investigations. These reactions are thus moderately efficient near room temperature, but the scalings of their rate coefficients and product branching ratios with temperature are essentially unknown. The reactions relevant to high temperature air have been well studied by shock tube techniques, and most of the rate coefficients are generally known to a factor of 2 at temperatures of 2000 to 3000 K. However, scalings to higher temperatures, and third body efficiencies where relevant (i.e., dissociation reactions), are not well known. Finally, information on specific product state excitation and deactivation is very limited, and is confined mainly to low temperature chemiluminescence experiments. Since the product internal state distributions are very sensitive to the detailed dynamics of the reagent molecules' approach and collision with one another, the chemical excitation and deactivation processes may have complex temperature dependencies which are virtually impossible to predict with any confidence using simple kinetic arguments.

In this evaluation, we attempt to provide high temperature extrapolations of the existing data using reasonable assumptions of simple kinetic theory, and to define conservative uncertainty bounds. The resulting data base should then be used in systematic modeling sensitivity studies to determine the impact of key kinetics uncertainties on predictions for a given scenario. In the following, we discuss the reactions of Table 1 on a case-by-case basis, assess ranges of uncertainty and key research requirements, and present plots of rate coefficients in Arrhenius form.

2. ELECTRON-INITIATED CHEMISTRY

2.1 Precursor Formation

The primary formation of NO precursors at high altitude (≈ 100 to 300 km) is through electron impact processes giving rise to the metastables $N(^2D)$ and $N(^2P)$. These species react with O_2 to provide the primary source of NO in the thermosphere. The principal $N(^2D, ^2P)$ formation processes are listed in Table 1, Reactions (1a.1) to (1a.5). In the quiescent daytime thermosphere, $N(^2D)$ is produced mainly by $e^- + NO^+$, with additional contributions from $N_2^+ + O$ and $e^- + N_2$, and significant contribution from $e^- + N_2^+$ above 250 km. [1] During an auroral bombardment, Reactions (1a.1), (1a.3), and (1a.4) provide roughly equal contributions between 110 and 200 km, the altitude range in which most of the NO formation occurs. [2,3] In a strong bombardment, where the electron number densities are large enough for dissociative recombination of N_2^+ to compete with charge transfer, Reaction (1a.2) supplants (1a.3) and (1a.4) as the major source of N^* . [4] Thus the relative importance of the various source terms depends upon the bombardment scenario in question.

The customary method for evaluating N^* production rates is through detailed modeling of the electron energy deposition, using various electron fluxes and energy distributions (describing the strength and penetration of the bombardment) together with measured electron impact cross sections. While it is beyond the scope of the present paper to critically review this complex data base, we provide here a brief review emphasizing key uncertainties in defining N^* production rates.

2.1.1 Auroral Bombardment

A considerable body of data exists on the high altitude excitation of $N(^2D)$ and $N(^2P)$, principally through radiometric observations of dipole-forbidden emissions from these states at 520, 346.6, and 1040 nm in weak overhead auroras. In addition, $N(^2D)$

excitation has been modeled by several investigators, of whom only a few are cited here. Unfortunately, there is little quantitative closure between the models and the measurements because of unknown factors affecting the measurement interpretation (O-atom number densities, electron hardness, vertical altitude profiles corresponding to overhead brightness, ion pair production rates) and uncertainties in the kinetic models (incorrect O quenching rate coefficients, uncertain radiative transition probabilities).

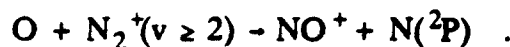
Caledonia and Kennealy [5] modeled $N(^2D, ^2P)$ production in an IBC II aurora (~ 8 kR overhead brightness at 391.4 nm) with the results shown in Figure 1. The total N^* production, which was taken to be $N(^2D)$ only, was computed to be $\sim 1.5 N(^2D)/\text{ion pair}$. The data sources were measurements of Kley et al. [6] for Reaction (1a.3), estimates of Frederick and Rusch [1] for Reactions (1a.4) and (1a.5), and theoretical predictions of Porter et al. [7] for Reaction (1a.1). The yield of $N(^2D, ^2P)$ from dissociative excitation of N_2 , 0.57 atoms/ion pair, is slightly larger than the value of 0.47 ($0.3 N(^2D) + 0.17 N(^2P)$) determined by Zipf et al. [8] from measurements of the electronic excitation cross sections by Zipf and McLaughlin [9] together with pre-dissociation considerations.

Predictions by Rusch and Gerard [2] for a weak nighttime aurora (< 0.3 kR overhead brightness at 391.4 nm) are generally consistent with the results of Caledonia and Kennealy; however, notwithstanding the authors' claims of good agreement between their predictions and their data, Rusch and Gerard's reported overhead brightnesses at 427.8 and 520 nm indicate an apparent $N(^2D)$ production rate on the order of ~ 10 atoms/ion pair, or about an order of magnitude larger than the model prediction. Similarly, brightness ratios reported by Sivjee and Marshall [10] for ground-based measurements of weak auroras at 346.6 nm and 520 nm indicate $N(^2D)/N(^2P)$ production rate ratios on the order of 100, as opposed to the factor of ~ 6 implied by the models cited above. More recent calculations by Rees and Romick [3] for a weak nighttime aurora (~ 4 to 5 kR at 391.4 nm) give altitude dependent yields which asymptote above 140 km to $0.12 N(^2P)/\text{ion pair}$, $0.59 N(^4S)/\text{ion pair}$, and 1.32

$N(^2D)$ /ion pair; however, in contrast to the other model predictions cited above, the main contributors to $N(^2D)$ production are predicted to be Reactions (1a.3) and (1a.4), with dissociative excitation of N_2 playing only a minor role. Thus the total N^+ production rates predicted by the models are all near 1.5 atoms/ion pair, but the branching fraction for $N(^2P)$ production is not well understood and may be a sensitive function of the hardness of the dosing, at least for weak auroras (see Zipf et al. [8], Rees and Romick [3]). In addition, the available data for auroral $N(^2D)$ production appear to be highly uncertain at best, and do not corroborate the model predictions.

The measurements of Zipf et al. [8] provide useful data on the auroral production efficiency of $N(^2P)$ in a moderate aurora. These measurements consist of rocketborne observations of overhead brightness at 346.6 and 391.4 nm as functions of altitude through an IBC II aurora (10 kR at 391.4 nm, overhead brightness from 110 km). Since the primary loss process for $N(^2P)$ is quenching by O, whose room temperature rate coefficient is now well known (vide infra), it is straightforward to apply steady-state kinetics to the Zipf et al. data to solve for an auroral production efficiency. Unfortunately, the atomic oxygen number density profile was not measured and must be treated parametrically. Our procedure was to convert their observed volume emission rates at 391.4 and 346.6 nm into ion pair production rates and $N(^2P)$ number densities as functions of altitude. We then corrected the $N(^2P)$ number densities for quenching by O and O_2 and radiative loss to obtain steady-state production rates for $N(^2P)$. The major term in this correction is O quenching, and we used several multiples of the atomic oxygen profile given by the U.S. Standard Atmosphere [11]. This profile is similar to measured O profiles characteristic of the auroral thermosphere [12]. The resulting ratios of $N(^2P)$ and ion pair production rates are plotted in Figure 2. The median value is $\sim 0.3 N(^2P)$ /ion pair; to achieve the value of 0.17 atoms/ion pair deduced by Zipf et al. from modeling the dissociative excitation of N_2 would require an O profile at about half the USSA number density. For comparison, $N(^2P)$ production rates inferred from observations of 1040 nm emission are reported to be 0.38 [13] and 0.33 [14] atoms/ion pair, in reasonable agreement with the value of 0.3 we infer above from 346.6 nm data.

Unfortunately, because the O number densities for the measurements are not known, the measured efficiency is uncertain by about a factor of 2 to 3. However, the data provide a reasonable indication that the $N(^2P)$ production rate is significantly larger than the modeled $e^- + N_2$ contribution. This would suggest another source, and Zipf et al. have suggested

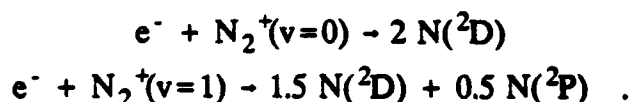


There are no experimental data to confirm this reaction path. Alternatively, perhaps the $N(^2P)$ yield from dissociative excitation of N_2 , which is a sensitive function of dosing hardness for very weak bombardments, is also sensitive to the electron energy distributions in the range encountered for IBC II-III auroras, and increases with average electron energy. This possibility is not supported by the Zipf cross sections. In any case, it seems likely that the $N(^2P)$ production efficiency in moderate to strong auroras is larger than commonly believed: we have shown [15] that, even assuming 0.3 $N(^2P)$ /ion pair, it is difficult to account for high-rotation $NO(v,J)$ radiances observed [16] in an overhead IBC II+ aurora, presumably arising from the reaction of $N(^2P)$ with O_2 [17].

2.1.2 Nuclear Bombardment

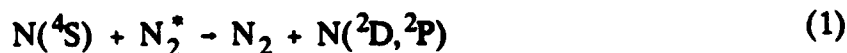
The electron impact chemistry for strong bombardment scenarios has been treated extensively by Gilmore [4,18] and we adopt his recommendations here. For large electron number densities, where electron-molecule reaction rates are larger than molecular charge transfer rates, N production occurs primarily through Reactions (1a.1) and (1a.2). As time progresses and the electron number densities decrease through recombination, the system relaxes toward the auroral case described above, and the ion-molecule reactions become more important. Thus different reactions will dominate at different times during the bombardment, and the corresponding N^* production efficiencies will vary accordingly.

Gilmore's computed N^* yields from dissociative excitation, based on the cross sections given by Zipf and coworkers [8,9], are 0.42, 0.25, and 0.62 atoms/ion pair for $N(^2D)$, $N(^2P)$, and $N(^4S)$, respectively. These values are similar to those obtained by Zipf et al. [8] for auroral conditions, with a 30 to 50% increase in dissociation rate but essentially no changes in computed relative $N(^4S, ^2D, ^2P)$ branching ratios for the more energetic bombardment conditions. Gilmore's predicted yields for the dissociative recombination of N_2^+ are based on theoretical branching ratio predictions of Michels [19], as well as on the rate coefficient measured by Mehr and Biondi [20] and on the code prediction [4] of 0.64 N_2^+ /ion pair. However, in contradiction to the Michels prediction of 1.08 $N(^2D)$ and 0.92 $N(^4S)$ per N_2^+ recombination, measurements by Queffelec et al. [21] show N^* metastable yields in excess of 1.85 per recombination. Indeed, more thorough analysis of Queffelec et al.'s results leads to the following:



These results certainly have a significant effect on predictions of the net N^* yields for the strong bombardment case, and we recommend modifying Gilmore's values to incorporate the large $N(^2D)$ yields observed by Queffelec et al. In addition, it is likely that significant $N(^2P)$ is also produced, depending on the vibrational distribution of the N_2^+ ; this could result in as much as a doubling of the predicted production rate of $N(^2P)$.

Finally, in view of the poor comparison between predictions and auroral data, it is important to consider other potential sources of $N(^2D, ^2P)$. One such class of processes is the family of reactions



where N_2^* is vibrationally and/or electronically excited N_2 . States above $N_2(X^1\Sigma_g^+, v=9)$ and $N_2(X, v=14)$ are sufficiently energetic to excite $N(^4S)$ to $N(^2D)$ and $N(^2P)$,

respectively. As an example of such a reaction, Piper [22] has shown that the reaction of N with $N_2(A^3\Sigma_u^+, v=0,1)$ proceeds at room temperature with a rate coefficient of $(4.0 \pm 0.5) \times 10^{-11} \text{ cm}^3 \text{ molecule}^{-1} \text{ s}^{-1}$, with an $N(^2P)$ yield of essentially unity. Indeed, an apparent excess of $N(^2P)$ production observed by Piper suggests either an error in the $N(^2P - ^4S)$ transition probability or significant production of $N(^2P)$ by $N_2(X,v)$ present in the reactor. However, to provide a significant source of N^* in an upper atmospheric bombardment, Reaction (1) would have to compete successfully with rapid removal of $N(^4S)$ by NO and with quenching of N_2^* , primarily by O and to a lesser extent by O_2 . Evaluations of these processes are discussed in later sections of this report. Evaluation of the role of Reaction (1) in the disturbed upper atmosphere would require supplemental data on N_2^* excitation, not covered in this report. These processes have been carefully modeled by Cartwright [23] for auroras and by Gilmore [4,18] for strong bombardments.

2.1.3 Recommendations

Our recommended N^* production rates, in atoms/ion pair, are listed in Table 2 for the auroral and strong bombardment limits. We note that these rates will actually be fairly sensitive to altitude at the lower edge of the dosing penetration, and treatment of these effects should involve detailed modeling of the electron deposition. Relevant (but not critically reviewed) kinetic data and literature sources are listed in Table 3. Scaling formulae for species production rates for electron bombardment of dissociated and ionized air, as suggested by Gilmore [18], are listed in Table 4.

A complete review of excitation cross sections, modeling calculations, and supporting laboratory and aeronomic data is beyond the scope of the present report; however, we recommend that such a critical review be performed in order to evaluate the aeronomic and laboratory data base, and to provide a more objective determination of the uncertainties of the predictions. At the present time, we subjectively ascribe an overall confidence of \pm a factor of 2 in the recommended production rates. However,

this confidence is not supported by any auroral or experimental data. and we further recommend a series of auroral and laboratory experiments designed to verify the predictions of the electron deposition models. Additional unknown factors which are required to properly interpret such measurements include the absolute transition probabilities for $N(^2D - ^4S)$, 520 nm, $N(^2P - ^4S)$, 346.6 nm, and $N(^2P - ^2D)$, 1040 nm; these are known only from the theoretical work of Garstang [24,25] (see Table 3), and should be determined experimentally and/or verified theoretically.

We also note that the present factor-of-2 uncertainty in the auroral predictions, together with the poor comparisons to the data base, allow room for the existence of hitherto unidentified N^* source reactions (particularly for $N(^2P)$) which could scale to greater significance in the strong or intermediate bombardment cases. Missing sources of $N(^2P)$ could have profound effects on predictions of high-rotation $NO(v,J)$ spectral signatures (vide infra).

It is also important for the nuclear case to consider the effects of high vibrational and gas-kinetic temperatures on the cross sections and product branching ratios for dissociative excitation, dissociative recombination, and ion-molecule reactions. In particular, in the electron impact processes where Franck-Condon factors affect the excitation to dissociative or predissociative electronic states, vibrational excitation of the reactant molecule can open new channels for product atomic state formation which would not be observed in room temperature interactions. This is clearly the case for the dissociative recombination of N_2^+ as described above. Vibrational temperature effects are potentially very important and could lead to marked increases in $N(^2P)$ production efficiencies in a heated atmosphere. We recommend theoretical and experimental investigations of the effects of reactant vibrational energy on the product branching ratios for dissociative excitation of N_2 and dissociative recombination of N_2^+ and NO^+ .

2.2 Precursor Loss

The primary high-altitude N^* loss processes are listed in Table 1, Reactions (1b.1) through (1b.11). In the auroral atmosphere, the main loss processes for $N(^2D, ^2P)$ are quenching by O and O_2 . There are now good kinetic data for these reactions at room temperature, but reliable information on temperature dependencies is practically non-existent. Thus extrapolation of the room temperature data to strong bombardment conditions is highly uncertain. However, superelastic quenching by electrons will dominate even gas-kinetic molecular/atomic quenching at electron densities above about 10^{10} cm^{-3} , so the molecular processes will be most important in the cooler recombination regions of the plasma where the electron densities are approaching ambient conditions.

The rate coefficient for quenching of $N(^2D)$ by O is a critical aeronomic parameter and has been the subject of controversy for the past 15 years [26]. Rate coefficient values have been inferred many times from aeronomic models of thermospheric NO and 520 nm airglow/auroral data, and tend to be erroneously low, in the $10^{-13} \text{ cm}^3 \text{ s}^{-1}$ range. However, in view of the significant uncertainties in $N(^2D)$ production rates and (usually) in the atomic oxygen number densities used in these models, it is inappropriate to treat the quenching rate coefficient as an adjustable parameter to be determined from the model. Laboratory measurements [27-30] generally agree on a room temperature value in the range $(1-2) \times 10^{-12} \text{ cm}^3 \text{ s}^{-1}$. A recent controversial laboratory determination of $2.1 \times 10^{-11} \text{ cm}^3 \text{ s}^{-1}$, reported by Jusinski et al. [31], is seriously incompatible with modeling of atmospheric $N(^4S)$, $N(^2D)$, $O(^1D)$, and NO profiles [32], and is subject to several likely experimental artifacts [29,30]. We consider the result reported by Piper [29], $(1.06 \pm 0.26) \times 10^{-12} \text{ cm}^3 \text{ s}^{-1}$ at room temperature, to be the most precise and incontrovertible result available, because of the use of resonance fluorescence to diagnose well-defined $N(^2D)$ decays at very low reagent number densities, the careful avoidance of mixing and flow artifacts, and the use of three different techniques for chemical generation of O in the reactor. This value is in

excellent agreement with most of the other laboratory measurements [27,28,30] as well as with recent aeronomic results [32]. In addition, Davenport et al. [27] reported some evidence for a temperature dependence (activation energy) of 1.0 ± 0.5 kcal/mole, which we adopt here. However, we stress that the temperature dependence data are meager at best, and the uncertainty in this rate coefficient at high temperature is large even though the value at room temperature is very well determined. The uncertainty is illustrated in Arrhenius form in Figure 3.

Quenching of $N(^2P)$ by O is less well understood. Rate coefficients derived from laboratory [33,34] and aeronomic [8] measurements are in the $\approx 1 \times 10^{-11}$ range. Very recent results of Piper [35] give a value of $(1.7 \pm 0.3) \times 10^{-11} \text{ cm}^3 \text{ s}^{-1}$ at room temperature. The relatively large rate coefficient for this reaction is surprising in view of the much smaller values for $N(^2D) + O$ and for most other $N(^2P)$ quenching reactions [26]. Golde and Thrush [33] suggested that the large rate coefficient resulted from a chemi-ionization product channel to form NO^+ , and Piper [36] reports observation of NO^+ as a major product of the quenching process. However, Bates [37] has argued on theoretical grounds that the chemi-ionization channel does not occur. Aeronomically, this channel, Reaction (1b.4), is indistinguishable from (1b.3), since the primary fate of NO^+ is to form $N(^2D)$ via Reaction (1a.3); however, the resulting $N(^2D)$ production rate is perhaps an order of magnitude larger than one might expect for physical quenching of $N(^2P)$ to $N(^2D)$. The absolute NO^+ yield has not yet been quantified by Piper; we have assumed it to be unity. There are no data on the temperature dependence for this reaction, and we assume there is no activation energy. Thus the extrapolation of the rate coefficient and product branching ratios to elevated temperatures is highly uncertain, as shown in Figure 3.

The room temperature quenching of $N(^2D)$ by O_2 has been studied by several investigators [28,39-43] with results that agree well within the various experimental uncertainties as shown in Figure 4. Again, the result of Piper and coworkers [44], $(4.6 \pm 0.5) \times 10^{-12} \text{ cm}^3 \text{ s}^{-1}$, appears to be the most accurate owing to the resonance

fluorescence/discharge flow techniques used. Unfortunately, information on temperature dependence is limited to an estimate by Slinger et al. [43] of near-zero activation energy over a limited temperature range near room temperature. Consequently, extrapolation to higher temperatures is quite uncertain. Furthermore, the possible occurrence of a reactive channel with significant activation energy could cause an increase in the temperature dependence of the overall quenching process at higher temperatures, as discussed further in Subsection 2.3. This possibility is supported by COCHISE observations of NO(v) formation [17], which imply a low-temperature rate coefficient of $(4-12) \times 10^{-13} \text{ cm}^3 \text{ s}^{-1}$ at 80 K. The resulting range of uncertainty in the recommended rate coefficient is shown in Figure 5. We will discuss the contributions from the reactive channel (NO formation) in Subsection 2.3, and the NO(v) excited state distributions in Section 4.

The rate coefficient for quenching of N(^2P) by O₂ is somewhat less well studied than that for N(^2D), but the available measurements [28,34,40,46], all at room temperature, agree to well within a factor of 2, as shown in Figure 6. The recent measurements of Piper [35] offer the best precision owing to his high measurement sensitivity and his use of a "clean" N(^2P) chemical generation technique, rather than the more commonly used discharge afterglow approach which is complicated by secondary reactions generating N(^2P). The rate coefficient reported by Piper [35] is $(2.2 \pm 0.3) \times 10^{-12} \text{ cm}^3 \text{ s}^{-1}$ at room temperature. There are no data on the temperature dependence of the total quenching reaction; by analogy with the N(^2D) reaction, we have assumed zero activation energy. COCHISE observations [17] of rovibrationally excited NO(v,J) apparently produced in this reaction imply a rate coefficient of $(1.5-9) \times 10^{-12} \text{ cm}^3 \text{ s}^{-1}$ at 80 K, which is consistent with small or negative activation energies, as illustrated in Figure 7. We will discuss the reactive channel in more detail in Subsection 2.3, and the NO(v,J) excited state distributions in Section 4.

The quenching of N(^2D , ^2P) by N₂ is inefficient at room temperature [26] and is unlikely to impact any high altitude scenario. N(^2D) quenching is less than 10^{-4} x gas

kinetic, and $N(^2P)$ quenching is at least two orders of magnitude slower than that. These rate coefficients probably increase with temperature, and perhaps also with vibrational quantum of $N_2(v)$ (consider microscopic reversibility of Reaction (1)); however, given the larger rate coefficients for quenching by O and e^- , it is unlikely that N_2 quenching would be significant in either auroral or nuclear-disturbed conditions. Recommended room temperature rate coefficients are listed below; we offer maximum recommended activation energies, but we also recommend high temperature measurements of these rate coefficients to confirm our assertion of their unimportance at high altitudes.

The quenching of $N(^2D, ^2P)$ by NO may contribute to N^* deactivation rates in specialized, post-nuclear conditions when $[NO]$ is large ($10^{11-12} \text{ cm}^{-3}$) and $[e^-]$ is small. However, for the most part, these reactions contribute more significantly as NO loss processes, and perhaps as possible NO excitation reactions. The recommended kinetics will be discussed in Subsection 2.4 and Section 4.

The quenching of $N(^2D, ^2P)$ by superelastic collisions with electrons is highly efficient, and will dominate N^* loss kinetics for $[e^-] > 10^{10} \text{ cm}^{-3}$, i.e. nuclear bombardment conditions. We recommend the rate coefficient parameters determined from theoretical calculations of Berrington and Burke [47]. These expressions, listed in Table 5, have been partially verified by experimental measurements of Queffelec et al. [21], who inferred a value for the quenching of $N(^2D)$ at 3900 K (electron temperature) that was 78% of the theoretical value. Owing to the lack of more extensive experimental verification, we assign factor-of-2 uncertainty limits for the theoretical rate coefficients; however, it seems likely that these are generous bounds.

It is interesting to note that, at higher electron temperatures, quenching by electrons does not discriminate against $N(^2D)$ (compared to $N(^2P)$) as strongly as does low-temperature quenching by atomic oxygen. This means that the relative contribution to NO excitation from the $N(^2P) + O_2$ reaction, which results in a high degree of

rotational as well as vibrational excitation, will be greater in the strong bombardment case than is commonly observed in auroras.

Recommendations: The recommended rate coefficient parameters and uncertainties for high altitude N^* collisional loss processes are listed in Table 5. Note that the radiative loss rates, listed in Table 3, do not contribute to N^* loss at any altitude where measurable NO formation can occur. The recommended rate coefficients are plotted in Arrhenius format for $N(^2D)$ quenching in Figure 8 and for $N(^2P)$ quenching in Figure 9. The primary uncertainties lie in the temperature dependencies and product branching ratios of the atomic and molecular quenching reactions, in particular for Reactions (1b.1) through (1b.6) of Table 1. This uncertainty is most important in the range of normal thermospheric conditions, 200 to 1000 K, where most of the NO is formed from N^* and superelastic quenching by electrons is not the dominant loss of N^* . We therefore recommend a series of experimental measurements of the rate coefficients for quenching of $N(^2D, ^2P)$ by O and O_2 over the nominal temperature range 200 to 1000 K. We further recommend that the product channels for $N(^2P) + O$ quenching be determined within this temperature range. Our further recommendations concerning the product channels for the reactions of N^* with O_2 are given in Subsection 2.3. As issues of lesser but significant importance, we recommend experimental verification of the superelastic quenching kinetics and of the high temperature quenching by N_2 .

2.3 NO Formation

The reaction sequence initiated by electron impact excitation results in the formation of NO by excited state chemistry. Since excited state chemical reactions are typically highly exoergic, the NO that is formed initially can have a high degree of internal (vibrational, rotational, electronic) excitation. The excitation and deactivation of $NO(v,J)$ are discussed in detail in Section 4; we examine here the kinetics of total NO formation via electron-initiated excited-state chemistry, Reactions (1c.1) through (1c.7) in Table 1.

It is generally accepted that the main source of NO in the auroral and sunlit upper atmosphere is the reactive quenching of $N(^2D)$ by O_2 . However, although the overall quenching kinetics are fairly well characterized (cf. Subsection 2.2), there are as yet no definitive measurements of the efficiency and temperature dependence of NO production. The primary quenching pathway is presumably via chemical reaction to form NO and O, as reported by Lin and Kaufman [39]. However, their measurement is not well documented and appears to be far from conclusive. It does not appear that they corrected their O-atom production data for the extensive $N(^2D)$ quenching losses at the flow tube wall, hence their reported observation of 1.2 O-atoms per $N(^2D) + O_2$ reaction is a lower bound by a significant factor. This would suggest that they could have been observing significant O production by other reactions in the active nitrogen flow. This is consistent with our own experience [17,48], where we have observed copious O production by hitherto unidentified reactions upon addition of O_2 and CO_2 to flowing afterglows of discharge-excited nitrogen. The occurrence of these "mystery" reactions precludes any of the attempts to date to determine the product branching ratios for $N(^2D) + O_2$ quenching, and we consider this to be an open question at this time.

Rawlins et al. [17], based on observations of $NO(v)$ product state distributions at cryogenic temperatures in the COCHISE reactor, argue on molecular dynamics grounds that there may be a significant activation energy for $NO(v)$ formation from $N(^2D) + O_2$ which, when taken together with the Slinger et al. [43] observation of zero activation energy for the overall quenching reaction, supports the possibility of a non-reactive energy transfer channel (e.g., excitation of $O_2(b^1\Sigma_g^+)$ or lower states of O_2). This possibility has been suggested by Torr et al. [49] from aeronomic data on high altitude O_2^+ emissions, but their interpretation has been vigorously contested by Slinger et al. [50,51].

COCHISE data on $NO(v)$ production rates at 80 K give estimated values for the $N(^2D) + O_2$ rate coefficient as shown in Figure 5; these estimates also support the possibility of a significant activation energy for the reactive channel. While these results

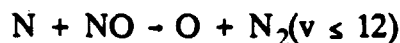
are far from conclusive, they raise the possibility of an increase in both the NO branching fraction and the overall activation energy above room temperature, and impose large uncertainties on the extrapolation of the kinetic data to higher temperatures.

The reaction of $N(^2P)$ with O_2 is a secondary source of NO in the auroral upper atmosphere, but appears to be an important source of highly rovibrationally excited $NO(v,J)$ [17]. The NO branching fraction and temperature dependence for this reaction are essentially completely unknown. Rate coefficients at 80 K inferred from COCHISE measurements of $NO(v,J)$ production rates are shown in Figure 7, and suggest the possibility of zero (NO branching fraction of unity) or negative activation energy for the chemical reaction branch. A negative activation energy is consistent with molecular dynamics considerations based on the COCHISE observations of randomized product energy distributions, which imply a long-lived reaction complex at low temperature. However, these observations do not rule out the possibility of a direct reaction with higher activation energy (and possibly different $NO(v,J)$ state distributions), which could dominate at higher temperatures. Thus the recommendation of rate coefficients and uncertainties for this reaction is a highly speculative endeavor.

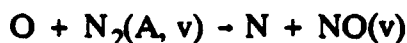
We also consider the possibility that NO can be formed by reactions of excited nitrogen, N_2^* , with O and O_2 . The primary candidates for N_2^* are the vibrationally excited ground and first electronically excited states, $N_2(X^1\Sigma_g^+, v)$ and $N_2(A^3\Sigma_u^+, v)$, although other persistent states such as $W^3\Delta_u$ and $a'^1\Sigma_u^-$ cannot be ruled out. There are currently no definitive experimental data to confirm or deny NO production from such reactions; this is in large part due to the difficulty of eliminating NO formation via impurities during the discharge excitation of N_2^* . However, simple reaction dynamics considerations rule out the possibility of NO formation from $N_2^* + O_2$ since a metathetic four-center exchange would be required. Such processes are severely dynamically hindered, and are known to have large activation energies and small steric

factors for product formation. In contrast, reactions of O with $N_2(v)$ and $N_2(A,v)$ offer intriguing possibilities which should be further investigated.

The reaction



is efficient (see Subsection 2.4) and is known to produce a high degree of vibrational excitation (at least six quanta with equal probability) [52]. By microscopic reversibility, one could expect the reverse reaction, involving $N_2(v \geq 13)$, to also be fast, unless additional dynamic constraints such as unfavorable reactant translational and rotational energies apply. In addition, the reaction



has often been speculated upon but never seriously examined in the laboratory. The total quenching rate coefficients at room temperature have been determined [53] to be (2.8 ± 0.4) and $(3.4 \pm 0.6) \times 10^{-11} \text{ cm}^3 \text{ s}^{-1}$ for $v=0$ and 1, respectively, with a 0.75 to 0.80 branching fraction for energy transfer to $O(^1S)$ [54,55]. However, the product channels for the remaining 20 to 25% of the reaction and the scaling with $N_2(A)$ vibrational level are unknown. Based on the predictions of Cartwright [23] for $N_2(A)$ formation in an IBC II+ aurora, reaction of O with $N_2(A, v=0-8)$ could give NO production rates on the order of $10^{4-5} \text{ cm}^{-3} \text{ s}^{-1}$, which is comparable to values expected for $N^* + O_2$ under these conditions. We therefore recommend upper-bound rate coefficients for this reaction.

Finally, we consider reactions between N^* (primarily $N(^2D)$) and excited states of O_2 such as $O_2(X^3\Sigma_g^-, v; a^1\Delta_g; b^1\Sigma_g)$. Such reactions have never been observed, but may be very fast with copious product excitation. The reduced collision rate imposed by the requirement of O_2 excitation can be substantially offset if the rate coefficients are

near gas-kinetic. Such reactions are probably not important in most auroral conditions, but may contribute significantly in nuclear scenarios.

Recommendations: The recommended rate coefficients for NO formation processes are listed in Table 6. For lack of a better alternative, we recommend NO branching fractions of unity at all temperatures for Reactions (1c.1) and (1c.3), with rate coefficient expressions and uncertainties given in Table 5 for the total quenching. Unfortunately, the level of sophistication that can be brought to bear on this seminal aspect of high altitude NO chemistry is appallingly poor. In each case, it is impossible to base a recommendation on anything more than speculation about likely product channels. Together with the NO excitation efficiencies (see Section 4), the chemistry of NO production represents the area of most critical uncertainty in the prediction of NO radiative signatures in the upper atmosphere. We recommend a series of laboratory and in situ auroral measurements, coupled with modeling predictions, to quantify the NO production channels for the $N^* + O_2$ and $O + N_2^*$ reactions. As a minimum, this should be done near room temperature; additional temperature dependence data are also required where possible in the range 200 to 2000 K. In addition, but with lower priority, we recommend experimental investigations of the reactions of N^* with excited forms of O_2^* to assess their viability as sources of NO(v).

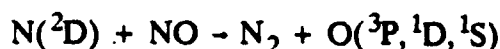
2.4 NO Loss Processes

The primary chemical loss of NO in the upper atmosphere is through reaction with $N(^4S)$, Reaction (1d.1) in Table 1. Additional processes which can contribute to NO removal under certain bombardment conditions include $N(^2D) + NO$, ultraviolet (UV) photoionization and photodissociation, and electron impact ionization and dissociation, Reactions (1d.2) through (1d.6). Additional high temperature loss processes, viz. reaction with O and thermal dissociation, become significant above 2000 K and are addressed in Section 3.

Since N and NO mutually destroy each other, the two species follow a complex interrelationship in the upper atmosphere. The reaction of $N + NO$ is well studied, with a critically evaluated [56] rate coefficient of $((3.1 \pm 1.0) \times 10^{-11}) \exp((0 \pm 100)/T) \text{ cm}^3 \text{ s}^{-1}$. For weak bombardments, where $[N]$ is comparable to or greater than $[NO]$, this reaction limits the $[NO]$ produced. However, in stronger auroral or nuclear bombardments, $[NO]$ can grow rapidly to exceed $[N]$, and the $N + NO$ reaction further depletes $[N]$ with little reduction in $[NO]$. Under these conditions, $[NO]$ continues to increase during the bombardment, and is ultimately limited by relatively slow processes such as horizontal and vertical transport, and photon- or electron-induced ionization and dissociation. Dissociation tends to be more effective at removing NO than ionization (via UV photons, electron impact, or charge transfer), since the energetic threshold is lower, and each dissociation gives $N(^4S)$ which removes another NO molecule while at least half of the NO^+ ions lead to NO reformation through the dissociative recombination sequence. In the quiescent upper atmosphere, the photochemical time constant for NO is about $1\text{-}2 \times 10^5 \text{ s}$; this competes with eddy diffusion losses below 100 km, but is significantly slower than transport by high altitude zonal (longitudinal) winds [57]. Thus, it is unlikely that photochemical destruction of NO will be very important, even in the nuclear case, but electron impact processes may become significant in strong bombardments.

A critical treatment of the NO dissociation and ionization processes would be lengthy and is beyond the scope of the present review; we provide here a brief summary of a few key references. The UV photoionization cross sections are tabulated by Watanabe et al. [58]; UV photodissociation via inverse predissociation is discussed in detail and modeled by Cieslik and Nicolet [59]. Electron impact ionization cross sections for NO have been reported by Kim et al. [60]. Electron impact excitation cross sections for NO, which can be used to derive cross sections for predissociation, are reported at length in two papers by Ajello et al. [61].

It is interesting to consider the reaction



as a possible NO chemical destruction pathway. Under conditions of large [NO], the $\text{N}(^2\text{D})$ and $\text{N}(^4\text{S})$ number densities can become comparable, and the destruction rates of NO by the two species can have similar magnitudes. The reaction has a recommended [26,30] rate coefficient of $(6.3 \pm 2.0) \times 10^{-11} \text{ cm}^3 \text{ s}^{-1}$ at 300 K. In addition, the reaction of $\text{N}(^2\text{P})$ with NO has a rate coefficient of $(3.0 \pm 0.5) \times 10^{-11} \text{ cm}^3 \text{ s}^{-1}$ at 300 K [26].

Recommendations: The necessary kinetics for low-temperature chemical removal of NO at high altitudes are reasonably well understood, and tend to be slower than transport for most bombardment conditions. The relevant rate coefficients are listed in Table 7. The high temperature kinetics of the N+NO reaction are covered further in Section 3. Destruction rates by photochemical and electron impact processes should be evaluated from cross section data available in the literature, and should be compared to transport losses for various bombardment conditions. High temperature NO removal through reaction with O and thermal dissociation are discussed in Section 3.

3. THERMALLY INITIATED CHEMISTRY

At the high temperatures ensuing from a high altitude nuclear burst, copious NO is formed from the chemistry of hot, thermally dissociated air. This chemistry follows the well-known Zel'dovich mechanism listed in Table 1, Reactions (2.1) through (2.6). NO is produced by reactions of ground-state O and N (formed by thermal dissociation of O_2 and N_2) with N_2 and O_2 , and is destroyed by thermal dissociation and reaction with O. The general temperature range in which these reactions are important is above about 2000 K. Zel'dovich chemistry diminishes in importance with increasing temperature above about 5000 K since the molecular species are largely dissociated. These reactions have been studied by many investigators for several decades, with the most reliable results obtained using shock tube techniques in the 2000 to 7000 K range.

Additional NO production chemistry involving N_2O and NO_2 requires three-body formation reactions for these species, and will not be important at high altitudes, although such reactions could contribute to N_2O and NO_2 radiative signatures. Other reactions involving odd-hydrogen species (HO_x) can also occur, but are not significant in terms of NO formation and destruction since odd-hydrogen number densities are small above 80 km. Such reactions could contribute to HO_x destruction and signatures from species such as NH or HNO. The chemical kinetics of the high-temperature H/N/O system have been extensively reviewed by Baulch et al. [62] and, more recently, by Hanson and Salimian [63]; we draw extensively from those reviews for the material presented here.

3.1 Precursor Formation

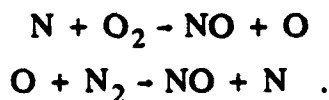
The Zel'dovich reaction sequence is initiated by thermal dissociation of O_2 and N_2 to produce O and N. These reactions have been reviewed by Baulch et al. [62], and we reproduce their Arrhenius plots in Figures 10 and 11. While there is anywhere from a factor of 2 to an order of magnitude spread among the different rate coefficient

evaluations, the most significant problem is that the rate coefficients are generally not well determined for the important high-altitude collision partners O, N₂ and O₂. This is because the shock tube technique requires dilution in an inert bath gas, usually Ar, and it is difficult to distinguish the effects of other, more dilute, gases. Thus while data for M=Ar are obtained over wide temperature ranges and are moderately well characterized, collision partner effects are usually determined in a relative sense over limited T ranges and are expressed as temperature-invariant multiplicative factors. This approach may be adequate for M=N₂O₂ but could cause serious errors in the estimation of O effects, which may exhibit different temperature dependencies if collisions proceed on attractive potential surfaces.

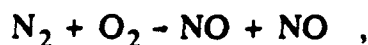
It can be seen from the data in Figures 10 and 11 that radical atomic collision partners are roughly an order of magnitude more effective at promoting dissociation than the molecular species, so we therefore expect O to be the dominant collision partner for dissociation above about 100 km. As a result, the kinetics data base required to predict collisional dissociation rates in the heated upper atmosphere is very limited and highly uncertain. The uncertainty increases further if one considers collisions of non-thermal, fast atoms with O₂ and N₂. We recommend use of the expressions and scaling factors given in Baulch et al. [62]; however, there is no basis for a recommendation on the dissociation of N₂ by O or O(fast). The recommended expressions are compared in Figure 12.

3.2 NO Formation

NO is formed at high temperatures by the reactions



The $N + O_2$ reaction has the larger rate coefficient, but its rate is limited by low $[N]$ (slow N_2 dissociation), so both reactions contribute to NO production near 1500 to 2000 K. The four-center exchange reaction,



though reviewed by Baulch et al. [62], certainly does not occur, due to strong dynamic constraints.

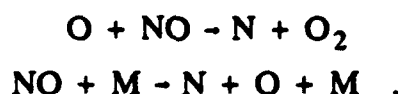
The $N + O_2$ reaction is reviewed by Baulch et al. [62] as shown in Figure 13. New data on the reverse $O + NO$ reaction, discussed by Hanson and Salimian [63] (see Subsection 3.3), indicate that the Baulch et al. expression for $N + O_2$ is accurate up to 2000 K and is low by less than a factor of 2 at 3000 K. We recommend the use of the Baulch et al. expression with factor-of-2 uncertainty above 3000 K, or, alternatively for the higher temperatures, evaluation by detailed balance from the recommended rate coefficient for $O + NO$ as given below. The rate coefficients for $N(^4S, ^2D, ^2P) + O_2$ are compared in Figure 14. Based on expected ratios of $[N]/[N^*]$, the ground state reaction will compete with the metastable reactions at temperatures of 900 to 1100 K, and will dominate at higher temperatures.

The $O + N_2$ reaction is reviewed by Hanson and Salimian [63] with the results shown in Figure 15. Their recommendation is based on recent direct observations of this reaction rate at 2000 to 4000 K, and is about a factor of 2 greater than the Baulch et al. [62] recommendation. Note that this expression can also be used to determine a high temperature rate coefficient for the reverse reaction, $N + NO$, which is about a factor of 2 larger than the value recommended in Table 7 from low temperature data [56]. This result is contradicted by recent work of Koski et al. [64], who determined a high-temperature (1600 to 2500 K) rate coefficient for the $N + NO$ reaction of $(2.2 \pm 0.3) \times 10^{-11} \text{ cm}^3 \text{ s}^{-1}$, in agreement with the low temperature extrapolation [62]. The recommended rate coefficients for the high-temperature NO production reactions are

compared in Figure 16. Based on expected $[O]/[N]$ and $[N_2]/[O_2]$ ratios, the $O + N_2$ reaction will be negligibly slow below 1500 K but will dominate the $N + O_2$ pathways for NO production at 2000 K and above.

3.3 NO Removal

The primary high-temperature NO removal reactions are reaction with O and thermal dissociation:



The $O + NO$ reaction is reviewed by Hanson and Salimian [63] as shown in Figure 17. Data from several different groups are seen to provide excellent agreement between 1500 and 5000 K. This reaction is fast enough above about 1000 K to compete with $N + NO$ and transport losses, and provides a significant chemical sink up to about 3000 K because, in this temperature range, the principal fate of the N atoms produced is reaction with excess NO to regenerate O. Above 3000 K, the reverse reaction of N with O_2 regenerates much of the NO so there is less net loss.

Rate coefficients for the thermal dissociation of NO, as reviewed by Hanson and Salimian [63] and by Baulch et al. [62], are plotted in Figures 18 and 19, respectively. Here the data base is very poor, with only limited experimental data for $M=Ar$ and no direct observations for $M=O, N_2, O_2$. The total spread in the uncertainty is about two orders of magnitude. We use the centrally located expression of Wray and Teare [65], but we note that both the Baulch and the Hanson reviews considered the data base to be too poor to provide a recommended rate coefficient expression. However, unless the rate coefficient is an order of magnitude or more larger than our suggested value, it seems that chemical reaction with O is the dominant loss process, at least below 5000 K. At higher temperatures, where the major collision partner is O, NO dissociation may

become fast enough to compete with the $O+NO$ reaction, since dissociation provides a more permanent sink for NO while chemical reaction forms O_2 , some of which regenerates NO instead of dissociating. It is thus important to determine the dissociation rate coefficients at high temperatures, since this process may limit the chemical lifetime of NO above 5000 K. Our recommended rate coefficients for the NO removal reactions are compared in Figure 20.

3.4 Recommendations

The recommended rate coefficient expressions for high-temperature NO production and removal are summarized in Table 8 and are plotted in Figures 12, 16, and 20 above. The data base for the thermal atom-molecule reactions is quite good, with uncertainties of a factor of 2 or less in the nominal range 2000 to 5000 K. However, the data base is poor for the thermal dissociation of O_2 , N_2 , and especially NO; we particularly note the need for kinetic data on the effects of the atmospheric collision partners O, N_2 , and O_2 . In addition, there are no data relevant to the collisional effects of fast O and N atoms in the 1 eV range, other than extrapolation of the thermal rate coefficient expressions well beyond their range of validity.

To improve the data base, we recommend experimental investigations of the kinetics of thermal dissociation of NO, O_2 , and N_2 with the atmospheric collision partners O, N_2 , and O_2 in the temperature range 3000 to 7000 K. We further recommend experimental measurements of the collisional and chemical effects of non-thermal, fast O and N atoms in Reactions (3.1) through (3.6) to extend the data base into the 1 to 2 eV range as encountered in high-altitude nuclear conditions. We point out that both the thermal and non-thermal measurements of atomic effects are difficult to perform, and will probably require the development of non-conventional and/or innovative experimental approaches to generate the required atomic collision partners.

4. EXCITATION OF NO(v,J)

The high-altitude excitation of vibrational states of NO can occur through a variety of non-thermal (low temperature) and thermal (high temperature) processes, listed as Reactions (3.1) through (3.13) in Table 1. The reactions may be grouped into categories of chemiexcitation via exoergic chemical reaction, energy transfer to NO(v=0) from internally or translationally excited species, and radiative excitation of NO by photon absorption. A considerable body of data now exists on these processes at low temperatures relevant to auroral observations, but many key issues remain unresolved, and little of this information is sufficiently quantitative to support reliable kinetics recommendations. In addition, there is essentially no information on temperature dependence, which could strongly impact the prediction of detailed product state distributions in many instances. We discuss below the most likely processes which should be considered, and provide tabulations of the product state distribution data where available. Rate coefficient data for most of these reactions (neglecting NO state distributions) have already been discussed in the preceding sections.

4.1 Chemiexcitation

The primary chemiexcitation processes to consider are the reactions of N(⁴S, ²D, ²P) with O₂, the speculated reaction of O with excited N₂^{*}, and the radiative recombination of N and O.

N + O₂ The reaction



has been studied at room temperature by several groups using infrared chemiluminescence (IRCL) [66,67], laser-induced fluorescence (LIF) [68], and multi-photon ionization (MPI) [69] to determine NO(v) product state distributions. A graphical

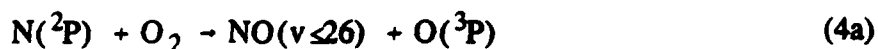
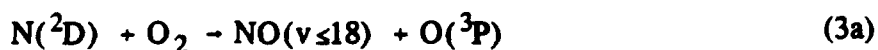
comparison of the results from these studies may be found in the paper by Winkler et al. [69]. The relative vibrational distributions determined from the various experiments agree to a factor of 2 to 3, and scatter about a roughly statistical distribution up to the energetic limit at $v=7$. Relative population factors for $v=0$ disagree by over an order of magnitude, with the lower result of Winkler et al. falling at about 75% of the statistical value. The total rate coefficient as determined by Winkler et al. from the $\text{NO}(v)$ yields is about 65% of the correct value, suggesting that these investigators underestimated their $\text{NO}(v=0)$ yields due to an error in their limiting-slope analysis of the kinetic data.

In general, the relative populations determined in all of these investigations are clouded by many uncertainties in the data analysis, including historical choices of IRCL infrared and LIF ultraviolet transition probabilities (which are now known to much better accuracy), MPI spectral interpretations [70] and variations of NO ionization cross sections with v , effects of $\text{NO}(v)$ deactivation on reactor walls, and possible generation of $\text{NO}(v)$ by secondary metastable chemistry in the nitrogen afterglow. Thus, a complete critical assessment of $\text{NO}(v)$ yields from $\text{N}(^4\text{S}) + \text{O}_2$ would require a substantial reanalysis of these data. In the absence of such a reanalysis, we suggest the use of the results as given by Winkler et al. [69], with the understanding that the populations are only accurate to about a factor of 2. Alternatively, a statistical product distribution (also given in Winkler et al.) would probably be adequate for modeling purposes.

In any event, we expect $\text{NO}(v)$ signatures from $\text{N}(^4\text{S}) + \text{O}_2$ chemiluminescence to be relatively unimportant in high altitude scenarios. As pointed out above, the reaction is too slow to compete with $\text{N}^* + \text{O}_2$ chemiluminescence below 1000 K. Above that temperature, excitation of $\text{NO}(v)$ by thermal $\text{O} + \text{NO}$ up-pumping (see below) will dominate $\text{NO}(v)$ signatures. Thus the reaction $\text{N}(^4\text{S}) + \text{O}_2$, while a significant source of total NO between 1000 to 2000 K, will provide only minor direct contributions to the high altitude $\text{NO}(v)$ distributions.

Similar reasoning applies to the other major high-T ($T \geq 2000$ K) NO-producing reaction, $O + N_2$; there are no data on NO(v) distributions produced in this reaction, but such data are probably not required since thermal NO(v) excitation processes will control NO(v) distributions at these temperatures. If such data are required for $O + N_2$ for modeling purposes, we suggest the use of a statistical vibrational distribution (see formulae given by Rawlins et al. [17]).

$N^* + O_2$. NO(v) chemiluminescence from the reactions



has been extensively studied in the COCHISE infrared chemiluminescence facility at cryogenic temperatures (80 to 120 K) [17,71]. The recent paper of Rawlins et al. [17] clarifies some uncertainties in Reaction (3) identified in the earlier work of Kennealy et al. [71], and tentatively identifies Reaction (4) as the source of highly rotationally excited NO(v,J) observed in the spectra. This rotational excitation appears in the form of sharp R-branch band heads well to the blue of the band center for each of eight vibrational bands, accompanied by less pronounced, extended P-branch transitions progressing to the red as far as 8 to 9 μm . The mechanism for rovibrational excitation identified in COCHISE experiments appears [15] to be at least partially responsible for similar band head excitation observed [16] for NO in an aurora.

The observed laboratory spectra show excitation of up to 14 observable vibrational levels, with the first 8 excited levels exhibiting 2 to 3 eV of rotational excitation. The

spectral distributions signify that much of the exoergicity of Reaction (3) appears as electronic excitation of $O(^1D)$, and much of the exoergicity of Reaction (4) appears as rotation rather than vibration. Although Rawlins et al. [17] modeled these rotational distributions with a 10,000 K Boltzmann distribution, subsequent work [72] indicates that a statistical nascent rotational distribution may provide a better representation.

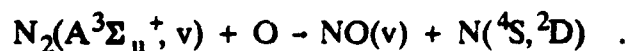
The relative initial vibrational populations for Reactions (3) and (4), determined by Rawlins et al. from surprisal analysis of their data, are given in Table 9. These distributions indicate a direct, atom abstraction reaction between $N(^2D)$ and O_2 , dynamically favoring $O(^1D)$ formation (75% of the total reaction rate) with maximum v excitation, and an indirect reaction of $N(^2P)$ with O_2 via a long-lived complex, with statistical partitioning of the exoergicity in product electronic, vibrational, rotational, and translational states. The production of $O(^1D)$ from Reaction (3) is relevant to the aeronomy of auroral $O(^1D)$ emission; however, a variety of modeling analyses have achieved conflicting and inconclusive results on this process, as reviewed by Solomon [73].

We emphasize that the COCHISE observations are not definitive in several respects and need to be verified by independent laboratory and auroral measurements. First, the identification of the contributions of the various reactions is not definitive, since $N(^2D, ^2P)$ were not directly measured and their contributions to the observed $NO(v)$ production were not independently separable. Indeed, the contribution of Reaction (4) as the source of the rotational excitation could only be identified by process of elimination and intuitive arguments. Second, and perhaps most important, the COCHISE measurements are applicable only to ~ 100 K, and there are reasonable concerns that the product state distributions might be substantially different near and above room temperature. As discussed by Rawlins et al. [17], Reaction (3a), which is a 25% branch at 100 K, may become a more important channel at higher temperatures owing to the possible presence of an energy barrier. Furthermore, the indirect, statistical dynamic mechanism for Reaction (4), which is favored at low temperatures, may give

way at higher temperatures to a direct abstraction mechanism over an energy barrier. Such changes in dynamic mechanism at higher temperatures would undoubtedly result in changes in the nascent NO(v) distributions. Finally, as discussed in Subsection 2.3, it has not yet been determined that NO(v) formation constitutes 100% of the total quenching reactions. For current modeling applications, we suggest the use of the COCHISE NO(v,J) distributions for Reactions (3) and (4) as described in Table 9, with the caveat that there is presently no basis for the extrapolation of these distributions to or above room temperature.

The relevant temperature range over which more data are required extends from the mesopausal minimum of ~ 200 K to roughly 1000 K or more. Near 1000 K, O+NO up-pumping is the dominant NO(v) excitation process for the lowest 7-10 excited vibrational levels (assuming post-burst NO number densities near $10^{11-12} \text{ cm}^{-3}$) as discussed in Subsection 4.2. Thus, the metastable reactions will continue to dominate the direct production of the higher vibrational levels and high rotational states at temperatures above 1000 K. Metastable production of NO(high v) probably becomes unimportant at about 1500 to 2000 K, but super-equilibrium production of NO(v,high J) may be important at all temperatures, subject only to precursor formation and quenching.

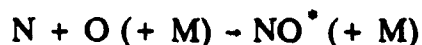
O + N₂^{*}. The possible (but undemonstrated) reactions of O with vibrationally and/or electronically excited N₂^{*} were discussed in Subsection 2.3 as potential sources of NO. Such reactions could be sufficiently exoergic to provide substantial NO(v) excitation. One of the more interesting possibilities is the reaction



For N₂(A,v=0), the maximum exoergicity at 300 K is sufficient to excite NO(v ≤ 14); higher vibrational levels of N₂(A) present in an auroral or nuclear bombardment could of course excite higher levels of NO(v) (or N^{*}). Unfortunately, there are no data

available on the kinetics or product state distributions for this reaction (cf. Table 6 for upper bound recommendation), nor is there a good way to make even a reasonable suggestion for possible NO(v) distributions.

N + O. The recombination of N and O



will provide the most significant source of NO(v) radiation in the highly dissociated atmosphere, at temperatures above 5000 K where the thermal lifetime of NO is too short for thermal up-pumping to dominate. The mechanisms of N + O recombination afterglows have been reviewed by Golde and Thrush [74] and, more recently, by Kenner and Ogryzlo [75]. The relevant electronic states of NO formed in recombination, shown in Figure 21, are the doublets $X^2\Pi$, $A^2\Sigma^+$, $B^2\Pi$, $C^2\Pi$, and the quartets $a^4\Pi$ (a metastable state) and $b^4\Sigma^-$. By rapid radiative cascade and collisional processes, these states populate NO(X,v), which can radiate in the infrared prior to thermal dissociation. However, as discussed below, the mechanisms by which the recombination occurs are quite complicated, and it is difficult to predict the exact NO(v) distributions that would result.

In the two-body mechanism, which is more relevant to the high altitude problem, the recombination is believed to occur by inverse predissociation from the $a^4\Pi$ surface into the (C,v=0) state. With a radiative lifetime somewhere between 15 and 50 ns, the C state undergoes rapid radiative cascade to the A and X states, with 20 to 40% of the cascade going into the A state. The A state in turn radiates promptly to NO(X,v) with a radiative lifetime of about 200 ns. Thus, to determine populations of NO(X,v), one must know the (C → X)/(C → A) branching ratio [76] and the relative transition probabilities for the (C,v=0) → (X,v), C(v=0) → (A,v), and (A,v) → (X,v) transitions. These factors have been addressed theoretically by Du and Dalgarno [77].

In addition, the a, b, and B states may become involved, especially if significant collisional coupling can occur. There is no evidence of a-state formation in two-body recombination at room temperature, but this cannot be ruled out at higher collision energies. The a-state is known to be formed by radiative cascade ($\tau \geq 6 \mu\text{s}$) from NO(b) formed in three-body recombination (NO(b) is formed by collisional crossing from the NO(a) potential surface). NO(a) is metastable and is a potential $10 \mu\text{m}$ radiator through its vibrational bands. In addition, NO(a) is collisionally quenched into the doublet manifold, to form NO(B,v) and probably NO(A,v) and NO(X,v) as well. NO(B,v) radiates to NO(X,v) with a radiative lifetime of $\approx 3 \mu\text{s}$ and characteristic $v' \rightarrow v''$ branching ratios.

A complete assessment of the NO(X,v) production rates from $\text{N} + \text{O}$ recombination requires a critical review and uncertainty evaluation of the rather copious literature on NO electronic state radiative lifetimes, relative $v' \rightarrow v''$ electronic transition probabilities, and collisional coupling effects. Particular attention should be paid to evaluation of the transition branching ratios. The vibrational level dependent transition probabilities can be determined from the usual equations [78] relating transition probability to the product of the Franck-Condon factor for the transition, the cube of the transition frequency, and the square of the electronic transition moment. Numerically computed Franck-Condon factors for all the required transitions except $\text{C} \rightarrow \text{A}$ are reported by Nicholls [79]; however, these were computed from Morse potentials and are likely to be less accurate than those computed from RKR wavefunctions. RKR Franck-Condon factors for a number of transitions, including at least $\text{A} \rightarrow \text{X}$ and $\text{B} \rightarrow \text{X}$, have been computed by Albritton et al. [80], but these are not published and are informally distributed throughout the community in the form of photocopied computer printout. Additional transition moments and radiative lifetimes have been computed by Du and Dalgarno [77].

Recent work by Piper and coworkers has established the presence of significant variations in the transition moments as functions of r -centroid (mean internuclear

separation) for both the A - X [81] and B - X [82] transitions. Such variations had not been considered in previous, commonly accepted documentations of these transition probabilities, and result in significant changes in the relative populations of lower-state vibrational levels by radiative transitions from a common upper-state vibrational level. It is likely that the C - A, C - X, and b-a transitions are similarly affected, but carefully calibrated spectral measurements are required to quantify this effect. Thus the relative populations resulting from the A - X and B - X transitions can now be treated with high accuracy using the Piper results [81,82] (which are coupled with accurate radiative lifetime measurements from other sources), but the remaining transitions can only be treated to a factor of 2 to 3 without further experimental work.

Since the previous investigations of N + O recombination were done near room temperature, an assessment of the temperature dependence relevant to the nuclear case is highly speculative. One might expect the rate coefficient for the two-body inverse predissociation process to have the form

$$k(T) \sim AT^{-1/2} \exp(-\Delta E/k_B T) \quad .$$

However, ΔE , which is the energy difference between the initial recombination state and the separated atoms, is small for $N + O \sim NO(C, v=0)$, so the exponential goes to unity at high temperatures. Based on the data given by Kenner and Ogryzlo [75], and neglecting collisional redissociation, this gives an estimate for the two-body rate coefficient:

$$k_{O+N} \sim 10^{-17} (300/T)^{1/2} \text{ cm}^3 \text{ s}^{-1} \quad .$$

Three-body recombination often follows stronger negative temperature dependencies, but the available data between 200 and 400 K [62] suggest a similar temperature dependence for the three-body process:

$$k_{O+N+M} = 10^{-32} (300/T)^{1/2} \text{ cm}^6 \text{ s}^{-1}$$

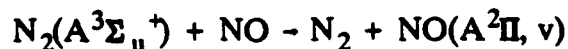
Statistically, 2/3 of the recombinations proceed through the $a^4\Pi$ state and the remaining 1/3 populate $\text{NO}(X,v)$ initially.

The two- process can be expected to dominate at number densities below 10^{15} cm^{-3} , i.e., altitudes above 70 km. In effect, this means that, if these temperature dependencies persist to high temperatures, two-body recombination of N and O dominates $\text{NO}(v)$ formation in the 5000 to 10000 K range following a high altitude nuclear burst. The estimated two-body rate coefficient is plotted in Figure 22.

4.2 Energy Transfer

There are numerous possible processes for $\text{NO}(v)$ excitation by collisional energy transfer which could be important in auroral or nuclear bombardments, but only a few have been definitely shown to occur, and high temperature information can only be obtained by scaling from room temperature data. It is especially interesting to consider the class of reactions in which $\text{NO}(v)$ is excited by energy transfer to $\text{NO}(v=0)$ from vibrationally and/or electronically excited states of N_2^* , N^* , O_2^* , and O^* produced by electron bombardment. Such processes could contribute significantly to $\text{NO}(v)$ vibrational luminescence at temperatures below about 1000 K, especially when $[\text{NO}]$ is large.

The most concrete example of such a process is the well known reaction



followed by the equally well understood radiative cascade (see discussion above)



Both processes have been recently investigated by Piper and coworkers [81,83]; results for the quenching and excitation kinetics are summarized in Table 10. The energy transfer is near gas-kinetic, and probably has no significant temperature dependence. In addition, a significant fraction of the excess energy is taken up in vibrational and rotational excitation within the A state. The measurements extend only up to $N_2(A, v=2)$, but indicate that with increasing v the excitation of $NO(A)$ is more distributed to higher v and $NO(B)$ excitation becomes more significant. Similar effects may occur with increasing temperature. Initial $NO(X, v)$ populations formed by this mechanism, calculated from the data in Table 10 and the $A \rightarrow X$ transition probabilities given by Piper et al. [81], are shown in Figure 23 and tabulated in Table 11. This reaction may contribute to $NO(v)$ excitation in strong auroras or nuclear afterglows where both $[NO]$ and $[N_2(A)]$ are large, especially at higher altitudes (≥ 110 km) where the increasing O/O_2 ratio discriminates against the $N^* + O_2$ mechanism.

Similar reactions involving metastable N_2^* states such as $N_2(v)$ or $N_2(a')$ may also excite $NO(v)$ or $NO(v, J)$, by analogy with energy transfer excitation observed for $N_2^* + CO$ in COCHISE experiments [72]. In addition, the quenching of N^* ,



may occur at least partially through an energy transfer channel, most likely via reactive atom exchange. This reaction could contribute to $NO(v)$ excitation when $[NO] \sim [O_2]$, as can occur at high altitudes (above 130 km) when the total NO number density is large. Preliminary experiments, performed by the author and coworkers on the COCHISE apparatus, indicate copious low- J and high- J rovibrational excitation of $NO(v, J)$ by energy transfer from discharge-excited nitrogen; although detailed investigation is still in progress, this appears to occur through energy transfer to NO from one or more states of (N^*, N_2^*) .

Similar reactions should be considered involving energy transfer to NO from vibrationally/electronically excited O_2^* and O^* . However, it is not clear that these

would be significant contributors since O_2^* quenching by NO is relatively inefficient, O^* quenching by the major atmospheric species is fast, and the behavior of oxygen metastables in the disturbed upper atmosphere is not known very well. Thus, further consideration of O_2^*/O^* energy transfer processes should await definitive laboratory measurements and a clearer assessment of the kinetics of metastable oxygen in the electron bombarded upper atmosphere.

The collisional up-pumping of $NO(v)$, by transfer of kinetic energy to $NO(v=0)$ from thermal or translationally fast O, is a major source of $NO(v)$ excitation in both the quiescent and disturbed upper atmosphere, over the entire temperature range in which NO is thermally stable. This process is well known as the major source of $NO(v=1)$ emission in the non-auroral thermosphere; computed excitation rates, following the model of Caledonia and Kennealy [5], are shown in Figure 24. The rate coefficient is determined by detailed-balance inversion of the rate coefficient for $NO(v=1)$ deactivation by O at room temperature, as measured by Fernando and Smith [84], which is reportedly accurate to $\pm 10\%$. At elevated temperatures, this reaction will provide a significant source of excitation to higher v ; unfortunately, the data base does not exist to support reliable extrapolations to higher v and T. We estimate the up-pumping rate coefficients by detailed-balance inversion of rate coefficients for $O + NO(v)$ deactivation as estimated from a simple model described below in Section 5. Briefly, this model assumes the Fernando and Smith [84] value for deactivation of $v=1$, together with a slight negative temperature dependence estimated as described in Section 5, and equal rate coefficients for multi-quantum deactivation of all higher v to the $v=0$ level. This gives rise to the $O + NO$ up-pumping rate coefficient expressions listed in Table 12 and plotted in Figure 25. It can be seen that this process is very important, and essentially governs most of the $NO(v)$ distribution at temperatures where thermal NO production exceeds the chemiluminescent contributions. For post-burst NO number densities of $10^{11-12} \text{ cm}^{-3}$, $O+NO$ up-pumping gives the dominant $NO(v)$ excitation rate for up to $v \sim 10$ near 1000 K, and for higher vibrational levels at higher temperatures.

The collisional excitation of NO by non-thermal, fast O will also be important in nuclear bombardments, but has not been investigated experimentally. Crude guesses of the relevant rate coefficients may be obtained by extrapolation of the expressions of Table 12 to the required collision energies. For the larger collision energies, it is conceivable that substantial rotational excitation of NO could occur as well as vibrational excitation. This is consistent with experimental [86] and theoretical [87] results for the analogous interaction between fast H and NO. Clearly, definitive measurements are required for multiquantum O + NO up-pumping at high temperatures (300 to 5000 K) and/or high collision energies (up to 1 to 2 eV).

4.3 Radiative Excitation

Radiative excitation of NO(v) is generally not significant in the quiescent or auroral upper atmosphere, but may be somewhat more significant in the nuclear case due to intense UV/IR radiation from the fireball region. In the non-nuclear atmosphere, NO(v) is radiatively excited by IR photons upwelling from the earth and/or lower atmosphere, so-called "earthshine", and to a lesser extent by solar UV photons.

The earthshine excitation rate may be estimated by the method of Caledonia and Kennealy [5], who approximate the absorption process as irradiation of a high altitude column by light from a low altitude grey-body slab. The radiative excitation rate is given by

$$R_e = \pi I_v S / (h c \nu N_L), s^{-1}$$

where πI_v is the upwelling earthshine flux in $W cm^{-2} (cm^{-1})^{-1}$, as predicted by LOWTRAN models for various model atmospheres [88], S is the absorption band-strength in $cm^{-1} cm^{-2}$, ν is the transition frequency in cm^{-1} , and h, c, and N_L are Planck's constant, the speed of light, and Loschmidt's number, respectively. More detailed treatments of the high altitude radiative transport problem give similar results [89]. For the fundamental band of NO at $1876 cm^{-1}$ ($5.4 \mu m$), we use the absorption

strength of $137.3 \pm 4.6 \text{ amu}^{-1} \text{ cm}^{-2}$ reported by Holland et al. [90]. LOWTRAN predictions of the upwelling radiation at $5.4 \mu\text{m}$ give I_{ν} ranging from 1.5 to $3.0 \times 10^{-7} \text{ Wcm}^{-2} \text{ sr}^{-1} (\text{cm}^{-1})^{-1}$ for subarctic winter to tropical conditions. This gives earthshine excitation rates of 0.7 to $1.4 \times 10^{-4} \text{ s}^{-1}$ (per $[\text{NO}]$) for $\text{NO}(v=1)$. It can be seen from Figure 24 that this rate is significant only below 110 km , and is overwhelmed by $\text{O} + \text{NO}$ up-pumping above that altitude. Due to low number densities of $\text{NO}(v \geq 1)$, successive radiative pumping of higher levels in the fundamental band is insignificant. Similarly, radiative excitation of $\text{NO}(v=2)$ by earthshine at $2.7 \mu\text{m}$, the first overtone band, is also insignificant.

A small degree of $\text{NO}(v)$ excitation can occur through UV solar absorption and resonance fluorescence in the A-X transition. From data given in McEwan and Phillips [91], the $\text{NO}(v)$ excitation rate for this process is on the order of 10^{-5} s^{-1} ; this would be distributed over several vibrational levels of $\text{NO}(v)$, as determined by the A - X relative transition probabilities as described above. The relevant transition probabilities are tabulated by Piper and Cowles [81]. The solar excitation of $\text{NO}(v > 1)$ would be IR-observable in non-auroral conditions with overhead sun and large NO number densities, and could exceed auroral excitation rates for weak auroras (i.e., $10^{3-4} \text{ cm}^{-3} \text{ s}^{-1}$ for $[\text{NO}] \sim 10^{8-9} \text{ cm}^{-3}$).

Solar excitation of $\text{NO}(v)$ by IR absorption at 2.7 and $5.4 \mu\text{m}$ is insignificant. In nuclear conditions, UV and IR radiation from the fireball, as well as $5.4 \mu\text{m}$ radiation from overhead $\text{NO}(v)$, may cause significant $\text{NO}(v)$ excitation at low altitudes, below the high-temperature atomic oxygen layer (i.e., below $\sim 90 \text{ km}$ or so). However, there is typically not very much NO expected at those altitudes, so these processes contribute in only a minor way to the total $\text{NO}(v)$ burden.

4.4 Recommendations

Although the current data base on NO(v) excitation kinetics does not support a set of firm recommendations, we provide suggested kinetic parameters as summarized in Table 13. Our principal recommendations are for further, more quantitative laboratory measurements, as follows.

For low temperature mechanisms involving metastable reaction dynamics, we recommend room temperature measurements to verify the product NO(v,J) state distributions and absolute yields from the reactions of N(²D) and N(²P) with O₂. Wherever feasible, these measurements should be extended to higher temperatures, preferably to at least 1000 K. We also recommend experimental measurements to determine the NO(v,J) state distributions and yields for reactions of O with excited N₂^{*} and for energy transfer to NO from metastable states of N₂, N, O, and O₂. These "discovery" measurements should be coupled with auroral modeling and assessments of the existing auroral data base to determine the relevance of the results to the aeronomic data base. To expand this data base, we recommend a series of aeronomic measurements of aurorally excited NO(v,J) yields and distributions. These measurements should be designed to give detailed supporting information on auroral strength, metastable excitation yields for a variety of species (at least N(²D), N(²P), N₂(A), and O(¹D, ¹S)), and O and NO number densities, all as functions of altitude, for a variety of auroral and atmospheric conditions (IBC II-III arcs, high/low penetration, pre-dosed regions, high/low [O], high/low [NO]). Such a systematic series of measurements, coupled with interpretive modeling and incorporation of current/emerging kinetic data, will guide the establishment of the key excitation mechanisms and kinetics, and will put an end to the current level of guesswork regarding the auroral excitation efficiency of NO.

For high temperature NO(v) excitation, we recommend experimental measurements of the kinetics of collisional up-pumping of NO by O at high temperatures. 1000

to 7000 K. and by translationally excited O at high collision energies, 1 to 5 eV. These results should be coupled to results from recommended low-temperature O + NO(v) deactivation experiments to be discussed in Section 5. In addition, we recommend high temperature (or high collision energy) measurements of the yield and temperature dependence for the two-body recombination of N and O. Particular attention should be paid to the initial C-state yields at high temperature, as well as to any evidence for participation of the $a^4\Pi$ and B states not previously observed at low temperatures. This work should be preceded by a critical review of the room temperature data, including careful reevaluation of the necessary transition probabilities in the radiative cascade sequence.

5. DEACTIVATION OF NO(v,J)

Once formed in the upper atmosphere, vibrationally and rovibrationally excited NO(v,J) are lost through collisional and radiative deactivation, Reactions (4.1) through (4.6) in Table 1. The primary deactivation paths are through collisions with O, which are only partially understood, and radiative cascade in the infrared fundamental band, which is fairly well characterized for thermal rotational distributions. Radiative and collisional deactivation kinetics of superthermal high-J components are not understood at all, and our present level of knowledge does not support any reasonable recommendations.

5.1 Collisional Deactivation

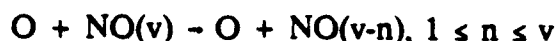
The principal path for collisional deactivation of NO(v) in the upper atmosphere is by collisions with O. This is a highly efficient process, and is the only collisional deactivation reaction whose rates can compete with radiative losses at typical thermospheric altitudes and temperatures. Furthermore, the potential for this process to proceed by multiquantum deactivation rather than single-quantum cascade can profoundly affect the NO(v) state distribution at lower altitudes. Unfortunately, the kinetics of this deactivation are not understood for higher vibrational levels.

The rate coefficient for



has been determined by Fernando and Smith [84] to be $(6.5 \pm 0.7) \times 10^{-11} \text{ cm}^3 \text{ s}^{-1}$ at 300 K. This relatively large rate coefficient is consistent with values determined for isotope exchange and high-pressure recombination, and thus indicates that vibrational deactivation occurs through formation and subsequent dissociation of a loosely bound O-NO complex. This could involve both redissociation and reactive atom exchange,

neither of which is likely to result in single-quantum deactivation of the $\text{NO}(v)$ as is commonly found in repulsive $V - T$ exchange. For higher v , we expect



with a distribution of n for each value of v . Based on statistical phase space arguments given by Quack and Troe [85], one might expect the most favored value of n to be v in each case, i.e., total deactivation of each level to $\text{NO}(v=0)$. However, the outcome is probably sensitive to details of the dynamic interaction along the potential surface(s), and a distribution of multiquantum n values is the most likely result. Since there are no experimental data to characterize this, we assume the statistical limit of Quack and Troe, $n=v$. We further assume, following Quack and Troe, that the rate coefficient is independent of v . This is consistent with experimental observations in electron-irradiated N_2/O_2 mixtures [92]. It is interesting to note that these assumptions in aeronomic modeling of auroral $\text{NO}(v)$ production provide a good comparison to collisionally coupled $\text{NO}(v)$ distributions observed [93] in a strong aurora [5,15].

The temperature dependence of $\text{O} + \text{NO}(v)$ is also not well known, but is likely to be small. Fernando and Smith [84] argue for a slightly negative temperature dependence due to the complex association step; Glänzer and Troe's [94] measured value of $(3.7 \pm 1.7) \times 10^{-11} \text{ cm}^3 \text{ s}^{-1}$ at 2700 K is consistent with this hypothesis. We have used the 300 and 2700 K values to estimate a temperature dependence for the overall rate coefficient, as shown in Figure 26. However, it is possible that repulsive single-quantum deactivation collisions will become increasingly important at the higher temperatures. Clearly, kinetic data on rate coefficients and product v distributions are sorely needed at both low and high temperatures.

Deactivation of $\text{NO}(v)$ by N_2 and O_2 is negligible in the normal thermosphere, but may become more important at the elevated temperatures following a high altitude nuclear burst. Owing to the mismatch between vibrational frequencies, the deactivation

proceeds primarily by V - T (vibration to translation) energy transfer, which occurs through impulsive collisions on a repulsive potential surface [95]. This type of energy transfer is relatively inefficient, with typical probabilities of $10^{-(5-6)}$ near room temperature, and results in single-quantum deactivation. Measured rate coefficients for N_2 and O_2 at 300 K are listed in Table 14. It is interesting to note that the values for O_2 [92] are relatively large and increase with v^2 rather than $v^{1.0}$ as predicted from SSH theory [95]; this may be a reflection of the approach of the system to V - V resonance between $O_2(v=0 \rightarrow 1)$ and $NO(v=12 \rightarrow 11)$.

The temperature dependencies of deactivation by N_2 and O_2 are difficult to assess with any confidence. Typically, V - T rate coefficients tend to scale as $A \exp(-BT^{-1/3})$ [95], but we are aware of no adequate high temperature data to establish the scalings for these collision partners. Taylor [96] recommended the expression $k = 6.75 \times 10^{-7} \exp(-182.83/T^{1/3})$ for deactivation of $NO(v=1)$ by both N_2 and O_2 based on his own unpublished data; however, this expression is highly suspect, since it gives room temperature values which are orders of magnitude below the subsequently measured ones, and it does not account for the two-order-of-magnitude difference between O_2 and N_2 . A temperature dependence plot is shown in Figure 27, comparing data for Ar, NO, N_2 and O_2 together with Taylor's expression. For N_2 extrapolation of the low-temperature data of Doyenette and Margottin-Maclou [97] indicates $k(N_2)$ values in the 10^{-13} range at high temperatures, in which case deactivation by N_2 will be unimportant (compared to O) in high altitude nuclear scenarios. On the other hand, if $k(N_2)$ follows a temperature dependence similar to $k(Ar)$, we might expect $k(N_2) \sim 3 \times 10^{-12} \text{ cm}^3 \text{ s}^{-1}$ at 5000 K, in which case $NO(v) + N_2$ can become a significant contributor to $NO(v)$ deactivation (or, conversely, collisional up-pumping) near and below 100 km. Use of the Taylor expression would suggest even larger contributions by N_2 at high temperatures.

In the case of deactivation by O_2 , $k(O_2)$ may follow a temperature dependence similar to that of $k(NO)$, due to open-shell attractive forces and/or V - V contributions,

resulting in $k(\text{O}_2) < 10^{-11} \text{ cm}^3 \text{ s}^{-1}$ even at temperatures up to 8000 K; since typical high altitude post-burst O/O_2 ratios are near unity or greater, it appears that $\text{NO}(\nu) + \text{O}_2$ does not play a major role in collisional deactivation of $\text{NO}(\nu)$ at any temperature. Use of the Taylor expression gives larger rate coefficients, but still probably not large enough compared to $k(\text{O})$ to offset the large O/O_2 ratios expected at these temperatures. However, we are unable to justify recommendations for specific temperature dependencies for $k(\text{N}_2)$ and $k(\text{O}_2)$, and we suggest that theoretical scaling estimates and/or high-temperature experimental measurements be performed.

We now turn to the deactivation of high-rotation states of NO, for which there is no adequate data base. As discussed in detail in Section 4, there is now ample evidence from laboratory and in situ auroral measurements that auroral NO production results in the formation of rovibrationally excited $\text{NO}(\nu, J)$, where the rotational J-states are sufficiently excited to form R-branch band heads in the vibrational transitions for each of several vibrational levels. (Strictly speaking, NO has half-integral rotational quantum numbers $K=J+\Omega$, where $\Omega=(1/2, 3/2)$ is the spin-orbit quantum number; in discussions of very high rotational states, we approximate this using J for convenience and simplicity.) The rotational line positions within these band heads follow Fortrat parabolas as described by Herzberg [78], with vertices near $J \sim 80$. Lines for $J \sim 60$ to 110 can contribute to the band head intensity, and excitation of up to $J \sim 120$ or higher cannot be ruled out. Excitation in excess of $J \sim 100$ represents more than 2 eV of rotational energy; this energy is extremely large relative to kT , and can be expected to profoundly affect the collisional deactivation kinetics. Collisional deactivation of $\text{NO}(\nu, J)$ can proceed by two pathways: rotational cooling within a given vibrational level, or vibrational deactivation to lower (ν, J) levels (retaining or losing rotational excitation).

Normally, one expects rotational thermalization to be rapid, proceeding with near-gas-kinetic collision efficiencies via $R \rightarrow T$ (rotation to translation) energy transfer. This occurs for relatively low-to-mid-J levels, where rotational spacings are much less than kT , and several multiquantum channels are thermally available. For such

conditions, rotational deactivation rate coefficients can be estimated using one of several scaling laws available in the literature [98]. For NO at 300 K, levels above $J \sim 40$ can proceed only by single-quantum deactivation, with concomitant reductions in their rate coefficients by more than an order of magnitude. The R - T deactivation efficiencies continue to decrease as the energy spacings approach kT , and, finally, for $J \geq 80$ the spacings exceed kT . At this point the classical statistical and energy gap formulas fail, and one must consider deactivation by collision partners in the high energy tail of the Boltzmann distribution. This means that rotational deactivation of the set of band head states will be prohibitively slow, for two reasons: (1) the deactivation probability is small because of the energetic mismatch, and (2) many successive single-quantum deactivation steps are required to remove a given molecule from the set of band head states.

Meanwhile, thermalization of the mid-to-low J states will occur fairly efficiently, perhaps on the scale of tens of collisions, resulting in a strongly bimodal rotational distribution. This is discussed by Rawlins et al. [17] and by Taherian et al. [99], who inferred effective rate coefficients of $\sim 10^{-11} \text{ cm}^3 \text{ s}^{-1}$ for thermalization of high- J states of NO in inert bath gases. At higher temperatures, R - T deactivation of band head states will become more efficient; above 500 K, the energy spacings between the band head states are exceeded by kT , and more efficient thermalization should ensue. Clearly, a series of measurements analogous to those of Taherian et al. [99] at 300 K and elevated temperatures would clarify the picture, as would theoretical estimates of the scalings of rate coefficients to high J .

Vibrational deactivation effects for band head states are much more uncertain. This can proceed through V - T transfer, where J remains essentially unchanged, or through R-V transfer where some of the rotational energy is converted to vibrational energy within the NO molecule. By analogy to the atmospheric deactivation of rotationally thermal NO(v), we expect collisions with O to dominate the collisional deactivation of NO(v , high J) in the thermosphere. However, comparisons between model predictions [15] and auroral spectral measurements [16] suggest that NO(v , J) may

be relatively immune to collisional deactivation by O. Such behavior would not be surprising, since the mismatch between the rotational and translational Fourier components of the interacting O--NO pair may prohibit entry into the attractive potential wells, resulting in less efficient impulsive collisions. This is a very important factor in assessing the collisional stability of the high-J spectral features in the upper atmosphere, and definitive experimental measurements are clearly required, both at room temperature and at elevated temperatures.

5.2 Radiative Deactivation

Radiative decay in the fundamental vibration-rotation band, $\Delta v=1$, near $5.4 \mu\text{m}$, controls the loss rate of NO(v) at altitudes above about 120 km. In addition, the transition probabilities in this and in the first overtone band, $\Delta v=2$, near $2.7 \mu\text{m}$, determine the intensity of NO(v) radiation at 5 to 7 and 2.5 to $3.5 \mu\text{m}$ for a given vibrational distribution. There are several reliable measurements of the $(v',v'') = (1,0)$ and $(2,0)$ band strengths (see below), and scalings of these values to higher v' via the theoretical dipole moment function of Billingsley [100] has been commonly accepted by the user community. However, recently emerging results from COCHISE, together with the newly realized need to determine transition probabilities for high-J states, indicate that the dipole moment function is still inadequately described at both small and large internuclear distances. This leads to significant uncertainties in the vibrational scaling of both the fundamental and the overtone transition probabilities, and in the extrapolation of these transition probabilities to higher J-states (and rotational temperatures). We will therefore discuss in some detail the currently accepted data base followed by the recently available results from COCHISE experiments.

Most of the experimental data base on NO(v) transition probabilities comes from absorption measurements on the $(1,0)$ and $(2,0)$ transitions. These are listed in Table 15. The measurements for the $(1,0)$ transition tend to fall into three groups: those with $S_{0,1} \sim 130$ to $140 \text{ cm}^{-2} \text{ am}^{-1}$, those with 120 to 130, and a few early measurements of 70 to

80. A weighted mean of 12 selected values from Table 15 gives $S_{0,1} = 132.0 \pm 1.5 \text{ cm}^{-2} \text{ ama}^{-1}$ or $A_{1,0} = 13.04 \pm 0.15 \text{ s}^{-1}$. The most recent work of Holland et al. [90], together with the extrapolated line-by-line data of Mandin et al. [101] as reported by Rothman et al. [102], tend to confirm the higher values, giving $A_{1,0} = 13.2$ to 13.6 s^{-1} . We recommend use of the intermediate value, $A_{1,0} = 13.4 \text{ s}^{-1}$ at 300 K. This quantity appears to be extremely well determined, and our recommended value is probably accurate to $\pm 10\%$ or better.

The (2,0) transition probability is less well determined. A weighted mean of six measurements gives $S_{0,2} = 2.16 \pm 0.97 \text{ cm}^{-2} \text{ ama}^{-1}$ or $A_{2,0} = 0.84 \pm 0.23 \text{ s}^{-1}$, which happens to coincide with the best available result, that of Chandraiah and Cho [103]. We note, however, that their result for the (1,0) band appears to be about 10 to 12% low. We will base our recommendation for $A_{2,0}$ on the COCHISE data as described below.

In a series of papers, Billingsley [100,104] determined a dipole moment function for NO from ab initio theoretical calculations, and used it to derive line-by-line and band-integrated Einstein transition probabilities for the fundamental and first overtone transitions up to $v' = 20$ and $J' = 33$. Billingsley's dipole moment function is illustrated in Figure 28. One of his more important conclusions was that the individual line strengths departed only slightly from Hönl-London scaling, and as a result the band-integrated Einstein coefficients were virtually independent of rotational temperature, at least below 600 K. Billingsley also provided scalings of the fundamental and overtone Einstein coefficients with v' , as listed in Table 16, and compared his results to those obtained from the semi-empirical dipole moment functions of Michels [105] and Chandraiah and Cho [103], which were derived from absorption data probing near-equilibrium internuclear separation. Recent measurements by Green et al. [106] of the overtone-to-fundamental ratios, $A_{v',v'-2} / A_{v',v'-1}$, gave results in excellent agreement with the Billingsley predictions for $v' = 3-7$, and clearly showed that the Michels scaling was incorrect. This measurement has commonly been interpreted as verification of the

shape of the Billingsley dipole moment function at medium to large internuclear separation, even though both the predicted absolute magnitudes of $A_{2,0}$ and $A_{1,0}$ and their ratio are much lower than the absorption data base indicates.

In a previous review of the transition probabilities of NO, Rothman et al. [102] recommended the values listed in Table 16. These values are based on the Chandraiah and Cho [103] results for the (2,0) band, the high resolution data of Mandin et al. [101] for the fundamental band, and the Billingsley [100] scalings to higher v' . However, we note that values recommended by Rothman et al. for the (3,1) and (4,2) transitions do not follow the Billingsley scalings, nor are they consistent with the overtone/fundamental ratios measured by Green et al. These values cause a physically unrealistic "kink" in a plot of the overtone Einstein coefficients versus v' . Furthermore, we question the physical consistency of adopting the Billingsley scaling for the overtone transition probabilities, which depend on the second derivative of the dipole moment function, when his predicted value for $A_{2,0}/A_{1,0}$, 0.043, is a factor of ~ 1.5 below the experimental value. This factor alone suggests that either the Billingsley dipole moment function is incorrect, at least at the second derivative level, or that all the experimental data are wrong.

To date, there have been two key factors missing from the experimental data base: a reliable measurement of $A_{2,0}$ (or $A_{2,0}/A_{2,1}$), and transition probability data extending to $v > 7$ to verify the Billingsley extrapolations to high v . Data recently obtained on the COCHISE facility [107] give an accurate measure of the overtone/fundamental ratios for $v'=2-13$ for a rotational temperature of 60 K. Such measurements have been elusive in the past due to complications from interfering radiators and bimodal high-J contributions; these complications are eliminated in the present data by use of high spectral resolution to isolate competing radiators and a helium background pressure to thermalize the rotational distributions. The observed overtone/fundamental ratios are plotted in Figure 29, compared to previously measured and predicted values. The agreement with Green et al. [106] is excellent over the range $3 \leq v' \leq 7$ where their data

have reasonable precision. However, the measured values deviate significantly from the Billingsley scaling at both low and high v' , even hinting at the presence of a maximum near $v' = 11$. The implications of these results are that the shape (second derivative) of the Billingsley dipole moment function is incorrect over much of the relevant range of internuclear separation, and that even the slope (first derivative, affecting fundamental band Einstein coefficient scaling with v') may have substantially increasing error at larger separations.

We presume that the Billingsley scaling is sufficient to give an accurate ratio of $A_{2,1}/A_{1,0}$, which we apply to the observed [107] value of $A_{2,0}/A_{2,1}$ to obtain $A_{2,0} = 0.94 \pm 0.11 \text{ s}^{-1}$. This is consistent with the results of Chandraiah and Cho [103], and is our recommended value. To provide a reliable set of values of $A_{v',v'}$ for higher v' , it will be necessary to derive an empirical dipole moment function which best reproduces the COCHISE overtone/fundamental measurements; this work is still in progress. Meanwhile, to provide a temporary recommendation, we suggest the values listed in Table 17. These are determined from the COCHISE data [107] using our recommended value for $A_{1,0}$ and assuming Billingsley scaling with v' for the $\Delta v=1$ Einstein coefficients. The Einstein coefficients determined in this fashion are plotted in Figure 30, in comparison with other values. Although it is essentially impossible to estimate the uncertainty of these values until the dipole moment function work has been completed, the values in Table 17 are probably accurate to within about 10% at low v' , and increasingly uncertain to about $\pm 40\%$ at $v' = 13$. There is presently no basis for extension of these values beyond $v' = 13$; this must await more complete evaluation of the experimental dipole moment function. Such an extrapolation is especially sensitive to the possibility of a downturn in the overtone transition probabilities in this region.

The values in Table 17 are appropriate for rotational temperatures below 100 K, and are probably reliable for temperatures up to at least 300 K. The extension of these values to higher rotational temperature (or higher J) is presently highly uncertain. At some temperature, $A_{v',v'}$ will become sensitive to rotational distribution, since the

scaling of $A(J)$ becomes more divergent from Hönl-London scaling as J increases. Whether this occurs for 1000, 5000, or 10000 K is impossible to know without more detailed evaluation of the dipole moment function and its effects on the line-by-line transition probabilities. It is likely that high- J distributions resulting in R-branch band heads ($J = 60$ to 120) are profoundly affected, since these states sample the extremes of internuclear separation where curvature in the dipole moment function will be more pronounced. Thus, there is at present little basis for estimating the effects of rotational distribution on transition probability. However, based on Billingsley's [100,104] prediction of near Hönl-London behavior for $J \approx 30$, $v' \leq 20$ for both the fundamental and the overtone, it is reasonable to guess that at least the fundamental band values in Table 17 are not seriously perturbed at temperatures up to about 1000 K. More definitive statements must await detailed evaluations in progress.

5.3 Recommendations

The recommended kinetic parameters for $\text{NO}(v)$ deactivation processes are listed in Table 18. However, few of these recommendations can be made with high or even well determined confidence, and much more definitive data are needed for all of the key processes. The most important deactivation processes for which definitive measurements are required are collisional deactivation of $\text{NO}(v)$ by O, collisional deactivation of high- J states, and radiative transition probabilities for high- v and high- J states. Specific questions which need to be answered are:

1. O+NO(v): What are the multiquantum product state distributions at low temperature? What is the temperature dependence of the rate coefficient up to ~ 5000 K? Does a single-quantum V - T deactivation mechanism become more important than multiquantum deactivation at high temperature?

2. $\text{NO}(\nu) + \text{O}_2, \text{N}_2$: What are the rate coefficients at high T. 3000 to 5000 K, and are they large enough for these processes to compete with O for deactivation/ up-pumping of $\text{NO}(\nu)$?
3. $\text{NO}(\nu, J) + \text{M}$: Does deactivation of high-J states occur predominantly through R - T, R - V, or (V,R) - T energy transfer? How do the rate coefficients vary with J and T? What are the effects of O?
4. Radiative Transition Probabilities: What are the overtone transition probabilities? What is the detailed shape of the dipole moment function, and how does it affect scaling of fundamental and overtone transition probabilities with ν and J? How do the band-integrated transition probabilities vary with rotational temperature, and what are the effects of very high-J states? What are the quantitative uncertainties in high-J, high- ν transition probabilities due to uncertainties in the dipole moment function at large and small internuclear separations?

We recommend that further experimental and theoretical efforts be pursued to answer these questions.

6. SUMMARY AND CONCLUSIONS

We have reviewed the chemistry and kinetics of the processes most directly relevant to the production of infrared radiation from vibrationally excited nitric oxide in the disturbed upper atmosphere. We have categorized these processes in terms of electron-initiated NO formation and removal (including metastable precursor production and quenching), high temperature thermal NO formation and removal, and NO(v) excitation and deactivation processes. We have provided recommended kinetic parameters and uncertainty estimates wherever possible, but we emphasize that many of these recommendations are highly speculative and are not well supported by the available data base. We have also given recommendations for specific areas where a great deal of further work is required to resolve key issues. Our specific recommendations may be found in the text in Subsection 2.1.3 (metastable precursor production), Subsection 2.2 (metastable precursor quenching), Subsection 2.3 (NO production from metastable chemistry), Subsection 2.4 (low temperature NO chemical removal), Subsection 3.4 (high temperature NO formation and removal), Subsection 4.4 (NO(v) excitation), and Subsection 5.3 (NO(v) deactivation). Recommended kinetic parameters are tabulated in Tables 2, 5, 6, 7, 8, 13, and 18.

Bombardment production of NO(v) can occur through three basic mechanisms which are roughly separable by temperature regime. At low temperatures, the dominant mechanism is through electron-impact initiated metastable chemistry, in which highly excited NO(v) is produced by energetic reactions involving electronically excited species. At least two such reactions have been identified to date, and several more are possible. Such processes tend to give rise to highly non-equilibrium, super-thermal vibrational and rotational distributions, which slowly relax toward equilibrium conditions by radiative and collisional decay. These reactions are efficient at low temperatures and have small temperature dependencies, so the metastable mechanism dominates NO(v) production in the auroral atmosphere and in the cooler electron-bombarded regions around a high altitude nuclear burst. At intermediate to high temperatures, most of the NO is

produced by thermally initiated chemistry of heated air, and is collisionally pumped up to and down from higher vibrational levels by atomic oxygen. This mechanism tends to produce subthermal, collision-limited vibrational distributions. Finally, at very high temperatures where the atmosphere is dissociated and the thermal lifetime of NO is short, NO(v) radiation can still be produced by radiative, two-body recombination of N and O. This occurs through radiative cascade from higher electronic states, resulting in non-equilibrium population of several vibrational levels.

Our understanding of atmospheric NO excitation has progressed greatly in the last 5 to 10 years, especially in the areas of metastable quenching and chemiexcitation mechanisms, high temperature N₂/O₂ kinetics, and the radiative properties of NO. However, many key elements of the above mechanisms are still poorly or marginally understood. A list of the more important gaps in the data base is given in Table 19. Foremost among these are the temperature dependencies of the rate coefficients and product channels for the metastable quenching and chemiexcitation reactions, the kinetics and product channels of O+NO up-pumping and O+NO(v) deactivation at all temperatures, the radiative and collisional kinetics of highly rotationally/vibrationally excited NO(v,J), the mechanisms and efficiencies of N(²D) and N(²P) production in electron-irradiated air as functions of dosing and vibrational temperature, the collisional and chemical kinetic effects of superthermal, translationally fast O and N, and the kinetics of high temperature NO dissociation and radiative recombination.

The potential methods for investigation of these problems deserve some comment. None of the issues we have raised are easy to resolve, and significant progress can only be made through application of thorough and novel experimental and theoretical methods. Product vibrational/rotational state distributions from metastable chemiexcitation and energy transfer reactions can be investigated by infrared chemiluminescence methods at low temperatures and by active probes such as laser-induced fluorescence near room temperature and above. The temperature dependencies of excited state quenching and chemiexcitation reactions can be

investigated to a significant extent in variable-temperature discharge flow reactors; however the requirements for short residence times and extensive optical access make such experiments very difficult and probably limited to temperatures below 800 to 1000 K. Flash photolysis techniques can perhaps be used to extend the temperature range to ~ 1500 K provided suitable photochemical precursors to the species of interest can be identified.

For kinetic measurements of thermal reactions above ~ 1000 K, carefully diagnosed shock tube techniques are the methods of choice. However, studies of metastable chemistry would require an external, non-thermal metastable excitation source (flash photolysis or electric discharge), and investigations of collision partner effects in vibrational relaxation and dissociation reactions would have to discriminate effectively against competing effects of the diluent bath gas (usually Ar). Fast atom effects can be studied with advanced crossed molecular beam techniques and, perhaps, by flash photolysis of suitable precursors; these methods are complicated by difficulties in controlling and specifying the interaction energies actually obtained.

State-of-the-art theoretical analyses can also be applied to a number of the more experimentally difficult problems, to predict trends and to guide our chemical intuition into these complex processes. Useful theoretical investigations would include potential energy surface and trajectory calculations for N^+-O_2 , $O-NO$, and $O-N_2^+$ interactions over a wide range of collision energies, extensions of vibrational deactivation rate coefficients to high temperature, the dynamics of highly rotationally/vibrationally excited species, and the behavior of the NO dipole moment function at extremes of internuclear separation.

In addition, we encourage the use of "integrated whole" experiments, in the form of well-diagnosed laboratory simulations and auroral flight measurements, to examine the overall process of $NO(v)$ production in electron-irradiated N_2/O_2 mixtures. Laboratory simulations could take the form of pulse radiolysis or electron-beam irradiation of N_2/O_2 mixtures; these could be similar to those previously reported [108,109], but at low

pressures, variable temperatures, and with more complete diagnostics of electron energy deposition and metastable, atomic oxygen, and total NO number densities. Similarly, high altitude auroral measurements of NO(v) distributions could be analogous to those previously performed [16,93] but with more complete supporting diagnostics of auroral deposition profiles, N(²D) and N(²P) emissions, and atomic oxygen number densities. Measurements of this type can provide a robust data base which shows trends with dosing, temperature, atomic oxygen effects, and atmospheric/auroral variability, and would place sufficient constraints on the model predictions to permit unambiguous conclusions about the viability of a postulated mechanism.

Finally, we recommend kinetic modeling studies, including numerical simulations and systematic sensitivity calculations, for specific auroral and nuclear scenarios. From the data provided in this report, it is possible to assemble a first-order estimate of a reaction mechanism describing NO(v) formation and destruction over the entire temperature range encountered in high altitude bombardments. This can be used in a systematic way to examine the relative importance of each reaction rate as a function of temperature and bombardment conditions. It is unlikely that every rate coefficient needs to be known from 200 to 10000 K, and information on the range of conditions over which specific reactions are most important would be extremely valuable in helping experimenters to focus their efforts on the most relevant conditions. Sensitivity calculations, employing the rate parameter and mechanistic uncertainties estimated here, can be used to evaluate the effects of the largest unknowns on predicted scalings of specific bandpass radiation with dosing, temperature, altitude, etc. This would also provide key information which would help to prioritize further investigations.

The problem of NO(v) radiation in the disturbed upper atmosphere is clearly a complex and partially understood one, even for relatively simple and accessible auroral conditions. After a significant amount of detailed experimental and theoretical investigation, our knowledge has reached the level at which we can specify what we still need to learn in order to have a reliable predictive understanding. Considering that NO

is arguably the best understood disturbed-atmosphere molecular infrared radiator, it is clear that our general knowledge of high altitude infrared signatures and excitation mechanisms is far from complete. Continued pursuit of these issues should challenge experimentalists, aeronomers, and theorists for some time to come.

7. REFERENCES

1. J.E. Frederick and D.W. Rusch, "On the Chemistry of Metastable Atomic Nitrogen in the F Region Deduced from Simultaneous Satellite Measurements of the 5200-Å Airglow and Atmospheric Composition," *J. Geophys. Res.* **82**, 3509 (1977).
2. D.W. Rusch and J-C. Gerard, "Satellite Studies of N(²D) Emission and Ion Chemistry in Aurorae," *J. Geophys. Res.* **85**, 1285 (1980).
3. M.H. Rees and G.J. Romick, "Atomic Nitrogen in an Aurora: Production, Chemistry, and Optical Emissions," *J. Geophys. Res.* **90**, 9871 (1985).
4. F.R. Gilmore, "Initial Species in Bombarded Air," memorandum dated 14 January 1985; "Bombardment Heating Efficiency of Air between 60 and 90 km Altitude," memorandum dated 9 April 1985.
5. G.E. Caledonia and J.P. Kennealy, "NO Infrared Radiation in the Upper Atmosphere," *Planet. Space Sci.* **30**, 1043 (1982).
6. D. Kley, G.M. Lawrence, and E. Stone, "The Yield of N(²D) Atoms in the Dissociative Recombination of NO⁺," *J. Chem. Phys.* **66**, 4157 (1977).
7. H.S. Porter, C.H. Jackman, and A.E.S. Green, "Efficiencies for Production of Atomic Nitrogen and Oxygen by Relativistic Proton Impact in Air," *J. Chem. Phys.* **65**, 154 (1976).
8. E.C. Zipf, P.J. Espy, and C.F. Boyle, "The Excitation and Collisional Deactivation of Metastable N(²P) Atoms in Auroras," *J. Geophys. Res.* **85**, 687 (1980).
9. E.C. Zipf and R.W. McLaughlin, "On the Dissociation of Nitrogen by Electron Impact and by EUV Photo-absorption," *Planet. Space Sci.* **26**, 449 (1978).
10. G.G. Sivjee and R.A. Marshall, "NI[3466Å] and NI[5200Å] Emissions from Various Nighttime and Daytime Auroras," *J. Geophys. Res.* **88**, 3153 (1983).
11. U.S. Standard Atmosphere, 1976, NOAA-S/T 7601562 (U.S.G.P.O. 1976).
12. G. Brasseur and D. Offermann, "Recombination of Atomic Oxygen near the Mesopause: Interpretation of Rocket Data," *J. Geophys. Res.* **91**, 10818 (1986); D. Offermann, "The Energy Budget Campaign 1980: Introductory Review," *J. Atmos. Terr. Phys.* **47**, 1 (1985).
13. W. Pendleton, Jr., P. Espy, J. Hartman, M. Fetrow, and G. Sivjee, "Nitrogen I 3F (²P^o - ²D^o) Emissions in the Aurora," *J. Geophys. Res.* **94**, 2595 (1989).

14. A. Vallance Jones and R.L. Gattinger, "The Relative Intensity of the [NI] 1.04 μm Multiplet as an Indicator of the Mean Height of Auroral Forms," *J. Geophys. Res.* 84, 1315 (1979).
15. M.E. Fraser, W.T. Rawlins, W.A.M. Blumberg, and S.M. Miller, "Auroral Production of Rovibrationally Excited Nitric Oxide in the Upper Atmosphere," *EOS* 70, 414 (1989); related work in progress, 1990.
16. R.H. Picard, J.R. Winick, R.D. Sharma, A.S. Zachor, P.J. Espy, and C.R. Harris, "Interpretations of Infrared Measurements of the High-Latitude Thermosphere from a Rocket-Borne Interferometer," *Adv. Space Res.* 7, 23 (1987).
17. W.T. Rawlins, M.E. Fraser, and S.M. Miller, "Rovibrational Excitation of Nitric Oxide in the Reaction of O_2 with Metastable Atomic Nitrogen," *J. Phys. Chem.* 93, 1097 (1989).
18. F.R. Gilmore, "Approximate Ion Production Rates in Air that is Partially Dissociated or Ionized, or Has a Higher than Standard Oxygen/Nitrogen Ratio," memorandum dated 3 April 1987.
19. H.H. Michels, "Theoretical Determination of Electronic Transition Probabilities for Diatomic Molecules," Air Force Weapons Laboratory, AFWL-TR-72-1, May 1972 (AD-901-449L).
20. F.J. Mehr and M.A. Biondi, "Electron Temperature Dependence of Recombination of O_2^+ and N_2^+ Ions with Electrons," *Phys. Rev.* 181, 264 (1969).
21. J.L. Queffelec, B.R. Rowe, M. Morlais, J.C. Gomet, and F. Vallee, "The Dissociative Recombination of $\text{N}_2^+(v=0,1)$ as a Source of Metastable Atoms in Planetary Atmospheres," *Planet. Space Sci.* 33, 263 (1985).
22. L.G. Piper, "The Excitation of $\text{N}(^2\text{P})$ by $\text{N}_2(\text{A}^3\Sigma_u^+, v=0,1)$," *J. Chem. Phys.* 90, 7087 (1989).
23. D.C. Cartwright, "Vibrational Population of the Excited States of N_2 Under Auroral Conditions," *J. Geophys. Res.* 83, 517 (1978).
24. R.H. Garstang, "Multiplet Emissions for the Lines $^4\text{S}-^2\text{D}$ of OI, OII and NI," *Astrophys. J.* 115, 506 (1952).
25. R.H. Garstang, The Airglow and the Aurorae, Pergamon, New York, 1956.
26. K. Schofield, "Critically Evaluated Rate Constants for Gaseous Reactions of Several Electronically Excited Species," *J. Phys. Chem. Ref. Data* 8, 723 (1979).

27. J.E. Davenport, T.G. Slanger, and G. Black, "The Quenching of $N(^2D)$ by $O(^3P)$," *J. Geophys. Res.* 81, 12 (1976).
28. M.P. Iannuzzi and F. Kaufman, "Rates of Some Reactions of $N(^2D)$ and 2P near 300 K," *J. Chem. Phys.* 73, 4701 (1980).
29. L.G. Piper, "The Rate Coefficient for Quenching $N(^2D)$ by $O(^3P)$," *J. Chem. Phys.* 91, 3516 (1989).
30. S.M. Miller, W.A.M. Blumberg, C.P. Fell, and J.I. Steinfeld, "Rate Constants for the Quenching of N^* by $O(^3P)$," *J. Chem. Phys.* 92, 4768 (1990).
31. L.E. Jusinski, G. Black, and T.G. Slanger, "REMPI Measurements of $N(^2D)$ Quenching by $O(^3P)$," *J. Phys. Chem.* 92, 5977 (1988).
32. C.G. Fesen, J.-C. Gerard, and D.W. Rusch, "Rapid Deactivation of $N(^2D)$ by O: Impact on Thermospheric and Mesospheric Odd Nitrogen," *J. Geophys. Res.* 94, 5419 (1989); D. Bates, "Rapid Deactivation of $N(^2D)$ by $O(^3P)$ and 630 nm Emission," *Planet. Space Sci.* 37, 1145 (1989).
33. M.F. Golde and B.A. Thrush, "General Discussion," *Faraday Discussions Chem. Soc.* 53, 233 (1972).
34. R.A. Young and O.J. Dunn, "The Excitation and Quenching of $N(^2P)$," *J. Chem. Phys.* 63, 1150 (1975).
35. L.G. Piper, "Rate Coefficients for Quenching $N(^2P)$ by $O(^3P)$ and O_2 ," *EOS* 70, 414 (1989).
36. L.G. Piper, private communication, 1990.
37. D. Bates, "Theoretical Considerations Regarding Some Inelastic Atomic Collision Processes of Interest in Aeronomy: Deactivation and Charge Transfer," *Planet. Space Sci.* 37, 363 (1989).
38. M.P. Iannuzzi and F. Kaufman, "Rates of Some Reactions of $N(^2D)$ and 2P near 300 K," *J. Chem. Phys.* 73, 4701 (1980).
39. C.L. Lin and F. Kaufman, "Reactions of Metastable Nitrogen Atoms," *J. Chem. Phys.* 55, 3760 (1971).
40. D. Husain, S.K. Mitra, and A.N. Young, "Kinetic Study of Electronically Excited Nitrogen Atoms, $N(2^2D, 2^2P_J)$ by Attenuation of Atomic Resonance Radiation in the Vacuum Ultraviolet," *J. Chem. Soc. Faraday II* 70, 1721 (1974).

41. B. Fell, I. V. Rivas, and D.L. McFadden, "Kinetic Study of Electronically Metastable Nitrogen Atoms, $N(2^2D_J)$, by Electron Spin Resonance Absorption," J. Phys. Chem. 85, 224 (1981).
42. G. Black, T.G. Slanger, G.A. St. John, and R.A. Young, "Vacuum Ultraviolet Photolysis of N_2O . IV. Deactivation of $N(2^2D)$," J. Chem. Phys. 51, 116 (1969).
43. T.G. Slanger, B.J. Wood, and G. Black, "Temperature Coefficients for $N(2^2D)$ Quenching by O_2 and N_2O ," J. Geophys. Res. 76, 8430 (1971).
44. L.G. Piper, M.E. Donahue, and W.T. Rawlins, "Rate Coefficients for $N(2^2D)$ Reactions," J. Phys. Chem. 91, 3883 (1987).
45. R.A. Young and O.J. Dunn, "The Excitation and Quenching of $N(2^2P)$," J. Chem. Phys. 63, 1150 (1975).
46. C.M. Phillips, J.I. Steinfeld, and S.M. Miller, "Remeasurement of $N(2^2P) + O_2$ Reaction Rate Using Multiphoton Ionization Detection of Nitrogen Atoms," J. Phys. Chem. 91, 5001 (1987).
47. K.A. Berrington and P.G. Burke, "Effective Collision Strengths for Forbidden Transitions in e-N and e-O Scattering," Planet. Space Sci. 29, 377 (1981).
48. L.G. Piper, H.C. Murphy, and W.T. Rawlins, "Development of COCHISE UV Absorption System," Air Force Geophysics Laboratory, AFGL-TR-81-0318, ADA111828, Hanscom AFB, MA, December 1981; W.T. Rawlins, L.G. Piper, A. Gelb, G.E. Caledonia, P.E. Nebolsine, G. Weyl, H.C. Murphy, L.M. Cowles, and B.D. Green, "COCHISE Atmospheric Nitrogen/Oxygen Excitation Studies, Air Force Geophysics Laboratory, AFGL-TR-85-0322, Hanscom AFB, MA, December 1985, pp 3-8 to 3-13, ADA172234.
49. M.R. Torr, B.Y. Welsh, and D.G. Torr, "The O_2 Atmospheric Dayglow in the Thermosphere," J. Geophys. Res. 91, 4561 (1986).
50. T.G. Slanger, E.J. Llewellyn, I.C. McDade, and G. Witt, "Comment on 'The O_2 Atmospheric Dayglow in the Thermosphere' by M.R. Torr, B.Y. Welsh, and D.G. Torr," J. Geophys. Res. 92, 7753 (1987).
51. M.R. Torr, J.K. Owens, and D.G. Torr, "Reply," J. Geophys. Res. 92, 7756 (1987).
52. K. Donahue and L.G. Piper, "Observations on the Chemical Production of $N_2(X,v)$ Using a $He(2^3S)$ Penning Ionization Diagnostic," manuscript in preparation, 1990.
53. L.G. Piper, G.E. Caledonia, and J.P. Kennealy, "Rate Constants for Deactivation of $N_2(A^3\Sigma_u^+, v'=0,1)$ by O," J. Chem. Phys. 75, 2847 (1981).

54. L.G. Piper, "The Excitation of $O(^1S)$ in the Reaction between $N_2(A^3\Sigma_u^-)$ and $O(^3P)$," *J. Chem. Phys.* 77, 2373 (1982).
55. A.R. DeSouza, G. Gousset, M. Touzeau, and T. Khiet, "Note on the Determination of the Efficiency of the Reaction $N_2(A^3\Sigma) + O(^3P) \rightarrow N_2 + O(^1S)$," *J. Phys. B: At. Mol. Phys.* 18, L661 (1985).
56. R. Atkinson, D.L. Baulch, R.A. Cox, R.F. Hampson, Jr., J.A. Kerr, and J. Troe, "Evaluated Kinetic and Photochemical Data for Atmospheric Chemistry: Supplement III," *J. Phys. Chem. Ref. Data* 18, 881 (1989).
57. G. Brasseur and S. Solomon, Aeronomy of the Middle Atmosphere, D. Reidel Publishing Co., Boston, 1984, p. 260.
58. K. Watanabe, F.M. Matsunaga, and H. Sakai, "Absorption Coefficient and Photoionization Yield of NO in the Region 580 to 1350Å," *Appl. Opt.* 6, 391 (1967).
59. S. Cieslik and M. Nicolet, "The Aeronomical Dissociation of Nitric Oxide," *Planet. Space Sci.* 21, 925 (1973).
60. Y.B. Kim, K. Stephan, E. Märk, and T.D. Märk, "Single and Double Ionization of Nitric Oxide by Electron Impact from Threshold up to 180 eV," *J. Chem. Phys.* 74, 6771 (1981).
61. J.M. Ajello, K.D. Pang, B.O. Franklin, S.K. Howell, and N.J. Bowring, "A Study of Electron Impact Excitation of NO: The Middle Ultraviolet from 170 to 270 nm," *J. Geophys. Res.* 94, 9105 (1989); "A Study of Electron Impact Excitation of NO: The Vacuum Ultraviolet from 40 to 170 nm," *J. Geophys. Res.* 94, 9093 (1989).
62. D.L. Baulch, D.D. Drysdale, D.G. Horne, and A.C. Lloyd, Evaluated Kinetic Data for High Temperature Reactions. Volume 2. Homogeneous Gas Phase Reactions of the H_2 - N_2 - O_2 System, Butterworths, London, 1973; D.L. Baulch, D.D. Drysdale, J. Duxbury, and S. Grant, Evaluated Kinetic Data for High Temperature Reactions. Volume 3. Homogeneous Gas Phase Reactions of the O_2 - O_3 System, the CO - O_2 - H_2 System, and of Sulphur-Containing Species, Butterworths, London, 1976.
63. R.K. Hanson and S. Salimian, "Survey of Rate Constants in the N/H/O System," Combustion Chemistry, W.C. Gardiner, Jr., ed., Springer-Verlag, New York, 1984, pp 361-421.
64. M. Koshi, M. Yoshimura, K. Fukuda, H. Matsui, K. Saito, M. Watanabe, A. Imamura, and C. Chen, "Reactions of $N(^4S)$ Atoms with NO and H_2 ," *J. Chem. Phys.* 93, 8703 (1990).

65. K.L. Wray and J.D. Teare, "Shock Tube Study of the Kinetics of Nitric Oxide at High Temperatures," *J. Chem. Phys.* **36**, 2582 (1962).
66. M.E. Whitson, Jr., L.A. Darnton, and R.J. McNeal, "Vibrational Energy Distribution in the NO Produced by the Reaction of N(⁴S) with O₂," *Chem. Phys. Lett.* **41**, 552 (1976).
67. A. Rahbee and J.J. Gibson, "Rate Constants for Formation of NO in Vibrational Levels $v=2$ through $v=7$ from the Reaction N(⁴S) + O₂ → NO(v) + O," *J. Chem. Phys.* **74**, 5143 (1981).
68. R.R. Herm, B.J. Sullivan, and M.E. Whitson, Jr., "Nitric Oxide Vibrational Excitation from the N(⁴S) + O₂ Reaction," *J. Chem. Phys.* **79**, 2221 (1983).
69. I.C. Winkler, R.A. Stachnik, J.I. Steinfeld, and S.M. Miller, "Determination of NO($v=0-7$) Product Distribution from the N(⁴S) + O₂ Reaction Using Two-Photon Ionization," *J. Chem. Phys.* **85**, 890 (1986).
70. C.S. Feigerle and J.C. Miller, "Multiphoton Ionization of Vibrationally Hot Nitric Oxide Produced in a Pulsed Supersonic Glow Discharge," *J. Chem. Phys.* **90**, 2900 (1989).
71. J.P. Kennealy, F.P. Del Greco, G.E. Caledonia, and B.D. Green, "Nitric Oxide Chemiexcitation Occurring in the Reaction between Metastable Nitrogen Atoms and Oxygen Molecules," *J. Chem. Phys.* **69**, 1574 (1978).
72. M.E. Fraser, W.T. Rawlins, and S.M. Miller, "Rovibrational Excitation of Carbon Monoxide by Energy Transfer from Metastable Nitrogen," *J. Chem. Phys.* **92**, 1758 (1990).
73. S.C. Solomon, "Optical Aeronomy," U.S. National Report to International Union of Geodesy and Geophysics 1987-1990, Review of Geophysics, Supplement, pp. 1088-1109, April 1991.
74. M.F. Golde and B.A. Thrush, "Afterglows," *Rep Prog. Phys.* **36**, 1285 (1973).
75. R.D. Kenner and E.A. Ogryzlo, "Chemiluminescence in Gas Phase Reactions," Chemi- and Bioluminescence, J. G. Burr, ed., Marcel Dekker, Inc., New York, 1985, pp. 45-185.
76. W.E. Sharp and D.W. Rusch, "Chemiluminescence of Nitric Oxide: The NO(C²Π-A²Σ⁺) Rate Constant," *J. Quant. Spectrosc. Radiat. Transfer* **25**, 413 (1981).
77. M.L. Du and A. Dalgarno, "The Radiative Association of N and O Atoms," *J. Geophys. Res.* **95**, 12265 (1990).

78. G. Herzberg, Molecular Spectra and Molecular Structure. I. Spectra of Diatomic Molecules, Van Nostrand Reinhold Co., New York, 1950.
79. R.W. Nicholls, "Franck-Condon Factors to High Vibrational Quantum Numbers IV: NO Band Systems," J. Res. Nat. Bureau of Standards A. Physics and Chemistry 68A, 535 (1964).
80. D.L. Albritton, A.L. Schmeltekopf, and R.N. Zare, private communication to L.G. Piper via D.W. Setser, 1985.
81. L.G. Piper and L.M. Cowles, "Einstein Coefficients and Transition Moment Variation for the NO($A^2\Sigma^+X^2\pi$) Transition," J. Chem. Phys. 85, 2419 (1986).
82. L.G. Piper, T.R. Tucker, and W.P. Cummings, "Electronic Transition Moment Variation and Einstein Coefficients for the NO($B^2\Pi-X^2\Pi$) System," J. Chem. Phys. 94, 7667 (1991).
83. L.G. Piper, L.M. Cowles, and W.T. Rawlins, "State-to-State Excitation of NO($A^2\Sigma^+$, $v'=0,1,2$) by $N_2(A^3\Sigma_u^+$, $v'=0,1,2$)," J. Chem. Phys. 85, 3369 (1986).
84. R.P. Fernando and I.W.M. Smith, "Vibrational Relaxation of NO by Atomic Oxygen," Chem. Phys. Lett. 66, 218 (1979).
85. M. Quack and J. Troe, "Complex Formation in Reactive and Inelastic Scattering: Statistical Adiabatic Channel Model of Unimolecular Processes III," Ber. Bunsenges. Physik. Chem. 79, 170 (1975).
86. C.A. Wight and S.R. Leone, "Vibrational State Distributions and Absolute Excitation Efficiencies for T-V Transfer Collisions of NO and CO with H Atoms Produced by Excimer Laser Photolysis," J. Chem. Phys. 79, 4823 (1983); C. A. Wight, D. J. Donaldson, and S. R. Leone, "A Two-Laser Pulse-and-Probe Study of T-R,V Energy Transfer Collisions of H+NO at 0.95 and 2.2 eV," J. Chem. Phys. 83, 660 (1985).
87. M.C. Colton and G.C. Schatz, "Theoretical Studies of Fast H Atom Collisions with NO," J. Chem. Phys. 83, 3413 (1985).
88. F.X. Kneizys, E.P. Shettle, W.O. Gallery, J.H. Chetwynd, Jr., L.W. Abreu, J.E.A. Shelby, R.W. Fenn, and R.A. McClatchey, "Atmospheric Transmittance/Radiance: Computer Code LOWTRAN 5," Air Force Geophysics Laboratory, AFGL-TR-80-0067, Hanscom AFB, MA, 1980, ADA088215.
89. T.C. Degges and H.J.P. Smith, "A High Altitude Infrared Radiance Model," Air Force Geophysics Laboratory, AFGL-TR-77-0271, Hanscom AFB, 1977, ADA059242.

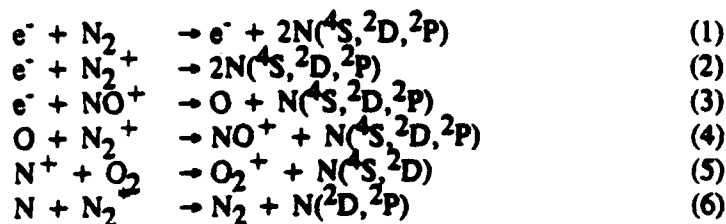
90. R.F. Holland, M.C. Vasquez, W.H. Beattie, and R.S. McDowell, "Absorptivity of Nitric Oxide in the Fundamental Vibrational Band," *J. Quant. Spectrosc. Radiat. Transfer* **29**, 435 (1983).
91. M.J. McEwan and L.F. Phillips, Chemistry of the Atmosphere, John Wiley and Sons, New York, 1975, p. 114.
92. B.D. Green, G.E. Caledonia, R.E. Murphy, and F.X. Robert, "The Vibrational Relaxation of NO($v=1-7$) by O₂," *J. Chem. Phys.* **76**, 2441 (1982).
93. W.T. Rawlins, G.E. Caledonia, J.J. Gibson, and A.T. Stair, Jr., "Infrared Emission from NO($\Delta v=1$) in an Aurora: Spectral Analysis and Kinetic Interpretation of HIRIS Measurements," *J. Geophys. Res.* **86**, 1313 (1981).
94. K. Glänzer and J. Troe, "Vibrational Relaxation of NO in Collisions with Atomic Oxygen and Chlorine," *J. Chem. Phys.* **63**, 4352 (1975).
95. J.T. Yardley, Introduction to Molecular Energy Transfer, Academic Press, New York, 1980.
96. R.L. Taylor, "Energy Transfer Processes in the Stratosphere," *Can. J. Chem.* **52**, 1436 (1974).
97. L. Doyenette and M. Margottin-Maclou, "Vibrational Relaxation of NO($v=1$) by NO, N₂, CO, HCl, CO₂, and N₂O from 300 to 600 K," *J. Chem. Phys.* **84**, 6668 (1986).
98. T.A. Brunner and D. Pritchard, "Fitting Laws for Rotationally Inelastic Collisions," Dynamics of the Excited State, K.P. Lawley, ed., John Wiley and Sons, New York, 1982, pp. 589-641.
99. M.R. Taherian, P.C. Cosby, and T.G. Slanger, "Photodissociation of NO₂ at 157.6 nm," *J. Phys. Chem.* **91**, 2304 (1987).
100. F.P. Billingsley II, "Calculated Vibration-Rotation Intensities for NO($X^2\Pi$)," *J. Mol. Spectrosc.* **61**, 53 (1976).
101. J.Y. Mandin, C. Amiot, and G. Guelachvili, *Ann. Phys. (Paris)* **5**, 91 (1980).
102. L.S. Rothman, A. Goldman, J.R. Gillis, R.R. Gamache, H.M. Pickett, R.L. Poynter, N. Husson, and A. Chedin, "AFGL Trace Gas Compilation: 1982 Version," *Appl. Opt.* **22**, 1616 (1983).

103. G. Chandraiah and C.W. Cho, "A Study of the Fundamental and First Overtone Bands of NO in NO-Rare Gas Mixtures at Pressures up to 10,000 PSI," J. Mol. Spectrosc. 47, 134 (1973).
104. F.P. Billingsley II, "Multiconfiguration Self-Consistent-Field Calculation of the Dipole Moment Function and Potential Curve of NO($X^2\Pi$)," J. Chem. Phys. 62, 864 (1975); "Improved MCSCF Dipole Moment Function for NO($X^2\Pi$)," J. Chem. Phys. 63, 2267 (1975); "Calculated Vibration-Rotation Intensities and Line Positions for Ground State Nitric Oxide," Air Force Geophysics Laboratory, AFCRL-TR-75-0586 (Physical Sciences Research Papers, No. 651), Hanscom AFB, MA, November 1975, ADA019790.
105. H.H. Michels, "Calculation of the Integrated Band Intensities of NO," J. Quant. Spectrosc. Radiat. Transfer 11, 1735 (1971).
106. B.D. Green, G.E. Caledonia, and R.E. Murphy, "A Determination of the Nitric Oxide Einstein Coefficient Ratios," J. Quant. Spectrosc. Radiat. Transfer 26, 215 (1981).
107. W.T. Rawlins, M.E. Fraser, S.M. Miller, and W.A.M. Blumberg, "Branching Ratios for Infrared Vibrational Emission from NO($X^2\Pi$, $v=2-13$)," J. Chem. Phys., submitted for publication, 1991.
108. R.G. MacDonald and O.A. Miller, "Low Dose-Rate Radiolysis of Nitrogen: Yield of Nitrogen Atoms, N(4S) and N(2D , 2P)," Radiat. Phys. Chem. 26, 63 (1985).
109. B.D. Green, G.E. Caledonia, W.A.M. Blumberg, and F.H. Cook, "Absolute Production Rates and Efficiencies of NO in Electron-Irradiated N_2/O_2 Mixtures," J. Chem. Phys. 80, 773 (1984).

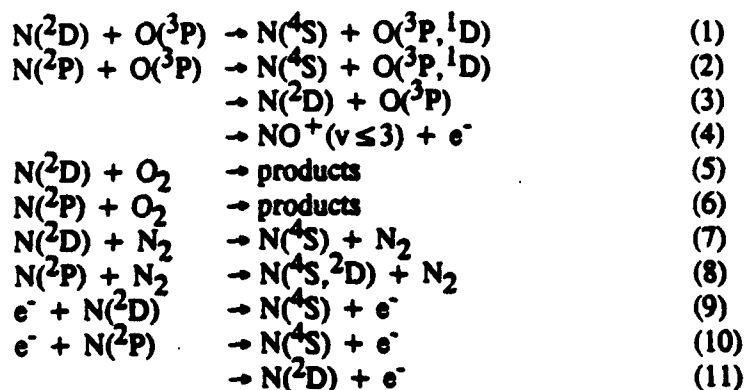
Table 1. High Altitude NO Chemistry

1. Electron-initiated chemistry

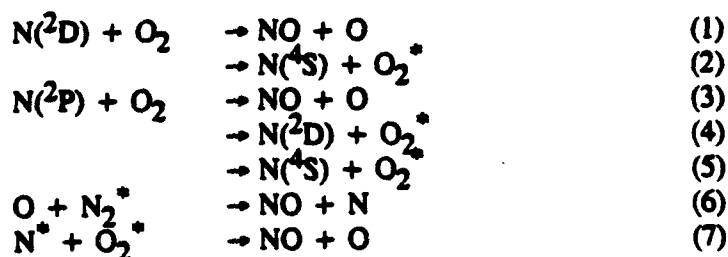
a. Precursor Formation



b. Precursor Loss



c. NO Formation



d. NO Destruction

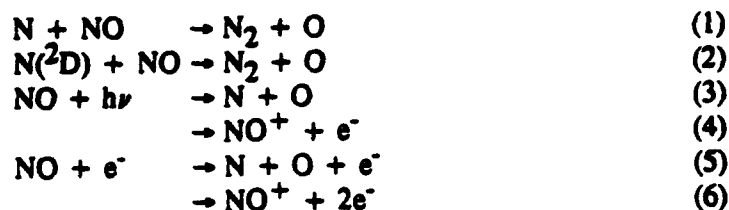
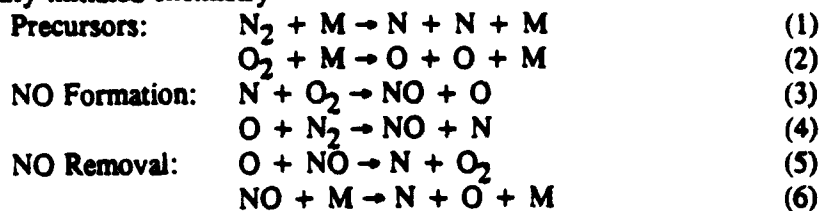


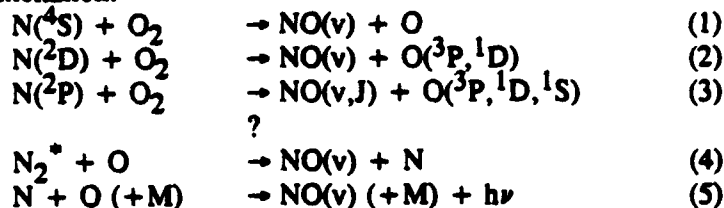
Table 1. High Altitude NO Chemistry (Continued)

2. Thermally initiated chemistry

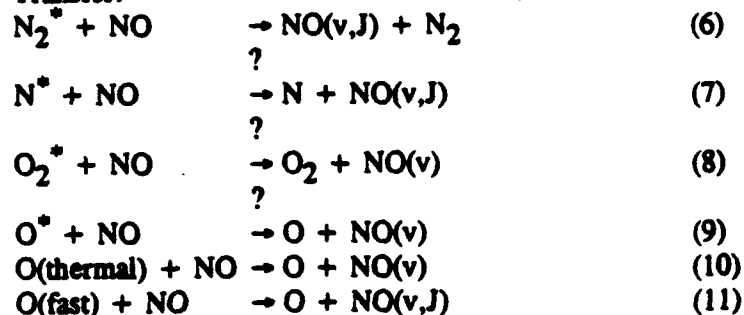


3. Excitation of NO(v,J)

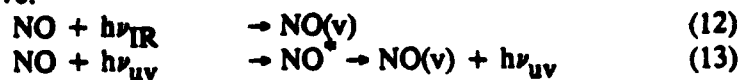
Chemiexcitation:



Energy Transfer:

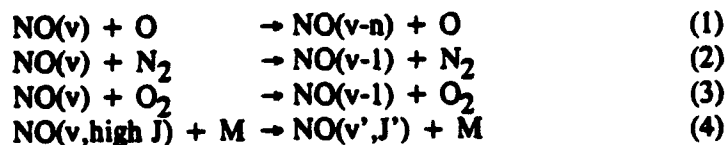


Radiative:



4. Deactivation of NO(v,J)

Collisional:



Radiative:

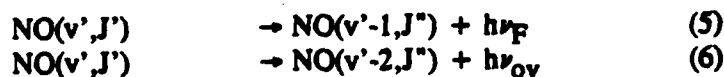


Table 2. Recommended Average N^* Production Rates, Atoms/Ion Pair^a

Process	Auroral ^b			Nuclear		
	$N(^4S)$	$N(^2D)$	$N(^2P)$	$N(^4S)$	$N(^2D)$	$N(^2P)$
$e^- + N_2$	0.5	0.3	0.2	0.62	0.42	0.25
$e^- + N_2^+$	0	0	0	0	1.3 ^e	e
$e^- + NO^+$	0.17	0.5	c	0	0.06 ^f	c,f
$O + N_2^+$	0	0.5	d	0	f	d,f
$N^+ + O_2$	0.01	0.03	0	0.02	0.06	0
Total	0.67	1.38	≥ 0.2	0.64	1.84	≥ 0.25

a. Overall confidence X/+ 2

b. Altitudes ≥ 110 km; yields at lower altitudes depend on dosing profile

c. May be produced from NO^+ ($v \geq 3$)

d. May be produced from N_2^+ ($v \geq 2$)

e. $N(^2D)/N(^2P)$ branching ratio depends on vibrational distribution of N_2^+

f. Small in strong bombardment limit; may contribute significantly in relaxation regions

Table 3. Representative Kinetic Parameters Relevant to N* Production

Reaction	k ^a	References
$e^- + N_2 \rightarrow e^- + N + N(^4S, ^2D, ^2P)$	b	Zipf and McLaughlin (1978) [9]; Zipf et al. (1980) [8]
$e^- + N_2^+(v=0) \rightarrow N(^2D) + N(^2D)$ $e^- + N_2^+(v=1) \rightarrow N(^2D) + N(^2D)$ $\quad \quad \quad \rightarrow N(^2D) + N(^2P)$	$1.66(-6) T_e^{-0.39}$ $1.1(-6) T_e^{-0.39}$ $5.6(-7) T_e^{-0.39}$	Mehr and Biondi (1968) [20]; Queffelec et al. (1985) [21]
$e^- + NO^+ \rightarrow O + 0.25 N(^4S)$ $\quad \quad \quad + 0.75 N(^2D)$	$4.0(-7)$ $(T_e/300)^{-0.9}$	Kley et al. (1977) [6]; Alge et al. (1983) ^d
$O + N_2^+ \rightarrow N(^2D) + NO^+$	$1.4(-10)$ $(T/300)^{-0.44}$	Frederick and Rusch (1977) [1]; McFarland et al. (1974) ^e
$N^+ + O_2 \xrightarrow{36\%} O_2^+ + N(^2D)$ $\quad \quad \quad \xrightarrow{15\%} O_2^+ + N(^4S)$ $\quad \quad \quad \xrightarrow{43\%} NO^+ + 0.15 O(^1D)$ $\quad \quad \quad \quad \quad + 0.85 O(^1S)$ $\quad \quad \quad \xrightarrow{6\%} O(^4S) + NO$	6×10^{-10}	Langford et al. (1985, 1986) ^f
$N(^4S) + N_2^+ \rightarrow N_2 + N(^2P)$	4×10^{-11} $(T/300)^{1/2}$	Estimated from Piper (1989) [22]

Table 3. Representative Kinetic Parameters Relevant to N* Production (Continued)

Reaction	k ^a	References
N(² D) → N(⁴ S) + hν (520 nm)	1.07(-5) ^c	Garstang (1956) [24,25]
N(² P) → N(⁴ S) + hν (346.6 nm)	5.4(-3) ^c	
N(² P) → N(² D) + hν (1040 nm)	7.9(-2) ^c	

a. Units are cm³ s⁻¹ unless otherwise noted; T_e signifies electron temperature; 1.66(-6) reads 1.66 x 10⁻⁶.

b. Cross sections must be convolved with a dosing-characteristic electron energy distribution to determine scene-specific rate coefficients and product branching ratios.

c. Units are s⁻¹.

d. E. Alge, N.G. Adams, and D. Smith, "Measurements of the Dissociation Recombination Coefficients of O₂⁺, NO⁺, and NH₄⁺ in the Temperature Range 200 to 600 K," J. Phys. B: Atom Molec. Phys. **16**, 1433 (1983).

e. M. McFarland, D.L. Albritton, F.C. Fehsenfeld, E.E. Ferguson, and A.L. Schmeltekopf, "Energy Dependence and Branching Ratio of the N₂⁺ + O Reaction," J. Geophys. Res. **79**, 2925 (1974).

f. A.O. Langford, V.M. Bierbaum, and S.R. Leone, "Auroral Implications of Recent Measurements on O(¹S) and O(¹D) Formation in the reaction of N⁺ with O₂," Planet. Space Sci. **33**, 1225 (1985); "Branching Ratios for Electronically Excited Oxygen Atoms Formed in the Reactions of N⁺ with O₂ at 300 K," J. Chem. Phys. **84**, 2158 (1986).

Table 4. Gilmore Mixing Rules for Ion and Excited State Production Rates by Electron Bombardment in Dissociated or Ionized Air [18]

Species	Numbers Produced Per Ion Pair (34 eV) ^{a,b}
N_2^+	$1.62 [N_2]/n$
O_2^+	$1.33 [O_2]/n$
N^+	$(0.38 [N_2] + 1.22 [N])/n$
O^+	$(0.57 [O_2] + 1.22 [O])/n$
$N_2(v=1)$	$19 [N_2]/n$
$O_2(a^1\Delta)$	$3.4 [O_2]/n$
$N(^2D)$	$(1.06 [N_2] + 5 [N])/n$
$N(^2P)$	$(0.63 [N_2] + 0.8 [N])/n$
^a Square brackets denote number density in molecules/cm ³ ^b Total nuclei: $n = 2 [N_2] + 2 [O_2] + [N] + [O]$ for dissociated air; $n = 2 [N_2] + 2 [O_2] + [N] + [O] + [N^+] + [O^+]$ for ionized air.	

Table 5. Recommended Kinetic Parameters for N* Collisional Loss Processes^a

$$k(T) = k(300) \left(\frac{T}{300} \right)^n \exp \left[- \frac{E}{R} \left(\frac{1}{T} - \frac{1}{300} \right) \right]$$

Reaction	k (T)	Upper/Lower Uncertainty Limits		Uncertainty Factor		
		T > 300 K	T < 300 K	1000 K	2000 K	5000 K
1b.1 N(² D) + O → N(⁴ S) + O(³ P, ¹ D)	k(300) = 1.1(-12)	1.4/ _{0.8} (-12)	T ≤ 300 K	5.4	7.0	8.3
	n = 0	0	0			
	E/R = 500	750/ ₂₅₀	250/ ₇₅₀			
1b.4 N(² P) + O → NO ⁺ (v ≤ 3) + e ⁻	k(300) = 1.7(-11)	2.0/ _{1.4} (-11)	2.0/ _{1.4} (-11)	8.4	12.5	16.5
	n = 0.5	0	0			
	E/R = 0	750/ ₀	0/ ₇₅₀			
1b.5 N(² D) + O ₂ → all products	k(300) = 4.6(-12)	5.1/ _{4.1} (-12)	5.1/ _{4.1} (-12)	20.5	37.3	53.4
	n = 0.5	0	0			
	E/R = 0	1200/ ₀	0/ ₂₅₀			
1b.6 N(² P) + O ₂ → all products	k(300) = 2.2(-12)	2.5/ _{1.9} (-12)	2.5/ _{1.9} (-12)	60	120	150
	n = 0.5	0	0/ _{0.5}			
	E/R = 0	1400/ ₁₈₀	-140/ ₀			

Table 5. Recommended Kinetic Parameters for N* Collisional Loss Processes^a (Continued)

Reaction	k (T)	Upper/Lower Uncertainty Limits		Uncertainty Factor		
1b.7 N(² D) + N ₂ → N(⁴ S) + N ₂	k(300) = 2.0(-14) n = 0 E/R = 2200(?)	2.5/1.5(-14) 0 3300/0	- - -	3700	2(4)	5(4)
1b.8 N(² P) + N ₂ → N(² D, ⁴ S) + N ₂	k(300) = 1(-16) n = 0 E/R = 3800?	Upper Bound		-	-	-
1b.9 e ⁻ + N(² D) → e ⁻ + N(⁴ S)	k(300) = 3.9(-10) n = 0.81	X/÷ 2		4	4	4
1b.10 e ⁻ + N(² P) → e ⁻ + N(⁴ S)	k(300) = 2.0(-10) n = 0.85	X/÷ 2		4	4	4
1b.11 e ⁻ + N(² P) → e ⁻ + N(² D)	k(300) = 9.5(-9) n = 0.0	X/÷ 2		4	4	4
^a Rate coefficients are in cm ³ molecule ⁻¹ s ⁻¹ .						

Table 6. Recommended Kinetic Parameters for NO Formation Reactions^a

Reaction	k (T)	Uncertainty Range
1c.1 $N(^2D) + O_2 \rightarrow NO + O$	Table 5 x 1.0	Table 5 x (0.5 to 1.0)
1c.2 $\rightarrow N(^4S) + O_2^*$	0.0	Table 5 x (0.0 to 0.5)
1c.3 $N(^2P) + O_2 \rightarrow NO + O$	Table 5 x 1.0	Table 5 x (0.5 to 1.0)
1c.4 $\rightarrow N(^2D) + O_2^*$	0.0	Table 5 x (0.0 to 0.5)
1c.5 $\rightarrow N(^4S) + O_2^*$	0.0	Table 5 x (0.0 to 0.5)
1c.6 $O + N_2^* \rightarrow NO + N$	$\leq 3 \times 10^{-11}$	Upper Bound
1c.7 $N^* + O_2^* \rightarrow NO + O$	$\leq 3 \times 10^{-10}$	Upper Bound
^a Rate coefficients are in $cm^3 \text{ molecule}^{-1} s^{-1}$		

Table 7. Recommended Kinetic Parameters for NO Removal Processes^a

Reaction	K (T)	Uncertainty Range
1d.1 $N + NO \rightarrow N_2 + O$	$(3.1 \pm 1.0) \times 10^{-11} \exp [(0 \pm 100)/T]$ Alternative for $T > 1000$ K: $6.3 \times 10^{-11} \exp [-390/T]$	X/ +2
1d.2 $N(^2D) + NO \rightarrow N_2 + O$	$(6.3 \pm 2.0) \times 10^{-11}$	X/ +2
1d.3 $NO + h\nu \rightarrow N + O$	Cross sections evaluated by Cieslik and Nicolet [59]	-
1d.4 $\rightarrow NO^+ + e^-$	Cross sections tabulated by Watanabe et al. [58]	-
1d.5 $NO + e^- \rightarrow N + O + e^-$	Cross sections tabulated by Ajello et al. [61]	-
1d.6 $\rightarrow NO^+ + 2e^-$	Cross sections tabulated by Kim et al. [60]	-
^a Rate coefficients are in $cm^3 \text{ molecule}^{-1} s^{-1}$.		

Table 8. Recommended Kinetic Parameters^a for High-Temperature NO Formation and Removal Reactions

$$k(T) = AT^n \exp (-E/RT)$$

Reaction	k (T)			Uncertainty Factor
	A	n	E/R	
2.1 N ₂ + M → N + N + M M = N ₂ M = Ar M = O, O ₂	6.1(-3)	-1.6	113200	X/+3, 6000 K ≤ T ≤ 15,000 K Additional X/ + 2 -
	k(N ₂) x 0.4 No recommendation			
2.2 O ₂ + M → O + O + M M = Ar M = N ₂ M = O ₂ M = O	3.0(-6)	-1.0	59380	X/ + 2, 3000 K ≤ T ≤ 8000 K Additional X/ + 2 Additional x 10, + 1 Additional x 10, + 1
	k(Ar) x 1.0 k(Ar) x 1.0 k(Ar) x 3.6			
2.3 N + O ₂ → NO + O	1.1(-14)	1.0	3150	±30%, 300-1500 K, increasing above 1500 K to X/ + 2 at 3000 K and above
	Alternative for T ≥ 2000 K:			
	2.5(-14)	1.0	4394	±30%, 2000-5000 K, incorrect for T < 1500 K
2.4 O + N ₂ → NO + N	3.0(-10)	0.0	38370	±35%, 2000-4000 K
2.5 O + NO → N + O ₂	6.3(-15)	1.0	20820	±30%, 1500-5000 K
2.6 NO + M → N + O + M M = Ar, O ₂ , N ₂ M = O, N, NO	6.6(-4)	-1.5	75500	X/ + 10 Additional X/ + 2
	k = 20 k(Ar)			
^a Rate coefficients are in cm ³ molecule ⁻¹ s ⁻¹ .				

Table 9. Surprisal Predictions of Relative Initial Populations of NO(v) in the Reactions of N(²D, ²P) with O₂ (from Ref. 17)

N _v /ΣN _v		
v	N(² D) + O ₂ ^a	N(² P) + O ₂ ^b
0	1.36(-02)	2.67(-01)
1	2.49(-02)	1.85(-01)
2	4.37(-02)	1.18(-01)
3	7.22(-02)	7.10(-02)
4	1.12(-01)	5.72(-02)
5	1.58(-01)	5.03(-02)
6	1.87(-01)	4.37(-02)
7	1.53(-01)	3.77(-02)
8	1.24(-01)	3.21(-02)
9	5.51(-02)	2.69(-02)
10	2.84(-02)	2.23(-02)
11	1.44(-02)	1.81(-02)
12	7.17(-03)	1.44(-02)
13	3.47(-03)	1.13(-02)
14	1.62(-03)	8.82(-03)
15	7.11(-04)	7.50(-03)
16	2.83(-04)	6.43(-03)
17	9.01(-05)	5.43(-03)
18	1.51(-05)	4.50(-03)
19		3.67(-03)
20		2.88(-03)
21		2.23(-03)
22		1.67(-03)
23		1.13(-03)
24		9.00(-04)
25		3.20(-04)
26		6.00(-05)
^a k(O ³ P)/k(O ¹ D) = 0.285 ^b k(O ³ P)/k(O ¹ D) = k(O ¹ S)/k(O ¹ D) = 1		

Table 10. Energy Transfer Kinetics for $\text{N}_2(\text{A}^3\Sigma_u^+) + \text{NO}$

N ₂ (A) v'	Total Quenching ^a	NO(A) v'			NO(B, v'=0)
		0	1	2	
0	(6.6 ± 1.0)(-11)	1 ^b	0.094 ± 0.006	0.003	0.0032 ± 0.0007
1	~ k(v'=0)	1.11 ± 0.07	0.22 ± 0.03	0.024	0.033 ± 0.007
2	-	0.29 ± 0.07	0.032 ± 0.03		

^aRate coefficients are in cm⁻³ molecule⁻¹ s⁻¹

^b"1" corresponds to (9 ± 3) x 10⁻¹¹ cm³ molecule⁻¹ s⁻¹

Table 11. Initial $\text{NO}(X^2\Pi, v)$ Populations from $\text{N}_2(\text{A}^3\Sigma_u^+) + \text{NO}$

NO(v)	$N_v / \Sigma N_v$					
	$\text{N}_2(\text{A}) v' = 0:1:2$ Relative Populations					
	1:0:0	1:1:0	1:1:1	0:1:0	0:0:1	1:0.5:0.2
0	0.224	0.235	0.254	0.243	0.326	0.238
1	0.262	0.251	0.236	0.242	0.178	0.249
2	0.207	0.195	0.176	0.186	0.106	0.192
3	0.137	0.132	0.124	0.127	0.096	0.131
4	0.081	0.081	0.083	0.081	0.088	0.092
5	0.044	0.047	0.052	0.049	0.070	0.048
6	0.023	0.027	0.032	0.029	0.051	0.027
7	0.011	0.015	0.019	0.018	0.035	0.015
8	0.006	0.009	0.012	0.012	0.024	0.009
9	0.003	0.005	0.008	0.008	0.016	0.005
10	0.001	0.003	0.005	0.005	0.011	0.003

Table 12. Estimated Rate Coefficients for Excitation of NO(v) by
O + NO(v=0) Collisions^a

$$k(v) = 3.5 \times 10^{-11} \exp \left[- \left(\frac{E_v}{0.695} - 190 \right) / T \right]$$

v	E _v , cm ⁻¹	E _{net} /R
1	1876.1	2509
2	3724.2	5069
3	5544.3	7787
4	7336.4	10366
5	9100.5	12904
6	10836.5	15402
7	12544.4	17860
8	14224.5	20277
9	15876.2	22654
10	17499.9	24990
^a Rate coefficients are in cm ³ molecule ⁻¹ s ⁻¹ .		

Table 13. Suggested Kinetic Parameters for NO(v,J) Excitation Processes^a

Reaction	k (T)	NO(v) Populations	Comments
3.1 $N(^4S) + O_2 \rightarrow NO(v) + O$	Table 8	Winkler et al. [69]	Populations good to factor of 2 for 300 K; need to re-evaluate data base.
3.2 $N(^2D) + O_2 \rightarrow NO(v) + O(^3P, ^1D)$	Tables 5,6	Table 9	Populations applicable to low T only; need direct measurements for T \geq 300 K.
3.3 $N(^2P) + O_2 \rightarrow NO(v,J) + O(^3P, ^1D, ^1S)$	Tables 5,6	Table 9	Populations applicable to low T only; need direct measurements for T \geq 300 K.
3.4 $N_2^* + O \rightarrow NO(v) + N$	Table 6	?	No basis for recommendations; need direct measurements.
3.5 $N + O \rightarrow NO(v) + h\nu$	$10^{-17} (300/T)^{1/2}$	-	Populations via cascade need to be evaluated; need high T measurements; uncertainty X/ + 10.
3.6 $N_2^* + NO \rightarrow NO(v,J) + N_2$	Table 11 for $N_2(A)$		Uncharacterized for most forms of N_2^*
3.7 $N^* + NO \rightarrow NO(v,J) + N$	Table 7, upper bound for $N(^2D)$?	Unknown
3.8 $O_2^* + NO \rightarrow NO(v,J) + O_2$	$O_2(a^1\Delta_g): 4.5(-17)$ $O_2(b^1\Sigma_g^+): 3(-13)$	$v=4$ only ?	Quenching data at 300 K only.
3.9 $O^* + NO \rightarrow NO(v,J) + O$	$O(^1D): 1.5(-10)$ $O(^1S): 8(-10)$? ?	Quenching data at 300 K only; no observations of NO(v) excitation.
3.10 $O + NO \rightarrow NO(v) + O$	Table 12	Table 12	Estimated upper bounds from simplified scaling of limited data for reverse reaction; need direct measurements at high T.

Table 13. Suggested Kinetic Parameters for NO(v,J) Excitation Processes^a (Continued)

Reaction	k (T)	NO(v) Populations	Comments
3.11 O(fast) + NO → NO(v,J) + O	3(-11)	Same for all v; J statistical	Guess. Need direct measurements.
3.12 NO + hν (IR) → NO(v)	See Table 15 for IR absorption coefficients	v = 1 only.	-
3.13 NO + hν (UV) → NO(v)	-	-	NO(A→X) transition probabilities in Piper and Cowles [81]
^a Rate coefficients are in cm ³ molecule ⁻¹ s ⁻¹ .			

Table 14. Measured Rate Coefficients for Deactivation of NO(v) by N₂ and O₂ at 300 K^a

NO(v=1) + N ₂ → NO(v=0) + N ₂					
					<u>k(v=1)</u>
Stephenson (1973) ^b					(1.4 ± 0.15) × 10 ⁻¹⁶
Murphy et al. (1975) ^c					(1.7 ± 0.7) × 10 ⁻¹⁶
Kosanetsky et al. (1980) ^d					(1.3 ± 0.1) × 10 ⁻¹⁶
Doyenette and Margottin-Maclou (1986) ^e					(1.4 ± 0.1) × 10 ⁻¹⁶
NO(v) + O ₂ → NO(v-1) + O ₂					
v	Murphy et al. (1975) ^c	Stephenson and Freund (1976) ^b	Kosanetzky et al. (1980) ^d	Fernando and Smith (1981) ^f	Green et al. (1982) ^g
1	(2.4 ± 1.5)(-14)	(2.8 ± 0.25)(-14)	(2.6 ± 0.15)(-14)	(2.9 ± 0.5)(-14)	(2.2 to 3.1)(-14)
2					(5.9 to 7.4)(-14)
3					(1.2 to 1.5)(-13)
4					(2.5 to 2.9)(-13)
5					(3.7 to 6.5)(-13)
6					(5.1 to 7.7)(-13)
7					(4.4 to 15)(-13)
<p>^aRate coefficients are in cm³ molecule⁻¹ s⁻¹.</p> <p>^bJ.C. Stephenson, "Vibrational Energy Transfer in NO," J. Chem. Phys. 59, 1523 (1973).</p> <p>^cR.E. Murphy, E.T.P. Lee, and A.M. Hart, "Quenching of Vibrationally Excited Nitric Oxide by Molecular Oxygen and Nitrogen," J. Chem. Phys. 63, 2919 (1975).</p> <p>^dJ. Kosanetsky, U. List, W. Urban, H. Vormann, and E.H. Fink, "Vibrational Relaxation of NO(X²Π, v=1) Studied by an IR-UV-Double-Resonance Technique," Chem. Phys. 50, 361 (1980).</p> <p>^eRef. [97].</p> <p>^fR.P. Fernando and I.W.M. Smith, "Relaxation of NO(v=1) by Radical Species," J. Chem. Soc. Faraday Trans. II, 77, 459 (1981).</p> <p>^gRef. [92].</p>					

Table 15. Absorption Coefficients and Transition Probabilities for the $\Delta v=1$ and $\Delta v=2$ Transitions of NO

Investigator	Citation	$S(0-1)$ $\text{cm}^{-2} \text{Ama}^{-1}$	$S(0-2)$ $\text{cm}^{-2} \text{Ama}^{-1}$	$A(1-0)$ s^{-1}	$A(2-0)$ s^{-1}
Havens (1938)	Ph.D. Dissertation, U. of Wisconsin	121		12.0	
Dinsmore and Crawford (1949)	U. of Minnesota Report No. NR-019-104	145 \pm 29		14.3 \pm 2.9	
Dinsmore (1949)	Ph.D. Thesis, U. of Minnesota		2.57 \pm 0.51		1.0 \pm 0.2
Penner and Weber (1953)	J. Chem. Phys. <u>21</u> , 649	70 \pm 7	2.3 \pm 0.6	6.9 \pm 0.7	0.9 \pm 0.2
Vincent-Geisse (1954)	Compt. Rend. <u>232</u> , 251	82		8.1	
Breene (1958)	J. Chem. Phys. <u>28</u> , 11; <u>29</u> , 512	70	2.7	6.9	1.1
Schurin and Clough (1963)	J. Chem. Phys. <u>38</u> , 1835	111 \pm 7		11.0 \pm 0.7	
Breeze and Ferriso (1964)	J. Chem. Phys. <u>41</u> , 3420	76 \pm 7	2.8 \pm 0.5	7.5 \pm 0.7	1.1 \pm 0.2
James (1964)	J. Chem. Phys. <u>40</u> , 762	138 \pm 6		13.6 \pm 0.6	
Fukuda (1965)	J. Chem. Phys. <u>42</u> , 521	74 \pm 4		7.3 \pm 0.4	
Ford and Shaw (1965)	Appl. Opt. <u>4</u> , 1113	115 \pm 9		11.4 \pm 0.9	
Alamichel 91966)	J. Phys. (Paris) <u>27</u> , 345	132 \pm 3		13.0 \pm 0.3	
Schurin and Ellis (1966)	J. Chem. Phys. <u>45</u> , 2528		2.11 \pm 0.1		0.82 \pm 0.04
Varanasi and Penner (1967)	J. Quant. Spectrosc. Radiat. Transfer <u>7</u> , 279	128 \pm 10		12.6 \pm 1.0	
Oppenheim et al. (1967)	Appl. Opt. <u>6</u> , 1305	125 \pm 8		12.4 \pm 0.8	
Feinberg and Camac (1967)	J. Quant. Spectrosc. Radiat. Transfer <u>7</u> , 581	124 \pm 22		12.3 \pm 2.2	
Green and Tien (1970)	J. Quant. Spectrosc. Radiat. Transfer <u>10</u> , 805	125		12.4	
Michels (1971)	Ref. [105]	134 \pm 2	2.0 \pm 0.6	13.2 \pm 0.2	0.78 \pm 0.23
King and Crawford (1972)	J. Quant. Spectrosc. Radiat. Transfer <u>12</u> , 443	135 \pm 5		13.3 \pm 0.5	

Table 15. Absorption Coefficients and Transition Probabilities for the $\Delta v = 1$ and $\Delta v = 2$ Transitions of NO (Continued)

Investigator	Citation	$S(0-1)$ $\text{cm}^{-2} \text{Ama}^{-1}$	$S(0-2)$ $\text{cm}^{-2} \text{Ama}^{-1}$	$A(1-0)$ s^{-1}	$A(2-0)$ s^{-1}
Chandraiah and Cho (1973)	Ref. [103]	121 ± 6	2.17 ± 0.11	12.0 ± 0.6	0.54 ± 0.04
Garside et al. (1976)	Appl. Opt. <u>16</u> , 398	124 ± 9		12.3 ± 0.9	
Billingsley (1976)	Ref. [100]	113.3	1.31	10.78	0.46
Kunimori et al. (1977)	J. Quant. Spectrosc. Radiat. Transfer <u>19</u> , 127	122 ± 6		12.1 ± 0.6	
Mandin et al. (1980)	Ref. [101,102]	134.4		13.3	
Holland et al. (1983)	Ref. [90]	137.3 ± 4.6		13.6 ± 0.5	

Table 16. Predicted Einstein Coefficients for NO($\Delta v=1,2$) Transitions^a

$\Delta v=1$				$\Delta v=2$		
v'	Billingsley ^b	Chandraiah ^c	Rothman ^d	Billingsley ^b	Chandraiah ^c	Rothman ^d
1	10.78	11.8	13.25	-	-	-
2	20.43	22.3	25.33	0.460	0.842	0.84
3	29.11	31.4	36.22	1.513	2.416	1.29
4	36.49	39.4	46.35	3.100	4.607	3.85
5	42.93	46.2	55.19	4.900	7.330	6.24
6	48.54	52.0		7.285	10.479	9.31
7	53.54			9.633		
8	57.48			12.500		
9	60.55			15.678		
10	62.77			19.143		
11	64.15			22.936		
12	64.61			27.150		
13	64.23			31.879		
14	63.17			36.932		
15	61.66			41.894		
16	59.80			46.409		
17	57.59			50.496		
18	54.95			54.343		
19	51.90			58.102		
20	48.46			61.812		

^aEinstein coefficients are in s⁻¹

^bRef. [100]

^cRef. [103], reported in Ref. [100]

^dRef. [102]

Table 17. Suggested Einstein Coefficients for NO($\Delta v=1,2$) Transitions,
 $T < 1000 \text{ K}^a$

v'	$A(v, v-1)$ s^{-1}	$A(v, v-2)$ s^{-1}
1	13.4	-
2	25.4	0.94
3	36.2	2.7
4	45.4	4.6
5	53.4	7.0
6	60.3	9.7
7	66.6	13
8	71.5	17
9	75.3	22
10	78.0	25
11	79.7	28
12	80.3	28
13	79.8	27
≥ 14	No recommendation	No recommendation
^a uncertainty = $\pm 10\%$ for $v' \leq 3$, increasing to $\pm 40\%$ for $v'=13$.		

Table 18. Recommended Kinetic Parameters for Deactivation of NO(v)^a

Reaction	K (T)	NO(v) Dependence	Comments
4.1 NO(v) + O → NO(v-n) + O	$\sum_n k_n(v) +$ $(6.5 \pm 0.7) \times 10^{-11}$ $\cdot \exp \left[190_{-130}^{-210} \left(\frac{1}{T} - \frac{1}{300} \right) \right]$	$n = v;$ $k(v) \propto v^0$	No data on variation of k with v; no data on distribution of n values for each v.
4.2 NO(v) + N ₂ → NO(v-1) + N ₂	$1 \times 10^{-12} \exp [-75/T^{1/3}]$	$k(v) \propto v^2;$ $\Delta v = 1$	No data T > 600 K; no data on v-dependence; uncertainty X/ ÷ 3 for T > 2000 K.
4.3 NO(v) + O ₂ → NO(v-1) + O ₂	$1.7 \times 10^{-10} \exp [-75/T^{1/3}]$	$k(v) \propto v^{(1.6 \pm 0.2)}$ $\Delta v = 1$	Estimated upper bound. k(300 K) = $(2.7 \pm 0.2) \times 10^{-14} (1.6 \pm 0.2)$. No data on T dependence.
4.4 NO(v, high J) + M → NO(v', J') + M	No recommendation		No data on v-deactivation; limited data on high-J thermalization suggests k(Δv=0) ~ 10 ⁻¹¹ for He and Ar.
4.5 NO(v', J') → NO(v'-1, J'') + hν _F 4.6 NO(v', J') → NO(v'-2, J'') + hν _{QV}	Table 17		Recommendations only for v ≤ 13 and T < 1000 K. Need more data for extension to high v, high J.
^a Rate coefficients are in cm ³ molecule ⁻¹ s ⁻¹ .			

Table 19. Key Unknown Factors in High-Altitude NO(v) Chemistry

Precursor Formation	<ul style="list-style-type: none"> - $N(^2D, ^2P)$ production efficiencies, ratios - Missing sources of $N(^2P)$? - Laboratory/auroral coverification - $N(^2D, ^2P)$ transition probabilities - Effects of v, T on $e^- + N_2, N_2^+, NO^+$
$N(^2D, ^2P)$ Chemistry	<ul style="list-style-type: none"> - T dependence and detailed product channels for $N(^2D, ^2P) + O, O_2$ - Superelastic quenching versus T_e - Is $O + N^+$ source of NO? - Viability of N_2^+ for NO source
High Temperature Chemistry	<ul style="list-style-type: none"> - High T dissociation of O_2, N_2, NO, especially by O - Fast atom (O,N) chemistry - High T chemical loss rates for NO, compared to transport losses
NO(v) Excitation	<ul style="list-style-type: none"> - $N^+ + O_2$: production efficiency of NO(v,J) states versus T - changes in dynamic mechanisms? - Excitation by electronic energy transfer: N^+, N_2^+, O^+, O_2^+ - Effects of O, O(fast) - $N + O$ as high-T source
NO(v) Deactivation	<ul style="list-style-type: none"> - $O + NO(v)$ kinetics - Effects of high-J on collisional deactivation kinetics - Transition probabilities: scale to high v, high J, high T

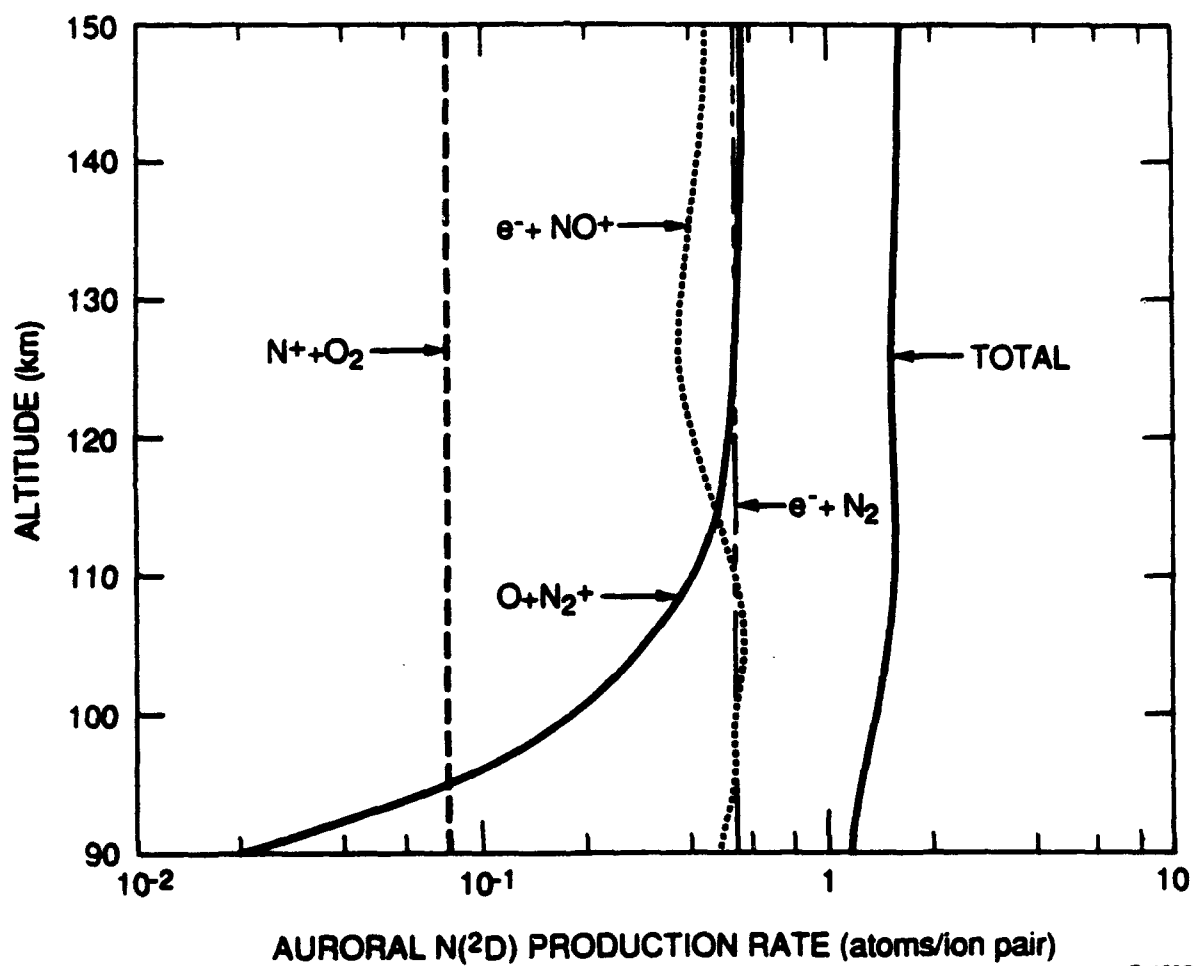
LIST OF FIGURES

- Figure 1 Auroral $N(^2D)$ production rates as modeled by Caledonia and Kennealy [5] for an ICB II aurora
- Figure 2 Auroral $N(^2P)$ production efficiencies based on data from Zipf et al. [8] and multiples of the U.S. Standard Atmosphere [11] atomic oxygen profile
- Figure 3 Recommended rate coefficients and uncertainties for quenching of $N(^2D, ^2P)$ by O
- Figure 4 Recent measurements of the rate coefficient for $N(^2D) + O_2$ quenching at 300 K. References: (a) [27], (b) [28], (c) [40], (d) [41], (e) [44], (f) [31].
- Figure 5 Rate coefficients and uncertainties for reaction of $N(^2D)$ with O_2
- Figure 6 Measurements of the rate coefficient for $N(^2P) + O_2$ quenching at 300 K. References: (a) [34], (b) [40], (c) [28], (d) [46], (e) [35].
- Figure 7 Rate coefficients and uncertainties for reaction of $N(^2P)$ with O_2
- Figure 8 Recommended rate coefficients for quenching of $N(^2D)$. Rate coefficients for quenching by e^- are plotted versus electron temperature.
- Figure 9 Recommended rate coefficients for quenching of $N(^2P)$. Rate coefficients for quenching by e^- are plotted versus electron temperature.
- Figure 10 Evaluated rate coefficients for $O_2 + M$ dissociation, extracted from Baulch et al. [62]
- Figure 11 Evaluated rate coefficients for $N_2 + M$ dissociation, extracted from Baulch et al. [62]
- Figure 12 Recommended rate coefficients and uncertainties for $O_2 + M$ and $N_2 + M$ dissociation
- Figure 13 Rate coefficients for the reaction of $N(^4S)$ with O_2 , extracted from Baulch et al. [62]
- Figure 14 Comparison of recommended rate coefficients for reaction of O_2 with $N(^4S)$, $N(^2D)$, and $N(^2P)$
- Figure 15 Rate coefficient data for the reaction of O with N_2 , extracted from Hanson and Salimian [63]

- Figure 16 Recommended rate coefficients and uncertainties for the $N + O_2$ and $O + N_2$ reactions. HS = rate coefficients for $N + O_2$ determined by detailed balance from the values of $O + NO$ recommended by Hanson and Salimian [63]
- Figure 17 Rate coefficient data for the reaction of O with NO , extracted from Hanson and Salimian [63]
- Figure 18 Rate coefficient data for $NO + M$ dissociation, extracted from Hanson and Salimian [63]
- Figure 19 Evaluated rate coefficients for $NO + M$ dissociation, extracted from Baulch et al. [62]
- Figure 20 Recommended rate coefficients and uncertainties for NO removal reactions: (a) above 300 K; (b) above 2000 K. HS = rate coefficients for $N + NO$ determined by detailed balance from the values for $O + N_2$ recommended by Hanson and Salimian [63].
- Figure 21 Potential energy curves for the low-lying states of NO , extracted from Kenner and Ogryzlo [75].
- Figure 22 Recommended rate coefficients and uncertainties for two-body recombination of N and O
- Figure 23 Relative $NO(v)$ populations produced in the energy transfer between $N_2(A^3\Sigma_u^+)$ and NO , from the data of Piper and co-workers [81,83]
- Figure 24 Predicted excitation rates for $NO(v=1)$ in the undisturbed upper atmosphere
- Figure 25 Estimated rate coefficients for collisional excitation of $NO(v)$ by O , compared to the rate coefficient for chemical reaction. Uncertainties are shown only for $v=1$; values for higher v are estimated upper bounds. Values for $v=9,10$ are nearly coincident with those for chemical reaction. The data points are from experimental measurements for $v=1$ deactivation as described in the text.
- Figure 26 Recommended rate coefficients and uncertainties for deactivation of $NO(v)$ by O . The rate coefficients are summed over all values of n and are assumed to be independent of v . The data points are from the experimental measurements cited in the text.
- Figure 27 Comparison of temperature dependences for deactivation of $NO(v=1)$ by O_2 , N_2 , NO , and Ar . References: N_2 , O_2 ; see Table 13; Doyennette: Ref.

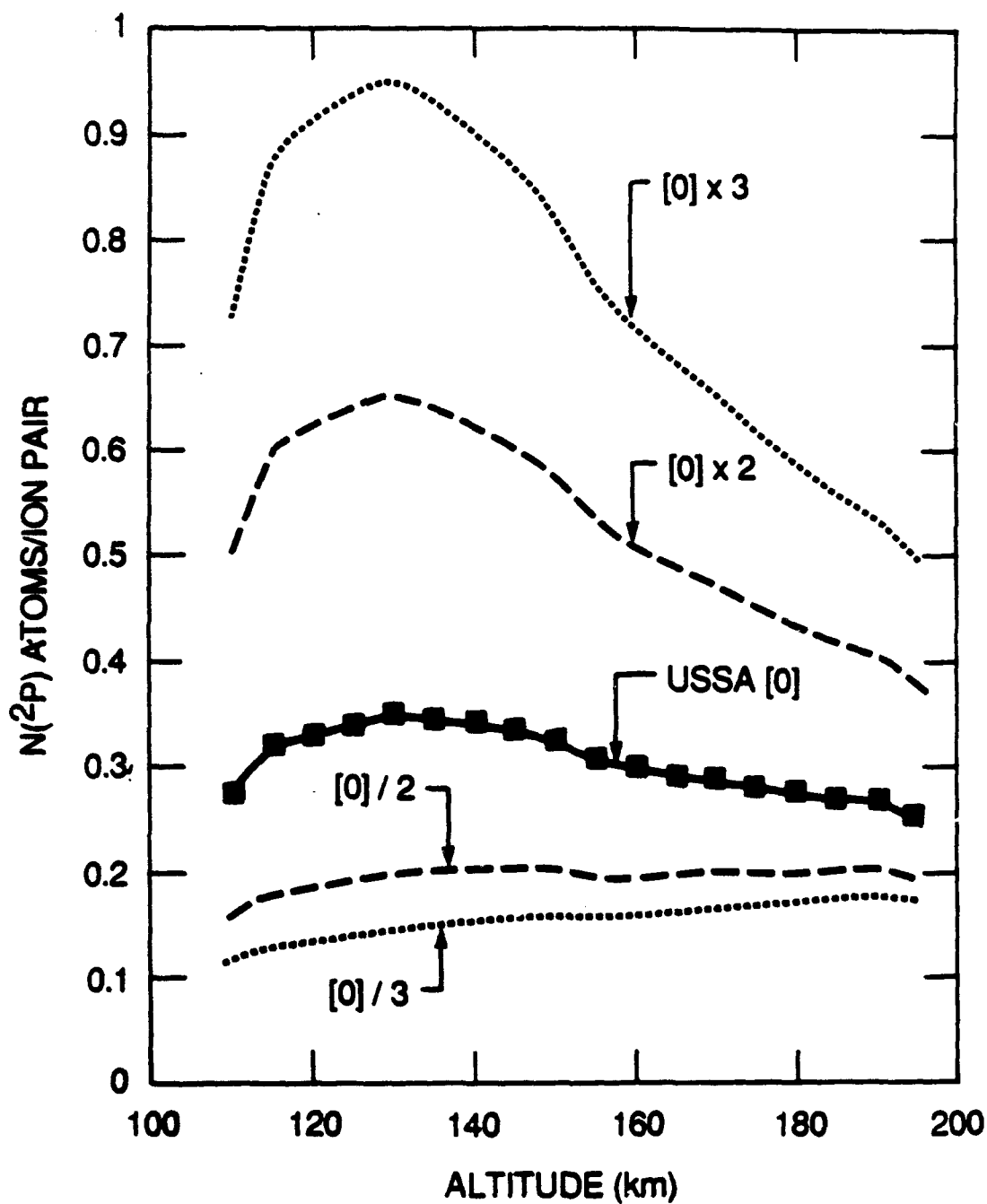
[97]; Taylor, Ref. [96]; Wray: J. Chem. Phys., 36, 4707 (1973); Troe: Ref. [94].

- Figure 28 Theoretical dipole moment function of Billingsley [104] (dashed curve) compared to potential curve for NO($X^2\Pi$)
- Figure 29 Comparison of observed and predicted overtone/fundamental branching ratios. References: COCHISE, Ref. 107, LABCEDE, Ref. 106; Billingsley, Ref. 100; Chandraiah, Ref. 103; Rothman, Ref. 102. Error bars on the COCHISE data represent two standard deviations about the weighted mean
- Figure 30 NO Einstein coefficients for the fundamental and first overtone sequences. The COCHISE values were estimated as described in the text. References are as cited in Figure 29.



B-4606

Figure 1 Auroral $N(^2D)$ production rates as modeled by Caledonia and Kennealy [5] for an ICB II aurora



B-4606

Figure 2 Auroral $N(2P)$ production efficiencies based on data from Zipf et al. [8] and multiples of the U.S. Standard Atmosphere [11] atomic oxygen profile

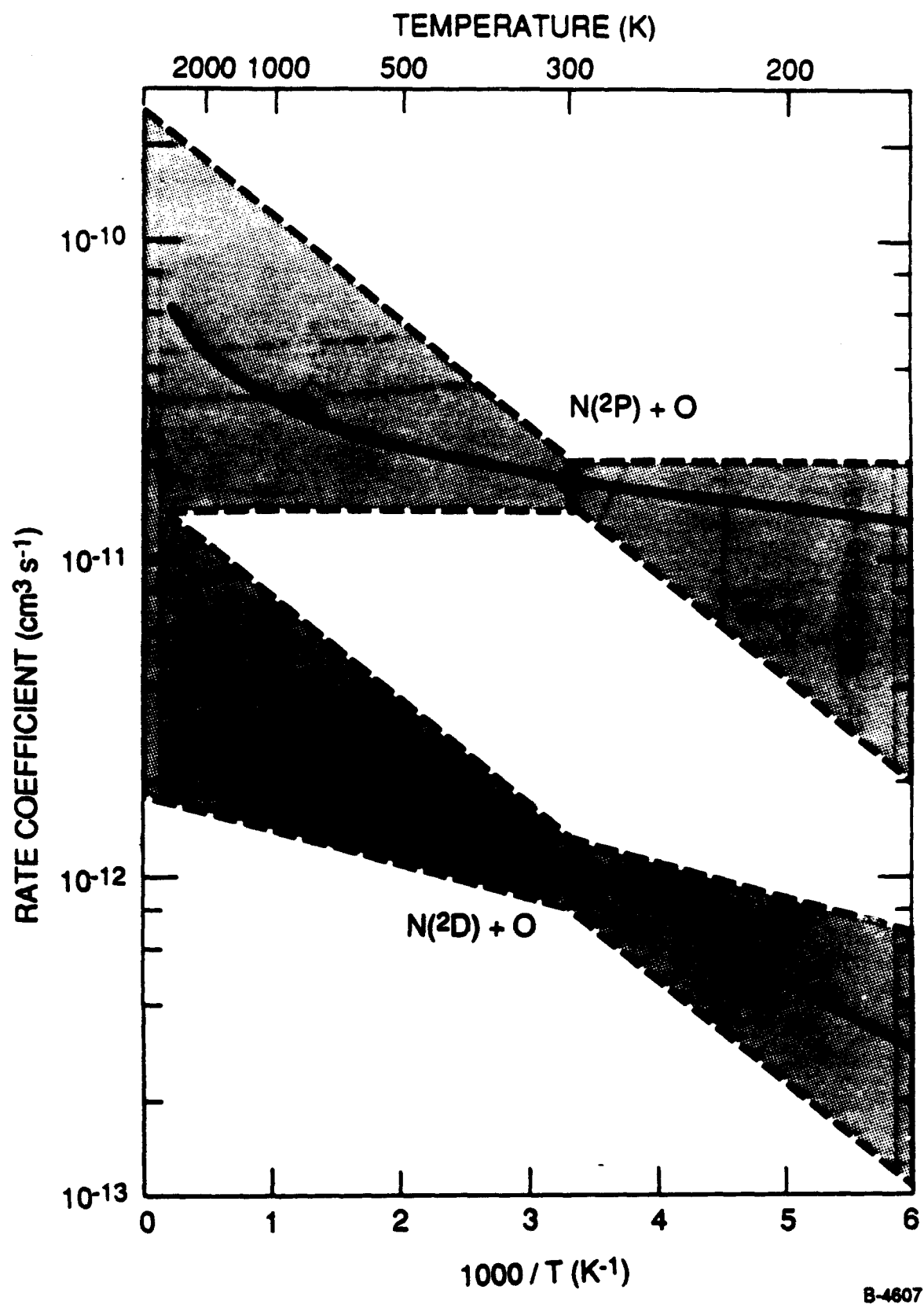
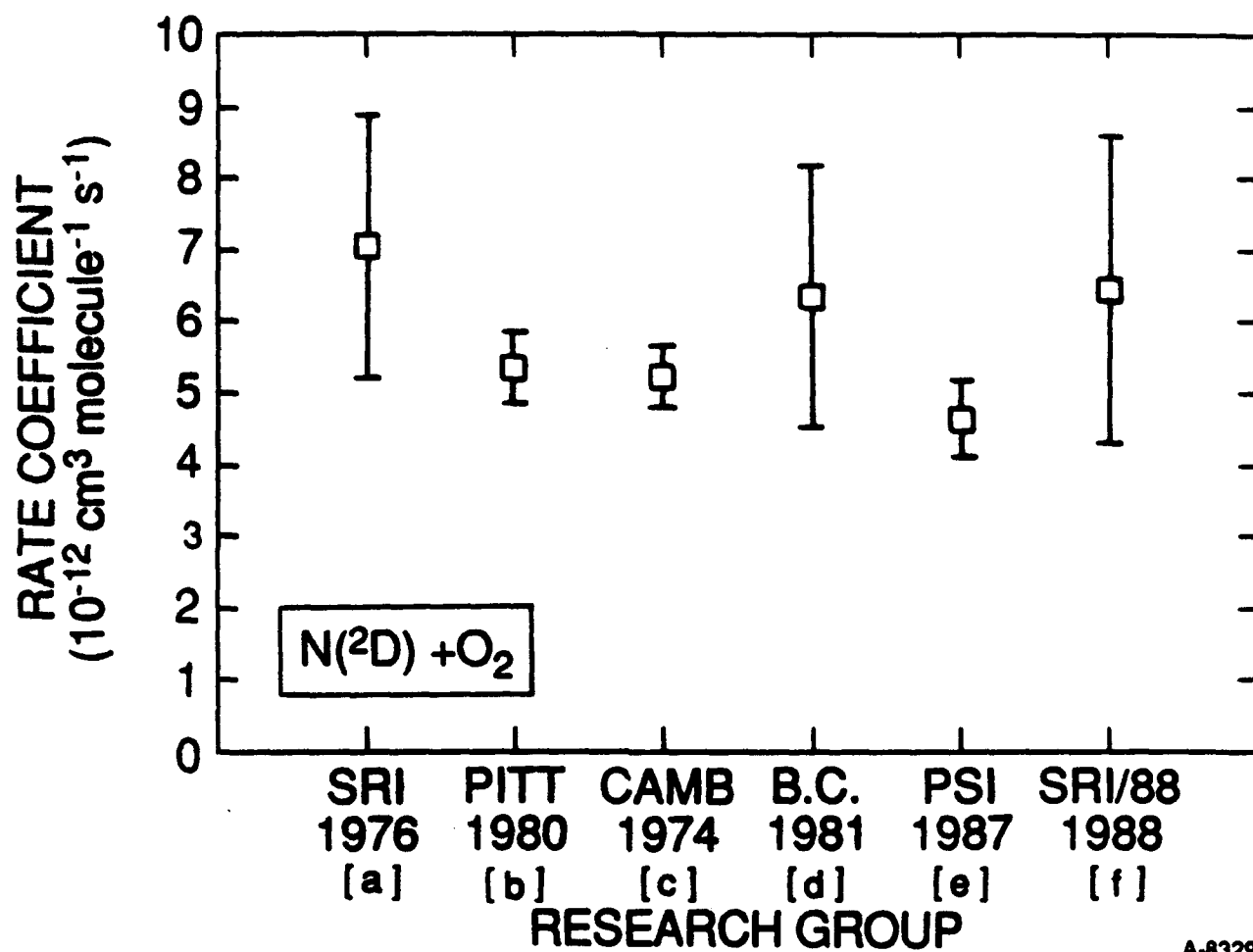


Figure 3 Recommended rate coefficients and uncertainties for quenching of N(²D, ²P) by O



A-8329

Figure 4 Recent measurements of the rate coefficient for $N(^2D) + O_2$ quenching at 300 K. References: (a) [27], (b) [28], (c) [40], (d) [41], (e) [44], (f) [31].

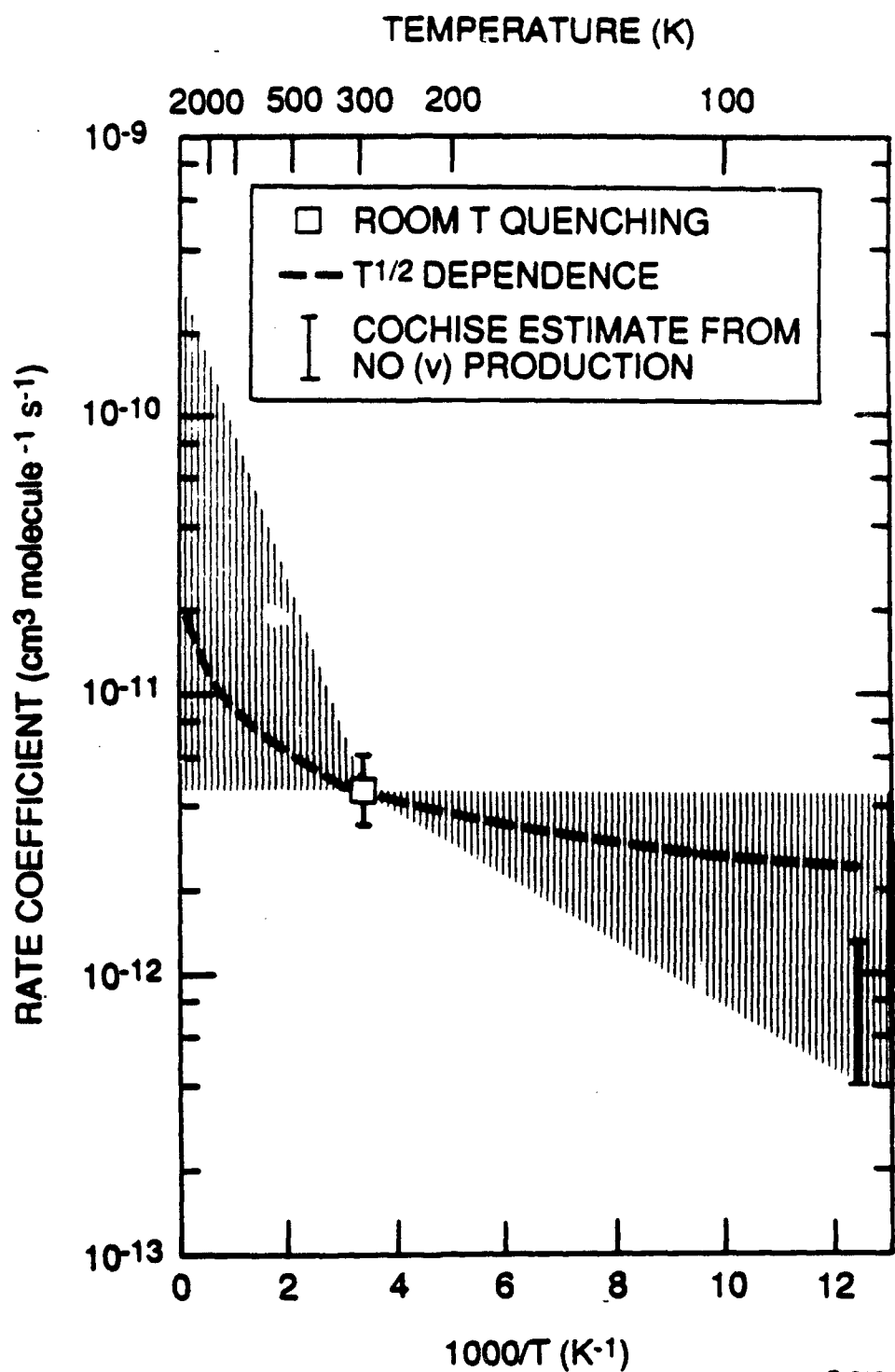
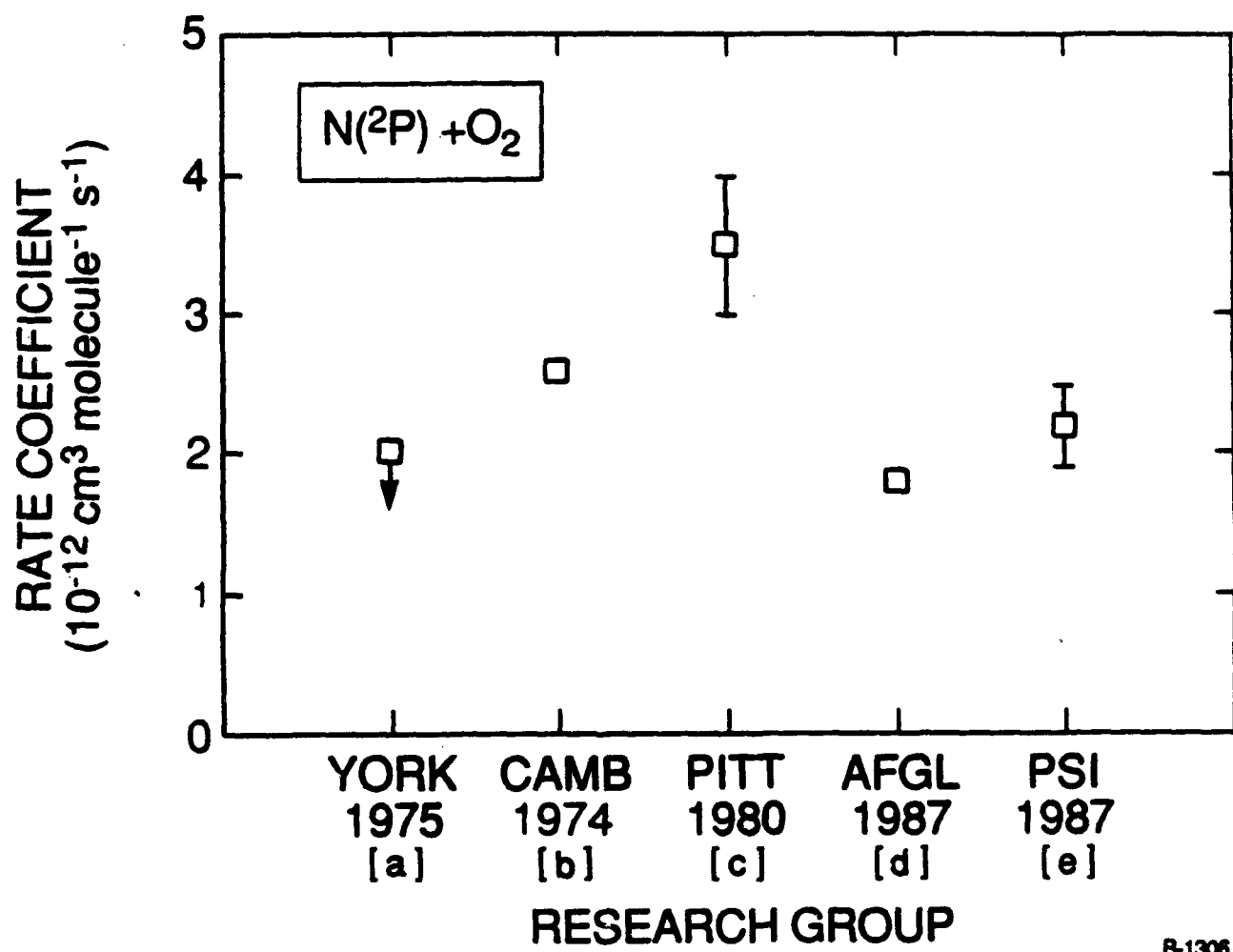


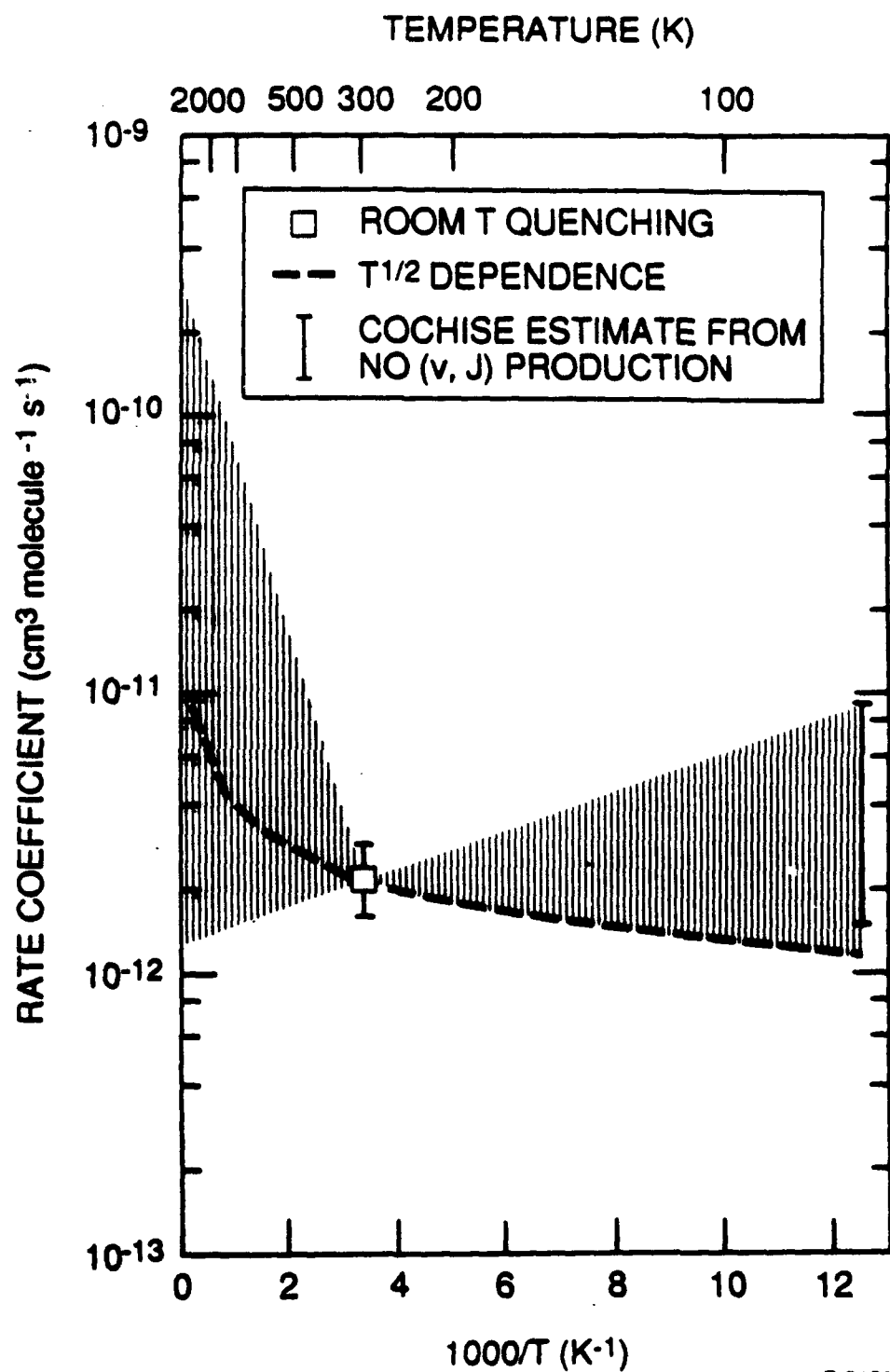
Figure 5 Rate coefficients and uncertainties for reaction of N(²D) with O₂



B-1306

Figure 6

Measurements of the rate coefficient for $N(^2P) + O_2$ quenching at 300 K.
References: (a) [34], (b) [40], (c) [28], (d) [46], (e) [35].



B-2130

Figure 7 Rate coefficients and uncertainties for reaction of N(²P) with O₂

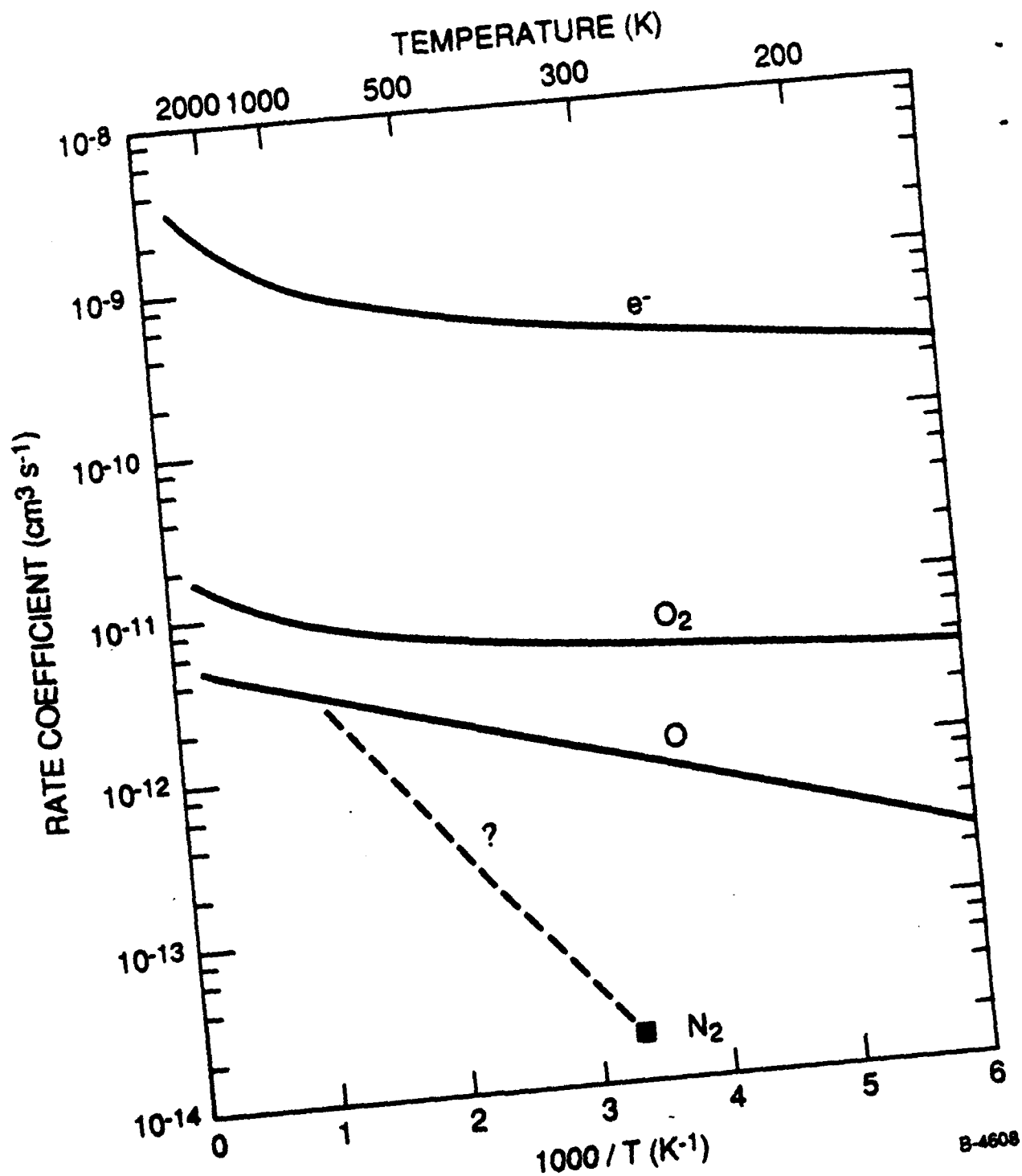


Figure 8

Recommended rate coefficients for quenching of $\text{N}(^2\text{D})$. Rate coefficients for quenching by e^- are plotted versus electron temperature.

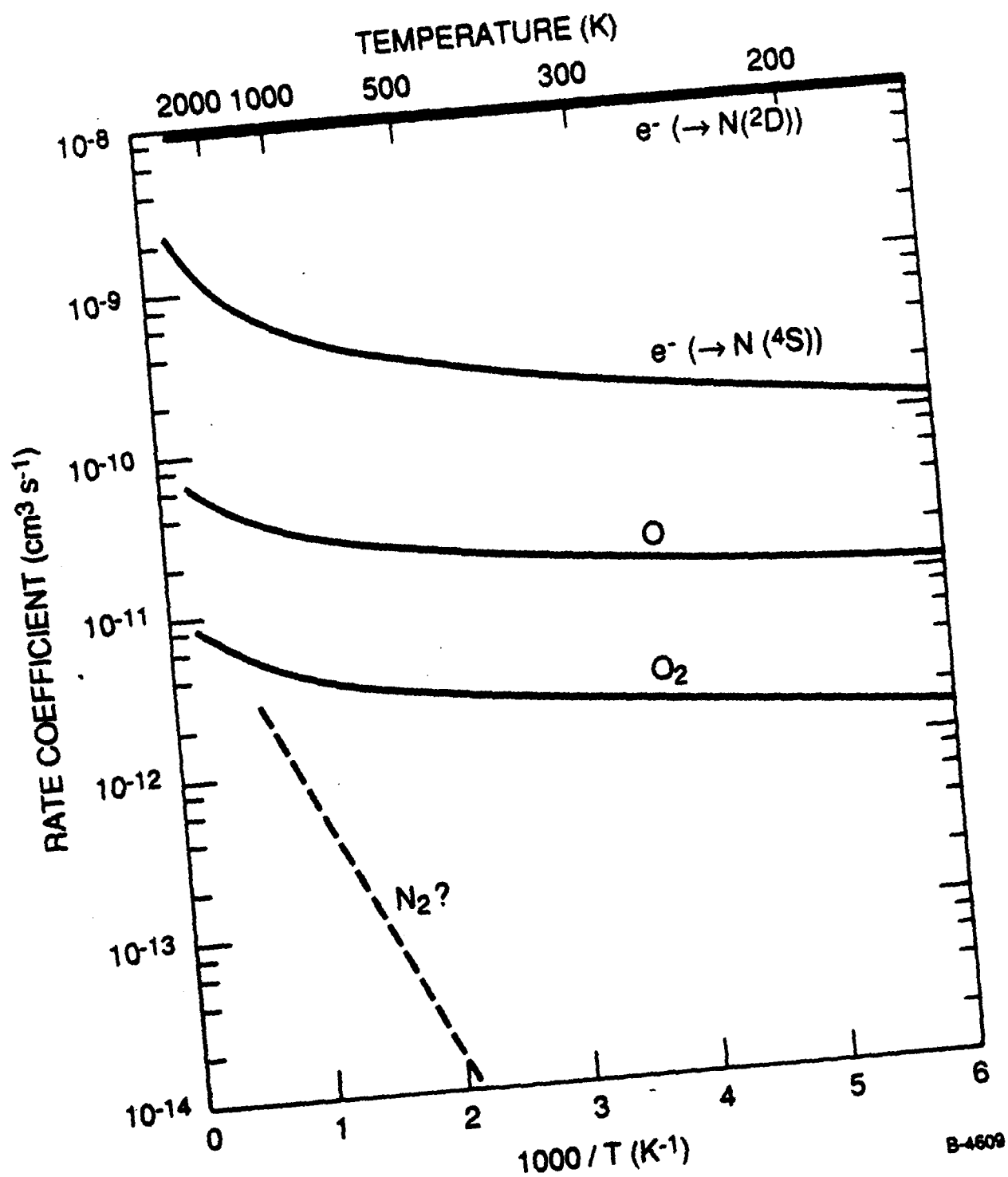


Figure 9 Recommended rate coefficients for quenching of $N(2P)$. Rate coefficients for quenching by e^- are plotted versus electron temperature.

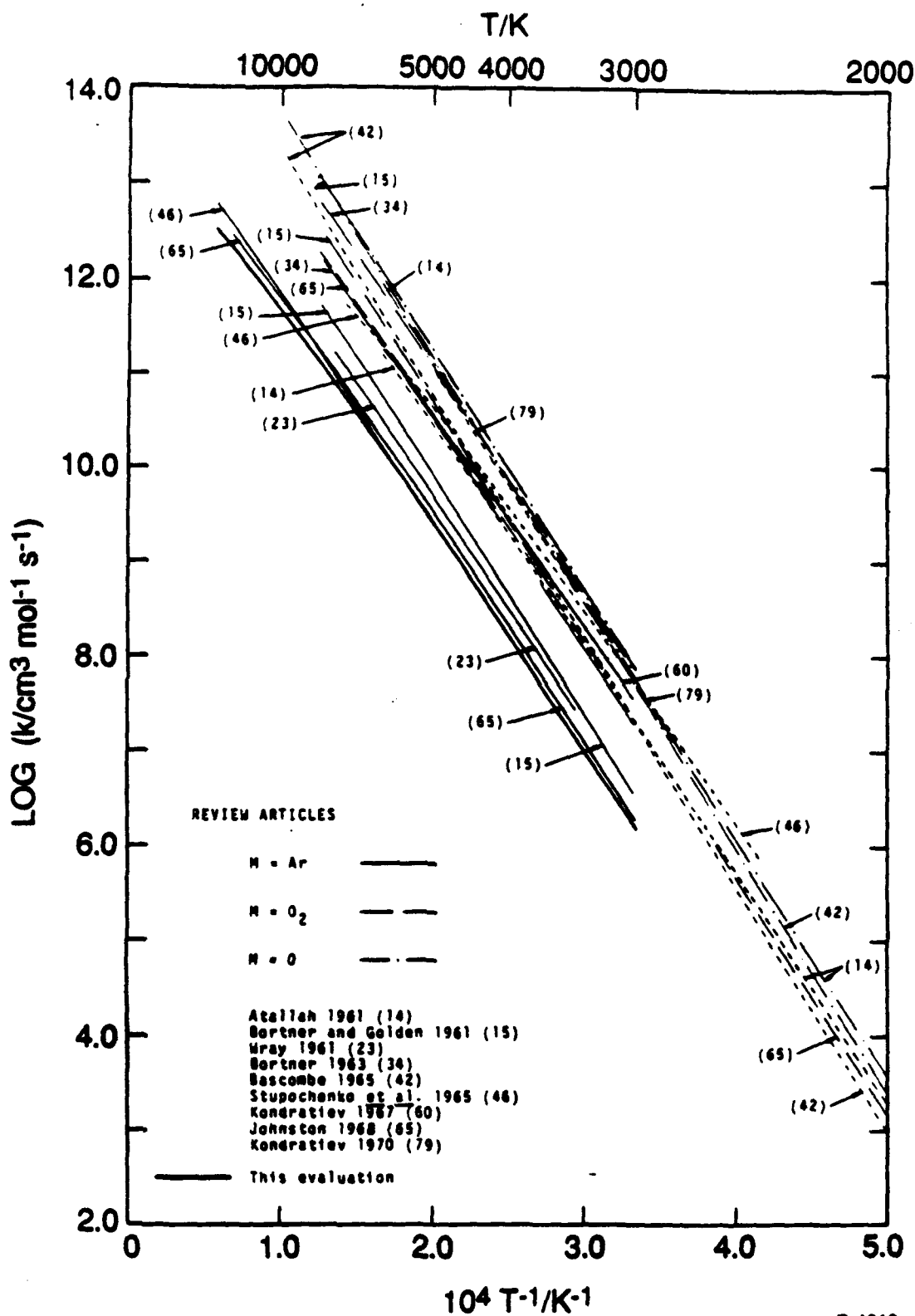
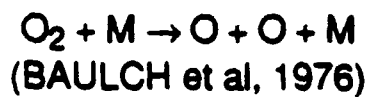


Figure 10 Evaluated rate coefficients for O₂ + M dissociation, extracted from Baulch et al. [62]

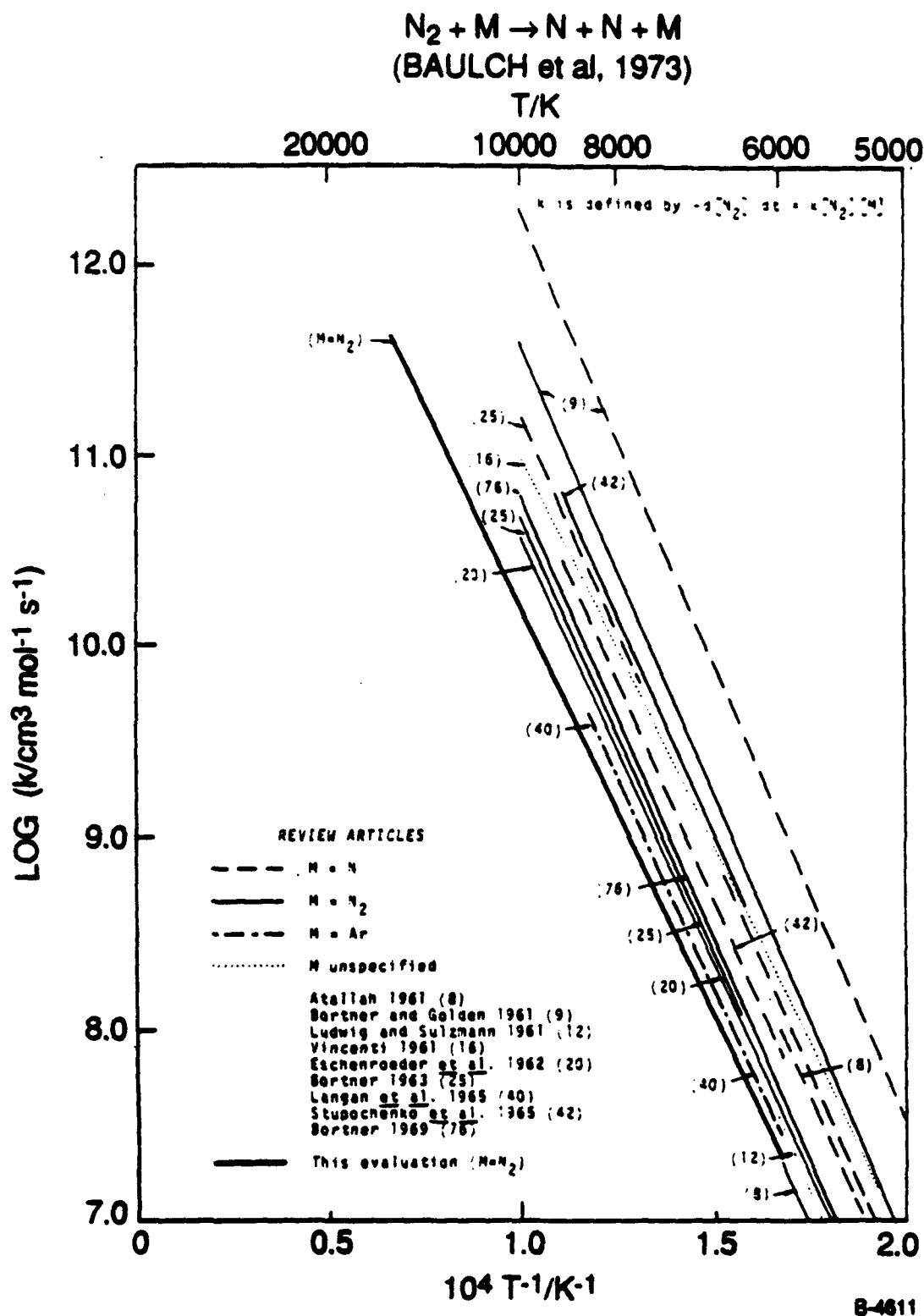


Figure 11 Evaluated rate coefficients for $\text{N}_2 + \text{M}$ dissociation, extracted from Baulch et al. [62]

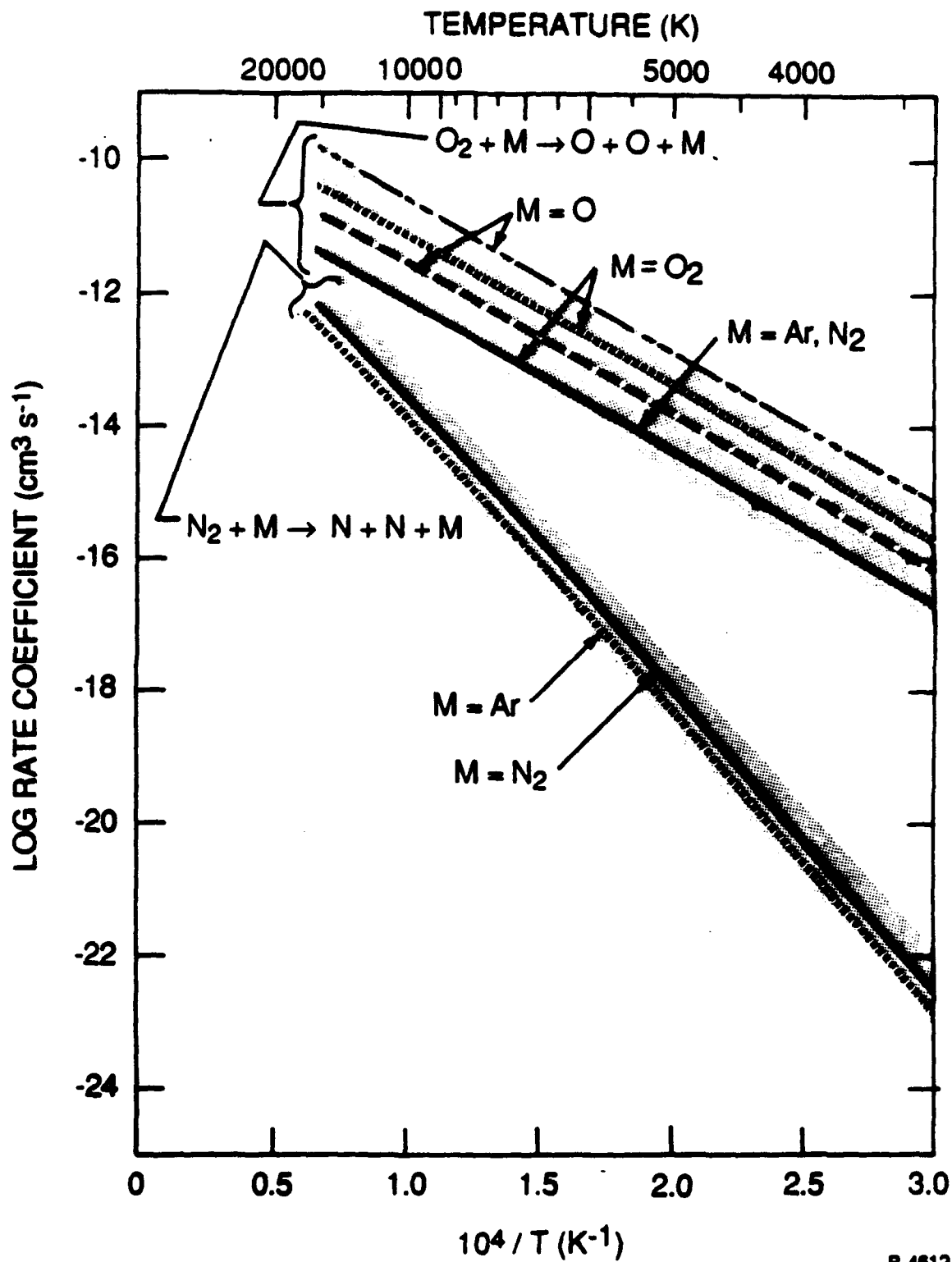


Figure 12 Recommended rate coefficients and uncertainties for $\text{O}_2 + \text{M}$ and $\text{N}_2 + \text{M}$ dissociation

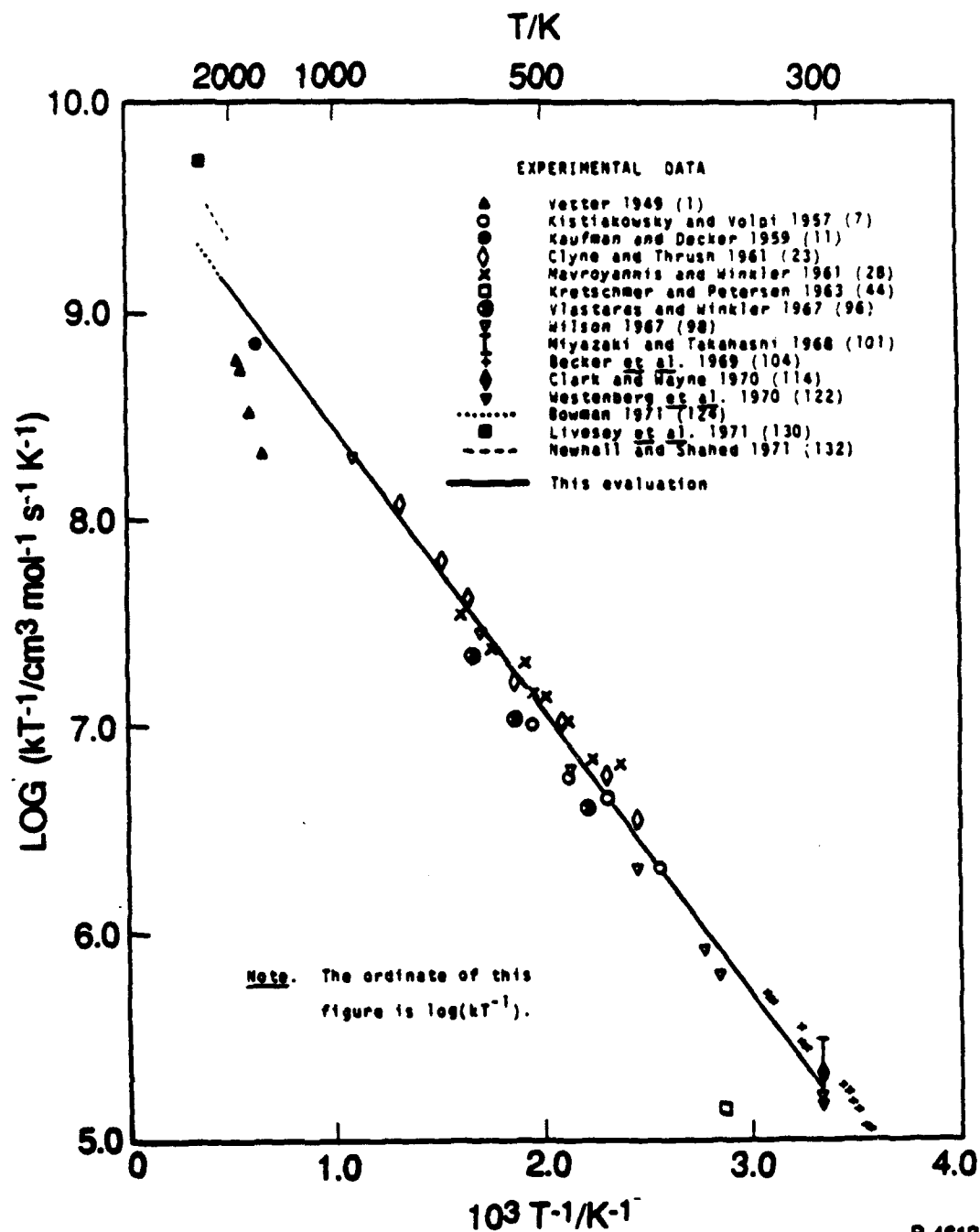
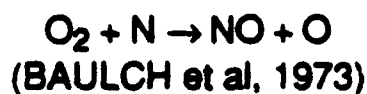


Figure 13 Rate coefficients for the reaction of $\text{N}(^4\text{S})$ with O_2 , extracted from Baulch et al. [62]

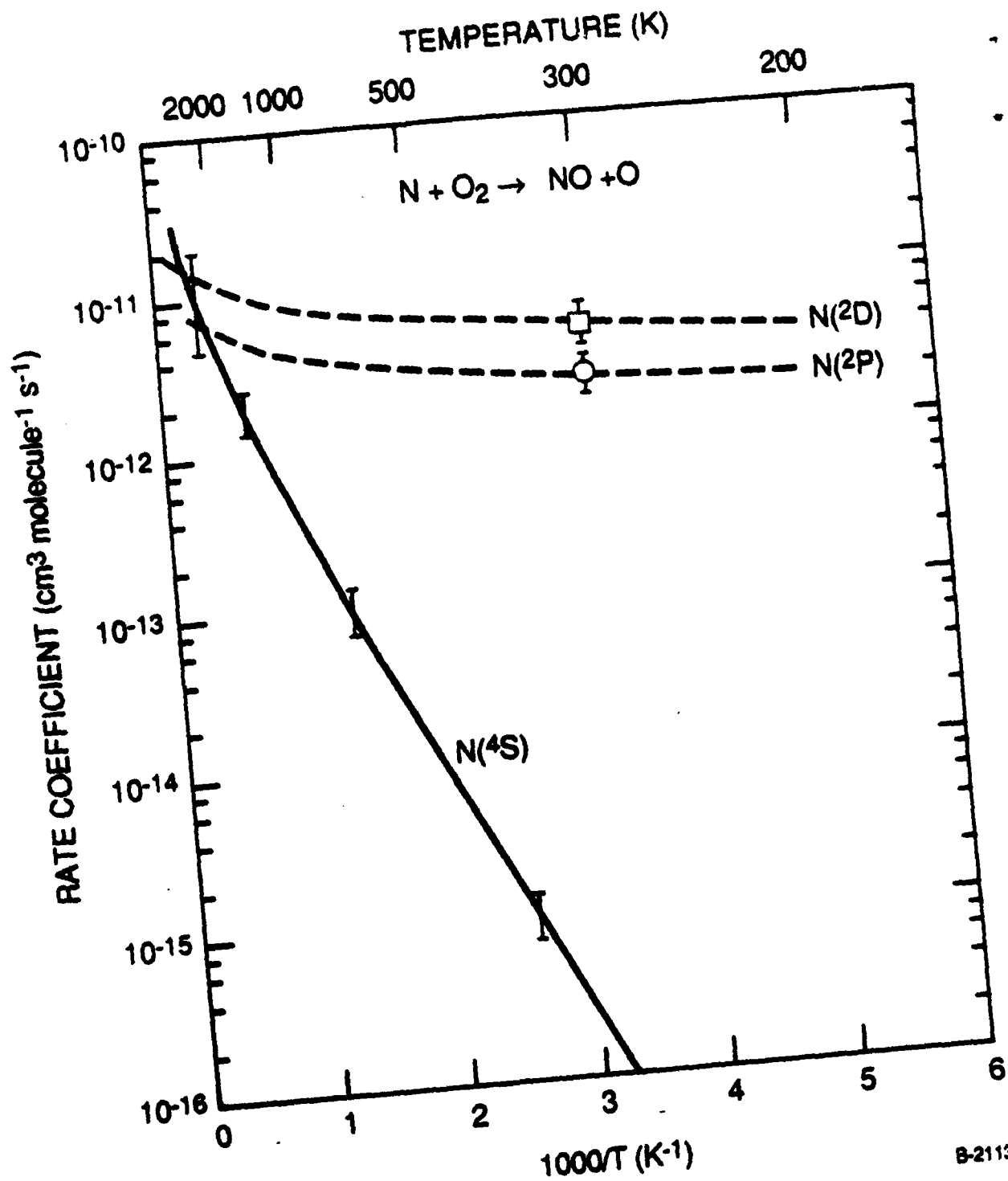


Figure 14 Comparison of recommended rate coefficients for reaction of O_2 with $N(^4S)$, $N(^2D)$, and $N(^2P)$

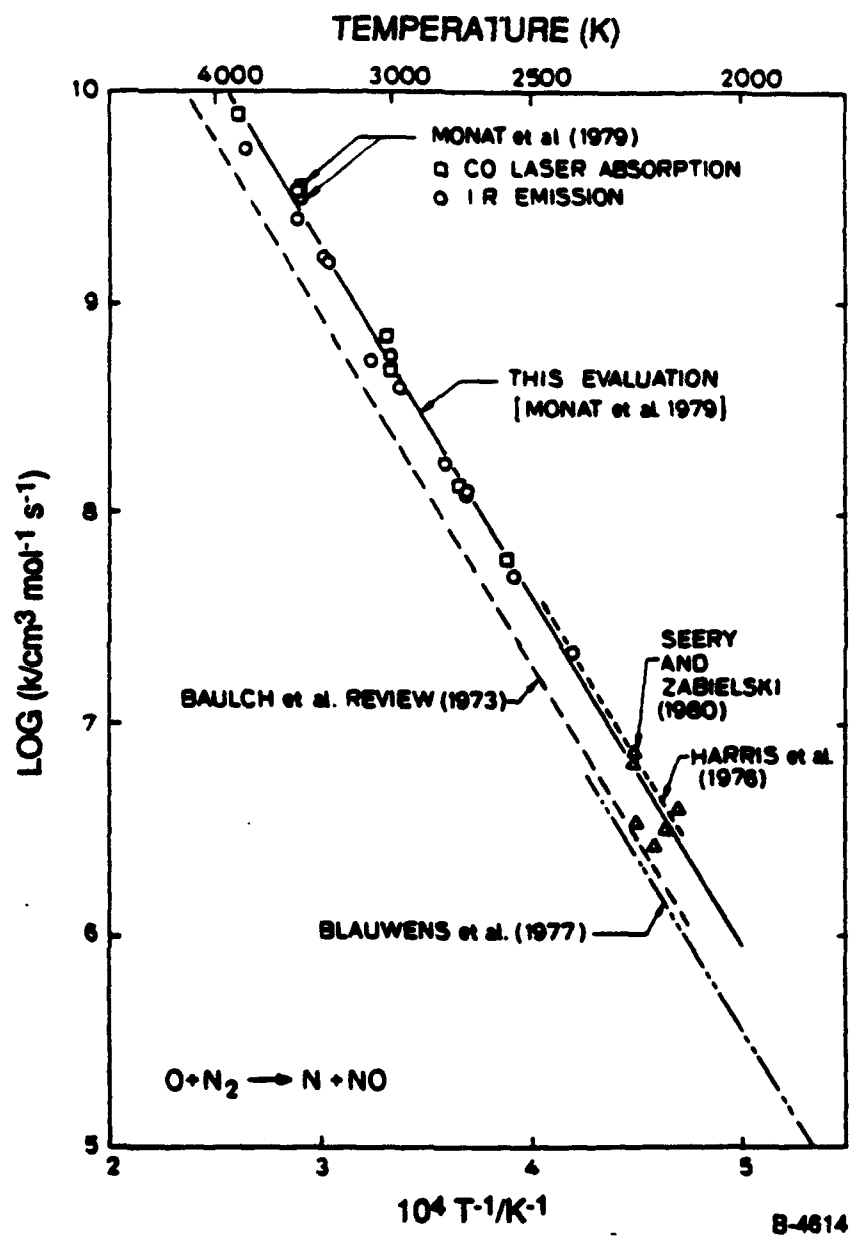
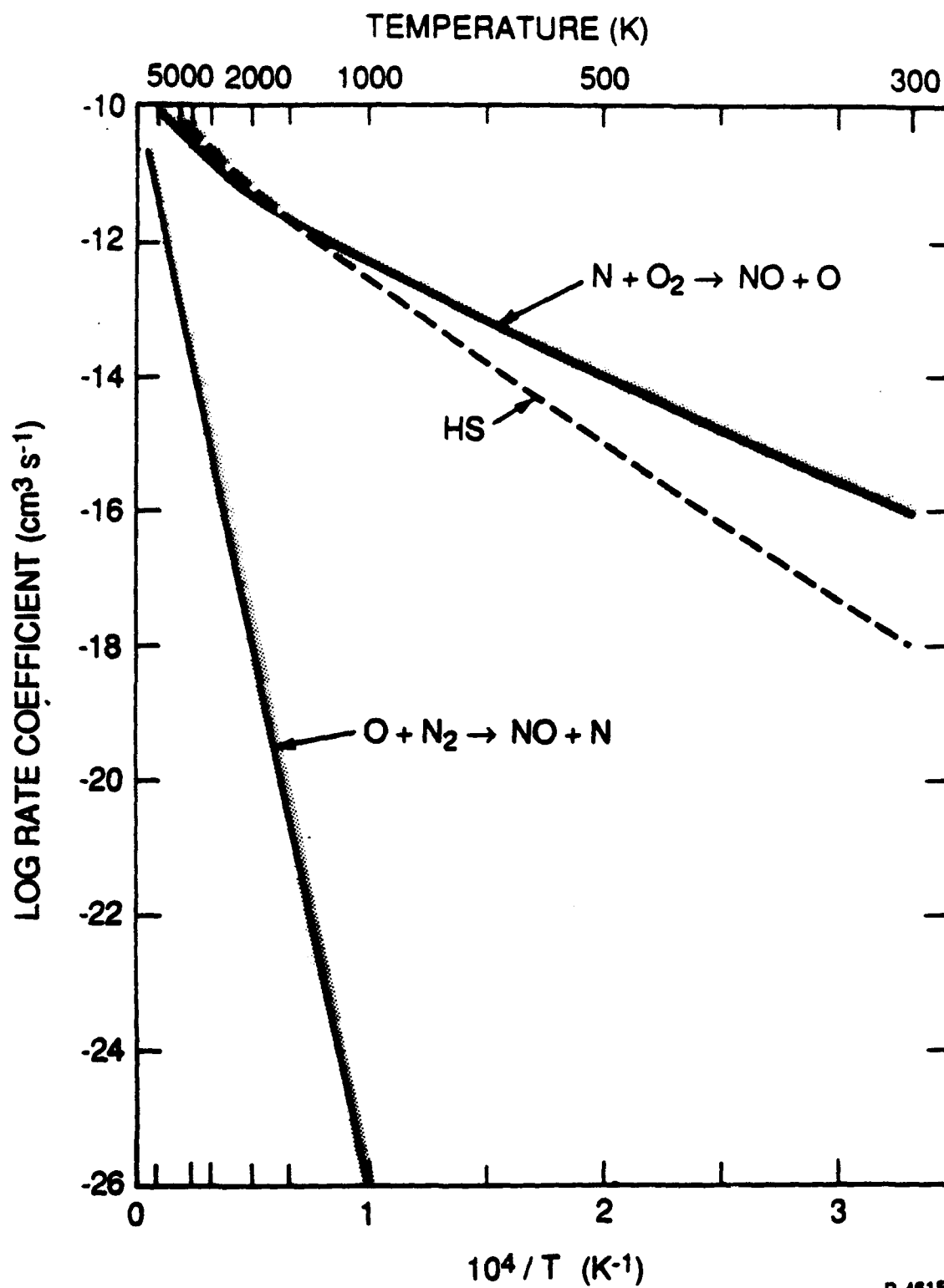


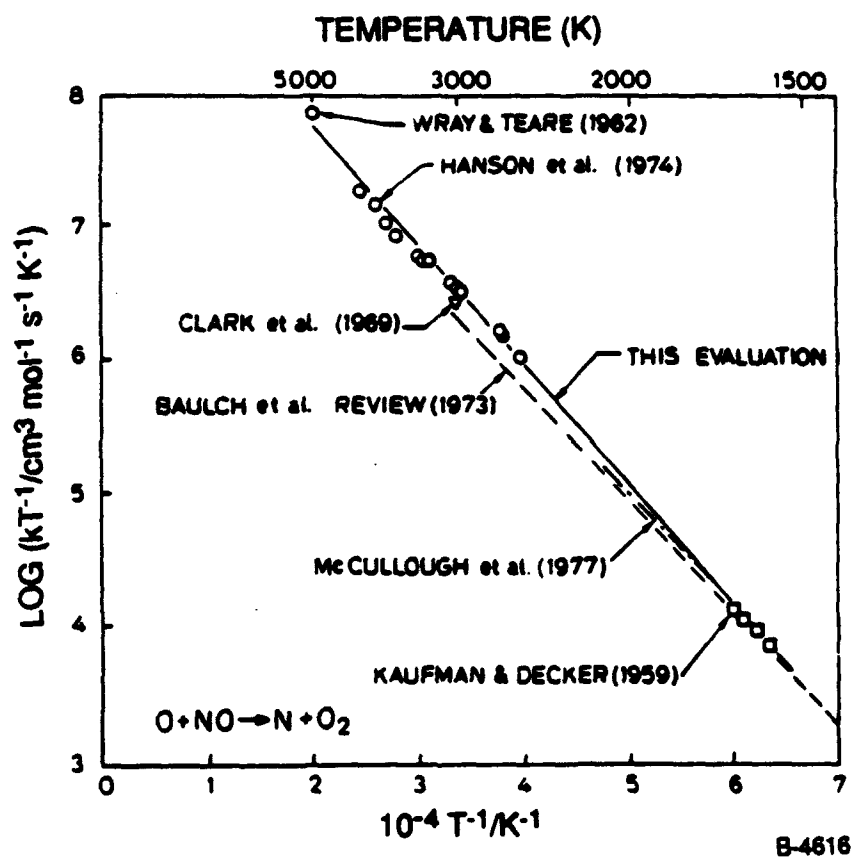
Figure 15 Rate coefficient data for the reaction of O with N_2 , extracted from Hanson and Salimian [63]



B-4615

Figure 16

Recommended rate coefficients and uncertainties for the $\text{N} + \text{O}_2$ and $\text{O} + \text{N}_2$ reactions. HS = rate coefficients for $\text{N} + \text{O}_2$ determined by detailed balance from the values of $\text{O} + \text{NO}$ recommended by Hanson and Salimian [63]



B-4616

Figure 17 Rate coefficient data for the reaction of O with NO, extracted from Hanson and Salimian [63]

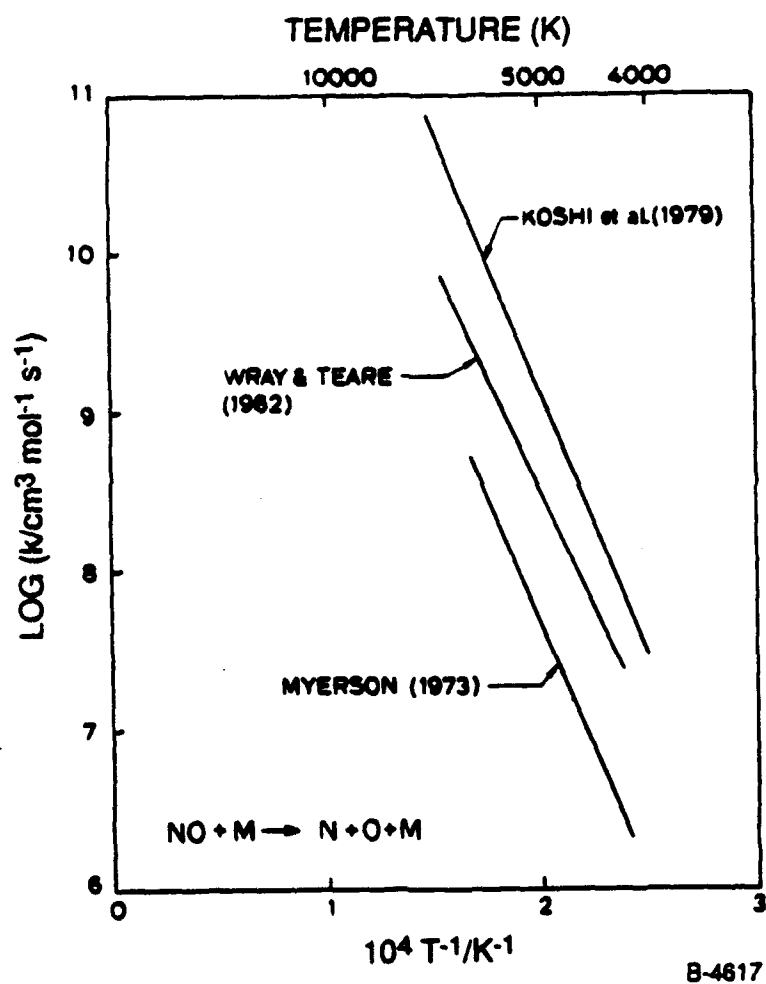
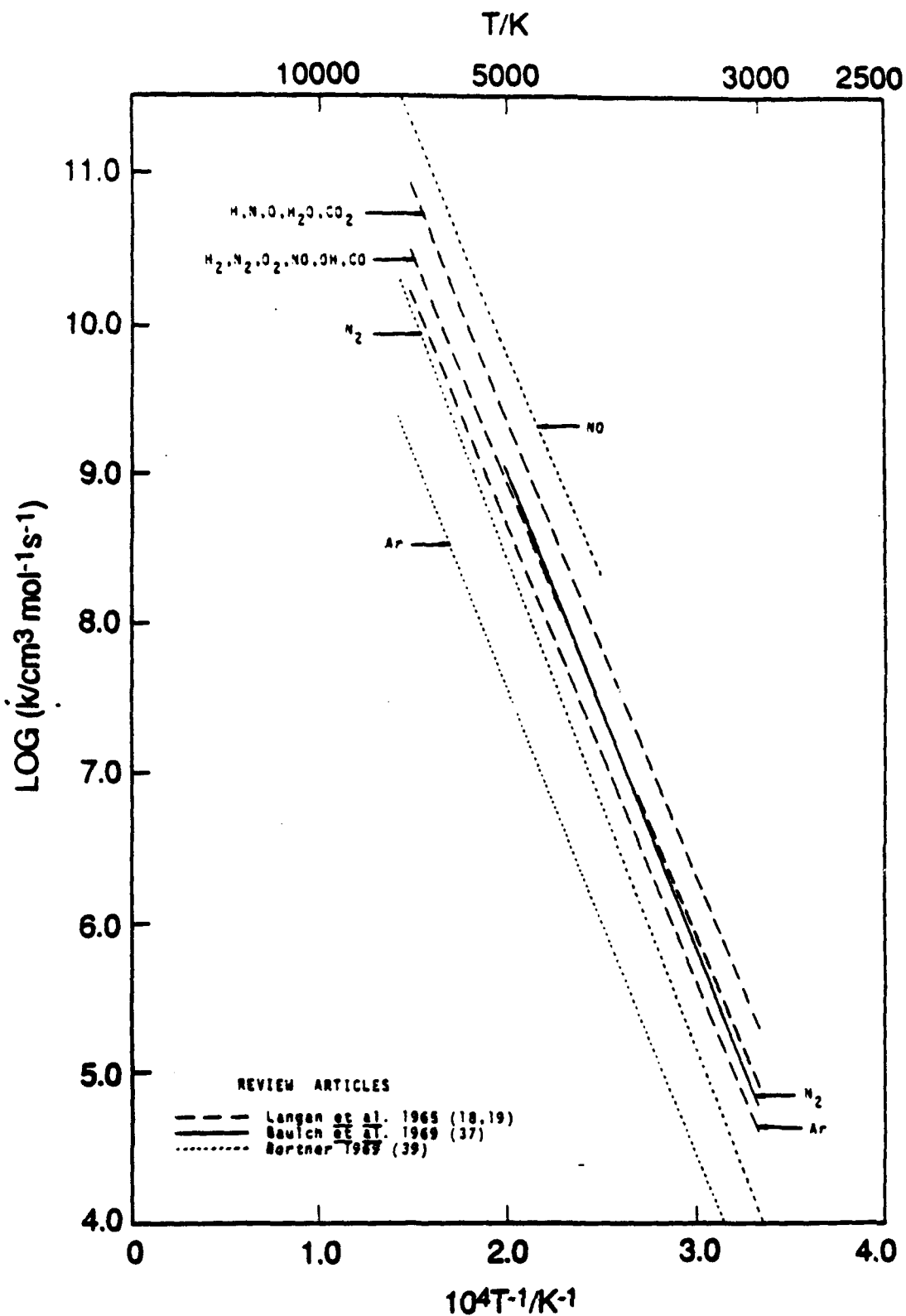
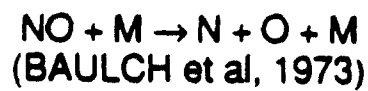


Figure 18 Rate coefficient data for $\text{NO} + \text{M}$ dissociation, extracted from Hanson and Salimian [63]



B-4618

Figure 19 Evaluated rate coefficients for NO + M dissociation, extracted from Baulch et al. [62]

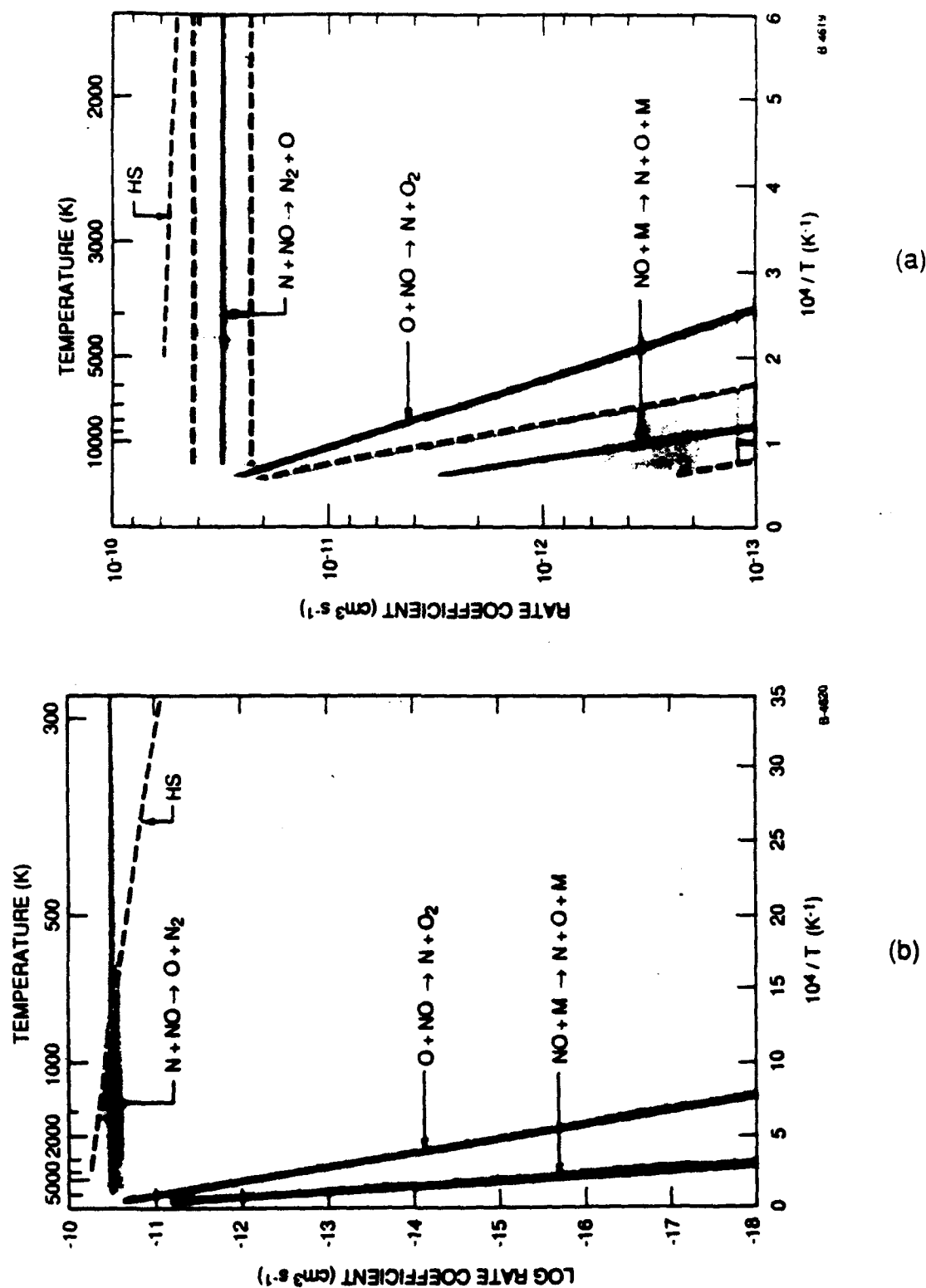


Figure 20 Recommended rate coefficients and uncertainties for NO removal reactions: (a) above 300 K; (b) above 2000 K. HS = rate coefficients for N + NO determined by detailed balance from the values for O + N₂ recommended by Hanson and Salimian [63].

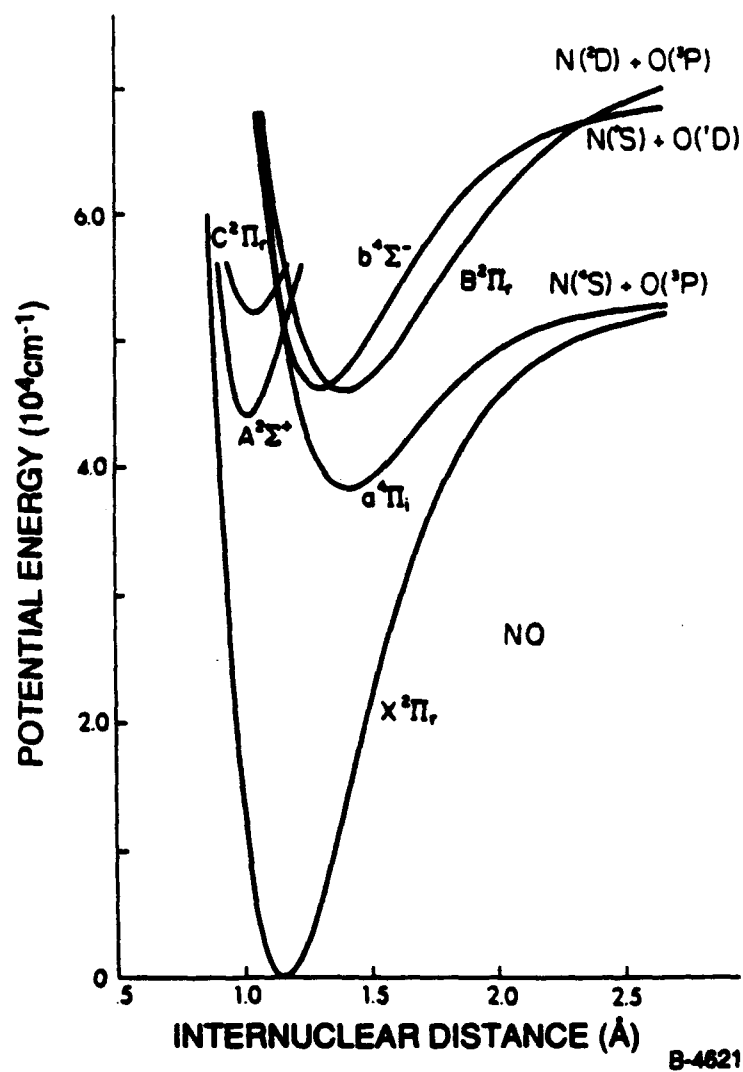


Figure 21 Potential energy curves for the low-lying states of NO, extracted from Kenner and Ogryzlo [75].

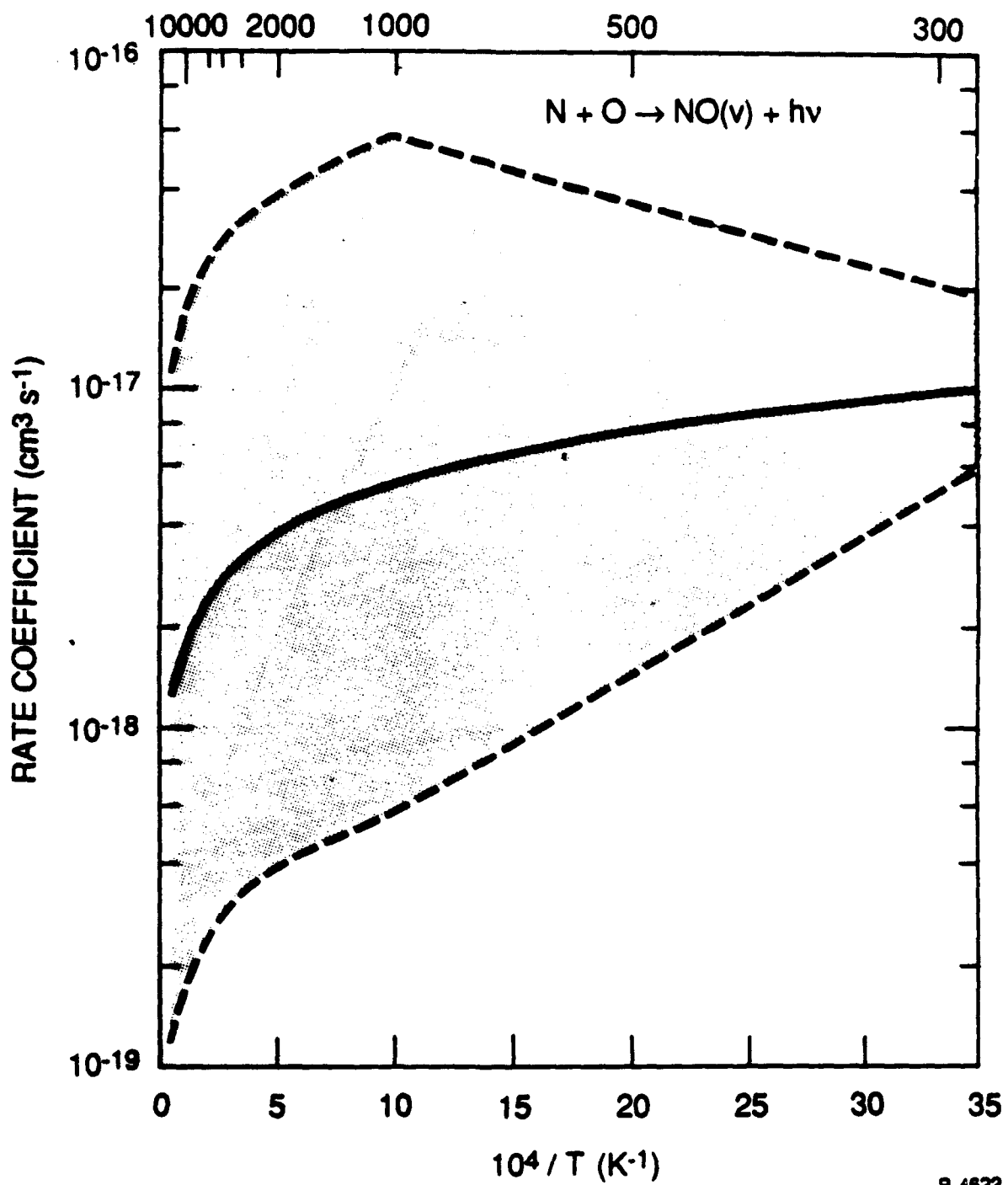
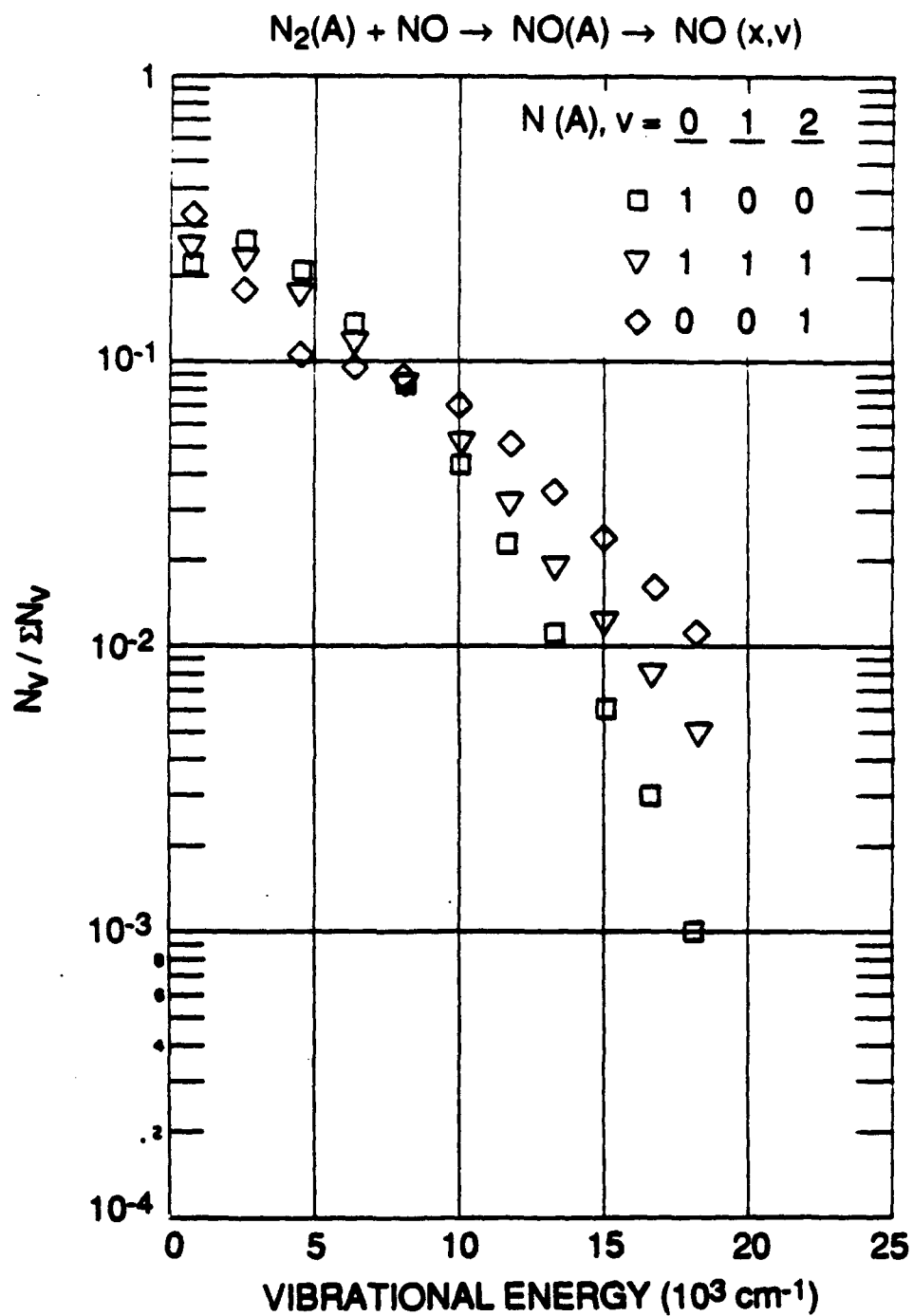


Figure 22 Recommended rate coefficients and uncertainties for two-body recombination of N and O



A3125

Figure 23

Relative $NO(v)$ populations produced in the energy transfer between $N_2(A^3\Sigma_u^+)$ and NO , from the data of Piper and co-workers [81,83]

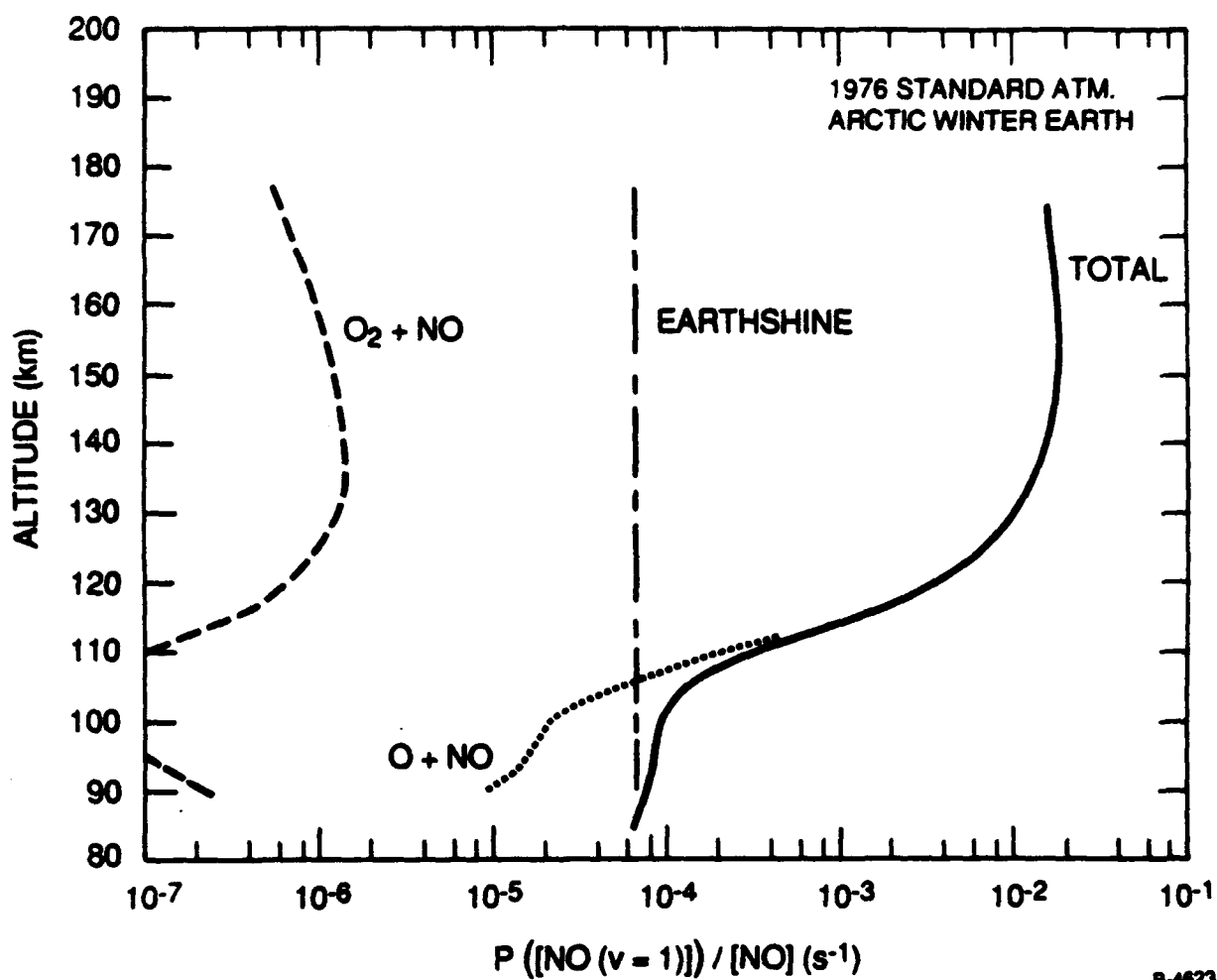


Figure 24 Predicted excitation rates for $NO(v=1)$ in the undisturbed upper atmosphere

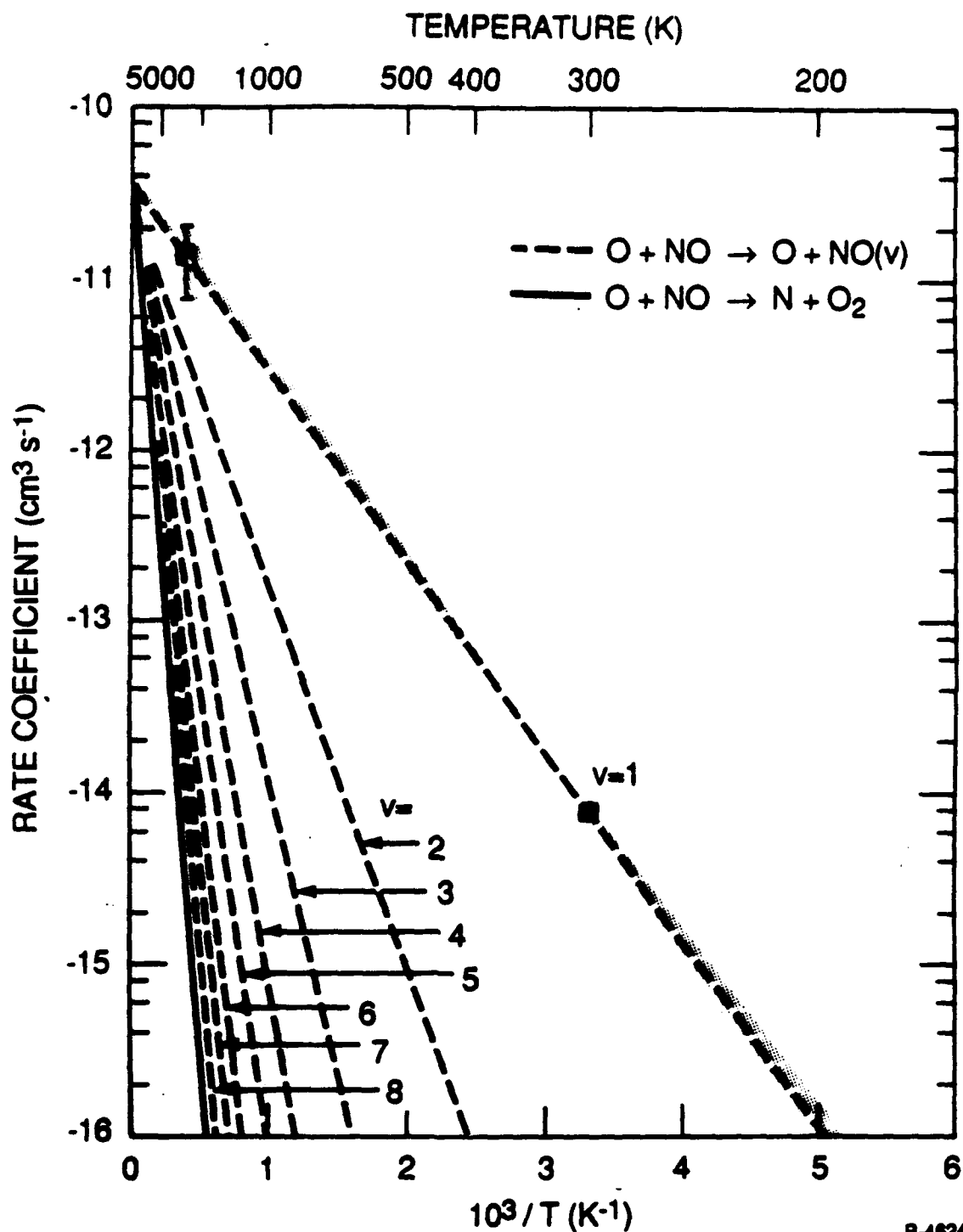
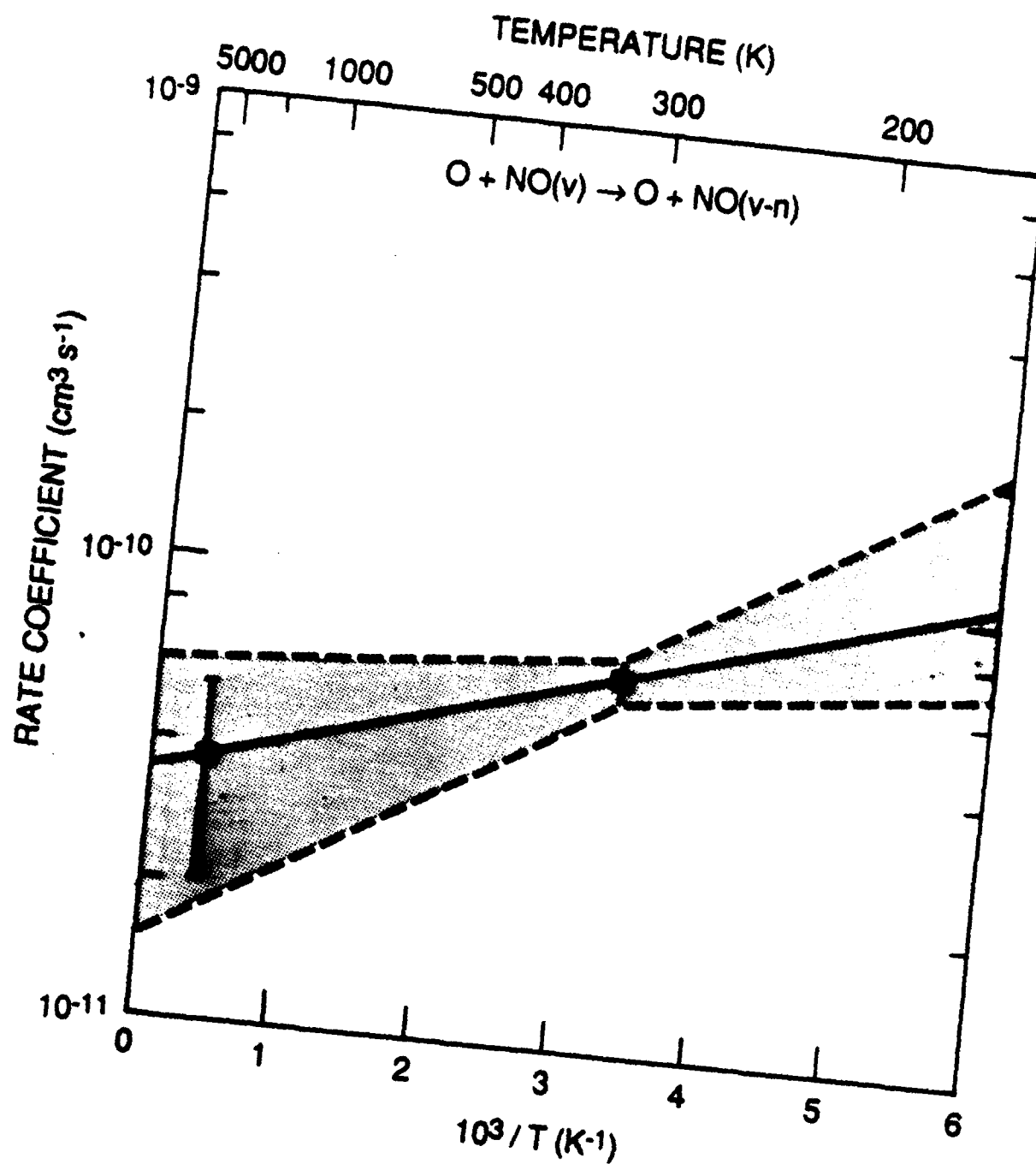


Figure 25 Estimated rate coefficients for collisional excitation of NO(v) by O, compared to the rate coefficient for chemical reaction. Uncertainties are shown only for v=1; values for higher v are estimated upper bounds. Values for v=9,10 are nearly coincident with those for chemical reaction. The data points are from experimental measurements for v=1 deactivation as described in the text.



8-4625

Figure 26 Recommended rate coefficients and uncertainties for deactivation of $\text{NO}(v)$ by O . The rate coefficients are summed over all values of n and are assumed to be independent of v . The data points are from the experimental measurements cited in the text.

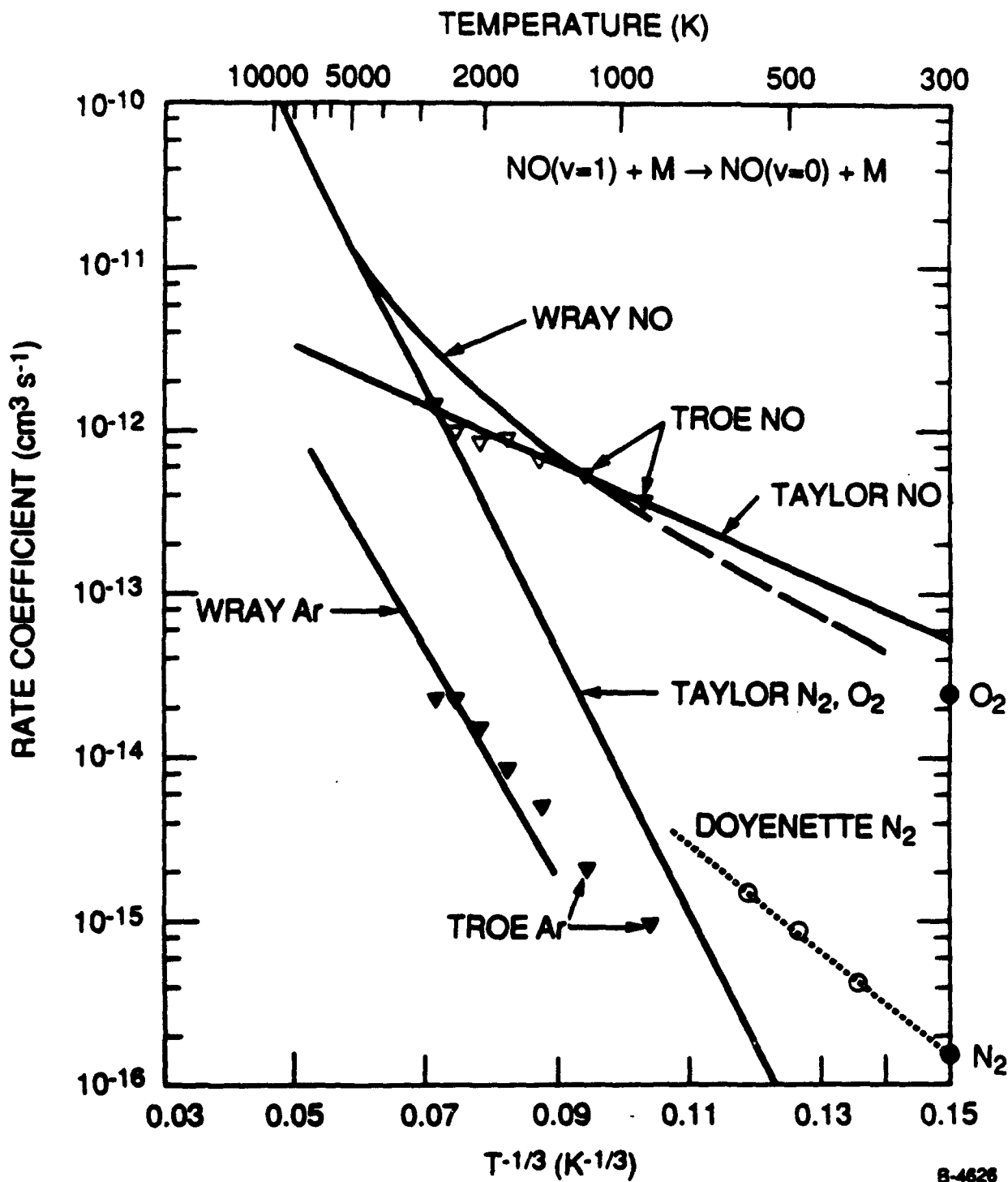
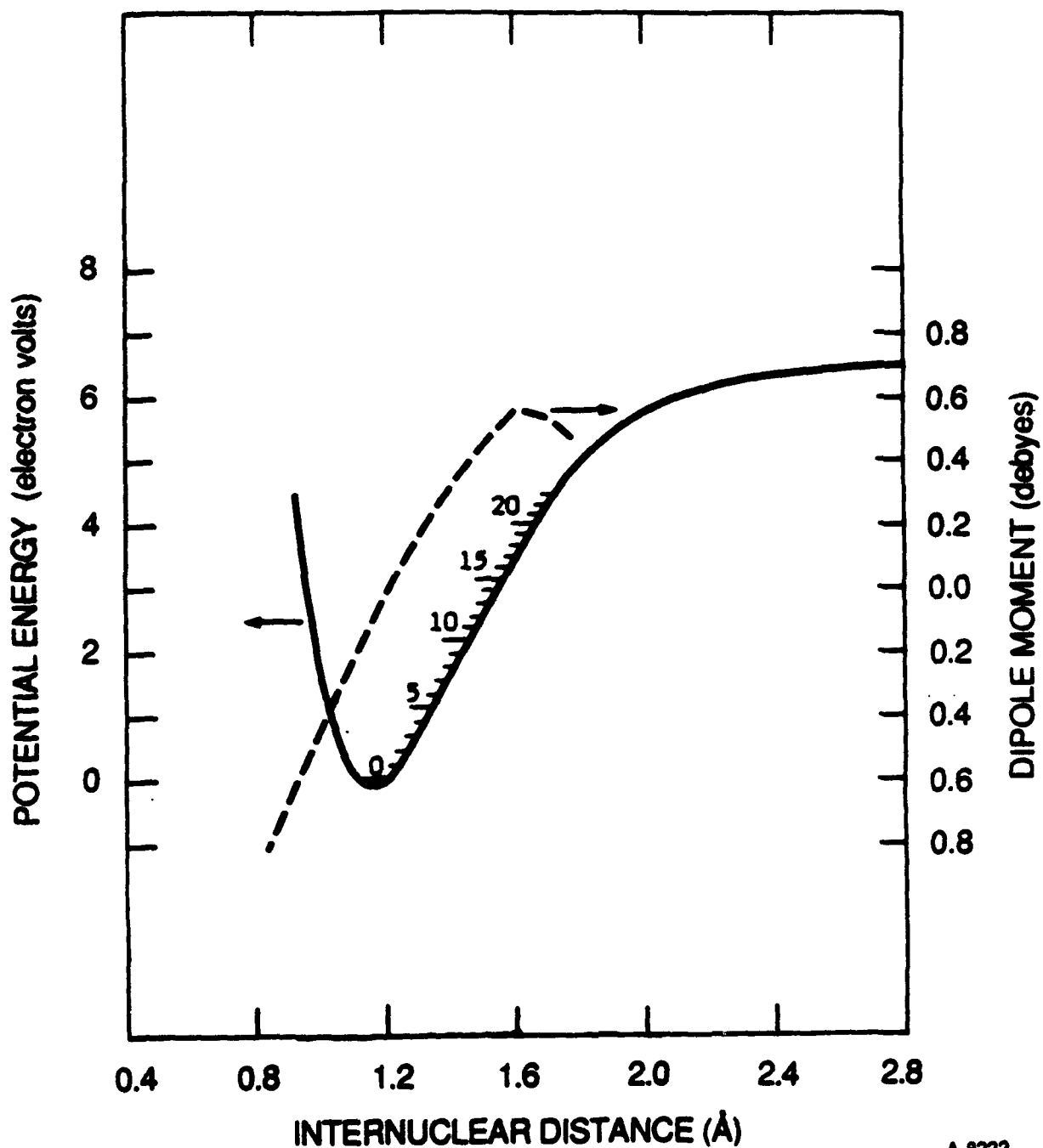
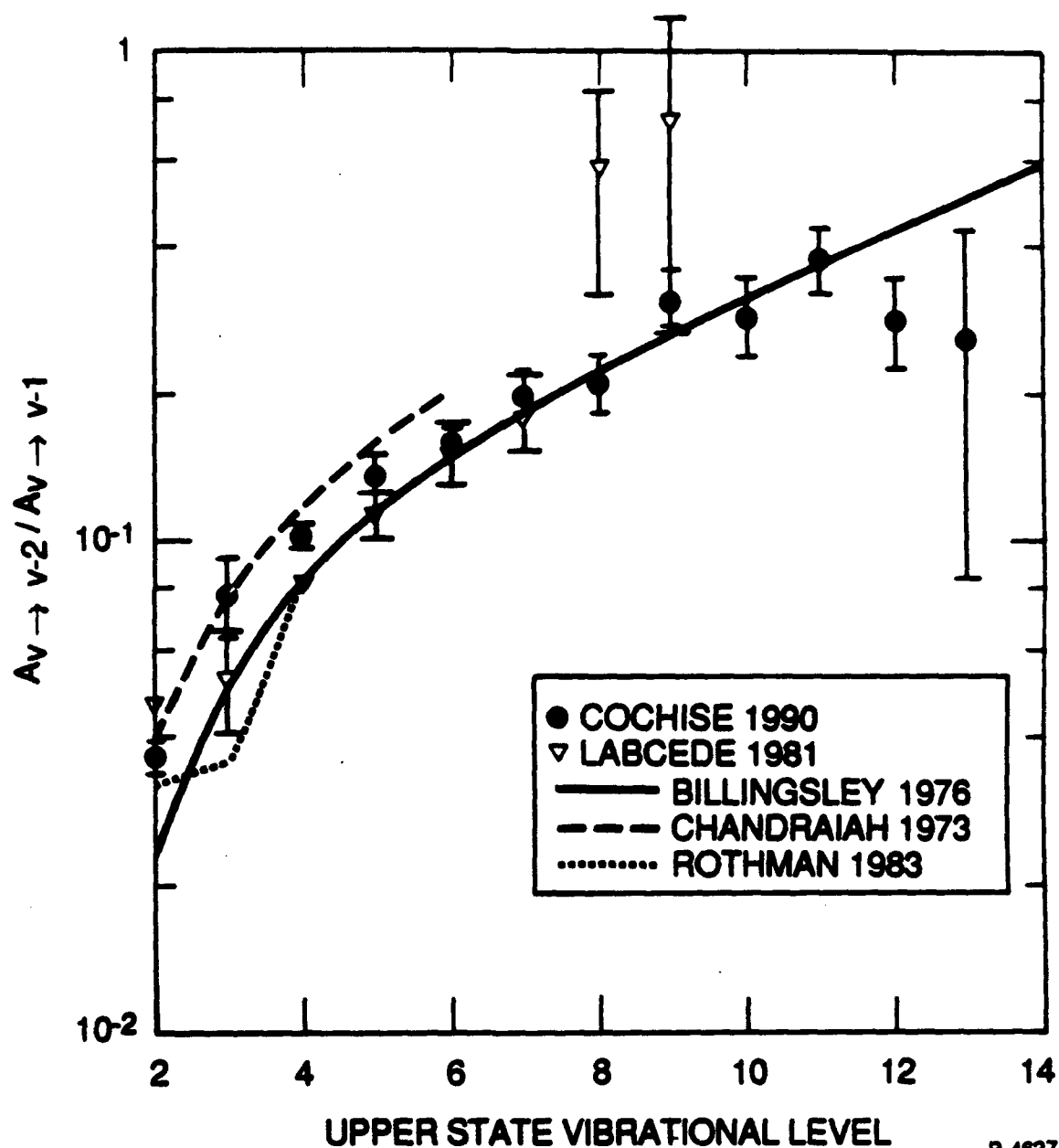


Figure 27 Comparison of temperature dependences for deactivation of $\text{NO}(v=1)$ by O_2 , N_2 , NO , and Ar . References: N_2 , O_2 : see Table 13; Doyenette: Ref. [97]; Taylor, Ref. [96]; Wray: J. Chem. Phys., **36**, 4707 (1973); Troe: Ref. [94].



A-8222

Figure 28 Theoretical dipole moment function of Billingsley [104] (dashed curve) compared to potential curve for NO(X²Π)



B-4627

Figure 29 Comparison of observed and predicted overtone/fundamental branching ratios. References: COCHISE, Ref. 107, LABCEDE, Ref. 106; Billingsley, Ref. 100; Chandraiah, Ref. 103; Rothman, Ref. 102. Error bars on the COCHISE data represent two standard deviations about the weighted mean

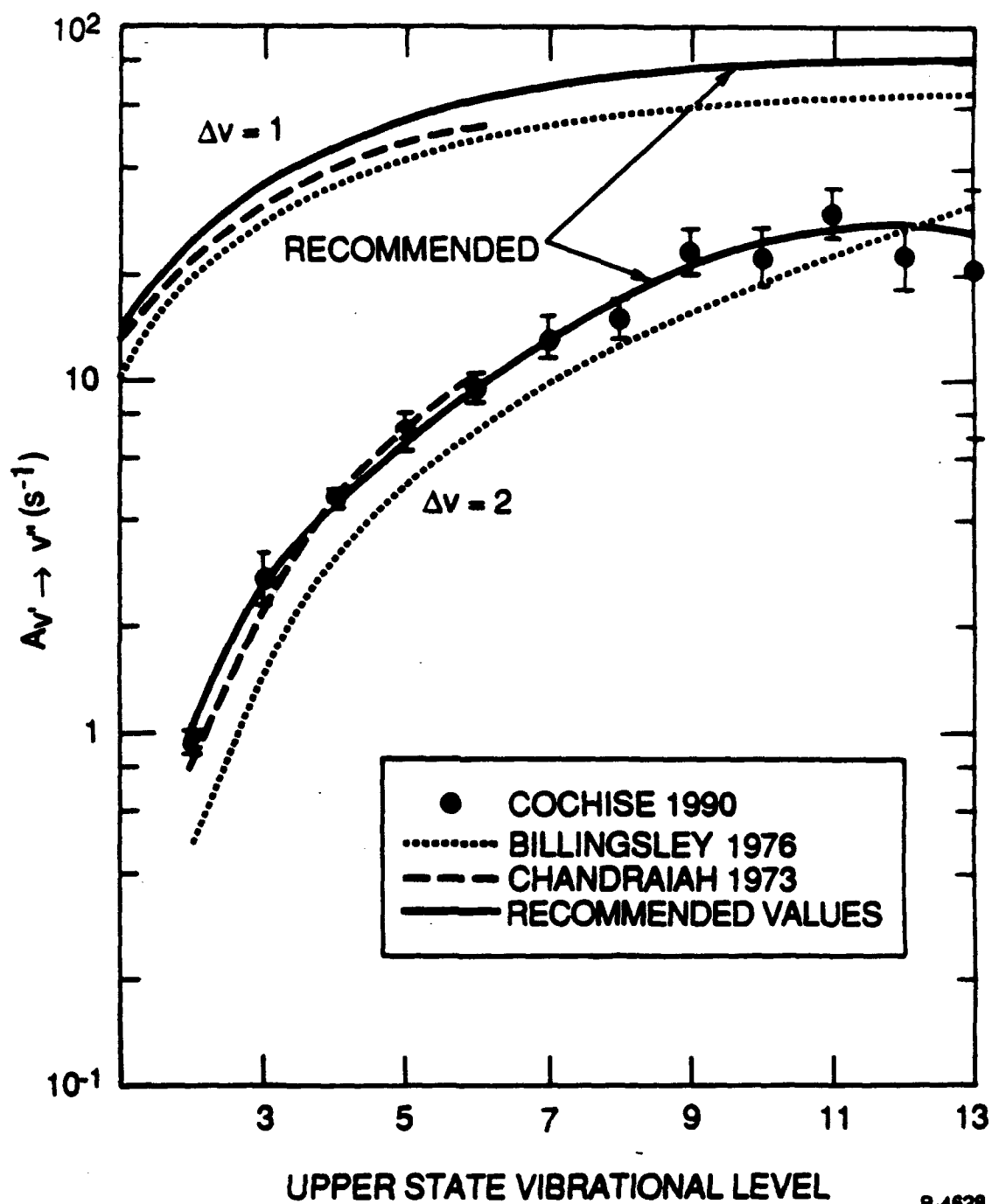


Figure 30 NO Einstein coefficients for the fundamental and first overtone sequences. The COCHISE values were estimated as described in the text. References are as cited in Figure 29.

APPENDIX M

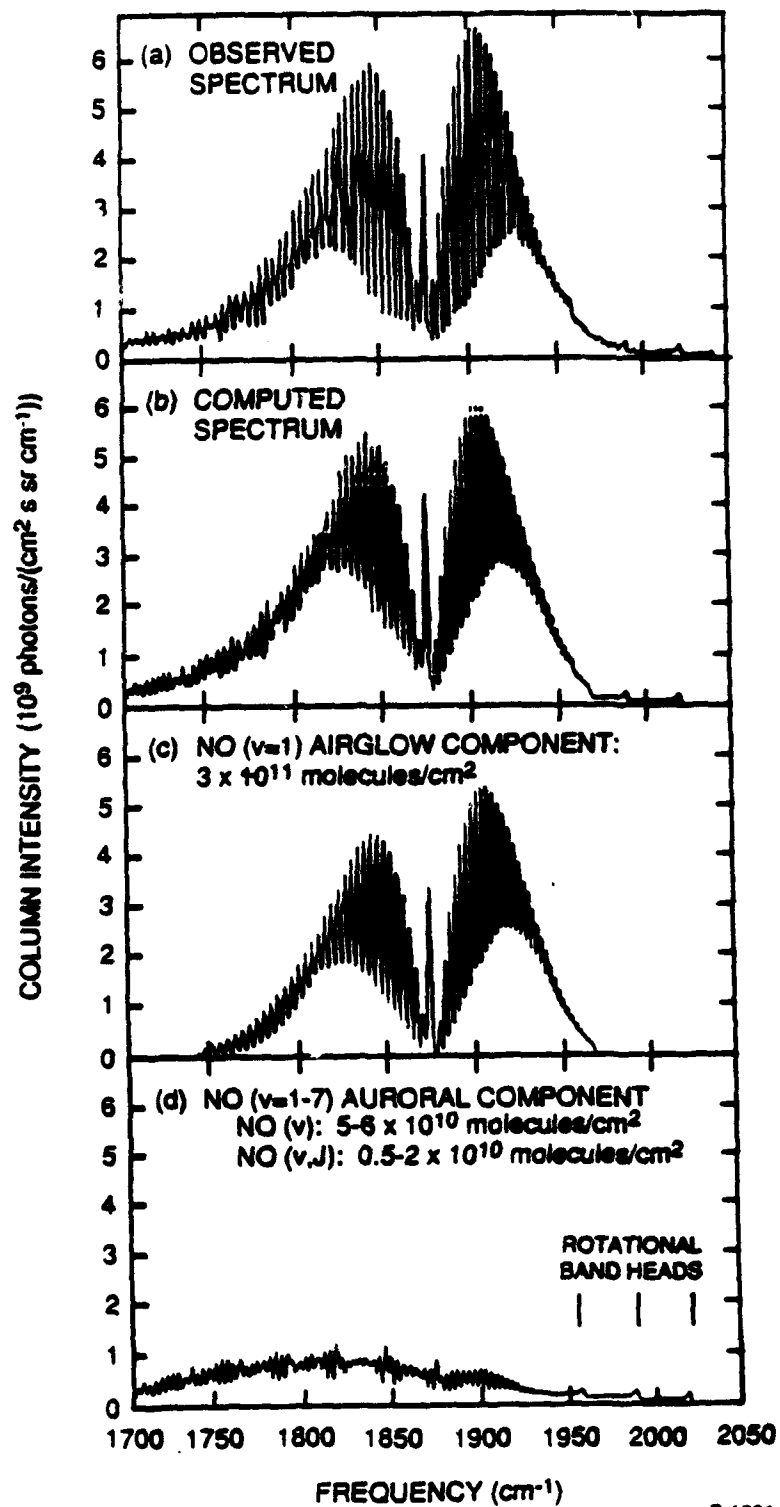
The Aeronomy of Aurorally Excited Infrared Fluorescence from Rovibrationally Excited Nitric Oxide

**W.T. Rawlins
M.E. Fraser**

THIS PAGE INTENTIONALLY LEFT BLANK

CLASS II⁺ AURORAL NO(v,J) EXCITATION

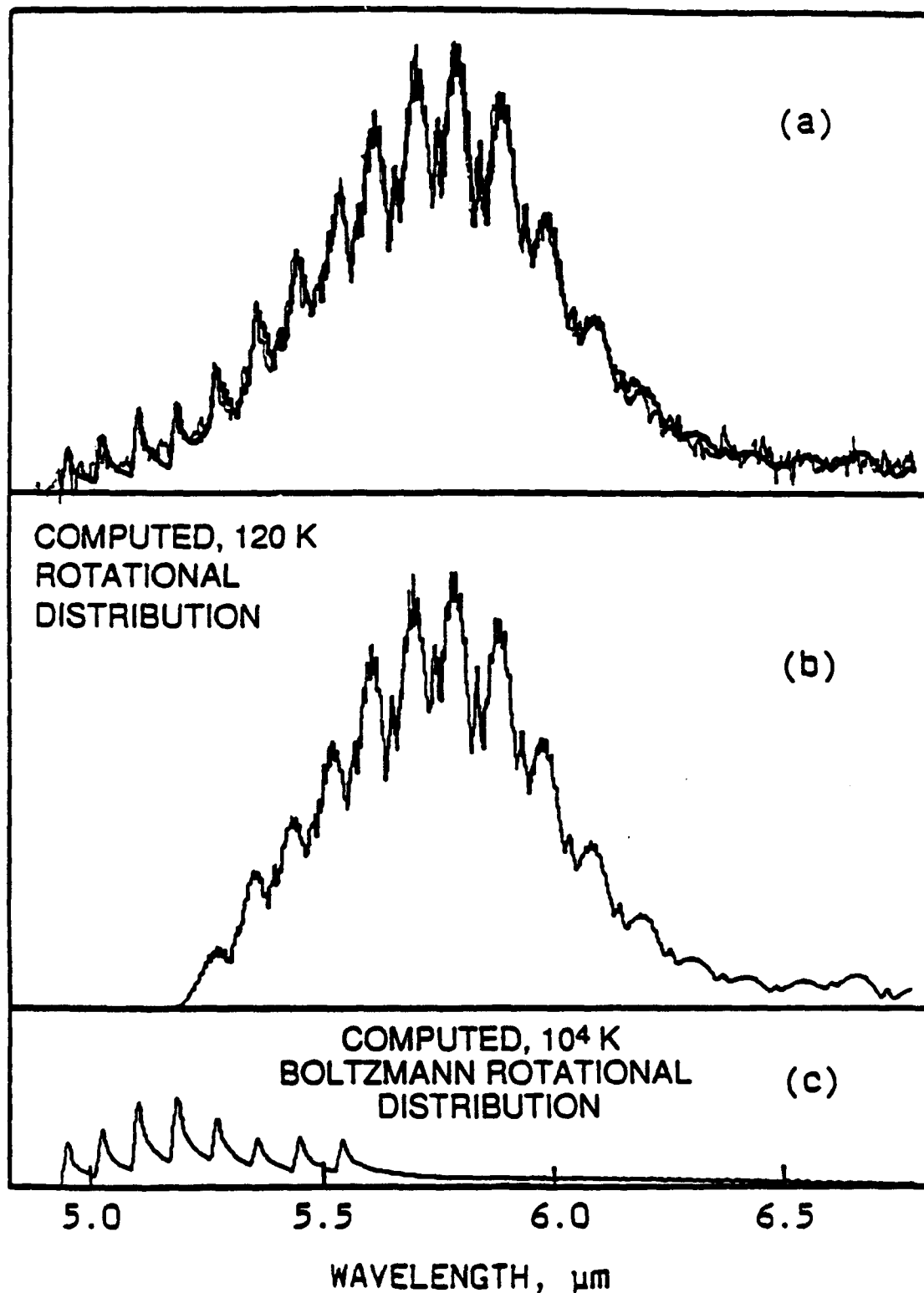
T-3124



B-1291

COMPARISON OF EXPERIMENTAL AND COMPUTED SPECTRA FOR NO(v, J)

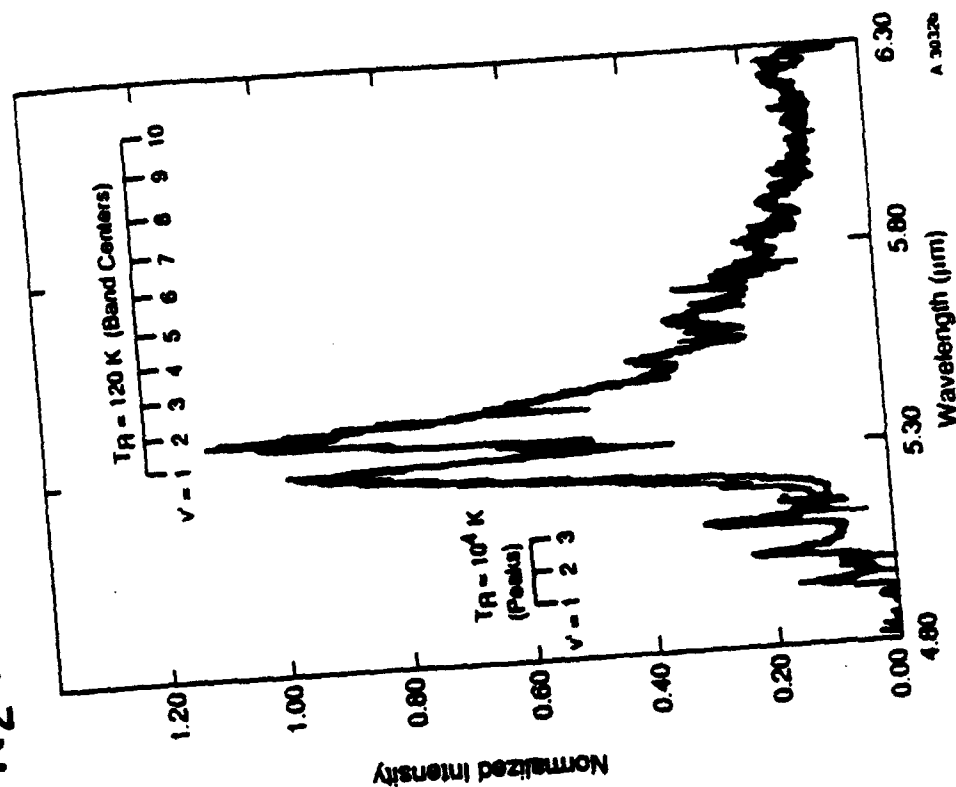
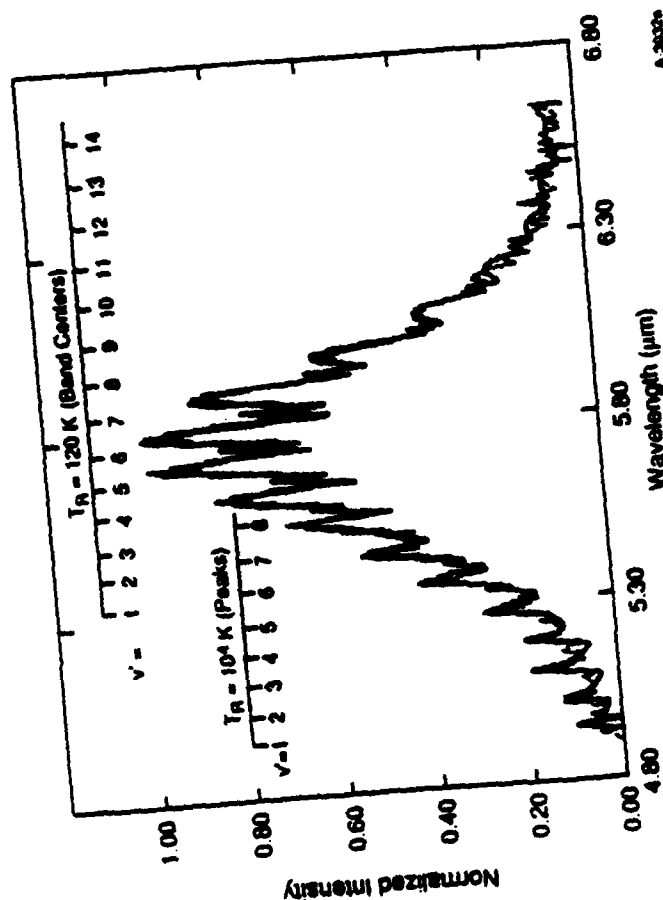
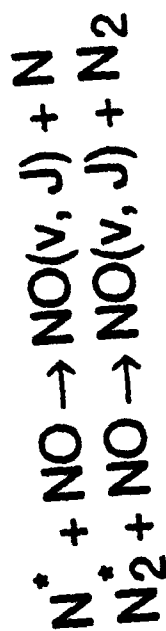
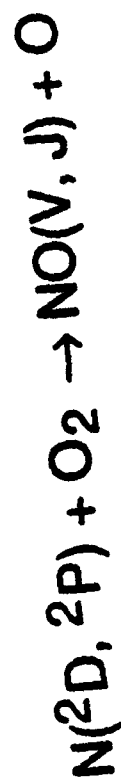
VG89-137



A-6944A

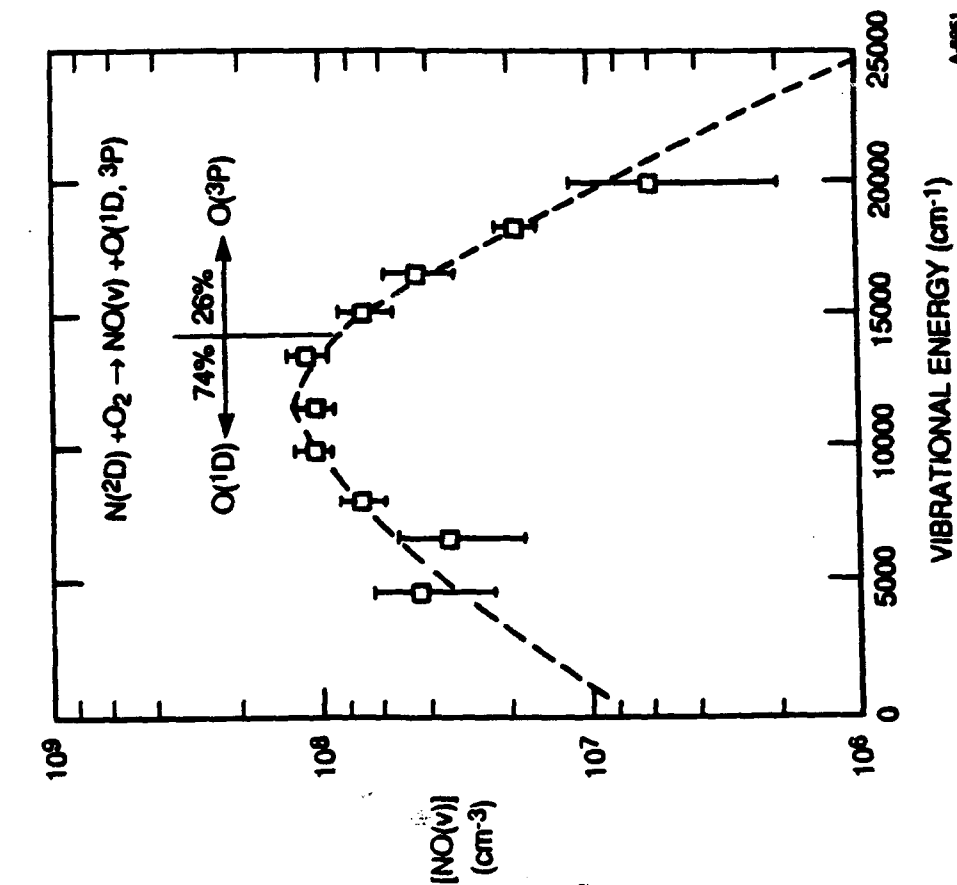
SOURCES OF NO(v, J) INFRARED CHEMILUMINESCENCE

T-14148

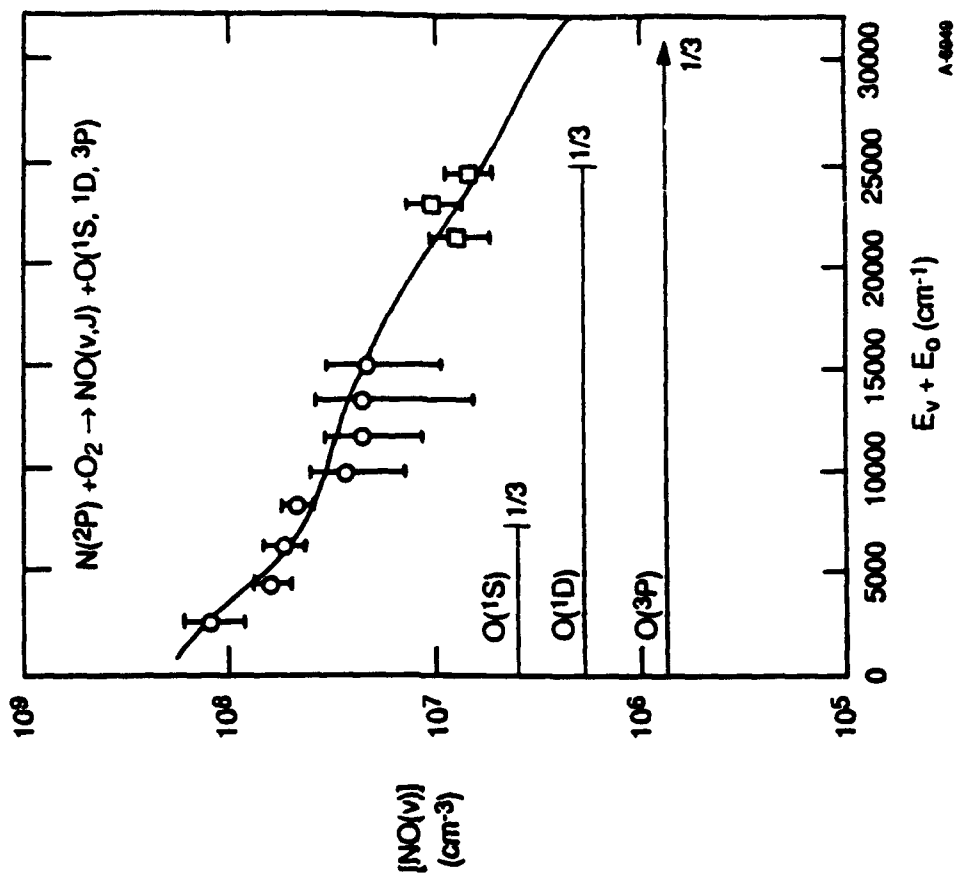


CHEMICAL FORMATION OF NO(v,J) NASCENT NO(v) PRODUCT DISTRIBUTION FOR $N^* + O_2$ REACTIONS

T-3129



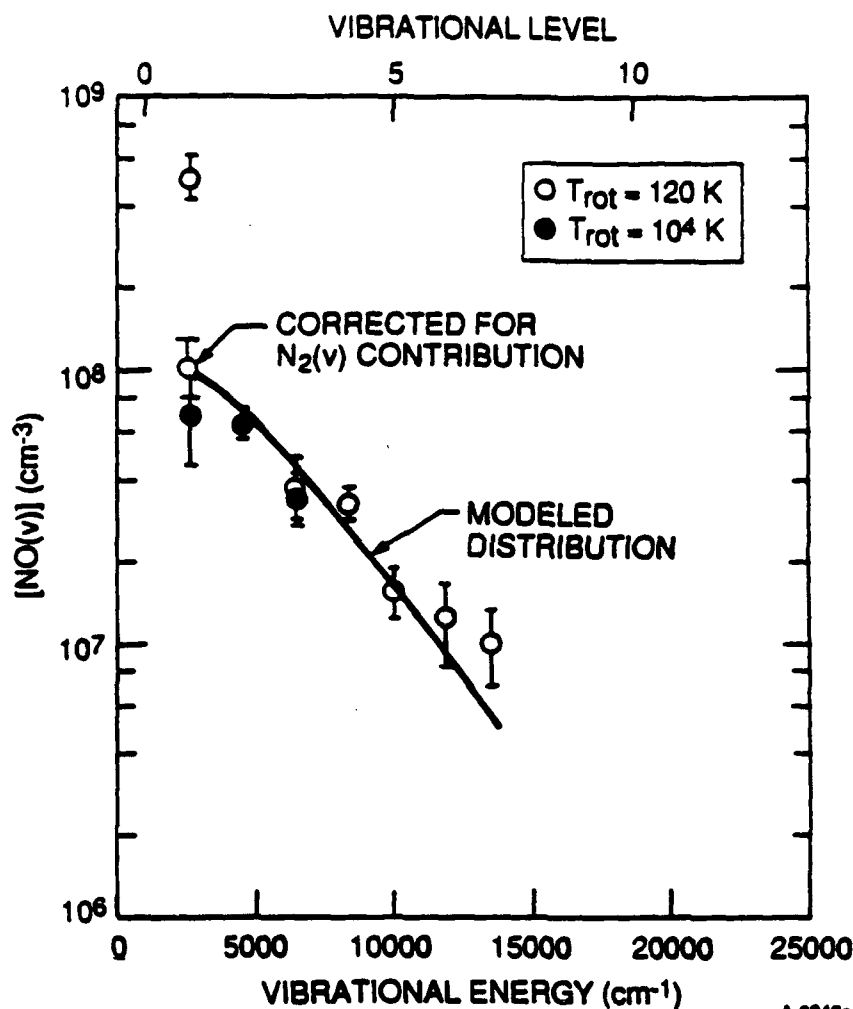
$N(2D) + O_2$ forms only rotationally thermalized NO(v) states



$N(2P) + O_2$ responsible for rovibrational excitation

ENERGY TRANSFER EXCITATION OF NO(v,J) $N^*, N_2^* + NO \rightarrow NO(v,J)$ AVERAGE POPULATIONS

T-3133

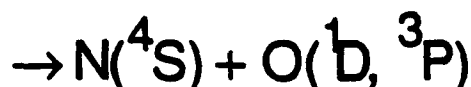
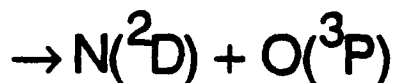
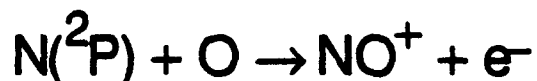
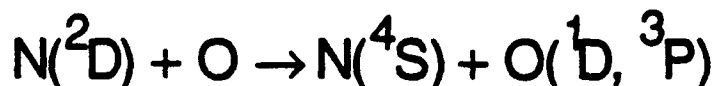
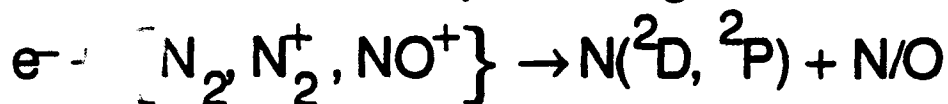


- NO(v=1) must be corrected for $N_2(v) + NO(v=0) \rightarrow NO(v=1) + N_2(v-1)$ contribution
- $v \leq 7$ rotationally thermalized bands; $v \leq 3$ rotational band heads observed
- Indicate energy transfer of ≤ 1.7 eV
- Modeled distribution is for $N_2(A) + NO \rightarrow NO(A) \rightarrow NO(v,J)$

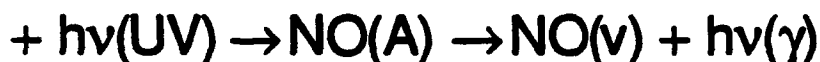
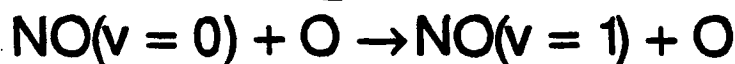
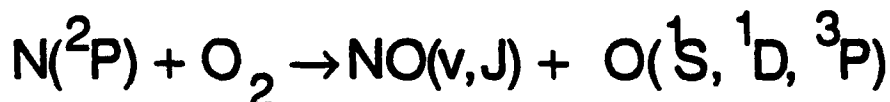
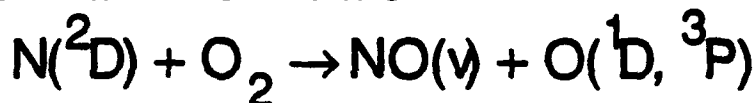
KEY REACTIONS FOR AURORAL NO(v) EXCITATION

T-3125

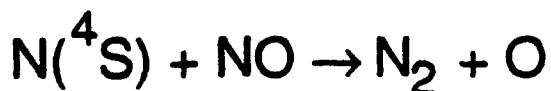
- Precursor formation/quenching:



- NO formation/excitation:



- NO loss/deactivation:



AUROLAL NO MODEL

VC80-245

- Airglow: radiative and collisional excitation/deactivation
- Auroral:
 - From COCHISE,
$$\text{N}(\text{}^2\text{D}) + \text{O}_2 \rightarrow \text{NO}(\text{v}) + \text{O}$$
$$\text{N}(\text{}^2\text{P}) + \text{O}_2 \rightarrow \text{NO}(\text{v},\text{J}) + \text{O}$$
 - Radiative/collisional deactivation of $\text{NO}(\text{v})$, $\text{NO}(\text{v},\text{J})$
 - New PSI/AFGL results for $\text{N}(\text{}^2\text{D}, \text{}^2\text{P})$ quenching
 - Model optimized for comparison to FWI data
- U.S. Standard Atmosphere (1976): representative auroral O-profile
- Uncertainties 8 to 9 $\mu\text{m} \Rightarrow$ lower bound
 - Contributions from high v ($\text{v} \geq 15$)
 - High J deactivation kinetics

AUROLAL NO CALCULATIONS

VC80-245

- Predicted number density versus altitude integrated along zenith sight path, $h \leq 90$ km

- Spectral resolution 2 cm^{-1} , $(\text{sinc})^2$ scan function

- Three airglow NO profiles

— High:	[NO] 110 km	$= 10^9 \text{ cm}^{-3}$
— Medium:	[NO] 110 km	$= 10^8 \text{ cm}^{-3}$
— Low:	[NO] 110 km	$= 10^7 \text{ cm}^{-3}$

- Four auroral conditions:

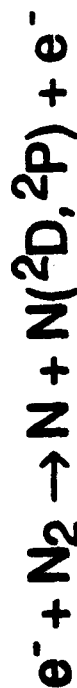
kR (391.4 nm) Overhead	Altitude of Peak Dosing
------------------------	-------------------------

380 kR	100 km
38 kR	105 km
38 kR	115 km
7.6 kR	115 km

N(²D, ²P) PRECURSOR KINETICS

T-14150

- Precursor formation



sometimes $e^- + N_2^+ \rightarrow 2N(^2D)$

— N(²D): 1 to 1.5 per ion pair

— N(²P): 0.2 to 0.3 per ion pair

— Is N(²P) enhanced by N₂(v), NO⁺(v), N₂⁺(v)?

- Precursor Quenching: O, sometimes e⁻

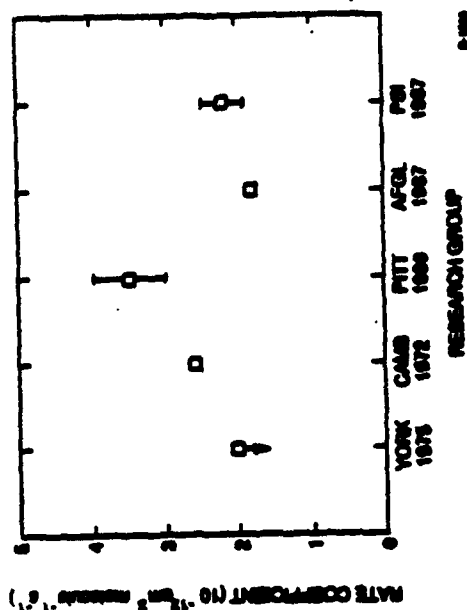
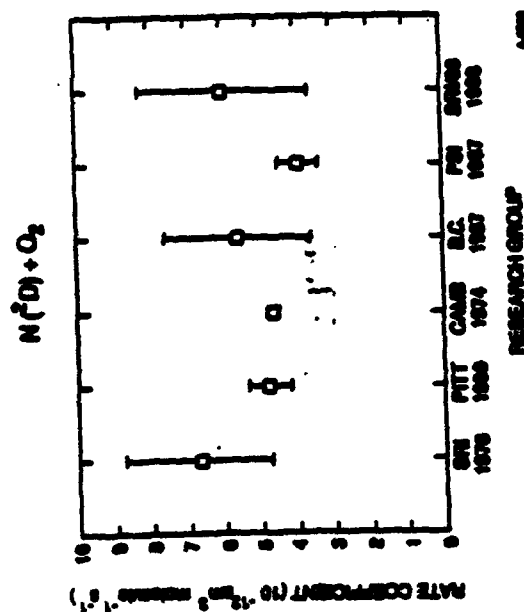
CANDIDATE ATMOSPHERIC EXCITATION REACTIONS

T-14149

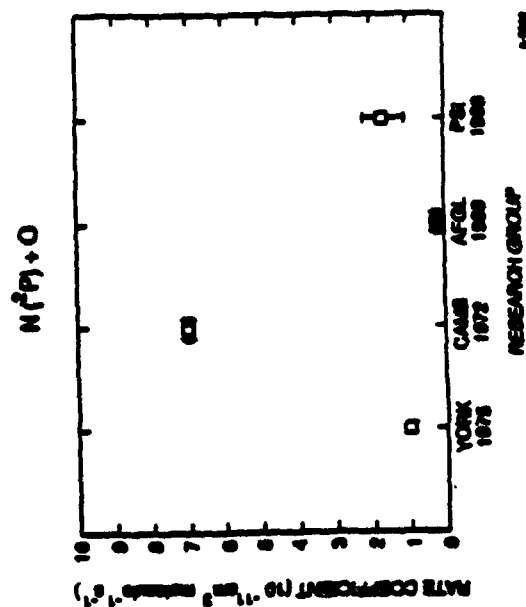
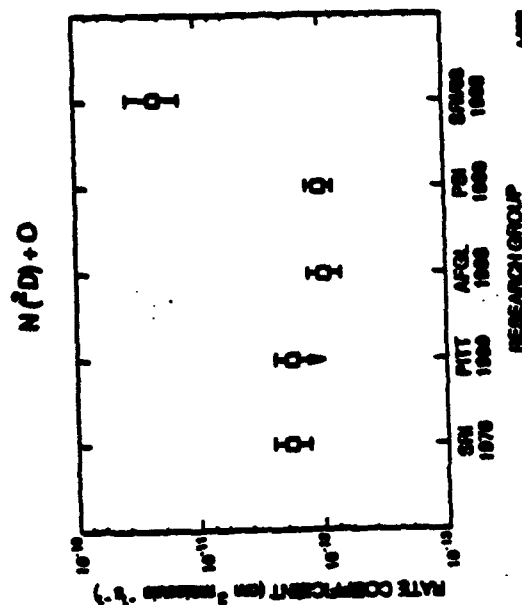
- Excitation of NO(v, J)
 - $\text{N}(^2\text{D}) + \text{O}_2 \rightarrow \text{O} + \text{NO} + 3.76 \text{ eV}$
 - $\text{N}(^2\text{P}) + \text{O}_2 \rightarrow \text{O} + \text{NO} + 4.96 \text{ eV}$
 - $\text{N}(^2\text{D}) + \text{NO} \rightarrow \text{N} + \text{NO} + 2.38 \text{ eV}$
 - $\text{N}_2(\text{A}^3\Sigma_u^+, v) + \text{NO} \rightarrow \text{N}_2 + \text{NO} + h\nu + (\sim 2) \text{ eV}$
 - $\text{N}_2(\text{A}^3\Sigma_u^+, v) + \text{O} \rightarrow \text{N} + \text{NO} + (3 \text{ to } 4) \text{ eV}$
- Deactivation of NO(v, J)
 - Collisional: O, N₂, O₂
 - Radiative: IR fundamental, overtone

RATE COEFFICIENTS FOR N_2 QUENCHING AT 300 K†

VG89-249



(a)



(c)

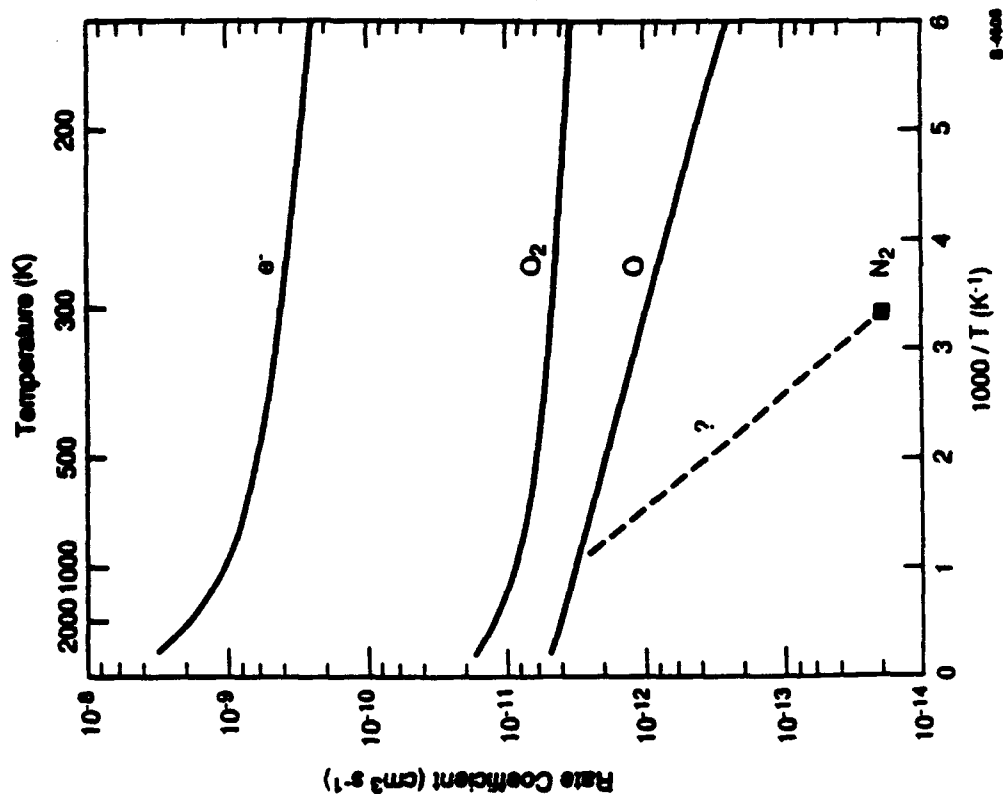
(d)

† L.G. PIPER AND COWORKERS, 1987-1989

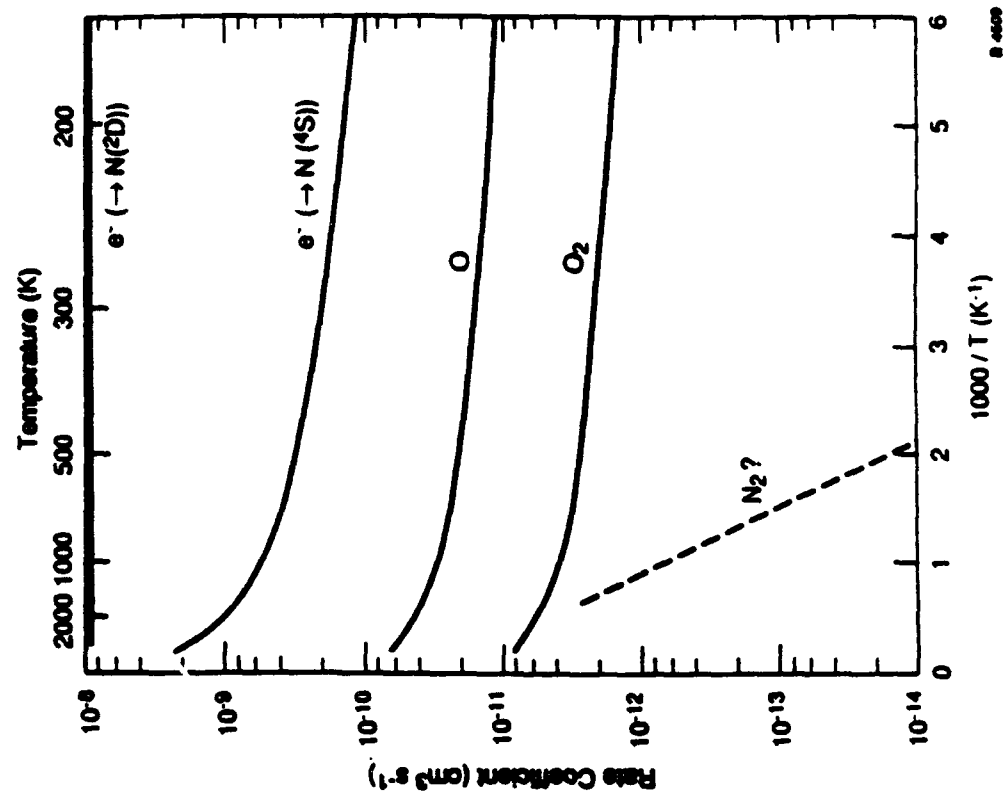
N(²D, ²P) QUENCHING KINETICS

T-14151

N(²D) Quenching

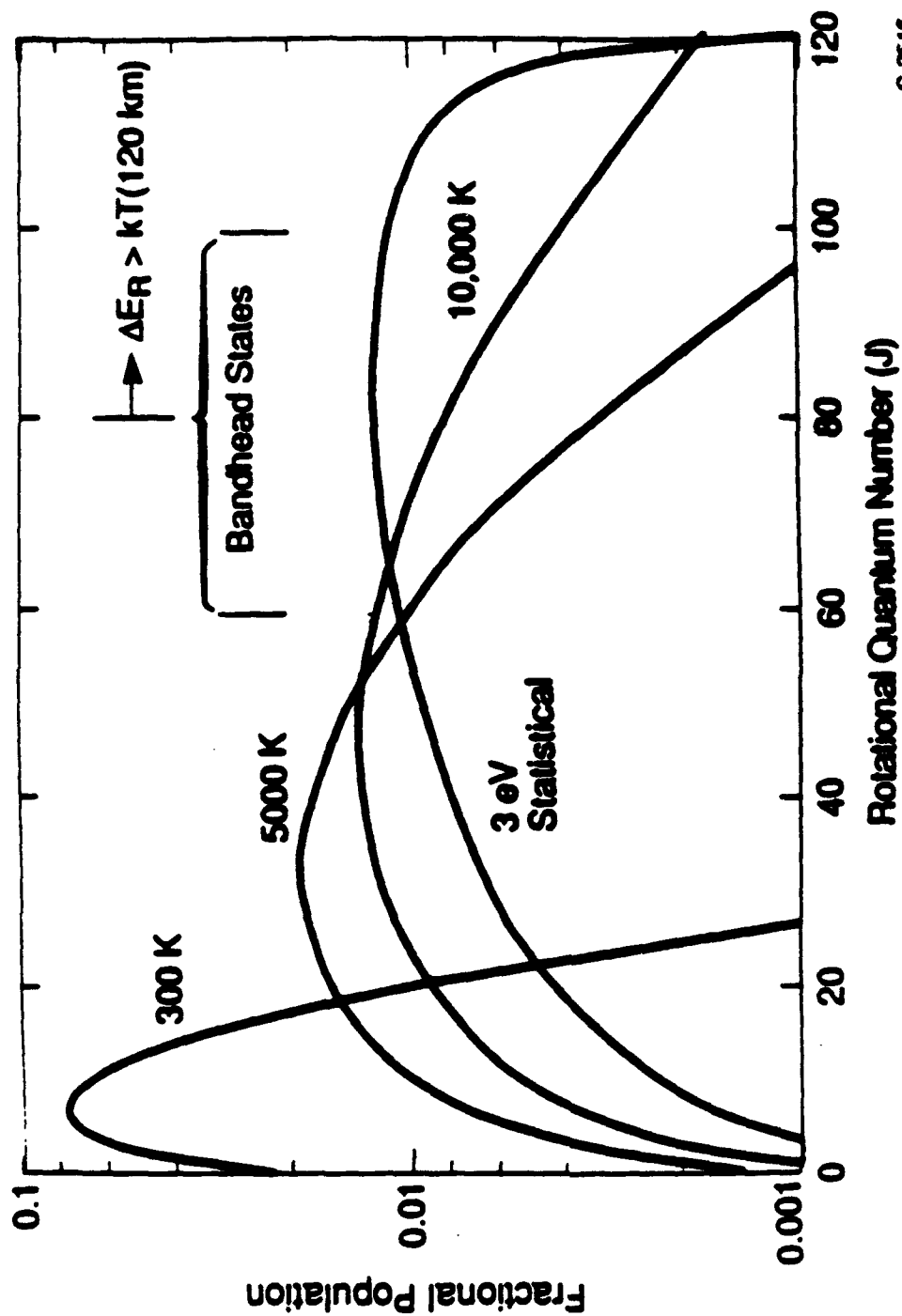


N(²P) Quenching



ROTATIONAL POPULATION DISTRIBUTIONS

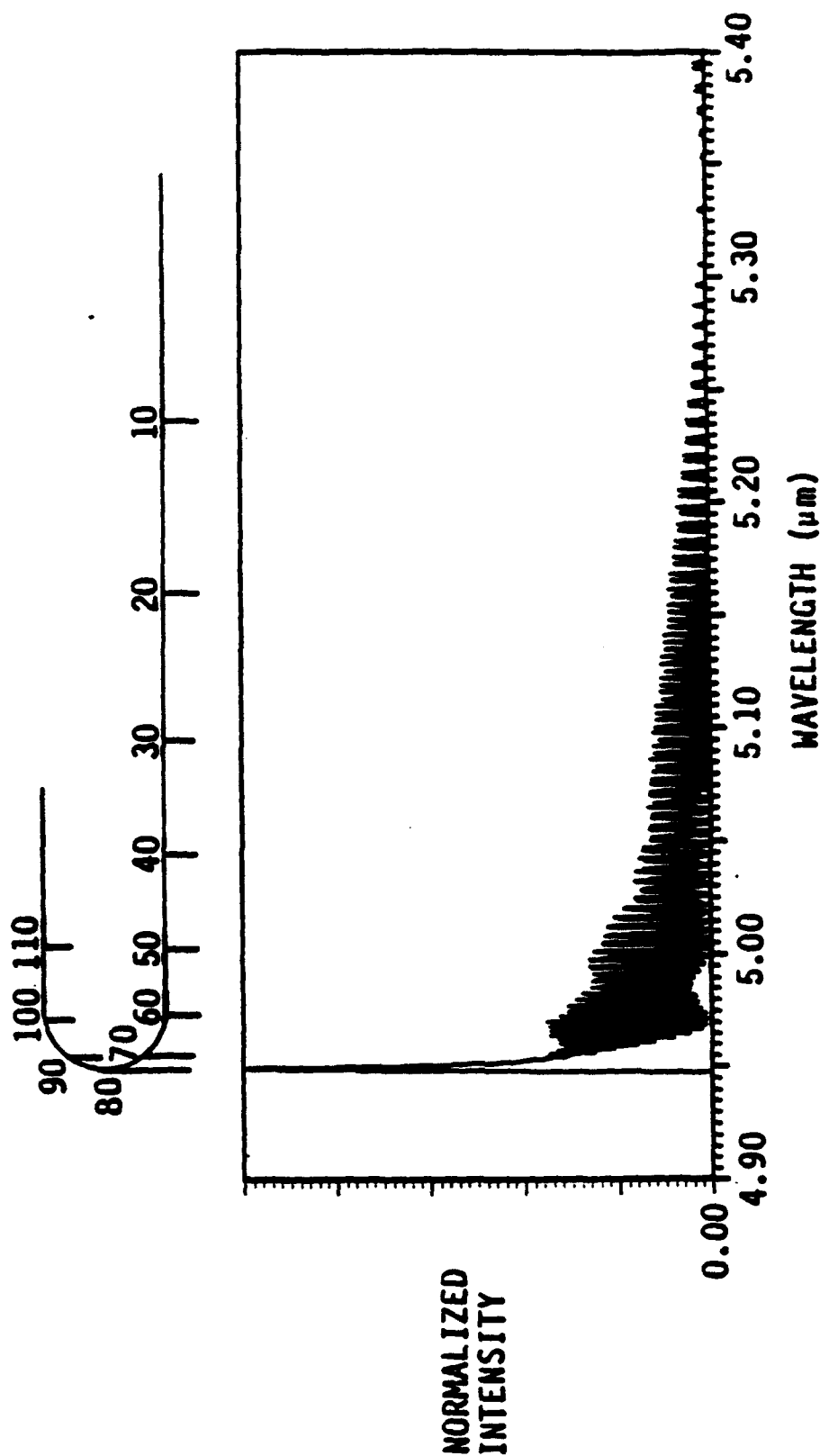
T-14152



C-2516

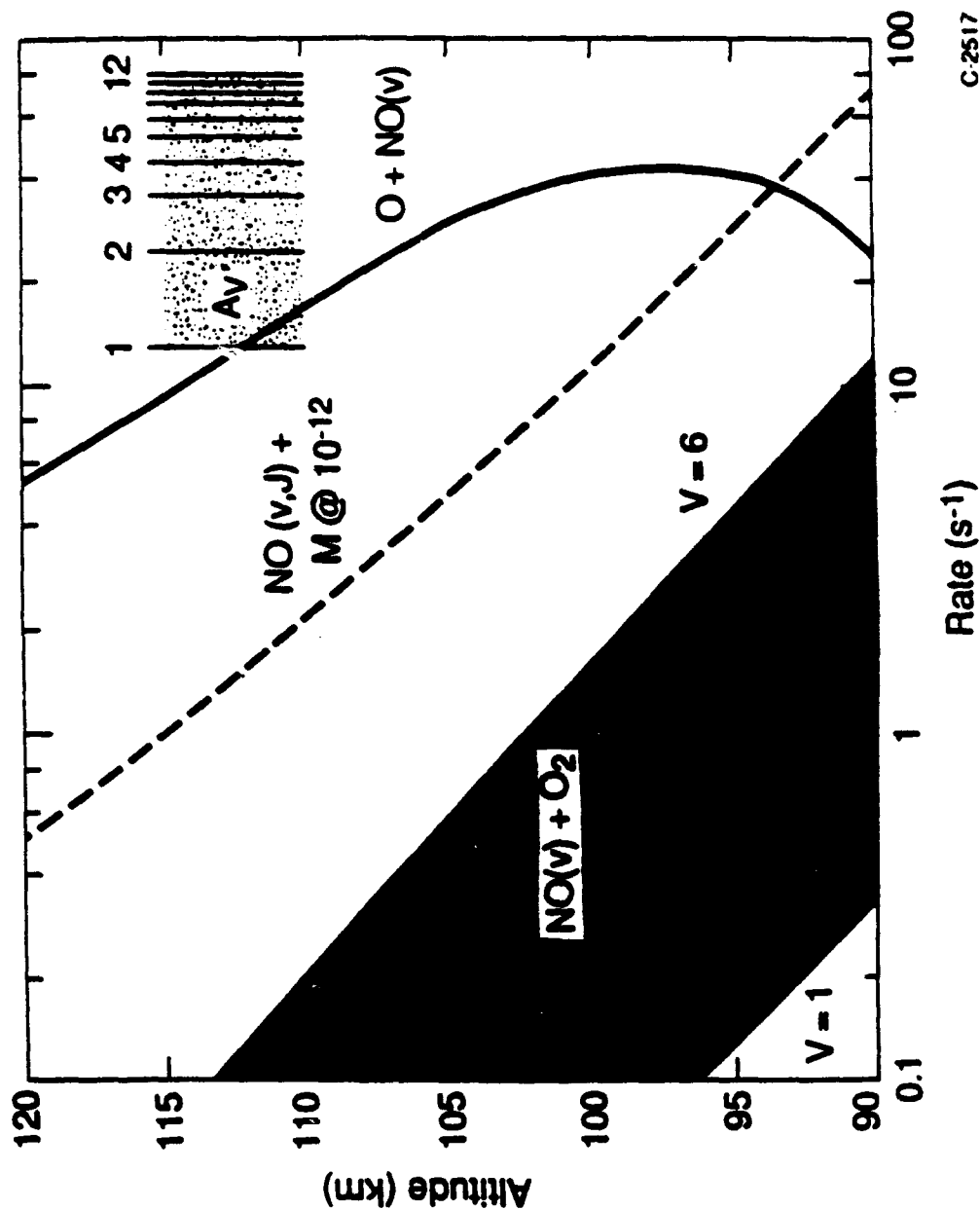
CALCULATED NO $v'=1$ $v''=0$ R BRANCH FOR $T_r=10,000$ K,

RESOLUTION=10A



NO(v) LOSSES

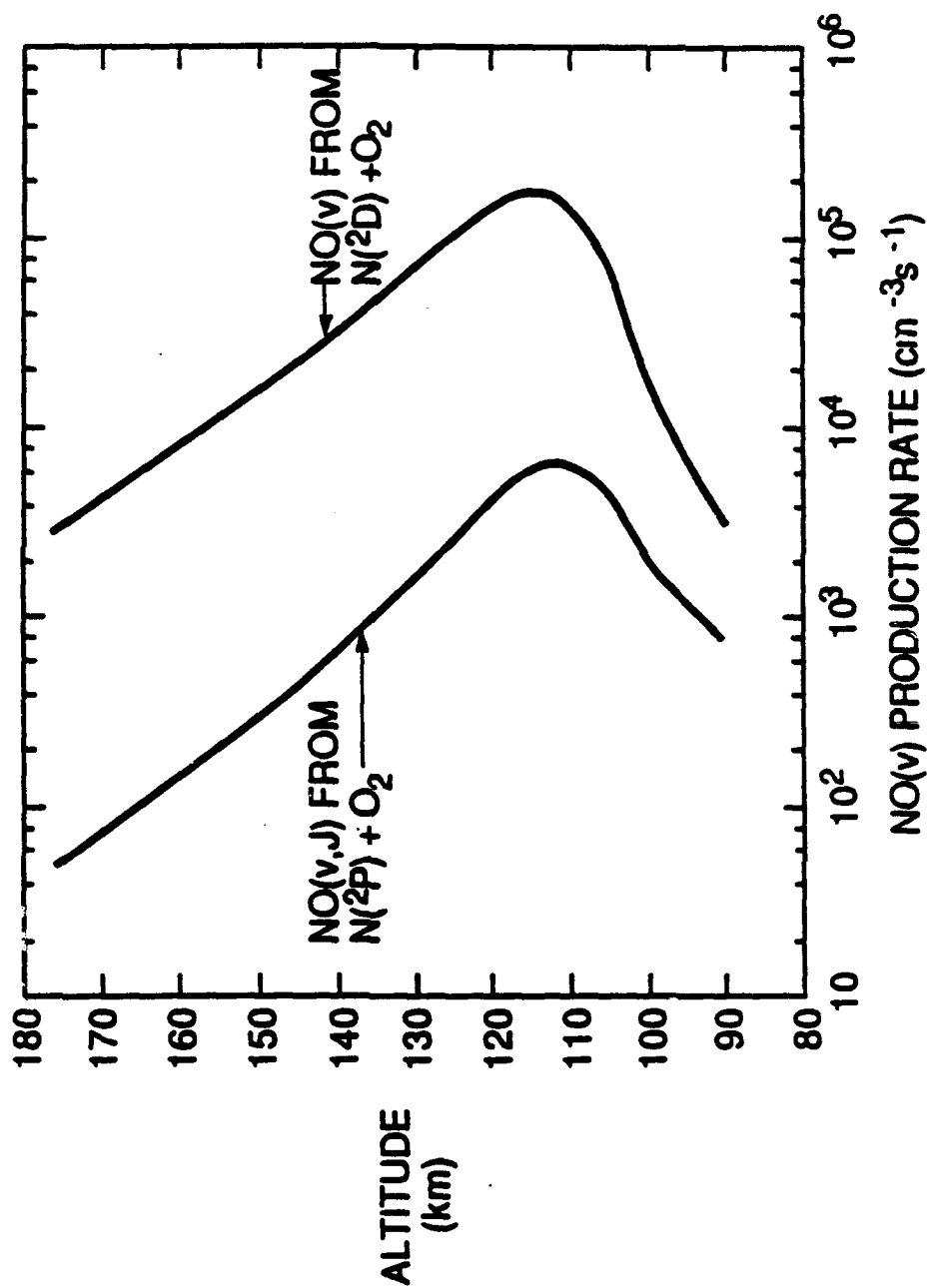
T-14153



C-2517

PREDICTED NO(v) PRODUCTION RATES CLASS II⁺ AURORAL COMPONENT

VG89-243



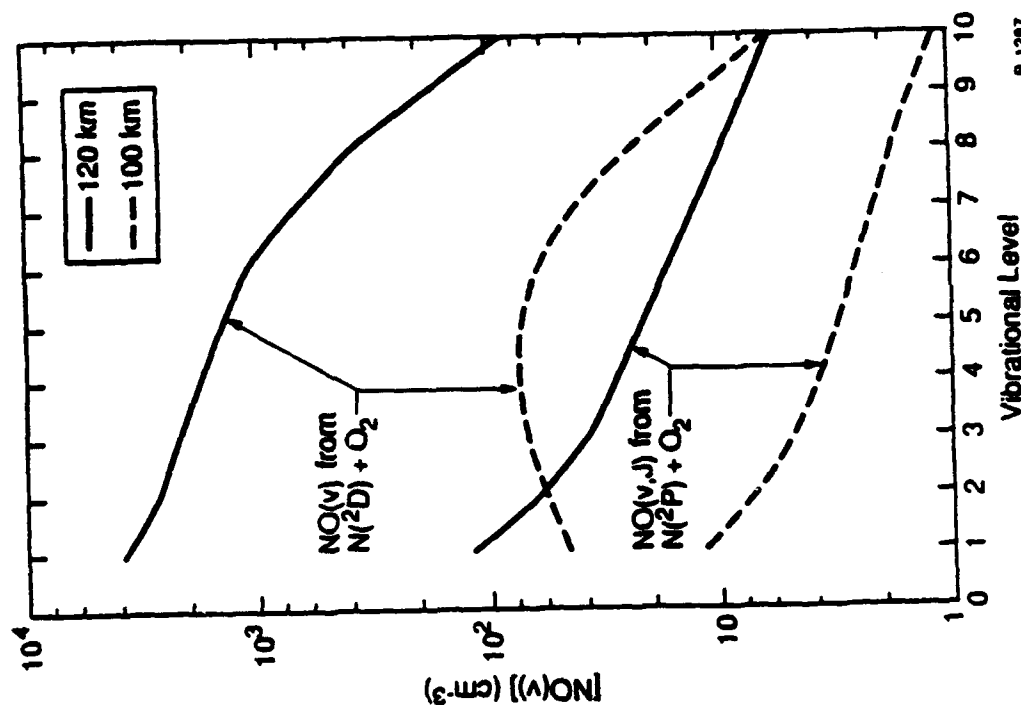
B-1290

PREDICTED AURORAL NO(v, J) PRODUCTION

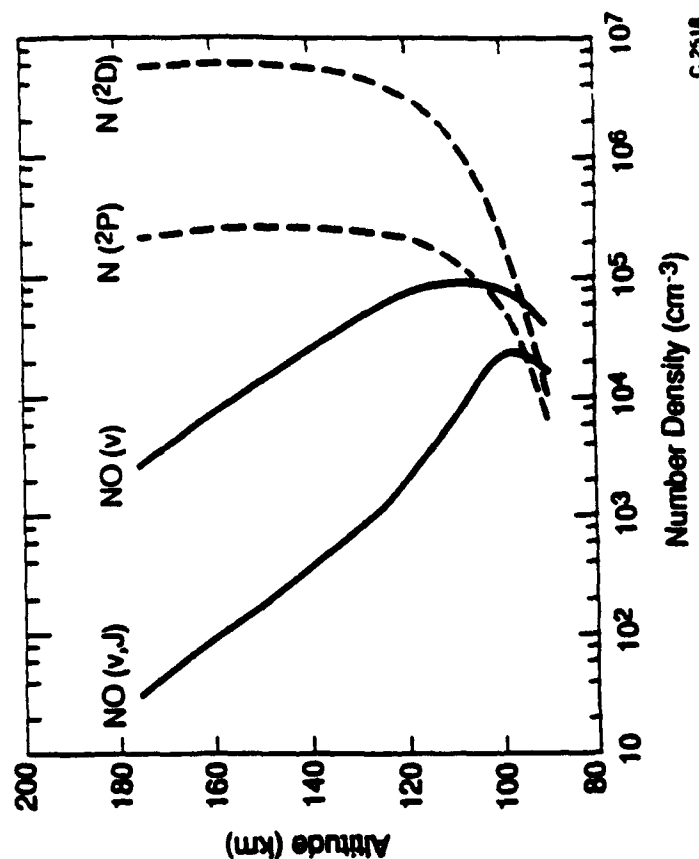
T-14154

Vibrational Distributions: IBC II

Number Densities: IBC III



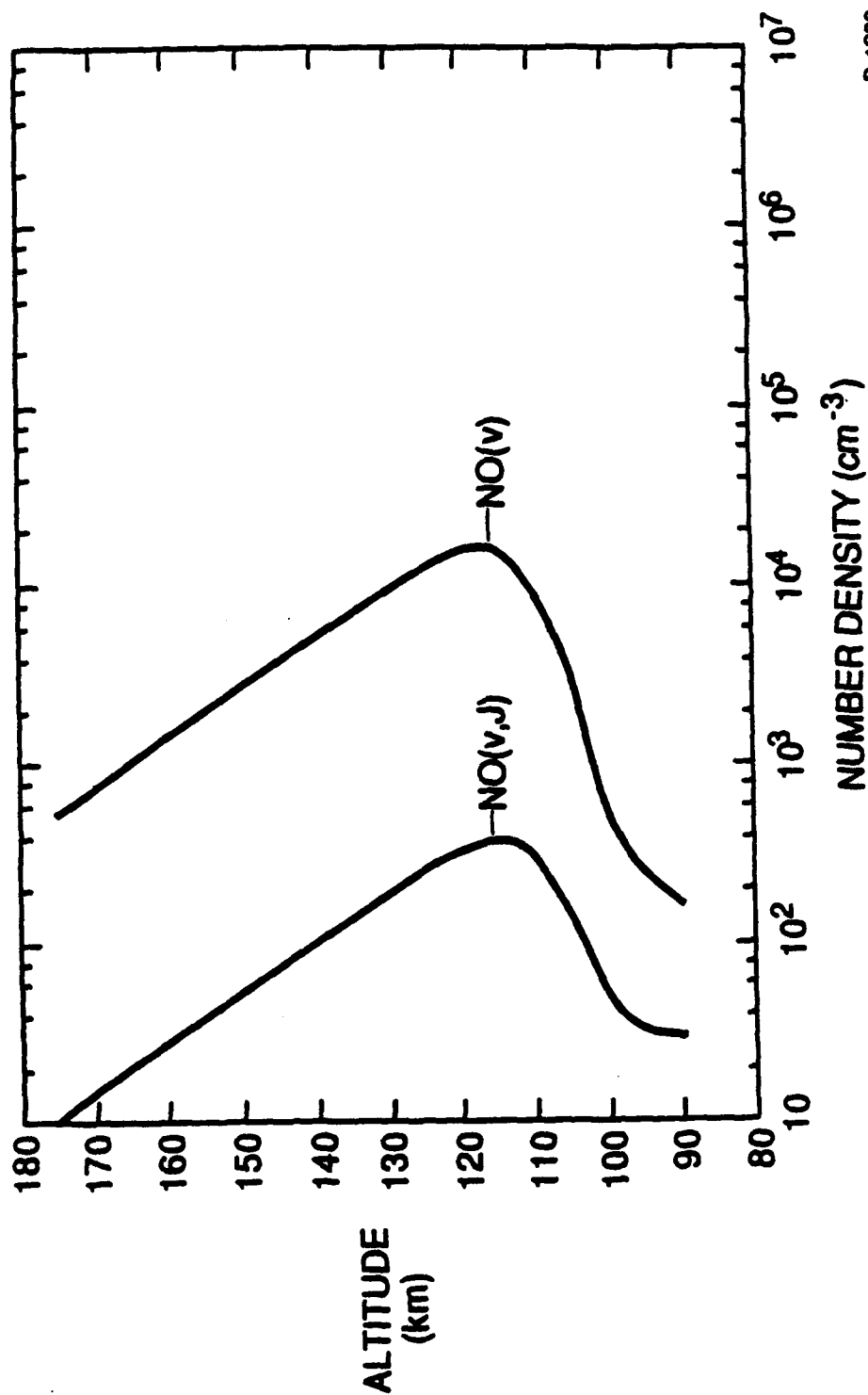
B-1287



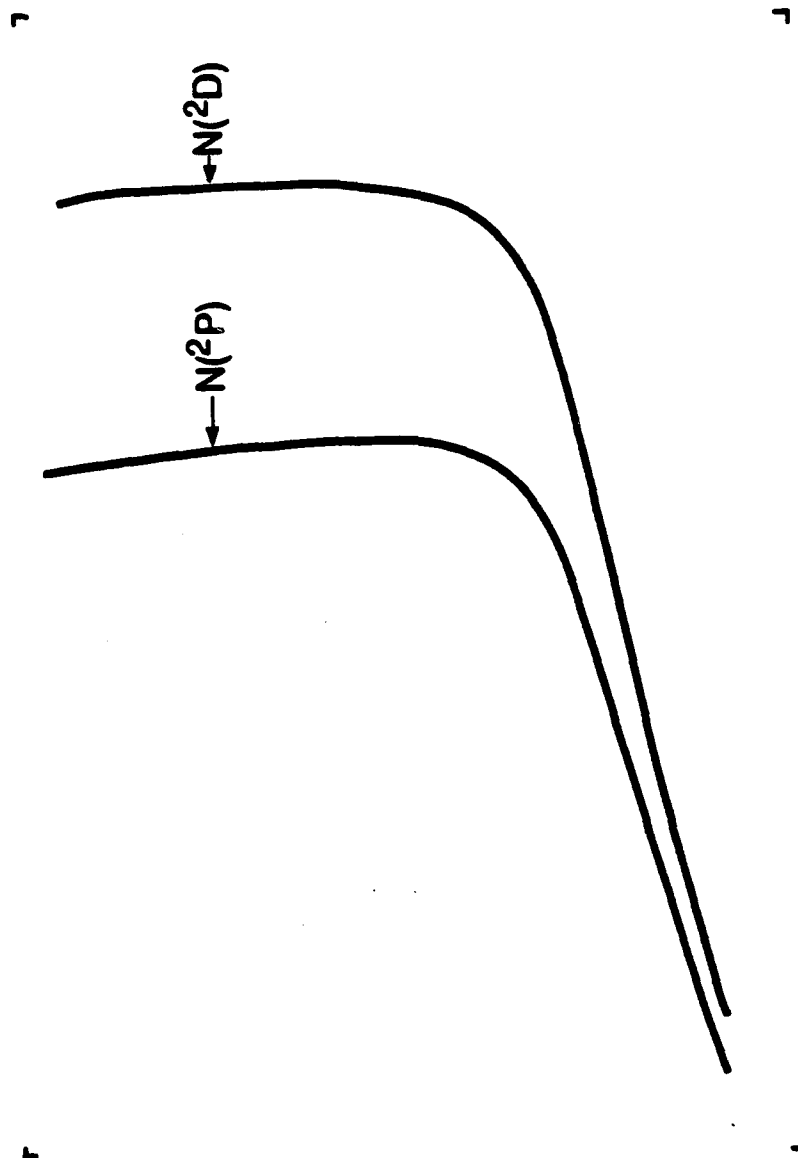
C-2518

PREDICTED NUMBER DENSITIES CLASS II⁺ AURORAL PRODUCTION

VG89-249



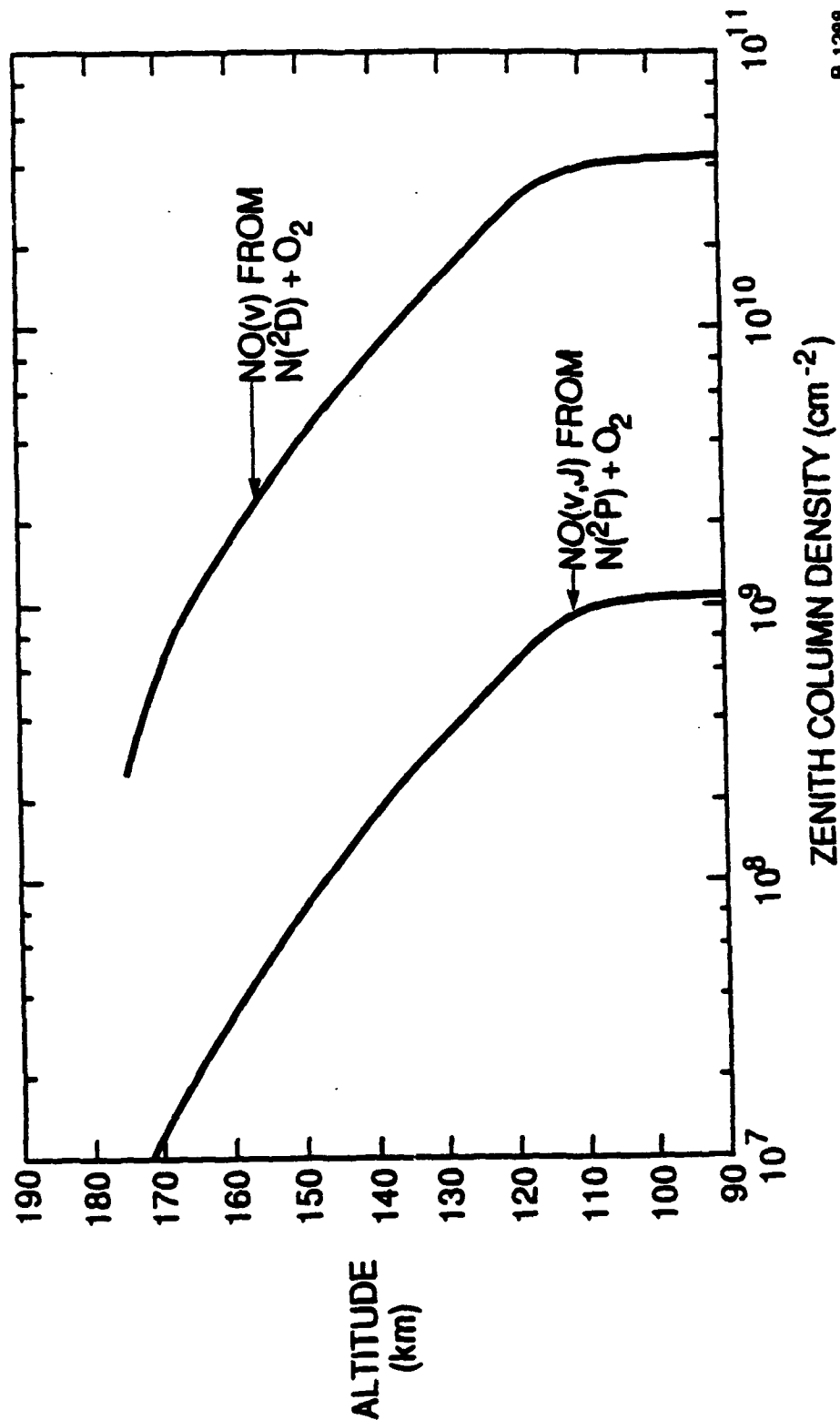
B-1289



PREDICTED AURORAL NO(v) PRODUCTION CLASS II+ AURORA

VG89-249

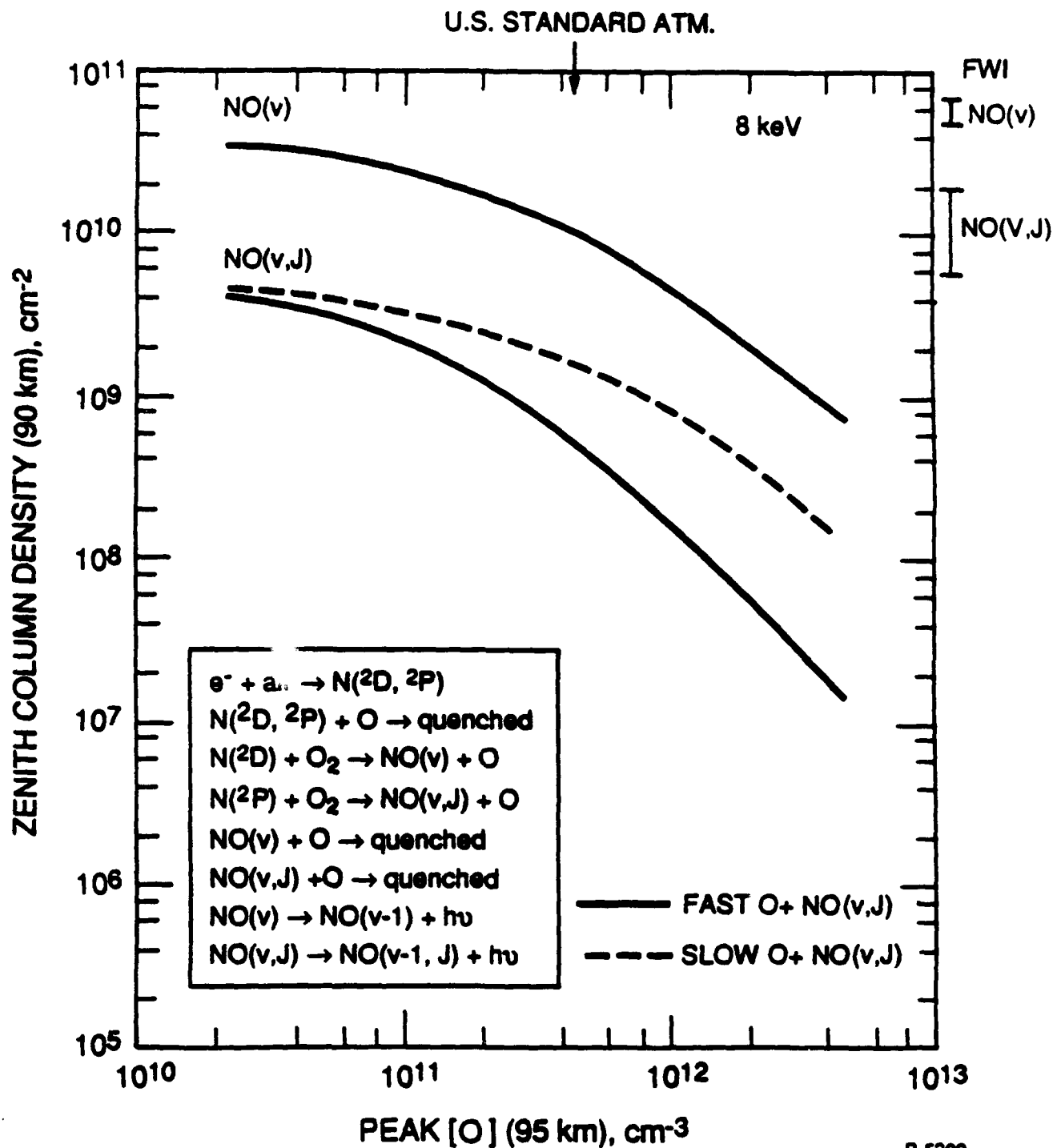
(40 kR AT 391.4 nm)



B-1288

EFFECT OF [O] ON NO(v) COLUMN DENSITY ZENITH COLUMN, $z \geq 90$ km 10 kR (391.4 nm)

T-1247

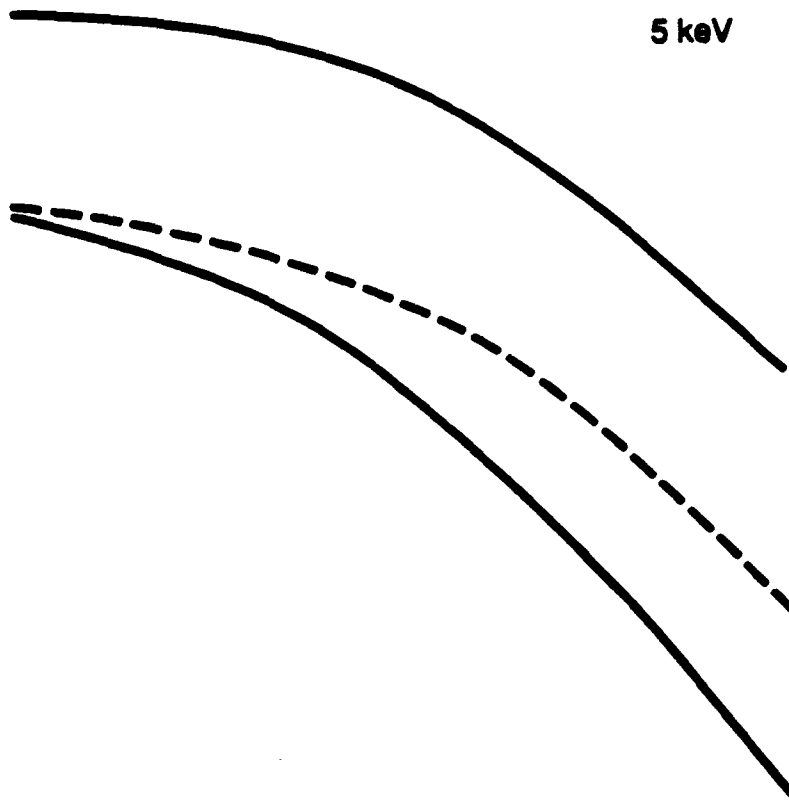


B-5299

┐

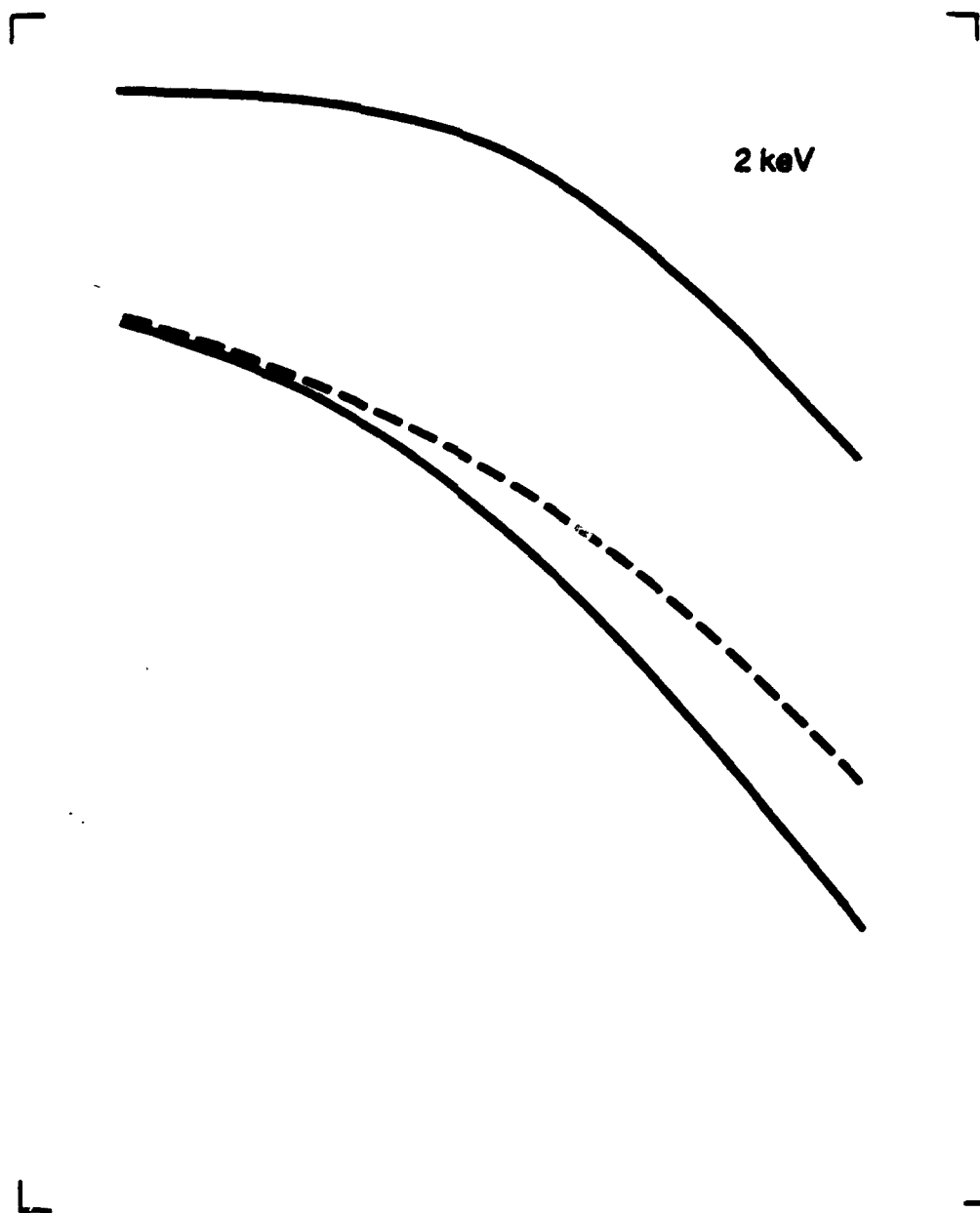
┐

5 keV



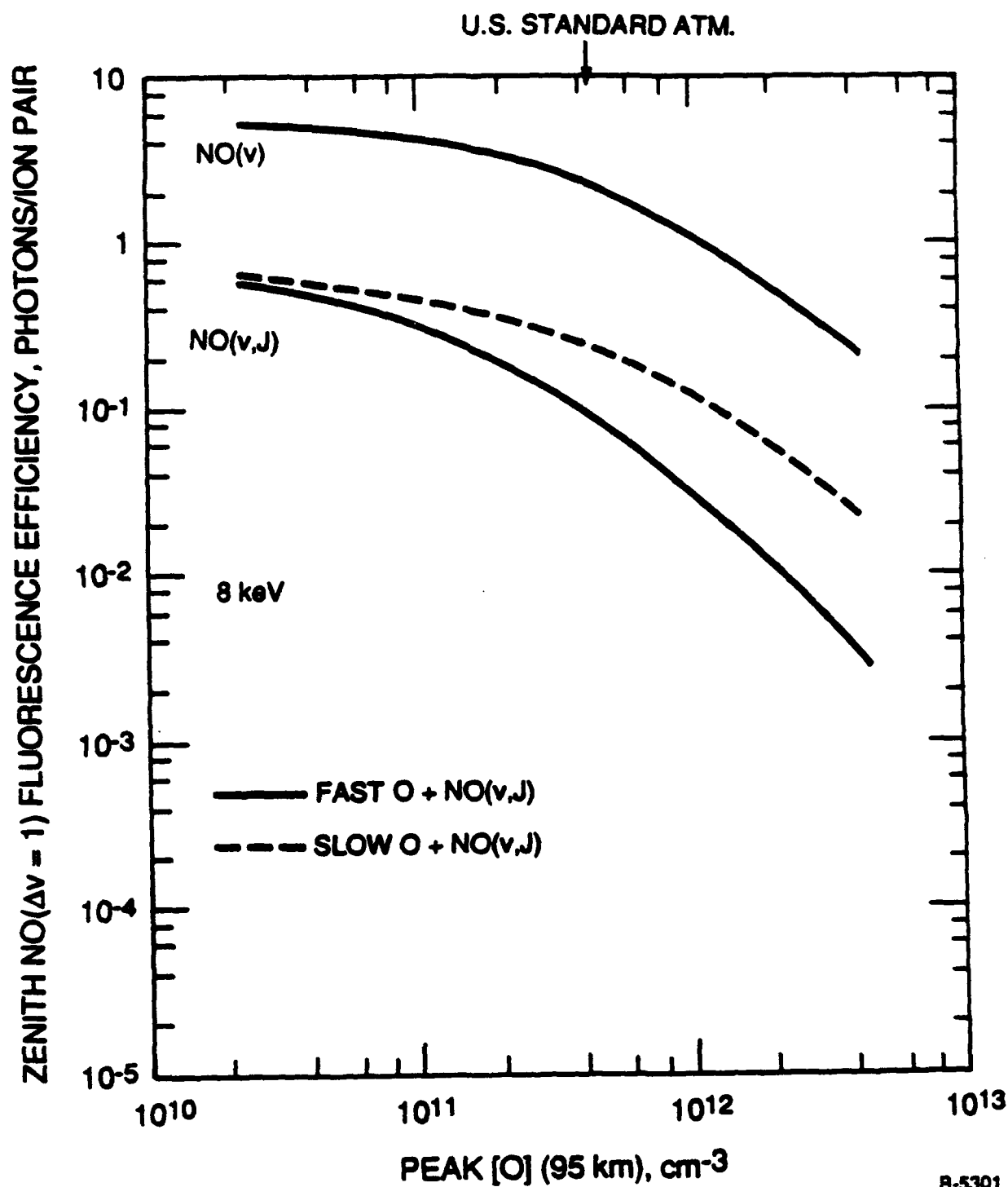
└

└



EFFECT OF [O] ON FLUORESCENCE EFFICIENCY ZENITH COLUMN, $z \geq 90$ km 10 kR (391.4 nm)

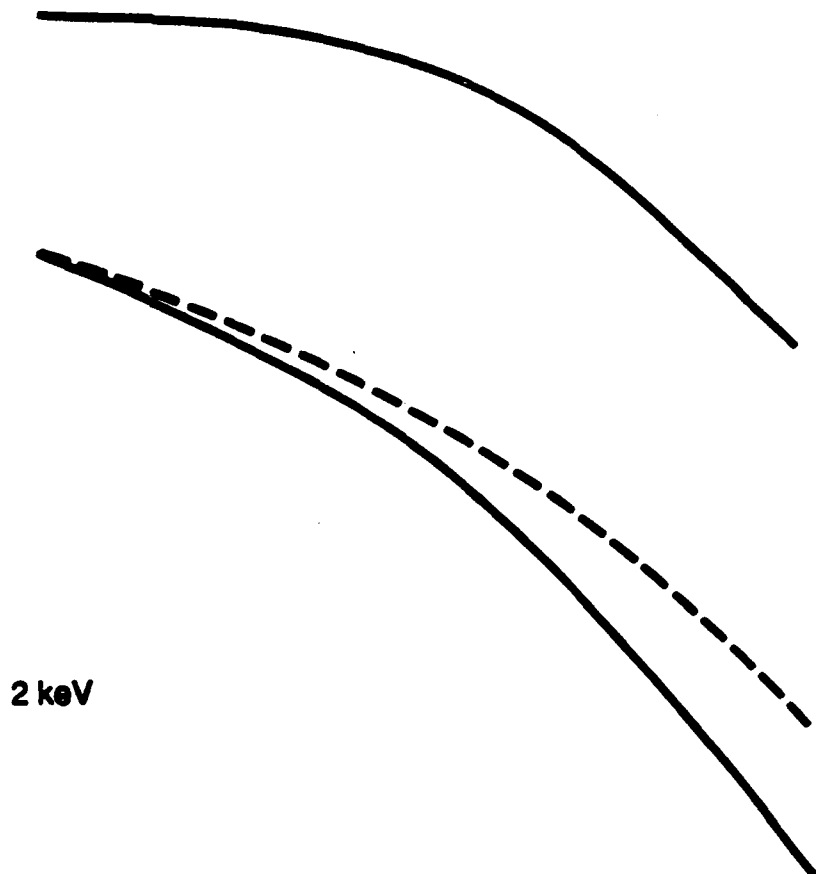
T-1248



B-5301

┐

┐



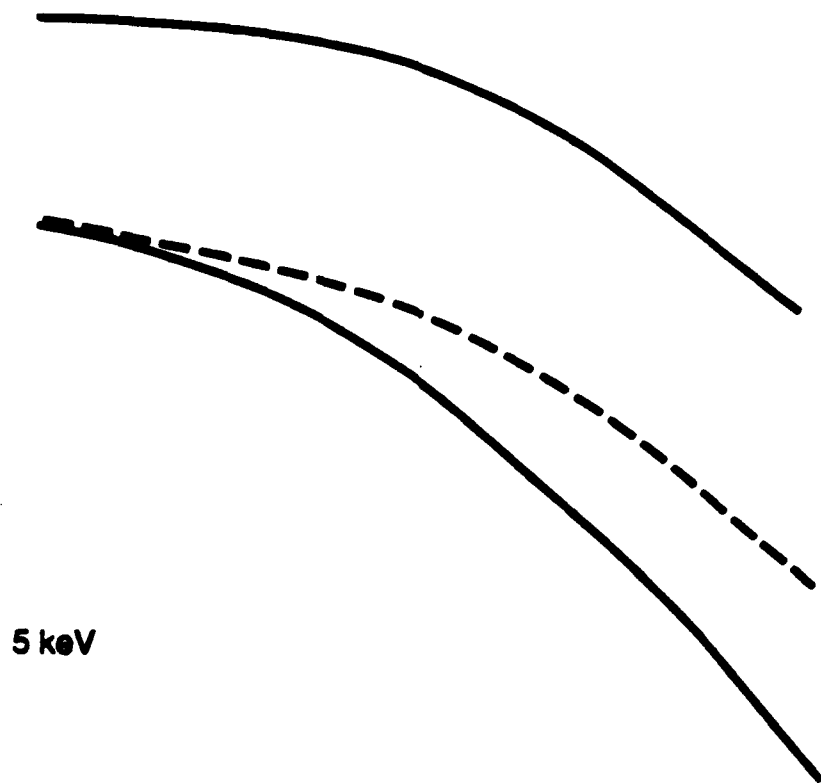
2 keV

└

└

┌

┐



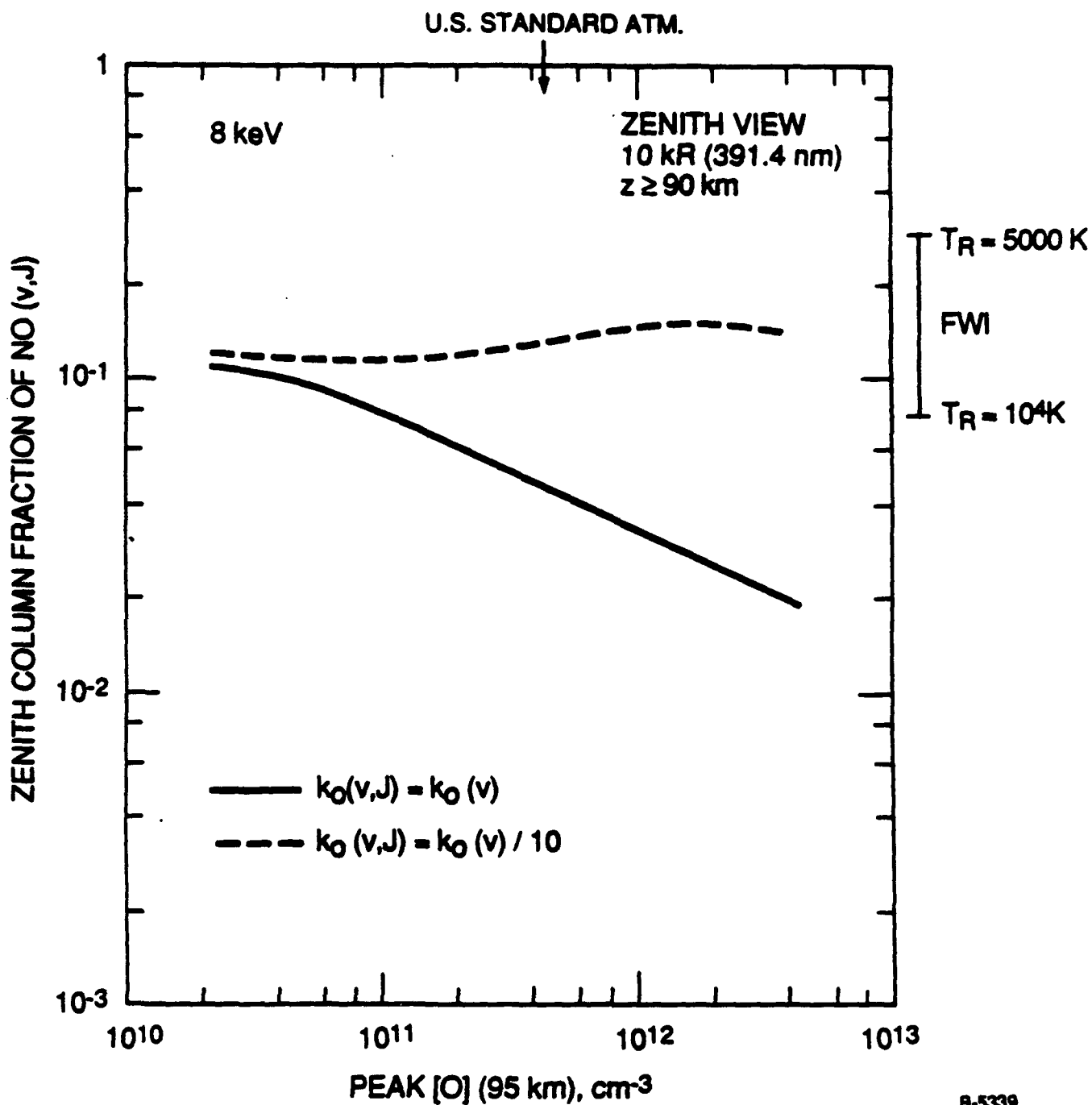
5 keV

└

┘

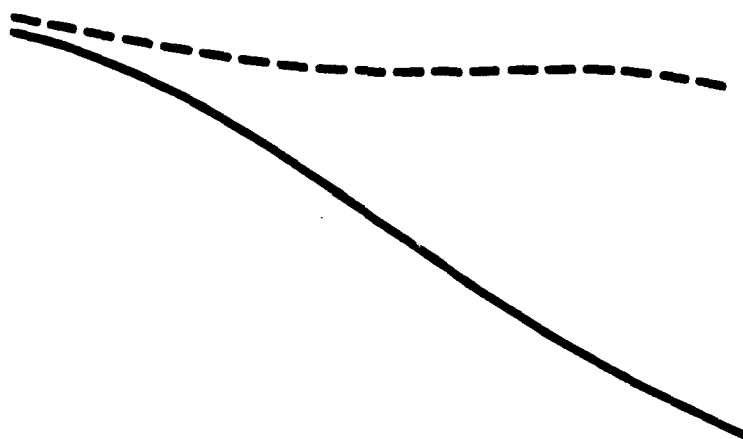
EFFECT OF [O] ON NO(v,J) CONTRIBUTION

T-1369

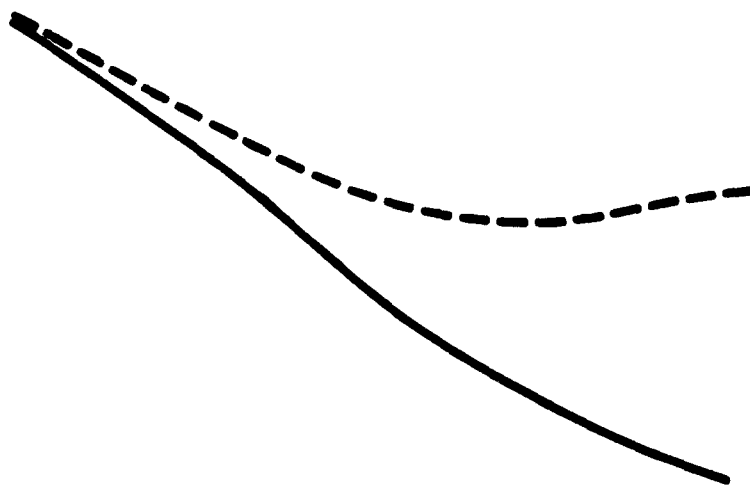


B-5339

5 keV

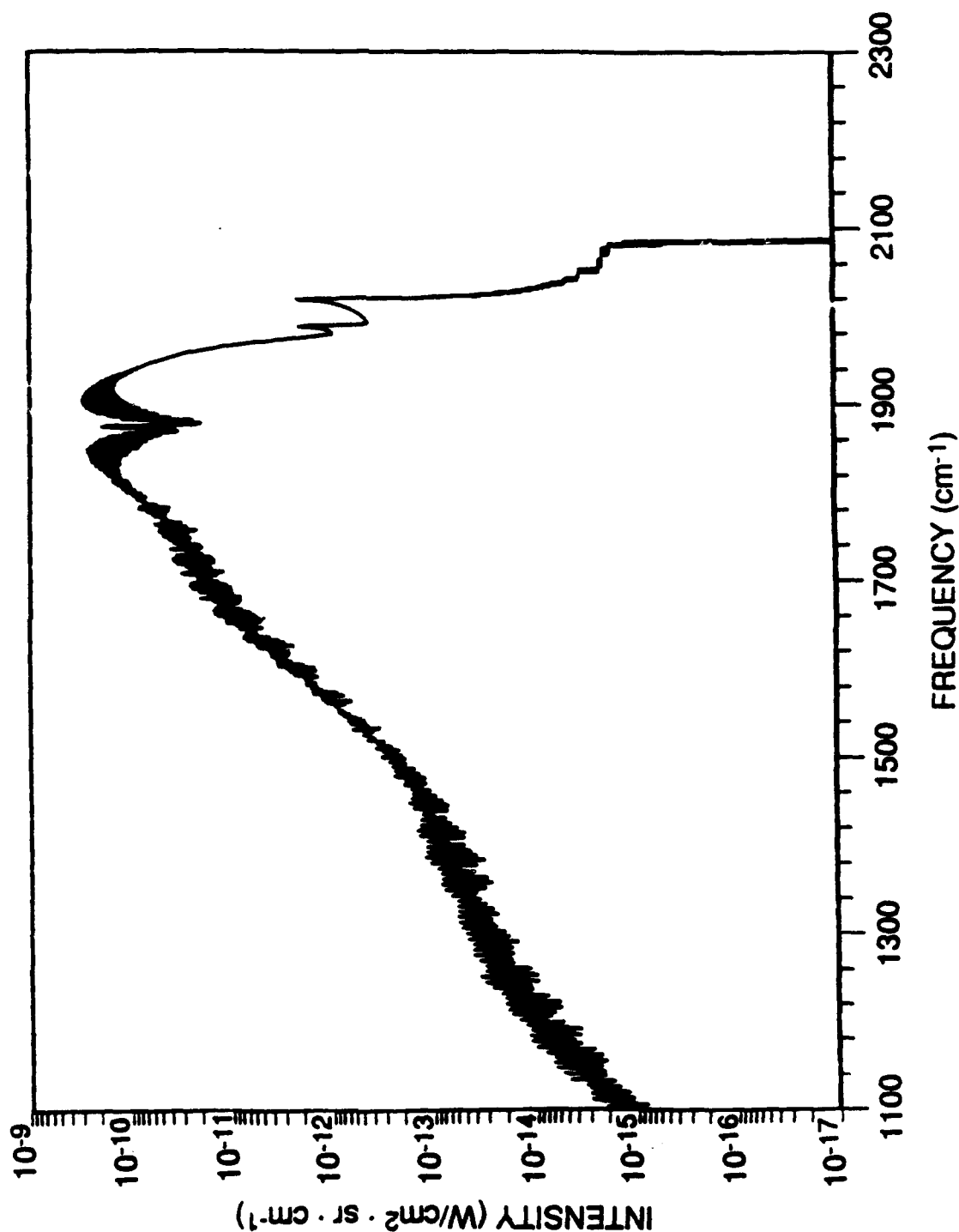


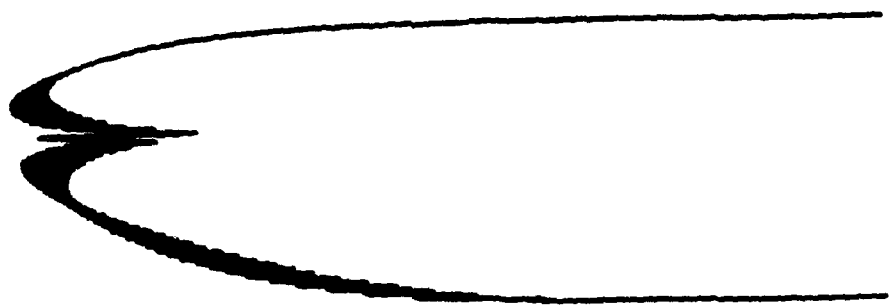
2 keV



**PREDICTED ZENITH NO RADIANCE,
IBC II+ (38 kR) AURORA, 105 km PEAK
DEPOSITION, HIGH [NO], U.S. STD. ATM.**

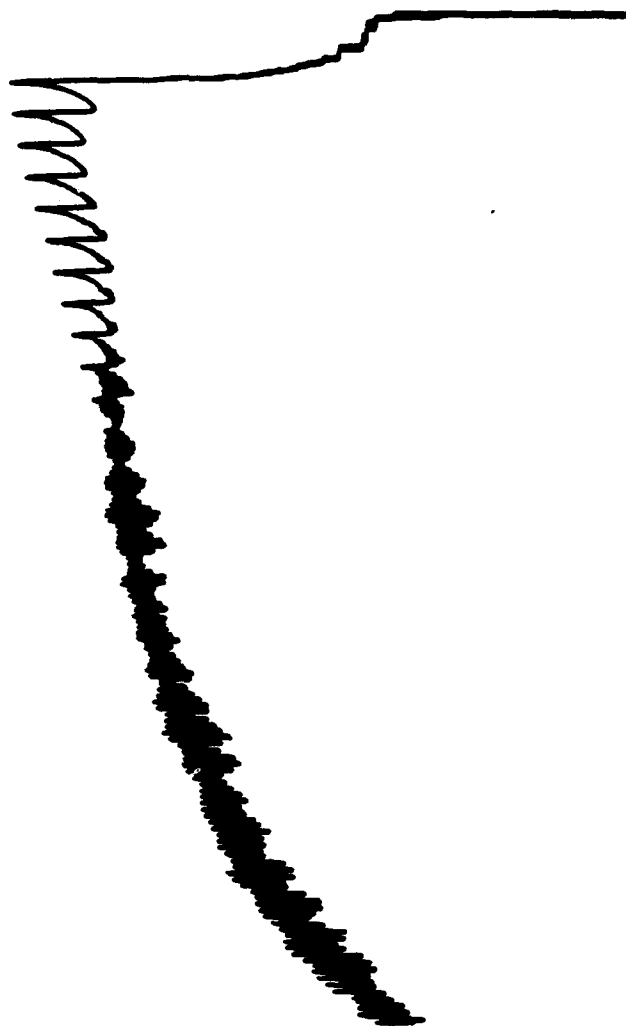
T-1247



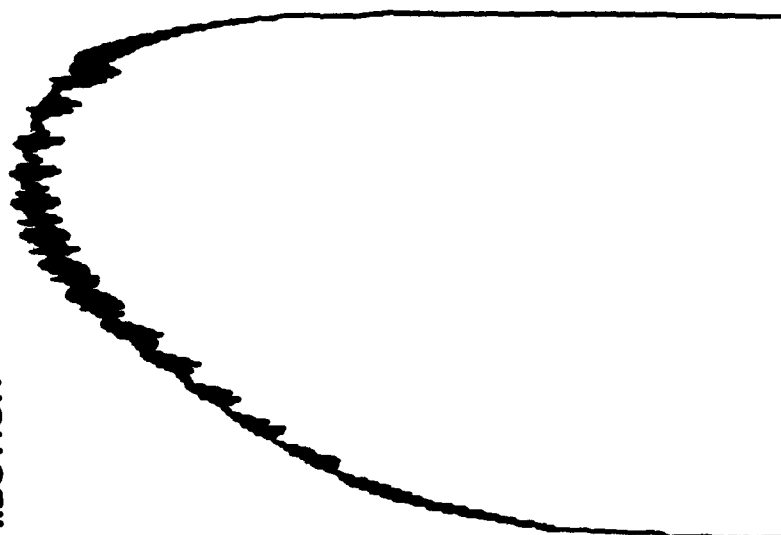


O + NO CONTRIBUTION

$N(^2P) + O_2$ CONTRIBUTION

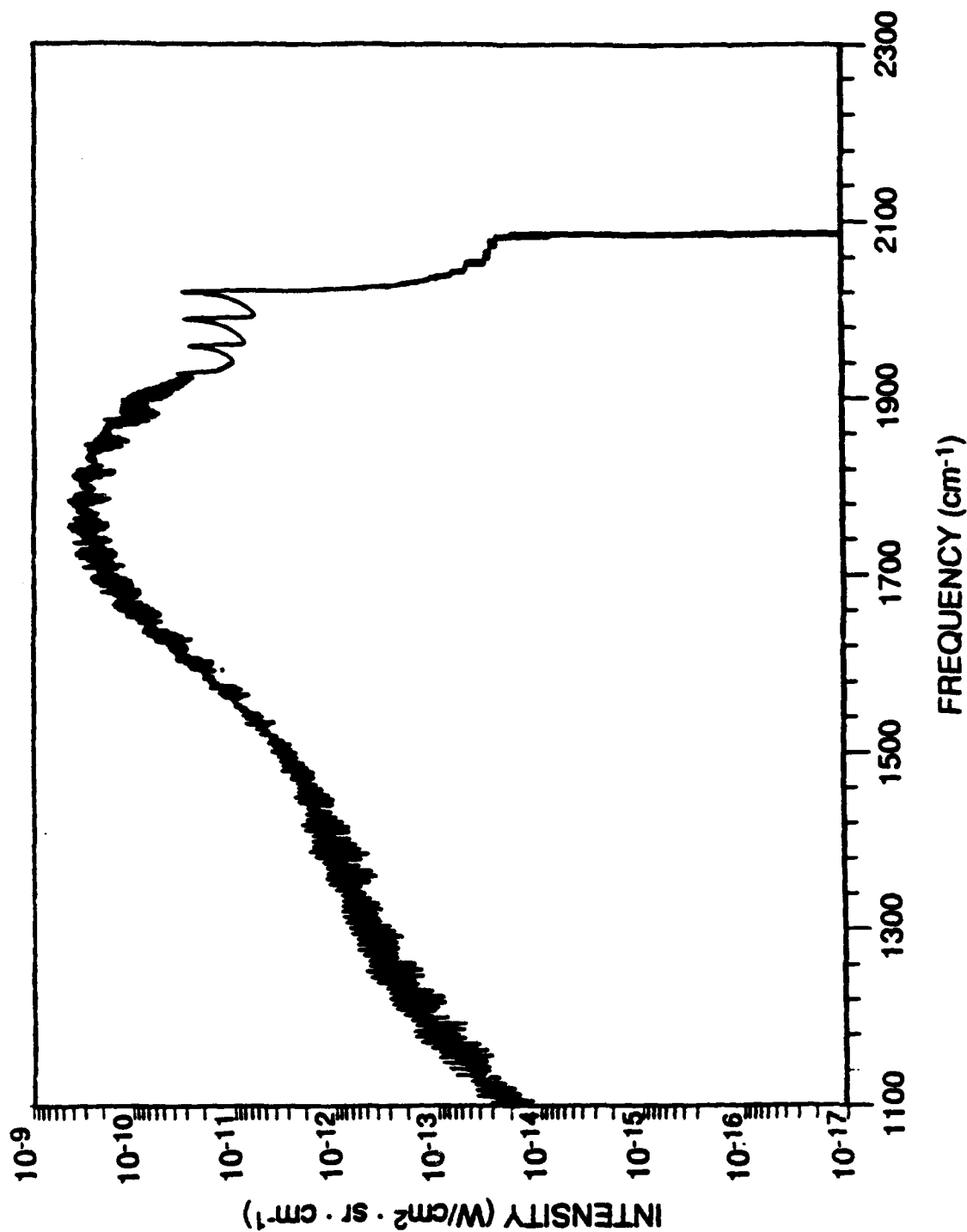


$N(^2D) + O_2$ CONTRIBUTION

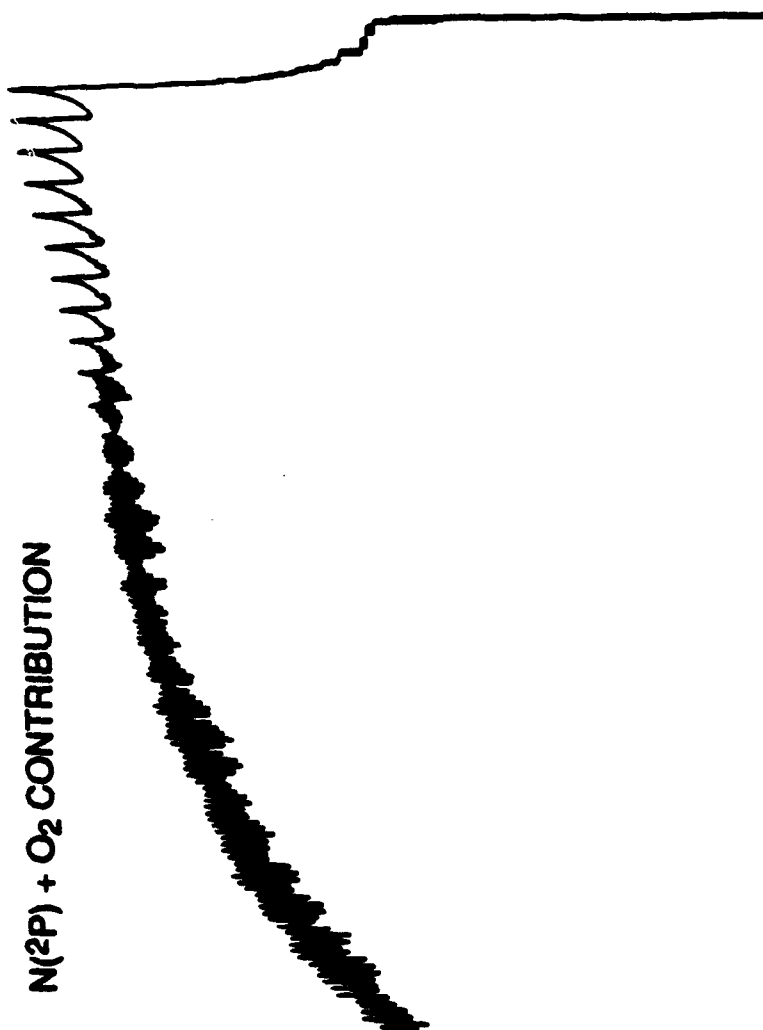


**PREDICTED ZENITH NO RADIANCE, IBC III⁺
(380 KR) AURORA, LOW [NO], U.S. STD. ATM.**

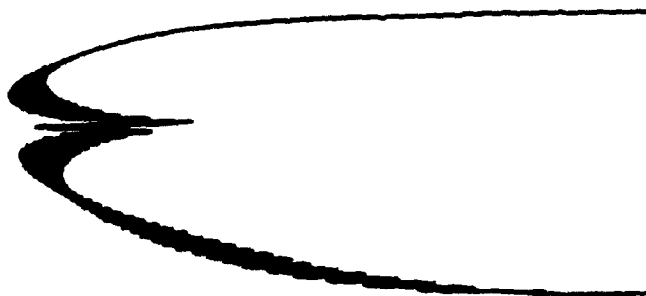
T-1246



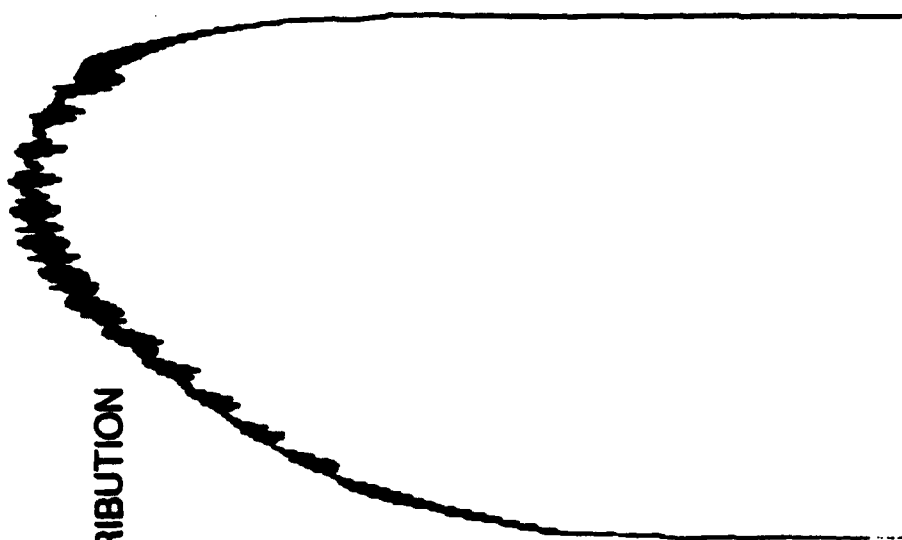
B-3976a



O + NO CONTRIBUTION

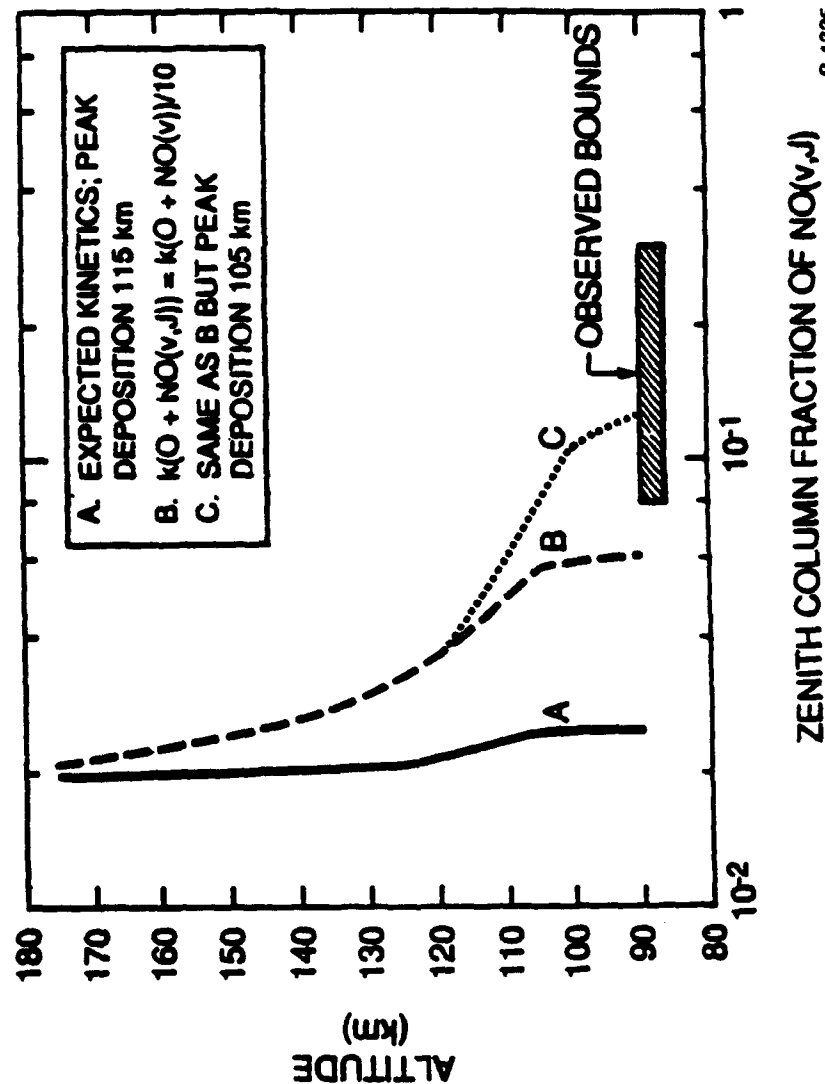


$\text{N}(^2\text{D}) + \text{O}_2$ CONTRIBUTION



PREDICTED FRACTIONAL CONTRIBUTION OF $\text{NO}(\nu, J)$ FROM $\text{N}(\text{}^2\text{D}, \text{}^2\text{P})$ SOURCES TO THE CLASS II⁺ AURORA

I-3130



B-1325

- $\text{N}(\text{}^2\text{P}) + \text{O}_2$ source of $\text{NO}(\nu, J)$ is insufficient to reproduce observed auroral data
- Agreement can be improved if collisional quenching is slow and auroral penetration is deeper
- Alternatively, there may be another $\text{NO}(\nu, J)$ source

ALTERNATIVE NO(v,J) SOURCES

T-3131

- Observation requires NO(v,J) production rate $\sim 10^{4-5} \text{ cm}^3 \text{ s}^{-1}$
near 110 to 120 km
- Possible reactions to form NO(v,J):

$(\text{N}^*, \text{N}_2^*) + \text{NO}$	Observed in COCHISE
$\text{O} + \text{N}_2^*$	Possible but never observed
$\text{O}_2 + \text{N}_2^*$	Four-center exchange unlikely
$\text{O}(\text{fast}) + \text{NO}$	Not enough O(fast)
$\text{O}(\text{fast}) + \text{N}_2$	Requires $> 4 \text{ eV}$
- $(\text{N}^*, \text{N}_2^*) + \text{NO}$ will contribute if $[\text{NO}] \geq 10^9 \text{ cm}^{-3}$ [these concentrations were observed for FWI aurora]

IMPLICATIONS OF HIGH-ALTITUDE NO(v,J) MODELING

T-1250

- $N(^2P) + O_2$ mechanism requires low $[O]$, deep auroral penetration
- Predicted NO(v) yields are lower than FWI observation
- $N(^2D, ^2P)$ auroral production efficiencies are critical unknowns
 - Requires field measurements
 - May be enhanced by predosing
- Other mechanisms for NO(v,J) formation may contribute
 - $(N_2^+, N^+) + NO$
 - $O + N_2 (A^3\Sigma)$
 - Need more laboratory/field data to evaluate these

FIELD MEASUREMENT REQUIREMENTS FOR NO(v,J)

T-1251

- IR fluorescence spectra
 - 1 to 2 cm^{-1} resolution
 - 4.9 to 8.0 μm
 - NESR $\sim 10^{-13} \text{W/cm}^2 \text{ sr cm}^{-1}$
 - Filter NO(v=1) band
- IBC II^+ and III^+ auroras
 - Zenith or partial limb views, 90 to 150 km
 - Peak deposition 105 km or lower (monitor by ground-based photometry)
 - Test for predosing effects
- Companion photometers:
 - $\text{N}_2^+(\text{B})$ 391.4 nm
 - $\text{N}(^2\text{P})$ 346.6 nm
 - $\text{N}(^2\text{D})$ 520.0 nm
 - $\text{N}_2(\text{A})$ V-K bands
 - $\text{NO}(\text{A})$ γ bands
- Atmospheric composition sounding
 - [O] essential, [NO] optional
 - Temperature, density
 - Ion concentrations: NO^+ , O_2^+ , O^+ , N_2^+

CONCLUSIONS

VG89-249

- HIGH-J ROTATIONAL EXCITATION ($\sim 10^4$ K) PERSISTS ABOVE 100 km: 10 TO 30 PERCENT OF TOTAL AURORAL NO(v) BUDGET
- EXPECTED $N(^2P) + O_2$ CONTRIBUTION IS 2 TO 10 PERCENT
- MOST ALTERNATIVE MECHANISMS SEEM UNLIKELY
- MAJOR UNKNOWN FACTORS
 - $N(^2D)/N(^2P)$ EXCITATION EFFICIENCIES
 - DEACTIVATION KINETICS/RADIATIVE RATES FOR NO(v, HIGH J)
 - T DEPENDENCE OF N^* KINETICS AND PRODUCT CHANNELS
 - KINETICS OF $O + NO(v)$
 - CONTRIBUTIONS FROM ENERGY TRANSFER MECHANISMS: $(N^*, N_2^*) + NO$